INVESTIGATING THE ROLE OF THE UBCH10 PROTO-ONCOGENE PRODUCT IN HIGH GRADE SEROUS OVARIAN CANCER

BY

RAWDA AHMED TAWFIQ MAHMOUD ELSHENNAWY

A thesis submitted to the University of Birmingham for the degree of

DOCTOR OF PHILOSOPHY

Institute of Cancer and Genomic Sciences
College of Medical and Dental Sciences
University of Birmingham
September 2023

ABSTRACT

High grade serous carcinoma (HGSOC) is the 5th leading cause of cancer related deaths in females worldwide. According to the Cancer Genome Atlas (TCGA), HGSOC is marked by early *TP53* mutation and has four molecular subtypes; Mesenchymal, Immunoreactive, Proliferative and Differentiated. Despite advances in our understanding of the molecular background of HGSOC, treatment modalities have not improved patient survival. UbcH10/Ube2C is an E2-conjugating enzyme that regulates cell-cycle progression, by promoting the degradation of mitotic regulators through the ubiquitin-proteasome pathway. UbcH10 is also a proto-oncogene whose aberrant expression has been reported in numerous cancers.

Research carried throughout this thesis aimed at investigating UbcH10 as a potential biomarker for the prognostication and molecular stratification of HGSOC. We aimed to study its relative protein expression in HGSOC, relation to *TP53* mutations, molecular subtypes of HGSOC and its effect on patient outcome. In addition, we aimed to identify its role in the progression of HGSOC by studying its expression in its precursor lesions; serous tubal intraepithelial carcinomas (STIC) and p53 signatures. Three experimental cohorts were investigated in the present study and the publicly available TCGA cohort of ovarian serous carcinomas was also interrogated.

Immunohistochemistry (IHC) was used to investigate UbcH10 and p53 protein expression in a training cohort which included 100 full-faced HGSOC sections and a validation cohort of 81 cases of tissue microarrays were used. UbcH10 was scored according to the IRS and H-scores, and the *X*-tile tool was used to generate biologically significant cut-off values. Ki-67 and CD8 IHC were used for molecular subtyping of the

training cohort according to TCGA groups. Multiplex IHC was used to investigate the co-expression of UbcH10/Ki-67 as well as UbcH10/p53 in a third cohort of 24 STIC samples and their matched HGSOC.

UbcH10 overexpression was detected in 29-33% and 16-17% of the training and validation cohorts respectively. In the training cohort, UbcH10 overexpression did not significantly impact survival nor correlate with p53 mutations, prognostic, or predictive parameters. Additionally, UbcH10 expression was positively correlated with Ki-67 index and significantly associated with the aggressive and treatment resistant Proliferative molecular subtype of HGSOC.

In the validation cohort, Ubch10 negatively impacted overall survival. The trend was maintained in progression-free survival but was not significant. Results from both cohorts therefore conclude that UbcH10 is significantly related to the proliferative state of the cell and has a borderline poor prognostic significance in HGSOC.

In STIC/HGSOC cohort, like p53, UbcH10 is expressed early in STICs and is positively correlated with Ki-67 index. A heterogeneous rather than a directly proportional relationship exists between p53 and UbcH10 in STICs and their corresponding HGSOC.

Analysis on TCGA cohort confirms results from the experimental cohorts at the gene level. *Ube2C* is significantly co-expressed with genes involved in cell-cycle regulation and has no impact on HGSOC mortality or progression. *Ube2C* gene expression levels do not correlate with *TP53* mutations and are significantly associated with the Proliferative molecular subtype of HGSOC. So, whilst UbcH10 is only a borderline prognostic marker in HGSOC, it is more beneficial as a predictor of treatment response when interpreted in the context of the molecular subgroup of HGSOC.

ACKNOWLEDGEMENT

First and foremost, I am deeply grateful to Allah the most gracious and most merciful for guiding me on my path and taking care of me through His unsleeping eye.

I would like to express my sincere gratitude to my supervisors, Dr Andy Turnell and Mr Jason Yap for their steadfast support, valuable guidance with my lab work, and for providing a warm and friendly work environment. Furthermore, I extend my gratitude to Dr Raji Ganesan for her support and help with all the pathology aspects of this work.

I am very thankful for the Newton-Mosharafa scholarship program and the International Society of Gynaecological Pathologists (ISGyP) for funding my work.

I would also like to extend my gratitude to:

The late Professor Naveena Singh for provision of material and data for the Barts cohort.

Dr Sayeed Haque, for training me on using the SPSS software for all statistical analyses in this study as well as his guidance with interpretation of data from both the Birmingham and Barts cohorts.

Dr Robert Camp for his help on analysing and interpreting data from the *X*-tile software.

Dr Martin Read, for training me on downloading, acquiring, and analysing TCGA cohort.

Dr Deena Gendoo for her help in using the Bioconductor package to assign molecular subtypes to TCGA cohort.

Dr Rachel Pounds and Dr Danielle O'Neill for provision of baseline survival data for the Birmingham cohort till 2018.

Dr Dean Larner and Mr Khalil Uddin for training me on all aspects related to slide sectioning and staining.

Professor Ahmed Ahmed from the University of Oxford, Dr Maria Pinna from the Andrew Beggs group and Dr Jianmin Zuo from the Paul Moss group for providing reagents, technical support, and assistance on culturing organoid models.

Last, but not least, I am eternally grateful for my loving family and their constant support without which this work would not have come to fruition.

TABLE OF CONTENTS

LIST OF FIGURES

LIST OF TABLES

ABBREVIATIONS

APC/C: Anaphase-Promoting Complex/Cyclosome

AJCC: American Joint Committee on Cancer

AURKA: Aurora Kinase A

AURKB: Aurora Kinase B

BAX: BCL2 associated X

BRCA1: Breast Cancer gene 1

BRCA2: Breast Cancer gene 2

BSO: Bilateral salpingo-oophorectomy

CA-125: Carbohydrate antigen 125

CCC: Clear cell carcinoma

CDK: cyclin-dependent kinase

CENP-A: Centromere protein A

C.I: Confidence interval

CRS: Chemotherapy response score

CTD: C-terminal domain

DAB: 3’,3'-Diaminobenzidine

DBD: DNA-binding domain

DDS: Delayed debulking surgery

DMEM: Dulbecco’s Modified Eagle Medium

DNE: Dominant negative effect

EC: Endometrioid carcinoma

EMT: Epithelial to Mesenchymal transition

EOC: Epithelial ovarian cancer

FBS: Foetal-bovine serum

FIGO: International Federation of Gynaecology and Obstetrics

FFPE: Formalin fixed paraffin embedded tissue blocks

FPKM: fragments per kilobase transcript per million

5-FU: 5-fluoro-uracil

GOF: Gain of function

H&E: Hematoxylin and Eosin

H-score: Histochemical score

HGSOC: High grade serous ovarian cancer

HIER: Heat induced epitope retrieval

HPA: Human Protein Atlas

HPF: High power field

HR: Hazard ratio

ICCR: International Collaboration on Cancer Reporting

IHC: immunohistochemistry

IRS: Immunoreactive score

KEGG: Kyoto Encyclopedia of Genes and Genomes

LGSOC: Low grade serous ovarian cancer

LOF: Loss of function

LOH: loss of heterozygosity

mIHC: multiplex immunohistochemistry

miRNA: micro-ribonucleic acid

MCC: Mitotic Checkpoint Complex

MMR: Mismatch repair

MYBL2: MYB protooncogene like 2

NACT: Neo-adjuvant chemotherapy

NE-GOF: no evidence of gain of function

NLS: Nuclear localization signal

NES: Nuclear exclusion sequence

NGS: Next generation sequencing

OS: Overall survival

PARP: poly ADP ribose polymerase

PBGOC: Pan-Birmingham Gynaecological Oncology Centre

PBST: Phosphate buffered saline with Tween

PCR: Polymerase chain reaction

PDS: Primary debulking surgery

PFS: Progression-free Survival

PLK1: Polo-like kinase 1

POLE: Polymerase DNA Epsilon

RCPath: The Royal College of Pathologists

RING: really interesting new gene

SAC: Spindle Assembly Checkpoint

siRNA: short interfering ribonucleic acid

SLH: sheet-loop-helix

SNP: Single nucleotide polymorphism

SPSS: Statistical Package for Social Sciences

STIC: Serous tubal intraepithelial carcinoma

TAH: Total abdominal hysterectomy

TCGA: The Cancer Genome Atlas

TD: tetramerization domain

TIGAR: *TP53*-inducible glycolysis and apoptosis regulator

TPS : tumour proportion score

TILs : Tumour infiltrating lymphocytes

TMA: Tissue microarrays

UAE: Ubiquitin-activating enzyme

UK: United Kingdom

Chapter 1. Introduction

1.1. Ovarian Cancer Incidence and Mortality rates

Ovarian cancer is the seventh most common cancer in females worldwide, and the eighth most common cause of cancer-related mortality. Among gynaecological malignancies, it is the third most common cancer following cervical and uterine cancer, respectively (1). According to Global Cancer Statistics, a total of 313,959 new cases of ovarian cancer were diagnosed in 2020, constituting 3.4% of all female cancers, with an Age-Standardized Incidence rate of 6.6 per 100,000 females (2). Ovarian cancer varies widely in frequency among the different geographic regions and ethnic groups. In general, the disease is more common in transitioned countries with a high Human Development Index (HDI), and low parity (2). The incidence rates per annum are highest particularly in the United States and Northern Europe with rates exceeding 9.3 and 16 per 100,000 females, respectively. Comparatively, the incidence rate in Eastern Africa including Egypt is 5.8 per 100,000 females (2). Historical data indicates, however, that there has been a small but steady increase in ovarian cancer incidence in Southern and Eastern Europe as well as Asia, with decreases in Northern Europe and North America. Among the various ethnic groups globally, White women tend to show higher rates than Asian and Black women (3).

Recent statistics in the UK indicate that ovarian cancer is the 6th most common cancer accounting for 4% of all new cancer cases among British females with around 7500 new cases diagnosed every year between 2016 and 2018 (Cancer Research UK). In the UK, ovarian cancer incidence rates are projected to increase between 2023-2025 and 2038-2040 (Cancer Research UK). Akin to the global trend, in England, ovarian

cancer incidence rates are lower in Asian and Black females compared to White females (4).

Although ovarian cancer ranks 3rd in incidence among female genital tract malignancies, it is the most lethal of all gynaecological cancers (3). Moreover, compared to the most common female malignancy, breast cancer, ovarian cancer is three times more fatal (5). The year 2020 recorded a total of 207,252 deaths from ovarian cancer worldwide, accounting for 4.7% of total cancer-related deaths in women and an Age-Standardized Mortality rate of 4.2 per 100,000 females (2).

With respect to mortality rates, the UK recorded 4100 deaths per annum from ovarian cancer between 2017 and 2019, constituting 5% of all cancer-related mortalities in British females (Cancer Research UK). Although incidence rates are high among countries in the Western hemisphere, mortality rates are declining especially in North America and Northern Europe (6). The UK alone showed a reduction in ovarian cancer-related mortality by 16% over the last decade (Cancer Research UK). In fact, mortality rates from ovarian cancer are projected to drop by 15% in the UK between 2023-2025 and 2038-2040. Similar to incidence rates, non-White ethnic minorities show lower mortality rates from ovarian cancer compared to White females in England and Wales (7).

Taken together, these numbers and figures highlight ovarian cancer as a significant contributor to morbidity and mortality among the global female population.

1.2. Types, Aetiology and Risk factors of Ovarian Cancer

1.2.1 Major morphological subtypes of ovarian cancer

Ovarian tumours comprise a very heterogeneous group of diseases. According to the World Health Organization (WHO) classification, major categories include: epithelial tumours, sex cord stromal tumours, germ cell tumours, mesenchymal tumours, mixed epithelial and mesenchymal tumours, and secondary tumours. Of these, surface epithelial ovarian neoplasms are the most prevalent (8).

The most recent 2020 WHO classification of ovarian tumours divided surface epithelial tumours into distinct diseases that differ in their histologic appearance and molecular features. Epithelial ovarian tumours are categorized as either serous, mucinous, endometrioid, clear cell, Brenner and seromucinous tumours. About 80% of these tumours are benign and occur in young females between the ages of 20 and 45 years. Borderline tumours are a distinct category of non-invasive neoplasms with an intermediate behaviour between benign and malignant tumours that occur in a slightly older age-group. Malignant surface epithelial tumours, typically referred to as epithelial ovarian cancers (EOCs), are invasive tumours that are more common in older women between 45 and 75 years of age (9).

The major morphological subtypes of EOCs include high-grade serous, low-grade serous, endometrioid (EC), clear cell (CCC) and mucinous carcinomas. Other subtypes include malignant Brenner tumours, undifferentiated and dedifferentiated carcinomas that occasionally occur but less frequently. Mixed carcinomas composed of two or more different morphological subtypes can also occur. In addition, carcinosarcomas previously categorised under the mixed mesenchymal and epithelial

category have now been identified to be of epithelial origin with divergent differentiation into malignant sarcomatous elements (8). Of all the types of ovarian malignancies, EOCs constitute the largest category (90%). In fact, in practice the term 'ovarian cancer' is used interchangeably with surface epithelial malignancies (10).

1.2.2 Aetiology and risk factors of Epithelial ovarian cancer

The rate of ovarian cancer increases with age (10). In fact, the main risk factor for ovarian cancer is older age which reflects cumulative DNA damage. In the UK, ovarian cancer incidence is particularly high in British females aged between 75 and 79 years (Cancer Research UK). In the USA, the median age at diagnosis is 63 years whilst the median age at death is 70 years. The mean age at diagnosis differs significantly between the different morphological subgroups as well between sporadic and hereditary ovarian cancer. Low-grade serous carcinomas for example are diagnosed at a younger age than high-grade serous carcinomas. *BRCA1/2* and Lynch syndrome associated ovarian cancer also typically presents earlier than sporadic ovarian cancer (10).

Other well-established risk factors for EOCs include early menarche and late menopause as well as nulliparity. On the other hand, multiparity and oral contraceptive pills (OCPs) appear to play a protective role in non-mucinous tumours especially endometrioid and clear cell carcinomas as compared to serous carcinoma (10). In fact, the observed decline in ovarian cancer incidence in North America and Northern Europe is mainly attributable to the widespread use of OCPs in these countries (11). These factors suggest a direct implicative role of ovulation-related events in causing the disease (12, 13).

Ovulation-related events are hypothesized to cause ovarian cancer through several mechanisms, the most common of which is traumatization of the ovarian surface epithelium (OSE) which predisposes malignant transformation (10). In addition, the follicular fluid released from incessant ovulation is a potential carcinogen due to its high content of reactive oxygen species (ROS). Recently, the fallopian tube has been implicated as the site of origin of high-grade serous ovarian cancer (HGSOC). The ROS in follicular fluid have been proposed to increase the risk of the malignant transformation of fallopian tube epithelium into HGSOC (14). More recent studies implicate surface inflammation induced by ovulation and pelvic inflammatory diseases as a cause of ovarian cancer, through induction of oxidative stress and DNA damage (15).These factors may explain why high parity and OCP use decrease the risk of ovarian cancer through decreasing the number of ovulations in the reproductive life of the female (16).

Obesity is among the preventable risk factors for ovarian cancer. In the UK, about 7% of ovarian cancer is caused by increased weight and the risk increases with each 5-unit increase in Body Mass Index (17, 18). The risk however seems to be more for EOCs other than HGSOC (19).

1.2.3 Hereditary ovarian cancer syndromes

About 90-95% of ovarian cancers are sporadic. Only about 5% to 10% of ovarian cancers are genetically predisposed i.e., hereditary. The latter include two well-known syndromes; Hereditary breast/ovarian cancer (HBOC), and Hereditary Non-Polyposis Colorectal Cancer (HNPCC, Lynch syndrome) (10).

HBOC is caused by germline mutations in the DNA repair genes *BRCA1* or *BRCA2* which are particularly common in Ashkenazi Jews. The lifetime risk of developing ovarian carcinoma by the age 80 years is higher for *BRCA1* than *BRCA2* mutation carriers, estimated at 44% and 17% respectively (20). Almost all these tumours are advanced stage HGSOC that occur at a younger age than sporadic cases (20).

BRCA1 and *BRCA2* genes are mapped to the long arms of chromosomes 17 and 13 respectively and they encode proteins that are implicated in homologous recombination repair, chromatin remodelling, and cell-cycle control through the regulation of ubiquitylation (10). Germline mutations are widely distributed throughout the whole length of the *BRCA* genes. These include small frameshift insertions/deletions in 89.5% of cases as well as large gene rearrangements in 10.5% of cases (Public Health England). Certain *BRCA* mutations are suggested to increase the risk of ovarian cancer. These include mutations between nucleotides 2401 and 4190 in the *BRCA-1* gene and between nucleotides 4075–6503 of exon 11 in the *BRCA-2* gene. Hence, these regions have been termed the “ovarian cancer cluster regions” (10).

HNPCC/Lynch syndrome is another hereditary ovarian cancer syndrome with an autosomal dominant pattern of inheritance. It is manifested by a predisposition to colon cancer without polypi, endometrial cancer and ovarian cancer albeit to a lesser extent than colon cancer (10).Similar to HBOC, Lynch syndrome-associated ovarian cancer typically present at a younger age than sporadic ovarian cancer. However, ovarian carcinoma in Lynch syndrome is predominantly of the endometroid and clear cell type and mostly presents at a low stage (21). HNPCC is predisposed by germline mutations involving the DNA mismatch repair (MMR) genes *hMSH2* or *hMLH1*, occurring in 70%

of patients, although germline mutations in *hPMS1*, *hPMS2,* and *hMSH6* also contribute towards HNPCC (21).

1.3 Subtype classification, Origin and Pathogenesis of Epithelial Ovarian Cancers

1.3.1 Subtypes, origin, and morphologic pathogenesis of EOC

The first WHO classification of ovarian tumours was published in 1973 and has, since undergone many revisions. This classification depended mainly on histogenesis and the morphological features of these tumours (22). For a long time, pathologists observed the resemblance of epithelial ovarian tumours to other histological structures in the female genital tract. For example, ovarian serous, endometrioid and mucinous tumours have been found to resemble fallopian tubal epithelium, the endometrium and endocervical lining epithelium, respectively. Consequently, a histogenetic theory was introduced according to which all epithelial ovarian neoplasms were deemed to arise from the OSE with questionable metaplasia to different morphological subtypes. Moreover, most investigators believed that all EOCs regardless of their morphological subtype developed through the sequential transformation of benign tumours into borderline and finally into malignant ovarian tumours (10).

However, advances in our understanding of the molecular mechanisms underlying the pathogenesis of these tumours, as well as the recognition of new precursor lesions have challenged this traditional stratification. Thus, various attempts have been made to re-classify and sub-classify ovarian cancer in a manner that reflects the biological behaviour of these tumours and correlates with their clinical course, such that common therapeutic strategies have been developed for different EOCs (23).

One breakthrough in this field has been the recognition that the origin of many subtypes of epithelial ovarian tumours is, in fact, extra-ovarian rather than the OSE (24). HGSOCs are now proven to originate from the fimbriated end of the fallopian tube, from putative precursor lesions known as serous tubal intraepithelial carcinomas (STICs). Endometrioid and clear cell tumours arise from endometriotic implants that pass from the uterine corpus through the fallopian tube to the ovaries. Mucinous and Brenner tumours originate from transitional type epithelial nests (Walthard cell rests) at the tubal-mesothelial junction through a process of metaplasia (24).

1.3.2 Model of epithelial ovarian cancer carcinogenesis

The biological characterization of ovarian epithelial carcinogenesis has led to a new dualistic model, which has been formally recognized in the 2014 WHO classification of ovarian tumours (Figure 1.1; (25). Type I tumours are thought to progress in a slow stepwise fashion, reminiscent of the classical adenoma-carcinoma sequence of colorectal cancer. This means they arise from benign precursor lesions namely borderline tumours and endometriotic implants and then progress to invasive low-grade carcinomas. On the other hand, type II tumours previously thought to arise “de novo” without identifiable precursors, have been shown to arise from identifiable extra-ovarian histological precursors (24).

Type I tumours include, low grade serous, low grade endometrioid, primary mucinous, clear cell carcinomas and malignant Brenner tumours. High grade serous carcinoma constitutes the majority of type II tumours. Other less frequent type II tumours include high grade endometrioid, undifferentiated carcinomas and carcinosarcomas. Studies show that undifferentiated carcinomas are probably variants of high-grade serous carcinomas, although evidence is inconsistent (26). Carcinosarcomas on the other

hand have been recognized in the latest WHO classification to arise from HGSOC with divergent differentiation as evidenced by the presence of identical *TP53* mutations in the carcinomatous and sarcomatous component (8). Moreover, evidence shows that like HGSOC they can arise from STIC lesions in the fallopian tube (10).

From a genomic perspective, type I tumours are genetically stable with rare *TP53* mutations. More commonly they show somatic mutations of switch proteins and protein kinases encoded by the following genes *KRAS, BRAF, PIK3CA*, and *ERBB2*. Other genes often found mutated in type I tumours encode signalling molecules such as *CTNNB1* (β-catenin) and *PTEN*. This contrasts sharply with type II tumours that are chromosomally unstable with frequent and early *TP53* mutations and infrequent *BRAF* and *KRAS* mutations (27, 28).

Clinically, type I tumours are indolent tumours that usually present at an early stage confined to the ovary. These tumours usually have a better prognosis and five-year survival rates than type II tumours. In contrast, type II tumours are aggressive tumours that usually present at an advanced stage from the outset with peritoneal dissemination, extra pelvic spread and distant metastasis (10).

Regarding their response to therapy, type I tumours are less sensitive to platinum-based chemotherapy in the adjuvant and neoadjuvant settings compared to type II tumours. This can be owed to their lower cellular proliferative index (8). Worthy of note is that CCC, although belonging to the type I category-due to its genetic similarity with these tumours and its origin from established precursors (endometriosis), is in fact clinically high grade with an aggressive behaviour displaying upfront resistance to chemotherapy (10). It has been concluded therefore, that low-grade (type I tumour)

and high-grade serous carcinomas (type II tumour) follow independent pathways; they are not two grades of the same neoplasm but are rather two distinct tumour types with different underlying pathogenesis and biological behaviour (28).

It is important to note however that on rare occasions, up to 3% of high-grade serous carcinomas can coexist with low grade components whether borderline tumours or low-grade serous carcinomas (LGSOC) (29). Similarly, LGSOC were associated on rare occasions with high grade serous carcinomas, undifferentiated carcinomas and carcinosarcomas. This shows that, although infrequently, HGSOC can evolve from LGSOC or arise directly from serous borderline tumours (30, 31). Nonetheless, this phenomenon is usually accompanied by the acquisition of *TP53* mutation (30).

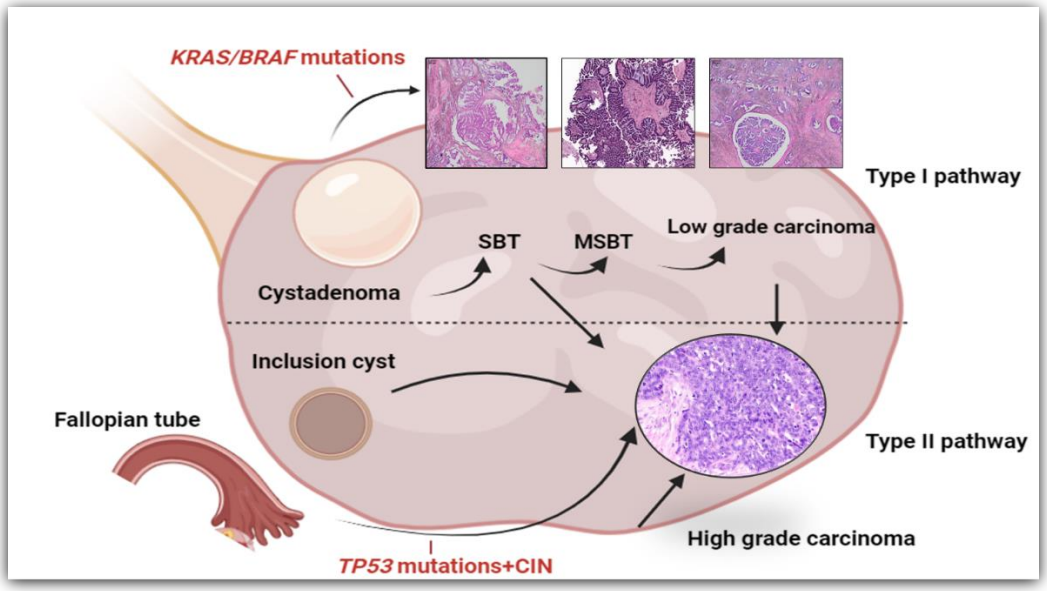

Figure 1. 1: A Schematic diagram demonstrating type I and type II pathways of ovarian epithelial carcinogenesis. Type I tumours develop in a stepwise fashion from benign and borderline precursor lesions into low grade carcinomas. They rarely show *TP53* mutations and more commonly show *KRAS/BRAF* mutations. Type II tumours on the other hand arise from extra-ovarian precursor lesions and are high grade carcinomas with chromosomal instability and frequent *TP53* mutations. CIN-chromosomal instability. SBT: Serous borderline tumour, MSBT: Micropapillary serous borderline tumour. Figure generated in BioRender using H&E images generated during this study. Adapted from Shih & Kurman, 2004 (27).

1.4 Prognostic and Predictive factors in ovarian cancer

Prognostic factors give a clue about the clinical outcome of the disease at the time of diagnosis, independent of therapy. In cancer patients they are indicators of growth, invasion, and metastatic potential. Predictive factors on the other hand portend the response to a given therapeutic modality. In Ovarian cancer patients, the two most powerful prognostic factors are FIGO (International Federation of Gynaecology and Obstetrics stage) and the volume of residual disease after surgery and debulking for stage IIIC and stage IV disease. Age is also a strong prognostic factor. Other debatable prognostic and predictive factors as well include cell type and histopathological grade (10). Measures of treatment response that have been found to be strongly correlated with patient outcomes in ovarian cancer include the chemotherapy response score (CRS) and resistance to platinum therapy (32-34).

1.4.1. FIGO stage and Volume of Residual disease

The newest FIGO staging for ovarian cancer recognizes the entire shift in paradigm regarding the origin and pathogenesis of EOCs. Therefore, the new staging system encompasses: ovarian, fallopian tubal and peritoneal carcinomas. The basis of the FIGO staging is the anatomical progression of ovarian cancer from those confined to the ovary (stage I), to those that spread locally in the pelvis (stage II), followed by peritoneal dissemination in the abdominal cavity with a specific predilection for the omentum (stage III) and finally to distant organs like the lung and liver (stage IV) (35). Most gynaecological oncologists use the FIGO staging system for ovarian cancers. Another widely used classification system is the TNM (primary Tumour, lymph Node, distant Metastasis) staging from the Union for International Cancer Control (UICC).

The 8th edition of the TNM staging has been used along the FIGO stage since 2018 (35). Table 1.1 summarizes the FIGO staging system and its corresponding TNM staging for ovarian, tubal, and peritoneal cancer.

Table 1. 1: The 2014 FIGO Ovarian, Fallopian tube, and Peritoneal Cancer Staging System and Corresponding TNM (35).

Stage I	**Tumor confined to ovaries or both fallopian tubes.[a]** **T1N0M0**
IA **T1aN0M0**	Tumor limited to one ovary (capsule intact) or fallopian tube; no tumor on ovarian or fallopian tube surface; no malignant cells in the ascites or peritoneal washings
IB **T1bN0M0**	Tumor limited to both ovaries (capsules intact) or fallopian tubes; no tumor on ovarian or fallopian tube surface; no malignant cells in the ascites or peritoneal washings
IC	Tumor limited to one or both ovaries or fallopian tubes, with any of the following:
IC1 **T1c1N0M0**	Surgical spill intraoperatively
IC2 **T1c2N0M0**	Capsule ruptured before surgery or tumor on ovarian or fallopian tube surface
IC3 **T1c3N0M0**	Malignant cells in the ascites or peritoneal washings
Stage II	**Tumor involves one or both ovaries or fallopian tubes with pelvic extension (below pelvic brim) or primary peritoneal cancer.[b]** **T2-N0-M0**
IIA **T2aN0M0**	Extension and/or implants on uterus and/or fallopian tubes and/or ovaries
IIB **T2bN0M**	Extension to other pelvic intra-peritoneal tissues including bowel serosa within the pelvis
Stage III	**Tumor involves one or both ovaries or fallopian tubes, or primary peritoneal cancer, with cytologically or histologically confirmed spread to the peritoneum outside the pelvis and/or metastasis to the retroperitoneal lymph nodes.** **T1/T2-N1-M0**
IIIA1	Positive retroperitoneal lymph nodes only (cytologically or histologically proven): **IIIA1(i)** Metastasis up to 10 mm in greatest dimension **IIIA1(ii**) Metastasis more than 10 mm in greatest dimension
IIIA2 **T3a2-N0/N1-M0**	Microscopic extra-pelvic (above the pelvic brim) peritoneal involvement with or without positive retroperitoneal lymph nodes
IIIB **T3b-N0/N1-M0**	Macroscopic peritoneal metastasis beyond the pelvis up to 2 cm in greatest dimension, with or without metastasis to the retroperitoneal lymph nodes (includes extension of tumor to capsule of liver and spleen without parenchymal involvement of either organ)
IIIC **T3c-N0/N1-M0**	Macroscopic peritoneal metastasis beyond the pelvis more than 2 cm in greatest dimension, with or without metastasis to the retroperitoneal lymph nodes (includes extension of tumor to capsule of liver and spleen without parenchymal involvement of either organ)
Stage IV	**Distant metastasis excluding peritoneal metastases & liver & spleen capsular metastasis** **Any T, any N, M1**
IVA	Pleural effusion with positive cytology
IVB	Parenchymal metastases and metastases to extra-abdominal organs (including inguinal lymph nodes and lymph nodes outside of the abdominal cavity).[c]

a: It is not possible to have stage I peritoneal cancer**, b:** Dense adhesions with histologically proven tumor cells justify upgrading apparent stage I tumors to stage II, **c:** Extra-abdominal metastases include transmural bowel infiltration and umbilical deposit.

The stage distribution of ovarian carcinomas differs according to the histological type. Type I tumours (mucinous carcinomas and 50% of clear and endometrioid carcinomas) constitute the largest proportion of stage I tumours. While the notorious HGSOC of type II tumours represents most stage III and stage IV cancers. In fact, early stage HGSOC are vanishingly rare and constitute only 3% of serous carcinomas (10). This is because HGSOC challenges the traditional concept of ovarian cancer progression from local disease to advanced malignancies. Investigators demonstrate that STICs, although in-situ and small lesions, are full-fledged malignancies capable of exfoliating malignant cells directly into the peritoneum, which then acquire metastatic potential to distant sites (36, 37).

Being the strongest prognostic indicator, FIGO stage correlates negatively with the survival of ovarian cancer females. In the UK the 5-year survival rate is 90% for stage I disease, and 42.8% for stage II disease. This contrasts sharply with the figures for stage III and stage IV disease, which are languishing at 18.6% and 3.5% respectively (Cancer Research UK).

For advanced stage ovarian cancer, the extent of residual disease after surgery (cytoreduction) is also a well-established prognostic factor. Optimal cytoreduction in the agenda of most gynaecological oncologists is defined as residual disease no larger than 1cm in greatest dimension and has demonstrated survival benefits for the patients (38).

1.4.2. Age

Epithelial ovarian cancer is primarily a disease of peri-menopausal and post-menopausal females. Some studies have shown that age is an independent prognostic

factor (39). This however is a debatable matter due to a myriad of other factors. Other studies argue that the age-related differences in prognosis among ovarian cancer females can be accounted for by the higher incidence of low grade, low stage, type I and optimally debulked tumours in younger females. Moreover, younger patients are generally healthier than older patients, who are more prone to comorbidities and are less responsive to treatment (40).

1.5 High-Grade Serous Ovarian Cancer and their precursor lesions

1.5.1 Clinical characteristics of HGSOC

The present study focuses mainly on HGSOC being the most common type of EOC and the prototype of type II tumours. HGSOC is the most common subtype of EOC accounting for about 70% of these tumours (10). According to the WHO, HGSOC is the 5th leading cause of cancer related deaths and is responsible for the majority of ovarian cancer deaths, globally (8).The disease most often presents in older females in the 6th and 7th decades of life. Additionally, most of these females present at an advanced FIGO stage, and their 10-year survival rate is a mere 15% (41). Because of the widespread peritoneal and abdominal dissemination at the time of presentation, females usually present with abdominal pain and distension (42).

Standard treatment for rare, early stage HGSOC includes surgery aimed at surgical staging of the tumour followed by adjuvant chemotherapy. Most of these tumours are upstaged following staging laparotomy. On the other hand, surgery for advanced stage HGSOC is aimed towards cytoreduction or debulking of these tumours, where cytoreduction is defined as an attempt to maximally resect all visible and palpable

tumour (38). The standard surgical procedure includes removal of the whole tumour intact, total abdominal hysterectomy (TAH), bilateral salpingo-oophorectomy (BSO) and omentectomy. Random peritoneal biopsies and lymphadenectomies are also performed. Primary debulking surgery (PDS) is the standard procedure in the USA for advanced stage disease. In Europe, however, pre-operative neoadjuvant chemotherapy (NACT) followed by interval debulking has been the mainstay of treatment for many years having a proven positive effect on the progression-free survival of these patients. Nonetheless, some centres in the UK do perform PDS in selected patients who are surgically fit with a good performance status and absence of co-morbid conditions (43). Currently, a combination of a platinum, cytotoxic compound, and a paclitaxel which inhibits cell-cycle progression is the best first line chemotherapy for advanced stage ovarian cancer (43). Although three-quarters of these patients respond initially to treatment, more than 80% will relapse within 48 months and develop chemo-resistance at some stage of their disease, and as such overall cure rates languish between 20% and 30% (38, 41).

1.5.2 Serous tubal intra-epithelial carcinoma (STIC)

As mentioned earlier, evidence has emerged that HGSOCs arise from precursor lesions in the fimbriated end of the fallopian tube known as a Serous Tubal Intraepithelial Carcinoma (STIC; Figure 1.2). Evidence for this was initially identified in *BRCA1/2* mutation carriers who have a well-known predisposition to HGSOC. These patients typically undergo prophylactic risk reducing salpingo-oophorectomy; their ovaries displayed small high grade serous carcinomas, whilst their tubes displayed in situ non-invasive serous carcinomas. Later studies found similar lesions in the tubes of patients with sporadic HGSOC (44, 45). Furthermore, identical *TP53* mutations have

been identified in these tubal lesions and ovarian serous carcinomas. Additionally, morphologically normal tubal epithelium that overexpresses p53, and can harbour *TP53* mutations have been postulated as precursors to STIC- termed the “p53 signature” (46).

Pathologically, STIC is diagnosed when pleomorphic serous type epithelium with loss of cilia is confined to the basement membrane and shows an aberrant p53 immunohistochemical (IHC) pattern with a high Ki-67 index of ≥10% (47). On the other hand, p53 signatures are diagnosed when a stretch of ≥12 secretory cells that are morphologically normal overexpress p53 by IHC and show a low Ki-67 index of <10% (46).

In routine diagnostic practice the primary site of origin of HGSOC is assigned after total pathological examination of both fallopian tubes. According to the criteria of the Royal College of Pathologists’ datasets, if either STIC or invasive carcinoma is present in the fallopian tube or if the tube is incorporated into the tubo-ovarian mass, the fallopian tube is considered the primary site of origin of HGSOC. An ovarian primary is assigned if an ovarian tumour does not fulfil the criteria above and a peritoneal primary is only given if tubal and ovarian origins are excluded. In other words, until proven otherwise, the fallopian tube is the primary site of origin of HGSOC (48).

Taken together, the above evidence establishes STICs as precursors of HGSOC and highlights the importance of *TP53* mutation as an early event in HGSOC (49).

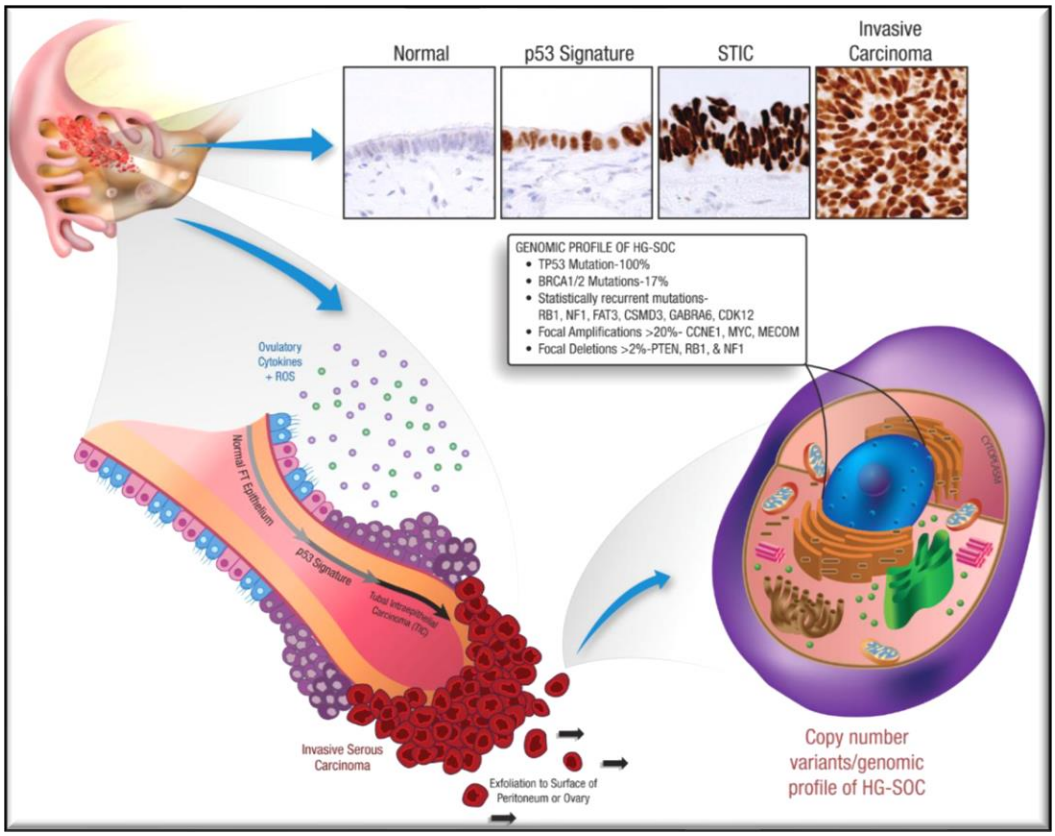

Figure 1. 2: Putative histopathological precursors of High grade serous ovarian cancer. The diagram illustrates the progression of High-grade serous ovarian cancer from histologically normal epithelium in the fallopian tube "p53 signature" to "Serous tubal intra-epithelial carcinoma" to invasive cancer**.** P53 signatures are morphologically normal but they overexpress p53 protein by immunohistochemistry. STIC are cytologically malignant serous epithelium which display an aberrant p53 IHC staining pattern; most commonly p53 overexpression. STIC: Serous Tubal Intra-epithelial Carcinoma. Figure taken from Jones & Drapkin, 2013 (46).

1.5.3 Molecular biology of HGSOC and STIC

The first study to revolutionize our understanding of the genetic background of HGSOC was launched in 2011 by TCGA investigators (50). Samples from over 300 patients were analysed using whole exome sequencing and determined that HGSOC is characterized by a high rate of *TP53* mutation. Additionally, *TP53* mutation is detected as early as the STIC stage of the model of HGSOC carcinogenesis. Therefore, it is the earliest molecular event essential for the initiation and development of HGSOC and

can be detected in more than 96% of HGSOC (51). As a result of early *TP53* mutations in these tumours HGSOC show pronounced chromosomal instability and a high prevalence of copy number alterations across their genome (49).

The second most common genetic alteration in HGSOC is *BRCA1/2* mutations whether germline or somatic which affect up to 15% of these tumours (10). Germline *BRCA1/2* mutations are more prevalent than somatic *BRCA* mutations in HGSOC affecting 22.6% and 13% of HGSOC, respectively (50, 52). It has also been reported that *BRCA-1* mutations are also more common than *BRCA-2* mutations (52). Most germline and somatic *BRCA1/2* mutations are small insertions/deletions rather than missense mutations. All functional domains of the *BRCA-1* gene are affected by mutations including RING, coiled-coil, and the C-terminal domain. Similarly, all functional domains of the *BRCA-2* gene are also affected by mutations; DNA-binding, oligonucleotide-binding and tower domains. The majority of *BRCA1/2* mutations are accompanied by a second hit in the form of allelic deletion or inactivation. Epigenetic silencing through promotor hypermethylation affects about 10-20% of HGSOC and they affect the *BRCA-1* rather than the *BRCA-2* gene. Additionally, *BRCA-1* promotor hypermethylation is mutually exclusive with *BRCA1/2* mutations (50, 53, 54).

More recently, several studies including the Cancer Genome Atlas (TCGA) project have shown that about 50% of HGSOC show genetic and epigenetic alterations of genes involved in homologous recombination repair (HRR) other than *BRCA1/2* (Figure 1.3*)*. These HRR gene include the DNA damage response genes such as *ATM, ATR*, *CHEK1* and *CHEK2*, Fanconi anaemia genes mainly PALB2 as well as core HR RAD genes such as *RAD50* and *RAD51C (50, 55)*.

Other genetic alterations that may confer HR deficiency through indirect modulation of the HR pathway include *PTEN* deletions, *EMSY* amplifications and inactivating mutations of *CDK12* (Figure 1.3). *PTEN* loss is reported to downregulate *RAD51* whereas *EMSY* amplifications inhibit the transcriptional activity of the BRCA-2 protein. *CDK12* inactivation confers HR deficiency through reduced transcriptional activation of *BRCA-1*. Finally, it has been reported that the overexpression of certain miRNA can induce HR deficiency through targeting and inhibition of BRCA-1, BRCA-2 and RAD51 proteins (55).

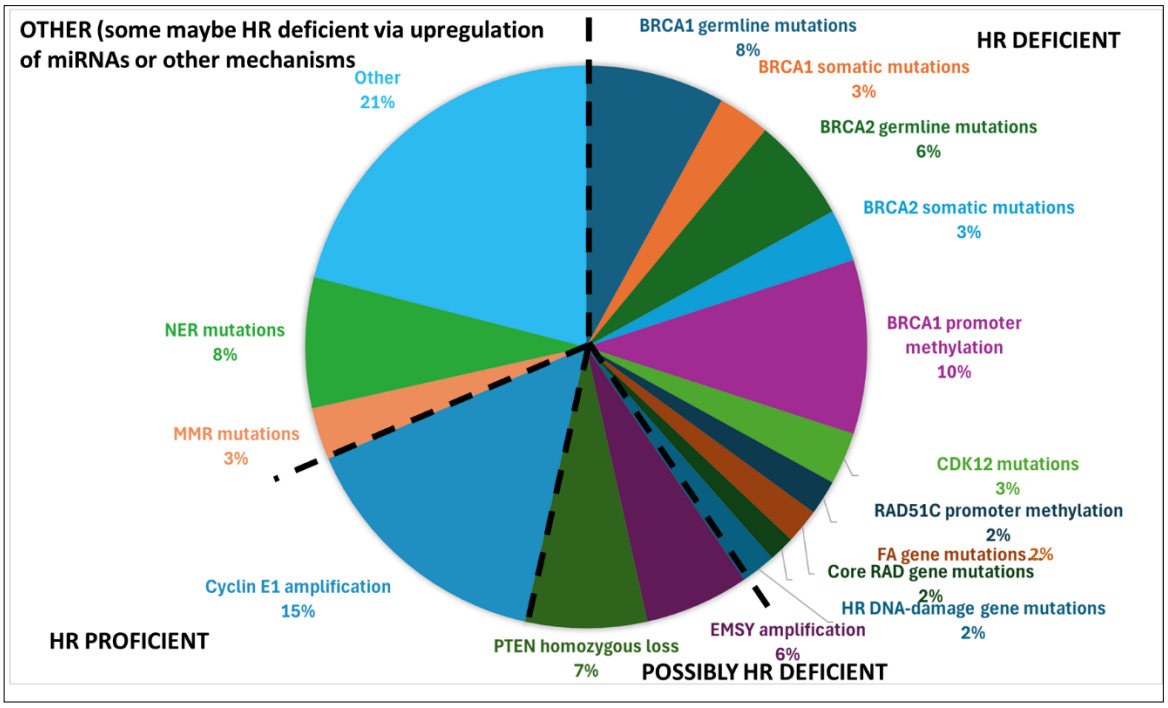

Figure 1. 3: A schematic demonstrating the various molecular alterations in HGSOC. About 50% of HGSOC are Homologous recombination deficient through genetic and epigenetic alterations in HR repair genes (Right hand side). Possible molecular alterations that confer HR deficiency include *EMSY* amplifications and *PTEN* loss (bottom centre). Some tumours may be HR deficient through overexpression of miRNA as well as other unknown mechanisms (top left). HGSOC with *CCNE1* amplifications are HR proficient (bottom left). Figure generated in Excel and adapted from Konstantinopoulos et al., 2015 (55).

Clinically, HR-deficient HGSOC including those with germline or somatic *BRCA1/2* mutations have a more favourable prognosis with better overall and progression-free survival. In addition, HR-deficient HGSOC show enhanced platinum sensitivity compared to HR-proficient HGSOC (56, 57). These tumours are also good candidates for Poly ADP ribose polymerase (PARP) inhibitors due to their high susceptibility to DNA damage.

About 15% of HGSOC are characterized by amplifications of *CCNE1* which have also been detected as early as the STIC precursor lesions (58, 59). HGSOC with *CCNE1* amplifications are HR-proficient and they run an aggressive clinical course compared to *BRCA1/2* mutant HGSOC. Moreover, unlike HR-deficient HGSOC, they do not respond to PARP inhibitors (55).

Initially investigated by TCGA research network, several studies have attempted to molecularly classify HGSOC based on gene expression patterns. These studies have identified 4 transcriptomic subtypes that were termed *Immunoreactive*, *Proliferative, Mesenchymal and Differentiated* (50, 60, 61). To date, the clinical applications of these subtypes are still controversial. HGSOC subtypes will be considered in more detail in chapter 7.

1.5.4 Pathological features of HGSOC

HGSOC can display a variety of architectural patterns, the most common of which is a complex papillary or labyrinthine pattern with slit like spaces (Figure 1.4 A and B). Other patterns include a villoglandular pattern reminiscent of endometrioid carcinoma as well as a transitional pattern reminiscent of urothelial carcinoma. The defining feature of HGSOC is the high-grade nuclear atypia and pleomorphism with more than threefold

variation in the nuclear size and shape. These tumours are also characterized by their high mitotic count (Figure 1.4C) which exceeds 12 mitoses per 10 high power fields (HPFs) including abnormal forms due to their high chromosomal instability (10).

A subset of HGSOC have been previously misclassified as either undifferentiated, endometrioid or transitional cell carcinomas (10). These tumours are now recognized as the “SET variant” of HGSOC including Solid, pseudo-Endometrioid and Transitional cell patterns (Figure 1.4 D). Characteristically, the SET pattern particularly when forming >25% of the tumour is more commonly associated with germline *BRCA1/2* mutations and homologous recombination deficiency (HRD). They also usually present in younger females and have a better prognosis (62, 63). Other features of HGSOC with SET features include necrosis, increased mitosis and intra-epithelial lymphocytosis which have been correlated with *BRCA-1* mutations particularly, but none of these features are diagnostic (62). Interestingly, similar features have been described in *BRCA-1* mutant triple negative breast cancer (64).

Other than the SET pattern, other histopathological features that have been described in association with somatic and germline *BRCA1/2* mutant HGSOC, include an invasive micropapillary architecture, a pushing pattern of invasion as well as high tumour-infiltrating lymphocytes (TILs). These features have been found to be more reliable in metastatic HGSOC rather than the primary tumour itself (62, 65).

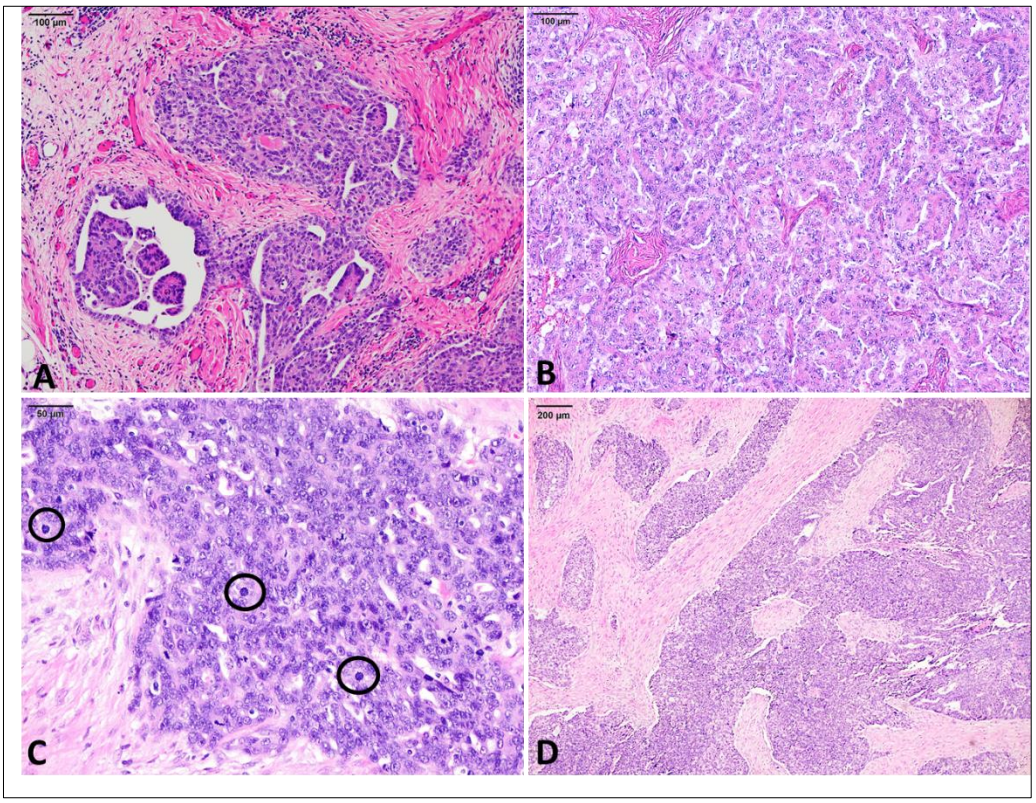

Figure 1. 4: The histopathological features of HGSOC from 4 different patients in the present study. A) Invasive high-grade serous carcinoma displaying a complex papillary architecture (H&E, x10 magnification). B) Another high-grade serous carcinoma with a compact papillary architecture imparting a labyrinthine pattern with slit-like spaces (H&E, x10 magnification). C) High-grade serous carcinoma displaying the characteristic high grade nuclear atypia with more than threefold variation in nuclear size and shape as well as an elevated number of mitoses (black circles, x20 magnification). D) HGSOC (SET variant) showing a solid growth pattern. This patient had a pathogenic *BRCA-1* mutation (H&E, x4 magnification).

1.6 *TP53* and High grade Serous Ovarian Cancer

1.6.1 Structure and function of the p53 protein

As mentioned earlier, *TP53* mutation is a universal and defining feature of HGSOC (49, 50). The *TP53* gene is located on the short arm of chromosome 17. The prototypic protein product of the *TP53* gene, p53 is a tumour suppressor protein that encodes a 393 amino acid protein, which is comprised of multiple structural domains, each

correlating with a specific function of the protein. These domains include two transactivation domains (TAD) within the N-terminal region, followed by a proline-rich domain (PRD), a central sequence-specific DNA-binding domain (DBD) and a C-terminal regulatory-domain (CTD; Figure 1.5). The PRD is encoded by exon 4 of the *TP53* gene and regulates the apoptotic activity of the protein. The CTD encodes the protein's nuclear localization signal (NLS) and a domain required for transcriptional activity known as the oligomerization domain (OD), which allows the p53 protein to oligomerise and act as a tetramer. The DBD is encoded by exons 5-8 of the *TP53* gene and is the key regulator of the transcriptional activity of p53 through binding to specific DNA sequences in p53 target genes (66). The DBD tertiary structure is divided into three loops and a sheet-loop-helix (SLH) motif which interact with the DNA double helix backbone (Figure 1.6) (67).

Three well-established target proteins whose expression is enhanced by p53 are: p21 a cyclin-dependent kinase inhibitor responsible for cell-cycle arrest at the G1/S checkpoint and post-replicative senescence; Bax, a pro-apoptotic protein involved in the intrinsic pathway of apoptosis; and MDM2 whose function is the promotion of p53 proteasomal degradation through an auto-regulatory negative feedback mechanism (66). These proteins define the role of *TP53* as a tumour suppressor gene that controls cell-cycle proliferation, apoptosis, and cellular senescence. Moreover, p53 regulates glycolysis and oxidative phosphorylation through a target gene known as TIGAR (*TP53*-inducible glycolysis and apoptosis regulator) (68).

Most of the mutations that affect p53 function occur in the central DNA binding domain. The most common type of these mutations are missense mutations resulting in amino acid substitutions. There are 5 major hotspot codons that are affected by missense

mutations (Figure 1.5) that usually result in substitution of arginine residues responsible for DNA contact (R175H, R248Q/W, R273H/C, R282W, G245S) (69).

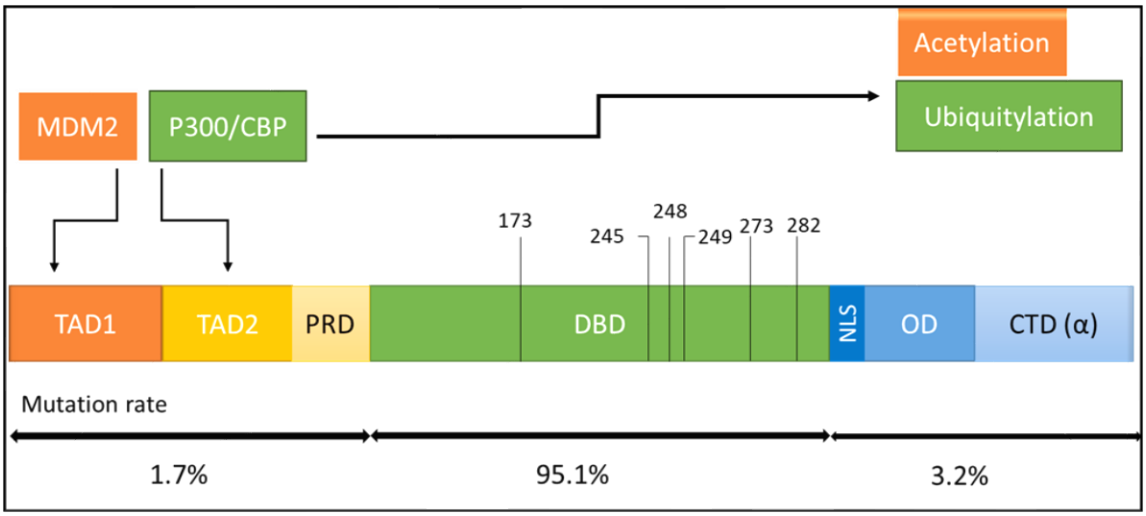

Figure 1. 5: A diagrammatic representation of the p53 protein with the frequency and site of tumour-associated mutations. The p53 protein possesses an N-terminal region including the transactivation domain, a central DNA-binding domain and a C-terminal regulatory domain that contains the oligomerization domain and nuclear-localization signals. Both amino- and carboxy-termini contain signals that regulate nuclear export of p53. Almost all mutations in p53 affect the DNA-binding domain, and the black bars represent some of the known missense mutations that affect this region. MDM2 and p300/CBP proteins interact with the N-terminal region of the p53 leading to posttranslational modifications within the C-terminal region; acetylation and ubiquitylation. TAD: Transactivation domain, PRD: Proline-rich domain, DBD: DNA-binding domain, NLS: Nuclear localization signal, OD: Oligomerisation domain, CTD: C-terminal domain. Figure generated in BioRender and adapted from Vousden & Lu, 2002 (70).

Because *TP53* is a tumour suppressor gene, inactivation of the second allele must occur to drive the clonal evolution of tumours with p53 missense mutations according to Knudson's two hit hypothesis. The second hit usually occurs through loss of heterozygosity (LOH), a phenomenon defined as the deletion of the wild type allele when a mutation affects the other allele. LOH can occur through whole chromosomal deletion, whole arm loss, sub-arm loss or uniparental disomy (66).

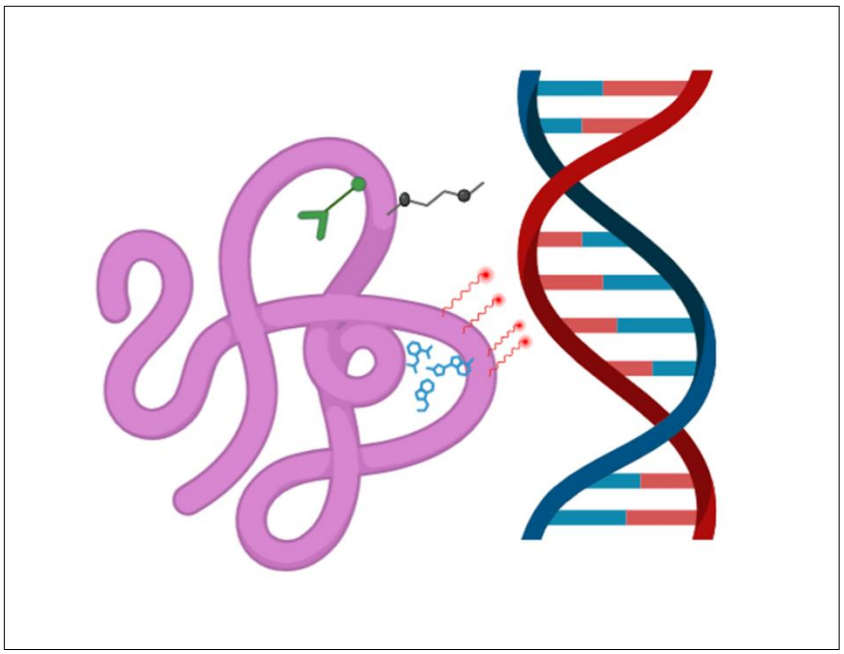

Figure 1. 6: A schematic of the p53 DNA-binding domain and its interaction with the DNA double helix. A ribbon model of the p53 DBD tertiary structure (purple) and wire schematic of the DNA double helix. **Red**: DNA major groove interacting residues. **Black:** DNA minor groove interacting residue (R248). **Blue**: SLH motif residues opposite the DNA major groove binding interface which serve to that support the tertiary structure at this location. **Green**: Zinc ion residues which also partially stabilize the DNA binding interface. Figure generated in BioRender; adapted from Seagle et al., 2015 (71)

Missense mutations affect p53 function in one of three different ways: a loss of function (LOF) of the p53 protein, a gain of function (GOF), or they exert a dominant negative effect (DNE). LOF mutations result in an improperly folded protein that has decreased ability to bind and activate target genes including p21, Bax and MDM2. Consequently, the mutated protein resists degradation by its inhibitor MDM2, which makes it more stable than the p53 wild-type protein that ultimately leads to an over-expressed non-functional protein in the affected cells (72), enabling its detection by IHC or q-PCR. The DNE can be explained by the fact that p53 functions as a tetramer. When certain mutations affect one allele of the *TP53* gene, the product is a mixed tetramer,

possessing both wild-type and mutant p53 proteins. In these instances, the mutant proteins negate the function of the wild-type species, hence the DNE. On the other hand, other hotspot missense point mutations result in all-mutant highly stable tetramers that *gain* function as onco-proteins and engage in novel protein-protein interactions and signaling pathways that promote tumourigenesis (73). A recent in vivo study in mice demonstrates that LOH is required for the stabilization of the mutant p53, and acquisition of oncogenic function. Mice tumours that showed LOH of the wild type allele exhibited accelerated time-to-tumour formation, compared to tumours that retained the wild type allele, where GOF activity was not observed (74).

About 25% of mutations that affect p53 function include nonsense or frameshift mutations that lead to truncated proteins subjected later to nonsense mediated decay (66). Other less common mutations include splice site mutations and in-frame deletions/insertions the biological significance of which is unclear (75).

1.6.2 *TP53* mutations in HGSOC

The majority of p53 mutations in human cancer affect the DNA-binding domain. In HGSOC around 70% of these mutations are missense mutations which result in amino acid substitutions (41). The most common missense mutation reportedly associated with HGSOC is R273C/H (66).

In around 25% of HGSOC, a LOF non-sense mutation will affect the *TP53* gene resulting in complete absence of the protein in the tumour cells. Another 4% of HGSOC will show a mutation affecting the NLS of the p53 protein resulting in its entrapment in the cytoplasm of the tumour cells. A further 5% of tumours will harbour truncating stop-

gain mutations affecting the CTD, yielding a small amount of non-functional p53 protein that simulates a wild-type staining pattern on IHC (41, 76).

Multiple studies have proven that the above-described mutation patterns of p53 correlate extremely well with its optimized immunohistochemical expression, showing a specificity of almost 100% (49, 77, 78). In fact, p53 IHC is established as a routine diagnostic marker in HGSOC. Table 1.2 summarizes the major immunohistochemical patterns of p53 expression in HGSOC and their correlation with the *TP53* mutation status.

Table 1. 2: The various p53 immunohistochemical staining patterns in tubo-ovarian high-grade serous carcinoma and their correlation with *TP53* mutational status. Table taken from Köbel et al., 2019 (76).

Staining pattern	*TP53* status	P53 IHC interpretation	% in tubo-ovarian HGSC
***TP53* mutation absent (wild type)**	No mutation	Normal/wild-type	0
***TP53* mutation present**			
Over-expression (>80% of tumor cell nuclei)	Non- synonymous missense mutation	Abnormal/aberrant/mutation-type	66
Complete absence (compared to positive normal controls e.g.: lymphocytes and stromal cells)	LOF frameshift or nonsense mutation	Abnormal/aberrant/mutation-type	25
Cytoplasmic	LOF mutation disrupting the nuclear localization domain	Abnormal/aberrant/mutation-type	4
Wild-type like	Truncating mutation	Abnormal/aberrant/mutation-type	5

IHC: immunohistochemistry, **LOF**: loss of function, **HGSC:** high-grade serous carcinoma.

1.6.3 The role of *TP53* mutations in ovarian cancer

Mutant *TP53* has been long linked to aggressive behaviour in human cancers. In ovarian cancer, *TP53* mutations are known to contribute to the metastatic potential of these tumours, and their resistance to chemotherapy. They also have a reported negative effect on the progression-free and overall survival of ovarian cancer females

(79). Furthermore, p53 GOF mutants have been hypothesized to contribute to the mechanisms that underlie chemo-resistance, such as suppression of apoptosis and upregulation of DNA repair pathways (80). Certain p53 GOF mutants have also been reported to promote metastasis and chemoresistance in HGSOC patients (81). Moreover, missense mutations in HGSOC patients grouped by their structural location within the DBD (Figure 1.6) have been reported to impact overall and progression-free survival in these patients (71). However, the literature is conflicting about the exact role of these different *TP53* mutations in predicting patient outcomes and chemoresistance in HGSOC patients (82, 83).

It is, therefore, clear that although *TP53* mutation is associated with aggressive behaviour and is established as a diagnostic marker for HGSOC, it alone falls short of being a prognostic marker for these tumours, much less as a predictor of response to therapy. Indeed, the role of p53 mutations and GOF mutants in predicting patient outcome and chemo-resistance are not fully understood and warrant further investigation. Furthermore, in the era of molecular subtyping of cancers, it has become crucial to establish a molecular classification of HGSOC that can stratify these tumours, and importantly, parallels their clinical outcome. In fact, as mentioned earlier new line of evidence stemming from genome expression profiling studies, identify HGSOC as a molecularly diverse disease that is genetically and clinically heterogeneous (61, 84). This is why there is an increasing need to identify new molecular targets that can establish a genetic signature for these tumours and hence demonstrate prognostic, predictive, and therapeutic relevance. A particular molecular target of interest to our laboratory is the E2 ubiquitin-conjugating enzyme, UbcH10

which is reportedly overexpressed in several human malignancies including HGSOC (85).

1.7 UbcH10 and the ubiquitin proteasome pathway

UbcH10 is a 19.6 kDa protein composed of 179 amino acids that functions as an E2 ubiquitin-conjugating enzyme for the multi-protein E3 ubiquitin ligase complex known as the Anaphase-Promoting Complex/Cyclosome (APC/C)(86). Together, they mark key mitotic regulators for degradation by the ubiquitin-proteasome system and coordinate the progression of the cell through mitosis and G1. In a highly coordinated temporal manner, the APC/C guarantees proper chromosomal segregation during mitosis, maintains genomic stability and averts aneuploidy, a well-known cause of malignancy (87).

Ubiquitin is a 76 amino acid protein that is central to the process of ubiquitylation, a common post-translational modification of proteins. Ubiquitin is characterized by seven lysine residues which can attach, and form iso-peptide linked poly-ubiquitin chains. The N-terminus can also mediate an eighth Met1-linked or linear chain with another ubiquitin molecule (88).

The ubiquitylation process is a mediated by a complex enzymatic cascade which can be divided into three steps:

1-Ubiquitin activation: an ATP-dependent reaction mediated by an E1 ubiquitin-activating enzyme (UAE). In this reaction a thioester bond is formed between ubiquitin and UAE.

2- Ubiquitin transfer from E1 to a cysteine residue in the E2 conjugating enzyme again through the formation of a thioester bond with the latter.

3- The ubiquitin together with the E2 interact with the appropriate E3 ligases which mediates the transfer of the ubiquitin to the lysine residues in the target protein substrate (Figure 1.7).

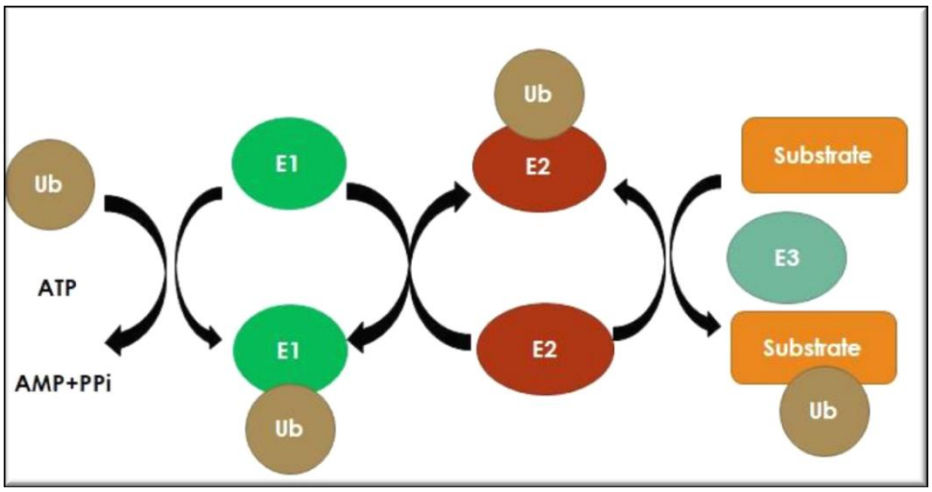

Figure 1. 7: The Ubiquitin-Proteasome System. Ubiquitylation is initiated by ubiquitin activation in an ATP-dependent reaction, followed by its conjugation to an E2 enzyme. An E3-ligase then interacts with both the ubiquitin and the E2 conjugating enzyme, resulting in the transfer of ubiquitin to the target substrate for degradation by the 26S proteasome. Figure generated in Microsoft PowerPoint and adapted from Barford, 2011 (89).

The APC/C belongs to the really interesting new gene (RING)-E3 ligase which concomitantly binds the E2 bound to ubiquitin and the substrate, and directly transfers ubiquitin from the E2 to the substrate (90). APC/C collaborates with two E2 ubiquitin-conjugating enzymes: UbcH10 and Ube2S. UbcH10 interacts with APC/C specifically and acts to initiate the mono-ubiquitinylation of substrates, while Ube2S acts on the pre-ubiquitylated substrate and extends the poly-ubiquitin chain on the substrate which is then targeted for degradation by the 26S proteasome (91).

The APC/C is a 1.5MDa multi-protein complex that is activated by one of two co-activators: Cdc20 and Cdh1. The APC/C and Cdc20 function together with the spindle

assembly checkpoint (SAC) to control metaphase to anaphase transition. The SAC is a multi-protein surveillance mechanism developed by the cell to ensure the fidelity of chromosomal segregation during mitosis. This is done mainly through a protein complex referred to as the mitotic checkpoint complex (MCC)(92). The main function of the MCC is to delay the transition of the cell from metaphase to anaphase by keeping the APC/C's activity in check, until all the chromosomes are properly attached by their kinetochores to the mitotic spindle. At the prometaphase of mitosis, the MCC inhibits Cdc20 one of the two co-activators of the APC/C. By the end of metaphase, the appropriate attachment of the last kinetochore to the mitotic spindle releases Cdc20 from the MCC which in turn activates the APC/C. Subsequently, the APC/C will target the mitotic regulators cyclin B and Securin for ubiquitin mediated degradation by the 26-S proteasome (93). The MCC is one of the main targets of the microtubule stabilizing agent paclitaxel used in ovarian cancer treatment. Paclitaxel induces mitotic arrest through activation of the MCC (94).

1.8 UbcH10, Human Cancer and p53

Normally, UbcH10 levels fluctuate in the cell-cycle, where the highest levels are observed right before the start of mitosis, and later declining during G1 phase as it is targeted for degradation by the APC/C-Cdh1 (95). Therefore, it is not surprising that UbcH10 expression levels are lowest in quiescent cells and normal tissue, and highest in rapidly dividing cells including malignant cells (96). In fact, UbcH10 has been identified as a proto-oncogene overexpressed in many human cancers including anaplastic thyroid, lung, gastric, breast, colorectal and ovarian cancers (96-101).

According to TCGA Pan Cancer Atlas database, the *Ube2C* gene which codes for the UbcH10 protein is among the most amplified genes in human malignancies including ovarian serous carcinomas (Figure 1.8).

Studies indicate that UbcH10 acts as a proto-oncogene by promoting chromosomal mis-segregation, genomic instability, and aneuploidy (93). It is thought that UbcH10 overexpression overrides the SAC and promotes the premature dissociation the MCC proteins from Cdc20 before proper chromosomal alignment at the metaphase plate. Cdc20 then activates the APC/C which results in the premature degradation of cyclin B1 and Securin, premature chromosomal segregation and exit from mitosis (102).

In EOCs, UbcH10 overexpression has been correlated positively with high tumour grade and poorly differentiated morphology. Immunohistochemically, UbcH10 levels of expression were nil in normal ovarian tissue and showed a steady increase from grade 1 well-differentiated tumours to grade 4 undifferentiated tumours. UbcH10 overexpression also has been demonstrated to have a negative impact on the overall survival of ovarian cancer patients (86). However, its prognostic and predictive role in HGSOC particularly has not been investigated before. Interestingly, short interfering RNA (siRNA) targeting of UbcH10 mRNA for degradation, leads to decreased cellular proliferation and growth in ovarian cancer cell lines, suggesting a possible role for UbcH10 in ovarian carcinogenesis (86). Indeed, in chemo-resistant breast cancer cell lines, the inhibition of UbcH10 has been shown to restore chemo-sensitivity (103). Taken together, these studies all emphasize the importance of UbcH10 as a cancer biomarker with potential prognostic, predictive and therapeutic advantages.

Moreover, recent studies demonstrate that p53 GOF mutants promote the transcriptional activation of UbcH10 in human cancer cell lines. In these studies, wild-type p53 expression induced by the DNA damaging agent 5-fluoro-uracil (5-FU) was found to repress the expression of UbcH10, through a direct effect on the promotor region of the *Ube2C* gene. Reciprocally, in the same setting, mutant GOF p53 promoted the upregulation of UbcH10 leading to SAC disruption, premature metaphase to anaphase transition and chromosomal abnormalities (104). In HGSOC however, the exact relationship between UbcH10 and p53 is yet to be established. A deeper investigation into this relationship might have therapeutic and prognostic implications for HGSOC.

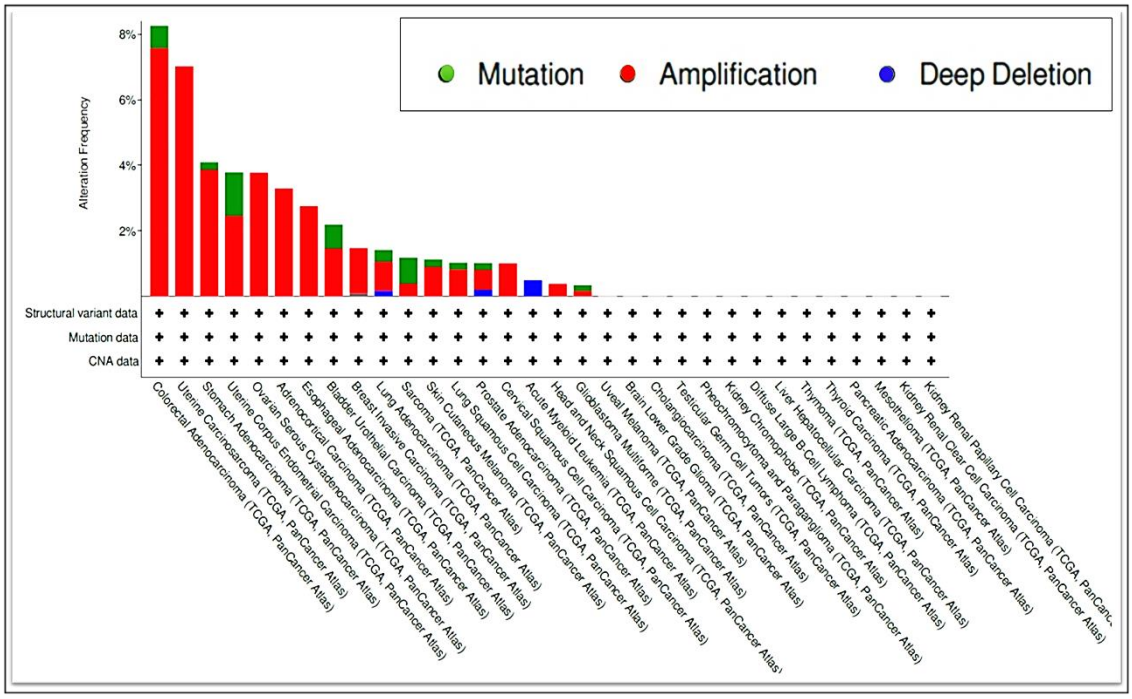

Figure 1. 8: *Ube2C* gene alterations in Pan Cancer Atlas studies. Across the cohorts of various malignancies from the Cancer Genome Atlas, the most common genetic alteration affecting *Ube2C* is amplification (red). Less commonly, it may show mutations (green) particularly in sarcomas as well as endometrial, bladder, colorectal carcinomas. Deep deletions (blue) occur in acute myeloid leukemia as well as prostatic, and lung adenocarcinomas. Figure generated from cBioportal (105).

1.9 Aims and Objectives

The primary aims of this project are to: determine whether UbcH10 can be used as an ovarian cancer biomarker and incorporated in the routine prognostication, stratification, and molecular classification of HGSOC; determine the predictive role of UbcH10 in HGSOC and its contribution to treatment resistance. Delivery of these objectives would impact significantly upon patient management and treatment protocols for HGSOC.

The principle aims of this project are, therefore, to:

1. Establish the proportion of HGSOC patients that display UbcH10 overexpression and identify a biologically significant immunohistochemical cut-off level for UbcH10 expression.

2. Explore the prognostic impact of UbcH10 on the survival of HGSOC patients and correlate it with established prognostic factors for ovarian cancer.

3. Explore the role of UbcH10 in predicting treatment response in HGSOC.

4. Identify the exact role that UbcH10 plays in the progression of HGSOC by studying its expression in the precursor lesions: STICs and p53 signatures and correlating it to the invasive tumours

5. Identify the exact relationship between UbcH10 expression status and p53 mutation status in HGSOC both at the protein and gene level.

6. Address the conflicting literature about the prognostic and predictive role of the different *TP53* mutations in HGSOC.

7. Establish a clinically significant molecular classification for HGSOC by use of immunohistochemistry.

8. Develop and validate techniques to generate new models to study the biological mechanism that underpin HGSOC development and progression primarily 3D organoid models.

Chapter 2. Materials and Methods

2.1 Tissue collection and analysis of retrospective cohorts

2.1.1 Study populations and tissue collection

The present study includes 4 main retrospective cohorts: the Birmingham cohort, the Barts cohort, the STIC cohort with corresponding HGSOC and the Cancer Genome Atlas (TCGA) cohort. A pilot cohort was used at the beginning of this project; however, work with this cohort was abandoned due to discrepant results, as described in section 2.2.3.

2.1.1.1 The Birmingham cohort

This cohort included 100 HGSOC females which included 90 women first diagnosed with HGSOC between 2008 and 2019. These women were identified from the clinical records at the Pan Birmingham Gynaecological Cancer Centre (PBGOC). An additional 10 patients were recruited from the Royal Wolverhampton hospital NHS Trust who were diagnosed between 2018 and 2019. Ethical approval for all tissue collected during this study was obtained from the relevant Ethics Committee (Health Resource Authority reference 18/NE/0011). For this cohort, formalin-fixed paraffin embedded (FFPE) tissue blocks were interrogated as full-faced whole tumour sections and stained immunohistochemically for UbcH10, p53, Ki-67 and CD8 [see section 2.2.1].

As such, a total of 100 Formalin-fixed paraffin-embedded (FFPE) tissue blocks were retrieved from the archives of the Birmingham Women's Hospital and the Royal Wolverhampton Hospital NHS trust. In this regard, tumour specimens had been fixed previously in 10% (v/v) neutral-buffered Formalin solution, before embedding in

paraffin and sectioning into 5µm thin full-faced sections using a microtome (Leica Biosystems) on coated slides (Colorfrost plus, Thermoscientific); coated slides were left to dry at room temperature.

The Haematoxylin and Eosin (H&E) stained slides corresponding to the sectioned tumour samples were examined by light microscopy first to identify and confirm the histo-pathological subtype and identify the most suitable block for immunohistochemical staining.

2.1.1.2 The Barts cohort

This cohort included a total of 1134 constructed tissue microarrays belonging to 81 HGSOC patients that were mounted on a total of 9 slides donated by Barts Health NHS trust. A total of 504 and 630 microarrays were obtained from the adnexal and omental tumours of these patients, respectively. To make results from this cohort comparable to the full-faced sections in the Birmingham cohort, at least 3 punches were taken from each site in the same patient and in most patients 6 punches were obtained from each site. Sections were stained for UbcH10 in this cohort by IHC. Necrotic and fibrotic tissue cores were excluded from immunohistochemical scoring and analysis.

2.1.1.3 Cohort of serous tubal intraepithelial carcinoma (STIC) and their corresponding tumours

This cohort included 24 females with HGSOC and matched tubal sections containing STIC. These included 10 patients form the Birmingham cohort and 14 newly retrieved cases between 2019 and 2021 identified from the Laboratory information system at the Birmingham Women's hospital. Full-faced whole tumour sections from FFPE tissue

blocks were examined for this cohort. This cohort was stained using multiplex IHC for UbcH10 and p53 as well as UbcH10 and Ki-67.

Right and left tubal blocks were collected from 10 and 12 patients respectively. In two patients, tubal disease was bilateral and both blocks were collected. Corresponding invasive tumour was chosen from the omentum in 5 patients, the right ovary in 8 patients, the left ovary in 10 patients and the left groin lymph node in one patient.

As a control group for this cohort, we also used 22 cases of normal ovarian and tubal sections, 4 serous cystadenomas and 1 serous borderline tumour.

Tissue blocks were sectioned full-faced and stained similar to the Birmingham cohort.

2.1.1.4 The Cancer Genome Atlas (TCGA) cohort

The TCGA cohort of ovarian serous carcinomas included 585 patients. For this cohort, no material was examined but publicly available normalised gene expression data on *Ube2C and* co-expressed genes generated from the Illumina RNA-seq platform as well as *TP53* mutational status were downloaded and analysed. Characteristics of this cohort are described in more detail in Chapter 5.

2.1.2 Clinico-pathological/treatment variables data collection

2.1.2.1 Extraction and documentation of clinico-pathological/treatment variables

For both the Birmingham and the STIC/HGSOC cohorts clinico-pathological information was collected from the clinical records at the PBGOC and the Laboratory information system at the Birmingham Women's hospital. The following data was collected for the Birmingham cohort: age at diagnosis, FIGO stage, Lymph node status, type of surgery performed, volume of residual disease after surgery (cytoreduction), chemotherapy response score, platinum resistance, *BRCA* mutation status and p53

immunohistochemical staining pattern. For the STIC/HGSOC cohort the same variables were collected but platinum resistance data was missing.

For the Barts cohort, only FIGO stage and the type of surgery performed was shared by the Barts NHS trust. Data was shared as excel sheets with a coded map to match microarrays from the same patient and clinical information with each other.

For TCGA cohort, in addition to *Ube2C* gene expression, *TP53* mutational status, only age at diagnosis, the American Joint Committee on Cancer (AJCC) stage, type of surgery performed, and chemotherapy administration was available. Data were downloaded from cBioportal (105) and Firebrowse (https://gdac.broadinstitute.org/runs/stddata__2016_01_28/).

Data were extracted and stored in password encrypted excel sheets on the office computer.

2.1.2.2 Definition of clinico-pathological/treatment variables

i. ***Age at diagnosis***: the patients' age was that recorded at the time of hospital admission.
ii. ***Stage of disease:*** Staging was extracted from the pathology reports and the clinical cords. Final staging was determined in a multidisciplinary team setting according to the 2014 FIGO staging system for ovarian, fallopian tube and primary peritoneal carcinoma (106). Patients diagnosed between 2008 and 2013 were re-staged according to the 2014 FIGO system for consistency.
iii. ***Pelvic lymph node (LN) metastasis***: the presence (N1) or absence (N0) of pelvic retroperitoneal lymph node involvement (para-aortic, common iliac, internal iliac, external iliac and obturator) was extracted from the pathology reports. When lymph

nodes were not submitted for pathological examination, this variable was considered to be undetermined (Nx).

iv. ***Type of surgery performed:*** Details of the cytoreductive surgical procedure were extracted from the operation records and confirmed by examination of the pathology reports. The following procedures were undertaken; primary debulking surgery or staging laparotomy and delayed/interval debulking surgery. Standard surgery in both cases involves removal of the whole tumour, TAH with BSO, and omentectomy. Random peritoneal biopsies and lymphadenectomies were also performed. In PDS the patient did not receive pre-operative chemotherapy whilst in DDS the patient received 3 to 6 cycles of a combination of carboplatin and paclitaxel before surgical debulking.

v. ***Volume of residual disease after surgery:*** After cytoreductive surgery, the volume of residual disease was estimated according to the size of the residual tumour deposits which were extracted from the operation notes. Complete cytoreduction (R0) was assigned when no gross residual disease was seen by the surgeon after surgery. Optimal cytoreduction (R1) was determined when any residual tumour deposit did not exceed 1 cm in maximum dimension. Any residual tumour deposit larger than 1cm in maximum dimension after surgery was determined to be suboptimal cytoreduction (R2).

vi. ***Chemotherapy response score (CRS):*** Patients receiving pre-operative chemotherapy were assessed as to the degree of response of their tumour to chemotherapy. Information on CRS was extracted from the pathology reports for the cases diagnosed after 2018. For the older cases, H&E-stained slides of the patients' omental biopsies were revisited, and a CRS was assigned by the two

pathologists in this study. The scoring was determined by comparing the amount of residual tumour to fibro-inflammatory changes following guidelines from the International Collaboration on Cancer Research (ICCR) and the Royal College of Pathologists (RCPath) (107). Table 2.1 summarises how CRS was determined.

vii. ***Platinum resistance:*** Data on platinum resistance was extracted from the clinical records. Patients who received platinum-based treatment whether pre- or post-operative and experienced disease recurrence within less than 6 months from completion of platinum-based chemotherapy were determined as platinum-resistant. This was calculated from the date of the last chemotherapy cycle to the time of disease relapse.

Table 2. 1: The chemotherapy response score in ovarian cancer specimens. Data is adapted from the ICCR and the Royal College of Pathologists' guidelines on the histopathological reporting of carcinomas and borderline tumours of the ovaries, fallopian tubes, and peritoneum (107).

Score	Criteria[a]	Tumour regression grading
1	Mainly viable tumour with minimal regression-associated fibro-inflammatory changes limited to a few foci.	No or minimal tumour response
2	Multifocal or diffuse regression-associated fibroinflammatory changes, with viable tumour ranging from diffuse sheets, streaks, or nodules to extensive regression with multifocal but easily identifiable residualtumour.	Partial tumour response
3	Mainly regression, with few irregularly scattered individual tumour cells or cell groups (all measuring <2 mm), or no residual tumour identified.	Near complete or complete response

a: assessed on H&E-stained sections of patients' omental biopsies.

viii. ***BRCA mutation status:*** Data on tumour *BRCA1/2* mutation testing were extracted from the clinical records and the pathology information system. The most appropriated FFPE tissue block was determined after patient consent based on a minimum neoplastic cell content of 40%. Tissue was sent to the West Midlands

Regional Genetics Laboratory for *BRCA1/2* mutation testing using Next Generation sequencing. Results on *BRCA* germline testing was not accessible to us in this study.

ix. ***p53 immunohistochemical staining:*** In a proportion of patients from both the Birmingham and STIC/HGSOC cohorts, p53 IHC staining was extracted from the pathology reports at the Birmingham Women's hospital. Staining at the Women's had been performed using the DO-7 clone which is raised against the N-terminal epitope of the p53 protein, similar to the DO-1 clone we use for our automated IHC. The staining patterns were recorded as per Table 1.2.

2.1.3 Survival Data

2.1.3.1 Definition of survival times and outcome variables

In the Barts cohort, survival data was shared as part of an encrypted excel sheet without calculations on our part. For the Birmingham cohort on the other hand, follow-up data was provided until 2018 by clinical colleagues and updating of the survival data was done by us till the census date (the 30th of October 2021). Patient follow-up for time-to-event measures were calculated according to the following parameters.

i. Overall survival (OS): the OS period was calculated from the date of diagnosis until death or the last recorded follow-up. The date of diagnosis in patients undergoing PDS was determined to be the date of the surgical procedure, whilst in patients undergoing DDS it was determined to be the date of the first pre-operative chemotherapy dose.

ii. Progression-free survival (PFS): the PFS period was calculated from the date of diagnosis until clinically unambiguous progression/recurrence. The date of diagnosis was determined similar to the OS. The date of progression/recurrence

was determined either by serum CA-125 elevation or radiologically confirmed disease recurrence whichever came first.

2.1.3.2 Extraction and documentation of survival dates

For the Birmingham cohort, information on the dates required to determine the survival times were extracted from the clinical records at the PBGOC and City hospital. Disease recurrence/progression for PFS calculation was determined from the records of the follow-up clinic visits. To determine the vital status for OS calculation of members of the cohort, certain measures were taken. The hospital notes were checked first for records of the date of death of the patients. If the date of death had not been recorded in the hospital notes the following steps were taken:

- If a referral had been indicated, the relevant hospital was contacted.
- The electronic database of Sandwell and City hospital was investigated for any recent outpatient or in-patient visit for reasons unrelated to ovarian cancer.
- Patients were contacted by telephone.
- The general practitioner of the patient was contacted.
- The remaining patients with undetermined vital status were matched with the records of the West Midlands Cancer Registry who receive regular notifications of death for patients registered with cancer in the West Midlands region.

If no death is recorded until the census date, patients were determined to be censored or lost to follow-up.

2.1.4 Statistical analysis and Bioinformatics

Data were analysed using the Statistical Package for Social Sciences (SPSS ver.29 Chicago, IL, USA). https://www.ibm.com/products/spss-statistics

Variables were categorized as either quantitative (numerical) or qualitative (categorical). Numerical variables were either continuous or discrete. Numerical continuous variables included age, immunohistochemical expression of UbcH10 by H-score, UbcH10 total tumour proportion score, Ki-67 index as well as gene expression levels in TCGA cohort. Numerical discrete variables included UbcH10 protein expression by IRS, CD8 count and the mitotic index. Categorical variables included marker expression categories, stage of disease, LN metastasis, type of surgery performed, volume of residual disease after surgery, CRS, *BRCA* mutation status, platinum resistance, p53 IHC staining patterns and molecular subtypes of HGSOC.

The distribution of numerical quantitative variables (UbcH10 expression by IRS and H-score, Ki-67 index) were tested for normality using Kolmogorov-Smirnov test, which revealed non-normally distributed data. Consequently, numerical variables were described using median (*Mdn*) and range, and non-parametric tests were used for analysis. Categorical data on the other hand were described using numbers and valid percent (percentage when missing data are excluded from calculations).

Association between categorical variables was tested using Pearson's Chi-square (X^2) test. Fisher's exact test was used in situations where the X^2 was invalid.

Comparing numerical variables between 2 groups was conducted using Mann-Whitney *(U)* test.

Comparing numerical variables between 3 or more groups was conducted using Kruskal-Wallis *(H)* test.

Correlations between numerical continuous variables were tested using Spearman's correlation coefficient *(ρ).*

The Wilcoxon signed ranks test was used to compare 2 sets of observations of a continuous variable from the same groups of patients at different time points.

For survival analysis, Kaplan-Meier curves were used to estimate survival rates across marker expression categories and clinico-pathological variables for both progression-free and overall survival. Median survival time defined as the time 50% of the patients progressed (PFS) or died (OS) was used to compare survival between different groups. The Log-Rank test (X^2) was used to statistically test survival functions between groups.

For each of the time-to-event measures described above, the ability of any clinico-pathological variable or tested marker to predict the hazard or risk of an event occurring was assessed using univariate Cox regression analysis and described using hazard ratio (HR) with a 95% confidence interval (95% C.I). Multivariate Cox regression analysis (Cox Proportional hazards model) was used to model tested marker expression with other co-variates to explore whether its impact was contingent on or independent of other clinico-pathological parameters.

In all statistical tests, a level of significance of 0.05 was used, below which the results were considered statistically significant; all calculated *p*-values were 2-sided.

For determination of an optimal cut-off for both UbcH10 protein expression (IRS and H-scores) in our experimental cohorts and *Ube2C* gene expression in TCGA cohort, we used the *X-tile* software (Version 3.6.1, Yale University) (108). This Bioinformatics tool was used to avoid the errors that arise from testing multiple cut-off points and eventually for dichotomisation of UbcH10/*Ube2C* expression into categories for statistical correlations. To determine the optimal cut-off point, survival data as well as marker expression values were fed into the software which subsequently generated

cut-off values based on survival differences between the 2 groups. In addition, *X*-tile cross validated the chosen cut-off point with thousands of random populations (Monte Carlo simulation).

2.2 Laboratory techniques

2.2.1 Immunohistochemistry

In the three experimental cohorts in this study, immunohistochemistry was the main method of study. Single as well as multiplex immunohistochemistry was applied in an automated setting in the Birmingham and the STIC/HGSOC cohorts, respectively. Manual immune staining was mainly used for the Barts cohort due to logistical issues encountered during the COVID-19 pandemic. Four main primary antibodies were used in the present study: UbcH10, p53, Ki-67 and CD8. Before staining, steps for optimisation and validation of these antibodies were taken.

2.2.1.1 Validation and optimization of primary antibodies for automated and manual immunohistochemistry

In the present study we had one in-house generated primary antibody: the rabbit polyclonal antibody against UbcH10. For p53, the mouse monoclonal antibody, clone DO-1 was originally sourced from David Lane. The Ki-67 and CD8 antibodies were commercially purchased from Leica Biosystems. Validation and optimisation of these antibodies for IHC use with respect to antigen specificity and linearity (optimal dilution) was performed following recommended guidelines (109), and using the following principles:

- Appropriate positive, negative and isotype controls were used for all antibodies.

- Experimenting with multiple heat-induced epitope retrieval (HIER) conditions and dilutions was done for all antibodies.
- An automated setting and commercially available validated kits were used.
- For both UbcH10 and p53, validation of the antibodies by another non-IHC technique (i.e. Western blot, immunofluorescent staining) using ovarian cancer lysates has been previously done in our laboratory.
  - For UbcH10, validation of antibody specificity was performed by knockdown of the UbcH10 gene in UbcH10-expressing cell lines. This is explained in further detail in section 2.2.2. Validation of the anti-UbcH10 antibody for Western blot had been performed previously (J.Foster, PhD thesis, University of Birmingham, 2018).

The automated stainer at the Birmingham Women's Hospital (Leica BOND-MAX) was used to optimise UbcH10 and p53 staining in the Birmingham cohort. For Ki-67 and CD8 the Leica BOND-MAX auto-stainer in the Institute of Cancer and Genomic Sciences was used. The BOND Polymer Refine Detection kit (No. DS9800) was used for all optimisation and single staining.

For UbcH10, tonsillar tissue and placental tissue were used as positive controls (Figures 2.1A and 2.1B, respectively) according to the Human Protein Atlas (HPA); normal ovarian and fallopian tube sections were also included in each run for comparison (Figure 2.1C). Additionally, negative reagent controls (omission of the primary antibody step) and a rabbit isotype control were used for UbcH10 to determine epitope specificity (Figure 2.2). Optimal HIER conditions were determined to be applying the BOND epitope retrieval solution at pH6 for 20 min at 95°C. To avoid

artefactual background staining, an optimal dilution of 1:200 for purified antibody was agreed upon by the two pathologists in this study.

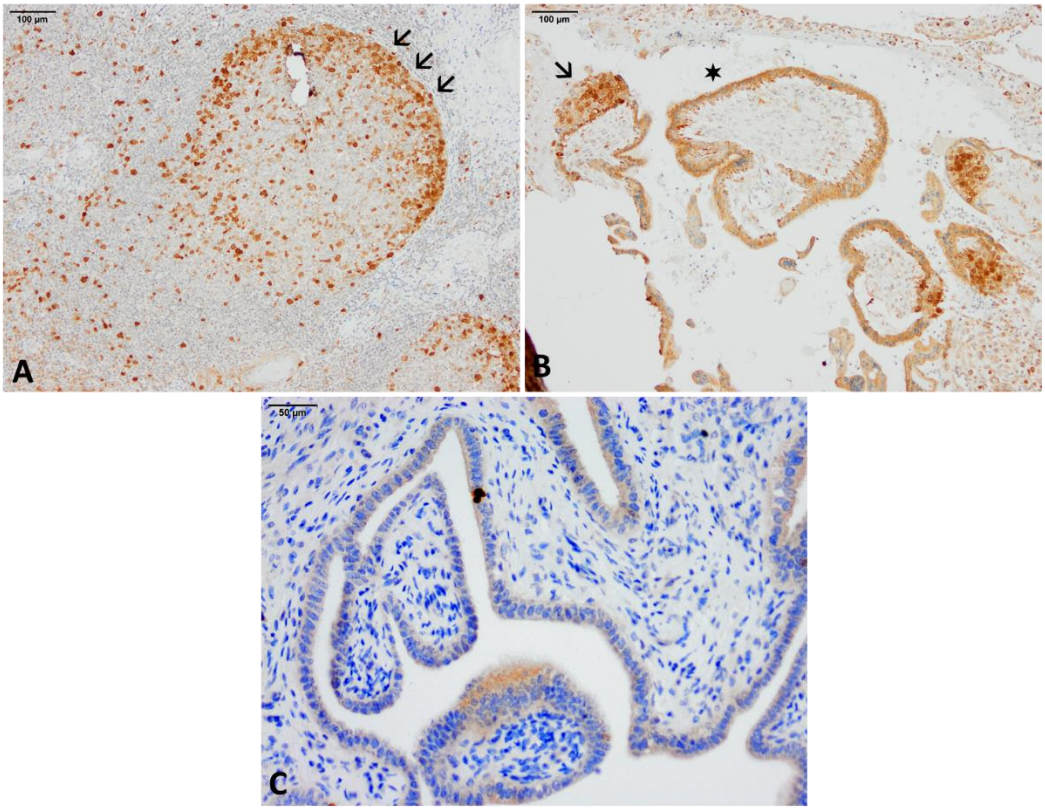

Figure 2. 1: Positive controls for UbcH10 optimization by immunohistochemistry. A) Tonsillar tissue demonstrating strong cytoplasmic and focal nuclear staining for UbcH10 with polarization of expression in the proliferative centroblasts of the germinal center (arrows, anti-UbcH10, x10 magnification). B) Products of conception showing strong cytoplasmic and nuclear staining in intermediate trophoblastic cells (arrow) and cytotrophoblasts (star, anti-UbcH10, x10 magnification). C) Normal fallopian tube epithelium control tissue showing mostly negative staining with only very focal strong cytoplasmic and nuclear staining as well as low intensity background cytoplasmic staining (anti-UbcH10, x20 magnification).

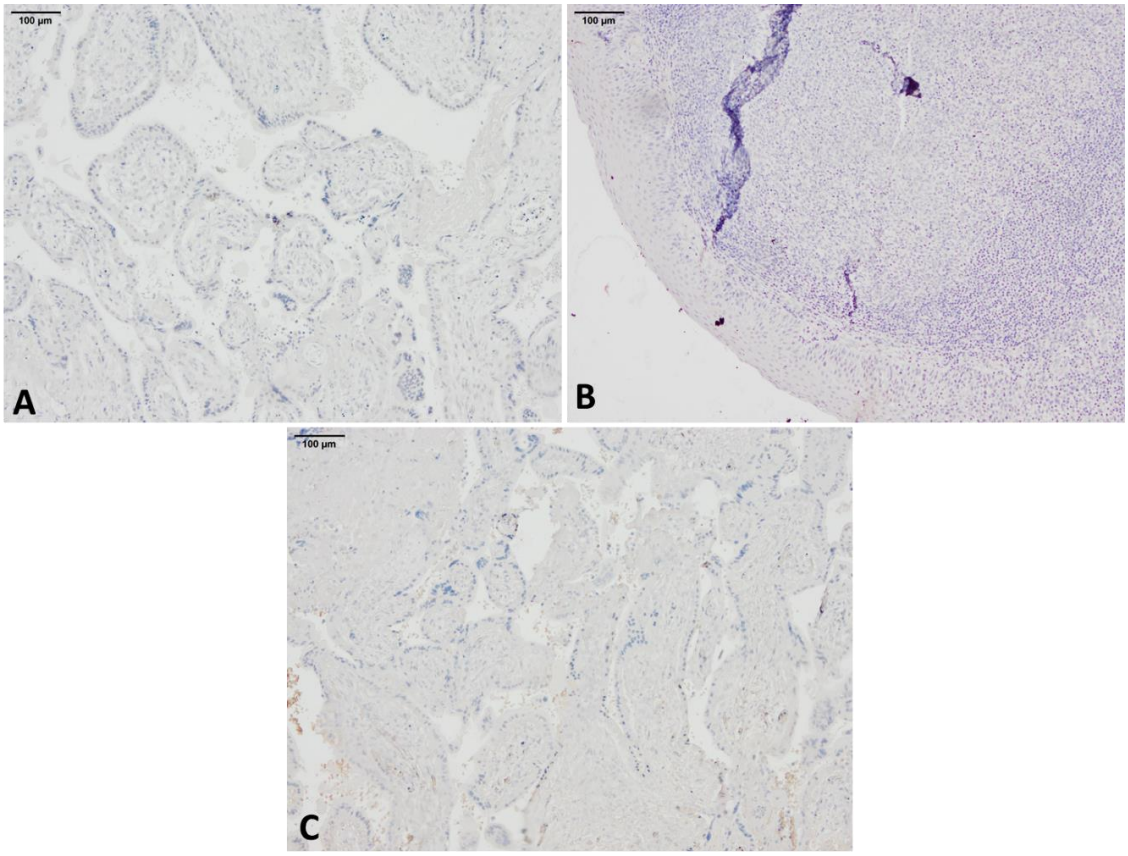

Figure 2. 2: Negative controls for UbcH10 optimization by immunohistochemistry. A) Products of conception used as a negative reagent control for UbcH10. Complete absence of staining is noted (no antibody control, x10 magnification). B) Tonsillar tissue used as a negative reagent control for UbcH10 Complete absence of staining is noted (no antibody control, x10 magnification). C) Products of conception stained with rabbit immunoglobulins used as an isotype control for UbcH10, no staining is noted denoting epitope specificity of our in-house UbcH10 antibody (rabbit IgG serum, x10 magnification).

For p53 (DO-1 clone), tonsillar tissue was used as a low expressor positive control (Figure 2.3A) to determine the lower limits of detection as recommended by Köbel *et al* (76). In addition, one well-established wild-type endometrioid carcinoma, one null and one over-expressor HGSOC were included in each run (Figure 2.3B, C & D). Optimal HIER conditions were determined to be applying the BOND epitope retrieval

solution at pH6 for 30 min at 95°C. A dilution of 1:2.5 of mouse hybridoma supernatant was found optimal for p53.

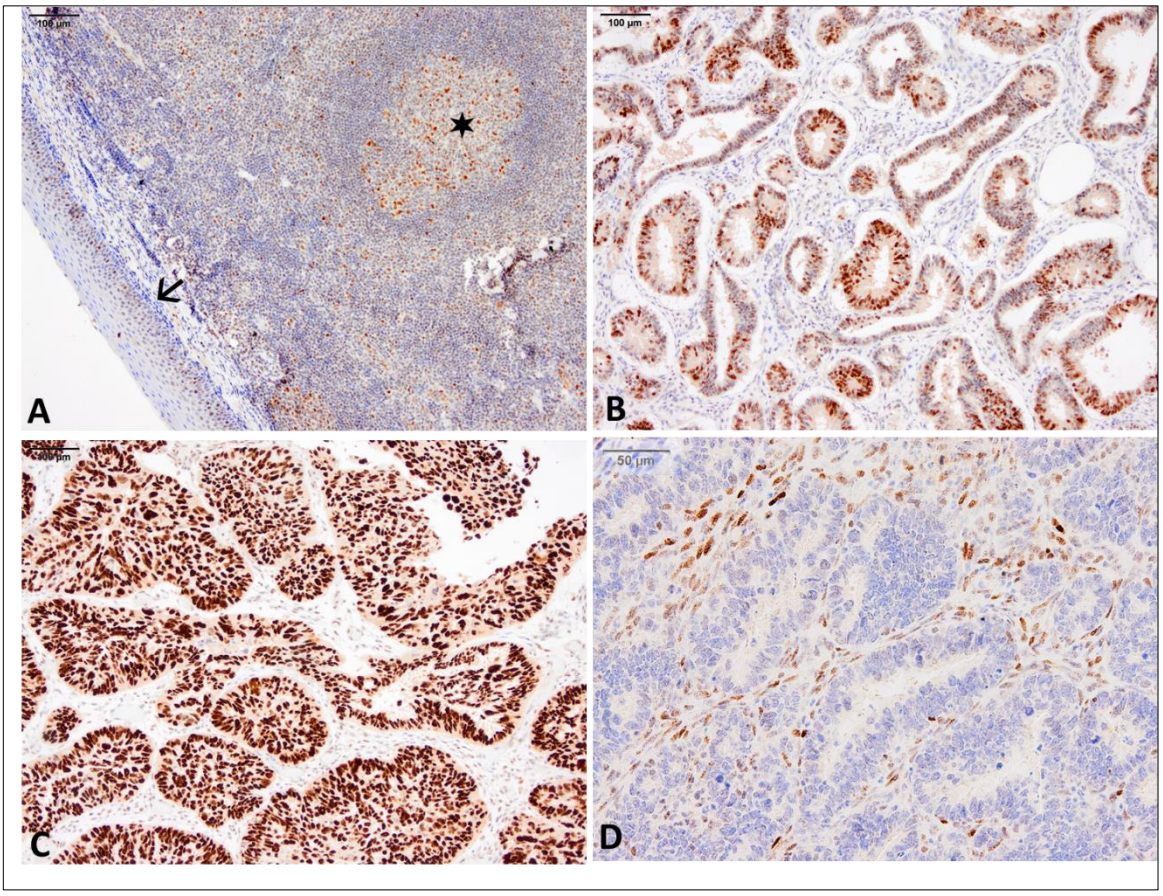

Figure 2. 3: Control tissue used for optimization of p53 by immunohistochemistry. A) Tonsillar tissue used as a low-expressor positive control showing nuclear staining for p53 in >20% of germinal center cells (star) and lower third of squamous epithelium (arrow, anti-p53, x10 magnification). B) Endometrioid carcinoma showing wild type staining for p53 few nuclei show strong staining, most show moderate to weak staining and some are negative) (anti-p53, x10 magnification). C) HGSOC over-expressor control showing diffuse strong nuclear staining for p53 in >80% of tumour nuclei (anti-p53, x10 magnification). D) HGSOC null control showing complete absence of nuclear staining for p53 in the tumour cells compared to wild type staining in the background stroma (anti-p53, x20 magnification).

For both Ki-67 and CD8, tonsillar tissue was used as a positive control. Optimal HIER conditions for both antibodies were determined to be the BOND epitope retrieval solution pH9 for 30 min at 95°C. A dilution of 1:100 and 1:50 was optimal for Ki-67 and

CD8, respectively. Table 2.2 summarizes the details of the primary antibodies used in this study.

Table 2. 2: Primary antibodies used for immunohistochemistry in the 3 experimental cohorts in this study.

Antibody	Dilution	Species	Automated HIER conditions (95°C)	Manufacturer
UbcH10	1:200	Rabbit	pH6, 20 min	Clone no.49 generated in-house
p53	1:2.5	Mouse	pH6, 30 min	Clone DO-1 originally sourced from David Lane
Ki-67	1:100	Mouse	pH9, 30 min	Clone MM1 Leica Biosystems product code: NCL-L-Ki67-MM1
CD8	1:50	Mouse	pH9, 30 min	Clone 4B11 Leica Biosystems product code: CD8-4B11-L-CE

HIER: Heat induced epitope retrieval.

Due to logistical issues encountered in accessing the automated IHC equipment in the Women's hospital during the COVID pandemic, we reverted to manual staining for the Barts cohort using the Leica Novolink Polymer detection kit (No. RE7140CE) which required re-optimisation and comparison with the Birmingham cohort to ensure that the IHC scoring observed between the two methods were equivalent.

To re-optimise UbcH10 for manual IHC, the Leica Novolink Polymer detection kit was used. The same positive, negative and isotype controls described in Figures 2.1 and 2.2 were used with different dilutions (1:50, 1:100 and 1:200) for the primary antibody. Additionally, using the same controls, multiple HIER conditions were used starting with no antigen retrieval and followed by antigen retrieval at pH9 using Tris-EDTA buffer

solution (Sigma-Aldrich) and finally at pH6 using sodium citrate buffer solution. To ensure results were comparable, two HGSOC cases from the Birmingham cohort with low and high UbcH10 expression were also included in the optimisation runs with different dilutions and HIER conditions.

UbcH10 was successfully optimised using the new kit with closely similar HIER conditions and primary antibody dilution applied. Manual staining for both the controls (Figure 2.4) and the two cases from the Birmingham cohort (Figure 2.5) were comparable to the automated staining. The final manual protocol applied for UbcH10 is described in the next section *2.2.1.2 (i).*

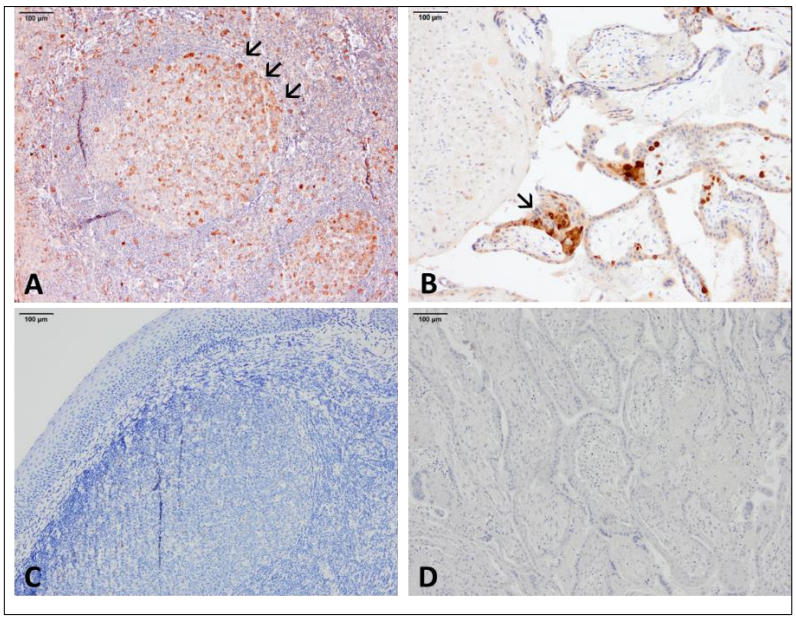

Figure 2. 4: Control tissue used for re-optimisation of UbcH10 for manual immunohistochemistry. A) Tonsillar tissue demonstrating strong cytoplasmic and focal nuclear staining for UbcH10 with polarization of expression in the proliferative centroblasts of the germinal center (arrows). Results are comparable to Figure 2.1A (anti-UbcH10, x10 magnification). B) Products of conception showing strong cytoplasmic and nuclear staining in intermediate trophoblastic cells (arrow) comparable to automated staining in Figure 2.1B (anti-UbcH10, x10 magnification). C) Tonsillar tissue used as a negative reagent control for UbcH10. No staining for UbcH10 is noted akin to Figure 2.2B (no antibody control, x10 magnification). D) Products of conception used as a negative reagent control for UbcH10. No staining for UbcH10 is noted akin to Figure 2.2A (no antibody control, x10 magnification).

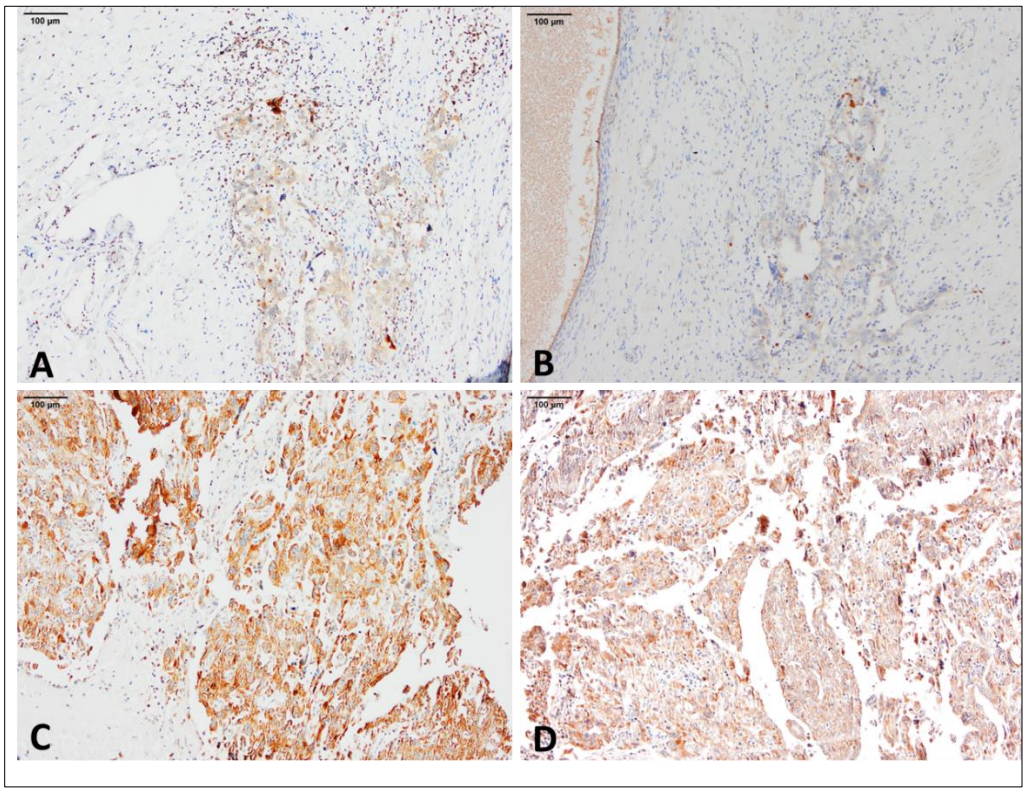

Figure 2. 5: Re-optimisation of UbcH10 for manual immunohistochemistry staining showing comparable results to automated staining in two HGSOC cases from the Birmingham cohort. A) A HGSOC case showing low levels of UbcH10 expression by manual staining (IRS 1, H-score 10; anti-UbcH10, x10 magnification). B) Automated UbcH10 staining for the same case in panel A with comparable levels of UbcH10 expression (anti-UbcH10, x10 magnification). C) A HGSOC case showing high levels of UbcH10 expression by manual staining (IRS 8, H-score 128; anti-UbcH10, x10 magnification). D) Automated UbcH10 staining for the same case in panel C showing comparable levels of UbcH10 expression (anti-UbcH10, x10 magnification).

2.2.1.2 Antigen retrieval and immunohistochemical staining steps

Optimisation and validation of the primary antibodies as well as staining of our tissue samples from the Birmingham and STIC/HGSOC cohorts followed an automated IHC protocol. A manual protocol was used for UbcH10 staining of the TMA slides from the Barts cohort. The principal steps for both the automated and manual IHC staining were similar.

i. The manual IHC protocol

The manual protocol was run over 2 days. On the first day, and after sectioning the tissue blocks into 5µm thin sections, the slides were immersed in a clearing agent; Histo-Clear II (National Diagnostics) for 15 min in a fume cupboard to deparaffinise the tissue. Slides were then taken out of the Histo-Clear II, gently shaken, and then immersed in 99% (v/v) Industrial Methylated Spirits (IMS, Thermo Fisher Scientific) for 10 min to re-hydrate the tissue and remove clearing agent residues. Subsequently, slides were gently rinsed under running tap water for 5 min. The slides were then laid out in a humidified chamber and covered with Leica peroxidase block [3–4%(v/v) Hydrogen peroxide, 2 drops/slide) for 30 min to block endogenous peroxidase activity. Slides were again washed with tap water for 5 min.

Heat-induced epitope retrieval (HIER) was then performed to break the cross links between antigen epitopes previously formed by formalin. To perform HIER for UbcH10, a beaker was filled with 800 ml of sodium citrate buffer [10mM of citric acid monohydrate (Sigma Aldrich) adjusted to a pH6 by 1M NaOH (Merck)]. The beaker with the citrate buffer was then covered with a plastic wrap with 6 to 8 holes to allow steam escape and heated in a microwave at full power (750W) for 12 min. The temperature was then checked by a thermometer to make sure it had reached 95°C. The slides were then lowered in the beaker and heated for another 12 min at medium power (500W). Then the beaker with the slides was taken out of the microwave and left to cool at room temperature for 30 min and then rinsed in running tap water for 1 min. After drying the slides, while avoiding the tissue sections, phosphate-buffered saline (Thermo Fisher Scientific) with 0.1%(v/v) Tween 20 (Sigma Aldrich, PBST) was gently pipetted on the tissue to avoid section drying. Leica Protein Block (0.4% (w/v)

Casein in phosphate-buffered saline, 2 drops/slide) was then applied for 30 min, thus negating non-specific antibody binding. Protein block was then tipped off the slides and 200µl of primary antibody, diluted in PBST, was applied to the tissue sections. For UbcH10, similar to the automated protocol an antibody dilution of 1:200 was optimal. Slides were then incubated in a humidified chamber overnight at 4°C.

The following day the slides were taken out of the fridge and washed in PBST three times for 15 min total. The Leica Post Primary block (Rabbit anti mouse IgG, 2 drops/slide) was then applied for 30 min and the slides were washed again in PBST three times 5 min each. The secondary antibody (Novolink Polymer, Anti-rabbit Poly-HRP-IgG, 2 drops/slide) was then applied to the tissue sections and incubated for 30 min at room temperature. The slides were then washed again in PBST three times, 5 min each. Antigens were visualised by applying the Novolink 3,3'-Diaminobenzidine (DAB) chromogen and its substrate (Novolink DAB Substrate Buffer) to the tissue for 5 min (50µl DAB to 1ml of substrate buffer for 10 slides). The slides were then washed three times in PBST to stop the reaction. Leica Haematoxylin (2 drops/slide) was then applied to the slides for 12 min for counterstaining and then washed in hot running tap water for 5 min.

To reverse the initial steps, the slides were then transferred to a fume cupboard and immersed in IMS, in 3 different Coplin jars 5 min each, to dehydrate the tissue. This was then followed by immersion in Histo-Clear II, in 2 different Coplin jars 5 min each, to remove the alcohol. Coverslips were then mounted on the slides using Omnimount (National Diagnostics) and left to dry for 30 min at room temperature before they were examined.

ii. The automated IHC protocol

For the automated protocol, the Leica BOND-MAX autostainer and the BOND Polymer Refine Detection kit (No. DS9800) were used. The BOND Polymer Refine Detection kit included the following reagents: Peroxide Block [3–4% (v/v) Hydrogen peroxide], Post Primary Block (Rabbit anti mouse IgG), Secondary antibody Polymer (Anti-rabbit Poly-HRP-IgG), DAB Part 1, DAB Part B and Haematoxylin. The automated protocol followed the same steps and principles of the manual protocol with some differences in the use of reagents and incubation times. Reagents used for the Leica BOND-MAX are detailed in Table 2.3. Antigen retrieval conditions and dilutions for the primary antibodies were determined as previously described in Table 2.2. The automated protocol was adjusted such that the primary and secondary antibodies were applied for 1 hr and 15 min, respectively. Additionally, Peroxidase Block and Post Primary Block were applied for 10 min and 15 min, respectively. Otherwise, incubation times for the remaining steps were as according to the manual protocol [see section 2.2.1.2 (*i*)].

iii. The multiplex IHC protocol

The multiplex IHC protocol used for the STIC/HGSOC cohort followed the same steps as the automated protocol. The Bond Polymer Refine detection kit (No. DS9800) was used for p53 and Ki-67 brown staining, whilst the Bond Polymer Refine Red detection kit (No. DS9390) was used for UbcH10 red staining. The red detection kit included the following reagents: Post Primary AP (Rabbit anti-mouse IgG), Polymer AP (Poly-AP anti-rabbit IgG), Red Part A activator, Red Part B Substrate, Red Part C Substrate, Red Part D Buffer solution and Haematoxylin.

Staining was performed in a sequential manner with shortening of the antigen retrieval conditions to avoid antigen denaturation. For multiplex p53/UbcH10 staining, initial dewaxing and rehydration of the tissue sections was performed as described previously [section 2.2.1.2 (*i*)]. The BOND brown protocol was then applied to stain for p53 [Peroxide Block (10min), HIER 20 min (pH6), p53 (1:2.5) for 1hr, Post Primary Block (15 min), Secondary antibody HRP Polymer (15 min), DAB and substrate (5 min), Haematoxylin (12 min)]. Subsequently, the BOND Red detection protocol was applied for UbcH10 [HIER 10 min (pH6), UbcH10 (1:200) for 1hr, Post Primary AP (15 min), Secondary Polymer AP (15 min), Red and substrate (5 min), Haematoxylin (12 min)]. Tissue sections were then dehydrated, cleared, mounted, and left to dry as described in the manual protocol [section 2.2.1.2 (*i*)].

For multiplex Ki-67/UbcH10 staining, Ki-67 staining was done initially and followed the same brown protocol described for p53, but HIER was done for 20 min at a pH9 and the dilution for Ki-67 was 1:100. UbcH10 staining was done subsequently using the BOND Red detection protocol described above.

Table 2. 3: The reagents used in the automated immunohistochemistry protocol for the Leica BOND-MAX autostainer compared to the manual IHC protocol.

Reagent for automated protocol	Counterpart in manual protocol	Application
Bond Dewax Solution **No. AR9222**	Histo-Clear II	Deparaffinization of tissue sections
Industrial Methylated Spirit 99% (v/v) (Thermo Fisher Scientific)	Industrial Methylated Spirit 99% (v/v)	Rehydration of tissue after deparaffinization
Bond TM Wash Solution 10X concentrate **No. AR9590**	Phosphate-buffered saline with Tween (PBST)	Wash between reagent incubation
Bond TM Epitope Retrieval solution-1 (pH6) **No. AR9961**	Citrate buffer, pH6	Heat induced epitope retrieval for UbcH10 and p53
Bond TM Epitope Retrieval solution-2 (pH9) **No. AR9640**	Not applicable	Heat induced epitope retrieval for Ki-67 and CD8
IHC Diluent **No. RE7133CE**	PBST	Primary antibody diluent

2.2.1.3 Immuno-histochemical scoring

In the present study we used two scoring systems for UbcH10 that we applied to all 3 experimental cohorts in this study; a modification of the Immunoreactive (IRS) score (110) and the Histochemical (H)-score as originally described (111).

i. The Immuno-reactive score (IRS)

This scoring system includes:

a) A proportion score (percentage of positive cells) scored as follows:

0= staining in less than 1% of tumour cells.

1= staining in 1 to 25% of tumour cells.

2= staining in 26% to 50% of tumour cells.

3= staining in 51% to 75% of tumour cells.

4= staining in >75% of tumour cells.

b) Intensity score (intensity of the staining reaction) scored as follows:

0= no colour reaction.

1= mild reaction.

2= moderate reaction.

3= strong reaction.

A total score was then calculated by the multiplication of the proportion and intensity scores to give a range of scoring from 0 to 12. To overcome the heterogeneous nature of staining for UbcH10, the percentage of cells with each intensity of staining were counted and scored independently in a standardized field area of $2mm^2$=10 high power fields (HPFs). An average percentage of cells with each intensity were then calculated and the results were summed (110).

ii. H-score

The H-score was applied in a similar manner to the IRS but with a wider range of the final scoring (0 to 300). The number of cells stained at each intensity were similarly counted in relation to the number of cells in 10 HPFs ($2mm^2$), an average percentage for each intensity was calculated and then the final score was calculated using the following formula: *1x percentage of weak staining cells+2 x percentage of moderate staining cells+ 3 x percentage of strong staining cells.*

In addition, a UbcH10 total tumour proportion score (TPS) was calculated as the total percentage of tumour cells expressing UbcH10 at any intensity in relation to the whole tumour.

P53 immunohistochemical staining was assessed as previously described in Table 1.2.

In both the Birmingham and STIC/HGSOC cohorts, scoring for a Ki-67 index was performed following previous recommendations (112). Tumour hot spots with the highest nuclear intensity of staining were chosen and 500-2000 tumour cells were assessed. The index was determined as an average percentage of positive tumour cells in 10 HPFs equivalent to $2mm^2$.

In the STIC/HGSOC cohort, we used a stepwise approach for immunohistochemical scoring assessment of Ki-67 and UbcH10. In the first instance, we used single staining to determine the Ki-67 index and the UbcH10 total tumour proportion score (TPS). We then applied multiplex staining to determine the percentage of tumour cells that co-expressed both proteins. A total tumour proportion score (TPS) was calculated as the percentage of tumour cells that expressed UbcH10 or Ki-67 either singly or dually in relation to the whole tumour. The percentage of tumour cells that co-expressed both proteins was then calculated in relation to the whole tumour (both positive and negative tumour cells) and in relation to the total TPS (only positive tumour cells).

As part of the molecular characterization for the Birmingham cohort a CD8 count of tumour infiltrating lymphocytes (TILs) was performed according to previous reports (113). TILs were categorized as peri-tumoral or ‘stromal’ and infiltrating into the

tumour or ‘intraepithelial’. Following recommendations from previous reports (113) (114), a total of 5 high power fields (x40 magnification equivalent to 0.196 mm^2 per HPF) with the most abundant TILs were chosen and the average CD8 count was taken. The CD8 count was then expressed as the number of CD8+ TILs per HPF.

Immuno-histochemical assessment of all markers was done using the Leica Bright field microscope Dm500 at the Birmingham Women’s hospital. Slides were stored in boxes at room temperature. Images were taken using the Olympus microscope BX53F2 (Tokyo, Japan).

2.2.2 Tissue culture and siRNA knockdown

2.2.2.1 Tissue culture and UbcH10 expressing cell lines

In this experiment, two UbcH10 expressing cell lines were used; RPE-1 (Retinal pigmented epithelial cells that are hTERT immortalized, ATCC number CRL-400) and H1299 (Human non-small cell lung carcinoma, ATCC number CRL-5803).

All procedures related to cell culture were performed in a safety hood under aseptic conditions. HEPES-buffered Dulbecco’s Modified Eagle Medium (DMEM; Sigma-Aldrich) was used to grow the cell lines in 10 cm tissue culture dishes (Falcon). The medium was supplemented with 8% (v/v) foetal-bovine serum (FBS; Sigma-Aldrich) and 2 mM L-glutamine (Sigma-Aldrich). The cells were grown in a humidified incubator at 37 ºC with 5% (v/v) CO2. At 80-90% confluence ($5x10^6$ cells/10cm plate), the cells were passaged. For passaging, the culture medium was aspirated, and the cells washed in D-PBS (Gibco) twice. To facilitate detachment, cells were then incubated in Trypsin (TrypLE express, Gibco) for 5 minutes at 37 ºC. To inactivate the trypsin, the detached cells were resuspended in medium and then centrifuged at 1600 rpm for 3

minutes. The cells were then resuspended in DMEM-HEPES medium and plated out at the appropriate passage density (0.7 x10^6 cells/10cm plate).

For long-term storage, cells were harvested at 80-90% confluence, transformed into a cell pellet and suspended in freezing medium [(50% growth medium, 40% FBS and 10% v/v DMSO (Sigma-Aldrich)]. The cells were then transferred to cryovials and left to cool in a Freezing container (Nalgene, MrFrosty) in a -80 freezer before they were transferred to liquid nitrogen.

2.2.2.2 siRNA knockdown

To perform a UbcH10 knockdown and confirm the specificity of our in-house generated antibody, three 10 cm dishes (one as a control and two for two different UbcH10 targeted siRNAs) were prepared for each of RPE-1 and H1299 cell lines. Cell lines were grown to 30% confluence in the dishes containing DMEM-HEPES medium supplemented with 8% (v/v) FBS and 2 mM L-glutamine. Knockdown of UbcH10 was done using two different small interfering RNA (siRNA); UbcH10-siRNA-1 (Ambion) and UbcH10 siRNA-2 (Dharmacon). Each siRNA targeted against Ubch10 was added to a final concentration of 40 nM and incubated with 200 µl of the low serum medium OptiMEM for 5 min at room temperature in an ependorf. In another ependorf, 15 µl lipofectamine RNAiMAX was incubated with 200µl OptiMEM at room temperature for 5 min. The lipofectamine-RNAiMAX mixture was then added to the siRNA-OptiMEM mixture and incubated at room temperature for another 30 min. The lipofectamine-RNAiMAX functions to increase the penetration of siRNA into the cells. Cells were then washed with 5 ml OptiMEM once and incubated in 5.5 ml fresh OpitMEM medium for another 15-20 min. The siRNA knockdown complex was then added to the respective cell lines in the non-control labelled dishes and incubated for 5 hours at 37 °C in 5%

(v/v) CO2. The OptimMEM-siRNA knockdown mixture was then aspirated and fresh DMEM-HEPES medium supplemented with 8% (v/v) FBS and 2 mM L-glutamine was added to the cells. Cells were incubated in a humidified incubator at 37 ºC with 5% (v/v) CO2 and harvested when 80-90% confluent at 72 hours later for immunohistochemical analysis.

2.2.2.3 Fixation of knockdown cells

To prepare the cells for IHC analysis, knockdown cells (RPE-1 and H1299) were harvested in accordance with the following protocol. The medium was aspirated from the cells which were then washed twice with warm Dulbecco's phosphate-buffered saline (D-PBS, Gibco). The cells were then trypsinized (TrypLE express, Gibco) for 5 minutes at 37 ºC to aid cellular detachment. The detached cells were resuspended in DMEM-HEPES medium, collected in a Falcon tube, and then centrifuged at 1000 rpm for 3 min to form a cell pellet. The supernatant was then discarded and 1 ml of 10% (v/v) neutral-buffered Formalin solution was added to the cell pellet for 1 hr to fix the cells. 10 ml of D-PBS was then added, and the cells were centrifuged again at 1000 rpm for 3 min and the supernatant discarded. 1ml of heated 3% (w/v) agar solution was then added dropwise to the fixed cell pellet and left to set at 4 ºC for 30 min. The agar solution was used to prevent the fragmentation of the fixed cell pellet during subsequent processing. The agar-embedded cell pellet was then placed in tissue cassettes and processed for paraffin embedding using the automated tissue processor at the Birmingham Women's hospital (Thermo Scientific Shandon Pathcentre). The FFPE tissue blocks containing the respective cell pellets were then sectioned into 3µm sections using a microtome onto coated slides.

2.2.2.4 Immunohistochemical staining of knockdown cells

To visualize UbcH10 knockdown in the RPE-1 and H1299 cells, immunohistochemical staining for Ubch10 was done on the respective fixed cell sections. Immunohistochemistry followed the automated protocol described in section 2.2.1.2. However, the steps were modified to suit the delicate nature of the cells. The BOND Polymer Refine detection kit was used. UbcH10 was diluted to 1:300 instead of 1:200 and HIER was done at pH6 for 10 min instead of the 20 min used on tissue sections. Figures 2.6 and 2.7 demonstrate decreased UbcH10 expression in knockdown RPE-1 and H1299 cells, respectively.

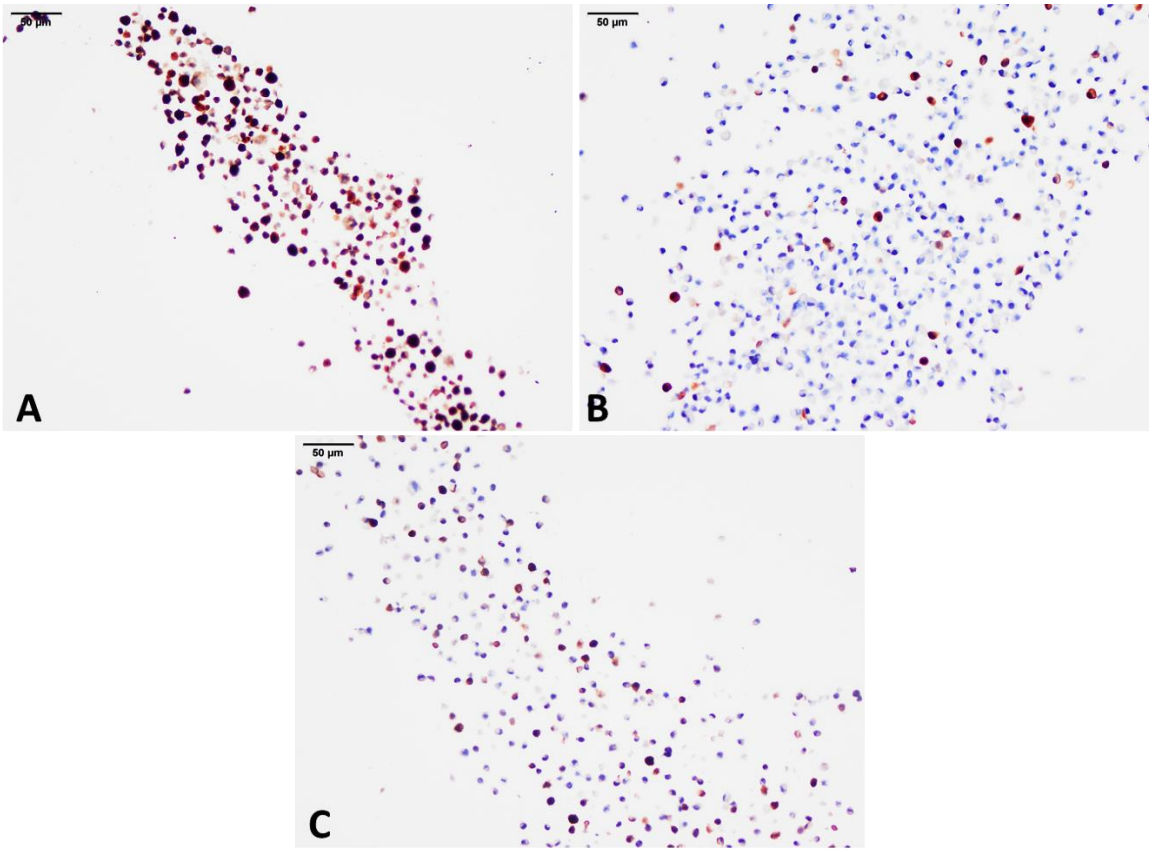

Figure 2. 6: UbcH10 knockdown using siRNA on RPE-1 cells demonstrating decreased UbcH10 expression after knockdown compared to the control. A) RPE-1 control cells not treated with siRNA showing strong diffuse UbcH10 expression (IRS 12, anti-UbcH10, x20 magnification). B) RPE-1 cells treated with UbcH10 siRNA-1 (Ambion) showing a significant reduction in the level of UbcH10 expression (IRS 5, anti-UbcH10, x20 magnification). C) RPE-1 cells treated with UbcH10 siRNA-2 (Dharmacon) showing similar levels of UbcH10 reduction (IRS 5, anti-UbcH10, x20 magnification).

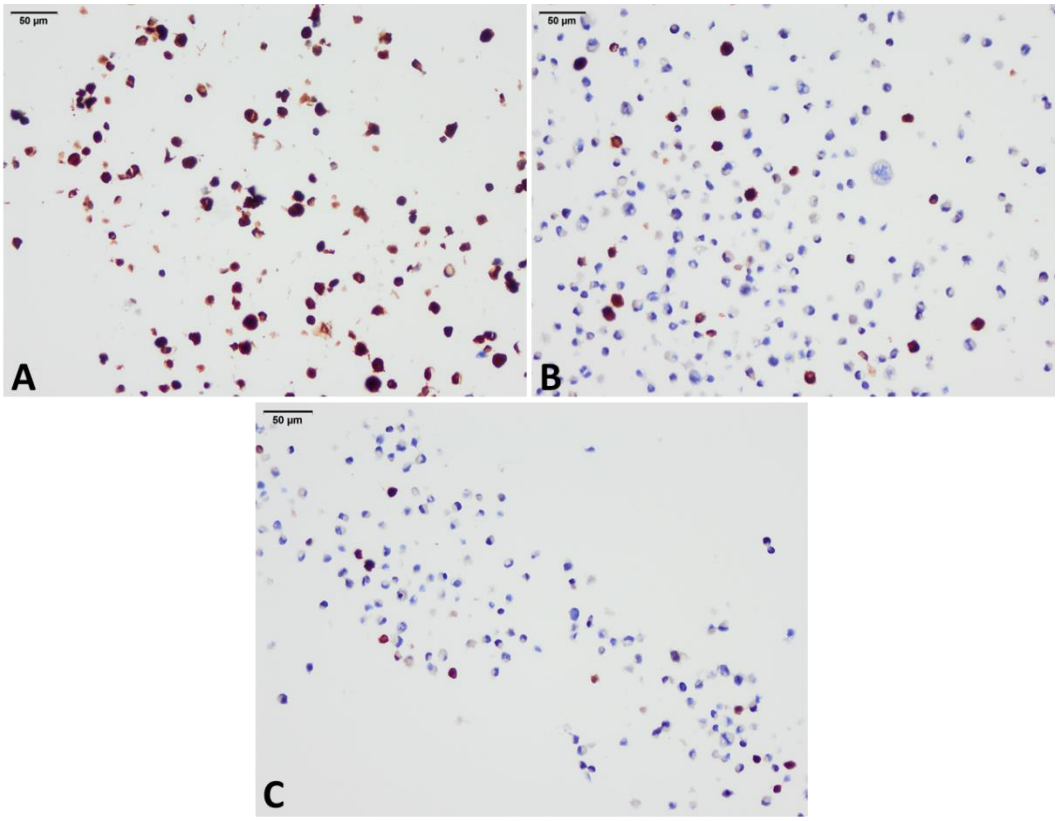

Figure 2. 7: UbcH10 knockdown using siRNA on H1299 cells demonstrating decreased UbcH10 expression after knockdown compared to the control. A) H1299 control cells not treated with siRNA showing strong diffuse UbcH10 expression (IRS 10, anti-UbcH10, x20 magnification). B) H1299 cells treated with UbcH10 siRNA-1 (Ambion) showing a marked reduction in the level of UbcH10 expression (IRS 3, anti-UbcH10, x20 magnification). C) H1299 cells treated with UbcH10 siRNA-2 (Dharmacon) showing decreased UbcH10 expression (IRS 5, anti-UbcH10, x20 magnification).

2.2.3 Western blot analysis

2.2.3.1 Protein extraction from Ovarian Cancer specimens

In the first 6 months of this project and as a pilot study, a total of 61 snap frozen samples were retrieved from liquid nitrogen. The samples had been collected by previous members of the laboratory from the ovary, omentum, peritoneum, and fallopian tube of 47 consenting ovarian cancer patients from the PBGOC. The samples were donated and ethically approved for research purposes from patients treated at both the Birmingham Women's Hospital and the Royal Wolverhampton Hospital NHS Trust. The samples had been put in Eppendorf tubes, labelled with the patient's study number, and stored at -80° C. Some patients had been sampled for ovarian and omental tumours simultaneously, whilst others had been sampled for the ovarian tumour and the fallopian tube, simultaneously. Of the 61 samples, 33 were collected from the ovary, 23 from the omentum, 3 were harvested from the peritoneum and 2 from the fallopian tube. Upon collection, samples were anonymised as to the pathological diagnosis and the clinical information to avoid bias.

To commence protein extraction, samples were retrieved on dry ice, cut-up into small tumour chunks, placed in individual tubes, to which 300-500 µl of UTB buffer [9M urea, 50 mM Tris (pH 7.4) and 0.15 M β-mercapto-ethanol] was added to each individual sample according to the size of the tumour chunk. Samples in UTB were then mechanically disrupted using a tissue disruptor for 1-3 min. The disrupted samples were then centrifuged at 16000 rpm at 4°C for 20 min. The fatty layer in omental specimens was carefully removed manually, and the protein lysate supernatant was placed in a new Eppendorf tube and stored at -80°C for 24 h. The following day, samples were sonicated for DNA/chromatin shearing and homogenization using

(Microson Ultrasonic Cell Disruptor) in continuous pulses for 15 sec, and then re-stored at -80°C.

2.2.3.2. Bradford Protein Assay

The Bradford assay was used to determine the protein concentration in the samples. Bradford reagent (BIO-RAD) was used to dilute Bovine Serum Albumin (BSA) (1mg/ml; Sigma Aldrich) to produce standard concentrations of 0, 5, 10, 20 and 30 µg/ml. A Cecil CE9200 spectrophotometer was then used to determine the absorbance of these standards at 595 nm wavelength. The results were used to generate a standard curve. A standard curve coefficient (R2) of 0.97 or more was deemed satisfactory. Then, 1000µl of Bradford reagent was added to 1-4µl of sonicated protein lysate from tumour tissue, and the absorbance at 595 nm was measured. The protein concentration of lysates was then determined by comparing their absorbance values to the standard curve.

2.2.3.3 SDS-PAGE and Western blotting

Sample buffer (1 volume of 10% (w/v) SDS, 2 volumes of UTB buffer, 0.1% (w/v) bromophenol blue) was added to 100 µg of protein lysate in an Eppendorf tube at a ratio of 1:1. Proteins were then heated at 95°C for 5 min to denature the proteins. The samples were then subjected to SDS-PAGE (sodium dodecyl sulphate- polyacrylamide gel electrophoresis) for approximately 16 h at 16mA for a double gel. The gel comprised 10% (v/v) acrylamide (37.5:1 acrylamide/bisacrylamide), 0.1 M Tris-Bicine pH 8.3, 0.1% (w/v) SDS, 0.3% (v/v) TEMED (N, N, N', N'-tetramethylethylenediamine) and 0.06% (w/v) ammonium per-sulphate and was run in the presence of running buffer (0.1M Tris-Bicine pH 8.3, 0.1% (w/v) SDS). We used a wet transfer method to electrophoretically transfer proteins to a nitrocellulose membrane, for 6 hours at 280

mA, using transfer buffer (24mM Tris, 193mM Glycine, 20% (v/v) Methanol). Membranes were then blocked using 5% (w/v) powdered milk in TBST [Tris-buffered saline (10mM Tris pH 7.5, 150mM NaCl) with 0.1% (v/v) Tween 20] for 45 min. Membranes were then cut at the appropriate molecular weights to ensure detection of the proteins of interest. The primary antibody (Table 2.4) was then diluted in 5% (w/v) powdered milk in TBST and applied to the blots in a polyethylene bag on a rocker, and incubated at 4°C. The following day, membranes were washed for 15 min with TBST, after which secondary antibodies conjugated to horseradish peroxidase (HRP) were prepared in 5% (w/v) powdered milk in TBST (Table 2.4) and added to the membranes for a further 3 h on a rocker at room temperature. The membranes were then washed for 45 min in TBST, which were then treated with ECL (Enhanced luminol-based chemiluminescence) reagent (Millipore) which reacts with HRP conjugated to the secondary antibody on the blots. This is followed by visualization of the protein bands on X-ray films using an X-ograph developer.

Table 2. 4: Primary and secondary antibodies used for Western blot analysis.

Antibody	Dilution	Species	Manufacturer
Ubch10	1:1000	Rabbit	Clone no. 49 generated In-house
p53	1:20	Mouse	Clone DO-1 originally sourced from David Lane
β-actin	1:30000	Mouse	Sigma-Aldrich
Anti-mouse Ig HRP	1:2000	Goat	Dako
Anti-rabbit Ig HRP	1:3000	Swine	Dako

HRP: Horseradish peroxidase, **Ig**: Immunoglobulin.

2.2.4 Molecular Biology

To verify results generated at the protein level in the Birmingham cohort including the mosaic p53 cases, we attempted to extract and amplify DNA from the FFPE-tissue blocks available to us from that cohort. The aim was to sequence and identify mutations in the *TP53* gene as well as amplifications/mutations in the *Ube2C* gene using Direct Sanger sequencing. To this end we started with 50 patients from the Birmingham cohort. Before these steps, macrodissection of the area of interest of the tumour was performed to maximise the neoplastic cell content.

2.2.4.1 Tumour macrodissection

In order to increase the DNA yield from the neoplastic cells, we had to pinpoint the area of the tumour with the maximum number of neoplastic cells and the least number of stromal and inflammatory cells. Additionally, because a considerable number of our tumours were from the omentum, areas of fatty tissue and necrosis had to be avoided where possible or reduced to a minimum.

To this end, we examined the H&E sections corresponding to the tumour blocks from the 50 patients under the microscope and then using a marker we traced the outline of the desired area of the tumour to be macro-dissected. For the cases with mosaic p53 expression, each area with a different IHC expression pattern was outlined separately. Subsequently, two 10μm thick serial sections of the tumour were sectioned using a microtome (Leica Biosystems) onto a coated slide. The outline of the desired area of the tumour was then re-traced on the newly sectioned slide using the H&E-stained slide as a guide. The outlined area of the tumour was then macro-dissected using a scalpel into a 1.5 ml microcentrifuge tube filled with 500 μl of 70% (v/v) ethanol. The

microcentrifuge tubes labelled with the patient study number were then centrifuged at 1000 rpm for 2 min. The ethanol was then aspirated from the tubes and the samples were left to dry for 20 min at room temperature.

2.2.4.2 DNA extraction from macro-dissected tumour

To extract DNA from the FFPE-tissue sections after macrodissection, the QIAamp DNA FFPE Advanced Kit (Qiagen, catalogue number 56604) was used.

Before starting, a thermomixer (Merck) was preheated at 56 °C and a heating block was pre-heated at 90 °C. Additionally, AW1 and AW2 buffers provided in the kit were reconstituted by adding 25 ml and 30 ml of 96-100% (v/v) ethanol to the bottles containing their respective concentrates.

In the first instance, the paraffin was removed from the FFPE tissue sections by adding 300 µl of Deparaffinization solution to the microcentrifuge tubes containing the samples. The microcentrifuge tubes were then vortexed vigorously for 10 seconds and pulse centrifuged for 1 min to bring the samples to the bottom of the tube. The samples were then incubated at 56 °C for 3 min and left to cool at room temperature.

A master mix consisting of 25 µl of FTB lysis buffer, 55 µl RNase-free Water, and 20 µl Proteinase K was then added to each individual sample to lyse the tissue and release nucleic acids from the cells. The samples were then vortexed, pulse centrifuged for 1 min and incubated inside the thermomixer for 1 hr at 56 °C and 1000 rpm. The samples were then incubated in the heating block for 1 hr at 90 °C without shaking to break the cross-links in the DNA formed by formalin fixation. The upper blue phase containing the Deparaffinization solution was then discarded and 150 µl of RNase-free Water was added to and mixed with the lower aqueous phase containing the lysate. Subsequently,

2 μl of RNase A was added to each individual sample and incubated for 2 min at room temperature. The aim of this step was to digest the RNA and focus on the extracted DNA. To ensure complete tissue lysis and increase the DNA yield, 20 μl of Proteinase K was added to each individual sample and incubated inside the thermomixer for 15 min at 65 °C and 450 rpm.

In the next steps we aimed to remove the unwanted debris (including lysed proteins and lipids) from the lysate and isolate and bind the genomic DNA. To do this, 250 μl of AL buffer and 250 μl of 96-100% (v/v) ethanol was added to each sample and vortexed to enhance DNA binding in the subsequent steps. Subsequently, 450 μl of the lysate was transferred to the QIAamp UCP MinElute column in a 2 ml collection tube, and centrifuge at 15000 x g for 30 sec. The remaining lysate was then transferred to the same QIAamp UCP MinElute column, and centrifuged at 15000 x g for 1 min. The flow-through containing the unwanted tissue debris was then discarded and the collection tube was reused. Subsequently, 500 µl of AW1 wash buffer was added to each spin column, and centrifuged at 15000 x g for 30 sec. The flow-through was again discarded and the collection tube reused. Then, 500 μl of AW2 wash buffer was added to the spin column and centrifuged at 15000 x g for 30 sec. The flow-through was discarded and the collection tube reused. Finally, 250 µl of 96–100% (v/v) ethanol was added to the spin column, and centrifuged at 15000 x g for 30 sec.The flow-through and the collection tube were discarded this time, and the spin column was placed into a new 2 ml collection tube and centrifuged for 3 min at 15000 x g to dry the membrane containing the bound DNA. The collection tube was discarded and the QIAamp UCP MinElute column was placed into a new 1.5 ml microcentrifuge tube. The lid of the column was opened and 50 μl of ATE buffer was added to the centre of the membrane

and left for 5 min at room temperature to elute the DNA. The column with the microcentrifuge tube were then centrifuged at 15000 x g for 1 min to increase the DNA yield. About 5 μl of the eluted DNA solution was set aside for quality control and DNA quantification testing and the rest of the material was used for subsequent DNA amplification.

2.2.4.3 DNA quantification

After DNA extraction from 50 patients from the Birmingham cohort, we checked the DNA for quantity and purity using NanoDrop Spectrophotometer. About 2 μl of the eluted DNA solution was placed on the pedestal of the Spectrophotometer and the amount of DNA was measured as ng/μl. The purity of the DNA was measured using the Optical Density at 260 nm/Optical Density at 280 nm ratio.

2.2.4.4 DNA amplification (Polymerase Chain Reaction)

After quantification of the DNA, we aimed to amplify the *TP53* and *Ube2C* genes in the genomic DNA using Polymerase Chain Reaction (PCR) to facilitate their subsequent sequencing. For a standard PCR reaction, a high-quality template DNA is needed in addition to forward and reverse primers to flank the segment of the DNA targeted for amplification. Therefore, we next proceeded to design primers to cover the whole length of the *TP53 (*9 exons*)* and *Ube2C* (6 exons) genes.

Primers were designed according to the following criteria: a length between 18 and 23 base pairs, GC content between 40-60%, annealing temperature between 55 to 63 °C, self-complementarity of not more than 10 and a resultant PCR product size between 250 and 500 base pairs. These properties facilitate specific primer binding to the targeted sequence and minimise the chances of non-specific binding to unwanted

sequences. Subsequently, the reference sequence for both the *TP53* and *Ube2C* genes was downloaded from the National Centre for Biotechnology Information (NCBI) website (https://www.ncbi.nlm.nih.gov). For *TP53*, we used the already designed primers from the West Midlands Regional Genetics laboratory as a guide and double checked their specificity against the reference sequence of the *TP53* gene using the Primer-BLAST function on the NCBI website. For *Ube2C*, we designed the primers ourselves using the primer designing tool on the NCBI website and Primer3 (https://primer3.ut.ee). Primers for both genes were then ordered from Sigma-Aldrich.

The PCR primer pairs for *TP53* and *Ube2C* are described in Tables 2.5 and 2.6 respectively.

Table 2. 5: List of primers used for the amplification of the *TP53* gene using PCR.

Primer number	Direction	Sequence (5'-3')	Exon	Annealing temperature	GC content (%)	PCR product length
TP53-1	Forward Reverse	TCTCATGCTGGATCCCCACT AGTCAGAGGACCAGGTCCTC	2-3	60.33 59.96	55 60	324
TP53-2	Forward Reverse	GTGGTGGGAAGGTTGGAAGT TGGGTGAAAAGAGCAGTCAG	2-3	59.81 57.74	55 50	499
TP53-3	Forward Reverse	TGCTCTTTTCACCCATCTAC ATACGGCCAGGCATTGAAGT	4a	55.06 59.74	45 50	353
TP53-4	Forward Reverse	TGAGGACCTGGTCCTCTGAC AGAGGAATCCCAAAGTTCCA	4b	60.25 56.02	60 45	413
TP53-5	Forward Reverse	TTCAACTCTGTCTCCTTCCT CAGCCCTGTCGTCTCTCCAG	5	55.40 61.94	45 65	248
TP53-6	Forward Reverse	GCCTCTGATTCCTCACTGAT TTAACCCCTCCTCCCAGAGA	6	56.7 58.90	50 55	181
TP53-7	Forward Reverse	TGTTCACTTGTGCCCTGACT GGAGGTCAAATAAGCAGCAGG	5-6	59.45 58.98	50 52.38	534
TP53-8	Forward Reverse	CTTGCCACAGGTCTCCCCAA AGGGGTCAGAGGCAAGCAGA	7a	62.07 63.05	60 60	237
TP53-9	Forward Reverse	AGGCGCACTGGCCTCATCTT TGTGCAGGGTGGCAAGTGGC	7b	64.36 66.02	60 65	177
TP53-10	Forward Reverse	TTCCTTACTGCCTCTTGCTT AGGCATAACTGCACCCTTGG	8	56.75 60.32	45 55	231
TP53-11	Forward Reverse	TTGGGAGTAGATGGAGCCT AGTGTTAGACTGGAAACTTT	8-9	56.95 51.92	52.63 35	395

Table 2. 6: List of primers used for the amplification of the *Ube2C* gene using PCR.

Primer number	Direction	Sequence (5'-3')	Exon	Annealing temperature	GC content (%)	PCR product length
Ube2C-1	Forward Reverse	CCGAGTTCCTGTCTCTCTGC GAGCTCCTGGTGTGTTCTCC	1	59.83 60.04	60 60	274
Ube2C-2	Forward Reverse	CCCATCCAGACTCCCAGGTA TGGGGCTAGGAAGTAGGGAC	2	60.03 60.03	60 60	328
Ube2C-3	Forward Reverse	GCTATGCCCAAAAGTGTACTCC AGCTGCCTTCTTGAGATCTGG	3	59.32 50.79	50 52.38	415
Ube2C-4	Forward Reverse	TTTGTCTACTGTCCGGTCCC CTGACAGGTTCCCAAGTTGC	4	59.03 59.05	55 55	375
Ube2C-5	Forward Reverse	GGAAAAGTGGTCTGCCCTGT GAGCCTTTGAAGGTTGGGGG	5	60.18 60.9	55 60	288
Ube2C-6	Forward Reverse	ACTGAGACCTGCCTGTTCTC AAAGACGACACAAGGACAGG	6	59.03 57.76	55 50	119

For PCR, the Q5 High-Fidelity PCR Kit was used (New England Biolabs, catalogue number E0555S). To prepare the primers for PCR, they were reconstituted using nuclease-free water according to the manufacturer's data sheet to make a 100 μM solution. The 100 μM primer solution was diluted again using nuclease-free water to yield a 10 μM solution.

For a standard PCR reaction, 25 μl of PCR components were used. The amount of each component needed, and their final concentration are included in Table 2.7 as per the manufacturer's recommendations.

Table 2. 7: Reagents for a standard 25 μl PCR reaction.

PCR component	25 μl PCR reaction	Final concentration
X5 Q5 reaction buffer	5 μl	x1
10 mM dNTPs	0.5 μl	200 μM
10 μM Forward Primer	1.25 μl	0.5 μM
10 μM Reverse Primer	1.25 μl	0.5 μM
Q5 High-Fidelity DNA Polymerase	0.25 μl	0.02 U/μl
X5 Q5 GC enhancer	5 μl	X1
Template DNA	1 μl	Variable*
Nuclease-free water	10.75 μl	-

dNTP: deoxynucleotide triphosphate

*Template DNA concentration in our samples ranged from 8.6 to 283 ng/μl.

To set-up a PCR reaction efficiently, a Master mix was first prepared with all the reagents needed except for the template DNA and Q5 DNA polymerase which were added in the last steps before the PCR. All reagents were assembled quickly on ice to provide optimal conditions for the DNA polymerase. The Master mix was prepared according to the formula: n+1 where n is the number of PCR reactions. For example, if one pair of primers was run with 6 different patient samples and a no template control was included to check for contamination, then a Master mix was prepared for n+1=8 PCR reactions. Each patient sample was run with the primer pairs described in Tables 2.5 and 2.6 to ensure full sequence coverage of *TP53* and *Ube2C* genes. The reaction was gently mixed and then transferred quickly to a thermocycler pre-heated to the

denaturation temperature (98 °C). The appropriate annealing temperature for each set of primers with the Q5 High-Fidelity DNA polymerase was calculated using the NEB Tm calculator. The thermocycling programme and steps for the PCR reaction are described in Table 2.8. After the PCR reaction, products were purified using the QIAquick PCR Purification Kit (Qiagen) according to the manufacturer's instructions.

Table 2. 8: Thermocycling conditions and steps for a standard PCR reaction.

Step	Temperature	Time
Initial Denaturation	98°C	30 seconds
25–35 Cycles (Annealing)	98°C	10 seconds
	50–72°C*	30 seconds
	72°C	20 seconds
Final Extension	72°C	1 minutes
Hold	4°C	10 minutes

*Annealing temperature was determined for each set of primers using NEB Tm calculator.

2.2.4.5 Agarose Gel Electrophoresis

To determine whether the PCR has worked and amplified the required amplicons we ran the samples on an agarose gel for later visualization under UV light. To do this, DNA fragments generated by PCR, were separated on an 0.8% (w/v) agarose gel. Electrophoresis-grade agarose (Life Technologies) was prepared in x1 TBE buffer (100 mM Tris, 100 mM boric acid, 2 mM EDTA, pH 8.3) and mixed with ethidium bromide (50 µg/ml) which intercalates with the DNA fragments allowing their visualisation. The agarose was then poured and allowed to polymerise inside a suitable tank for 50 min

which was then flooded with x1 TBE buffer. The PCR samples were then loaded onto the gel and an appropriate volume of x6 sample buffer (30% (v/v) glycerol, 0.25% (w/v) xylene cyanol FF) was added to the PCR samples before separation by electrophoresis. A 1 kb plus DNA ladder (Life Technologies) was used loaded in one lane next to the samples to confirm fragment size. The gel tank was connected to the power pack and the samples were run at 60v for 30 minutes. The DNA bands were then visualized using a UV transilluminator (GeneFlash, Syngene).

At this point, results were suboptimal as described later in Chapter 3 section 3.2.7 and Chapter 4 section 4.6.5. Therefore, we did not proceed with Sanger sequencing for either *TP53* or *Ube2C*.

Chapter 3. UbcH10 is a poor prognostic indicator of borderline prognostic significance that is aberrantly overexpressed in high grade serous ovarian cancer

3.1 Introduction

UbcH10 functions as an E2 ubiquitin-conjugating enzyme for the multi-protein E3 ubiquitin ligase complex known as the Anaphase-Promoting Complex/Cyclosome (APC/C) (86). Together, they mark key mitotic regulators for degradation by the ubiquitin-proteasome system and coordinate the progression of the cell through mitosis and G1. UbcH10 has also been identified as a proto-oncogene that is overexpressed in many human cancers including ovarian cancers (96-101). Studies indicate that UbcH10 acts as a proto-oncogene by promoting chromosomal mis-segregation, genomic instability, and aneuploidy (93).

In ovarian cancer, UbcH10 overexpression has been correlated positively with high tumour grade and poorly differentiated morphology (86). Taken together, these studies all emphasize the importance of UbcH10 as a cancer biomarker with potential prognostic, predictive, and therapeutic advantages. For more information see Chapter 1 sections 1.7 and 1.8.

Earlier studies have explored UbcH10 in cohorts of mixed ovarian cancer subtypes but have not considered fully its role in the most common and most lethal subtype; high grade serous carcinoma (86). Indeed, UbcH10 has yet to be investigated as a prognostic, predictive, and therapeutic marker in HGSOC.

Therefore, in this chapter we study two well-characterised cohorts of HGSOC women to consider whether UbcH10 is an HGSOC biomarker with prognostic value. For the purposes of this study, the first cohort was designated as the 'training set' and comprised 100 FFPE tissue blocks collected from consenting women at the PBGOC. The second cohort was designated as the 'validation set' and comprised constructed TMAs from 81 HGSOC patients and was donated by Barts Health NHS Trust. Immunohistochemical staining was performed using an in-house anti-UbcH10 antibody after proper optimization and validation (see Materials and Methods section 2.2.1). Scoring was done using two validated scoring systems IRS and H-scores. The *X*-tile software was used to generate biologically significant cut-off values for UbcH10 scoring based on survival differences. This was applied consistently in both cohorts to dichotomize UbcH10 into low and high expression categories for statistical analysis. Clinico-pathological and survival data were collected from the relevant archives and data analysis was performed (refer to Materials and Methods section 2.1.4).

3.2 The Birmingham cohort (training cohort)

3.2.1 Study population

This cohort included 100 HGSOC females diagnosed and collected as previously described in section 2.1.1.1.

3.2.2 Demography, clinico-pathological profile, and treatment variables

3.2.2.1 Age at diagnosis

The females were aged between 36 to 84 years with a median (*Mdn*) age of 64 years. The clinical and pathological features of this cohort, detailed herein, are summarised in Table 3.1.

3.2.2.2 Stage of disease

Staging was performed in a multidisciplinary team setting according to the 2014 FIGO staging system (Chapter 1 Table 1.1) (35). A total of 4 patients (4%) had stage I disease, 1% of which were stage IA (tumour limited to one ovary), and 3% were stage IC2 (pre-operative capsule rupture). All 3 stage II patients (3%) had stage IIA disease (with implants on the surface of the uterus or fallopian tube). Stage III patients represented the largest grouping (71%), of which, 2% were IIIA1(i), 2% were IIIA1(ii), 1% were IIIA2, 14% were IIIB and 52% were IIIC. Twenty-two patients (22%) had stage IV disease, 6% of which were stage IVA (pleural effusion with positive cytology) and 16% were stage IVB (extra-abdominal metastasis).

3.2.2.3 Lymph node (LN) metastasis

Lymph nodes were not submitted for 50% of patients (Nx). Retroperitoneal pelvic lymph nodes were submitted for histopathological examination in the outstanding 50% of patients. Of these 50 patients, 11% showed no lymph node metastasis (N0) and 39% had positive nodal disease (N1).

3.2.2.4 Type of surgery performed

Thirty-two patients (32%) underwent debulking/cytoreductive surgery in the primary setting prior to postoperative, adjuvant chemotherapy. Those patients were chosen based on their fitness for surgery and good general condition. In contrast, the remaining 68 patients (68%) initially received 3 to 6 cycles of neoadjuvant chemotherapy (NACT) with paclitaxel and carboplatin, and then underwent delayed debulking surgery as is standard practice in the UK.

3.2.2.5 Volume of residual disease after surgery

After cytoreductive surgery, the volume of residual disease was estimated. A total of 74 patients (74%) had complete cytoreduction with no gross residual disease. Eleven patients (11%) were optimally debulked with a volume of residual disease of ≤1 cm, whilst only 15 patients (15%) were sub-optimally debulked with a volume of residual disease of >1cm.

3.2.2.6 Chemotherapy response score

Patients receiving chemotherapy in the neo-adjuvant setting were assessed as to the degree of response of their tumour to chemotherapy (see Materials and Methods Table 2.1) (107). Of the 68 patients receiving NACT, 27 patients (39.7%) showed only a minimal response, 27 patients (39.7%) responded partially, and 14 patients (20.6%) responded completely.

3.2.2.7 Resistance to platinum therapy

Patients who received platinum-based (carboplatin) treatment whether in the adjuvant or neo-adjuvant setting and experienced disease recurrence within less than 6 months from the last chemotherapy cycle were classified as platinum resistant. Data was

available for only 79 patients. Of these, 24 patients (30.4%) were platinum resistant, and 55 patients (69.6%) were not.

3.2.2.8 BRCA mutation status

Tumour *BRCA1/2* mutation testing was performed for a total of 33 patients (33%) of the Birmingham cohort. Seventeen patients (51.5%) were *BRCA* wild type, and 16 patients (48.5%) were *BRCA* mutant. *BRCA* mutant patients included 9 patients (27.3%) with a *BRCA-1* mutation (one with a frameshift mutation in exon 11 and 8 unspecified mutations) and 7 patients (21.2%) with a *BRCA-2* mutation (one with a heterozygous pathogenic deletion in exons 14 and 16, one with a heterozygous frameshift mutation in exon 13, and 5 unspecified mutations).

3.2.2.9 p53 immunohistochemical staining.

We performed p53 immunohistochemical staining on 60% of the cases from this cohort and in the remaining 40%, staining was done by the Birmingham Women's hospital. We used the DO-1 while the Women's hospital used the DO-7 clone for p53. A total of 65 tumour sections (65%) showed aberrant diffuse overexpression of p53 in >80% of tumour cell nuclei. Twenty-four cases (24%) showed a null pattern with complete absence of p53 in tumour cell nuclei, 3 cases (3%) showed a cytoplasmic pattern of p53 expression, and 8 cases (8%) exhibited a heterogeneous/mosaic pattern of p53 expression (7 with a combination of overexpression and wild-like staining and 1 with overexpression and cytoplasmic staining). These phenotypic differences will be discussed more thoroughly in chapter 4.

Table 3. 1: The clinico-pathological features of the Birmingham HGSOC cohort.

Patient criteria	Number of patients	Valid Percentage	Total
Age, year			
≤64 (*Mdn*)	51	51	100
>64	49	49	
FIGO stage			
I	4	4	
II	3	3	100
III	71	71	
IV	22	22	
LN status			
Nx (not submitted)	50	50	
N0 (no LN metastasis)	11	11	100
N1 (LN metastasis	39	39	
Type of surgery			
PDS	32	32	100
DDS	68	68	
Cytoreduction			
R0	74	74	100
R1	11	11	
R2	15	15	
CRS			
Minimal	27	39.7	68*
Partial	27	39.7	
Complete	14	20.6	
Platinum resistance[a]			
Yes	24	30.4	79**
No	55	69.6	
***BRCA* status**			
Mutant	16	48.5	33***
Wild type	17	51.5	
P53, IHC			
Overexpression	65	65	
Mosaic[b]	8	8	100
Null	24	24	
Cytoplasmic	3	3	

Mdn: median**, PDS**: primary debulking surgery, **DDS**: delayed debulking surgery, **CRS**: chemotherapy response score, **R0** (complete):no gross residual disease, **R1** (optimal): gross residual disease between 0.1 to 1 cm, **R2** (sub-optimal): gross residual disease >1cm, **IHC**: immunohistochemistry.

a: defined as recurrence of disease within 6 months or less of the last chemotherapy dose.

b: heterogeneous p53 expression with a combination of overexpression and wild-like/cytoplasmic

*Data available for patients who underwent DDS only, ** missing data for 21 patients, ***missing data for 67 patients.

3.2.3 UbH10 is differentially and heterogeneously expressed in HGSOC with aberrant over-expression in a minority of patients.

Initially, we examined our cohort for UbcH10 expression using immunohistochemistry. The validated anti-UbcH10 antibody was applied to sections collected from various sites and then scored using IRS and H-scores. A total of 39 cases (39%) were collected from the right adnexa, 38 cases (38%) from the left adnexa and 13 cases (13%) from the omentum (12 being from the greater omentum and 1 from the lesser omentum). In addition, 10 cases were collected from other metastatic sites (6 from the pelvic wall peritoneum, one from the falciform ligament, one from an inguinal lymph node, one from the serosa of the caecum and one from the serosa of the rectosigmoid colon).

When applying the IRS to our HGSOC sections, scores ranged from 0 to 12 (*Mdn=6*), while the H-score in our cases ranged from 0 to 229 (*Mdn*=98.3). The UbcH10 TPS ranged from 0 to 89.6% (*Mdn*=46.9).

UbcH10 protein levels by IRS and H-score were higher in omental tumours compared to other sites, but the difference was not statistically significant. The median IRS for omental tumours was slightly higher (*Mdn*=7) than right and left adnexal tumours *(Mdn*=6) and other metastatic sites (*Mdn*=6). Similarly, the median H-score for omental tumours was higher (*Mdn*=120) than right and left adnexal tumours *(Mdn*=99.8) and other metastatic sites (*Mdn*=39.4). The difference however was not statistically significant as indicated in Table 3.2 and Figure 3.1.

Table 3. 2: The difference between UbcH10 protein levels in HGSOC specimens collected from different sites in the Birmingham cohort.

Site of tumour	Number of patients	UbcH10 protein expression *Mdn (Min, Max)*	Kruskal-Wallis test *(H)*
		IRS	**2.11 (*p*=0.347)**
Right and left adnexa	77	6 (0, 12)	
Omentum	13	7 (3, 12)	
Other metastatic sites*	10	6 (1, 11)	
Total	**100**	**6 (0, 12)**	
		H-score	**4.62 (*p*=0.099)**
Right and left adnexa	77	99.8 (0, 229)	
Omentum	13	120 (21.6, 206)	
Other metastatic sites	10	39.4 (5, 170)	
Total	**100**	**98.3 (0, 229)**	

Mdn: median, **Min:** minimum, **Max**: maximum,

*Include pelvic wall peritoneum, falciform ligament, inguinal lymph node, serosa of caecum and rectosigmoid colon

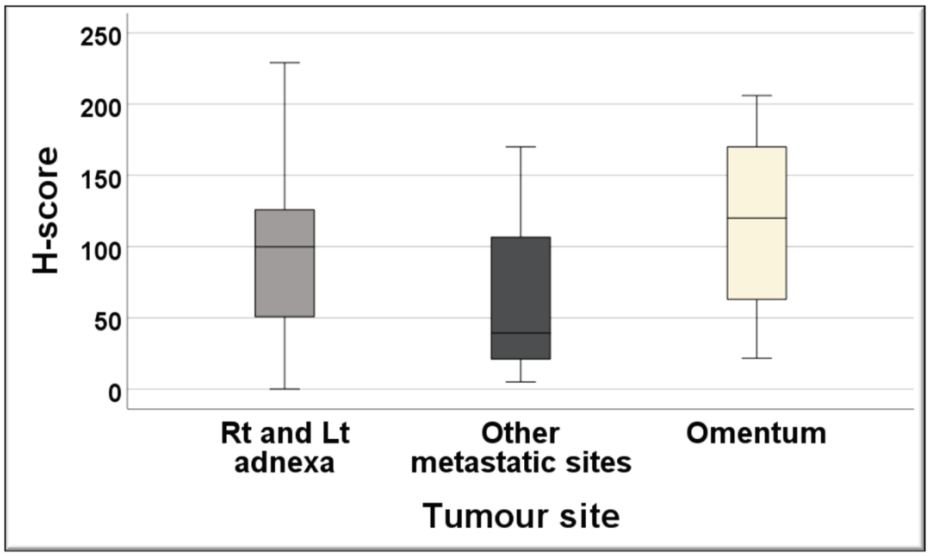

Figure 3. 1: The difference in UbcH10 protein levels by H-score between HGSOC specimens taken from different sites in the Birmingham cohort. The median UbcH10 H-score in omental tumours was higher (n=13, *Mdn*=120) than right and left adnexal tumours (n=77, *Mdn*=99.8) and other metastatic sties (n=10, *Mdn*=39.4, include pelvic wall peritoneum, falciform ligament, inguinal lymph node and serosa of caecum and rectosigmoid colon). The difference was statistically not significant (*H*=4.62, *p*=0.099).

The *X*-tile generated cut-offs for IRS and H-scores were 7 and 120 respectively. When applying the IRS cut-off to our cohort, it sub-divided the patients into high UbcH10 (29%) and low UbcH10 (71%) expression groups. Similarly, when applying the H-score cut-off, 33% of patients were assigned to the high UbcH10 and 67% were assigned to the low UbcH10 expression group (Figure 3.2).

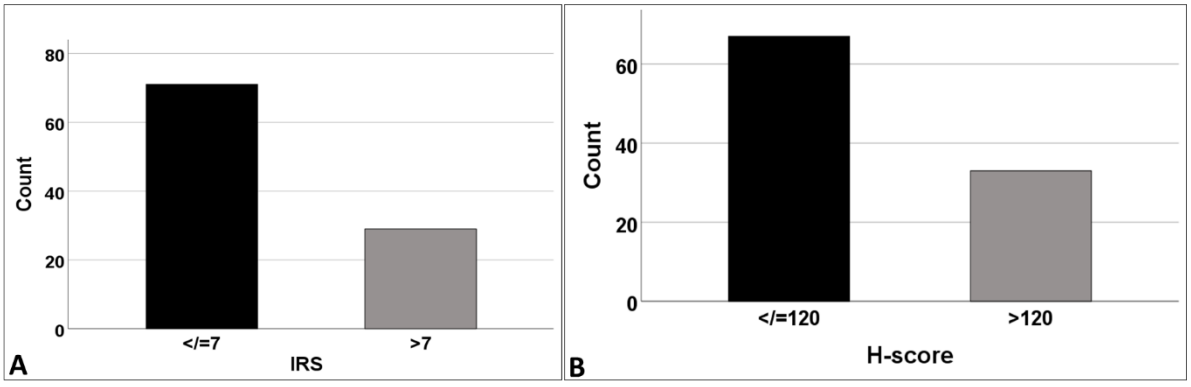

Figure 3. 2: The distribution of the Birmingham HGSOC cohort according to the X-tile generated cut-offs for A) IRS and B) H-score. High UbcH10 expression was noted in 29-33% of patients.

Tumour sections which contained adjacent normal ovary, fallopian tube or benign serous cystadenomas were either totally negative or focally positive for UbcH10 with an IRS ranging from 0-4 and an H-score ranging from 0 to 40 (Figure 3.3). We also determined cellular intra-tumoral heterogeneity of UbcH10 (Figure 3.4) as well as inter-tumoral heterogeneity between different patients (Figure 3.5). Representative images of individual patient tumours are shown to highlight typical UbcH10 staining patterns. UbcH10 expression was localised to both the nuclear and cytoplasmic subcellular compartments of the tumours in our study cohort (Figure 3.5D). These data indicate that UbcH10 is only over-expressed in malignant ovarian tissue and that more than 25% of HGSOC patients have high UbcH10 expression. In addition, it highlights the wide range of UbcH10 expression levels across different HGSOC specimens.

Taken together these data indicate that UbcH10 is heterogeneously expressed in a wide range of HGSOC with higher expression in metastatic sites. UbcH10 is only aberrantly overexpressed in a minority of patients.

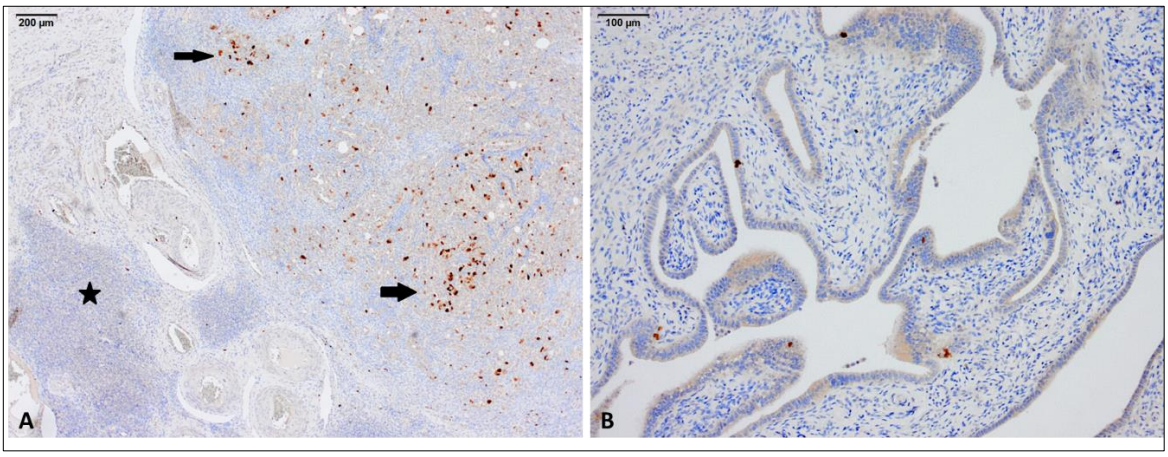

Figure 3. 3: UbcH10 is a feature of malignant tissue with low to nil expression in normal ovary and fallopian tube. A) HGSOC showing focal strong cytoplasmic and nuclear staining for UbcH10 in 10 % of the tumour cells (arrows), another 10% of the tumour shows moderate staining. This case was an assigned an IRS of 5 and an H-score of 50. The adjacent normal ovarian tissue (star) is totally negative. (anti-UbcH10, x4 magnification) B) Normal fallopian tube with very focal UbcH10 expression (anti-UbcH10, x10 magnification).

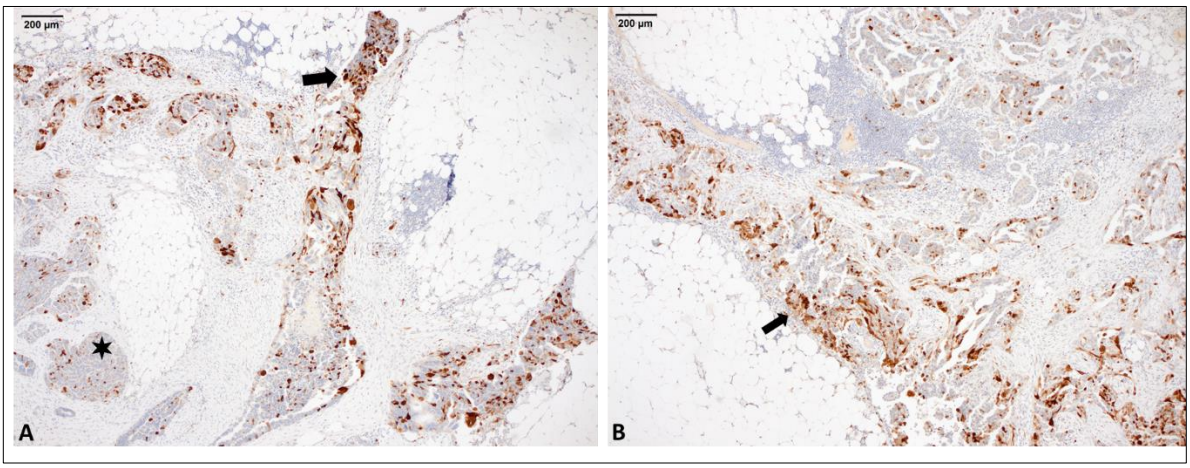

Figure 3. 4: Two foci from the same tumour that highlight the heterogeneous manner of UbcH10 expression in HGSOC. A) A deposit of high-grade serous carcinoma in the omentum showing graded expression of UbcH10 from negative and focal moderate (star) to more diffuse and strong staining (arrow). This case was assigned an IRS of 7 and H-score of 116. (anti-UbcH10, x4 magnification) B) Another focus in the same tumour showing accentuation of UbcH10 expression at the tumour-stroma interface (arrow). (anti-UbcH10, x10 magnification)

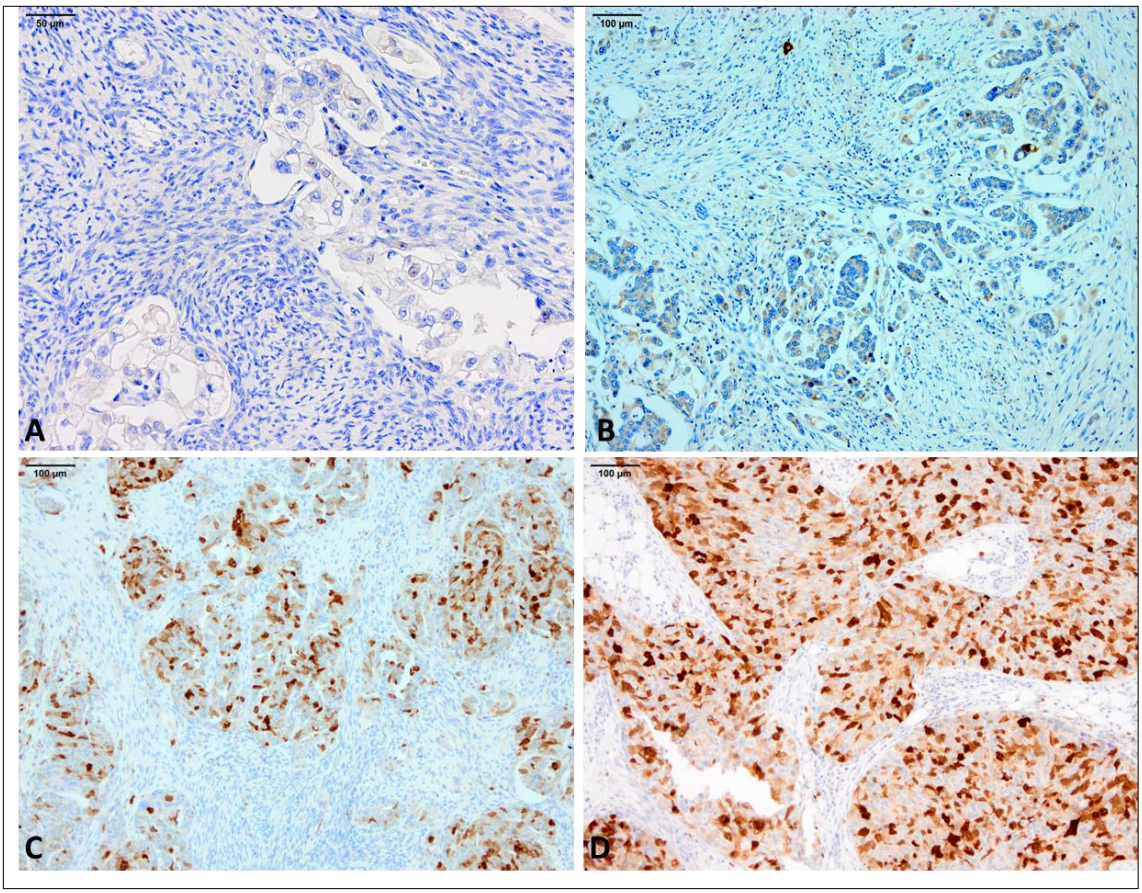

Figure 3. 5: Four different HGSOC patients demonstrating inter-tumoral heterogeneity of UbcH10 expression. A) A case of HGSOC with virtually no staining for UbcH10. This case was considered negative. (anti-UbcH10, x20 magnification). B) Another case with low UbcH10 expression. This was assigned an IRS of 2 and H-score of 30 (anti-UbcH10, x10 magnification). C) A third patient with moderate UbcH10 expression (IRS=7, H-score=141) (anti-UbcH10, x10 magnification). D) A fourth case which had high UbcH10 expression (IRS=12, H-score=206). Note both the cytoplasmic and nuclear localisation of UbcH10 staining in the tumour (anti-UbcH10, x10 magnification).

3.2.4 The correlation between UbcH10 and clinico-pathological/treatment variables in the Birmingham cohort

3.2.4.1 Overview

To explore the prognostic value of UbcH10 protein levels for HGSOC patients we next proceeded to correlate UbcH10 expression levels with the well-established prognostic and predictive parameters in ovarian cancer. In the first instance, analysis was carried out using the IRS and H-scores for UbcH10 as continuous variables without cut-offs to enhance statistical power. Mann-Whitney *(U)* test, Kruskal-Wallis (*H)* test and Spearman's correlation coefficient (*ρ)* were used for this analysis. This was followed by dichotomisation of UbcH10 into high and low expression groups to draw more biologically significant conclusions. Pearson's Chi-square (X^2) was used for this type of analysis. Fisher's exact test was used when Chi-square was not valid due to limited number of observations in the subgroups. Details about the statistical analyses used throughout this study are discussed more thoroughly in the materials and methods section 2.1.5.

3.2.4.2 UbcH10 protein levels correlate weakly with older patient age

When correlating the UbcH10 IRS with the age of the female patients at diagnosis, no significant statistical correlation was found (ρ=0.026, p=0.797). When dividing the females into two groups based on the median age and UbcH10 expression by H-score category; UbcH10 expression was significantly higher in female patients aged above 64 years (Figure 3.6). Because the p-value was not significant across the different types of statistical tests applied, we therefore concluded that this correlation was weak and only borderline significant.

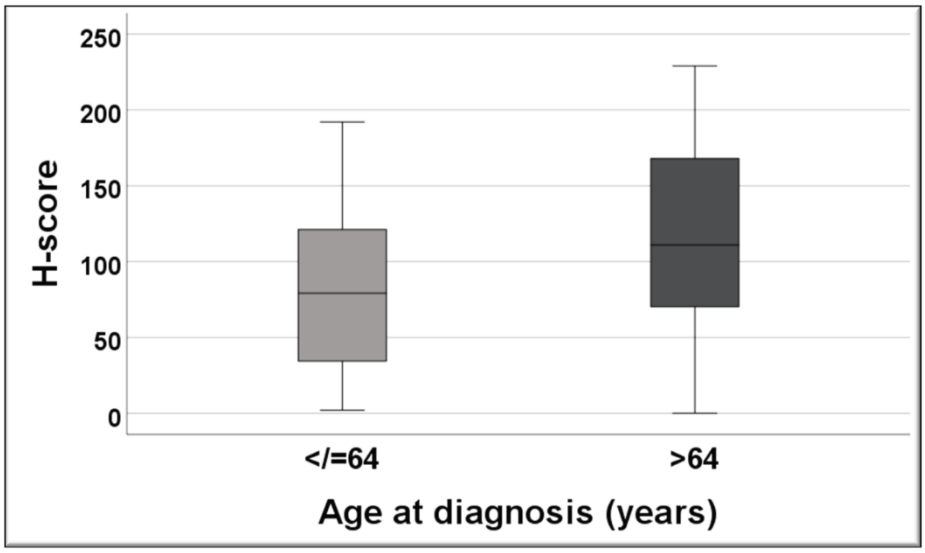

Figure 3. 6: A box plot diagram demonstrating the correlation between UbH10 expression by H-score and the age group of patients in the Birmingham cohort. The median H-score was significantly higher in the females aged above 64 years (*Mdn*=111) compared to younger females (*Mdn*=79.2) (*U*=905, *p*=0.018).

3.2.4.3 UbcH10 protein levels do not correlate significantly with FIGO stage but was higher in early stage disease

UbcH10 expression levels were next correlated with the strongest prognostic factor in ovarian cancer; FIGO stage. The median score of UbcH10 expression was higher in early (I &II) (*Mdn* IRS=7, *Mdn* H-score=113.6) compared to late (III & IV) FIGO stage patients (*Mdn* IRS=6, *Mdn* H-score=95.2). However, this difference was not statistically significant [for IRS (*U*=263, *p*=0.39), for H-score (*U*=220.5, *p*=0.156)]. No significant association between IRS or H-score categories and FIGO stage was found (Table 3.3).

Table 3. 3: The association between UbcH10 expression by IRS and H-score categories and FIGO stage in the Birmingham cohort

UbcH10 protein expression	Early FIGO stage (I&II)	Late FIGO stage (III & IV)	Total	Fisher's exact 2-sided significance
IRS category				
≤7	4	68	**72**	***p*=0.396**
>7	3	25	**28**	
Total	**7**	**93**	**100**	
H-score category				
≤120	4	63	**67**	
>120	3	30	**33**	***p*=0.681**
Total	**7**	**93**	**100**	

3.2.4.4 UbcH10 protein levels do not correlate significantly with Lymph node metastasis

Lymph node metastasis is another important prognostic parameter that we correlated with UbcH10 protein levels. UbcH10 expression was higher in patients with N0 disease compared to those with N1 disease. This difference was not statistically significant. The median IRS was 7 in N0 disease, compared to 6 in N1 and Nx disease (H=0.7, p=0.69). On the other hand, median H-score was 111 in N0 patients, 85.6 in N1 patients, and 104.9 in Nx patients (H=1.5, p=0.46). This means that UbcH10 levels were higher in patients with negative nodal disease compared to those with nodal disease, although statistically not significant. Similarly, no significant association was found between IRS and H-score categories and LN status (Table 3.4).

Table 3. 4: The association between UbcH10 expression by IRS and H-score categories and Lymph node metastasis in the Birmingham cohort

UbcH10 protein expression	LN status			Total	Pearson Chi-square (X^2) test
	N0	N1	Nx		
IRS category					**0.626 (*p*=0.731)**
≤7	9	28	35	**72**	
>7	2	11	15	**28**	
Total	**11**	**39**	**50**	**100**	
H-score category					**0.454 (*p*=0.797)**
≤120	8	27	32	**67**	
>120	3	12	18	**33**	
Total	**11**	**39**	**50**	**100**	

N0: no LN metastasis, **N1**: LN metastasis, **Nx**: LN not submitted.

3.2.4.5 UbcH10 protein levels are significantly affected by pre-operative chemotherapy administration

To examine the effect of chemotherapy on UbcH10 levels, we then compared UbcH10 expression between patients who underwent PDS without prior chemotherapy administration and those who underwent DDS with NACT treatment. UbcH10 levels were significantly higher in patients who underwent PDS compared to those who underwent DDS (Table 3.5). When applying IRS and H-score categories, patients who underwent DDS polarized to the low UbcH10 expression group while patients who underwent PDS polarized to the high UbcH10 expression group (Figure 3.7). These data indicate that UbcH10 levels are significantly reduced by chemotherapy administration.

Table 3. 5: The association between UbcH10 expression and the type of surgery performed in the Birmingham cohort

Type of Surgery	Number of patients	UbcH10 protein expression *Mdn (Min, Max)*	Mann-Whitney test *(U)*
		IRS	**541.5 (*p*=<0.001)***
PDS	32	8 (0, 12)	
DDS	68	6 (1, 11)	
Total	**100**	**6 (0, 12)**	
		H-score	**523 (*p*=<0.001)***
PDS	32	128.4 (0, 229)	
DDS	68	75 (2,190.8)	
Total	**100**	**98.3 (0, 229)**	

PDS: Primary debulking surgery, **DDS**: delayed debulking surgery, **Mdn**: median, **Min**: minimum, **Max**: maximum.

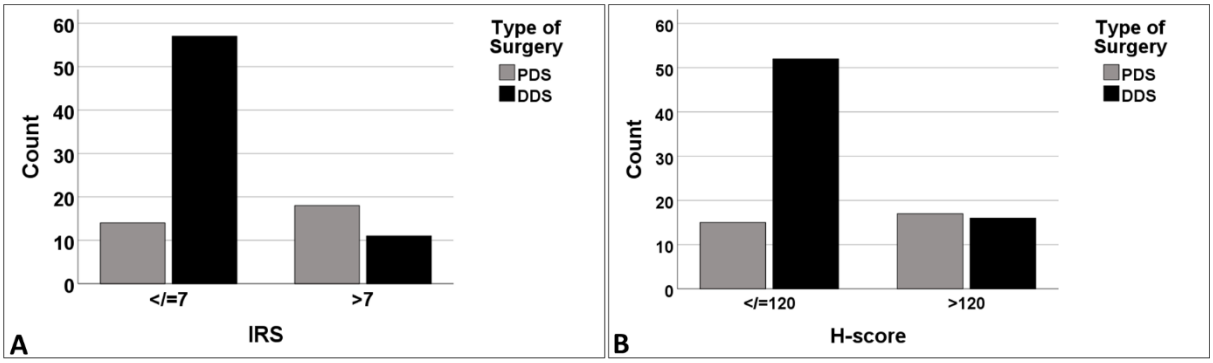

Figure 3. 7: The association between UbcH10 expression categories by IRS (A) and H-score (B) and the type of surgery performed in the Birmingham cohort. Patients who underwent DDS mostly had low UbcH10 expression levels (IRS ≤7, H-score ≤120), while patients who underwent PDS had mostly high UbcH10 expression (IRS>7, H-score >120). This difference was statistically significant (X^2 for IRS=16.97, p=<0.001, X^2 for H-score=8.62, p=0.003).

3.2.4.6 UbcH10 protein levels do not correlate significantly with the volume of residual disease after surgery

We next investigated the relationship between UbcH10 expression and the volume of residual disease after surgery. Patients with complete (R0) and optimal (R1) cytoreduction were placed in one group and compared to sub-optimally (R2) cytoreduced patients. The median UbcH10 expression by IRS did not differ between R0, R1 and R2 patients (*Mdn*=6 for all three categories, *U*=633, *p*=0.96). The median H-score on the other hand was higher for R2 patients (*Mdn*=113.6) compared to R0 and R1 patients as one group (*Mdn*=96.8). The difference however was not statistically significant (*U*=576.5, *p*=0.56). IRS and H-score categories did not correlate significantly with cytoreduction (Figure 3.8). These data indicate that UbcH10 levels were slightly higher in sub-optimally debulked patients, but that difference did not achieve statistical significance.

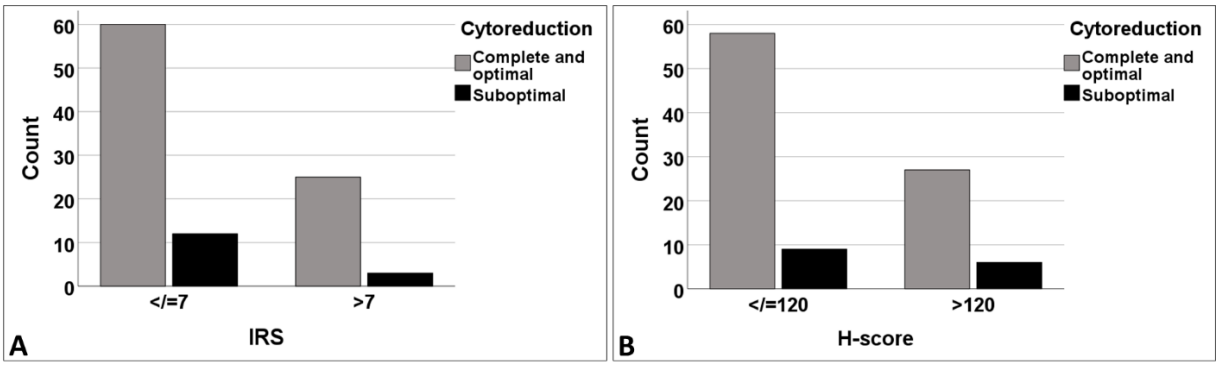

Figure 3. 8: The distribution of the Birmingham cohort according to to the level of cytoreduction after surgery and IRS (A) and H-score (B) category for UbcH10 expression. No significant association was found between the two variables (For IRS Fisher's exact 2-sided significance=0.55, for H-score Fisher's exact 2-sided significance= 0.56).

3.2.4.7 UbcH10 protein levels are not predictive of chemotherapy response

After correlating UbcH10 with the prognostic indicators of ovarian cancer, we then investigated its relationship with measures of treatment response. When assessing the CRS in our cohort, patients with complete response had a slightly higher median UbcH10 expression by IRS (*Mdn*=6.5) compared to those with partial response (*Mdn*=6) and minimal response (*Mdn*=6). This difference was not statistically significant (*H*=0.817, *p*=0.66). Similarly, the median H-score was higher in complete responders (*Mdn*=99.3), compared to partial (*Mdn*=79.2) and minimal responders (*Mdn*=57.8). Again, the difference was not significant (*H*=1.4, *p*=0.49). H-score category did not correlate significantly with CRS (Table 3.6). For IRS category analysis partial and complete responders were grouped into one group and compared to minimal responders due to limited number of observations in each group (Figure 3.9). These data highlight that patients with improved response to chemotherapy, showed increased UbcH10 expression levels, although statistically not significant.

Table 3. 6: The association between UbcH10 expression by H-score category and chemotherapy response score in the Birmingham cohort

UbcH10 protein expression (H-score category)	Chemotherapy response score			Total	Pearson Chi-square test (X^2)
	Minimal response	Partial response	Complete response		
≤120	21	21	9	**51**	**1.079 (*p*=0.583)**
>120	6	6	5	**17**	
Total	**27**	**27**	**14**	**68**	

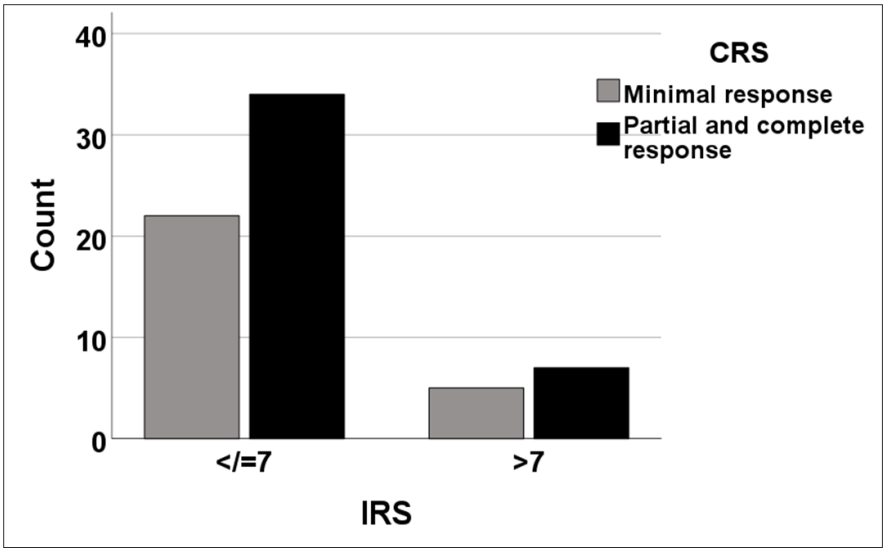

Figure 3. 9:The distribution of the Birmingham cohort according to the CRS and IRS category for UbcH10 expression. No significant association was found between CRS and UbcH10 expression (Fisher's exact 2-sided significance=1).

3.2.4.8 UbcH10 protein levels are not predictive of resistance to platinum therapy

Platinum resistance was another important measure of treatment response that we correlated with UbcH10 protein levels. Patients who experienced platinum resistance had lower UbcH10 levels (*Mdn* IRS=6, *Mdn* H-score=81.2) compared to those that were platinum sensitive (*Mdn* IRS=7, *Mdn* H-score=106). This difference was not statistically significant [for IRS (*U*=589, *p*=0.44), for H=score (*U*=575.5, *p*=0.36)]. The UbcH10 IRS and H-score categories did not correlate significantly either with platinum resistance (Figure 3.10).

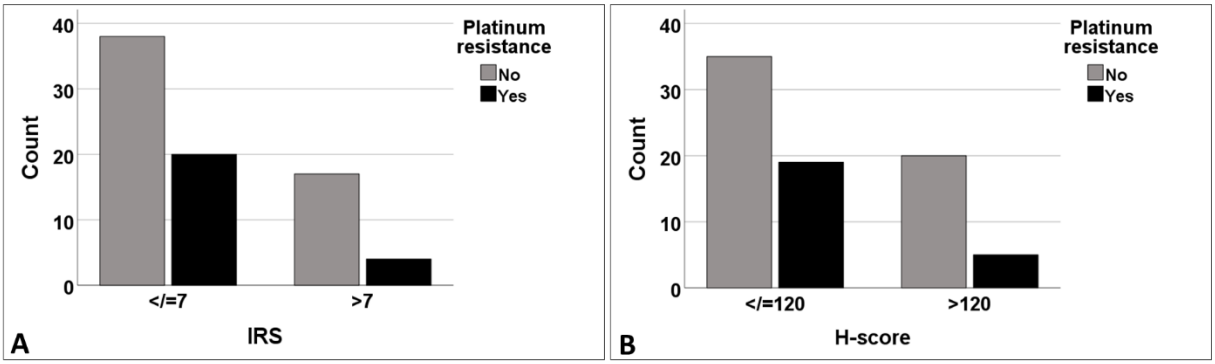

Figure 3. 10: The distribution the 79 HGSOC patients from the Birmingham cohort with platinum resistance data according to A) IRS and B) H-score categories of UbcH10 expression. No significant association was found between platinum resistance and UbcH10 expression (X^2 for IRS=1.737, p=0.188, X^2 for H-score=1.863, p=0.172).

3.2.4.9 UbcH10 protein levels are not significantly associated with BRCA mutation status

Other than CRS, the only other good prognostic indicator available in this cohort was the *BRCA* mutation status. UbcH10 levels were compared in *BRCA* wild type versus *BRCA* mutant patients. The median UbcH10 expression by IRS was slightly higher in *BRCA* mutant (*Mdn*=7) compared to *BRCA* wild type patients (*Mdn*=6). This difference was not statistically significant (U=119, p=0.53). This applies to the H-score as well (Figure 3.11). IRS and H-score categories did not correlate with *BRCA* mutation in this cohort (Table 3.7).

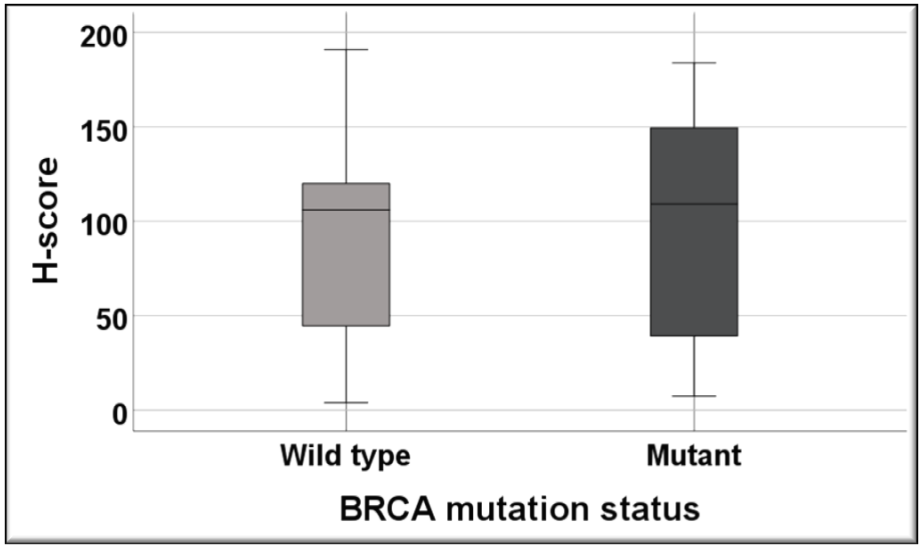

Figure 3. 11: A box plot demonstrating the correlation between the BRCA mutation status in the Birmingham cohort and UbcH10 expression by H-score. The median H-score was slightly higher in *BRCA* mutant patients (n=16, *Mdn*=109) compared to *BRCA* wild type patients (n=17, *Mdn*=106), and this difference was statistically not significant (*U*=121, *p*=0.589).

Table 3. 7: The association between UbcH10 expression by IRS and H-score categories and the BRCA mutation status in the Birmingham cohort.

UbcH10 protein expression	BRCA mutation status		Total	Pearson Chi-square test (X^2)
	Wild type	Mutant		
IRS category				**0.243 (*p*=0.622)**
≤7	10	12	**22**	
>7	6	5	**11**	
Total	**16**	**17**	**33**	
H-score category				**2.456 (*p*=0.114)**
≤120	8	13	**21**	
>120	8	4	**12**	
Total	**16**	**17**	**33**	

3.2.5 Survival analysis and patient outcomes in the Birmingham cohort

3.2.5.1 Overview

After correlating UbcH10 with the various prognostic/predictive indicators and before we investigate its effect on patient survival, we will consider, in general terms, the survival data from this cohort. In the Birmingham cohort, the OS period ranged from 1.9 to 126.1 months [Median OS=49.77*, 95% C.I* (37.8, 60.7)]. The PFS period ranged from 1.5 to 126.1 months [Median PFS=16.1, 95% C.I (13.2, 19.1)]. At the end of the follow-up period there had been 70 patient deaths (70%), and 78 patients (78%) had experienced progression in the form of recurrence or metastatic disease (Figures 3.12 and 3.13).

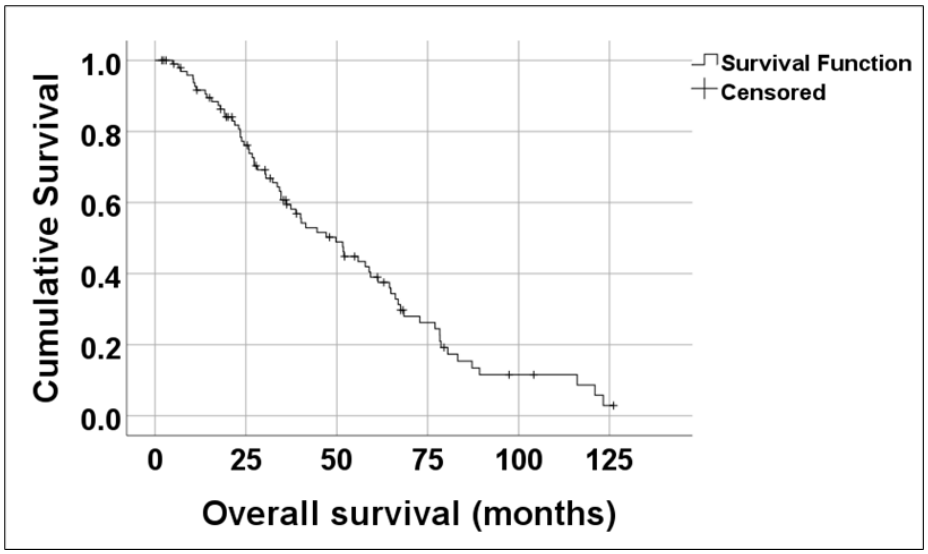

Figure 3. 12: A Kaplan-Meier curve for Overall survival of the Birmingham cohort. A total of 50% of patients were alive at 49.7 months (median OS). The proportion of patients that were still alive after 5 years (60 months) was 39%. Censored data are patients who did not die but were lost to follow-up at different time points during the study.

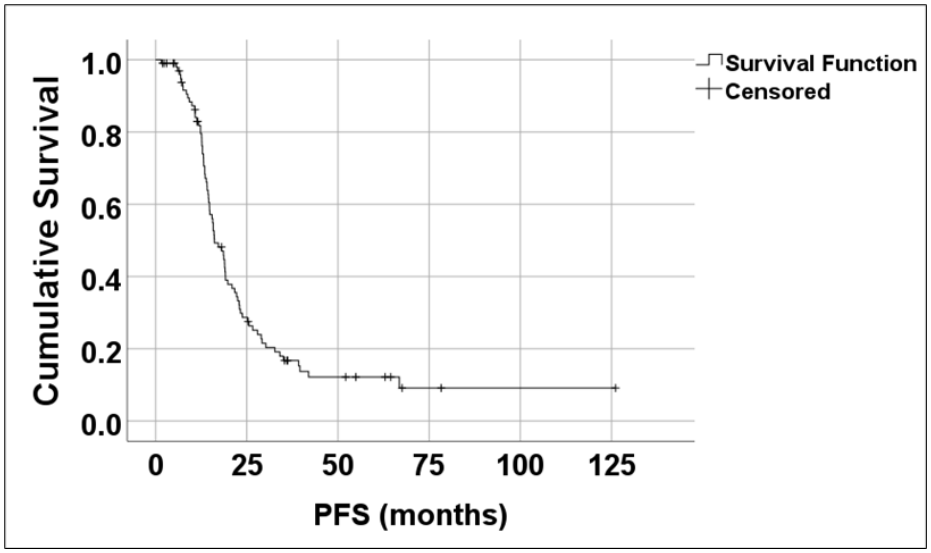

Figure 3. 13: A Kaplan-Meier curve for progression-free survival of the Birmingham cohort. Median PFS was 16.1 months. A total of 17% of patients experienced disease progression in the first year and 64% in the first 2 years of follow up. Censored data are patients who did not progress but were lost to follow-up at different time points during the study.

Before investigating the effect of UbcH10 on patient outcome in this cohort, we explored the impact of all the clinico-pathological/treatment variables on patient survival. The aim of this analysis was to determine which of these variables, either alone or in combination, were likely to explain the findings of subsequent UbcH10 impact on patient outcomes. Univariate Cox regression analysis and hazard ratio were used to identify the prognostic variables that influence OS and PFS in the Birmingham cohort.

3.2.5.2 The prognostic impact of the various clinico-pathological/treatment variables on patient survival

3.2.5.2.1 Univariate analysis of overall survival

Univariate analysis revealed only platinum resistance to be a strong predictor of mortality of HGSOC patients in the Birmingham cohort. Females who developed

platinum resistance within 6 months of their treatment were at a much higher risk of dying compared to those that were platinum sensitive. This is demonstrated in the Kaplan-Meier curve shown in Figure 3.14. FIGO stage, type of surgery and volume of residual disease after surgery were only weak predictors of mortality in this cohort. Although statistically not significant, patients with partial or complete chemotherapy response were at a lower risk of dying than those with minimal response. *BRCA* mutant patients were also at a lower risk of dying than *BRCA* wild type patients. The results are summarized in Table 3.8

These data highlight the positive and negative predictors of mortality in the Birmingham cohort.

Table 3. 8: A summary of the univariate analysis of potential predictors of HGSOC mortality in the Birmingham cohort

Variable	Overall survival	
	HR (95% C.I)	***p*-value**
Age at diagnosis ≤ 64 (Ref. category) > 64	1.15 (0.72, 1.89)	0.553
FIGO stage I & II (Ref. category) III & IV	1.35 (0.49, 3.72)	0.564
LN status Nx & N0 (Ref. category) N1	0.73 (0.45, 1.19)	0.22
Type of Surgery PDS (Ref. category) DDS	1.25 (0.73, 2.16)	0.411
Cytoreduction R0 and R1 (Ref. category) R2	1.68 (0.90, 3.12)	0.101
CRS Minimal (Ref. category) Partial and complete	0.74 (0.42, 1.29)	0.293
Platinum resistance No (Ref. category) Yes	6.89 (3.68, 12.82)	**<0.001***
BRCA mutation Wild type (Ref. category) Mutant	0.67 (0.22, 2.03)	0.479

HR: Hazard ratio, **C.I**: confidence interval, **N0**: no LN metastasis, **N1**: LN metastasis, **Nx**: LN not submitted, **PDS:** Primary debulking surgery, **DDS**: delayed debulking surgery, **R0**: complete cytoreduction, **R1**: optimal cytoreduction, **R2**: suboptimal cytoreduction, **CRS**: chemotherapy response score. **Ref. category**: reference category.

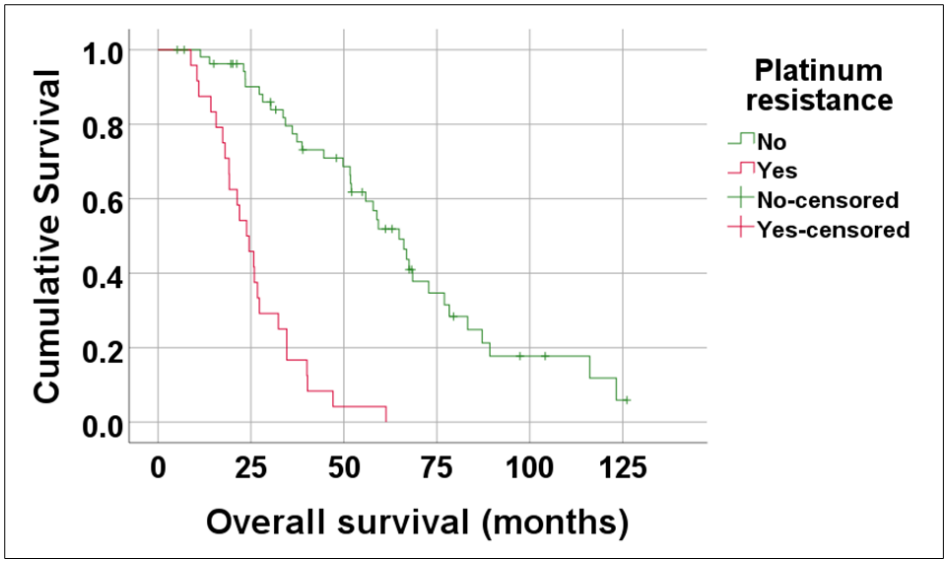

Figure 3. 14: A Kaplan-Meier curve demonstrating the effect of platinum resistance on HGSOC mortality in the Birmingham cohort. All 24 platinum resistant patients (red line) experienced death from disease compared to 55 platinum sensitive patients (green line) where 35 experienced deaths from disease. The median OS of platinum resistance patients (23.8 months) was significantly shorter than that of platinum sensitive patients (63.8 months, Log rank X^2=46.5, p=<0.001).

3.2.5.2.2 Univariate analysis of progression-free survival

A total of 78 patients (78%) in this cohort had experienced progression of their disease in the form of recurrence or metastasis. Sixty-four of these patients (64%) experienced recurrence within the first 2 years of their treatment. Univariate analysis revealed 4 prognostic factors that influence the risk of progression in these females: advanced FIGO stage, delayed debulking surgery, suboptimal cytoreduction, and platinum resistance, as indicated in the Kaplan-Meier curves shown in Figures 3.15 to 3.18. Patients older than 64 years, partial and complete chemotherapy responders and *BRCA* mutant patients had a lower risk of progression although statistically, not significant. These results are summarized in Table 3.9. These data highlight the positive and negative predictors of progression in the Birmingham cohort.

Table 3. 9: A summary of the univariate analysis of potential predictors of progression of HGSOC in the Birmingham cohort

Variable	Progression-free survival	
	HR (95% C.I)	***p*-value**
Age at diagnosis ≤ 64 (Ref. category) > 64	0.85 (0.54, 1.33)	0.465
FIGO stage I & II (Ref. category) III & IV	5.9 (1.44, 24.29)	**0.014***
LN status Nx & N0 (Ref. category) N1	1.35 (0.86, 2.12)	0.186
Type of Surgery PDS (Ref. category) DDS	2.38 (1.37, 4.13)	**0.002***
Cytoreduction R0 and R1 (Ref. category) R2	2.10 (1.13, 3.76)	**0.019***
CRS Minimal (Ref. category) Partial and complete	0.62 (0.36, 1.05)	0.075
Platinum resistance No (Ref. category) Yes	4.92 (2.88, 8.41)	**<0.001***
BRCA mutation Wild type (Ref. category) Mutant	0.85 (0.39, 1.88)	0.698

HR: Hazard ratio, **C.I**: confidence interval, **N0**: no LN metastasis, **N1**: LN metastasis, **Nx**: LN not submitted, **PDS:** Primary debulking surgery, **DDS**: delayed debulking surgery, **R0**: complete cytoreduction, **R1**: optimal cytoreduction, **R2**: suboptimal cytoreduction, **CRS**: chemotherapy response score. **Ref. category**: reference category.

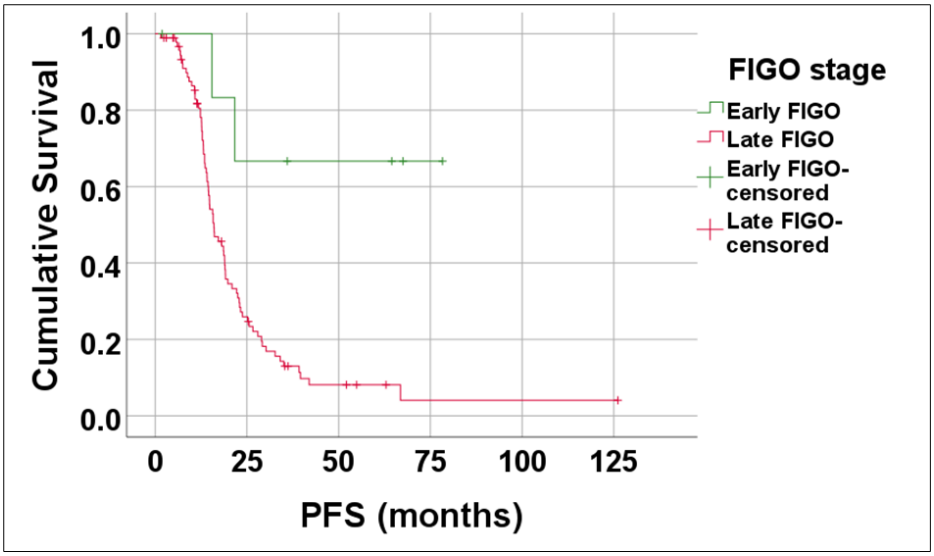

Figure 3. 15: A Kaplan-Meier curve demonstrating the prognostic effect of FIGO stage on the progression-free survival of HGSOC females in the Birmingham cohort. Out of 93 late FIGO stage patients (red line) 76 patients had experienced disease progression compared to 7 early FIGO stage patients (green line) where only 2 patients showed disease progression. The difference was statistically significant (Log rank X^2=7.75, p=0.005). Median PFS for late FIGO stage patients was 16 months but was not reached in early FIGO stage patients.

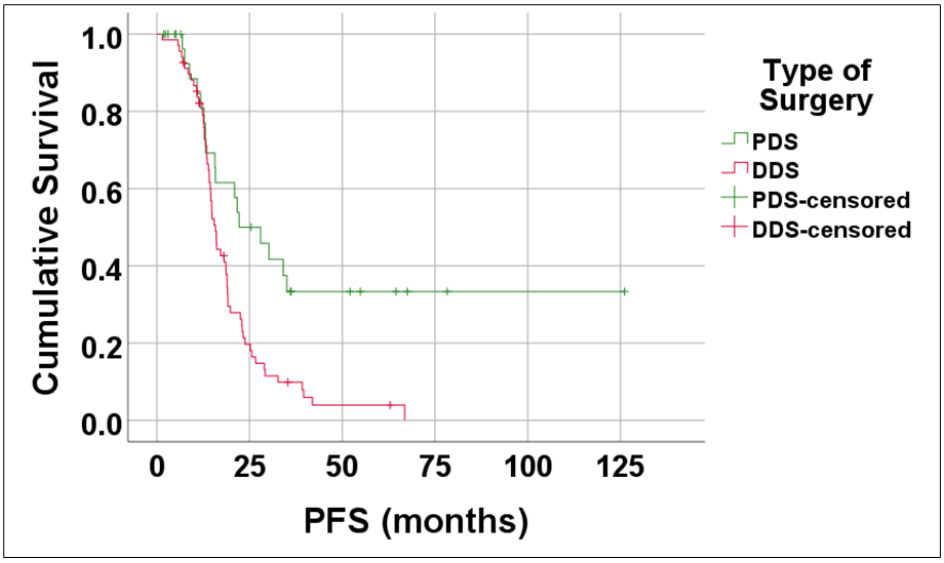

Figure 3. 16: A Kaplan-Meier curve demonstrating the prognostic effect of debulking surgery on the progression-free survival of HGSOC in the Birmingham cohort. Patients who underwent DDS (red line) experienced a higher event rate (61 out of 68 patients) compared to those who underwent PDS (green line, 17 out of 32 patients). Additionally, median PFS was significantly worse for patients who underwent DDS (15.8 months) compared to patients who underwent PDS (22.2 months, Log rank X^2=10.05, p=0.002).

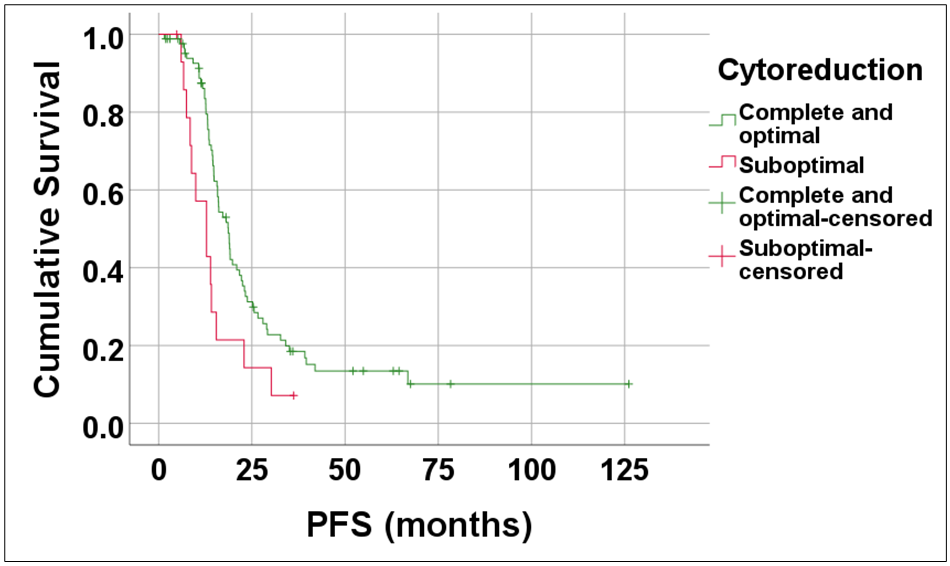

Figure 3. 17: A Kaplan-Meier curve demonstrating the prognostic effect of extent of cytoreduction after surgery on the progression-free survival of HGSOC females in the Birmingham cohort. Patients with sub-optimal cytoreduction (red line) experienced a higher event rate (13 out of 15 patients) compared to patients with complete and optimal cytoreduction (green line, 65 out of 85 patients). Additionally, median PFS for patients with sub-optimal cytoreduction (12.8 months) was significantly shorter than that for patients with complete and optimal cytoreduction (18.6 months, Log rank X^2=5.77, p=0.016).

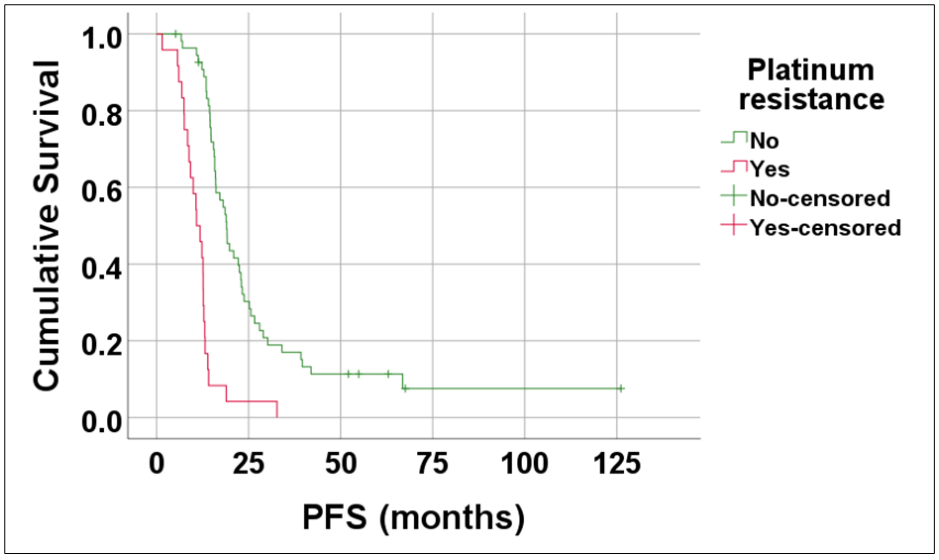

Figure 3. 18: A Kaplan-Meier curve demonstrating the prognostic effect of platinum resistance on progression-free survival of HGSOC in the Birmingham cohort. Platinum resistant patients (red line) experienced a higher event rate (24 out of 24 patients) compared to platinum sensitive patients (green line, 48 out of 55 patients). The median PFS of platinum resistant patients (10.8 months) was also significantly shorter than that of platinum sensitive patients (19 months, Log rank X^2=39.87, p=<0.001).

3.2.6 The effect of UbcH10 on patient outcomes in the Birmingham cohort

3.2.6.1 Overview

After exploring the various prognostic/predictive indicators in the Birmingham cohort, we next proceeded to investigate the effect of UbcH10 expression on HGSOC mortality and progression. Kaplan-Meier curves were constructed to explore the difference in OS and PFS amongst those patients with high UbcH10 protein levels (IRS>7, H-score >120) and those with low or absent UbcH10 protein levels (IRS≤7, H-score≤120). UbcH10 was then analysed as a continuous variable without cut-offs using Univariate Cox regression analysis to identify the HR related to UbcH10 protein overexpression. This was then followed by multi-variate analysis to identify whether the effect of UbcH10 protein levels on patient outcome was independent or contingent on other prognostic factors.

3.2.6.2 UbcH10 expression did not influence HGSOC mortality

When comparing OS among the low and high UbcH10 expression groups, a higher event rate was, perhaps, unexpectedly found in the low UbcH10 group, and thus the OS was better for patients with a high UbcH10 (IRS>7 and H-score>120) compared to the low or absent UbcH10 group (Figure 3.19). The difference was statistically, however, found not to be significant.

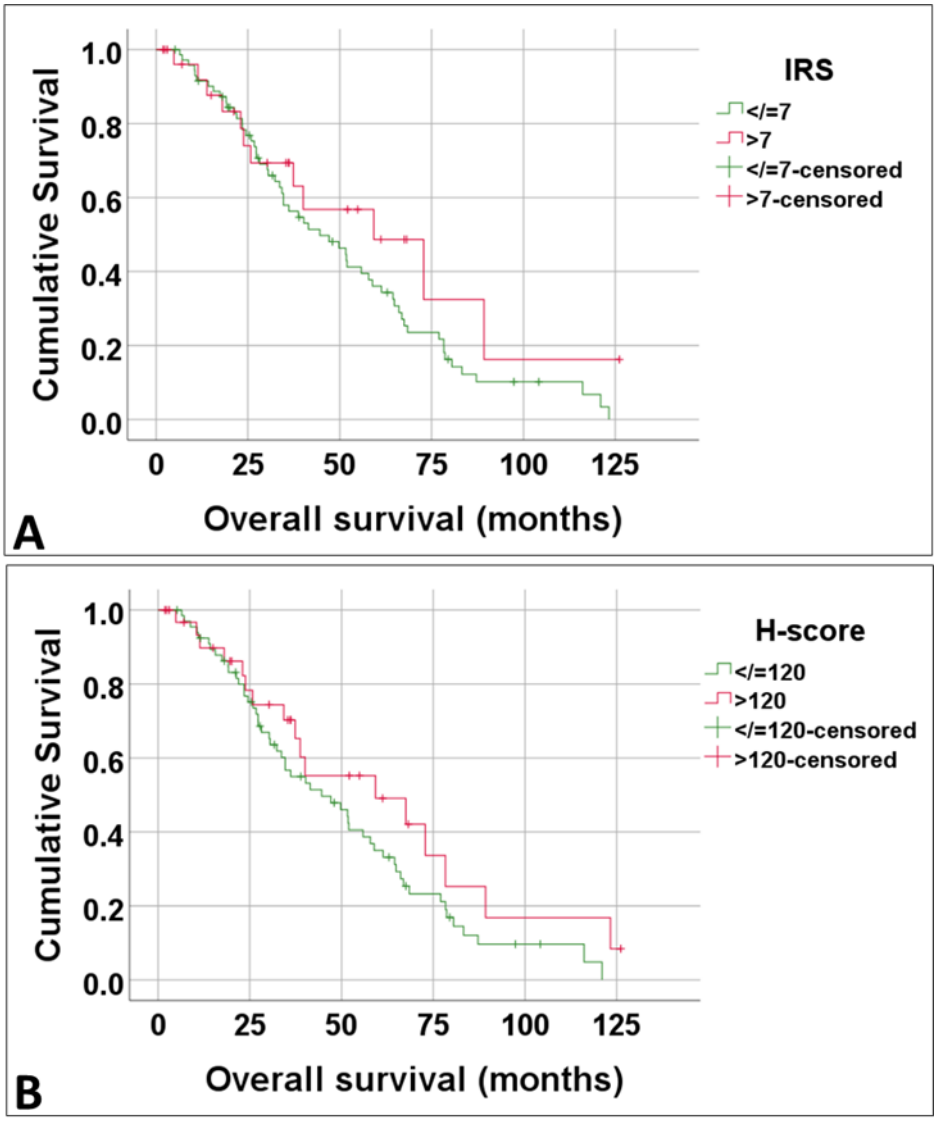

Figure 3. 19: Kaplan-Meier curves demonstrating the effect of UbcH10 expression by A) IRS B) H-score on HGSOC mortality in the Birmingham cohort. The OS period ranged from 1.9 to 126 months. In curve A the OS survival was worse in the low UbcH10 group (n=72 with a total of 58 events) compared to the high UbcH10 category (n=28 with 12 events). In curve B, patients with low UbcH10 expression again experienced a higher event rate (53 out of 67 patients) compared to patients with high UbcH10 expression (17 out of 33 patients). The median OS in both curves was shorter for low UbcH10 group (*Mdn*=44.6 months) compared to high UbcH10 group (*Mdn*=59.3 months). The difference between the two groups was statistically not significant [(For IRS Log rank X^2=1.85, p=0.174), (for H-score Log rank X^2=2.15, p=0.142)].

3.2.6.3 UbcH10 expression influenced HGSOC progression

Next, we explored the effect of UbcH10 expression on PFS of the Birmingham cohort. A higher recurrence rate and shorter median survival time was observed in the patients that displayed low UbcH10 expression (IRS ≤ 7 and H-score ≤120) compared to patients that displayed high UbcH10 expression. These differences were determined to be statistically significant (Figure 3.20). These results suggest that UbcH10 may have a *favourable* impact on HGSOC progression.

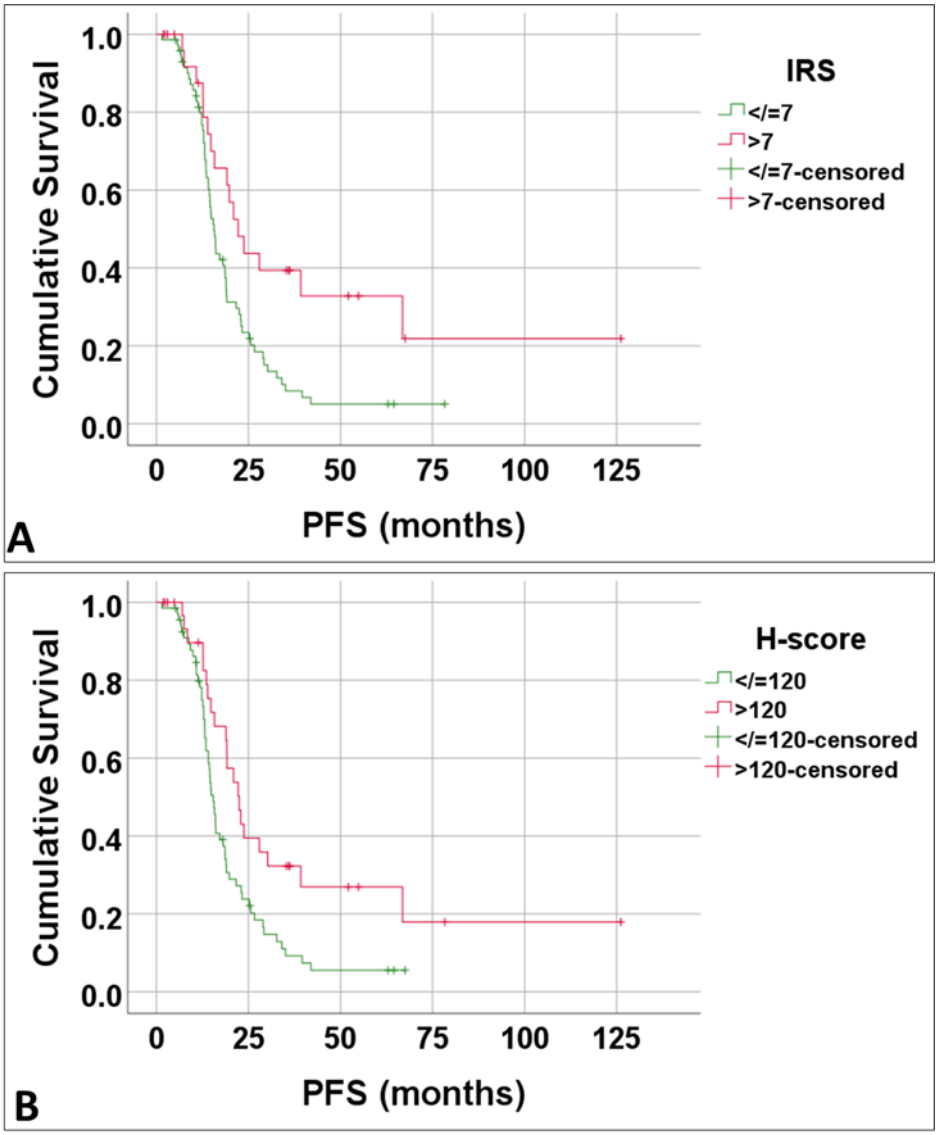

Figure 3. 20: Kaplan-Meier curves demonstrating the effect of UbcH10 expression by A) IRS B) H-score on HGSOC progression in the Birmingham cohort. The PFS period ranged from 1.5 to 126 months. The low UbcH10 group in curve A (n=72) exhibited a significantly and unexpectedly higher progression rate (62 events) and shorter median PFS (15.6 months) than the high UbcH10 group (n=28) with a total of 16 events and median PFS of 22.2 months (Log rank X^2=7.65, p=0.006). In curve B, the low UbcH10 group (n=67) again experienced a significantly higher event rate (57 events) compared to the high UbcH10 category (n=33 with a total of 21 events, Log rank X^2=6.93, p=0.008).

3.2.6.4 Univariate analysis of the effect of UbcH10 expression on progression-free survival

Because PFS was significantly worse for the low UbcH10 protein expression group in this cohort, we performed a univariate analysis of UbcH10 protein expression by IRS and H-scores as a continuous variable without dichotomisation. The main aim was to identify whether UbcH10 can be used as a biomarker to accurately predict progression in HGSOC. The HR for increased UbcH10 expression was found to be between 0.92 and 0.99. This indicates that high UbcH10 expression decreased the risk of disease progression in HGSOC females by a mere 1 to 8%. This was statistically borderline significant and hence, we concluded that quantification of UbcH10 protein levels by either IRS or H-score was a weak negative predictor of HGSOC progression in this cohort. (Table 3.10).

Table 3. 10: The results of univariate Cox-regression analysis of the effect of UbcH10 expression by IRS and H-score on progression-free survival (PFS) in the Birmingham cohort. The negativity of the regression coefficients indicates the decrease in the hazard of an event occurring (recurrence/metastasis) with increase in the value of the IRS and H-scores. Both models were statistically borderline significant. UbcH10 expression by IRS and H-scores is a borderline negative predictor of progression in this cohort.

UbcH10 protein expression	**B**	**SE**	***p*-value**	**HR**	**95% C.I**	**Chi-square (overall significance)**
IRS	-0.099	0.042	0.018	0.92	(0.83, 0.98)	**5.654 (*p*=0.017)**
H-score	-0.004	0.002	0.031	0.99	(0.99,1.00)	**5.580 (*p*=0.031)**

B: regression coefficient, **SE**: standard error, **HR**: hazard ratio, **95% C.I**: 95% confidence interval

3.2.6.5 Multivariate analysis of progression-free survival

To explore the results from the univariate analysis further, we next proceeded to measure UbcH10 as a continuous variable against the other co-variates in this cohort that significantly impacted disease progression outlined in Table 3.11. Platinum resistance was not used in this model although the strongest prognostic indicator because 21 patients lacked recorded data which would have weakened the model power. The model indicates that only FIGO stage and the volume of residual disease after surgery were independent poor prognostic indicators of progression in this cohort. This means that UbcH10 protein levels were ***not*** an independent negative predictor of progression in this cohort.

Table 3. 11: Multivariate Cox regression analysis of UbcH10 expression by IRS and H-score modeled with the prognostic factors in the Birmingham cohort to study their effect on HGSOC progression. The model is statistically significant as indicated by the Chi-square *p*-value. Only FIGO stage and cytoreduction were found to be *significant independent* predictors of PFS. UbcH0 expression by either IRS or H-score was not found to be independent predictors of progression in this cohort.

Co-variate	B	SE	*p-value*	HR	95% C.I	Chi-square test (*p*-value)
UbcH10 [a] (IRS)	-0.081	0.047	0.087	0.92	(0.84, 1.01)	**22.49 (*p*=<0.001)***
UbcH10 (H-score)	-0.003	0.002	0.167	0.99	(0.99, 1.01)	
Type of surgery[b]	0.493	0.324	0.128	1.64	(0.87, 3.09)	
Cytoreduction[c]	0.932	0.318	**0.003***	2.54	(1.36, 4.74)	
FIGO stage[d]	1.464	0.745	**0.049***	4.32	(1.10, 18.59)	

B: regression coefficient, **SE**: standard error, **HR**: hazard ratio, **95% C.I**: 95% confidence interval.

a: UbcH10 by IRS and H-scores was analyzed as a continuous variable and compared individually to the other 3 covariates.

b: Surgery was analyzed as PDS (reference category) vs DDS.

c: Cytoreduction was analyzed as complete and optimal cytoreduction (reference category) vs suboptimal cytoreduction.

d: FIGO stage was analyzed as stage I & II (reference category) vs stage III & IV.

3.2.7 Suboptimal results for *Ube2C* gene amplification

As previously described in section 2.2.4, we have attempted to amplify DNA extracted from FFPE-tissue blocks belonging to 50 patients from the Birmingham cohort. The aim was to validate IHC results on the molecular level. The amount of DNA extracted from these 50 samples was variable ranging from 8.6 ng/μl to 283 ng/μl. The purity of the DNA determined by the A260/A280 ratio was between 1.57 and 1.98. Two samples

with the highest UbcH10 expression by IHC (IRS 10 and 11) and with high DNA purity (A260/A280 ratio >1.8) and content (73.5 ng/μl and 283 ng/μl) were chosen for PCR. A total of 6 pairs of primers (Table 2.6) were run with the two samples to amplify the whole length of the *Ube2C* gene. When the DNA gel was run, the amplicons failed to be visualised at the correct band size according to the PCR product length. We resorted this failure in amplification to the poor quality and high fragmentation of the DNA extracted from the samples. Further testing was abandoned as the limited time remaining for the study did not allow further optimisation.

3.3 The Barts cohort (validation cohort)

3.3.1 Study population

To increase the robustness of our conclusions from the Birmingham cohort we next investigated UbcH10 protein levels in a distinct cohort of tissue microarrays belonging to 81 HGSOC females described in detail in section 2.1.1.2. A total of 15 (18.5%) patients had microarrays from their adnexal tumours only, 25 (30.9%) patients had microarrays from their omental tumours and 41 (50.6%) patients had microarrays from both sites. Microarrays form the adnexal and omental tumours of the same patient were cross referenced and the average IRS and H-scores were chosen from the highest expressing site in each patient for analysis.

3.3.2 Patient Characteristics

In the Barts cohort, the only available data were the type of surgery performed and FIGO stage of the patients (Table 3.12).

Table 3. 12: The clinico-pathological features of the Barts HGSOC cohort

Patient Criteria	Number of patients	Percentage	Total
Type of Surgery			
PDS	18	22.2	**81**
DDS	63	77.8	
FIGO stage			
I	2	2.5	
II	3	3.7	**81**
III	51	63	
IV	25	30.8	
UbcH10 expression (IRS)			
≤7	67	82.7	**81**
>7	14	17.3	
UbcH10 expression (H-score)			
≤120	68	84	**81**
>120	13	16	

PDS: primary debulking surgery, **DDS**: delayed debulking surgery

3.3.3 Heterogeneous UbcH10 protein expression

The protein levels of UbcH10, as determined by IHC, in the Barts cohort was heterogeneous, similar to the Birmingham cohort with IRS ranging from 0 to 11 (*Mdn*=4) and H-score ranging from 0 to 200 (*Mdn*=51; see Figures 3.21 and 3.22). The UbcH10 TPS ranged from 0 to 99% (*Mdn*=34.5).

When applying the *X*-tile generated cut-offs for IRS and H-score to this cohort, it unequally divided the patients into high UbcH10 (IRS >7 and H-score >120) and low UbcH10 expression groups. Similar to the Birmingham cohort, a minority of patients had high UbcH10 levels; 14 patients (17.3%) had an IRS >7 and 13 patients (16%) had an H-score >120 (Table 3.12).

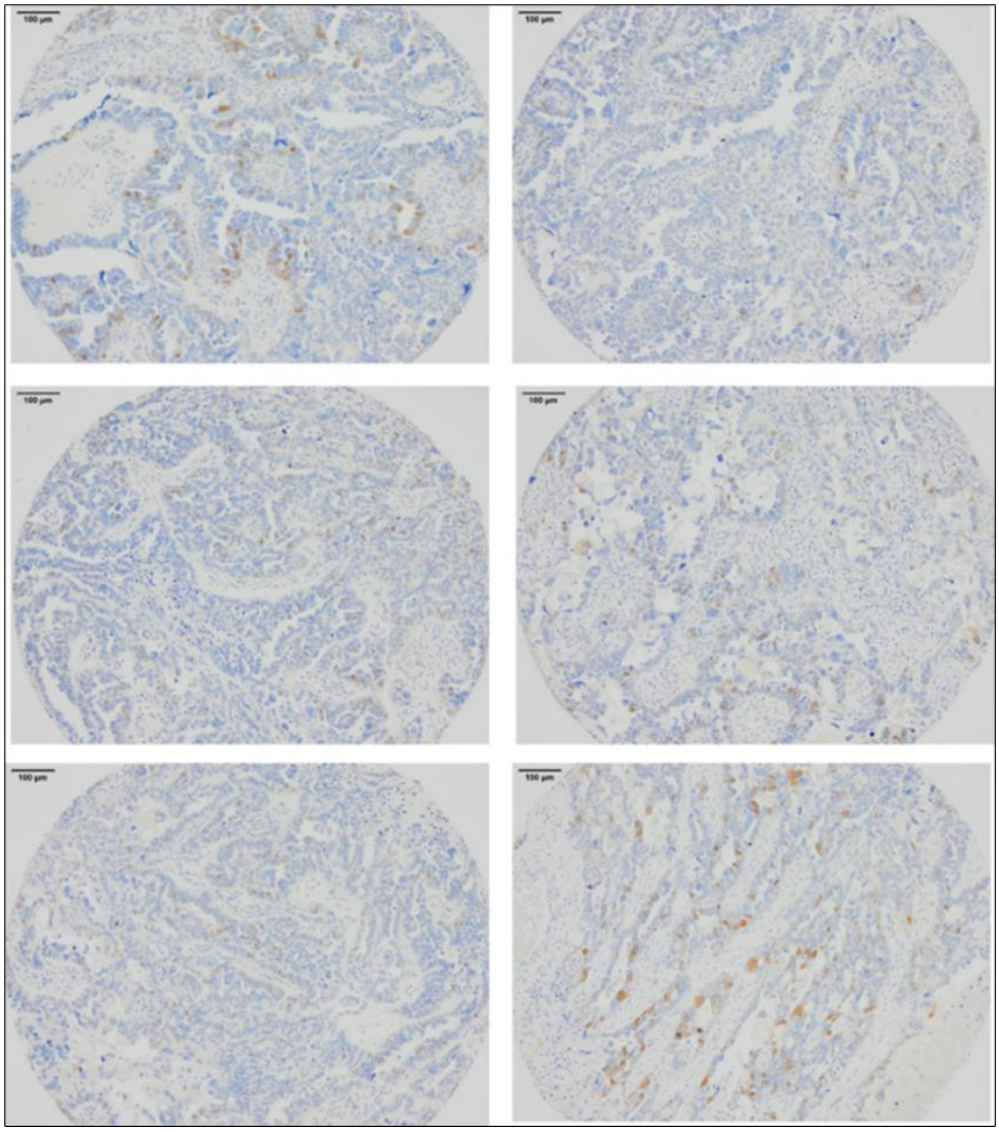

Figure 3. 21: HGSOC TMAs displaying weak UbcH10 expression from the Barts cohort. Six tissue microarrays from the ovary of one HGSOC patient from the Barts cohort. Sections show weak focal, and moderate cytoplasmic and nuclear staining in some parts of the tumour. This patient was assigned an IRS of 3 and H-score of 28 (anti-UbcH10, x10 magnification).

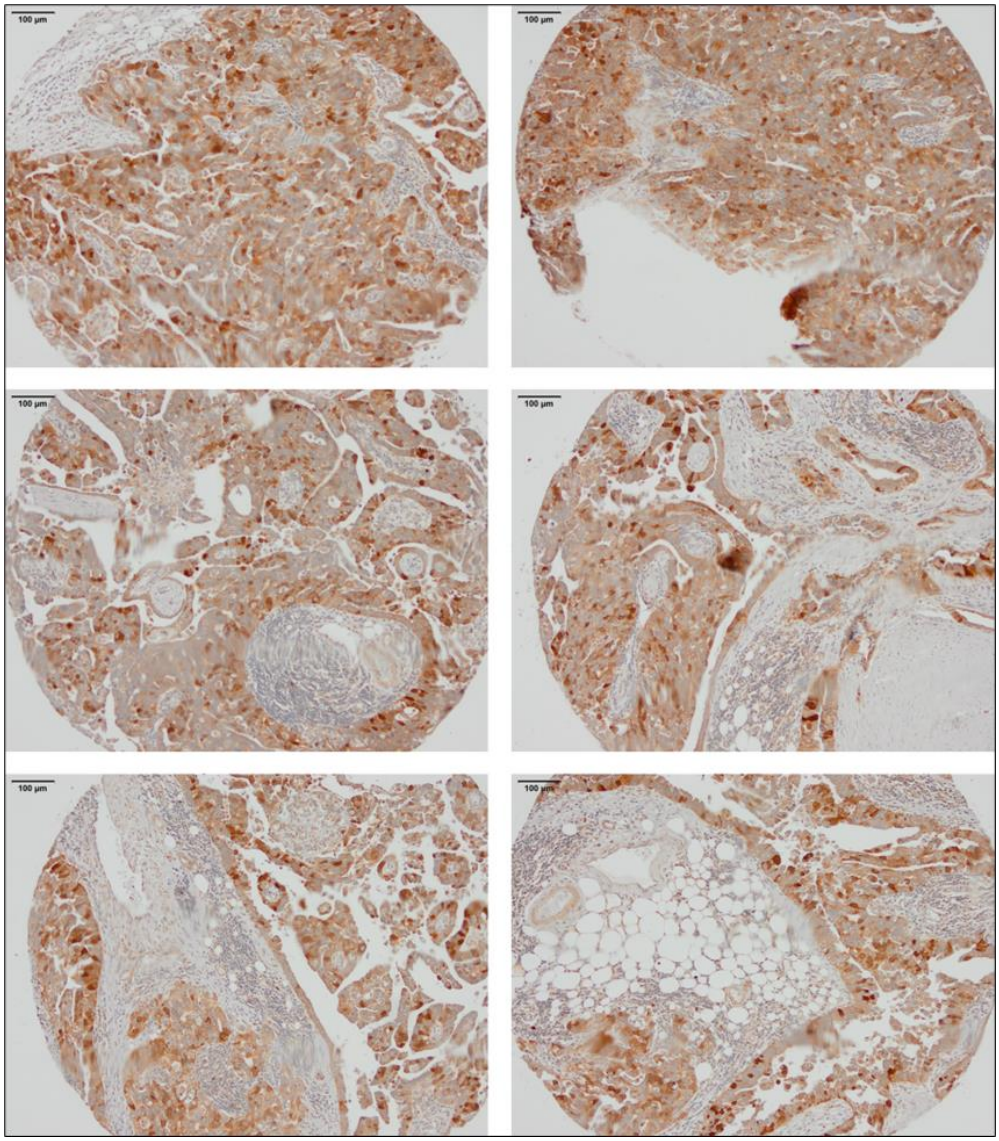

Figure 3. 22: HGSOC TMAs displaying high UbcH10 expression in the Barts cohort. Six tissue microarrays from the omentum of one HGSOC patient. The tumour sections show diffuse yet heterogeneous strong and moderate nuclear and cytoplasmic staining for UbcH10. This patient was assigned an IRS of 11 and H-score of 200 (anti-UbcH10, x10 magnification).

To study the role of UbcH10 in HGSOC progression we then compared UbcH10 expression using IRS and H-scores from the 41 patients that had both adnexal and omental tumours. We found significantly higher UbcH10 levels in omental tumours compared to adnexal primaries (Table 3.13).

Table 3. 13: The difference in UbcH10 protein levels between paired omental metastases and adnexal primaries in 41 patients from the Barts cohort. Omental tumours had significantly higher UbcH10 expression compared to their adnexal primaries.

Site of tumour	**UbcH10 protein expression** ***Mdn*** ***(Min, Max)***	**Wilcoxon signed rank test**
	IRS	
Adnexa	3 (0, 8)	**183 (*p*=0.029)**
Omentum	4 (0, 11)	
	H-score	
Adnexa	24.5 (0, 110)	**626.5 (*p*=<0.0.001)**
Omentum	51 (0, 200)	

Mdn: median, **Min**: minimum, **Max**: maximum.

Taken together these data highlight the heterogenous pattern of UbcH10 expression in HGSOC. UbcH10 is over-expressed in 16-17% of patients in this cohort and its levels are significantly higher in omental metastases compared to adnexal primaries.

3.3.4 The correlation between UbcH10 protein levels and clinico-pathological features in the Barts cohort

3.3.4.1 UbcH10 protein levels do not correlate significantly with FIGO stage

As opposed to the Birmingham cohort, UbcH10 expression in this cohort was slightly higher in late compared to early FIGO stage patients. When looking at its expression by IRS, it ranged from 1 to 6 (*Mdn*=3) in early FIGO stage patients. In late FIGO stage patients IRS ranged from 0 to 11 (*Mdn*=4). When applying H-score in early FIGO stage patients it ranged from 11 to 74 (*Mdn*=23.3), while in late FIGO stage patients it ranged from 0 to 200 (*Mdn*=54.1). However, this difference was not statistically significant [for IRS (*U*=157.5, *p*=0.52), for H-score (*U*=139.5, *p*=0.32)]. No significant association between IRS or H-score categories and FIGO stage was found (Table 3.14).

Table 3. 14: The association between UbcH10 protein expression by IRS and H-score categories and FIGO stage in the Barts cohort.

UbcH10 protein expression	Early FIGO stage (I&II)	Late FIGO stage (III & IV)	Total	Fisher' exact 2-sided significance
IRS category				
≤7	5	62	**67**	
>7	0	14	**14**	***p*=0.581**
Total	**5**	**76**	**81**	
H-score category				
≤120	5	63	**68**	
>120	0	13	**13**	***p*=0.587**
Total	**5**	**76**	**81**	

3.3.4.2 UbcH10 protein levels were reduced by pre-operative chemotherapy administration.

To explore the effect of pre-operative chemotherapy on UbcH10 levels in this cohort, we again compared its expression in PDS and DDS patients. UbcH10 levels by IRS were significantly higher in patients who underwent PDS compared to those who underwent DDS after NACT administration (Figure 3.23). The difference was borderline significant when applying the H-score (*U*=395, *p*=0.05). When applying IRS and H-score categories the difference was not statistically significant (Table 3. 15).

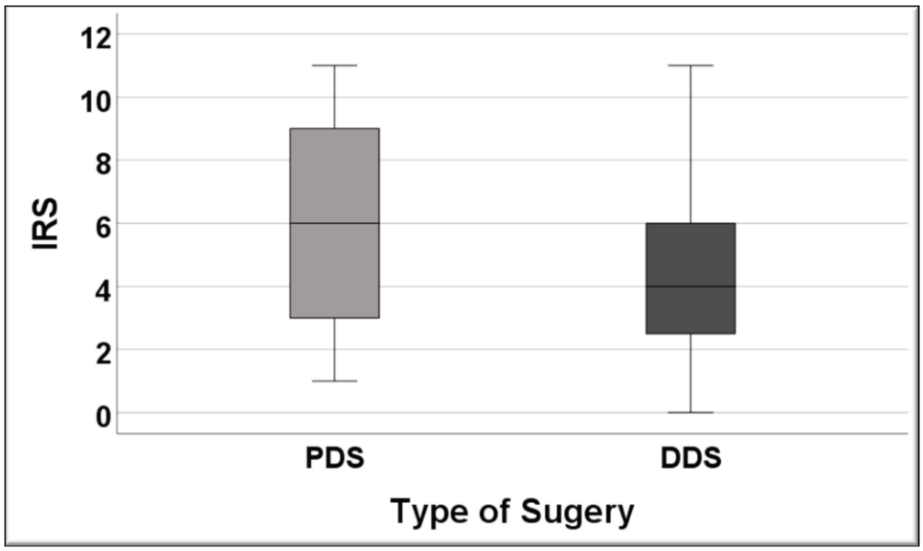

Figure 3. 23: A box plot diagram demonstrating the relationship between the type of surgery performed and UbcH10 expression by IRS in the Barts cohort. The median UbcH10 score in patients who underwent PDS was higher (n=18, *Mdn*=6) compared to those who underwent DDS (n=63, *Mdn*=4). This difference was statistically significant by Mann-Whitney test (*U*=367, *p*=0.022).

Table 3. 15: The association between UbcH10 expression categories by IRS and H-score and the type of surgery performed in the Barts cohort. No significant association was found between UbcH10 expression categories, and the type of surgery performed.

UbcH10 protein expression	PDS	DDS	Total	Fisher' exact 2-sided significance
IRS category				
≤7	12	55	**67**	***p*=0.071**
>7	6	8	**14**	
Total	**18**	**63**	**81**	
H-score category				
≤120	13	55	**68**	***p*=0.15**
>120	5	8	**13**	
Total	**18**	**63**	**81**	

PDS: Primary debulking surgery, **DDS**: delayed debulking surgery

3.3.5 Survival analysis and patient outcomes in the Barts cohort

3.3.5.1 Overview

Consideration of the Barts cohort survival data indicated that the OS period ranged from 0.5 to 85.8 months [(Median OS=37.7, 95% C.I (27.6, 47.8)] and PFS ranged from 0.5 to 73.7 months [Median PFS=15.2, 95% C.I (12.5, 17.8)]. At the end of the follow-up period there had been 50 deaths (61.7%) and 62 patients (76.5%) had experienced progression in the form of recurrence or metastasis (Figures 3.24 and 3.25)

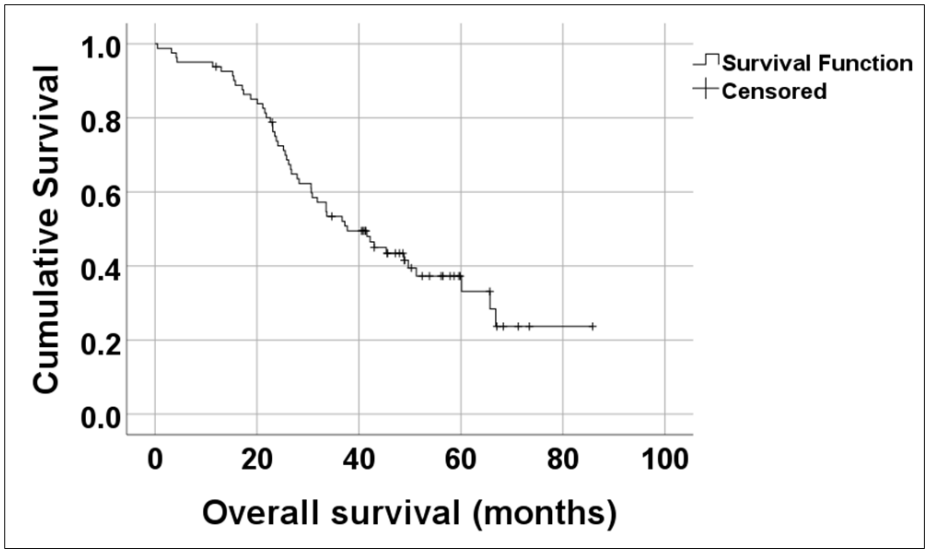

Figure 3. 24: A Kaplan-Meier curve for Overall survival of the Barts cohort. A total of 50% of patients were alive at 37.7 months (median OS). The proportion of patients that were still alive at 5 years (60 months) was 33%Censored data are patients who did not die but were lost to follow-up at various time points during the study.

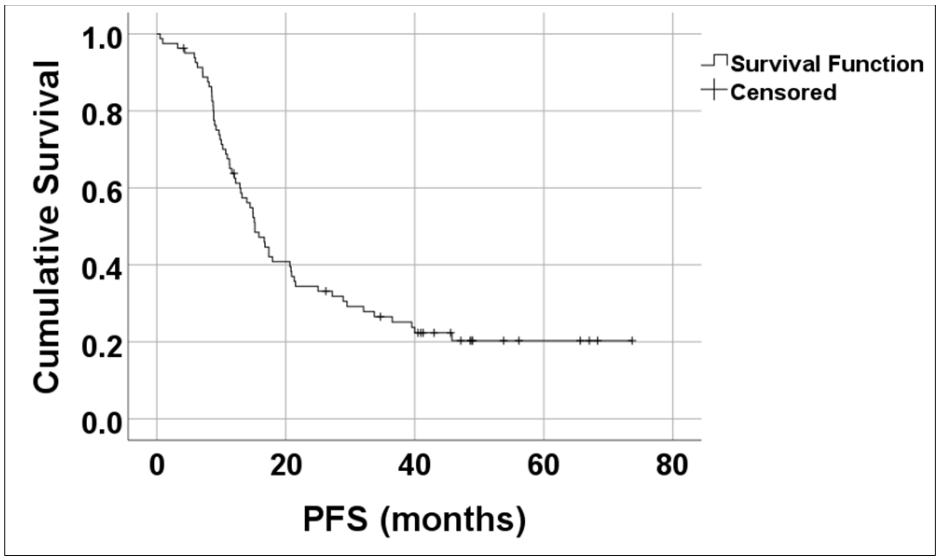

Figure 3. 25:A Kaplan-Meier curve for progression-free survival of the Barts cohort. Median PFS was 15.2 months. A total of 37% of patients experienced disease progression in the first year and 65.4% in the first 2 years of follow-up. Censored data are patients who did not progress but were lost to follow-up at various time points during the study.

3.3.5.2 The prognostic impact of FIGO stage and type of surgery performed on patient survival

As previously considered for the Birmingham cohort, univariate regression analysis was performed here to identify whether FIGO stage and the type of surgery performed influenced mortality and progression in the Barts cohort.

3.3.5.2.1 Univariate analysis of overall survival

Univariate analysis revealed FIGO stage to be the only significant predictor of mortality in this cohort. Due to the small number of early FIGO stage patients in this cohort (n=5), FIGO stage here was analysed as stages I, II & III versus stage IV. Patients with stage IV disease (n=25) had a significantly higher risk of mortality than patients with FIGO stages I, II and III [n=56, HR=1.8, 95% C.I (1.01, 3.23), p=0.046]. On the other hand, patients who underwent DDS (n=63) had a higher risk of mortality than those who underwent PDS (n=18), but the difference was not statistically significant [HR=1.79, 95% C.I (0.84, 3.84), p=0.13].

3.3.5.2.2 Univariate analysis of progression-free survival

A total of 62 patients (76.5%) had tumours that had recurred or metastasized at the end of their follow-up period, of which 53 (65.4%) experienced disease progression within the first 2 years of follow-up. Univariate analysis revealed delayed debulking surgery to be a stronger predictor of HGSOC progression than advanced FIGO stage in this cohort with both being statistically significant. Patients who underwent DDS had a significantly higher risk of progression [HR=2.83, 95% C.I (1.37, 5.82), p=0.005] compared to those who underwent PDS. Advanced FIGO stage patients also had a higher risk of progression [HR=8.1, 95% C.I (1.11, 58.52), p=0.03] compared to early FIGO stage patients.

3.3.6 The effect of UbcH10 on patient outcomes in the Barts cohort

3.3.6.1 Overview

As previously determined for the Birmingham cohort, we next investigated the effect of UbcH10 expression on HGSOC mortality and progression in the Barts cohort. Kaplan-Meier curves were constructed and the same cut-off values for IRS (7) and H-scores (120) were applied. This was followed by univariate and multivariate analysis.

3.3.6.2 UbcH10 was a predictor of HGSOC mortality in this cohort

We then explored the effect of UbcH10 on OS in the Barts cohort. In this cohort, a significantly higher death rate and shorter median OS was observed in patients that expressed *high levels of* UbcH10 relative to those patients that displayed *low levels* of UbcH10 (Figure 3.26)

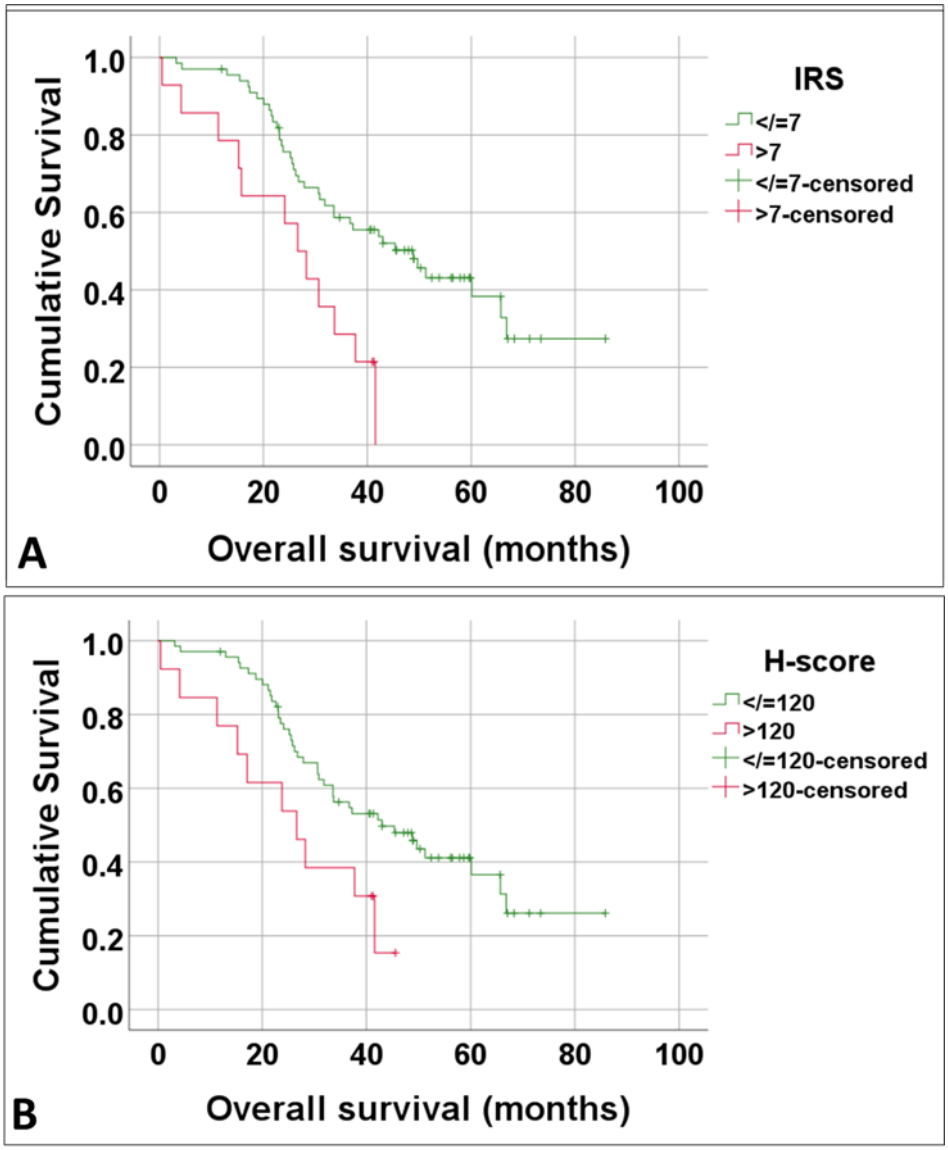

Figure 3. 26: Kaplan-Meier curves demonstrating the effect of UbcH10 expression by A) IRS B) H-score on HGSOC mortality in the Barts cohort. The OS period ranged from 0.5-85.6 months in both curves. In curve A, patients with high UbcH10 expression experienced a higher event rate (n=14 with a total of 12 events) and a significantly shorter median OS (26.6 months) than patients with low UbcH10 expression (n=67 with a total of 38 events, *Mdn* OS=43 months). In curve B, the high UbcH10 expression group again experienced a higher event rate (n=13 with a total of 10 events) and a significantly shorter median OS (26.6 months) than the low UbcH10 expression category (n=68 with 40 events, *Mdn* OS=43 months). The test of significance for IRS (Log rank X^2=9.049, p=0.003) and for H-score (Log rank X^2=5.187, p=0.023).

3.3.6.3. UbcH10 could not predict progression of HGSOC in this cohort

To investigate the effect of UbcH10 expression on PFS we compared survival in low and high UbcH10 expression groups. The recurrence rate in this cohort was slightly higher in the patients that expressed *high levels of* UbcH10 (IRS>7, H-score>120) relative to those patients that displayed *low levels* of UbcH10, but this was statistically not significant (Figure 3.27).

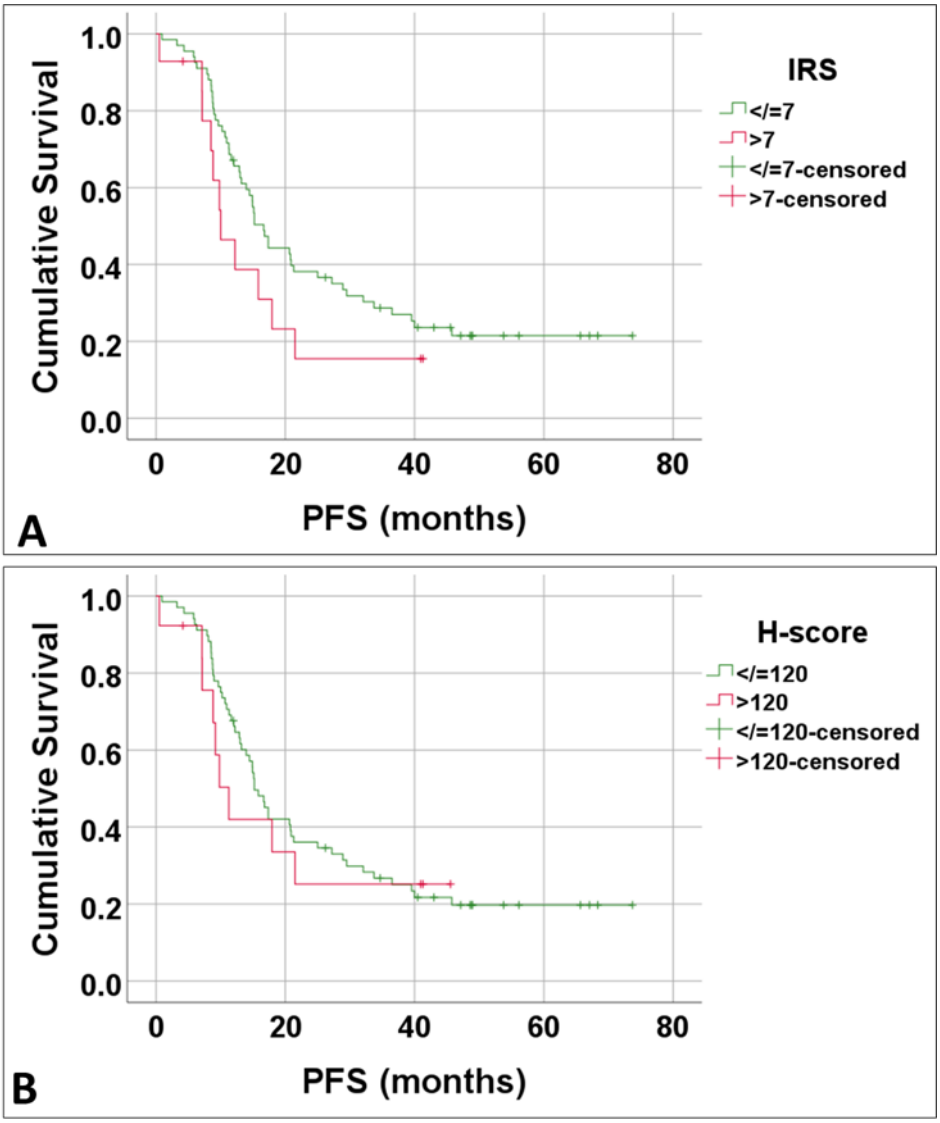

Figure 3. 27: Kaplan-Meier curves demonstrating the effect of UbcH10 expression by A) IRS B) H-score on HGSOC progression in the Barts cohort. The PFS period ranged from 0.5 to 73.7 months in both curves. The high UbcH10 group in curve A (n=14) exhibited a higher progression rate (11 events) and shorter median PFS (10 months) than the low UbcH10 group (n=67) with a total of 51 events and median PFS of 16.6 months. The difference was not statistically significant (Log rank X^2=1.95, p=0.163). In curve B, the high UbcH10 group (n=13) again experienced a significantly higher event rate (9 events) and a shorter median PFS (11.3 months) compared to the low UbcH10 category (n=68 with a total of 53 events, median PFS=15.2 months). The difference was not statistically significant (Log rank X^2=0.183, p=0.669).

We can infer from the data for this cohort that high UbcH10 expression has a *negative* impact on patient mortality which is different from the results obtained from the Birmingham cohort.

3.3.6.4 Univariate analysis of the effect of UbcH10 on overall survival

Because OS was worse for patients that expressed high UbcH10 relative to patients that expressed low UbcH10, we used univariate analysis to identify the effect of UbcH10 on OS in the Barts cohort. The HR for increased UbcH10 expression was found to be between 1.006 and 1.11. This means that high UbcH10 expression increased the risk of mortality in HGSOC in this cohort by only 0.6 to 11%. We can therefore deduce that both the IRS and H-scores are **positive, yet weak predictors** of HGSOC mortality in this cohort (Table 3.16).

Table 3. 16: The results of univariate Cox-regression analysis of the effect of UbcH10 expression by IRS and H-score on Overall survival in the Barts cohort. The positivity of the regression coefficient in both scores and borderline significant *p*-values indicate a significant but weak increase in the hazard of an event occurring (death) with increase in the value of IRS and H-scores.

UbcH10 protein expression	*B*	SE	*p*-value	HR	95% C.I	Chi-square (overall significance)
IRS	0.105	0.049	0.033	1.111	(1.008,1.223)	4.574 (*p*=0.032)
H-score	0.006	0.003	0.022	1.006	(1.001,1.012)	5.358 (*p*=0.021)

B: regression coefficient, **SE**: standard error, **HR**: hazard ratio, **95% C.I**: 95% confidence *interval.*

3.3.6.5 Multivariate analysis of overall survival

We then resorted to multivariate analysis to confirm the results obtained with univariate analysis, and to identify whether the impact of UbcH10 on patient outcome is

independent or dependent on the only other significant co-variate available in this cohort; FIGO stage. The model identifies both FIGO stage and UbcH10 as **independent** poor prognostic indicators of HGSOC in this cohort (Table 3.17).

Table 3. 17: Multivariate cox regression analysis of the effect of UbcH10 expression by IRS and H-scores and FIGO stage on OS of the Barts cohort. The model is statistically significant as indicated by the Chi-square *p*-value. The analysis indicates that UbcH10 expression is a weakly significant positive and independent predictor of HGSOC mortality in this cohort. FIGO stage was also an independent predictor of mortality in this cohort.

Co-variate	B	SE	*p*-value	HR	95% C.I	Chi-square (overall significance)
UbcH10 (IRS) [a]	0.106	0.047	0.025	1.110	(1.010, 1.220)	**9.932 (*p*=0.007)**
UbcH10 (H-score)	0.006	0.003	0.019	1.006	(1.001, 1.012)	
FIGO stage [b]	0.618	0.298	0.038	1.850	(1.034, 3.326)	

B: regression coefficient, **SE**: standard error, **HR**: hazard ratio, **95% C.I**: 95% confidence interval

a: UbcH10 by IRS and H-score were analyzed as continuous variables and compared individually to FIGO stage.

b: FIGO stage was analyzed as stages I, II & III vs stage IV.

3.4 The Pilot cohort of fresh ovarian cancer specimens

3.4.1. The Clinico-pathological profile of the 61 harvested samples

As a pilot study at the beginning of this project, we attempted to determine which protein technique was best for studying UbcH10 and p53. As previously described in section 2.2.3, after anonymously analysing 61 samples from 47 patients by Western blot analysis for both UbcH10 and p53, we retrospectively retrieved the pathological diagnoses for those patients. The Pathology reports of the patients were retrieved from the electronic archives of the respective Pathology departments in Birmingham Women's and Royal Wolverhampton's NHS Trust. Concerning histopathological diagnosis, the tumours from the 47 females included a wide range of ovarian cancer subtypes. These entailed 22 (46.8%) HGSOC, 11 (23.4%) mixed subtypes of EOCs (4 CCC, 3 LGSOC, 2 EC and 2 Carcinosarcoma), 6 (12.8%) benign and borderline tumours and 3 (6.4%) metastatic ovarian malignancies. Pathological information was missing on 5 (10.6%) of the samples. Clinical information for the 22 HGSOC were collected including age at diagnosis, FIGO stage and type of surgery performed. The remaining ovarian malignancies were excluded as they were outside the scope of this study.

The 22 HGSOC patients were aged between 40 and 82 years old, with a median age (*Mdn)* of 61 years. With regards to the stage distribution of the cases, all but one were advanced FIGO stages (III/IV). Of the 21 cases characterized, 5 (23.8%) were selected for PDS without prior chemotherapy, while the remaining 16 cases (76.2%) underwent NACT followed by DDS. The remaining HGSOC case was an early FIGO stage IIA, which was isolated by PDS.

We concluded from the above that around 50% of patients analysed by Western blot analysis included advanced stage HGSOC that mostly received pre-operative chemotherapy.

3.4.2 UbcH10 and p53 were overexpressed in a minority of HGSOC patients with interpretive difficulties.

Out of the 22 HGSOC patients analysed by Western blot, only 6 patients overexpressed UbcH10, and 5 patients overexpressed p53 (Appendix 10.1 shows representative blots from some of these patients). Several interpretive difficulties arose with the blots. Firstly, in the cases where no UbcH10 was noted, it was hard to determine whether UbcH10 was totally absent or just low as no quantitation of the amount of UbcH10 was feasible by Western blot. Similarly, for p53, a negative result on Western blot might indicate either a wild type p53, expressed at undetectable levels, or a non-expressed protein i.e. a null mutation. Secondly, UbcH10 and p53 expression levels differed, with variation in biopsy site, from the same patient. Patient RWT17, for instance, had overexpressed UbcH10 and p53 in the ovarian biopsy, whilst the omental deposit did not show detectable UbcH10 or p53 levels (Appendix 10.1). This was also found to be the case for two other HGSOCs (results not shown), which could indicate a difference in clonality between the ovarian tumour and the metastatic omental deposit from the same patient. Another plausible explanation would be the difference in cellular content between the omental biopsy and the ovarian biopsy. Omental samples tend to be high in adipose tissue that may interfere with the detection of the proteins on Western blot. Lastly, because sampling had been done as small snips in a fresh state intra-operatively, the tumour may have been missed and sampling errors could have accounted for the discrepant results.

Based on the literature, we also aimed to explore the relationship between UbcH10 and the prognostic and predictive parameters in ovarian cancer. We also wanted to explore the relationship between UbcH10 and p53 at the protein level. Because the majority of the HGSOC patients from this cohort (21 out of 22) were advanced FIGO stage and only 5 cases overexpressed UbcH10, it was hard to establish a statistical relationship between the two parameters. Similarly, it was hard to conclude any significant relationship between p53 and UbcH10. Therefore, a larger cohort was needed before doing any correlations. But before proceeding with further Western blot analysis and given the above-described interpretational difficulties with the technique, we had to validate the results using immunohistochemistry.

3.4.3 Discrepant results between Western blot analysis and immunohistochemistry

As mentioned above, the mutational status of p53 could not be specifically predicted by Western blot analysis. Moreover, Western blot analysis showed discrepant protein expression levels for both UbcH10 and p53 isolated from various biopsy sites in the same patient. To explain these results and validate our technique, we collected the FFPE tissue blocks corresponding to the analysed Western blot samples and stained them for both UbcH10 and p53.

Concerning UbcH10 expression, it was noted that the 6 cases that overexpressed UbcH10 by Western blot analysis showed high expression of UbcH10 by immunohistochemistry (IRS >7 and H-score>120). However, out of the 16 cases that showed no UbcH10 expression by Western blot analysis, only 2 cases showed completely absent UbcH10 expression on IHC. The remaining 14 cases showed a wide

range of UbcH10 expression levels with IRS ranging from 2 to 11 and H-score ranging from 20 to 190. This means that immunohistochemistry was more sensitive in the detection of UbcH10 expression than Western blot analysis, which seemed to detect only a portion of the tumours that overtly overexpressed UbcH10 whilst missing others. This could possibly be resorted to the heterogeneous manner of UbcH10 expression in different parts of the same tumour and the difficulties with equal protein loading/detection by Western blot due to contaminating lipid. It could also be related to sampling errors in the fresh state. Appendix 10.2 shows an example of two cases (RWT1 and RWT13) with discrepant UbcH10 expression on IHC compared to Western blot analysis.

Concerning p53 expression, 15 out of the 22 cases showed aberrant p53 overexpression by IHC compared to only 5 on Western blot analysis. In the remaining 7 cases, a null pattern was observed on IHC which was concordant with an absent p53 band on Western blot. This means that Western blot was not picking up a significant portion of HGSOC with p53 overexpression. Appendix 10.2 shows an example of a HGSOC case (RWT13) with discrepant p53 overexpression on IHC compared to Western blot analysis.

To conclude, the Western blot analysis results were not validated by immunohistochemistry. We therefore determined that immunohistochemistry was superior to Western blotting in detecting both UbcH10 and p53 given the heterogeneity of the tumours and the numerous pre-analytical and analytical factors that hindered proper detection of both proteins on Western blot analysis. Additionally, immunohistochemistry was more specific in the detection of p53 mutational status and offered a better visual aid to appreciate tumour heterogeneity. Moreover, it allowed for

a wider range of semi quantification and analysis of UbcH10 protein expression. As such, we expanded on the 22 HGSOC cases and collected further FFPE-tissue blocks that later constituted the Birmingham cohort described in section 2.1.1.1.

3.5 Discussion

HGSOC is the most frequent and most lethal of all gynaecological malignancies, being the fifth leading cause of cancer death among females worldwide (10, 115). To date, the behaviour of HGSOC, is characterized by aggressiveness, high propensity for local and distant metastasis, recurrence, and resistance to treatment (41). UbcH10 has been previously identified in several studies as a proto-oncogene whose over-expression was linked to aggressive behaviour in many human malignancies including ovarian cancer (86, 98-101). However, the relationship between UbcH10 and HGSOC has not been investigated extensively. To this end, the principle aim of the present study was to expand on former studies and investigate the prognostic and predictive relevance of UbcH10 in HGSOC in an attempt to stratify these tumours for treatment.

To this end we investigated UbcH10 levels in two patient cohorts of HGSOC by IHC using validated in-house anti-UbcH10 antibody and correlated our findings with clinico-pathological parameters and patient outcome.

3.5.1 UbcH10 is a feature of malignant tissue with heterogenous expression in HGSOC and higher expression in metastatic sites

Our data confirmed that UbcH10 is a feature of malignant ovarian tumours with absent, or low levels of UbcH10 protein in normal ovarian, fallopian tube epithelium (Figure 3.2) and even benign serous tumours (discussed in more detail in chapter 6). These findings conformed with previous studies on ovarian (86, 116) and non-ovarian

malignancies (96, 98, 117). Okamoto *et al (96)* were among the first to identify UbcH10 as a feature of malignant cells rather than normal tissue. Their study identified UbcH10 at high levels in cancerous cell lines from various organs, whilst normal tissue displayed low or undetectable UbcH10 levels by quantitative RT-PCR. Similarly, Pallante *et al (98)* demonstrated higher UbcH10 levels in anaplastic thyroid carcinomas compared to normal and benign thyroid tissue. With respect to EOCs, Berlingieri *et al (86)* detected the over-expression of UbcH10 protein in ovarian cancer cell lines compared to normal ovarian tissue. Gong *et al* (116) detected significantly higher UbcH10 protein levels in EOC samples compared to normal ovarian tissue and benign ovarian tumours.

In addition, we also detected a heterogeneous pattern of UbcH10 protein expression within HGSOC which was seen previously in the two former studies of UbcH10 in EOCs (86, 116). Importantly, we detect significantly higher UbcH10 levels in metastatic ovarian tumours compared to their primaries in one of our cohorts (Table 3.13) which points to an oncogenic role that UbcH10 might play in HGSOC. This oncogenic role could be explained at the molecular level where UbcH10 was found to promote chromosomal mis-segregation and genomic instability in transgenic mice (93). Furthermore, UbcH10 is hypothesized to promote tumour growth by overriding the SAC (96). It has also been suggested that UbcH10 over-expression upregulates N-cadherin and inhibits E-cadherin contributing to epithelial-to-mesenchymal transition (EMT), thus promoting invasion and metastasis (118) . We discuss the role of UbcH10 in HGSOC progression in more detail in chapter 6.

3.5.2 UbcH10 as a prognostic marker in HGSOC

With respect to the possibility that UbcH10 is a prognostic marker in HGSOC we used two independent datasets: one designated the 'training' set (Birmingham) and the other designated the 'validation' set (Barts) and compare the results obtained from both. The ability to compare two independent datasets to investigate any role for UbcH10 in the prognosis of HGSOC is a major strength of our study. Two factors were important to consider, in this regard, when considering UbcH10 as a prognostic marker: its correlation with the well-established prognostic factors in ovarian cancer and its effect on patient survival.

3.5.2.1 Comparison between the training and validation datasets

The relationship between UbcH10 and other prognostic factors in ovarian cancer was mostly consistent in both cohorts. In the Birmingham cohort, high UbcH10 protein levels correlated only weakly with advanced patient age at diagnosis (Figure 3.6) and did not correlate significantly with the well-known and established *poor* prognostic indicators of ovarian cancer; FIGO stage, LN metastasis, volume of residual disease after surgery. Moreover, UbcH10 protein levels did not correlate with the good prognostic indicator in this dataset; the *BRCA* mutation status. In addition, UbcH10 was not significantly associated with measures of treatment response namely CRS and platinum resistance. In the Barts cohort, we found no significant association between UbcH10 and FIGO stage, similar to the Birmingham cohort. Unfortunately, other clinico-pathological parameters were not available in this cohort for comparison with the training cohort.

Our analyses revealed that the survival data from the Birmingham cohort was not validated in the Barts cohort. In the Birmingham cohort, UbcH10 protein levels could

not predict mortality (Figure 3.19), while in the Barts cohort high UbcH10 expression significantly affected patient mortality. Furthermore, data from the Birmingham cohort seemed to suggest that high UbcH10 expression had a *favourable* impact on PFS of HGSOC patients. The Barts cohort data suggested the opposite; with high UbcH10 expression observed in patients with *worse* PFS. This brings us to the importance of multi-variate analysis in our cohorts. In the Birmingham cohort, although univariate analysis suggested that UbcH10 might be a negative predictor of progression, this could not be validated by multi-variate analysis (Table 3.11). This means that UbcH10 is ***not*** an independent negative predictor of progression in this cohort and therefore its effect on disease progression is contingent on other factors. Note that UbcH10 levels were significantly lower in patients who underwent DDS (Table 3.5), and those patients had a significantly worse PFS (Figure 3.16). Additionally, UbcH10 levels were lower in advanced FIGO stage (Table 3.3) and platinum resistant patients (Figure 3.10). All three factors; DDS, advanced FIGO stage and platinum resistance were significant predictors of disease progression in this cohort (Table 3.9). Consequently, the low UbcH10 group had inherently strong poor prognostic indicators that significantly affected their disease progression independent of UbcH10 levels. This means that the traditional *p*-value originally reported in Figure 3.20 overestimated the significance of UbcH10 as a favourable prognostic marker because it was not validated on multi-variate analysis. In other words, patients with high UbcH10 had more favourable outcome due to lower stage and higher platinum sensitivity and not because of high UbcH10 expression. Contrary to the Birmingham cohort however, we identified a weakly significant poor impact of high UbcH10 expression on HGSOC mortality but not

progression in the validation cohort (Table 3.16). This poor impact was independent of FIGO stage in multi-variate analysis (Table 3.17).

Taken together, these data argue against the use of UbcH10 as a prognostic marker in HGSOC as indicated in the other studies on EOCs (86, 116). Nevertheless, it is important to highlight the shortcomings of our study. The Birmingham cohort, although well characterised with many significant clinico-pathological variables available for analysis, had a sample size of only 100. We acknowledge that when studying biological markers, it is important to increase the sample size to at least double the current size to increase statistical power and the likelihood of detecting higher hazard ratios (119). In the Barts cohort, other important prognostic data were missing including CRS, cytoreduction, platinum resistance and patient age, which would have offered a good validation of the conclusion from this cohort and a more robust refinement of our multivariate analysis model.

3.5.2.2 UbcH10 in other studies on epithelial ovarian cancers

In consideration of other UbcH10 studies in EOC, a recent study presented comparable data to the Barts cohort findings. This study implicated the *Ube2C* gene among 9 other genes in the progression of EOCs and linked high UbcH10 expression to poor OS (120). When looking at their study design, they included different subtype of EOCs in their survival analysis: serous, endometrioid, clear cell and mucinous carcinomas. It is not clear however how many of each subtype they included in their survival analysis, nor is it clear what type of serous carcinoma they had in their cohort.

Two studies used IHC to study EOCs, the first being Berlingieri *et al (86)* which identified UbcH10 as a useful prognostic tool in ovarian cancer. They also reported a

significant association between high UbcH10 expression in EOCs and poor OS but not relapse-free survival. The second study was Gong *et al (116)* who reported a significant association of UbcH10 with FIGO stage in EOC but not with patient age. They also identified UbcH10 as an independent poor prognostic marker affecting the OS of ovarian cancer patients.

To explore these studies (86, 116) in more detail we compare our study design and methodology to theirs. Our study is the first of its kind to use two scoring systems for UbcH10: the IRS and H-score in ovarian cancer. Although both scoring systems have been used in other malignancies such as bone and breast cancer (121, 122), they have not been used in ovarian cancer before. Furthermore, identifying an appropriate cut-off was performed using the well-established *X*-tile software to identify patients who express low and high levels of UbcH10. In the study by Berlingieri *et al (86)* there was no clear definition of the scoring system used for immune-histochemical expression of UbcH10, whilst in the study by Gong *et al (116)*, they used a scoring system similar to the IRS with a range of scores from 0 to 12. Berlingieri *et al (86)* used the median UbcH10 expression to divide their cohort for survival analysis, while Gong *et al (116)* used an arbitrary cut-off of 2 on their scoring system to define positive and negative cases.

Concerning histological type, Berlingieri *et al (86)* reported low levels of UbcH10 in clear cell, endometrioid and serous cystadenocarcinomas, whilst expression levels were high in undifferentiated carcinomas; confirmed by RT-PCR analysis. Nevertheless, in their cohort of 60 ovarian cancer specimens, Berlingieri *et al (86)* used the old 4-tiered grading system for all their ovarian cancers, rather than the more recently adopted two-tiered grading system tailored for serous carcinomas (8).

Therefore, in addition to their smaller cohort, it is not clear whether their stated serous cystadenocarcinoma cases were low- or high-grade. Moreover, since undifferentiated carcinomas are likely to be a subtype of HGSOC (8)-a fact unbeknownst back then- it is probable that their undifferentiated cases were actually misclassified HGSOCs, while their serous cystadenocarcinoma cases were likely LGSOC. Gong *et al (116)* although included a larger sample size (n=180) than Berlingieri *et al (86),* they again included different histological subtypes of EOCs with a mixture of low and high grade cases and hence a good number of early and late FIGO stage cases as well. This means that these two studies compared survival between histotypes of EOCs which are biologically different tumours by definition and not part of a biological continuum (8, 10). We contend that the design of both studies and the conclusions drawn cannot be generalized on HGSOC cases which are-by definition-all high grade and largely late stage. In other words, both studies could be over-stating the significance of UbcH10 as prognostic indicator by conveniently comparing two groups that have stark differences in well-established prognostic factors.

As a counterargument, whilst it is true that the *X*-tile generated cut-offs in our study are robust and avoid statistical bias from randomly testing multiple cut points, survival analysis was not consistent in both cohorts of our study. It could be reasoned that the shortcomings of our cohorts such as the small sample size and missing prognostic parameters to model UbcH10 against affect our conclusions. Nevertheless, it is more likely that UbcH10 is not prognostic in HGSOC, but has borderline significance at best, which is why results from our two cohorts differ. Moreover, the differences in the survival results from our two cohorts provide a good example of how it is easy to claim falsely a marker as prognostic in one study and then fail to validate it in another study.

This is one of the advantages of using training and validation datasets and the strengths of using the *X*-tile software which applies the same principle (108). In their paper in 1994, Altman *et al (123)* highlighted the significant false positive rate that can arise from using an optimal cut-off point in assessing prognostic markers. Researchers use many different "optimal" cut-off points in an arbitrary manner which makes it difficult to compare different studies and quantify the prognostic effect of any new biomarker. Therefore, Altman *et al (123)* recommended the use of corrected *p*-values and univariate cox regression analysis of any new biomarker as continuous variable to minimise the bias in estimating its effect on survival. Our study managed to circumvent that problem by using the robust *X*-tile software (108) and using univariate regression analysis. Furthermore, the univariate analysis of the baseline clinico-pathological parameters performed before testing UbcH10 confirmed the robustness of the data collection process and the minimal bias in our methodology.

Another prospect for future studies would be to correlate UbcH10 protein levels with *Ube2C* gene expression levels which was not possible in the current cohorts due to the poor quality of FFPE tissue extracted nucleic acids as described in section 3.2.7. However, we explore this further by analysing *Ube2C* gene expression data extracted from the publicly available TCGA dataset in chapter 5.

3.5.2.3 UbcH10 in other malignancies

To consider UbcH10 expression in other cancers, UbcH10 protein expression was significantly correlated with high tumour grade and aggressive behaviour in colon cancer (101). This study included 150 neoplastic colonic specimens of various grades (G1-3) the majority of which were adenocarcinomas. In their study, UbcH10 did not correlate with patient age or lymph node metastasis similar to the Birmingham cohort,

but UbcH10 expression was significantly associated with grade 3 carcinomas. In the same study they also demonstrated an increase rate of cellular proliferation, and aberrant cell-cycle progression in colon cancer cell lines that over-expressed UbcH10. Their data indicate that the aggressive behaviour associated with UbcH10 overexpression in colonic cancer could be related to its proliferative properties.

Another study evaluated UbcH10 expression in 140 lung carcinoma patients which included a mixture adenocarcinomas and squamous cell carcinomas of various grades (100). It was noted again that UbcH10 protein levels progressively increased with decreased tumour differentiation and higher tumour grade.

In a study that included 209 invasive breast carcinomas of no special type (IBC, NST) of progressive grades (Grade 1 to 3), UbcH10 expression was again positively correlated with worse histological grade. This study used a semiquantitative IHC scoring system similar to the IRS used in our study. In addition, they significantly correlated high UbcH10 expression with clinical stage and LN metastasis in IBC, NST (124).

We can infer from the above studies and our own data that UbcH10 over-expression is mostly associated with high grade tumours. High grade tumours are characterised by both their high ability to invade and metastasise as well as their highly proliferative indices. This means that UbcH10 may play an oncogenic role through promotion of disease progression and metastasis, or it could be a proliferative marker that promotes tumour growth and proliferation. In fact, both the oncogenic and proliferative roles of UbcH10 may be closely intertwined because mitotic dysfunction is closely related to chromosomal instability and cancer progression (96). Accordingly, UbcH10 could be

more useful as a prognostic marker in tumours that show increasing histological grades and proliferative rates as part of their biological continuum like colorectal, lung and breast adenocarcinomas. On the other hand, it is only borderline significant in tumours that are all inherently high grade and highly proliferative such as HGSOC.

3.5.3 UbcH10 as a predictive marker in HGSOC

With respect to treatment factors, one parameter that was consistent in both the Birmingham and Barts cohorts was that UbcH10 expression levels were significantly lower in patients who underwent DDS compared to those who underwent PDS (Table 3.5 and figure 3.7). The fundamental difference between both groups was that patients who underwent DDS received pre-operative chemotherapy in the form of paclitaxel and carboplatin. We therefore concluded that UbcH10 levels were significantly reduced by pre-operative chemotherapy administration. This behaviour is akin to MIB-1 (Ki-67) a proliferative marker whose levels have been shown to decrease significantly after NACT in breast cancer (125-127). Having said that, it was also interesting to note that in tonsillar tissue sections (Figure 2.1 from Materials and Methods) UbcH10 polarized in the highly proliferative cells of the germinal centre in a similar manner to the known proliferative marker MIB-1 (Ki-67). The relationship between the two markers is investigated further in chapters 6 and 7.

When looking at treatment response, although we did not find a significant association between UbcH10 and CRS, UbcH10 protein levels were shown to be higher in patients with pathological complete or partial response to chemotherapy compared to those with minimal response (Table 3.6). Platinum-sensitive patients had higher UbcH10 levels than platinum-resistant patients although again not significant (Figure 3.10). We can discuss these findings from two points of view.

The first consideration is that UbcH10 is a possible proliferative marker that behaves in a similar fashion to the well-known proliferative marker Ki-67. Cytotoxic drugs that are cell-cycle phase-specific like paclitaxel have long been known to selectively kill highly proliferative tumour cells (128). Since all HGSOC are, by definition, highly proliferative tumours (8), we therefore consider that high levels of UbcH10 protein might correlate positively with a better response to chemotherapy due to the high proliferative rate of the cells. This view is supported by studies where high levels of Ki-67 predicted a pathological complete response in breast cancer patients receiving NACT (125, 129). In addition, UbcH10 knockdown inhibited the expression of Ki-67 in drug resistant breast cancer cell lines and promoted a better response to epirubicin and docetaxel (103). These studies further corroborate UbcH10 as a proliferative marker.

The second point of view to consider is with respect to platinum therapy. In gastric cancer cell lines, UbcH10 overexpression (99) has been associated with decreased apoptosis induced by cisplatin and hence platinum resistance. In our study, UbcH10 levels were higher in platinum sensitive patients. This might be explained by the fact that these patients are administered paclitaxel as well. Paclitaxel as mentioned earlier is a cytotoxic drug that exerts its anti-proliferative activity through inhibition of microtubule polymerisation (128). This means that high UbcH10 expression in platinum sensitive patients might be a direct result of paclitaxel-induced mitotic arrest (93, 128). Cells arrested in mitosis by paclitaxel later die by apoptosis or enter senescence (128). On the other hand, this does present us with a chicken and egg conundrum. Does high UbcH10 expression promote high cellular proliferation and hence a better response to

cytotoxic chemotherapeutic drugs like taxanes and platinum? Or do anti-proliferative drugs like taxanes promote mitotic arrest thus leading to high UbcH10 levels?

To address this dilemma, we revisited the difficulties that faced us whilst studying the role of UbcH10 as a predictor of chemotherapy response. Firstly, platinum resistance in our cohort was gauged as a clinical response and not determined at a cellular level like the above study (99). Correlation between the clinical and cellular response to platinum therapy would be a promising prospect for further studies. It is also important to study the relationship between UbcH10 and Ki-67- which we would discuss in later chapters-as well as the effect of carboplatin and paclitaxel used in HGSOC treatment on UbcH10 expression levels in ovarian cancer models. Secondly, CRS in our cohort was performed on omental patient biopsies as is standard of practice (32, 107). UbcH10 levels on the other hand, were measured in adnexal, omental, or sometimes distant metastatic sites in those patients. Treatment response in ovarian cancer varies considerably depending on tumour location as well as the number of NACT cycles administered (130, 131) which also varied considerably in our cohort. This is another limitation of our study. To study the relationship between UbcH10 levels and treatment parameters adequately, it is therefore important to standardize the site of biopsy and cycles of NACT administered in future studies. In addition, matched pre-and post-operative samples should ideally be used to further clarify the role of UbcH10 in chemotherapy resistance/sensitivity in HGSOC.

3.6 Conclusion

To conclude, in the present cohorts we use robust immunohistochemical scoring and sound statistical analysis. UbcH10 is a poor prognostic indicator in HGSOC of

borderline significance as outlined from the results of our two cohorts. UbcH10 likely behaves as a proliferative marker rather than a proto-oncogene in HGSOC as it shows many similarities to Ki-67 and, as such we explore the relationship between the two markers in later chapters. As a predictor of treatment, although UbcH10 was not significantly associated with CRS or platinum resistance, it is worth exploring this relationship in future studies in a more standardised cohort and comparing its effect in matched pre- and post-chemotherapy specimens and in ovarian cancer models.

Chapter 4. The heterogeneous relationship between UbcH10 and p53 at the protein level and implications on outcomes of HGSOC patients

4.1 Introduction

HGSOC is characterized by profound chromosomal instability and a high rate of *TP53* mutation (50). In fact, *TP53* mutation is an early event in HGSOC being present in more than 96% of HGSOC and their well-established precursors in the fallopian tube STICs (24, 49). This makes it a valuable marker used in the routine diagnosis of HGSOC.

As previously discussed in chapter 1 section 1.6, HGSOC can exhibit different types of p53 mutations that translate to four different protein expression profiles on immunohistochemistry: overexpression, null, cytoplasmic, and wild-like patterns. With optimised protocols, these immunohistochemical expression patterns of p53 correlate extremely well with the *TP53* mutation status (49, 77, 78). Furthermore, *TP53* mutations are known to contribute to the metastatic potential of ovarian cancers and their resistance to chemotherapy. Results however on the role of the different *TP53* mutations in predicting patient outcomes and chemoresistance in ovarian cancer have been conflicting (82, 83).

Moreover, recent studies have demonstrated that p53 GOF mutants promote the transcriptional activation of UbcH10 in human cancer cell lines (104). In HGSOC however, the exact relationship between UbcH10 and p53 has yet to be established. A

deeper investigation into this relationship might have therapeutic and prognostic implications for HGSOC.

In this chapter we explore the relationship between p53 and UbcH10 protein levels in the Birmingham cohort using a combination of regular and multiplex immunohistochemistry (Material and Methods section 2.2.1). We also investigate the effect of different p53 IHC staining patterns on patient outcomes and chemotherapy resistance in this cohort. P53 data for the Barts cohort was not available for consideration in our analysis.

4.2 The different p53 immuno-histochemical staining patterns in the Birmingham cohort and a newly recognised pattern in HGSOC

We first explored the different patterns of p53 protein expression in the HGSOC specimens from the Birmingham cohort. As mentioned briefly in section 3.2.2, we performed p53 immuno-histochemical staining for 60% of cases from the Birmingham cohort using the DO-1 clone, whilst the staining patterns for the remaining 40% was retrieved from the relevant slide archives. A total of 65 tumour sections (65%) showed aberrant diffuse overexpression of p53 in >80% of tumour cell nuclei (example shown in Figure 4.1). Twenty-four cases (24%) showed a null pattern with complete absence of p53 in tumour cell nuclei (example shown in Figure 4.2). A total of 3 cases (3%) showed a cytoplasmic pattern of p53 expression (example shown in Figure 4.3). Lastly, 8 cases (8%) exhibited a heterogeneous/mosaic pattern of p53 expression. These mosaic cases are a newly recognised pattern in HGSOC that is rarely reported in the literature which we will consider in more details later in this chapter. They included 7

cases that showed a combination of over-expression and wild type-like staining pattern (example shown in Figure 4.4), and one case with over-expression and cytoplasmic staining (Figure 4.5). These data highlight the different p53 protein expression patterns in HGSOC in our cohort with p53 overexpression being dominant in our cohort.

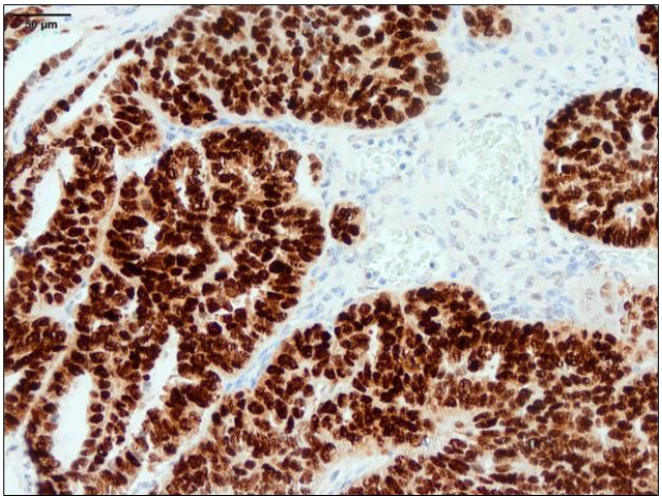

Figure 4. 1: A HGSOC case from the Birmingham cohort demonstrating aberrant p53 overexpression by immunohistochemistry. More than 80% of tumour nuclei exhibit strong staining for p53 (anti-p53, x20 magnification).

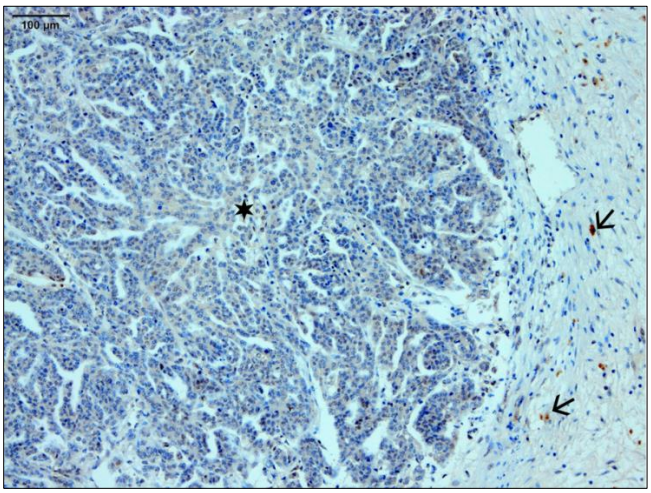

Figure 4. 2: A HGSOC case from the Birmingham cohort demonstrating aberrant null phenotype of p53 staining by immunohistochemistry. Note the complete absence of staining in tumour cell nuclei (star) compared to the scattered focal staining in the surrounding, non-cancerous stroma (arrows) that represents wild-type staining. Background wild-type staining is important because it indicates that the internal control reacted to the antibody and hence a true null pattern rather than a technical error (anti-p53, x10 magnification).

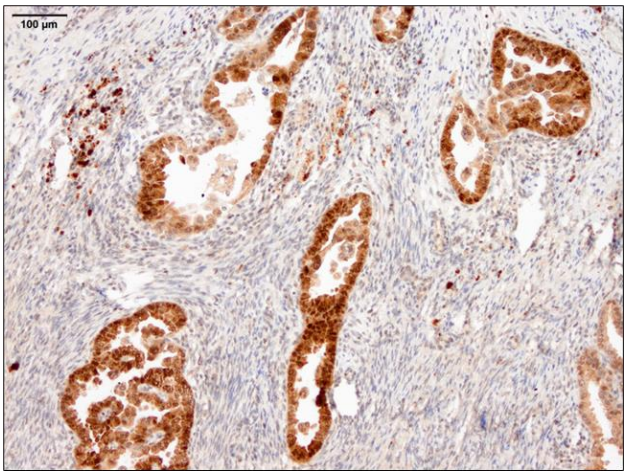

Figure 4. 3: A HGSOC case from the Birmingham cohort demonstrating cytoplasmic p53 staining. Cytoplasmic p53 staining here is unequivocal accompanied by variable nuclear staining but without nuclear overexpression (anti-p53, x10 magnification).

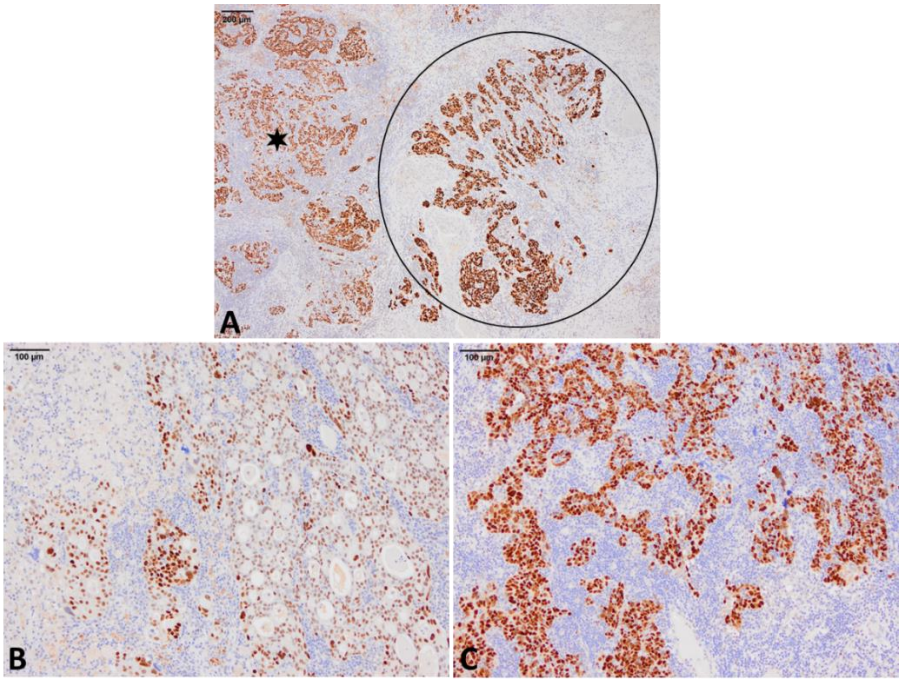

Figure 4. 4: A case of HGSOC from the Birmingham cohort showing mosaic pattern of p53 staining. A) Scanning view highlights an overexpression pattern (circle) and a wild-type like pattern (star) (anti-p53, x4 magnification). B) Higher power view of wild-type like type staining showing focal strong, some moderate but mostly weak nuclear staining (anti-p53, x10 magnification).C) Higher power view of the overexpression focus demonstrating strong diffuse nuclear staining in more than 80% of tumour cell nuclei (anti-p53, x10 magnification).

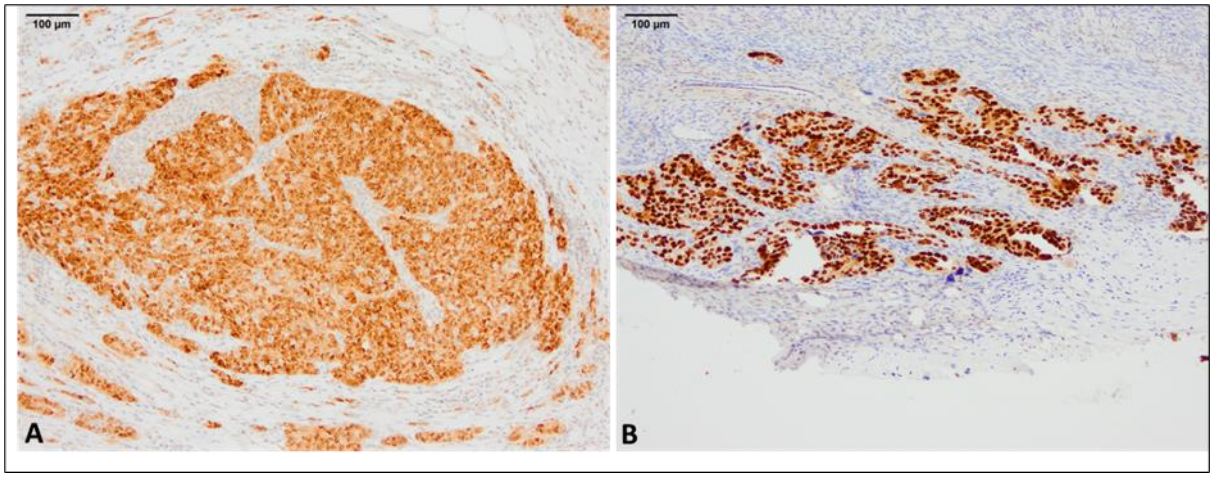

Figure 4. 5: Another case of HGSOC with the mosaic p53 expression pattern. A) A focus of cytoplasmic p53 expression in the tumour (anti-p53, x10 magnification). B) Another focus in the same tumour with strong nuclear overexpression of p53 (anti-p53, x10 magnification).

4.3 Heterogeneous relationship between p53 and UbcH10 at the protein level in HGSOC

4.3.1 Overview

We next proceeded to investigate the relationship between the different p53 IHC staining patterns and UbcH10 expression by IRS and H-scores. The main aim of this analysis was to explore whether p53 GOF mutants promoted high UbcH10 expression. We first analysed UbcH10 as a continuous variable to improve statistical power and explored the difference in its levels between the different p53 IHC staining patterns. For this analysis we applied the Kruskal-Wallis (*H*) test. This was then followed by applying the IRS and H-score cut-offs to see if biologically different UbcH10 expression groups correlated with p53 expression patterns. For this analysis we applied Pearson's Chi-square (X^2) test. As a rule, because the Chi-square test becomes invalid with smaller number of observations in the different subgroups, we combined subgroups to achieve statistical significance without impacting the validity of the Chi-square test.

4.3.2 UbcH10 levels do not differ significantly between p53 IHC staining patterns

When analysing UbcH10 as a continuous variable, the median UbcH10 expression levels were not significantly different between the different p53 expression groups including the p53 mosaic pattern (Table 4.1).

Table 4. 1: The relationship between p53 and UbcH10 at the protein level including the p53 mosaic pattern. When analyzing UbcH10 expression using IRS and H-scores as continuous variables without cut-offs, the median IRS score for cytoplasmic p53 was higher than the other three groups, but this difference was not statistically significant. The median H-score for UbcH10 expression was similarly highest in the cytoplasmic p53 pattern, followed by the null pattern, the overexpression pattern and lowest in the mosaic pattern. The difference was again statistically not significant.

P53 IHC expression category	**Number of patients**	**UbcH10 expression** ***Mdn*** ***(Min, Max)***	**Kruskal-Wallis test** ***(H)***
		IRS	
Overexpression	65	6 (0, 12)	**1.65** ***(p*=0.648)**
Null	24	6 (1, 11)	
Cytoplasmic	3	8 (6, 10)	
Mosaic	8	6 (4, 11)	
Total	**100**	**6 (0, 12)**	
		H-score	
Overexpression	65	95.2 (0, 229)	**0.739** ***(p*=0.864)**
Null	24	106.9 (3, 175.8)	
Cytoplasmic	3	120 (57.8, 180)	
Mosaic	8	81.1 (31.2, 170)	
Total	**100**	**98.3 (0, 229)**	

IHC: immunohistochemistry**, Mdn**: median, **Min:** minimum, **Max**: maximum, **a**: combination of overexpression and wild-like/cytoplasmic

4.3.3 Low and High UbcH10 protein levels do not correlate significantly with the aberrant p53 protein-staining patterns

4.3.3.1 p53 and UbcH10 using IRS

After analysing UbcH10 as a continuous variable we tried to see if UbcH10 expression groups based on IRS correlated with any of the p53 staining patterns. The samples which over-expressed UbcH10 protein (>7) represented a minority (29%) of the whole cohort, whilst 71% had low UbcH10 protein levels (≤7). Because mosaic p53 cases had p53 overexpression as a common component of their staining, they were combined with pure p53 overexpression cases for the purpose of this exercise. When considering the expression levels of both UbcH10 and p53, only 22% of this cohort showed p53 overexpression and high UbcH10 expression, while 19% showed low or absent UbcH10 levels (≤7) and absence of p53 expression. In fact, the majority of p53 overexpression cases (51%) polarized to the low UbcH10 expression category. Two of the cytoplasmic p53 cases had high UbcH10 expression and one had low UbcH10 expression (Figure 4.6 A)

4.3.3.2 p53 and UbcH10 using H-score

When considering UbcH10 expression by H-score, cases which overexpressed UbcH10 (>120) constituted 33% of the cohort whilst low UbcH10 cases (≤120) represented 67% of the cohort. The distribution of the p53 overexpressing HGSOC with respect to H-score was similarly shown to be heterogeneous with 24% showing both p53 and UbcH10 overexpression (including mosaic cases), and 16% showing p53-null and low or absent UbcH10 expression. A total of 49% of p53 overexpressing HGSOC cases polarized to the low UbcH10 expression category. One cytoplasmic p53 case had high and two had low UbcH10 expression (Figure 4.6 B)

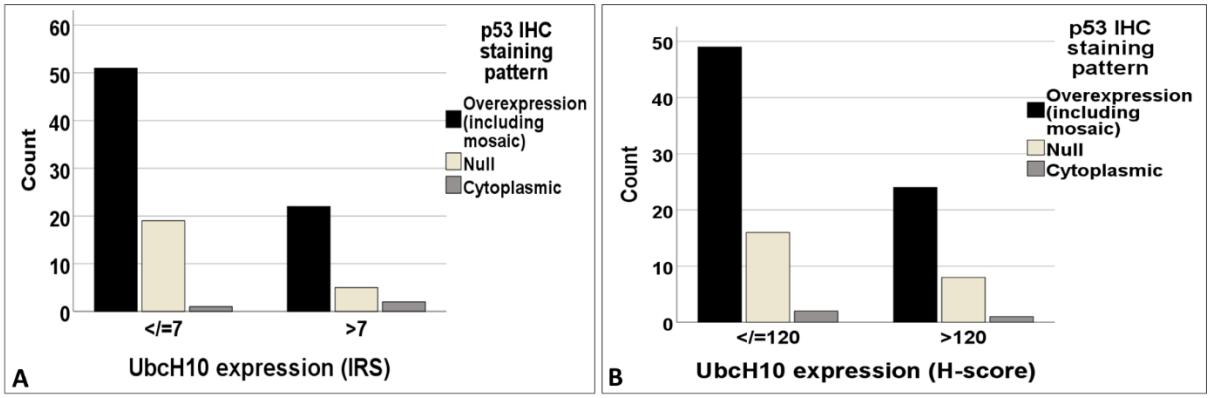

Figure 4. 6: The distribution of the HGSOC patients in the Birmingham cohort according to p53 immuno-histochemical staining pattern relative to UbcH10 expression levels A) IRS and B) H-score. The bar charts highlight the heterogeneous relationship between UbcH10 and p53 at the protein level. Only 22-24% of cases overexpressed both proteins, while 16-19% of cases showed low to absent levels of both proteins. A total of 51% of patients overexpressed p53 and polarized to the low UbcH10 expression group by IRS in Figure A, while 49% polarized to the low UbcH10 expression group by H-score in Figure B.

4.3.3.3 No significant association between UbcH10 protein levels and aberrant p53 protein expression groups

To explore the relationship between UbcH10 and p53 further, we combined p53 expression patterns into groups and compared those groups using the Chi-square test. For statistical reasons and due to the small numbers of cytoplasmic (3%) and mosaic (8%) p53 patterns, we combined patients with overexpression and mosaic into one group and those with cytoplasmic and null into a second group. There was no significant association between these combined p53 expression groups and the UbcH10 expression categories by IRS or H-score (Table 4.2). We can deduce from these data that this heterogeneous relationship does not corroborate a directly proportionate relationship between p53 and UbcH10 expression levels.

Figures 4.7 and 4.8 show correlative UbcH10 and p53 expression levels by immunohistochemistry to highlight the heterogeneous relationship between the two proteins.

Table 4. 2: The relationship between UbcH10 expression by both IRS and H-scores and p53 expression by IHC. UbcH10 expression categories did not correlate significantly with the p53 IHC expression patterns.

UbcH10 protein expression	**P53 IHC staining pattern**		**Total**	**Pearson Chi-square (X^2) test**
	Over-expression and mosaic[a]	**Null and Cytoplasmic**		
IRS category				**0.612 (*p*=0.434)**
≤7	51	21	**72**	
>7	22	6	**28**	
Total	**73**	**27**	**100**	
H-score category				**0.002 (*p*=0.966)**
≤120	49	18	**67**	
>120	24	9	**33**	
Total	**73**	**27**	**100**	

IHC: immunohistochemistry, **a**: combination of overexpression and wild-like/cytoplasmic

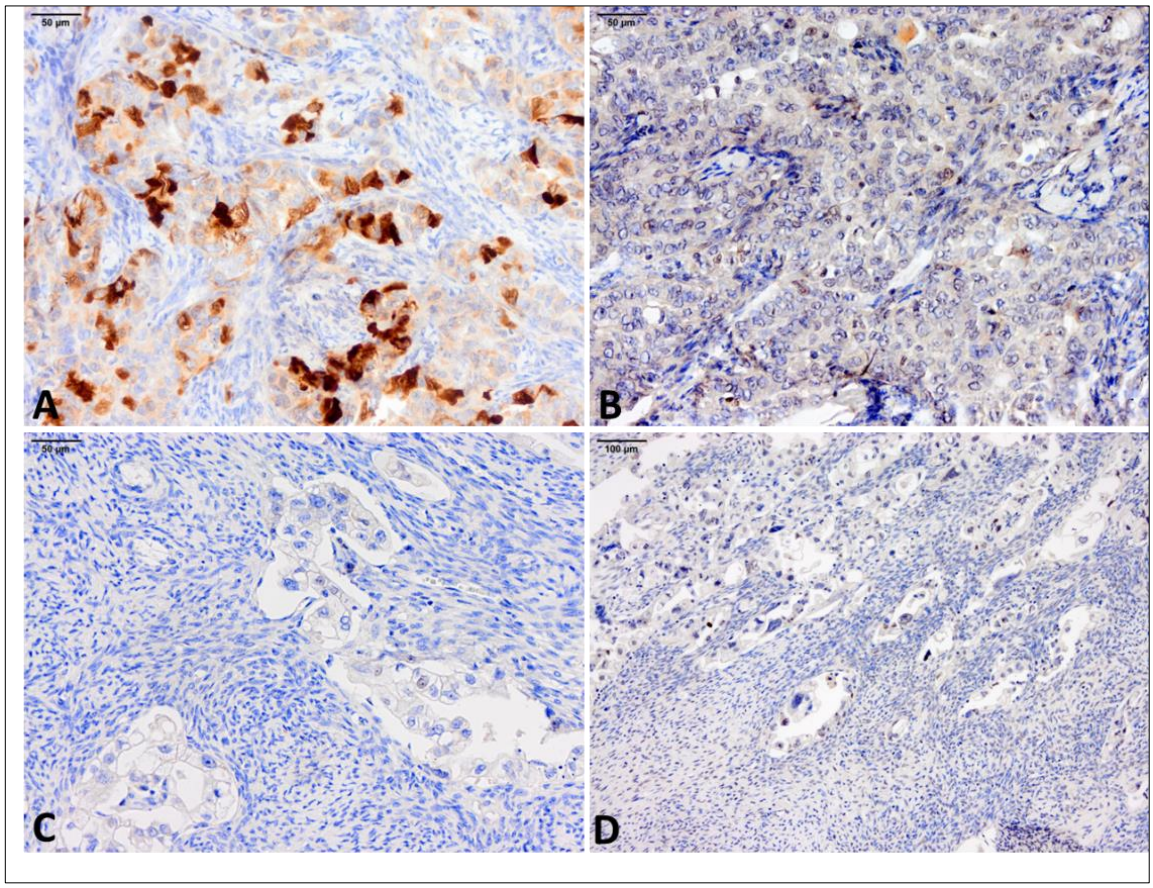

Figure 4. 7: The relationship between UbcH10 expression and p53 null mutant HGSOC in the Birmingham cohort. A) A HGSOC case showing high UbcH10 expression (IRS 8, H-score 120; anti-αUbcH10, x20 magnification). B) p53 of the HGSOC in panel A showing complete absence of nuclear staining (anti-p53, x20 magnification). C) Another HGSOC case showing absent staining for UbcH10 (anti-αUbcH10, x20 magnification). D) p53 staining of the HGSOC in panel C showing aberrant null pattern (anti-p53, x10 magnification).

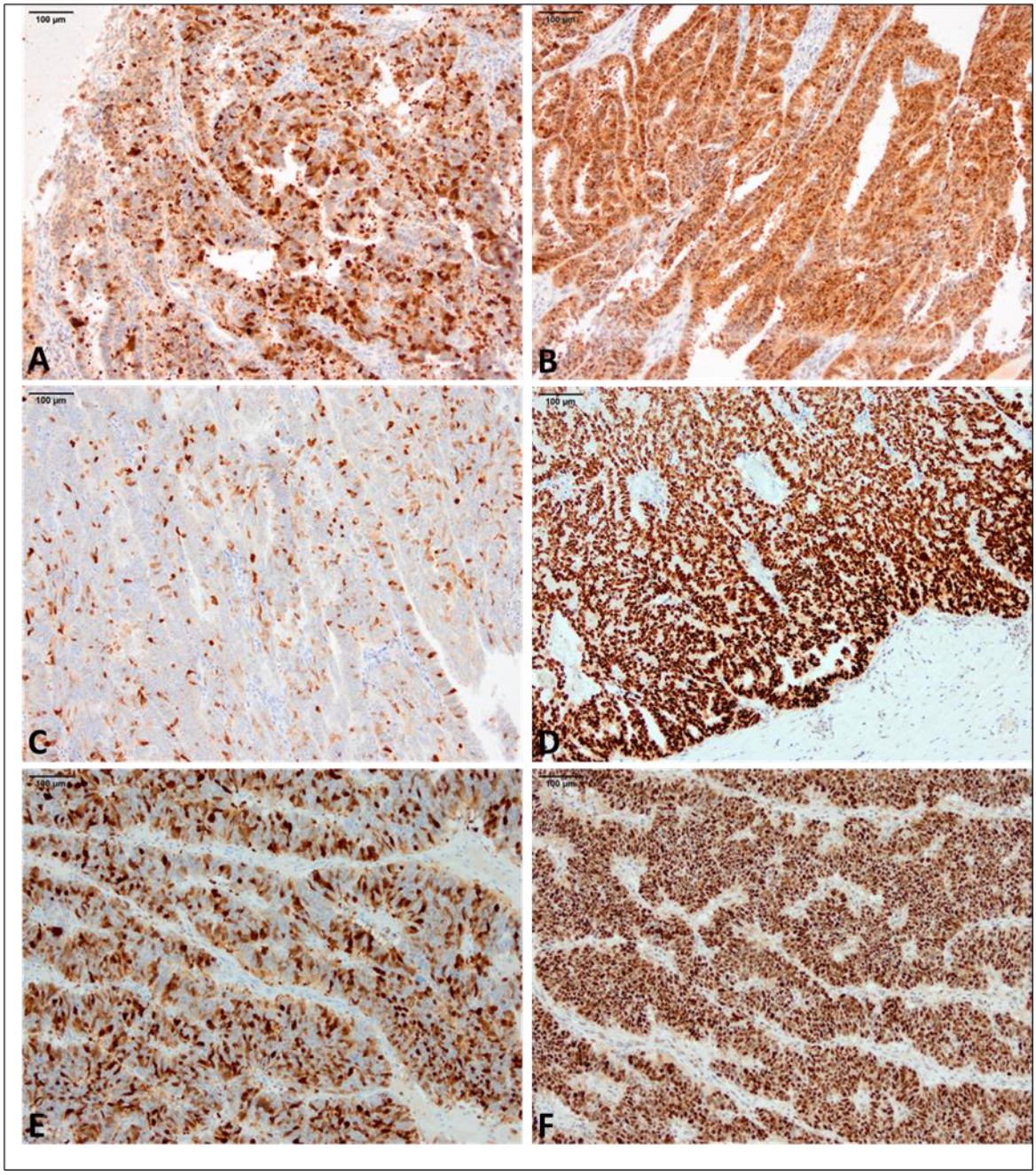

Figure 4. 8: The relationship between UbcH10 expression and aberrant p53 overexpression and cytoplasmic patterns in HGSOC in the Birmingham cohort. A) A case of HGSOC with high UbcH10 expression (IRS10, H-score180; anti-UbcH10, x10 magnification). B) Corresponding p53 from case A showing unequivocal cytoplasmic staining in the absence of strong nuclear staining (anti-p53, x10 magnification). C) A second case of HGSOC with low UbcH10 expression levels (IRS 6, H-score 95; anti-UbcH10, x10 magnification). D) strong nuclear staining for p53 in >80% of nuclei of case shown in panel C (anti-p53, x10 magnification). E) A third case of HGSOC with high UbcH10 expression (IRS 12, H-score 229; anti-UbcH10, x10 magnification). F) Corresponding p53 overexpression from the patient shown in panel E (anti-p53, x10 magnification).

4.4 The prognostic impact of aberrant p53 protein expression on patient survival in the Birmingham cohort

4.4.1 Overview

After investigating the relationship between UbcH10 and p53 at the protein level, we then explored the impact of the various p53 IHC staining patterns including the p53 mosaic pattern on OS and PFS in the Birmingham cohort. The aim of this analysis was to address the conflicting literature about the prognostic impact of p53 in HGSOC. Kaplan-Meier curves and the Log rank ($X^{2)}$ test were used to test the survival differences between the different p53 IHC staining patterns.

4.4.2 P53 immunohistochemical expression patterns did not influence HGSOC mortality

Firstly, we explored the impact of different p53 protein expression levels on overall survival of HGSOC patients in the Birmingham cohort. When comparing median overall survival between the different p53 IHC staining patterns, the patients with mosaic pattern of p53 staining had the shortest median OS whilst the patients with cytoplasmic p53 staining had the longest median OS (Figure 4.9). Moreover, p53 mosaic patients had the 2nd highest death rate while the p53 overexpression group exhibited the lowest death rate (Figure 4.9). These differences, however, were found to be statistically not significant (Table 4.3).

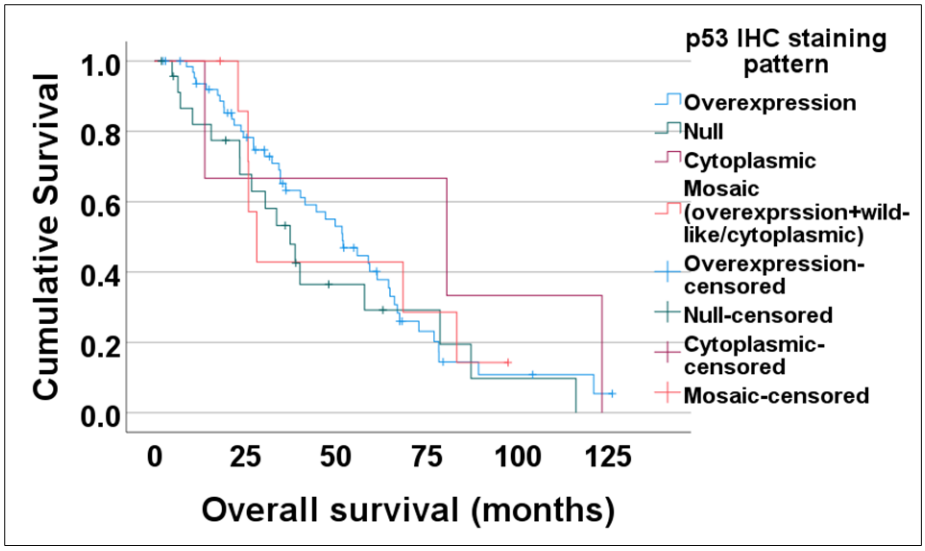

Figure 4. 9: A Kaplan-Meier curve demonstrating the effect of p53 immunohistochemical expression patterns on overall survival in the Birmingham cohort. The median OS survival was the worst for the mosaic group (orange line, Median OS=28.2 months), followed by the null pattern (green line, median OS=37.4 months). This was followed by the overexpression pattern (blue line) at a median OS of 51.8 months, while the longest median OS was for the cytoplasmic group (red line) at 80.5 months. These differences were not statistically significant (Log rank X^2=2.073, p=0.557).

Table 4. 3: The effect of p53 immuno-histochemical expression patterns on overall survival in the Birmingham cohort. The cytoplasmic expression group had the longest median OS but the highest death rate (100%) at the end of the follow-up period. The mosaic group had the shortest median OS and the 2nd highest death rate of 75%. The null pattern had a death rate of 70.8% and the overexpression group had the lowest death rate of 67.7%. These differences were not statistically significant (Log rank X^2=2.073, p=0.557).

P53 IHC staining pattern	Number of patients	Number of events	Median OS in months (95% CI)
Overexpression	65	44	51.8 (40.4, 63.2)
Null	24	17	37.4 (25.9, 48.8)
Cytoplasmic	3	3	80.5 (0.0, 187.2)
Mosaic	8	6	28.2 (22.4, 33.9)
Total	**100**	**70**	**49.7 (37.8, 61.7)**

IHC: immunohistochemistry**, OS:** overall survival, **95% C.I**: 95% confidence interval.

4.4.3 P53 immunohistochemical expression patterns did not influence HGSOC progression

Secondly, we investigated the role of p53 expression on HGSOC progression. When comparing the median PFS, the cytoplasmic p53 expression group had the shortest median PFS, while the null cases had the longest PFS. The recurrence rate was highest for the cytoplasmic group followed by the mosaic group. The null group had the lowest recurrence rate. The difference was statistically not significant (Figure 4.10 and Table 4.4).

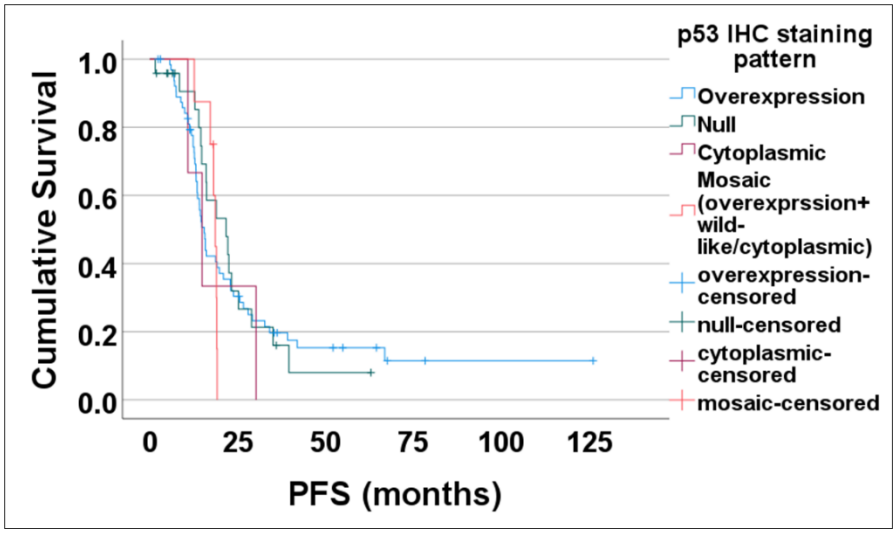

Figure 4. 10: A Kaplan-Meier curve demonstrating the effect of p53 immunohistochemical expression patterns on progression free survival in the Birmingham cohort. The median PFS was shortest for the cytoplasmic group (red line,14.9 months) followed by the overexpression group (blue line, median PFS=15.5 months). This was followed by the mosaic group (orange line, median PFS=18.6 months) and lastly the null group (green line, median PFS=21.7 months). These differences were not statistically significant (Log rank X^2=0.602, p=0.896).

Table 4. 4:The effect of p53 immuno-histochemical expression patterns on progression free survival in the Birmingham cohort. The cytoplasmic expression group experienced the shortest PFS and the highest recurrence rate (100%) at the end of the follow-up period. The mosaic group had the 2nd highest recurrence rate (87.5%). The overexpression group had a recurrence rate of 78.4% and the null group had the lowest recurrence rate at 70.8%. These differences were not statistically significant (Log rank X^2=0.602, p=0.896).

P53 IHC staining pattern	Number of patients	Number of events	Median PFS in months (95% CI)
Overexpression	65	51	15.5 (13.7, 17.3)
Null	24	17	21.7 (13.2, 30.2)
Cytoplasmic	3	3	14.9 (8.4, 21.3)
Mosaic	8	7	18.6 (17.4, 19.8)
Total	**100**	**78**	**16.1 (13.2, 19.1)**

IHC: immunohistochemistry**, PFS:** progression-free survival, **95% C.I**: 95% confidence interval.

We can conclude from the above data that p53 protein expression does not affect HGSOC OS or PFS in this cohort. Mosaic p53 HGSOC had relatively higher death and recurrence rates than p53 over-expression and null HGSOC, but the difference was not statistically significant. These results will be considered further in the discussion.

4.5 The predictive role of aberrant p53 protein expression in HGSOC chemotherapy response in the Birmingham cohort

4.5.1 Overview

After investigating the effect of aberrant p53 protein expression on patient survival, we then looked at its role in chemotherapy resistance in HGSOC patients from the Birmingham cohort. To try and achieve statistical significance, we combined p53 over-

expressing HGSOC with mosaic p53 cases into one group, and p53 null and cytoplasmic into a second group. This is due to the small number of observations in the p53 IHC staining pattern subgroups which would impact the validity of the Chi-square test.

4.5.2 Aberrant p53 protein expression was not predictive of chemotherapy response or resistance to platinum therapy

To investigate the role of p53 in predicting chemotherapy resistance, we examined p53 protein expression in relation to the CRS in the 68 females from the Birmingham cohort who received NACT. No significant association was found between the p53 expression groups and the degree of response to chemotherapy (Table 4.5).

We then examined the relationship between p53 protein expression and resistance to platinum therapy. Again, no significant association was found between the p53 expression groups and platinum resistance (Table 4.5).

Table 4. 5: The relationship between aberrant p53 protein expression patterns and the measures of treatment response in the Birmingham cohort. P53 protein expression did not correlate significantly with chemotherapy response score, or platinum resistance as indicated by the *p*-value of the Chi-square tests.

Chemotherapy response score	**P53 IHC staining pattern**		**Total**	**Pearson Chi-square test (X^2)**
	Over-expression and mosaic	**Null and Cytoplasmic**		
Minimal	20	7	27	**0.612 (*p*=0.434)**
Partial and complete	30	11	41	
Total	**50**	**18**	**68**	
Platinum resistance				**1.03 (*p*=0.310)**
Yes	20	4	24	
No	40	15	55	
Total	**60**	**19**	**79**	

IHC: immunohistochemistry

These data indicate that p53 protein expression cannot predict resistance to chemotherapy in HGSOC from this cohort.

4.6 The significance of mosaic p53 protein expression in HGSOC patients from the Birmingham cohort

4.6.1 Overview

We highlighted earlier (Table 4.1) that mosaic p53 immuno-histochemical staining pattern did not correlate significantly with UbcH10 protein levels. In addition, although patients with mosaic p53 pattern showed relatively higher death and recurrence rates compared to the p53 over-expressing and null patients, their survival did not differ significantly from the other p53 expression groups (Figures 4.9 and 4.10). We therefore

proceeded to explore the significance of the mosaic p53 pattern with respect to its relationship to the different clinico-pathological parameters in the Birmingham cohort. To do this, we included an additional patient, diagnosed with HGSOC more recently, with this new pattern to the 8 cases from the Birmingham cohort bringing the total to 9 mosaic/heterogeneous p53 cases.

4.6.2 Clinico-pathological features of HGSOC patients with mosaic p53 expression pattern

We looked first at the patient characteristics of the mosaic p53 expression pattern. The 9 HGSOC females with p53 mosaic expression were aged between 42 and 74 with (*Mdn*=64.5). All 9 (100%) patients had advanced FIGO stage disease. Five out of 9 patients (55.6%) had nodal disease, while 4 (44.4%) had no nodal disease or lymph nodes were not submitted. A total of 8 patients (88.9%) underwent DDS and one patient (11.1%) underwent PDS. The outcome of the surgery in all 9 (100%) patients was optimal or complete cytoreduction. Concerning the 8 patients that underwent DDS, 3 (37.5%) showed minimal response and 5 (62.5%) showed partial and complete response to NACT. Only 7 (77.8%) out of 9 patients had platinum resistance data, two (28.6%) of which experienced platinum resistance and 5 (71.4%) were non-platinum resistant. Only 5 (55.6%) out of 9 patients had *BRCA* mutation data available, 2 (40%) of which were wild type *BRCA-1 and BRCA-2,* and 3 (60%) were *BRCA* mutant. The *BRCA* mutant cases included one patient with a *BRCA-1* frameshift mutation in exon 11, one with an unspecified *BRCA-1* mutation and one with a *BRCA-2* frameshift deletion (*BRCA-2* variant c.4398_4402del p. frameshift deletion).

4.6.3 Mosaic p53 protein expression does not correlate with the clinico-pathological parameters from the Birmingham cohort

We then explored the relationship between the mosaic p53 expressing HGSOCs with the clinical and pathological parameters in the Birmingham cohort. To focus more on the mosaic patients as one group and to avoid statistical bias that arises when comparing 4 subgroups with limited number of observations, we had to omit two subgroups. We excluded the null and cytoplasmic p53 cases being the smaller subgroups from this analysis and compared the mosaic cases (9 patients) to the p53 over-expressing HGSOC cases (65 patients). We used the Mann-Whitney and Fisher's exact tests for this type of analysis. Analyses revealed that the mosaic p53 expression pattern did not correlate significantly with any prognostic or predictive parameter in the Birmingham cohort (Table 4.6).

Table 4. 6: The relationship between HGSOCs with mosaic p53 expression pattern and clinico-pathological parameters from the Birmingham cohort. The mosaic p53 cases were compared to the p53 overexpression group. The distribution of clinico-pathological parameters in this cohort did not differ significantly between the mosaic p53 cases and the p53 overexpression group.

Patient characteristic	Mosaic p53 pattern[a] (n=9)	P53 Overexpression (n=65)	Test of significance (*p*-value)
Age, year ***Mdn*** ***(Min, Max)***	 64.5 (42, 74)	 65 (40, 84)	Mann-Whitney=245 *p*=0.791
FIGO stage, *n* Early (I, II) Late (III, IV)	 0 9	 4 61	Fisher's exact 2-sided significance=1
LN status, *n* Nx & N0 N1	 4 5	 37 28	Fisher's exact 2-sided significance=0.455
Type of surgery, *n* PDS DDS	 1 8	 22 42	Fisher's exact 2-sided significance=0.096
Cytoreduction, *n* R0 & R1 R2	 9 0	 55 10	Fisher's exact 2-sided significance=0.588
CRS, *n* [b] Minimal Partial and Complete	 3 5	 17 25	Fisher's exact 2-sided significance=1
Platinum resistance, *n* [c] Yes No	 2 5	 18 35	Fisher's exact 2-sided significance=1
BRCA status, *n* [d] Mutant Wild type	 3 2	 11 11	Fisher's exact 2-sided significance=1

Mdn: median**, Min:** minimum**, Max:** maximum**, Nx**: LN not submitted**, N0:** no LN metastasis**, N1:** LN metastasis**, DDS:** delayed debulking surgery**, PDS:** primary debulking surgery**, R0:** complete cytoreduction**, R1:** optimal cytoreduction, **R2:** suboptimal cytoreduction**, CRS:** chemotherapy response score.
A: combination of overexpression and wild-like/cytoplasmic

b: data available for patients only undergoing DDS *n*=50 (8 mosaic cases and 42 overexpression cases)

c: data available for only *n*=60 patients (7 mosaic cases and 53 overexpression cases)

d: data available for only *n*=27 patients (5 mosaic cases and 22 overexpression cases)

4.6.4 Mosaic p53 expression in *BRCA* mutant HGSOC patients

4.6.4.1 Mosaic p53 expression correlates with different tumour morphology

Because of the small number of the mosaic cases and the scarcity of *BRCA* mutation data, we could not find a significant association at the statistical level. From a histopathological perspective however, it was interesting to note that the different p53 staining patterns correlated with different morphological patterns in *BRCA* mutant patients with mosaic p53 expression. Areas where the tumour assumed a glandular or pseudo-endometrioid pattern had mostly wild-type like p53 staining, while papillary areas showed p53 overexpression (Figure 4.11).

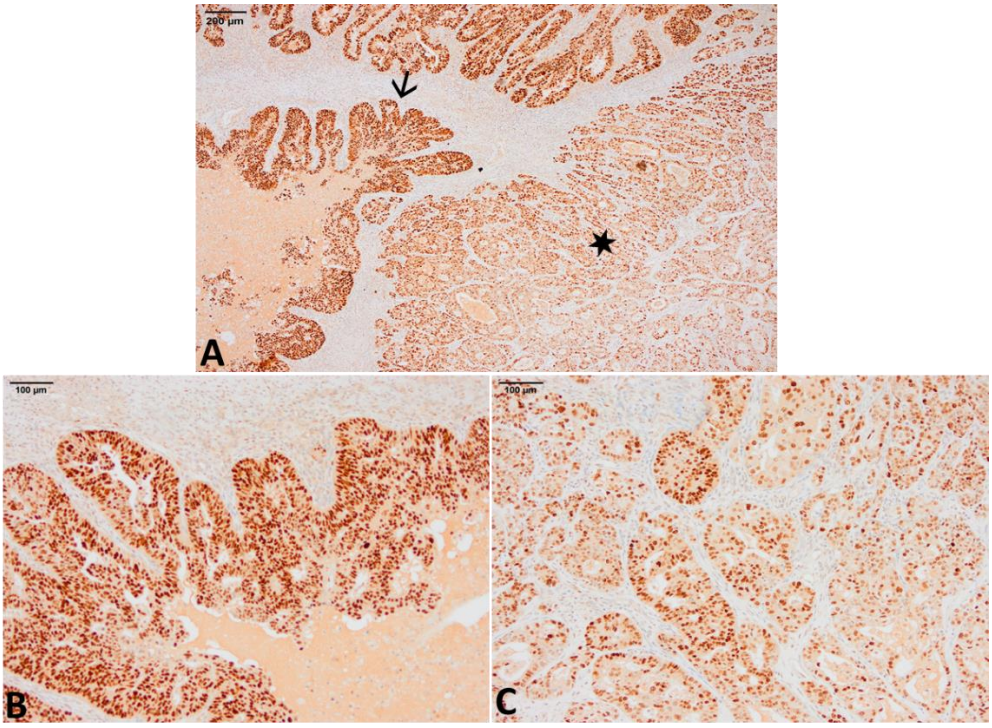

Figure 4. 11: Mosaic P53 expression in a *BRCA-2* mutant HGSOC patient. A) Scanning power view showing a combination of overexpression in the papillary component of the tumour (arrow) and wild-type like pattern in the glandular and pseudo-endometrioid component (star) of the tumour (anti-p53, x4 magnification). B) Higher power view of papillary p53 overexpressing focus from panel A (anti-p53, x10 magnification). C) Higher power view of the glandular pseudo-endometrioid component with wild-type like p53 staining pattern from panel A (anti-p53, x10 magnification).

4.6.4.2 Differential UbcH10 and Ki-67 expression in mosaic p53 cases

To explore the theme of mosaic p53 expression in *BRCA* mutant HGSOC patients further, we next used multiplex immunohistochemistry to ascertain whether HGSOC with different morphology and p53 expression patterns had different UbcH10 and Ki-67 expression levels. Both UbcH10 and Ki-67 protein expression levels were found to be different in the 2 components of p53 mosaic tumours. Papillary areas in the tumour which overexpressed p53 had high UbcH10 and Ki-67 expression, while glandular areas with p53 wild-type like staining had low UbcH10 and Ki-67 levels (Figure 4.12).

It is important to note that the number of *BRCA*-mutant patients with mosaic p53 expression is too small to achieve any solid statistical conclusion.

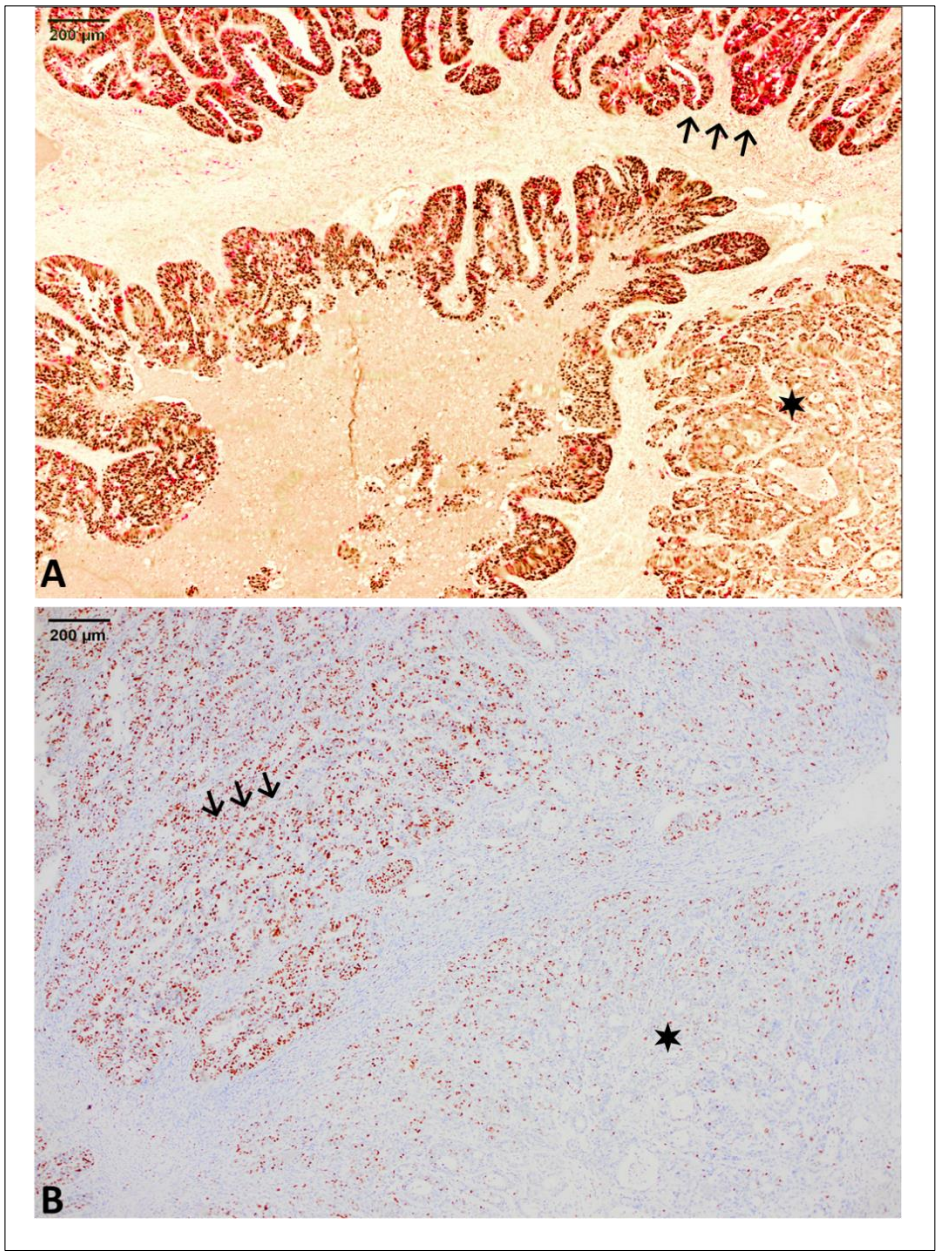

Figure 4. 12: Differential UbcH10 and Ki-67 expression in mosaic p53 expressing *BRCA-2* mutant HGSOC from the previous Figure 4.11. A) Multi-plex immunostaining for both p53 (brown) and UbcH10 (red) was performed. UbcH10 is noticeably elevated in p53 overexpressing papillary areas of the tumour (arrows, IRS 9, H-score 180) compared to the p53 wild-like staining glandular areas (star, IRS 6, H-score 92) (anti-UbcH10, anti-p53, x4 magnification). B) Ki-67 index was markedly elevated (53%) in papillary p53 overexpressing areas (arrows) compared to only 15% in the glandular areas [star, anti-Ki67(MM-1), x4 magnification].

4.6.5 Suboptimal results for *TP53* gene amplification in the mosaic p53 cases

We next proceeded to validate the findings of mosaic p53 expression by IHC at the molecular level. To do this, we first extracted the DNA from the different parts of the tumour with different p53 expression patterns in the 9 samples. Subsequently, we attempted to amplify the DNA binding domain of the *TP53* gene in those samples. We chose primer pairs 3 to 10 covering exons 4 to 8 in the *TP53* gene (Table 2. 6). Upon running of a DNA gel to visualize the amplicons after PCR reaction, the bands failed to be visualized. We reasoned that this could be to the poor quality of the DNA extracted from the samples similar to the previous failed attempts at *Ube2C* gene amplification. Direct sequencing of those cases was therefore not possible and further testing was not continued due to time restraints which did not allow further optimization of PCR.

4.6.6 Conclusion

We can conclude from the above data that our small series of HGSOC patients with mosaic p53 expression show different, albeit non-significant, biological behaviour from the other well-established p53 protein expression groups in terms of survival. Mosaic p53 cases in our series were all advanced stage and mostly received pre-operative chemotherapy and about 30% were BRCA mutant. They also show differential expression of UbcH10 and Ki-67 proteins. Numbers were too small to achieve statistical significance. Nevertheless, mosaic p53 expression holds promise for future research especially in patients with *BRCA* mutations.

4.7 Discussion

The Cancer Genome Atlas study on HGSOC in 2011 was among the first papers to revolutionise our understanding of the genetic background of HGSOC (50). This was preceded by a benchmark study in 2010 which identified *TP53* mutations as a ubiquitous driver mutation in pelvic high-grade serous carcinomas (132). Several subsequent studies confirmed *TP53* mutation as a universal and defining feature of HGSOC required for disease initiation (133). Although studies have linked *TP53* mutations to aggressive behaviour in human cancer including ovarian cancer, its role in HGSOC prognosis however is not well established (79, 134).Therefore, we studied the effect of p53 protein expression on patient outcome and chemotherapy resistance in the Birmingham cohort. In addition, we explored the relationship between UbcH10 and p53 at the protein level in the same cohort since previous reports identified p53 GOF mutants to upregulate UbcH10 expression (104) and because the exact relationship between the 2 protein is poorly understood in HGSOC patients.

4.7.1 Aberrant p53 protein expression in HGSOC

Our findings indicated that p53 over-expression was the dominant aberrant expression pattern in our cohort (65%) followed by the null pattern (24%). This was followed the mosaic pattern (8%) and lastly the cytoplasmic pattern (3%). Apart from the mosaic pattern, our data from section 4.2 is mostly consistent with previous reports on tubo-ovarian high grade serous carcinoma (76, 135).

4.7.2 P53 as a prognostic and predictive marker in HGSOC

With respect to the prognostic and predictive role of p53 aberrant protein expression, our findings are somewhat different from previous reports. We detected no significant

impact of aberrant p53 protein expression on HGSOC mortality or progression (Figures 4.9 and 4.10). Additionally, p53 was not predictive of chemotherapy response in HGSOC in the Birmingham cohort (Table 4.5). One previous study highlighted that *TP53* mutations contributed to the metastatic potential of ovarian cancer, and their resistance to chemotherapy. They also demonstrated a negative effect of *TP53* mutations on the PFS and OS of ovarian cancer patients (79). That particular study used fresh frozen tumour sections of a cohort of 178 EOCs of mixed subtypes who received only adjuvant chemotherapy. In addition, they detected *TP53* mutations (both missense and nonsense) in 56% of their patients. This means they were comparing survival between different *TP53* mutant EOCs (including HGSOC) and *TP53* wild-type ovarian cancer and not between different *TP53* mutation statuses in a single pathological tumour type like our cohort. Similarly, they used the same principal to correlate chemotherapy resistance with *TP53* mutant EOCs compared to *TP53* wild type. This might explain why their *TP53* mutant cases were more significantly chemo-resistant because wild-type p53 function is required for both platinum- and paclitaxel-induced apoptosis and cell death (136). Moreover, their results cannot be generalised on a *TP53* mutant cohort of HGSOC like the Birmingham cohort investigated herein. Another study investigated p53 protein expression using an immunofluorescence-based method in a cohort of 141 EOCs of mixed subtypes (137). That study did not investigate conventional IHC expression pattern, but rather divided p53 protein expression into high and low nuclear and cytoplasmic staining using the *X*-tile software we applied for UbcH10 analysis in Chapter 3. They associated high nuclear and cytoplasmic p53 expression levels with better 5-year overall survival and disease-free survival. We contend that their conclusions cannot be directly related to our cohort of

HGSOC as the defined parameters are different. In particular, their quantitative assessment of p53 expression is rather different from our more standardised and widely applicable immune-histochemical technique. In addition, it is not clear whether their p53 protein expression patterns correlated with *TP53* mutation status as opposed to the well-established immune-histochemical aberrant patterns used in our cohort. On the other hand, a study like the one presented here investigated a cohort of 43 EOCs, the majority of which were serous carcinomas of high histological grade. They used direct sequencing of the *TP53* gene from those samples and, like our study, found no role for *TP53* mutation status in chemoresistance or survival of ovarian carcinomas (82).

A more recent study related p53 immunohistochemistry from 3 different cohorts of HGSOC to clinical outcomes (135). They found a significant but weak reduced risk of recurrence in p53 overexpression compared to p53 null HGSOC in one of their cohorts (n=215 HGSOC) on both univariate [HR=0.72, 95% C.I (0.51, 1.00)] and multivariate analysis [HR=0.71, 95% C.I (0.51, 0.99)]. On combined analysis of the three cohorts for a total of 506 HGSOC patients, they found a significant more favourable impact of p53 overexpression on recurrence-free survival in multivariate analysis with stage, age, and residual disease after surgery [HR= 0.70, 95% C.I (0.55–0.89)]. As indicated by the 95% C.I and HR from this study, we contend that the role of p53 protein expression in survival of HGSOC is still only weak or borderline significant. Nevertheless, this highlights the fact that the weakly significant HR they found on initial analysis of one of their cohorts was improved when they combined their cohorts and hence increased their sample size. As such, our results and conclusions might be altered with a larger sample size which, unfortunately, was not available due to the

missing p53 data from the Barts cohort. Having said that, a very recent large multi-centre study on EOCs which included 6,678 cases of HGSOC, EC and CCC provide similar results to our own (138). They used the same IHC staining patterns we applied in our study, and they found no significant difference in the OS of HGSOC cases with abnormal p53 expression patterns which included overexpression, cytoplasmic and null patterns. On the other hand, they found that EC and CCC patients with abnormal p53 expression were at an increased risk of dying compared to those with p53 wild-type pattern. Similar to our conclusions, this study provides persuasive evidence that the abnormal p53 IHC patterns corresponding to *TP53* mutations do not affect HGSOC patients' mortality. The data from this study does indicate that p53 is prognostic in CCC and EC both of which evolve from normal p53 wild type function, acquire a *TP53* mutation, and develop abnormal p53 function. Consequently, *TP53* mutations are not early founder mutations in endometrioid, and clear cell carcinomas (8). In tumours where *TP53* mutations are an early founder mutation like HGSOC, it does not seem to play a strong prognostic role. This is perhaps not surprising since *TP53* mutations are invariably present in all these tumours. Our views are supported by the early study by Ahmed *et al* (132) on 123 high grade pelvic serous carcinomas of ovarian, fallopian tube and peritoneal origin. Ahmed *et al (132)* also found no significant impact of *TP53* mutations on the OS and PFS of high-grade serous carcinoma patients because of its early expression in all the cases. They also found no significant role of *TP53* mutations in chemoresistance in those patients. This role of p53 is very reminiscent of our theory on UbcH10 expression in HGSOC and its role in their prognosis (see Chapter 3).

One important limitation of our study is the lack of correlation of *TP53* variants with protein expression. While this was not possible in the Birmingham cohort, we discuss

this further in analyses done on the publicly available cohort of HGSOC from TCGA in chapter 5. Having said that, a recent study performed survival analysis on TCGA cohort of HGSOC (139). They compared OS between HGSOC with mutations in the DBD (n=428, mostly resulting in p53 overexpression by IHC) and those with mutations in the NLS, TD and NES (n=43, mostly resulting in cytoplasmic p53 by IHC) of the p53 protein. No significant difference in OS was found between the two groups. This highlights the importance of including both p53 protein expression and *TP53* mutation status in future studies on HGSOC.

4.7.3 Mosaic p53 expression; implications for HGSOC

The mosaic p53 expression pattern is an aberrant feature that has rarely been seen in HGSOC. Our cohort included 9 cases of this new pattern, which displayed both over-expression and cytoplasmic, or wild-type like staining (Figures 4.4 and 4.5). Heterogeneous p53 expression by immunohistochemistry is well reported in endometrial carcinomas of endometrioid type (76). In contrast to endometrial serous carcinomas where *TP53* mutation is an early event universally present in all tumours, endometrial endometrioid carcinomas have mostly wild type p53 expression (140). Only 18% of endometrial endometrioid carcinomas are high grade and have *TP53* mutations as an initiating mutation (8, 141). However, certain molecular subtypes of endometrioid carcinomas have a mutator phenotype with a high tumour mutational burden. Such endometrioid carcinomas are either POLE (polymerase DNA epsilon) ultra-mutated or MMR-deficient and thus can acquire sub-clonal *TP53* mutations later on (76, 142). These sub-clonal *TP53* mutations result in p53 overexpression in one part of the tumour in addition to the wild type staining originally present in the rest of the tumour. This ultimately leads to a heterogeneous pattern of p53 expression on IHC.

However, this cannot explain the heterogeneous pattern we observed in HGSOC where *TP53* mutation is an early founder mutation present in all subclones of the tumour. Moreover, the wild-type pattern we observe in our cases is not true wild type but rather wild-type like staining. This is because it likely corresponds to truncating mutations in the C-terminal domain (CTD). These CTD mutations result in a truncated p53 transcript that is not subjected to non-sense mediated decay but is rather detectable at a level similar to wild-type protein but with loss of function nonetheless (76, 139). This is supported by in-vitro experiments which highlighted that *TP53* mutations affecting the CTD resulted in retained p53 protein expression (143). Moreover, it is our experience that the wild-type like and cytoplasmic component of mosaic p53 cases was observed in one section of the tumour but not the other. Consequently, and given the rarity of both patterns and hence the interpretational difficulties when dealing with them in HGSOC (76, 139), we therefore contend that the mosaic pattern is probably overlooked during routine diagnosis, which is probably why we observed 9% of patients with this staining pattern.

As a counterargument, we could argue that our different methodology could be one of the reasons we detected mosaic p53 cases. While most studies applying p53 immunohistochemistry used the DO-7 clone, we used the DO-1 clone for our cohort because it was sourced from David Lane and hence was abundantly available to us (76, 139). However, previous reports have stated comparable results of both clones in FFPE tissue sections. This is because both clones are raised against the N-terminal epitope corresponding to amino acids 20-25 in the TAD of the p53 protein (144, 145). There is however an acceptable number of fallacies that arise from different IHC antibody clones, where some clones could yield weaker staining than others (146). To

overcome this however, we also ran our mosaic p53 cases using the DO-7 clone used in routine diagnostic services for comparison and the results were consistent. In addition, proper optimisation and validation of the DO-1 clone was done before application in IHC (Figure 2.3 Materials and Methods). Another important consideration to bear in mind is that most of our mosaic cases had received pre-operative chemotherapy (Table 4.6). Additionally, one might consider pre-analytical factors such as different levels of fixation in different parts of the tumour which may affect affinity for IHC staining resulting in p53 wild-like staining in an otherwise overexpressing tumour. Therefore, it could be argued that this mosaic pattern of p53 expression observed is just a treatment or fixation artifact. To discuss these three points, we will consider other studies. To overcome IHC fallacies, Park *et al (147)* correlated p53 immunohistochemical results with targeted next generation sequencing (NGS) in 202 cases of HGSOC among ovarian carcinomas of other subtypes. They detected IHC-sequencing mismatch in 9% of their cases and mostly arising due to mutations in the NLS and OD of the p53 protein. These are the mutations responsible for cytoplasmic and wild-like staining pattern in HGSOC (147). Interestingly, among these mismatch cases two cases showed a mosaic IHC staining pattern: one with wild-type like and cytoplasmic and one with overexpression and cytoplasmic similar to one of our patients (Figure 4.5). Moreover, a study compared p53 immunohistochemical expression in matched pre-and post-chemotherapy HGSOC omental samples and found 96% concordance between the paired tumours (148).Finally, To consider fixation artifacts, Köbel *et al* (76) who studied p53 IHC expression in endometrial biopsies and compared the results to their corresponding hysterectomy specimens, found that strong p53 staining is usually resistant to fixation issues and yields similar results in both samples.

This means that the mosaic p53 cases in our cohort could represent two genuinely different *TP53* mutational patterns rather than just a technical error or an effect of treatment. While Direct Sanger sequencing was not possible due to the poor quality of extracted DNA from the tissue blocks, it would be interesting to sequence the different components of our mosaic p53 cases using NGS for future endeavours to stratify these differences in protein staining patterns at the gene level.

4.7.4 Heterogeneous relationship between p53 and UbcH10 at the protein level

Because we were trying to determine the role of UbcH10 in HGSOC, and since p53 mutation is a founder mutation in these tumours, it was logical to address the relationship between the two proteins. Our results determined a heterogeneous relationship between p53 and UbcH10 with only 22-24% of our cases overexpressing both proteins (Figure 4.6); no significant association between UbcH10 and p53 overexpression at the protein level was observed (Table 4.2). In fact, most of the patients with p53 over-expression polarized with low UbcH10 expression. Our findings contradict previous studies on human cancer cell lines that identified certain GOF p53 mutants to upregulate UbcH10 expression through nuclear transcription factor-Y (NF-Y) (104). Observations in lung adenocarcinomas also correlated positively UbcH10 overexpression with p53 mutation (149). On the other hand, wild type p53 has been shown to repress UbcH10 expression in human cancer cell lines through a direct effect on the *Ube2C* gene promotor region (104). However, akin to our results, Gong *et al (116)* demonstrated UbcH10 over-expression in only 38.9% of EOCs, more than 75% of which were serous carcinomas with p53 missense mutation. This could possibly mean that whilst p53 is an early event in HGSOC, UbcH10 might play a later role in

progression, invasion, and metastasis. On the other hand, p53 did not impact HGSOC mortality and progression whilst UbcH10 was borderline significant in the Birmingham cohort. In addition, UbcH10 seems to behave like a proliferative marker in HGSOC as discussed in the previous chapter. This brings us to another possible theory; UbcH10 might also be expressed early in HGSOC and hence does not demonstrate a strong role in the prognostication of these tumours akin to p53. To address the role of UbcH10 in HGSOC progression/proliferation we will consider its co-expression with Ki-67 and p53 in HGSOC precursor lesions using mIHC in chapter 6. Lastly, while we could not investigate the relationship between specific p53 mutations and UbcH10 expression in our cohort, we will explore this relationship in the TCGA cohort detailed in Chapter 5.

4.8 Conclusion

The Birmingham cohort showed a wide range of aberrant p53 protein expression patterns including a newly identified mosaic/heterogeneous staining pattern. Our data do not corroborate a directly proportional relationship between p53 and UbcH10 protein expression but rather a heterogeneous relationship between the two proteins. P53 protein expression did not predict mortality or progression nor was it predictive of chemotherapy response of HGSOC patients. Mosaic p53 expression pattern in HGSOC is a very recently identified pattern that requires further investigation.

Chapter 5. Ube2C gene expression and its relationship with *TP53* mutations and clinico-pathological parameters in The Cancer Genome Atlas (TCGA) cohort of ovarian serous cancer

5.1 Introduction

According to TCGA database, the *Ube2C* gene is among the most amplified genes in human malignancies including ovarian serous carcinomas. In this regard, *Ube2C* gene amplification is also associated with chromosomal mis-segregation and promotion of cell-cycle progression (93). On the other hand, *TP53* is the most commonly mutated gene in human malignancies including HGSOC (Introduction sections 1.5 and 1.6). Various mutations can affect the *TP53* gene including missense and nonsense mutations, which are especially common in HGSOC (41). Other mutations include in-frame and frameshift insertions and deletions as well as splice site mutations (41).

As discussed in Chapter 1 section 1.6.1, the majority of p53 mutations in HGSOC affect the central DBD and most commonly they are missense mutations (41). Moreover, HGSOC patients having missense mutations grouped by their structural location within the DBD have been shown to have significantly different OS and recurrence rates (71). Concerning functional impact, missense mutations may result in LOF, or GOF mutants or mutants that exert a DNE (66). Missense mutations mostly result in p53 overexpression by immunohistochemistry (77). The null pattern on the other hand, occurs with LOF mutations including nonsense, frameshift, and splicing mutations

(139). Furthermore, certain p53 GOF mutants have been shown to promote metastasis and chemoresistance in HGSOC patients (81).

In the previous chapters, UbcH10 protein expression was found to be only of borderline prognostic significant in our cohorts while p53 aberrant protein expression was not prognostic at all. In addition, we did not find a significant directly proportional association between the two proteins. Given that p53 is a transcription factor and has been suggested to regulate *Ube2C* mRNA levels in earlier reports, we wanted to expand further on these studies and explore the relationship between p53 and UbcH10 at the gene level. Due to the expense involved, we could not apply this to our cohort, so we chose to interrogate TCGA database. Our main aim in this chapter is to explore the prognostic impact of *Ube2C* gene expression and p53 mutational status on patient outcome as well as the relationship between both genes in the publicly available TCGA cohort of ovarian serous carcinomas. Normalised gene expression data generated from the Illumina RNA-seq platform and clinico-pathological information were downloaded from cBioportal (105) and Firebrowse. (https://gdac.broadinstitute.org/runs/stddata__2016_01_28/). In addition, we investigate the *Ube2C* significantly co-expressed genes to clarify its relationship with other oncogenes and growth-promoting genes in HGSOC.

5.2 The Cancer Genome Atlas (TCGA) cohort of ovarian serous cystadenocarcinomas

5.2.1 Characteristics of TCGA cohort

The Cancer Genome Atlas cohort included 585 ovarian serous carcinomas. The majority of those comprise HGSOC but there are LGSOC as well. The exact number

of patients in each subtype however was not specified in the database as the cohort predates the new classification of ovarian serous carcinomas. Only 307 patients had normalized gene expression data for the *Ube2C* gene and other co-expressed genes. None of the samples in the cohort had matched normal ovarian tissue. In this cohort of 307 ovarian serous carcinoma, we first studied the *Ube2C* significantly co-expressed genes using Spearman's correlation coefficient (*ρ)* and performed initial OS analysis using Kaplan-Meier curves and the Log rank X^2 test.

5.2.2 *Ube2C* is significantly co-expressed with genes involved in mitosis, chromosomal segregation and cell-cycle regulation

To study the role of UbcH10 in ovarian serous carcinoma we first looked at the other co-expressed proteins in TCGA cohort of ovarian serous carcinoma. In the first instance we downloaded normalised gene expression data for 18882 genes in TCGA cohort of 307 ovarian serous carcinoma female patients. The following formula was used to transform gene expression values $\mathbf{[X=\log_2(X+1)]}$ where *X* represents the normalized fragments per kilobase transcript per million mapped reads (FPKM) values. We then used Spearman's correlation coefficient (*ρ)* to detect the *Ube2C* significantly correlated genes. A significant correlation was found between *Ube2C* and a total of 5391 genes but only 2509 were *positively* co-expressed with *the Ube2C* gene*.* We then quantified the correlation as very strong (*ρ>0.8)*, strong (*ρ=0.65-0.79), moderate (ρ=0.40-0.64) and weak (ρ=0.1-0.39).* In all correlations a *q*-value was calculated equivalent to a corrected *p*-value. *Ube2C* correlated strongly and moderately with 37 and 330 genes respectively. The remaining 2142 genes correlated only weakly with *Ube2C*. We then used the HPA and DAVID gene functional classification database to clarify the molecular and biological function of these proteins (150). UbcH10 was found

to be strongly and positively correlated with proteins involved in cell-cycle regulation, chromosomal segregation, and nuclear division examples of which are shown in Table 5.1. The strongest significant positive correlation was found between *Ube2C* and Centromere protein A (*CENP-A*) (*ρ=0.82, q-value=1.21 E^{-42}). CENP-A* is a centromeric protein required for progression through mitosis and chromosomal segregation (151). Figures 5.1 and 5.2 shows the correlation between *Ube2C* and *CENP-A* as well as *BRCA-1,* respectively. Both figures were generated from the cBioportal website (105).

Table 5. 1: The *Ube2C* significantly co-expressed genes in the Cancer Genome Atlas cohort of 307 ovarian serous cystadenocarcinoma.

Spearman's correlation coefficient (*q*-value)	***Ube2C* Co-expressed Genes**	**Molecular and Biological functions[a]**
Strong positive (0.65-0.79) (q=1.57E^{-20} - 4.11E^{-36})	MYBL2, TPX2, AURKB, AURKA, PLK1, CDK1, FAM83D, PIMREG, KIF2C, MND1, HJURP, CCNB2, CDC20, CDCA3, CKS1B, FAM72B, MTFR2, CDC25C, CCNB1, PTTG1, UBE2S, UBE2T, NCAPH, CCNA2, IRC5, MAD2L1, MCM10, NEIL3, NUF2, E2F1, SKA3, TOP2A, TROAP, H2AZ1, FAM72D, RAD51	Chromatin binding Kinase binding APC/C regulator APC/C substrate Purine ribonucleotide binding ↓ Mitosis, nuclear division, cell cycle regulation, chromosomal organisation, and segregation
Moderate positive (0.40-0.64) (q=9.10E^{-07}-2.17E^{-20})	NCAPG, CKS2, KIF4A, CKAP2, NUSAP1, TRIP13, SPC25, CENPM, CDKN3, EXO1, NEK2, NDC80, HMGB2, RACGAP1, PDRG1, MELK, DNTTIP1, KNSTRN, CDCA5, KPNA2, KIF18A, BUB1, CCNE1	Microtubule binding Protein serine/threonine kinase activity ↓ Nuclear division Chromosomal segregation
Weak positive (0.1-0.39) (q=1.9 E^{-05}-2.52E^{-06})	BRCA1, BRCA2	Tubulin and cytoskeleton protein binding ↓ DNA repair and damage response.

a: Molecular and biological function extracted from the Human Protein Atlas and DAVID gene functional classification database (150).

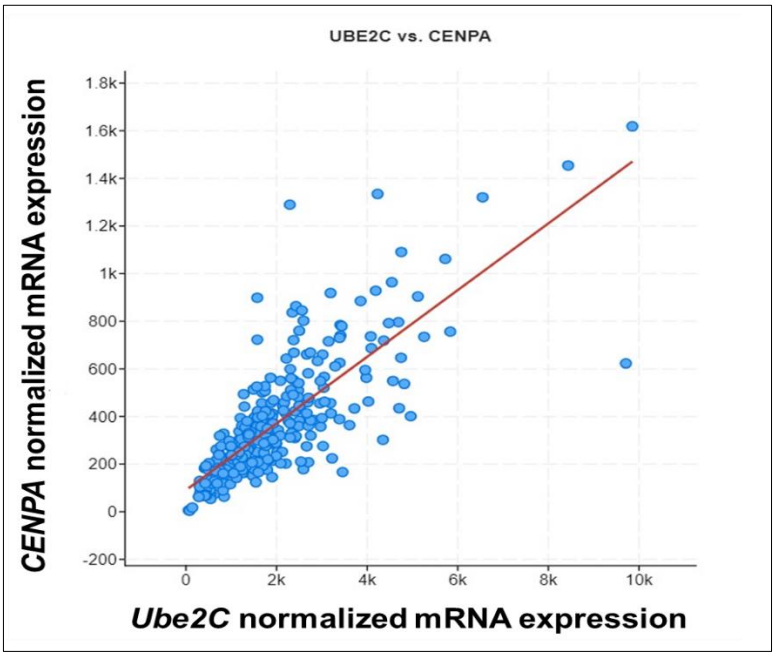

Figure 5. 1: A scatter plot depicting the very strong positive correlation between *Ube2C* and *CENP-A* gene expression levels [Spearman's correlation coefficient *(ρ)=0.82, q-value=1.21 E^{-42}]*.

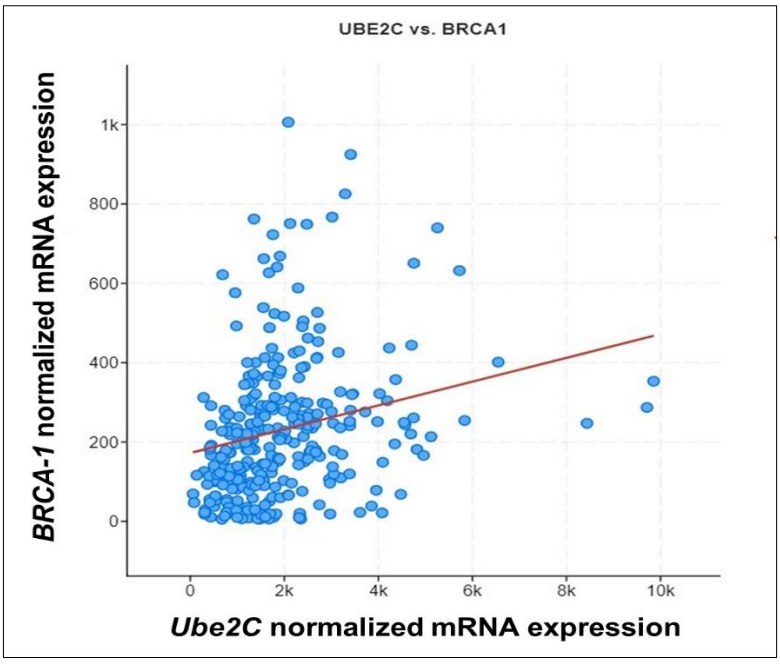

Figure 5. 2: A scatter plot showing the weak positive correlation between *Ube2C* and *BRCA-1* gene expression levels [Spearman's correlation coefficient *(ρ)=0.38, q-value=2.52E-06]*.

5.2.3 *Ube2C* gene expression did not significantly impact mortality of ovarian serous carcinoma patients from TCGA

We next investigated whether *Ube2C* normalised mRNA expression influenced the overall survival of patients form TCGA cohort. *Ube2C* Gene expression values were transformed as **$X=\log_2(X+1)$**. Log_2 expression values of normalized *Ube2C* gene expression ranged from 5.9 to 13.28. We then used a cut-off of 11 to divide the cohort into high (log_2 mRNA values >11) and low *Ube2C (log_2 mRNA values ≤11)* expression and compare survival differences. This cut-off value was generated by *X*-tile, and it closely mirrored the values generated by *X*-tile in the Birmingham cohort with the high expression group being roughly in the upper 30^{th} percentile (Figure 3.2). A total of 110 (36%) patients had high *Ube2C* gene expression and 197 (64%) patients had low *Ube2C* gene expression. Overall survival data was available for 302 patients (109 with high *Ube2C* and 193 with low *Ube2C* gene expression). We found no statistically significant difference in OS between patients with high *and* low *Ube2C* gene expression (Figure 5.3 and Table 5.2). These data indicate that *Ube2C* gene expression has no effect on the mortality of ovarian serous carcinomas from TCGA dataset.

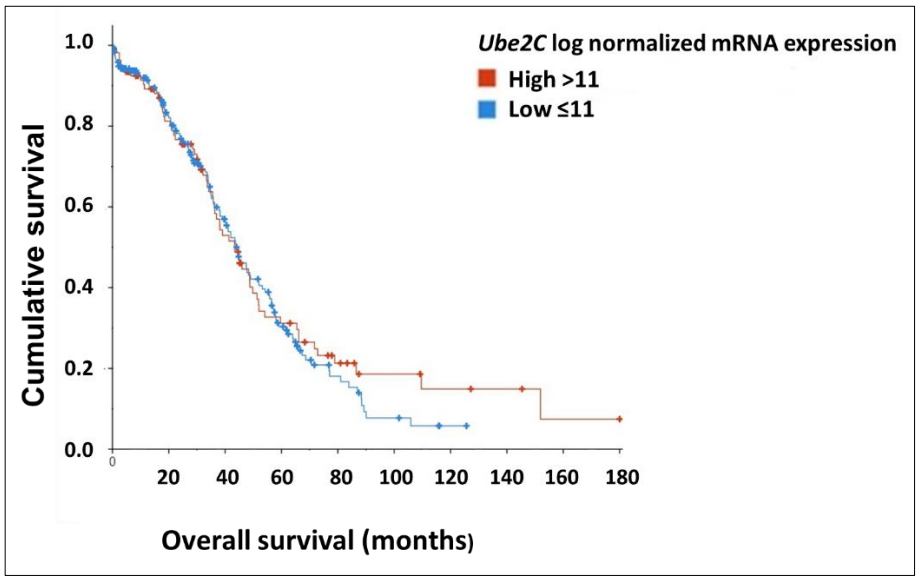

Figure 5. 3: A Kaplan-Meier curve demonstrating the effect of *Ube2C* gene expression on the mortality of ovarian serous carcinoma patients from TCGA. There was no statistically significant difference in overall survival between patients with high *Ube2C* gene expression and those with low expression (Log rank test *p*-value=0.565).

Table 5. 2: The effect of *Ube2C* gene expression on overall survival in the TCGA cohort of ovarian serous carcinoma. The median OS period and the death rate was not significantly different between the high and low *Ube2C* expression groups (Log rank *p*-value=0.557).

***Ube2C* gene expression group[a]**	**Number of patients**	**Number of events**	**Median OS (95% C.I)**
Low (≤11)	193	119	44.3 (38.0-52.0)
High (>11)	109	64	43.4 (36.3-51.33)
Total	**302**	**183**	**44.0 (35.1, 55.6)**

a: normalized mRNA expression data were calculated as $\log_2$ value using the formula: $X=\log_2(X+1)$

OS: overall survival, **95% C.I**: 95% confidence interval.

5.3 High grade serous carcinoma in the Cancer Genome Atlas cohort

In the previous section we used 307 ovarian serous carcinomas from TCGA which included a mixture of HGSOC and LGSOC. In order to focus on HGSOC we narrowed our cohort to ovarian serous carcinomas that showed *TP53* mutations, and which also had corresponding *Ube2C* normalized gene expression data. This downsized our cohort to 163 HGSOC patients.

5.3.1 Clinico-pathological and molecular profile of HGSOC patients from TCGA

5.3.1.1 Age at diagnosis

The cancer genome atlas cohort of HGSOC included 163 females aged between 34 and 87 years (*Mdn*=58). The clinical and pathological features of this cohort, detailed herein, are summarised in Table 5.3.

5.3.1.2 Type of surgery performed, stage of disease and chemotherapy administration

All patients in this cohort underwent PDS followed by adjuvant chemotherapy. The patients in this cohort were staged using the AJCC system (152). None of the patients had received pre-operative chemotherapy. A total of 10 patients (6.1%) had stage II disease, 1 of which (0.6%) was stage IIA, 3 (1.8%) were stage IIB and 6 (3.7%) were stage IIC. The largest stage category was stage III with a total of 130 patients (79.8%), of which 3 (1.8%) patients were stage IIIA, 8 (5%) were stage IIIB and 119 (73%) were stage IIIC. Lastly, a total of 23 patients (14.1%) had stage IV metastatic disease.

5.3.1.3 Ube2C gene expression

The log_2 value of normalised *Ube2C* gene expression ranged from 8.27 to 13.28 (*Mdn*=10.63). The *X*-tile software generated the cut-off value of 11.236 which divided the cohort into high (log_2 >11.236) and low *Ube2C* (log_2 ≤11.236) gene expression groups for later correlations and survival analyses. This cut-off value placed the high *Ube2C* expression group in the upper 25th percentile.

5.3.1.4 TP53 mutational status

We categorized the HGSOC patients into 5 major *TP53* mutation groups. The first two were missense and nonsense mutations both resulting from a single nucleotide polymorphism (SNP) mostly affecting the DBD. The other groups included frameshift deletions/insertions which resulted in disruption of the reading frame, splice site mutations and finally in-frame deletions where the reading frame was preserved. A total of 99 (60.7%) patients had missense mutations, 18 (11%) had nonsense mutations, 19 (11.7%) had frameshift deletions or insertions, 23 (14.1%) had splice site mutations and 4 (2.5%) had in-frame deletions.

With respect to functional impact, missense mutations resulted in a non-functional overexpressed p53 protein with Polyphen-2 (153) functional impact scores ranging between 0.5 and 1. On the other hand, nonsense mutations, frameshift deletions/insertions, splice site mutations and in-frame deletions resulted in a truncated p53 protein that is subjected to nonsense mediated decay.

Following previous reports (67, 71), the 99 cases with *TP53* missense mutations were further classified based on their structural location within the DBD into 9 groups detailed in Table 5.4.

Table 5. 3: The clinico-pathological and molecular profile of HGSOC patients from TCGA cohort.

Patient variable	Number of patients	Percentage	Total
Age, year			
≤58 *(Mdn)*	86	52.8	**163**
>58	77	47.2	
AJCC stage[a]			
II	10	6.1	**163**
III	130	79.8	
IV	23	14.1	
***Ube2C* gene expression**[b]			
≤11.236	123	75.5	**163**
>11.236	40	24.5	
***TP53* mutation category**			
Missense	99	60.7	
Nonsense	18	11	**163**
Frameshift deletion/insertion	19	11.7	
Splice site mutation	23	14.1	
In-frame deletion	4	2.5	

a: all patients underwent primary debulking surgery with no neoadjuvant chemotherapy administered.

B: normalized mRNA expression data were calculated as log2 value using the formula: $X=\log_2(X+1)$

AJCC: American Joint Committee on Cancer Staging

Table 5. 4: The classification of the 99 HGSOC patients from TCGA with missense mutations according to their location within the DNA-binding domain tertiary substructure of the p53 protein. The classification is based on previous reports (71).

Site of missense mutation in p53 DNA-binding domain	Mutation (protein change)	Frequency (%)
DNA major groove interacting residues	**R273H/C/L***, S241Y/F, C277F	12 (12.1)
DNA minor groove interacting residues	**R248Q/W/G**	5 (5.1)
Zinc (Zn) ion coordinating residues	**C176Y/F,** C238F/Y, H178N, H179Q/R, P177R	11 (11.1)
SLH (Sheet loop helix) motif stabilizers	**R282W,** S127Y, E286K	5 (5.1)
Loop2/Loop3 interactions stabilizers	**R175H**	7 (7.1)
Distal loop residues	**Y220C**, V157F	8 (8.1)
Loop 3 stabilizers	**G245C/D/R/S/V**, G244C/D	8 (8.1)
Hydrophobic residues	**I195T/N**, Y236C, V216M, L145R, F270L, I232N, Y234C	15 (15.1)
Other sites**	**Y163C/N**, G266V/R, K132E/N/M, H193R, P278R/H, V274D/G, V272M, P250L, V173L, D259Y, D208V, L194R, H214R, S215R, L130V, G262V, Y205C	28 (28.2)

*Mutations highlighted in bold are the most common in each group

**Mutations not belonging to the above 8 defined groups were categorized as 'other sites'

Additionally, we used the study by Kang *et al* (81) to identify p53 GOF mutants and apply another classification for HGSOC females with *TP53* missense mutations from TCGA (Table 5.5).

Table 5. 5: The classification of the 99 HGSOC patients from TCGA with missense mutations according to whether they generate Gain of Function (GOF) mutants based on previous reports (81).

***TP53* missense mutation type**	**Mutation (protein change)**	**Frequency (%)**
Gain of Function (GOF) mutants	**R248Q/W/G*, R273H/C/L, R282W** S127Y, Y163C/N, V173L, **R175H**, **C176Y**, H179R/Q, L194R, Y205C, H214R, **Y220C**, Y234C, S241F, **G245C/S/V/D**	51 (51.5)
No evidence of gain of function (NE-GOF) mutants	G244C/D, G245R, G266V/R, L130V, D208V, V157F, K132E/M/N, S215R, C238Y, **I195N/T**, Y236C, R337C, C238F, D259Y, V216G/M, E286K, L145R, V274D/G, P250L, V272M, I232N, P278H/R, S241Y, **C176F**, P177R, C277F, F270L, H178N, H193R	48 (48.5)

*Mutations highlighted in bold are the most frequent hotspot mutations.

5.3.2 Survival analysis and patient outcomes in HGSOC patients from TCGA

5.3.2.1 Overview

In this section we explore in general terms the survival data available in TCGA cohort of HGSOC patients

5.3.2.2 Overall survival

Overall survival data was available for 162 (99.4%) out of 163 patients from this cohort. The overall survival period in this cohort ranged from 0.3 to 180 months [Median OS=44.05, 95% C.I (36.40, 51.70)]. At the end of the follow-up period a total of 105 patients (64.8%) had died. The 5-year survival rate of these patients was 31.7%.

5.3.2.3 Progression-free survival

Progression-free survival data was available for 130 (79.7%) out of 163 patients. The PFS period ranged from 2 to 180 months [Median PFS=17.3, 95% C.I (14.6, 19.9)]. At the end of the follow-up period a total of 99 (76.2%) patients had experienced disease recurrence or progression. A total of 33% of patients had experienced disease recurrence or progression in the first year and 76% in the first two years of follow-up.

5.3.3 The prognostic impact of *Ube2C* gene expression on patient outcomes and its relationship with clinico-pathological variables in TCGA HGSOC cohort

5.3.3.1 Overview

In this section we investigate the relationship of *Ube2C* gene expression to the clinical variables from TCGA cohort as well as its impact on HGSOC mortality and progression.

5.3.3.2 Ube2C gene expression do not correlate significantly with age at diagnosis

In the first instance we analyzed *Ube2C* gene expression and age at diagnosis as two continuous variables. A negative but statistically non-significant correlation was found between the two variables using Spearman's correlation coefficient (ρ=*-0.01, p=0.901*). When dividing the females into two groups based on the median age, *Ube2C* gene expression was not significantly different between the two groups (Figure 5.4).

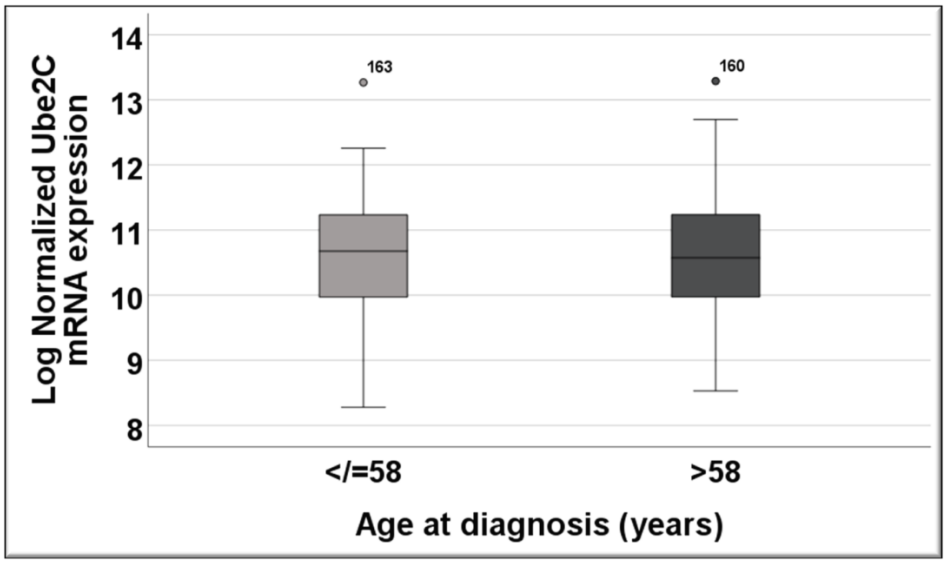

Figure 5. 4: A box plot diagram demonstrating the correlation between *Ube2C* mRNA expression and the age group of patients in TCGA cohort of HGSOC patients. The median log_2 normalized *Ube2C* mRNA expression was not significantly different between patients aged 58 years and below (*Mdn*=10.67) compared to those aged above 58 years (*Mdn*=10.57) (*U*=3292, *p*=0.95).

5.3.3.3 Ube2C gene expression do not correlate significantly with AJCC stage but was lowest in stage IV patients

We next correlated *Ube2C* gene expression with AJCC stage. Stage III patients had the highest median *Ube2C* gene expression, followed by stage II patients, and stage IV patients had the lowest *Ube2C* gene expression. However, the difference was not statistically significant (*H*=2.168, *p*=0.338). These data do not indicate a significant association between *Ube2C* gene expression levels and AJCC stage in TCGA cohort of HGSOC patients. Data are shown in Figure 5.5.

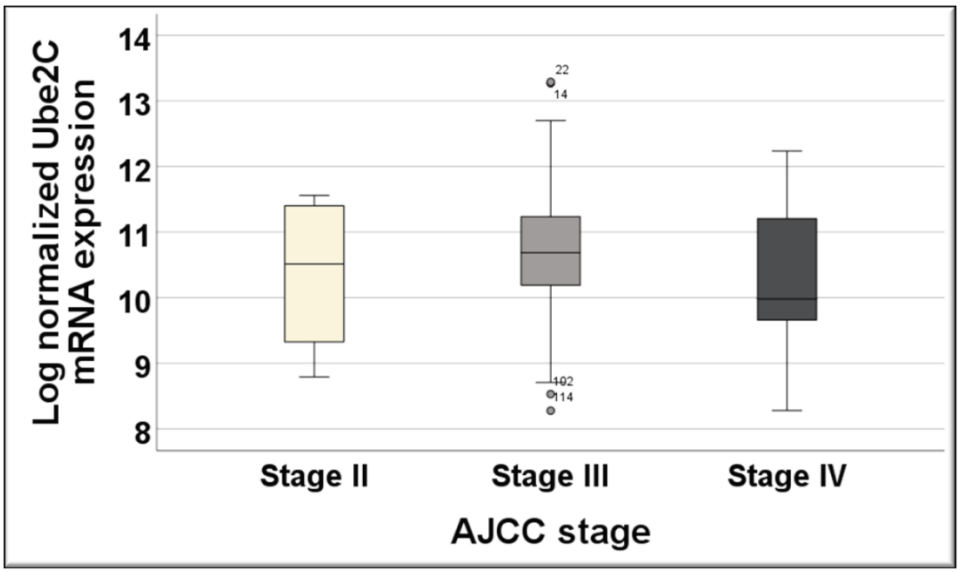

Figure 5. 5: A box plot diagram demonstrating the relationship between *Ube2C* gene expression and AJCC stage in TCGA cohort of HGSOC patients. The median log_2 normalized mRNA expression of *Ube2C* was lowest in stage IV patients (n=23, *Mdn*=9.97), followed by stage II patients (n=10, *Mdn*=10.51) and stage III patients had the highest median *Ube2C* expression (n=130, *Mdn*=10.69). The difference was not statistically significant (*H*=2.168, *p*=0.338).

5.3.3.4 Ube2C gene expression does not impact HGSOC mortality in TCGA cohort

We next investigated the effect of *Ube2C* mRNA expression on overall survival of 162 HGSOC patients from TCGA with OS data. We applied the *X*-tile generated cut-off value of 11.236 to divide the cohort into high (log_2 >11.236) and low *Ube2C* (log_2 ≤11.236) gene expression groups and compared survival using Kaplan-Meier curves.

The median OS was worse, and the mortality rate was higher for the low *Ube2C* expression group compared to the high expression group, although the difference was not statistically significant as indicated in Figure 5.6 and Table 5.6. Taken together, these data indicate that *Ube2C* mRNA expression levels do not impact HGSOC mortality in TCGA cohort.

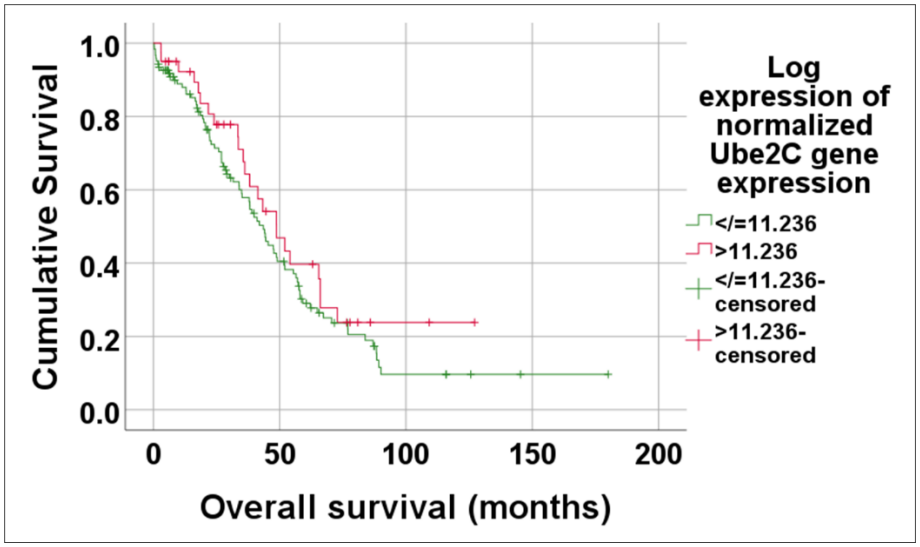

Figure 5. 6: A Kaplan-Meier curve demonstrating the effect of *Ube2C* gene expression on HGSOC mortality in TCGA cohort. Patients with low *Ube2C* gene expression (green line, n=122) had worse median OS (*Mdn*=43.5 months) compared to patients with high *Ube2C* gene expression (red line, n=40, *Mdn*=48.75 months). The difference was not statistically significant (Log rank X^2=1.16, *p*=0.282).

Table 5. 6: The effect of *Ube2C* gene expression on overall survival in the TCGA cohort of HGSOC patients. The median OS was shorter and death rate was higher (67.2%) for the low expression group compared to the higher expression group (57.5%). The difference however was not statistically significant (Log rank X^2=1.16, *p*=0.282).

***Ube2C* gene expression group[a]**	**Number of patients**	**Number of events**	**Median OS (95% C.I)**
Low (≤11.236)	122	82	43.50 (36.80-50.10)
High (>11.236)	40	23	48.75 (35.50-62.00)
Total	**162**	**105**	**44.05 (36.40, 51.70)**

a: normalized mRNA expression data were calculated as $\log_2$ value using the formula: $X=\log_2(X+1)$

OS: overall survival, **95% C.I**: 95% confidence interval.

5.3.3.5 Ube2C gene expression does not impact HGSOC progression in TCGA cohort

Using the same X-tile cut-off values for *Ube2C* gene expression we next explored the difference in PFS between high (log_2>11.236) and low *Ube2C* (log_2≤11.236*)* mRNA expression groups in 130 HGSOC females with PFS data. The median PFS was worse, and the progression rate was higher for the low *Ube2C* expression group compared to the high expression group, although the difference was not statistically significant (Figure 5.7 and Table 5.7). These data indicate that *Ube2C* mRNA expression levels do not impact progression/recurrence rates of HGSOC patients from TCGA cohort.

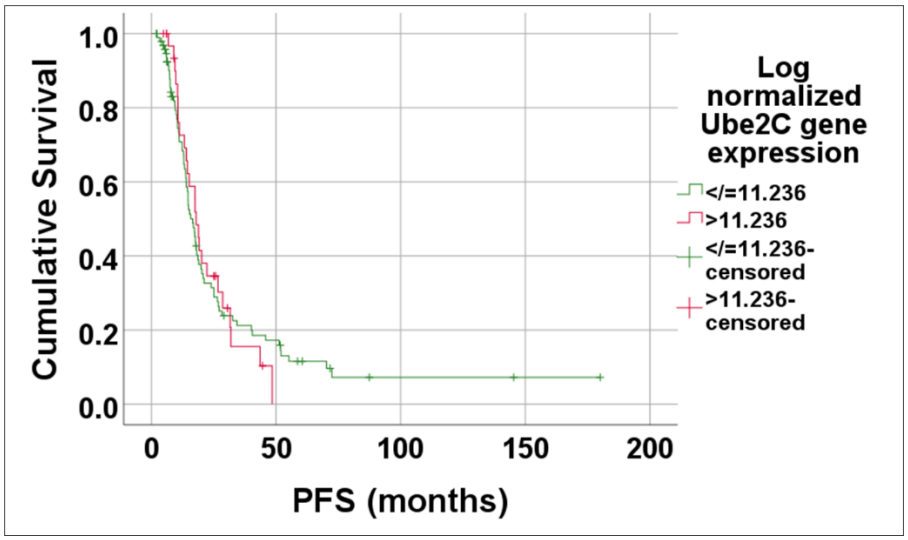

Figure 5. 7: A Kaplan-Meier curve demonstrating the effect of *Ube2C* gene expression on HGSOC progression in TCGA cohort. Patients with low *Ube2C* gene expression (green line, n=197) experienced a worse median PFS (*Mdn*=16.59 months) compared to patients with high *Ube2C* gene expression (red line, n=33, *Mdn*=17.97 months). The difference was not statistically significant (Log rank X^2=0.0, *p*=0.994).

Table 5. 7: The effect of *Ube2C* gene expression on progression-free survival in the TCGA cohort of HGSOC patients. The median PFS was shorter and progression/recurrence rate was higher (76.3%) for the low expression group compared to the higher expression group (75.8%). The difference however was not statistically significant (Log rank X^2=0.0, p=0.994).

***Ube2C* gene expression group[a]**	**Number of patients**	**Number of events**	**Median PFS (95% CI)**
Low (≤11.236)	97	74	16.59 (14.04-19.14)
High (>11.236)	33	25	17.97 (15.55-20.39)
Total	**130**	**99**	**17.30 (14.60, 19.90)**

a: normalized mRNA expression data were calculated as $\log_2$ value using the formula: $X=\log_2(X+1)$

PFS: progression-free survival, **95% C.I**: 95% confidence interval.

5.3.3.6 Ube2C gene expression is not a predictor of mortality or progression in HGSOC patients from TCGA cohort

After exploring the effect of *Ube2C* mRNA expression on OS and PFS in HGSOC patients form TCGA, we wanted to confirm our results by performing univariate Cox regression analysis on the *Ube2C* gene expression values as a continuous variable without cut-offs.

HGSOC patients with higher *Ube2C* gene expression levels were at a *lower* risk of dying (6%) than those with low gene expression levels. The difference was not statistically significant [HR=0.94,95% C.I (0.76, 1.15), p=0.536]. On the other hand, HGSOC patients with higher *Ube2C* gene expression levels had a slightly *higher* risk of progression/recurrence (2.3%) than those with low gene expression. The difference however was not statistically significant [HR=1.023, 95% C.I (0.84, 1.25), p=0.827]. We can therefore conclude that *Ube2C* gene expression levels are not predictors of mortality or progression in HGSOC patients from TCGA cohort.

5.3.4 The prognostic impact of *TP53* mutational status on patient outcomes of HGSOC patients from TCGA

5.3.4.1 Overview

In this section we explore the prognostic impact of the various *TP53* mutations highlighted previously (Tables 5.3, 5.4 and 5.5) on the survival of HGSOC patients from TCGA using Kaplan-Meier curves and the Log rank X^2 test.

5.3.4.2 TP53 mutations do not impact HGSOC mortality

Firstly, we investigated the impact of the 5 major *TP53* mutation groupings (Table 5.3) on the OS of 162 HGSOC patients from TCGA with OS data. The median OS period was shortest for missense mutations and longest for frameshift deletions/insertions. The mortality rate was highest for patients with splice site mutations followed by missense mutations, nonsense mutations, frameshift deletions/insertions and the lowest mortality rate was for in-frame shift deletions' patients. These differences however were not statistically significant as indicated in Figure 5.8 and Table 5.8.

To study the impact of the functional differences of *TP53* mutations on HGSOC survival, we combined LOF mutations that resulted in complete absence of p53 protein in one group (nonsense, frameshift deletions/insertions, splice site, and in-frame deletions) and compared them to missense mutations which resulted in overexpressed p53 protein. The difference in OS was again not statistically significant (Figure 5.9). We can conclude from these studies that *TP53* mutations including those with different functional impacts on the p53 protein do not influence the mortality of HGSOC patients included in TCGA.

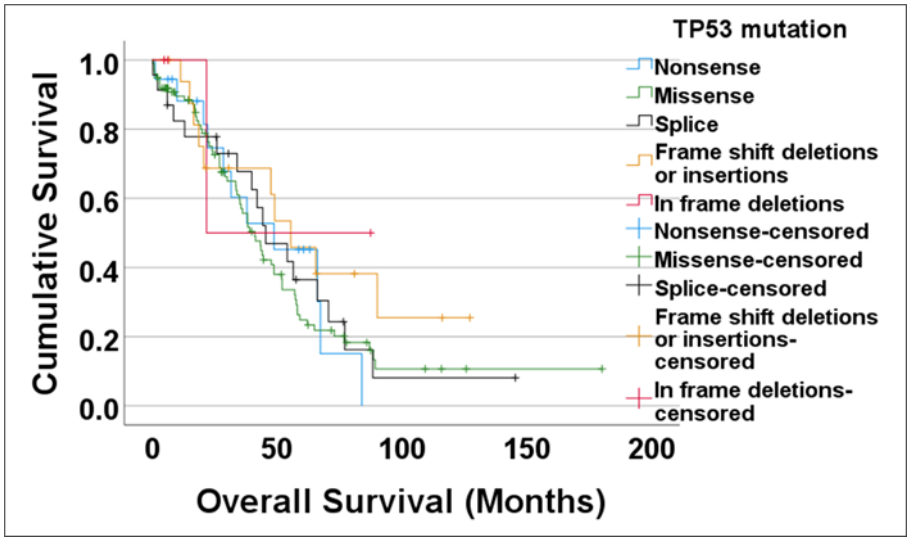

Figure 5. 8: A Kaplan-Meier curve demonstrating the effect of the 5 major *TP53* mutation groups on the mortality of HGSOC females from TCGA. Patients with missense mutations (green line, n=99) had the shortest median OS (*Mdn*=41.03 months). This was followed by patients with splice site mutations (black line, n=23) with a median OS of 45.47 months, and then patients with nonsense mutations (blue line, n=18) with a median OS of 48.75 months. The longest median OS (*Mdn*=55.45 months) was for patients with frameshift deletions/insertions (yellow line, n=18). The median OS was not reached in patients with in-frame deletions (red line, n=4). The difference between the 5 groups was not statistically significant (Log rank X^2=2.6, *p*=0.626).

Table 5. 8: The effect of *TP53* mutations on overall survival in TCGA cohort of HGSOC patients. Patients with splice site mutations had the highest death rate (74%) followed by missense mutations (66.7%), nonsense mutations (61.1%), and frameshift deletions/insertions (55.6%). The lowest event rate was for patients with in-frame deletions (25%). These differences however were not statistically significant (Log rank X^2=2.6, *p*=0.626)

***TP53* mutation**	**Number of patients**	**Number of events**	**Median OS (95% C.I)**
Nonsense	18	11	48.75 (18.89, 78.60)
Missense	99	66	41.03 (33.55, 48.50)
Splice site	23	17	45.47 (28.56, 62.37)
Frame shift deletions/insertions	18	10	55.45 (35.03, 75.86)
In-frame deletions	4	1	incalculable
Total	**162**	**105**	**44.05 (36.4, 51.7)**

OS: overall survival, 9**5% C.I**: 95% confidence interval

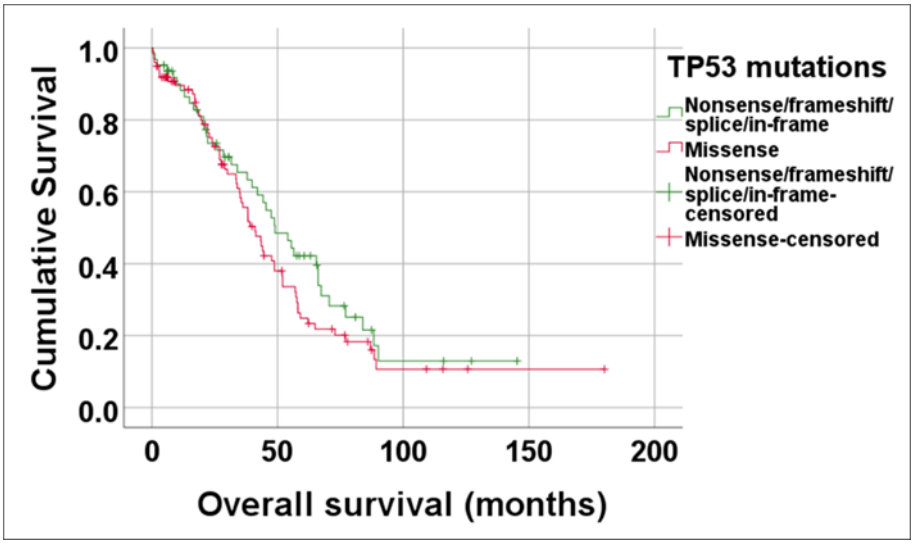

Figure 5. 9: A Kaplan-Meier curve demonstrating the difference in overall survival between patients with *TP53* mutations that have different functional impacts on the p53 protein. Patients with missense mutations that resulted in overexpressed p53 protein (red line, n=99) had a shorter median OS (*Mdn*=41.03 months) and higher event rate (66 out of 99 patients) than patients with the other 4 groups of mutations that resulted in completely absent p53 protein (green line, *Mdn* OS=49.01 months, event rate 39 out of 63 patients). The difference however was not statistically significant (Log rank X^2=1.38, p=0.239).).

5.3.4.3 TP53 mutations do not impact HGSOC progression/recurrence

Next, we investigated the impact of *TP53* mutations on the PFS of 130 HGSOC females from TCGA with PFS data available. Analyses revealed that there was no statistically significant difference in the progression/recurrence rate between the 5 major *TP53* mutational groups (Figure 5.10 and Table 5.9). Moreover, when we compared patients with missense mutations to the 4 other mutational groups combined, to investigate mutations with different functional impacts on the p53 protein, again the difference in PFS was not statistically significant (Figure 5.11). These data indicate that *TP53* mutations including those with different functional impacts on the p53 protein do not impact the progression/recurrence rate of HGSOC females from TCGA.

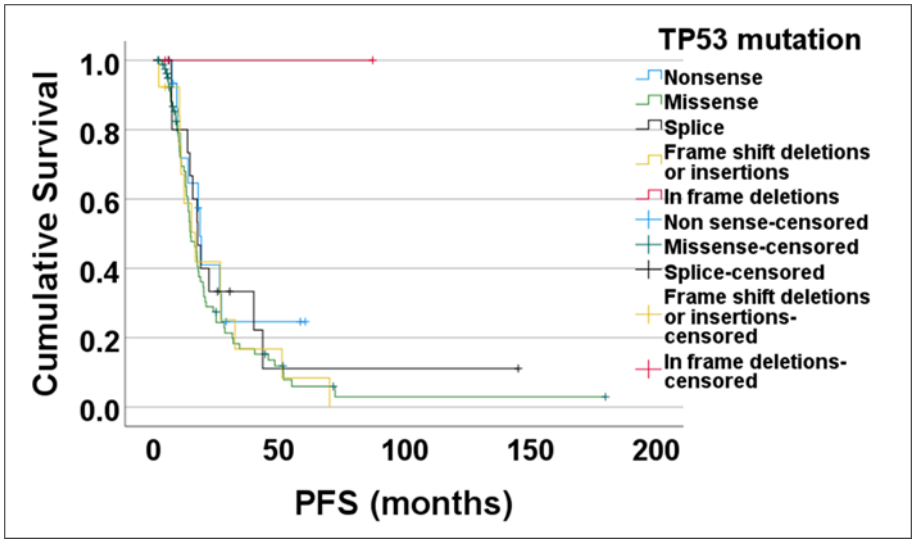

Figure 5. 10: A Kaplan-Meier curve demonstrating the effect of the 5 major *TP53* mutation groups on the progression of HGSOC females from TCGA. The median PFS was the shortest for patients with missense mutations (green line, n=82, *Mdn*=14.91 months), followed by patients with frameshift deletions/insertions (yellow line, n=13, *Mdn*=16.82 months). This was followed by patients with splice mutations (black line, n=16, *Mdn*=17.7 months), while patients with nonsense mutations had the longest median PFS (blue line, n=16, *Mdn*=18.66 months). Patients with in-frame deletions (red line, n=3) did not reach the median PFS. The difference in PFS was not statistically significant (Log rank X^2=5.1, p=0.277).

Table 5. 9: The effect of *TP53* mutations on the progression-free survival in TCGA cohort of HGSOC patients. Patients with frameshift deletions/insertions had the highest progression/recurrence rate (92.3%), followed by patients with missense mutations (79.2%), splice site mutations (75%) and nonsense mutations (62.5%). The lowest progression/recurrence rate was for patients with in-frame deletions (0%). These differences however were not statistically significant (Log rank X^2=5.1, p=0.277)

***TP53* mutation**	**Number of patients**	**Number of events**	**Median PFS (95% C.I)**
Nonsense	16	10	18.66 (16.73, 20.58)
Missense	82	65	14.91 (11.62, 18.20)
Splice site	16	12	17.71 (13.68, 21.73)
Frame shift deletions/insertions	13	12	16.82 (9.32, 24.31)
In-frame deletions	3	0	incalculable
Total	**130**	**99**	**17.30 (14.60, 19.90)**

PFS: progression-free survival, **95% C.I**: 95% confidence interval

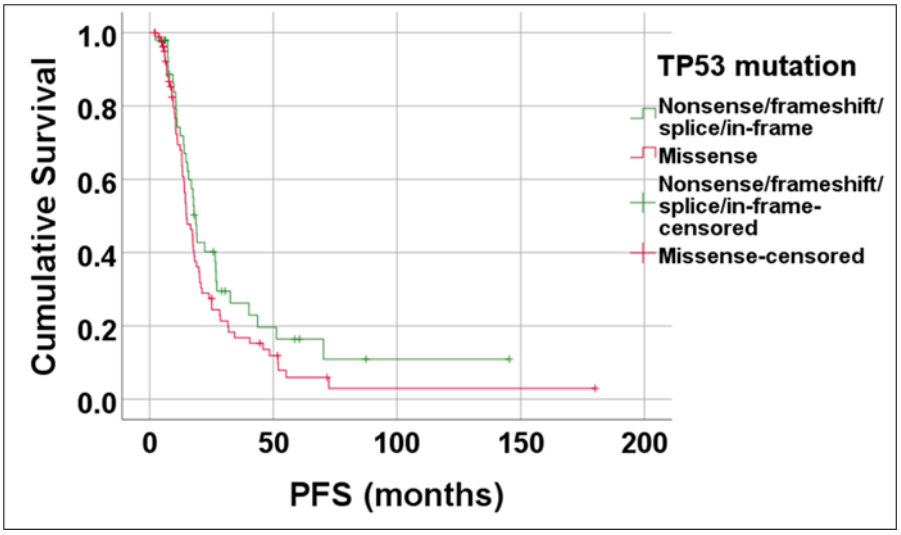

Figure 5. 11: A Kaplan-Meier curve demonstrating the difference in progression-free survival between patients with *TP53* mutations that have different functional impacts on the p53 protein. Patients with missense mutations that resulted in overexpressed p53 protein (red line, n=82) had a shorter median PFS (*Mdn*=14.91 months) and higher event rate (65 out of 82 patients) than patients with the other 4 groups of mutations that resulted in completely absent p53 protein (green line, *Mdn* PFS=18.66 months, event rate 34 out of 48 patients). The difference however was not statistically significant (Log rank X^2=2.25, p=0.134).

5.3.4.4 Structurally grouped TP53 missense mutations do not impact HGSOC mortality

In this section we discuss the impact of the various *TP53* missense mutations on the OS of HGSOC females (n=99) from TCGA. The mutations were grouped based on their location within the DBD tertiary substructure in the p53 protein as into 9 categories previously shown in Table 5.4. Because survival analysis on 9 groups is cumbersome, we performed initial OS analysis and grouped patients with similar median OS into 3 major groups. Patients with the shortest median OS were placed in the high-risk group, patients with the longest median OS were placed in the low-risk group, and patients in between were placed in the intermediate risk category (Table 5.10). Kaplan-Meier curves were constructed and the difference in OS between the three risk groups was

not statistically significant (Figure 5.12 and Table 5.11). We can conclude from these data that *TP53* missense mutations grouped by their structural location in the DBD of the p53 protein have no influence on HGSOS mortality from TCGA.

Table 5. 10: The Classification of the 99 HGSOC females from TCGA with *TP53* missense mutations grouped according to the median overall survival.

High risk group (n=17)	Intermediate risk group (n=58)	Low risk group (n=24)
-DNA major groove interacting residues -SLH (sheet loop helix) motif stabilizers	-Hydrophobic core residues -Loop 3 stabilizers -Loop2/Loop 3 interaction stabilizers -Other missense mutations	-DNA minor groove interacting residues -Distal loop residues -Zinc Ion coordinating residues

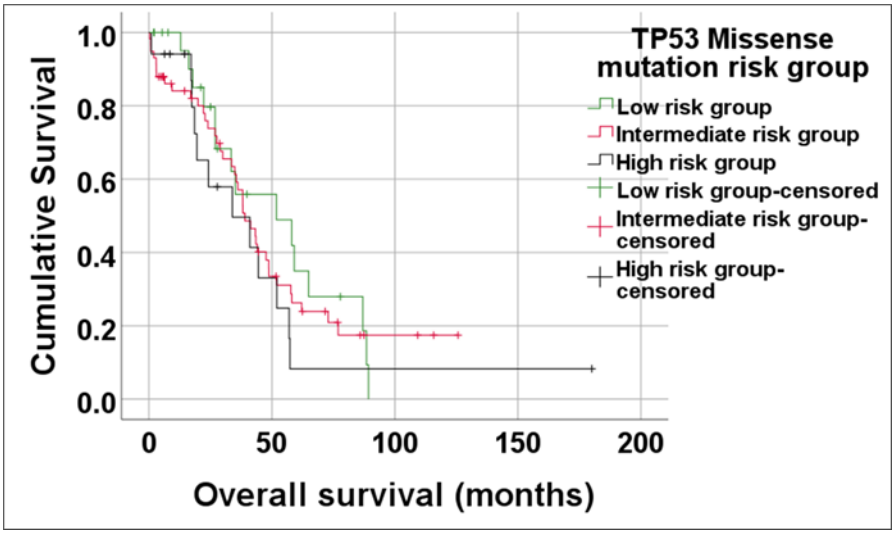

Figure 5. 12: A Kaplan-Meier curve demonstrating the effect of *TP53* missense mutation risk groups on the overall survival of HGSOC females from TCGA. Patients in the high-risk group (black line, n=17) had the shortest median OS (*Mdn*=33.94 months), followed by patients in the intermediate risk group (red line, n=58, *Mdn*=39.06 months). Patients in the low-risk group (green line, n=24) had the longest median OS (*Mdn*=51.87 months). The difference was statistically not significant (Log rank X^2=0.989, *p*=0.61).

Table 5. 11: The effect of *TP53* missense mutation risk groups on the overall survival of HGSOC females from TCGA. Patients in the high-risk groups had the highest death rate (70.6%), while patients in the low-risk group had the lowest death rate (62.5%). Patients in the intermediate risk group had a death rate of 67.2%. The difference was not statistically significant (Log rank X^2=0.989, *p*=0.61).

***TP53* missense mutation risk group**	**Number of patients**	**Number of events**	**Median OS (95% CI)**
Low risk[a]	24	15	51.87 (12.40-91.33)
Intermediate risk[b]	58	39	39.06 (31.19, 46.92)
High risk[c]	17	12	33.94 (6.75, 61.12)
Total	**99**	**66**	**41.03 (33.55, 48.50)**

OS: overall survival, 9**5% C.I**: 95% confidence interval

a: include DNA minor groove interacting residues, distal loop residues, and zinc ion coordinating residues.

b: include hydrophobic core residues, loop 3 stabilizers, loop2/loop 3 interaction stabilizers, and other missense mutations.

c: include DNA major groove interacting residues and SLH (sheet loop helix) motif stabilizers.

5.3.4.5 Structurally grouped TP53 missense mutations do not impact HGSOC progression/recurrence

After exploring the impact of *TP53* missense mutations on HGSOC mortality, we proceeded to apply the same principles to investigate their impact on progression-free survival. For these analyses data was available for only 82 (82.2%) out of 99 patients with *TP53* missense mutations. We compared PFS between the 3 risk groups previously shown in Table 5.10 and the difference was again not statistically significant (Figure 5.13 and Table 5.12). We conclude from these data that *TP53* missense mutations grouped by their structural location in the DBD of the p53 protein have no influence on HGSOC progression/recurrence from TCGA.

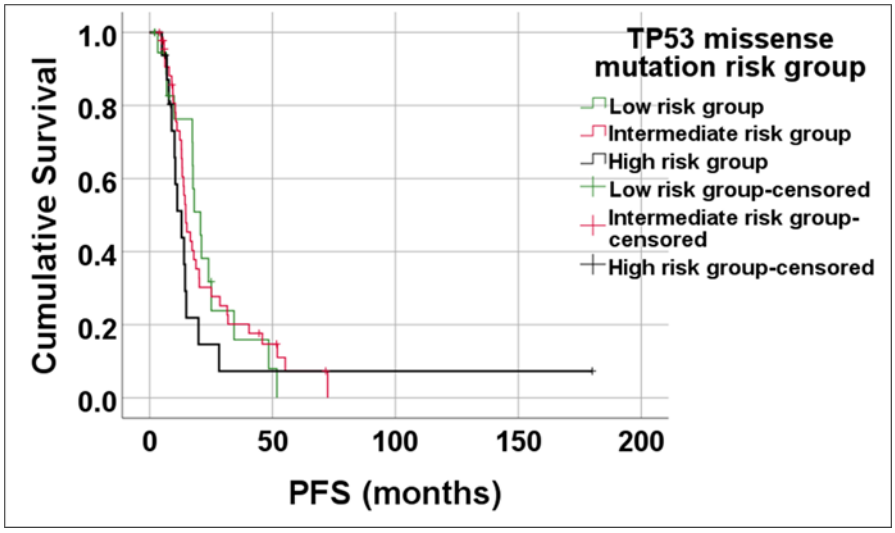

Figure 5. 13: A Kaplan-Meier curve demonstrating the effect of *TP53* missense mutation risk groups on the progression-free survival of HGSOC females from TCGA. Patients in the high-risk group (black line, n=16) had the shortest median PFS (*Mdn*=13.01 months), followed by patients in the intermediate risk group (red line, n=46, *Mdn*=14.72 months). Patients in the low-risk group (green line, n=20) had the longest median PFS (*Mdn*=20.73 months). The difference was statistically not significant (Log rank X^2=1.436, *p*=0.488).

Table 5. 12: The effect of *TP53* missense mutation risk groups on the progression-free survival of HGSOC females from TCGA. Patients in the high-risk groups had the highest progression/recurrence rate (81.25%), while patients in the low-risk group had the lowest death rate (75%). Patients in the intermediate risk group had a death rate of 80.4%. The difference was not statistically significant (Log rank X^2=1.436, p=0.488).

***TP53* missense mutation risk group**	**Number of patients**	**Number of events**	**Median PFS (95% CI)**
Low risk[a]	20	15	20.73 (14.80-26.65)
Intermediate risk[b]	46	37	14.72(11.52, 17.92)
High risk[c]	16	13	13.01 (8.50, 17.51)
Total	**82**	**65**	**14.91 (11.62, 18.20)**

PFS: overall survival, **95% C.I**: 95% confidence interval

a: include DNA minor groove interacting residues, distal loop residues, and zinc ion coordinating residues.

b: include hydrophobic core residues, loop 3 stabilizers, loop2/loop 3 interaction stabilizers, and other missense mutations.

c: include DNA major groove interacting residues and SLH (sheet loop helix) motif stabilizers.

5.3.4.6 Gain of function p53 mutants do not impact HGSOC mortality

In this section we investigate the effect of *TP53* missense mutations that result in GOF p53 mutants previously shown in Table 5.5 on the OS of HGSOC females (n=99) from TCGA. The OS of HGSOC females with GOF mutations were compared to those with NE-GOF and the difference was not statistically significant (Figure 5.14 and Table 5.13), indicating that p53 GOF mutants do not impact HGSOC mortality in TCGA cohort.

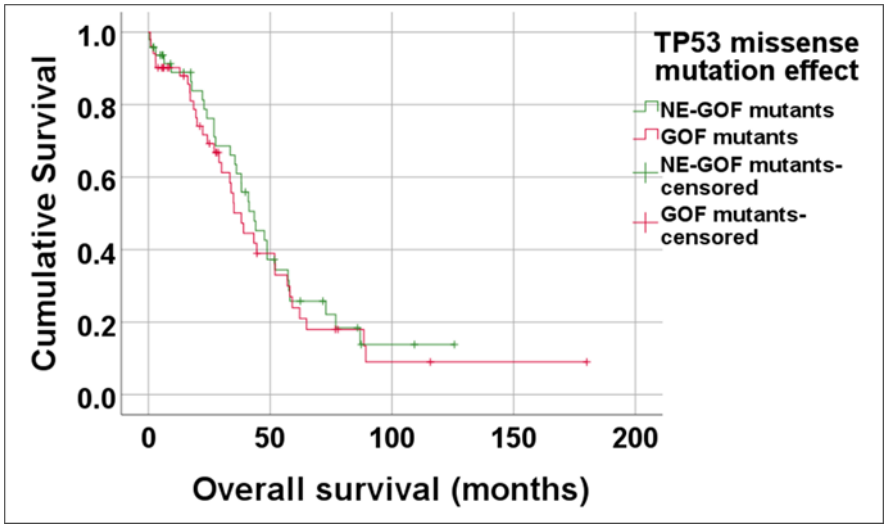

Figure 5. 14: A Kaplan-Meier curve demonstrating the effect of p53 gain of function mutants (GOF) on the overall survival of HGSOC females from TCGA. Patients with GOF mutants (red line, n=51) experienced a shorter median OS (*Mdn*=38.17 months) than patients who showed no evidence of GOF mutants (NE-GOF, green line, n=48, *Mdn* OS=43.5 months). The difference however was statistically not significant (Log rank X^2=0.29, p=0.59).

Table 5. 13: The effect of p53 GOF mutants on the overall survival of HGSOC females from TCGA. HGSOC females with *TP53* missense mutations that resulted in GOF mutants experienced a similar death rate (66.7%) compared to those with NE-GOF mutants. The difference was accordingly not statistically significant (Log rank X^2=0.29, p=0.59).

***TP53* missense mutation effect**	**Number of patients**	**Number of events**	**Median OS (95% CI)**
NE-GOF mutants[a]	48	32	43.50 (32.40-54.60)
GOF mutants[b]	51	34	38.17 (30.98-45.35)
Total	**99**	**99**	**41.03 (33.55, 48.50)**

OS: overall survival, 9**5% C.**I: 95% confidence interval, **GOF**: gain of function, **NE-GOF**: no evidence of gain of function.

a: includes the following mutations: G244C/D, G245R, G266V/R, L130V, D208V, V157F, K132E/M/N, S215R, C238Y, I195N/T, Y236C, R337C, C238F, D259Y, V216G/M, E286K, L145R, V274D/G, P250L, V272M, I232N, P278H/R, S241Y, C176F, P177R, C277F, F270L, H178N, H193R.

b: includes the following mutations: R248Q/W/G, R273H/C/L, R282W S127Y, Y163C/N, V173L, R175H, C176Y, H179R/Q, L194R, Y205C, H214R, Y220C, Y234C, S241F, G245C/S/V/D.

5.3.4.7 Gain of function p53 mutants do not impact HGSOC progression/recurrence

After exploring the impact of *p53 GOF* mutations on HGSOC mortality, we proceeded to apply the same principles to investigate their impact on PFS. Progression-free survival was available for only 82 (82.2%) out of 99 patients with *TP53* missense mutations. We compared PFS between patients with GOF mutants and those with NE-GOF mutants previously shown in Table 5.5 and the difference was again not statistically significant (Figure 5.15 and Table 5.14), indicating that p53 GOF mutants do not impact HGSOC progression/recurrence in TCGA cohort.

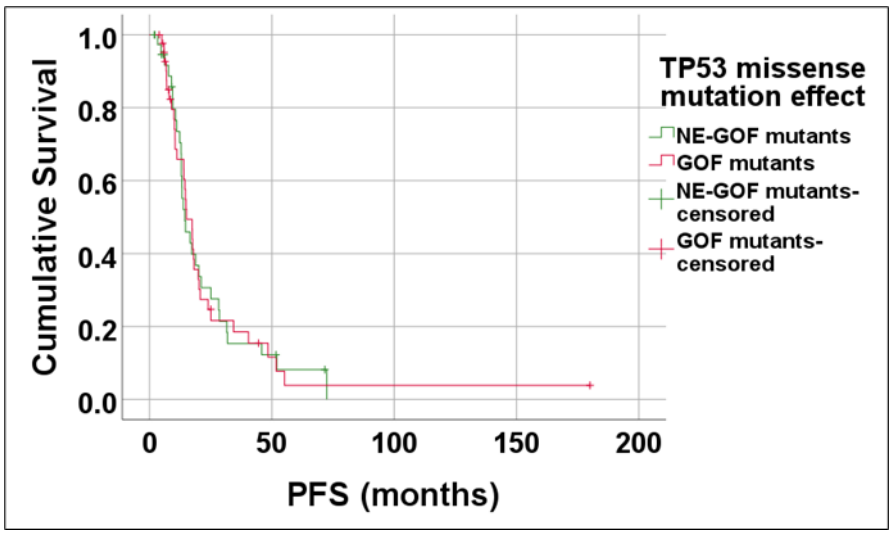

Figure 5. 15: A Kaplan-Meier curve demonstrating the effect of p53 gain of function mutants (GOF) on the progression-free survival of HGSOC females from TCGA. HGSOC females with GOF mutants (red line, n=43) experienced a slightly longer median PFS *(Mdn*=15.14 months) than patients with no evidence of GOF (NE-GOF) mutants (green line, n=39, *Mdn* PFS=14.42 months). The difference was not statistically significant (Log rank X^2=0.0, *p*=0.984).

Table 5. 14: The effect of p53 GOF mutants on the progression-free survival of HGSOC females from TCGA. HGSOC females with *TP53* missense mutations that resulted in GOF mutants experienced a slightly lower death rate (79.1%) compared to those with NE-GOF mutants (79.5%). The difference was accordingly not statistically significant (Log rank X^2=0.0, p=0.984).

***TP53* missense mutation effect**	**Number of patients**	**Number of events**	**Median PFS (95% CI)**
NE-GOF mutants[a]	39	31	14.42 (9.83, 19.00)
GOF mutants[b]	43	34	15.14 (11.54-18.73)
Total	**82**	**65**	**14.91 (11.62, 18.20)**

PFS: progression-free survival, 9**5% C.**I: 95% confidence interval, **GOF**: gain of function, **NE-GOF**: no evidence of gain of function.

a: includes the following mutations: G244C/D, G245R, G266V/R, L130V, D208V, V157F, K132E/M/N, S215R, C238Y, I195N/T, Y236C, R337C, C238F, D259Y, V216G/M, E286K, L145R, V274D/G, P250L, V272M, I232N, P278H/R, S241Y, C176F, P177R, C277F, F270L, H178N, H193R.

b: includes the following mutations: R248Q/W/G, R273H/C/L, R282W S127Y, Y163C/N, V173L, R175H, C176Y, H179R/Q, L194R, Y205C, H214R, Y220C, Y234C, S241F, G245C/S/V/D.

5.3.5 The relationship between *Ube2C* gene expression and *TP53* mutations in TCGA cohort of HGSOC patients

In the final section of this chapter, we explore the relationship between *Ube2C* mRNA expression levels and the various *TP53* mutations in TCGA cohort of HGSOC females. Our main aim is to expand on the previous studies that reported a positive correlation between p53 GOF mutants and UbcH10 overexpression.

5.3.5.1 Ube2C gene expression levels do not correlate significantly with TP53 mutations

In the first instance we investigated the *Ube2C* mRNA expression levels as a continuous variable in the 5 major groups of *TP53* mutations in 163 HGSOC patients from TCGA indicated in Table 5.3.

Log_2 normalized *Ube2C* mRNA expression levels were not significantly different between the 5 groups of *TP53* mutations (Table 5.15).

Table 5. 15: The relationship between *Ube2C* mRNA expression and *TP53* mutations in HGSOC females from TCGA. The median mRNA expression of the *Ube2C* gene was not statistically different between the 5 groups of *TP53* mutations as indicated by the *p*-value of the Kruskal-Wallis test.

***TP53* mutation category**	**Number**	***Ube2C mRNA expression[a] Mdn (Min, Max)***	**Kruskal-Wallis test *(H)* (*p*-value)**
Nonsense	18	10.77 (8.8, 12.3)	**0.344 *p*=0.987**
Missense	99	10.57 (8.3, 13.28)	
Frameshift deletion/insertion	19	10.71 (9.1, 12.69)	
Splice site	23	10.71 (8.7, 12.29)	
In-frame deletion	4	10.74 (9.4, 11.25)	
Total	**163**	**10.63 (8.27, 13.28)**	

Mdn: median, ***Min***: minimum, ***Max***: maximum

a: normalized mRNA expression data were calculated as log_2 value using the formula: $X=log_2(X+1)$

Next, we divided the cohort into high and low *Ube2C* mRNA expression categories based on the previously defined *X*-tile cut-off value of 11.236. The samples with high *Ube2C* gene expression (log_2 >11.236) represented a minority (24.5%) of the whole cohort, whilst 75.5% expressed *Ube2C* mRNA at low levels (log_2≤11.236). We then explored the relationship of these *Ube2C* gene expression groups to *TP53* mutations that had different functional impacts on the p53 protein and found no significant association. In fact, the relationship between *Ube2C* gene expression and *TP53*

mutations was heterogeneous and therefore, these data do not indicate a directly proportional relationship between *TP53* mutations and *Ube2C* gene expression (Figure 5.16).

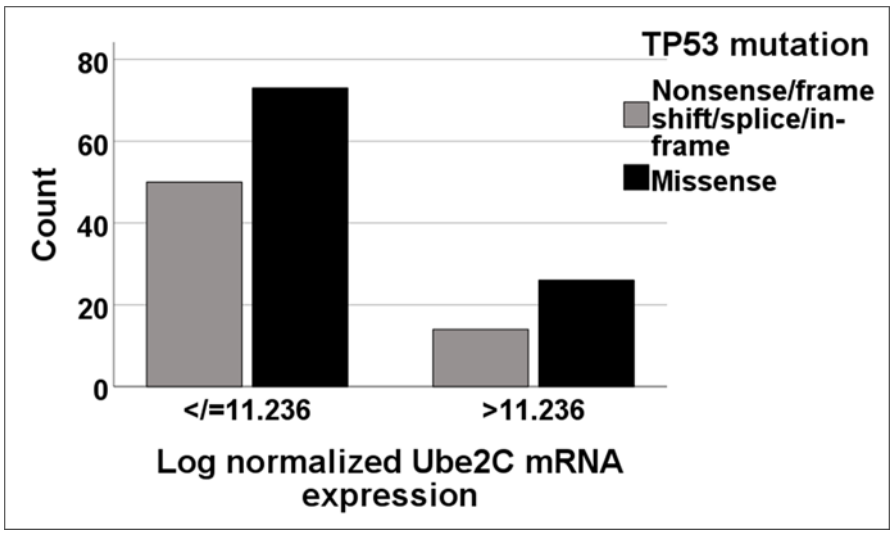

Figure 5. 16: The distribution of HGSOC females from TCGA according to the *Ube2C* mRNA expression categories and *T53* mutations with different functional impacts on the p53 protein. Patients with *TP53* missense mutations [99 patients (60.7%)] which resulted in overexpressed p53 protein and those which resulted in completely absent p53 protein [nonsense, frameshift deletions/insertions, splice-site, and in-frame deletions, 64 patients (39.3%)] were proportionately distributed between the high and low *Ube2C* gene expression categories. The association between the two variables was therefore found to be statistically not significant (Pearson X^2=0.404, p=0.525). The bar chart also highlights the heterogeneous relationship between *Ube2C* gene expression and *TP53* mutations. Only 26 patients (15.9%) had high *Ube2C* gene expression and *TP53* missense mutations that resulted in overexpressed p53 protein. On the other hand, 50 patients (30.7%) showed low *Ube2C* gene expression and *TP53* mutations that resulted in absent p53 protein. A total of 73 patients (44.8%) had missense mutations that resulted in p53 overexpression and polarized to the low *Ube2C* gene expression category.

5.3.5.2 Ube2C gene expression levels do not correlate significantly with structurally grouped TP53 missense mutations

In this section we explore the relationship between *Ube2C* gene expression and the various *TP53* missense mutations grouped according to their location within the DBD

of the p53 protein previously outlined in Table 5.4. For statistical reasons, we grouped those 9 categories into 3 major risk groups based on the median OS shown in Table 5.10. We then explored *Ube2C* mRNA expression levels as a continuous variable in those 3 major groups of *TP53* missense mutations. No statistically significant difference was found in *Ube2C* gene expression levels between the 3 risk groups of *TP53* missense mutations (Figure 5.17).

After investigating *Ube2C* gene expression levels as a continuous variable we divided the cohort into high and low *Ube2C* gene expression categories based on the cut-off value of 11.236 and correlated these two groups with the 3 *TP53* missense mutation risk groups. We could not find any statistically significant correlation between *Ube2C* gene expression groups and *TP53* missense mutation risk groups (Table 5.16).

We can therefore conclude that there was no statistically significant relationship between *Ube2C* gene expression and structurally grouped *TP53* missense mutations in TCGA cohort of HGSOC females.

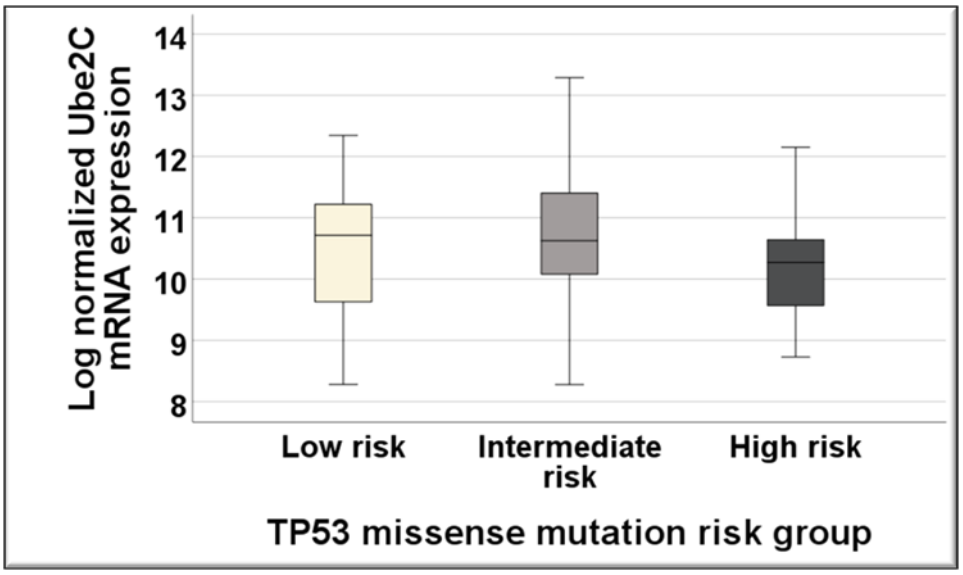

Figure 5. 17: A box plot diagram demonstrating the relationship between *Ube2C* gene expression levels and *TP53* missense mutation risk groups in 99 HGSOC females from TCGA. HGSOC patients in the high-risk group (DNA major groove interacting residues and SLH motif stabilizers, n=17) had the lowest median *Ube2C* mRNA expression levels (*Mdn*=10.27), while patients in the low-risk group (DNA minor groove interacting residues, Zn ion coordinating residues and distal loop residues, n=24) had the highest median *Ube2C* mRNA expression (*Mdn*=10.71). Patients in the intermediate risk group (Hydrophobic core residues, Loop 3 stabilizers, Loop2/Loop 3 interaction stabilizers and other missense mutations, n=58) had a median *Ube2C* mRNA expression level of 10.62. The difference between the 3 groups was not statistically significant (*H*=3.35, *p*=0.188).

Table 5. 16: The relationship between *Ube2C* gene expression and *TP53* missense mutation risk groups in 99 HGSOC females from TCGA. The *TP53* missense mutation risk groups were proportionately distributed between the high and low *Ube2C* gene expression categories. The association between the two variables was therefore statistically not significant as indicated by the p-value of the Chi-square test.

***Ube2C* gene expression group[a]**	***TP53* missense mutation risk group**			**Total**	**Pearson Chi-square test (X^2)**
	Low risk[b]	Intermediate risk[c]	High risk[d]		
Low (≤11.236)	18	40	15	**73**	**2.547**
High (>11.236)	6	18	2	**26**	***p*=0.28**
Total	**24**	**58**	**17**	**99**	

a: normalized mRNA expression data were calculated as $\log_2$ value using the formula: $X=\log_2(X+1)$

b: include DNA minor groove interacting residues, distal loop residues, and zinc ion coordinating residues.

c: include hydrophobic core residues, loop 3 stabilizers, loop2/loop 3 interaction stabilizers, and other missense mutations.

d: include DNA major groove interacting residues and SLH (sheet loop helix) motif stabilizers.

5.3.5.3 Ube2C gene expression levels do not correlate with p53 GOF mutants

In this final section we attempt to explore the relationship between *Ube2C* mRNA levels and *TP53* missense mutations that resulted in GOF mutants. The aim was to find out if GOF mutants positively affect *Ube2C* mRNA expression levels. We firstly analyzed *Ube2C* mRNA levels as a continuous variable and explored its expression levels in HGSOC females with GOF mutations and those with NE-GOF mutations. The *Ube2C* mRNA expression levels were in fact lower in HGSOC females with p53 GOF mutants. The difference, however, was not statistically significant (Figure 5.18).

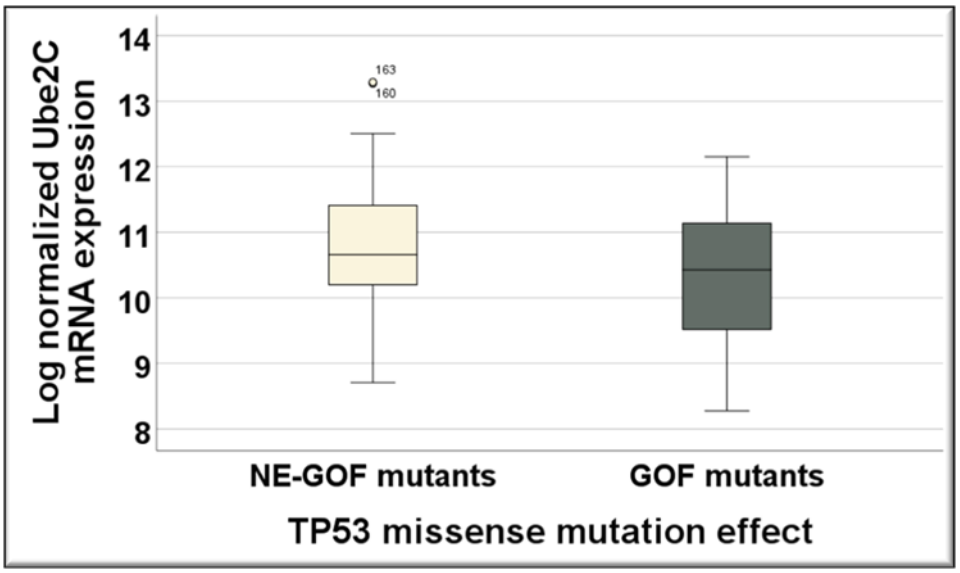

Figure 5. 18: A box plot diagram demonstrating the relationship between *Ube2C* gene expression levels and p53 gain of function (GOF) mutations in HGSOC females from TCGA. HGSOC patients with *TP53* missense mutations that resulted in GOF mutants (n=51) had lower median *Ube2C* mRNA expression levels (*Mdn*=10.42) compared to HGSOC patients with no evidence of GOF (NE-GOF) mutants (n=48, *Mdn*=10.65). The difference between the 2 groups was not statistically significant (*U*=951, *p*=0.056).

After investigating *Ube2C* gene expression levels as a continuous variable we divided the cohort into high and low *Ube2C* gene expression categories based on the cut-off value of 11.236 and correlated these two groups with p53 GOF mutations. We could not however, find any statistically significant correlation between *Ube2C* gene expression groups and p53 GOF mutants (Table 5.17). We can conclude from these data that p53 GOF mutants are not significantly associated with high *Ube2C* gene expression levels in HGSOC females from TCGA. Our data do not corroborate a directly proportional relationship between these genes.

Table 5. 17: The relationship between *Ube2C* gene expression and p53 GOF mutations in 99 HGSOC females from TCGA. HGSOC females with p53 GOF mutations were proportionately distributed between the high and low *Ube2C* gene expression categories. The association between the two variables was therefore statistically not significant as indicated by the p-value of the Chi-square test.

***Ube2C* gene expression group[a]**	***TP53* missense mutation effect**		**Total**	**Pearson Chi-square test (X^2)**
	NE-GOF mutants[b]	GOF mutants[c]		
Low (≤11.236)	32	41	**73**	**2.406**
High (>11.236)	16	10	**26**	***p*=0.121**
Total	**48**	**51**	**99**	

GOF: gain of function**, NE-GOF:** no evidence of gain of function.

a: normalized mRNA expression data were calculated as $\log_2$ value using the formula: $X=\log_2(X+1)$

b: includes the following mutations: G244C/D, G245R, G266V/R, L130V, D208V, V157F, K132E/M/N, S215R, C238Y, I195N/T, Y236C, R337C, C238F, D259Y, V216G/M, E286K, L145R, V274D/G, P250L, V272M, I232N, P278H/R, S241Y, C176F, P177R, C277F, F270L, H178N, H193R.

c: includes the following mutations: R248Q/W/G, R273H/C/L, R282W S127Y, Y163C/N, V173L, R175H, C176Y, H179R/Q, L194R, Y205C, H214R, Y220C, Y234C, S241F, G245C/S/V/D.

5.4 Discussion

We previously explored the prognostic and predictive role of UbcH10 and p53 protein levels in HGSOC females from two different cohorts (Birmingham and Barts) in chapters 3 and 4. In this chapter we expanded on these findings by using gene expression and mutational data form the publicly available cohort of ovarian serous carcinomas from TCGA.

5.4.1 *Ube2C* significantly co-expressed genes

We first explored the *Ube2C* significantly co-expressed genes in ovarian serous carcinomas from TCGA. We found more than 50 significantly and positively co-

expressed genes mostly involved in mitosis, chromosomal segregation, and cell-cycle regulation (Table 5.1). In fact, the strongest significant positive correlation was found between *Ube2C* and the genes that code for Centromere protein A (Figure 5.1), MYB protooncogene like 2 (MYBL2), and Aurora kinase A and B (AURKA, AURKB). CENP-A is a histone H3-like protein found specifically in the centromeric nucleosome. It is essential for assembling kinetochore proteins and hence required for progression through mitosis and chromosomal segregation (151). MYBL2 is a transcription factor also involved in cell-cycle progression (154). AURKA and AURKB are both serine/threonine-protein kinases that regulate the progression of the cell-cycle. AURKA interacts with the centrosome and spindle microtubule to ensure normal spindle positioning during mitosis (155). On the other hand, AURKB is a component of the chromosomal passenger complex which also binds to centromeric proteins to ensure the fidelity of chromosomal alignment and segregation (156). The function of these significantly co-expressed proteins is concordant with the role of UbcH10 as an E2 ubiquitin-conjugating enzyme for the APC/C (86). Together, they mark key mitotic regulators for degradation, guarantee proper chromosomal segregation during mitosis, maintain genomic stability, and avert aneuploidy (87). Other *Ube2C* significantly co-expressed genes include *CDC20* and *Ube2S* which were previously discussed in Chapter 1 section 1.7 as essential components of the ubiquitin proteasome pathway (91). These data indicate that UbcH10 is positively co-expressed with proteins upregulated during mitosis and essential for cell-cycle progression.

It is interesting to note that both CENP-A and MYBL2 have been shown to be upregulated in SKOV-3 and A2780 ovarian cancer cell lines. They also play an important role in the proliferation of these ovarian cancer cell lines (157, 158). This is

consistent with their molecular function, and like UbcH10 they seem to behave like proliferative markers in ovarian cancer cells. Gene expression data from the Human Protein Atlas which analysed samples from TCGA cohort also show that neither CENP-A nor MYBL2 are prognostic in ovarian cancer. In fact, like our findings for *Ube2C* gene expression (Figure 5.3) they do not seem to impact the OS of ovarian cancer females. In a recent study on TCGA cohort of breast carcinoma specimens (n=854), *Ube2C* mRNA expression was strongly and positively correlated with proliferation-related genes (*CDK1*, *CDKN2A, CCNB1, CCNE1, CCNE2, and CCNA1*) (159). This again closely aligns with results presented in Table 5.1 and further corroborates our theory that UbcH10 mostly behaves like a proliferative marker in ovarian serous carcinoma.

5.4.2 *Ube2C* gene expression as a prognostic marker in HGSOC

With respect to *Ube2C* gene expression as a prognostic marker in HGSOC females from TCGA, we found no significant association between *Ube2C* mRNA levels and the two prognostic parameters in that cohort: age at diagnosis and AJCC stage (Figures 5.4 and 5.5). This is mostly consistent with our data from the Birmingham and Barts cohorts. In the Birmingham cohort, we found a significant but weak association between UbcH10 protein expression and advanced age at diagnosis (Figure 3.6). We also found no significant association between UbcH10 protein expression and FIGO stage (Table 3.3). Additionally, in the Barts cohort we could not find a significant association between UbcH10 protein levels and FIGO stage (Table 3.14). Although FIGO stage is more universally implemented in the staging of ovarian cancer, the AJCC staging system closely mirrors FIGO stage (8). Furthermore, TCGA cohort has an important advantage compared to the Birmingham and Barts cohorts. None of the patients from TCGA received pre-operative chemotherapy. Consequently, the previous

concern of reduced UbcH10 levels after pre-operative chemotherapy (Table 3.5 and Figure 3.23) that we found in our cohorts was eliminated in TCGA cohort. This means that conclusions from TCGA are more robust and with limited pre-analytical confounding factors. We therefore contend that the significant weak correlation we found between UbcH10 protein levels and advanced age in the Birmingham cohort is probably confounded by the pre-operative chemotherapy administered in those patients. Patients older than 64 years in the Birmingham cohort were mostly patients who underwent PDS and did not receive preoperative chemotherapy. On the other hand, patients younger than 64 years at diagnosis mostly received NACT and later underwent DDS. This association was found to be statistically significant (X^2=5.21, p=0.023). Since UbcH10 protein levels were significantly higher in patients who underwent PDS (Table 3.5), this could account for the significant weak association between high UbcH10 levels in patients older than 64 years. This further corroborates our previous argument that UbcH10 is not prognostic in HGSOC or only borderline significant at best. Accordingly, studies that previously advocated UbcH10 as a prognostic parameter in ovarian cancer (86, 116) are mostly biased and the prognostic effect of UbcH10 found was probably contingent on other well established prognostic parameters in ovarian cancer like stage, grade and histotype.

Our analysis on ovarian serous carcinomas (n=307) and HGSOC females (n=163) from TCGA also indicate that *Ube2C* gene expression levels do not significantly impact the OS or PFS of those females (Figures 5.3, 5.6 and 5.7). These data are concordant with data from the HPA where analysis was also performed on ovarian serous carcinomas from TCGA. The HPA cohort included 373 ovarian serous carcinoma females (mostly high grade) divided by the median FPKM value of the *Ube2C* gene

expression level (67.09), as well as the best expression cut-off (100.66) that yielded the maximum survival difference at the lowest log-rank *p*-value (<0.001). When considering the median *Ube2C* expression value, the 5-year survival rate of patients with high *Ube2C* expression (>67.09, n=186) was ***worse*** (29%) compared to patients with low *Ube2C* expression (≤67.09, n=187) at 35%. The difference was statistically not significant (Log rank *p*-value=0.66). When considering the best expression cut-off value, the 5-year survival rate of patients with high *Ube2C* expression (>100.66, n=97) was ***better*** (38%) than patients with low *Ube2C* expression (≤100.66, n=276) at 30%. The difference was again not statistically significant (Log rank *p*-value=0.10). It is worth noting that the best expression cut-off value placed patients with high U*be2C* gene expression (n=97) from the HPA/TCGA cohort in the upper 25th percentile. This closely mirrors our own cut-off value (log_2=11.236) in TCGA cohort, and the cut-off value previously generated by *X*-tile for UbcH10 protein expression in the Birmingham cohort. The fact that changing the cut-off value for *Ube2C*/UbcH10 expression changes the difference in OS between high and low *Ube2C* expression groups further corroborates our conclusion that *Ube2C*/UbcH10 is not a strong prognostic marker or predictor of mortality and progression in HGSOC patients.

5.4.3 *TP53* mutations and patient outcomes in HGSOC

Our analysis on the 163 HGSOC females from TCGA revealed that the 5 major groups of *TP53* mutations do not affect the mortality or progression rates of those females (Figures 5.8 and 5.10). In addition, missense mutations grouped by their functional impact on the p53 protein had no impact on OS or PFS of those females (Figures 5.9 and 5.11). Furthermore, missense mutations that resulted in p53 GOF mutants did not significantly impact mortality or progression of HGSOC females (Figures 5.14 and

5.15). The prognostic role of *TP53* mutations in HGSOC has been a matter of debate in the literature. When looking at the study by Kang *et al* (81) which we used as the basis for the classification of p53 GOF mutants in our own analysis, they also performed analysis on TCGA cohort. However, they included a total of 301 HGSOC females in their analysis. They downloaded whole exome sequencing and *TP53* mRNA expression data from TCGA and identified 185 patients with missense mutations. They then categorised 31 hotspot missense mutations in the DBD of the p53 protein to be GOF mutations resulting in activation of genes normally repressed by wild type p53 and/or oncogenic transformation of mouse embryonic fibroblasts. In their analysis, a total of 101 out of 185 HGSOC patients had p53 GOF mutants. Accordingly, the number of patients in each category were slightly higher than our own because they were not limited by the number of patients with *Ube2C* gene expression data. Nonetheless, when they compared the OS and PFS of the HGSOC females with those p53 GOF mutants to non-GOF mutants, like our results no statistically significant difference was found. Mandilaras *et al (160)* used six different classifications for *TP53* mutations on a cohort of 229 HGSOC females and still found no significant association with OS in those females. More recently, Tuna *et al* (161) used a larger combined population of 791 HGSOC females (which partly included TCGA patients) to explore the impact of *TP53* mutations on HGSOC survival. But again, similar to our results they could not find a significant difference in OS and recurrence-free survival between the 5 major *TP53* mutation groups. In addition, when they compared missense mutations to the other 4 mutation groups that resulted in truncated p53 protein, no significant difference in survival was found. These studies on HGSOC in addition to our own analysis form TCGA corroborate our results from the Birmingham cohort in chapter 4

which showed that the survival of patients with overexpressed or cytoplasmic p53 protein by IHC was not significantly different from patients with a null p53 pattern (Figures 4.9 and 4.10). Nonetheless, it was interesting to note that Tuna *et al (161)* identified certain hotspot missense mutations (G266, Y163, R282) to be associated with worse OS in HGSOC females. While the number of such mutations in our cohort of HGSOC females from TCGA are too low to achieve any robust conclusions, this might point that individual mutation analysis might be more clinically relevant than lumping mutations based on their functional impact on the p53 protein. In the era of personalised medicine, these might even represent attractive targets for therapy. Whether targeted *TP53* mutational analysis could be incorporated into clinical practice is an important question. While it might be more cumbersome than the routinely applied IHC staining, nevertheless, it does hold prospect for future research.

To expand on this further, we attempted to group *TP53* missense mutations based on their location within the DBD and their OS difference into 3 major groups as indicated in Table 5.10. We then explored their impact on OS and PFS of HGSOC females from TCGA. No significant association was found between these structurally grouped *TP53* missense mutations and the survival of those females (Figures 5.12 and 5.13). This analysis was attempted previously by Seagle *et al (71)* who also used TCGA cohort of HGSOC females. However, contrary to our results they demonstrated differences in OS and PFS of those patients with structurally grouped *TP53* missense mutations. Seagle *et al* (71) included 185 HGSOC females from TCGA with *TP53* missense mutations while we included 99 patients only because we limited our analysis to patients who had corresponding *Ube2C* expression data. We could argue that the difference in sample size might be a reason for the discrepant results. However, their

characterisation of HGSOC from TCGA is vastly different from our own methodology. In their cohort, they include a significant number of what they call HGSOC with wild type p53 from TCGA. We contend that these patients are probably misclassified LGSOC as TCGA includes both serous carcinoma subtypes. So, in essence this could be one of the sources of bias in their survival analysis as they have included LGSOC patients who inherently have better survival than HGSOC patients. Another important consideration is that Seagle *et al* (71) excluded ovarian cancer females that were sub-optimally debulked from their survival analysis which is another source of bias in their conclusions.

Taken together the above studies support the notion that functional and structural groups of *TP53* mutations do not impact survival in HGSOC, while individual mutation analysis might be a more promising prospect for future investigation.

5.4.4 The relationship between *Ube2C* gene expression and *TP53* mutations

Our analysis on the relationship between *Ube2C* mRNA expression and the various *TP53* mutations yielded non-significant results (Table 5.15). Only 15.9% of HGSOC females had *TP53* mutations that resulted in overexpressed p53 protein and high *Ube2C* mRNA levels. In fact, most patients with *TP53* missense mutations polarized to the low *Ube2C* mRNA expression category (Figure 5.16). This supports a heterogeneous rather than a directly proportional relationship between the two proteins. Findings from the TCGA cohort are consistent with our previous results from the Birmingham cohort (Figure 4.6). Only 22-24% of patients from the Birmingham cohort overexpressed both p53 and UbcH10 and 49-51% of patients overexpressed

p53 and had low UbcH10 expression. Our findings contradict previous studies on non-ovarian malignancies. In one study on non-small cell lung carcinomas (NSCLC), the median UbcH10 expression was found to be significantly higher in specimens with mutant p53 compared to p53 wild type (149). Similarly, in breast carcinoma specimens high UbcH10 expression was positively correlated with high p53 expression (159). We can explain the differences between our finding and these two studies by looking at the methodology applied. Pallante *et al* (149) compared UbcH10 protein levels in NSCLC specimens that had wild type and those that had p53 mutation whereas we are comparing HGSOC samples with different forms of p53 mutations. In addition, Pallante *et al* (149) found a significant positive association between UbcH10 and Ki-67 index supporting the notion that UbcH10 behaves as a proliferative marker. Since NSCLC specimens that are p53 mutant are more proliferative by nature (162) than those with wild type p53, this could explain the higher UbcH10 levels. On the other hand, Kariri *et al* (159) who correlated high UbcH10 expression with p53 expression in breast carcinomas (n=619) did not specify how they estimated p53 expression. They describe p53 expression as positive and negative which is rather ambiguous. It is not clear whether they are comparing p53 mutant to wild type or p53 overexpression to null pattern. Nevertheless, they did correlate high UbcH10 expression with high Ki-67 expression in their cohort. This seems to be a recurring theme for UbcH10: how it is positively co-expressed with cell-cycle proliferative proteins and how it correlates significantly with well-established proliferative markers. Accordingly, we explore this relationship further in chapters 6 and 8.

To explore the relationship between p53 and UbcH10 further, we found that p53 GOF mutants characterized by previous studies (81) did not significantly impact *Ube2C*

mRNA expression levels in HGSOC females from TCGA. In fact, *Ube2C* gene expression levels were paradoxically higher in HGSOC with NE-GOF mutants (Figure 5.18). This again does not suggest a directly proportional relationship between the two genes. This contradicts previous studies on human cancer cell lines where certain GOF p53 mutants (R273H and R175H) were found to upregulate UbcH10 expression through nuclear transcription factor-Y (NF-Y) (104). On the other hand, wild type p53 has been shown to repress UbcH10 expression through a direct effect on the *Ube2C* gene promotor region (104). These two GOF mutants (R273H and R175H) were among the hotspot mutations in HGSOC females from TCGA. They also do not seem to impact the survival of those females or upregulate *Ube2C* mRNA expression levels. However, as previously highlighted by Tuna *et al (161)*, certain *TP53* missense mutations might prove prognostic in larger cohorts. Similarly, studying these specific mutations in larger cohorts might yield results that conform with studies on cancer cell lines. One study on breast cancer cell lines found that p53 R273H mutations specifically promoted cancer cell proliferation, invasion, and resistance to chemotherapeutic drugs (163). This means that mutations at a single codon in the p53 protein can have vastly different functional and clinical implications. This also highlights the importance of correlating *in vivo* tumour studies with *in vitro* functional studies on ovarian cancer cell models to identify the exact relationship between p53 GOF mutants and *Ube2C* gene expression.

5.5 Conclusion

Analysis of gene expression and mutational data from TCGA cohort of HGSOC reveals that *Ube2C* mRNA expression levels do not impact patient prognosis, mortality, or progression rates. In addition, the various *TP53* mutations including those structurally

grouped based on their location within the DBD and those that result in GOF of the p53 protein do not influence HGSOC survival from that cohort. Correlative analysis does not indicate a directly proportional or significant relationship between *Ube2C* gene expression and any type of *TP53* mutation. Individual *TP53* missense mutational analysis both *in vivo* and *in vitro* represents a promising prospect for future studies.

Chapter 6. UbcH10 is expressed early in serous tubal intraepithelial carcinomas and its relationship to p53 expression and the proliferative state of these tumours.

6.1 Introduction

Over the last decade, cumulative evidence supported an extraovarian origin of high-grade serous carcinomas. It is now accepted that most HGSOCs arise from precursor lesions in the fimbrial end of the fallopian tube known as Serous Tubal Intraepithelial Carcinoma (STIC; ((8)). Furthermore, identical *TP53* mutations have been identified in STICs and their corresponding ovarian serous carcinomas further cementing *TP53* mutations as a universal early occurrence in HGSOC (8). Consequently, diagnosis of STIC is currently based on the identification of unequivocally malignant serous type epithelium limited to the tubal basement membrane which displays aberrant p53 immunohistochemical expression and a high Ki-67 index (≥10%) (47). Additionally, a putative precursor of STIC has been described termed “p53 signature”. These p53 signatures are morphologically normal tubal epithelium that overexpresses the p53 protein. Reportedly, p53 signatures can also harbour *TP53* mutations but have a low Ki-67 index (46). Overexpression of p53 in these signature lesions is thought to be due to early DNA damage in the secretory cell cells (164). For more information refer to Chapter 1 section 1.5.2.

One of the main objectives of this study was to identify the exact role that UbcH10 plays in the progression of HGSOC. Consequently, one objective was to study its

expression in the precursor lesions and correlate its expression to the invasive tumours. Pertinent to this study we have already noted that UbcH10 IHC staining patterns are reminiscent of the proliferation marker, Ki-67 (see Chapters 2 and 3). As such, UbcH10 is polarised to the proliferative cells in tonsillar germinal centres (Figure 2.1) and is significantly reduced in levels in response to chemotherapy (Table 3.5). Given these similarities, in the present study we also address the relationship between UbcH10, Ki-67 and p53 in these precursor lesions and their invasive carcinomas.

6.2 Study population

To study the role of UbcH10 in HGSOC progression and its relationship to Ki-67 and p53 we used a cohort of 24 females with HGSOC and matched tubal sections containing STIC previously described in section 2.1.1.3. A total of 9 (37.5%) patients from this cohort also had p53 signatures adjacent to STIC in their fallopian tube fimbriae.

STICs were identified by their morphological abnormality and their abnormal p53 protein expression pattern, whilst p53 signatures were identified by staining normal tubal sections for p53 to identify an abnormal p53 staining pattern. Figure 6.1 demonstrates an example of STIC and p53 signature taken from the same tubal section in one HGSOC patient.

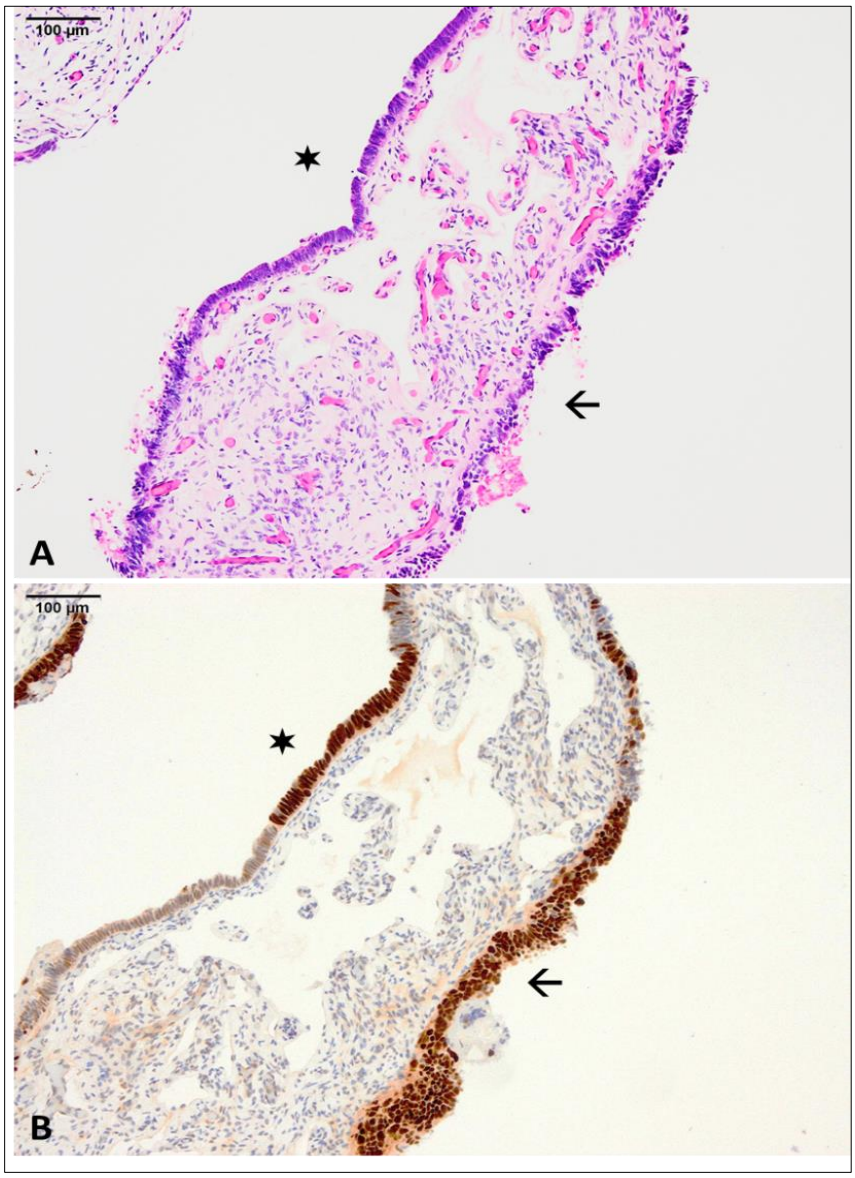

Figure 6. 1: A section form the fallopian tube fimbriae of a HGSOC patient demonstrating both serous tubal intra-epithelial carcinoma (STIC) and p53 signature. A) Hematoxylin and Eosin image showing a focus of STIC (arrow) on one side with nuclear enlargement, hyperchromasia and stratification limited to the tubal basement membrane. Ciliated cells are characteristically absent (H&E, x10 magnification). The other side shows a stretch of tubal epithelium composed of ≥12 consecutive secretory cells that lack cytological atypia (star). B) p53 is overexpressed in both the STIC (arrow) and the p53 signature (star, anti-p53, x10 magnification).

6.3 Demography, clinico-pathological profile, and treatment variables in HGSOC patients with STIC

To get an idea of the characteristics of the 24 HGSOC patients with STIC, we found it important to look at their clinical and pathological features.

6.3.1 Age at diagnosis

These HGSOC patients were aged between 47 and 75 years (*Mdn*=68). The clinical and pathological features of this cohort, detailed herein, are summarised in Table 6.1.

6.3.2 FIGO stage

A total of 5 patients (20.8%) had FIGO stage I disease, 4 (16.6%) of which were stage IC3 (with positive peritoneal cytology) and 1 (4.2%) was stage IC2 (with spontaneous ovarian capsular rupture). A total of 14 patients (58.4%) had FIGO stage III disease, 3 (12.5 %) of which were stage IIIB (with omental metastasis less than 2 cm in maximum diameter) and 11 (45.9%) cases were stage IIIC (with omental metastasis more than 2 cm in maximum diameter). Lastly, 5 (20.8%) patients had stage IV disease, 4 (16.6%) of which were stage IVB (with extra-abdominal metastasis) and 1(4.2%) had stage IVA (with cytologically proven malignant pleural effusion).

6.3.3 Lymph node (LN) metastasis

A total of 6 (25%) out of 24 patients had metastatic disease to regional LNs (internal and external iliac) whilst 1 (4.2%) patient had no evidence of nodal disease. In the remaining 17 (70.8%) cases, no LNs were submitted for pathological examination.

6.3.4 Type of surgery performed

Eleven (45.8%) patients underwent primary debulking surgery followed by adjuvant chemotherapy, whilst the remaining 13 (54.2%) patients received NACT before undergoing delayed debulking.

6.3.5 Volume of residual disease after surgery

A total of 14 (58.3%) patients had complete R0 disease, 7 (29.2%) patients had optimal cytoreduction (R1), and only 3 (12.5%) patients had suboptimal cytoreduction (R2).

6.3.6 Chemotherapy response score

Of the 13 patients receiving NACT, 5 patients (38.5%) showed a minimal response, 7 patients (53.8%) responded partially, and only 1 patient (7.7%) responded completely.

6.3.7 p53 immunohistochemical staining

The majority of the patients [19 patients, (79.2%)] showed aberrant p53 overexpression pattern. On the other hand, 2 (8.3%) patients showed a null pattern, 2 (8.3%) showed a wild type-like pattern, and 1 (4.2%) patient showed cytoplasmic p53 expression. The p53 IHC staining pattern was identical in both STICs and their corresponding tumours (Figure 6.2).

Table 6. 1: Clinico-pathological features of the 24 HGSOC females with serous tubal intraepithelial carcinomas in their fallopian tubes.

Patient characteristic	Number of patients	Valid Percentage	Total
Age, year			
≤68 (*Mdn*)	13	54.2	24
>68	11	45.8	
FIGO stage			
I	5	20.8	24
III	14	58.4	
IV	5	20.8	
LN status			
Nx (not submitted)	17	70.8	24
N0 (no LN metastasis)	1	4.2	
N1 (LN metastasis)	6	25	
Type of surgery			
PDS	11	45.8	24
DDS	13	54.2	
Cytoreduction			
R0	14	58.3	24
R1	7	29.2	
R2	3	12.5	
CRS			
Minimal	5	38.5	13*
Partial	7	53.8	
Complete	1	7.7	
p53, IHC			
Wild type-like	2	8.3	
Overexpression	19	79.2	24
Null	2	8.3	
Cytoplasmic	1	4.2	

Mdn: median**, PDS**: primary debulking surgery, **DDS**: delayed debulking surgery, **CRS**: chemotherapy response score, **R0** (complete): no gross residual disease, **R1** (optimal): gross residual disease between 0.1 to 1 cm, **R2** (sub-optimal): gross residual disease >1cm, **IHC**: immunohistochemistry.

*Data available for patients who underwent DDS only.

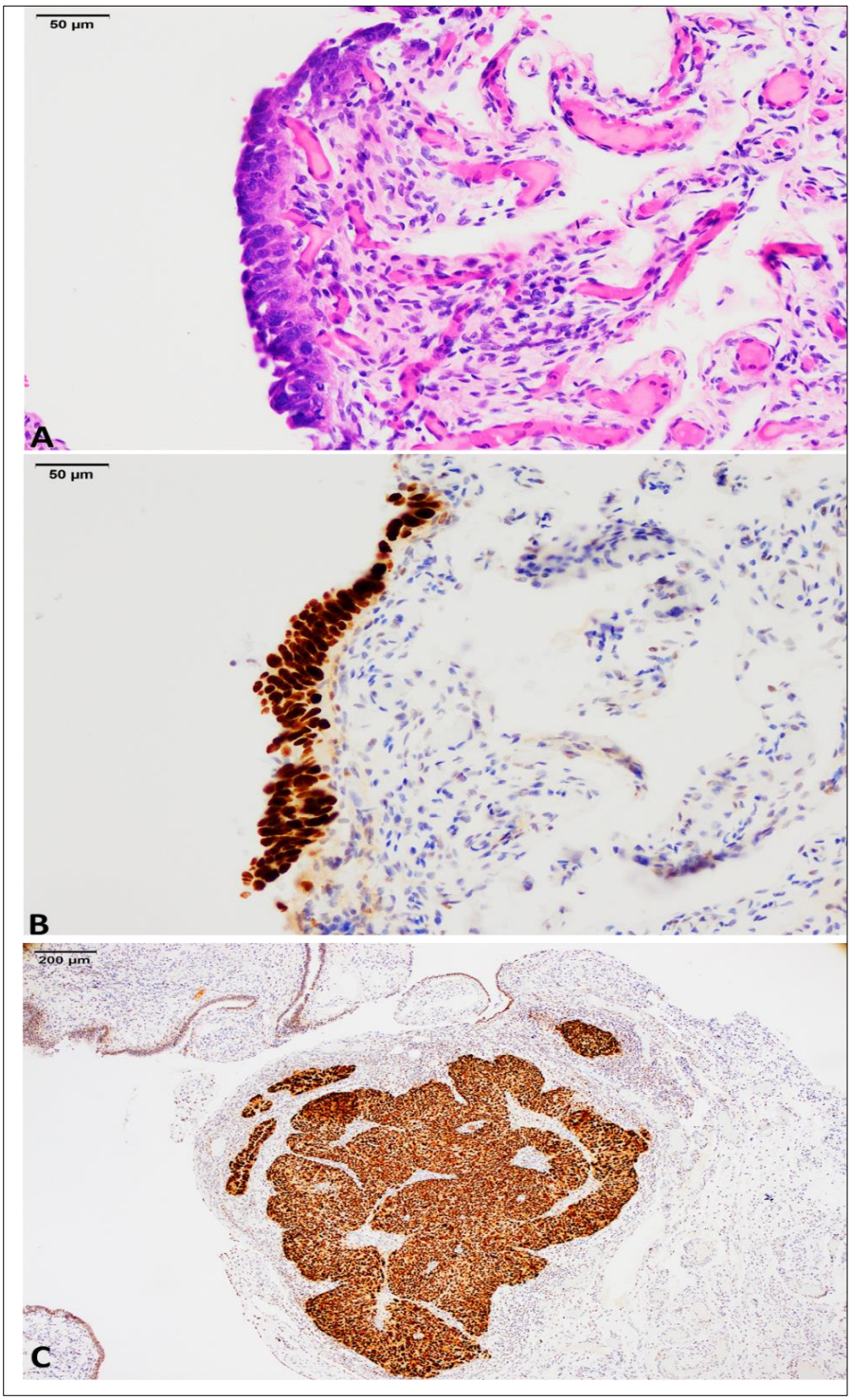

Figure 6. 2: A HGSOC patient showing similar p53 IHC expression patterns in both STIC and invasive malignancy. A) A focus of serous tubal intra-epithelial carcinoma demonstrating nuclear enlargement, hyperchromasia and stratification. Ciliated cells are absent (H&E, x20 magnification). B) p53 shows an aberrant pattern with diffuse expression in>80% of nuclei in STIC focus (anti-p53, x20 magnification). C) Invasive high grade serous carcinoma in the tube of the same patient showing aberrant p53 overexpression similar to STIC in panel B (anti-p53, x4 magnification).

6.4 UbcH10 is expressed early in HGSOC and is differentially expressed between normal, benign and malignant lesions

6.4.1 Overview

To identify the role of UbcH10 in HGSOC progression, we compared UbcH10 expression between p53 signatures, STICs and their corresponding invasive tumours. In addition, we stained normal tissue, benign and borderline serous tumours for UbcH10 as a control group.

6.4.2 UbcH10 protein expression is very low in normal tissue, benign and borderline serous tumours

When looking at UbcH10 protein expression in the 22 cases of normal ovarian tissue and tubal epithelia, very low to absent expression was noted. In normal tissue, UbcH10 IRS ranged from 0 to 3 (*Mdn*=2) and its H-score ranged from 0 to 20.4 (*Mdn*=7). The UbcH10 tumour proportion score (TPS) ranged from 0 to 10.2% (*Mdn*=2.8) Similarly, in the 5 cases of benign serous cystadenomas and borderline serous tumours, UbcH10 expression levels were noticeably low to absent. In benign and borderline tumours, UbcH10 IRS ranged from 0 to 2 (*Mdn*=2), whilst its H-score ranged from 0 to 40 (*Mdn*=4). The UbcH10 TPS in these tumours ranged from 0 to 40% (*Mdn*=2). Figure 6.3 demonstrates UbcH10 protein expression in a benign serous cystadenoma.

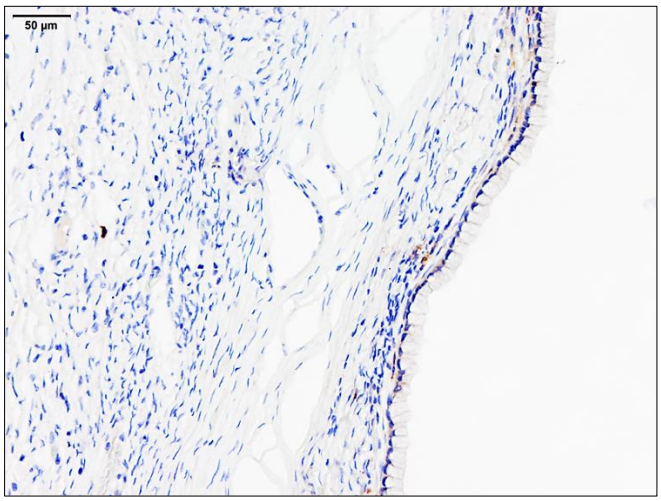

Figure 6. 3: A case of benign serous cystadenoma with mostly absent and focally weak UbcH10 expression (IRS 1, H-score 3, x20 magnification).

6.4.3 UbcH10 protein expression in p53 signatures is comparable to normal tubal epithelium

When looking at p53 signatures (9 cases) as the postulated earliest step in HGSOC pathogenesis, UbcH10 expression was slightly higher but still comparable to normal tissue. The UbcH10 IRS ranged from 2 to 6 (*Mdn*=4) and the H-score ranged from 4 to 40 (*Mdn*=12). The UbcH10 TPS ranged from 2 to 20% (*Mdn*=4) Figures 6.4 and 6.5 demonstrate examples of UbcH10 expression in p53 signatures. These data show that UbcH10 expression in p53 signatures is comparable to normal tubal epithelium.

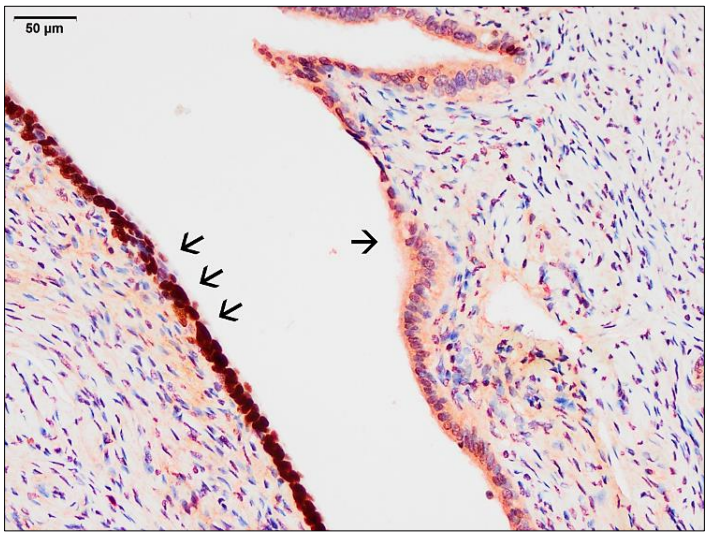

Figure 6. 4: Negligible UbcH10 expression in p53 signature. Dual staining for UbcH10 (red) and p53 (brown) in a focus of p53 signature was performed. The focus of p53 signature (arrows) demonstrates nuclear p53 overexpression (brown) and barely any UbcH10 expression. Note the stretch of normal tubal epithelium opposite the p53 signature (arrow) with negligible UbcH10 expression comparable to p53 signature (anti-p53, anti-UbcH10, x20 magnification).

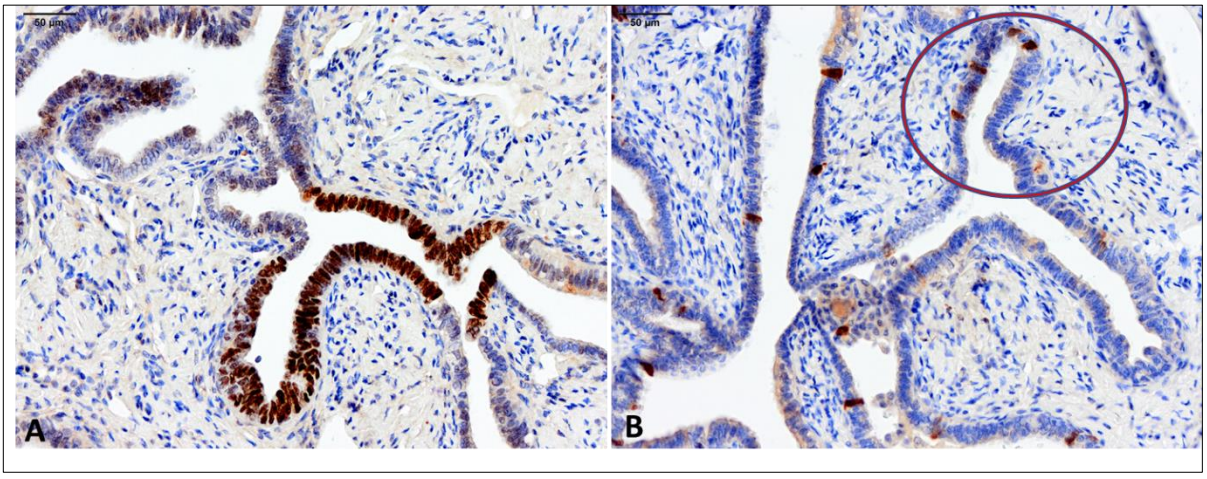

Figure 6. 5: Low UbcH10 expression in p53 signature is comparable to normal tubal epithelium. A) Normal fallopian tube epithelium showing p53 nuclear overexpression in one part of the epithelium characteristic of a p53 signature. The rest of the epithelium shows scattered weak to moderate nuclear staining characteristic of wild type p53 (anti-p53, x20 magnification). B) Focal UbcH10 expression (IRS 3, H-score 9) in the p53 signature focus (red circle). UbcH10 expression levels in the p53 signature is comparable to its focal staining pattern in the background normal tubal epithelium (anti-UbcH10, x20 magnification).

6.4.4 High UbcH10 protein expression in STIC

Inspection of the 24 cases of STICs, indicated a notable increase in UbcH10 protein levels in comparison to normal tissue and p53 signatures. The IRS for UbcH10 ranged from 2 to 11 (*Mdn*=7), while the H-score ranged from 20 to 195 (*Mdn*=117). The UbcH10 TPS in STICs ranged from 10 to 95% (*Mdn*=58.75). Figures 6.6 to 6.8 show different examples of STICs with variable UbcH10 expression levels.

6.4.5 High UbcH10 protein expression in HGSOC

Although the highest UbcH10 expression levels were observed in well-established HGSOCs their corresponding STICs also expressed high levels of UbcH10. Indeed, UbcH10 IRS levels ranged from 2 to 11 (*Mdn*=8), while H-scores ranged from 20 to 198 (*Mdn*=136). In HGSOC, the UbcH10 TPS ranged from 10 to 95% (*Mdn*=73.6).

Taken from the data presented so far, we can deduce that UbcH10 protein levels are absent or very low in normal ovarian tissue, tubal epithelia as well as benign and borderline serous tumours. In p53 signatures, UbcH10 protein levels were found to be slightly higher but still comparable to normal tubal tissue. However, high UbcH10 protein levels were observed in STICs and in their corresponding invasive malignancies.

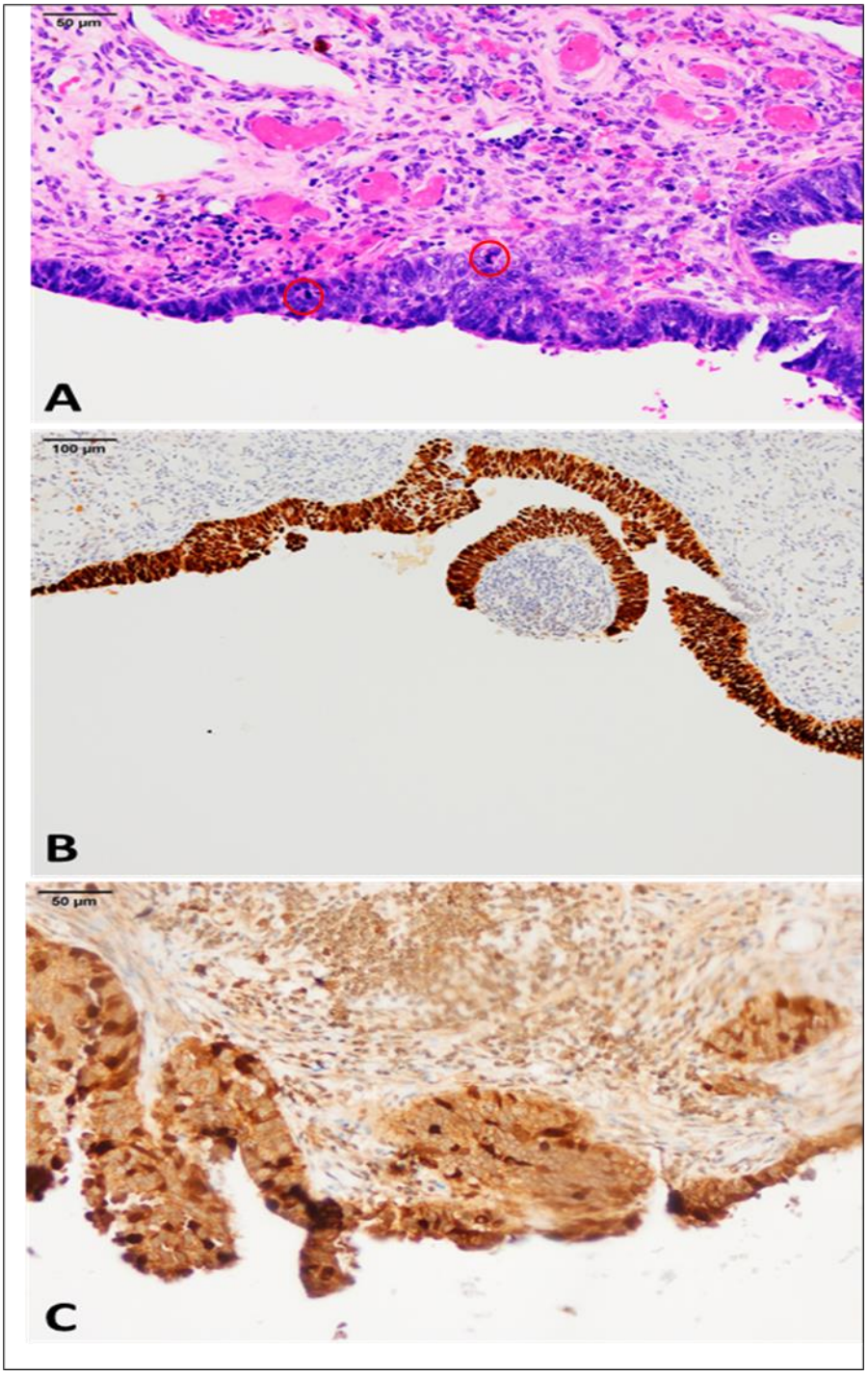

Figure 6. 6: A focus of serous tubal intra-epithelial carcinoma with high UbcH10 expression. A) Intra-epithelial carcinoma (STIC) with nuclear stratification, hyperchromasia and mitotic figures (red circles, H&E, x20 magnification). B) STIC demonstrating aberrant p53 overexpression in almost 100% of its nuclei (anti-p53, x10 magnification). C) High nuclear and cytoplasmic UbcH10 expression in STIC (IRS 10, H-score 162, anti-UbcH10, magnification).

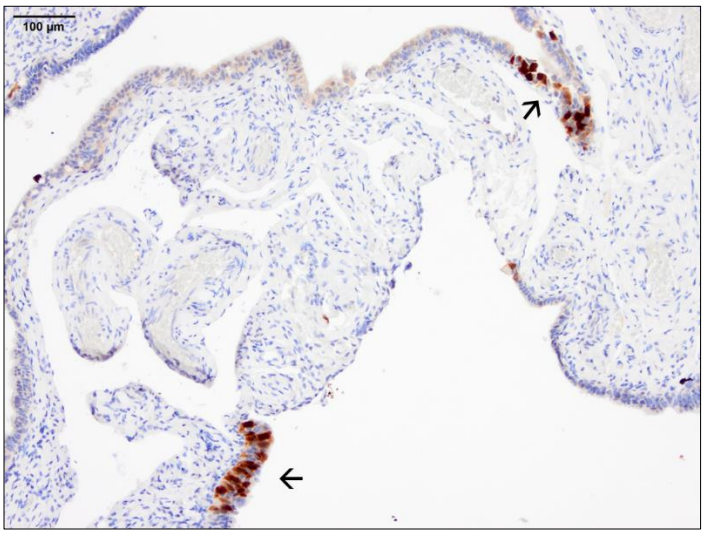

Figure 6. 7: Multi-focal serous tubal intra-epithelial carcinoma with moderate to high UbcH10 expression in the same patient. The upper right arrow points to a focus of STIC with moderate UbcH10 expression levels (IRS 8, H-score 140). The lower left arrow points to a focus of STIC with high UbcH10 expression (IRS 9, H-score 195). Note the normal tubal epithelium between the two foci with absent UbcH10 expression (anti-UbcH10, x10 magnification).

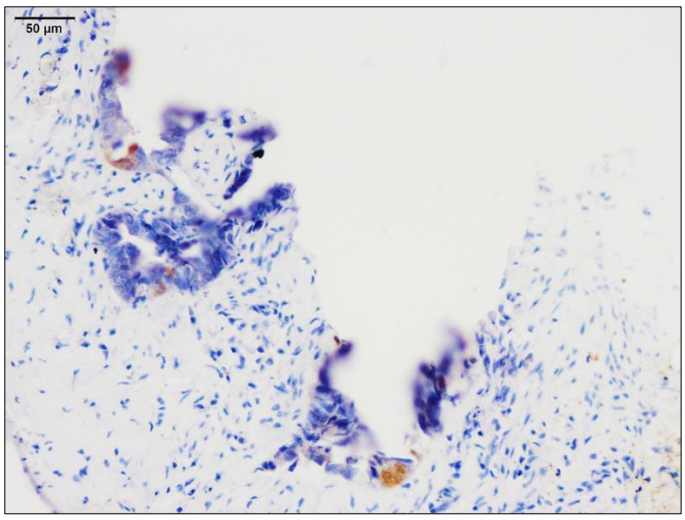

Figure 6. 8: A serous tubal intra-epithelial carcinoma with low UbcH10 expression (IRS2, H-score 20) (anti-UbcH10, x20 magnification).

6.4.6 UbcH10 is a feature of tubo-ovarian serous malignancy and is differentially expressed between normal, benign and malignant lesions

Given the differential UbcH10 staining patterns observed we statistically compared UbcH10 protein expression levels between normal tissue, benign serous cystadenomas, borderline serous tumours, p53 signatures, STICs and HGSOC. UbcH10 expression levels by both IRS and H-scores were significantly higher in STICs and HGSOC compared to p53 signatures, benign and borderline serous tumours as well as normal ovarian and tubal tissue, thus confirming the significance of our immunohistochemical observations (Table 6.2 and Figure 6.9). When we used the Mann-Whitney test to compare UbcH10 protein expression by IRS and H-scores between p53 signatures and STICs respectively, the difference was statistically significant [for IRS (U=20.5, p=<0.001, for H-score (U=4, p=<0.001)]. This confirms that the rise in UbcH10 expression is significant between the p53 signatures and the STIC stage of the HGSOC carcinogenesis model. Figure 6.10 is a representative image demonstrating the progressive increase in UbcH10 expression levels from normal tubal tissue to STIC and finally to invasive HGSOC in the same patient, whilst Figure 6.11 demonstrates higher UbcH10 expression in STIC compared to p53 signature from the same patient.

Table 6. 2: UbcH10 is differentially expressed between malignant tubo-ovarian serous lesions, p53 signatures, benign and borderline tumours, and normal tissue. UbcH10 expression by both IRS and H-scores are lowest in normal ovarian and tubal tissue as well as benign and borderline serous tumours. Expression in p53 signatures is slightly but not significantly higher than normal tissue. A statistically significant rise in UbcH10 expression is noted in high grade malignant serous lesions whether intra-epithelial (STICs) or invasive malignancies (HGSOC) as indicated by the *p*-value of the Kruskal-Wallis test.

Type of sample	**Number of samples**	**UbcH10 expression** ***Mdn (Min, Max)***	**Kruskal Wallis test** ***(H)***
		IRS	**60.52 *(p=<0.001)***
Normal ovary and Fallopian tube[a]	22	2 (0, 3)	
Serous cystadenoma and Serous borderline tumour[a]	5	2 (0, 2)	
P53 signature[b]	9	4 (2, 6)	
STIC[c]	24	7 (2, 11)	
HGSOC[c]	24	8 (2, 11)	
Total	**84**		
		H-score	**58.88 *(p=<0.001)***
Normal ovary and Fallopian tube	22	7 (0, 20.4)	
Serous cystadenoma and Serous borderline tumour	5	4 (0, 40)	
P53 signature	9	12 (4, 40)	
STIC	24	117 (20, 195)	
HGSOC	24	136 (20, 198)	
Total	**84**		

Mdn: median, **Min:** minimum, **Max**: maximum, **STIC:** serous tubal intra-epithelial carcinoma, **HGSOC**: high-grade serous ovarian cancer.

a: normal, benign, and borderline tumours were used as a control group from separate patients.

b: p53 signatures were found adjacent to STICs in 9 out of 24 patients.

c: STICs and HGSOC were matched from the same 24 patients.

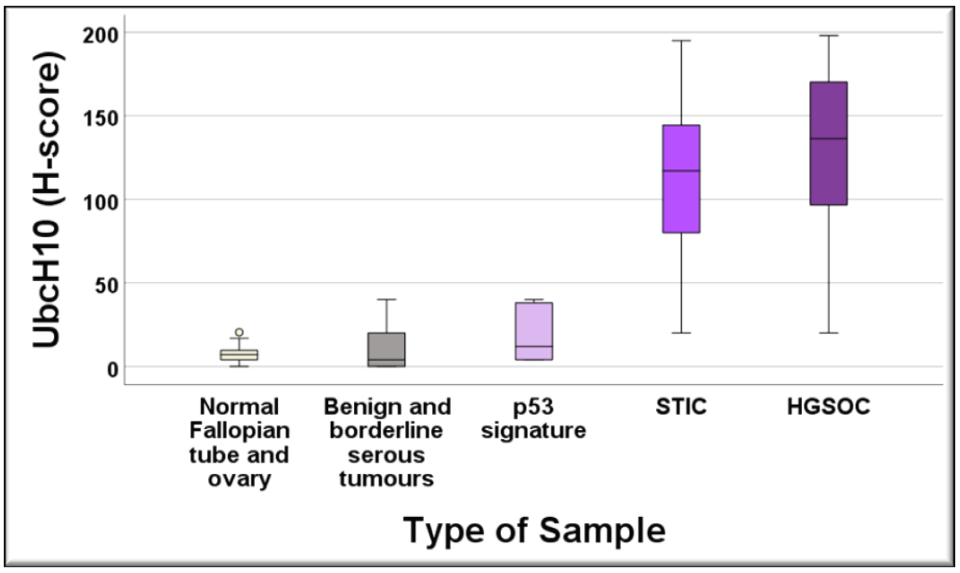

Figure 6. 9: A box plot diagram demonstrating the differential pattern of UbcH10 expression by H-score between malignant tubo-ovarian serous lesions, p53 signatures, benign and borderline tumours, and normal tissue. The median UbcH10 expression by H-score was lowest in normal ovarian and tubal tissue (n=22, *Mdn*=7) as well as benign and borderline serous tumours (n=5, *Mdn*=4). P53 signatures had a slightly but not significantly higher median UbcH10 expression (n=9, *Mdn*=12). The highest median UbcH10 expression was noted in serous tubal intra-epithelial carcinomas (n=24, *Mdn*=117) and their invasive high grade serous carcinomas (n=24, *Mdn*=136). This difference was statistically significant compared to p53 signatures, benign and borderline tumours as well as normal tissue (*H*=58.88, *p*=<0.001).

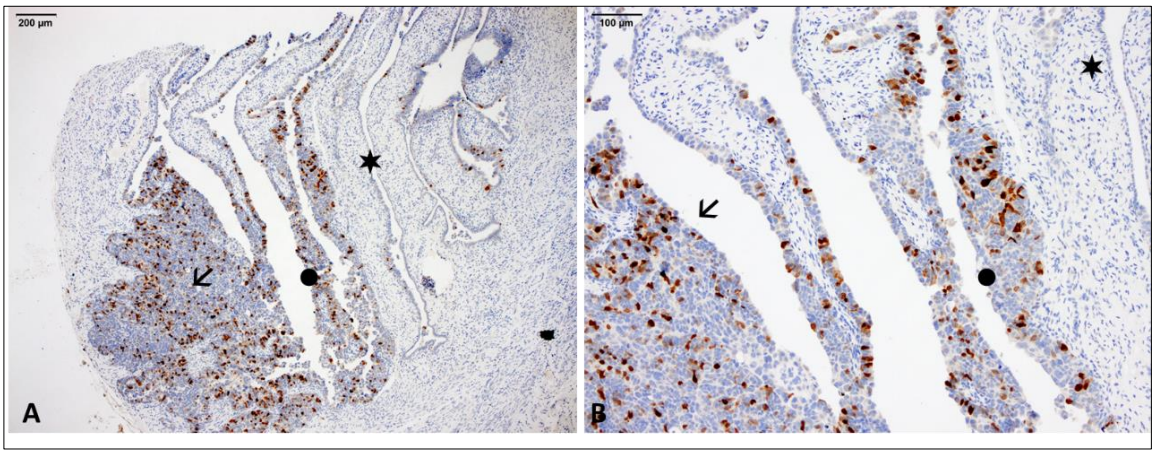

Figure 6. 10: Differential UbcH10 expression between normal tubal epithelium, STIC and invasive carcinoma from the same HGSOC patient. A) scanning power view showing UbcH10 expression in normal tubal tissue (star) followed by STIC (dot) and invasive carcinoma (arrow, anti-UbcH10, x4 magnification). B) Higher power view showing absent UbcH10 expression in normal tubal epithelium (star). UbcH10 expression was higher in STIC (dot, IRS 8, H-score 138.8) and highest in HGSOC (arrow, IRS 10, H-score 166) (anti-UbcH10, x10 magnification)

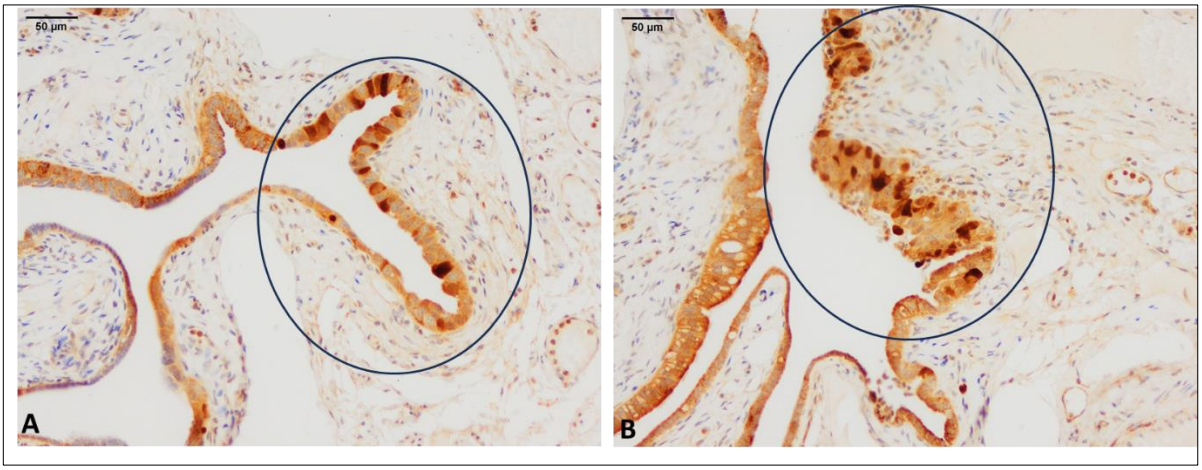

Figure 6. 11: Differential UbcH10 expression between STIC and p53 signature from the same HGSOC patient. A) A focus of p53 signature (circle) demonstrating low UbcH10 expression (IRS 5, H-score 35) (anti-UbcH10, x20 magnification). B) A focus of intraepithelial carcinoma from the same patient (circle) showing higher UbcH10 expression (IRS 7, H-score 109) (anti-UbcH10, x20 magnification).

These data confirm that UbcH10 is a feature of malignant high grade serous lesions whether precursor intra-epithelial carcinomas (STICs) or invasive high-grade serous carcinomas when compared to UbcH10 protein levels in p53 signatures, and normal and benign ovarian tissue.

6.4.7 UbcH10 protein expression in STICs is comparable to their corresponding invasive malignancies

As we have shown that high UbcH10 expression is a feature of malignant high grade serous lesions whether intra-epithelial carcinomas or invasive HGSOC, we next aimed to explore whether UbcH10 played a role in STIC progression to invasive carcinomas. To do this we compared UbcH10 expression levels by IRS and H-scores in STICs and their corresponding tumours using the Mann-Whitney test. Although UbcH10 expression levels were higher in HGSOC, its levels were not significantly different to their corresponding intra-epithelial carcinomas (Figures 6.12 and 6.13). In fact, UbcH10 expression in STICs were mostly comparable to their invasive malignancies. Figures 6.14, 6.15 and 6.16 demonstrate correlative UbcH10 expression in STICs and their corresponding HGSOC samples from three different patients.

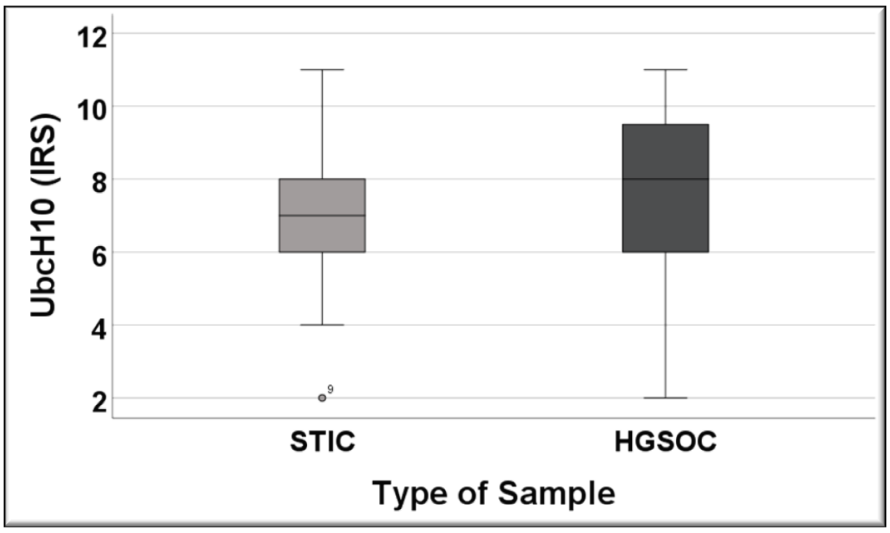

Figure 6. 12: A box plot diagram demonstrating comparable UbcH10 protein expression by IRS in 24 patients with STIC and their corresponding HGSOC. The median UbcH10 expression in HGSOC specimens was slightly higher (*Mdn*=8) compared to its median expression in STIC samples (*Mdn*=7) from the same patients. The difference was not statistically significant (*U*=220, *p*=0.156).

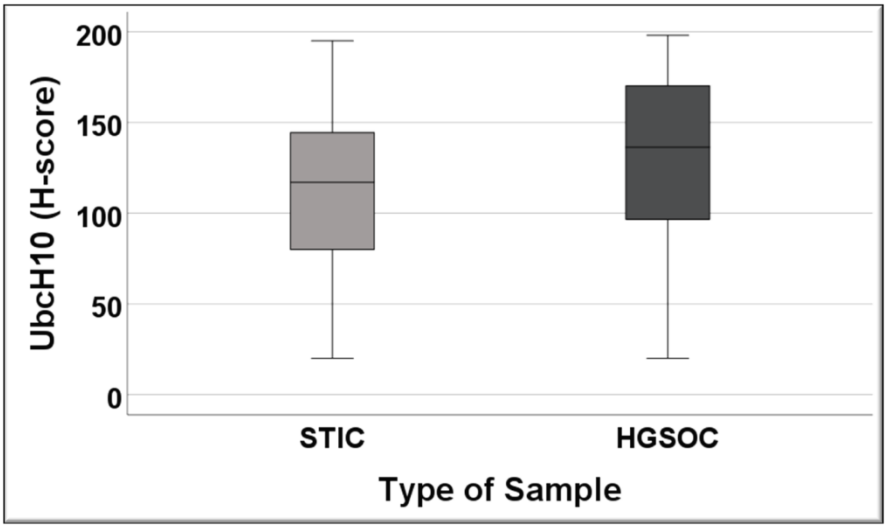

Figure 6. 13: A box plot diagram demonstrating comparable UbcH10 protein expression by H-score in 24 patients with STIC and their corresponding HGSOC. The median UbcH10 expression in HGSOC specimens was slightly higher (*Mdn*=136) compared to its median expression in STIC samples (*Mdn*=117) from the same patients. The difference was not statistically significant (*U*=233, *p*=0.261).

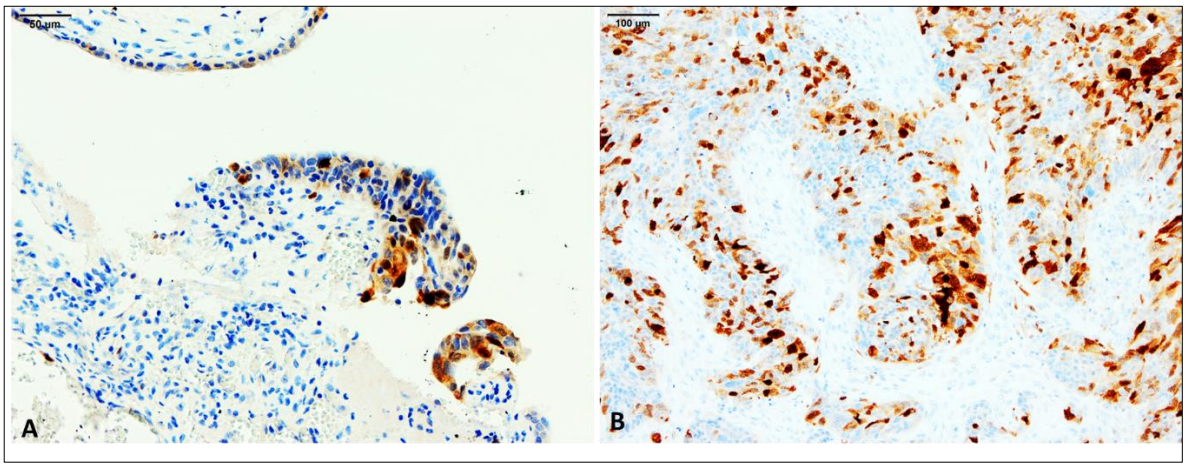

Figure 6. 14: A case showing comparable expression of UbcH10 in serous tubal intra-epithelial carcinoma (STIC) and corresponding HGSOC. A) A focus of STIC showing strong and moderate staining for UbcH10. This case was assigned IRS of 5 and H-score of 49 (anti-UbcH10, x20 magnification). B) The corresponding HGSOC from the same patient was assigned an IRS of 7 and H-score of 114.8 (anti-UbcH10, x10 magnification).

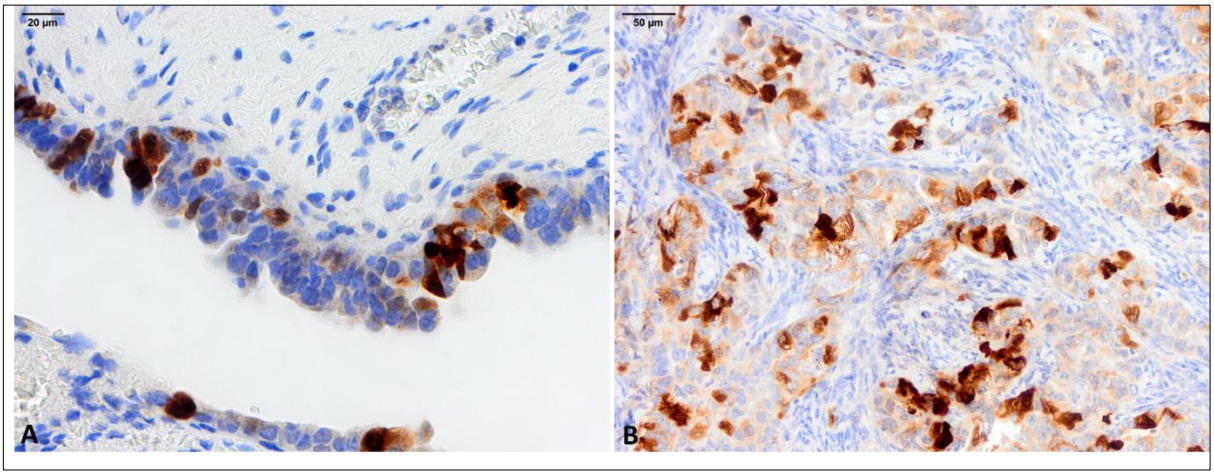

Figure 6. 15: A case showing very close UbcH10 immunohistochemical profile between STIC and its corresponding HGSOC. A) A focus of STIC with moderate UbcH10 nuclear and cytoplasmic expression (IRS 6, H-score 90) (anti-UbcH10, x40 magnification). B) The corresponding invasive carcinoma from the same patient with comparable UbcH10 expression (IRS 6, H-score of 106) (anti-UbcH10, x20 magnification).

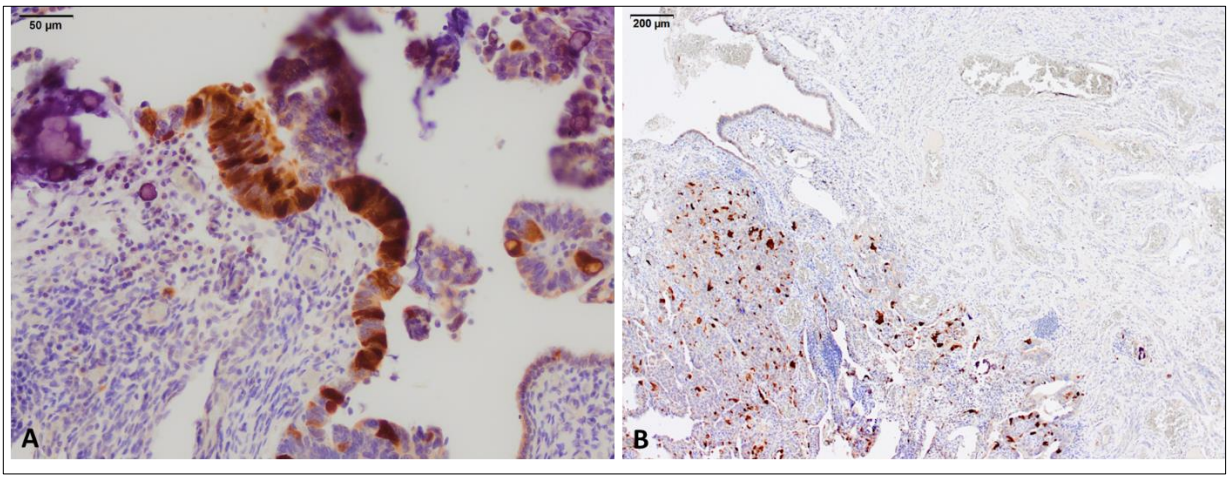

Figure 6. 16: An outlier case demonstrating paradoxical higher expression of UbcH10 in the serous tubal intra-epithelial carcinoma compared to the invasive carcinoma from the same patient. A) A focus of STIC showing strong diffuse UbcH10 expression (IRS 9, H-score 180) (anti-UbcH10, x20 magnification). B) Comparatively, in the invasive HGSOC UbcH10 expression levels were lower (IRS 5, H-score 93.8) (anti-UbcH10, magnification). It is worth noting that this patient was FIGO stage IV and had received neoadjuvant chemotherapy. The Ki-67 index in the STIC was similarly higher (50%) than the invasive tumour (30%).

We can conclude from these data that UbcH10 expression is comparable in STICs and their invasive HGSOC. Taken together, we can conclude that in the model of HGSOC carcinogenesis (p53 signature→STIC→HGSOC), UbcH10 is expressed as early as the p53 signature stage but with levels comparable to normal tubal epithelium. This means that UbcH10 is ***not*** overexpressed in p53 signatures but rather rises significantly in the STIC stage followed by invasive HGSOC. UbcH10 expression levels are not significantly higher in HGSOC compared to STICs. This might indicate that UbcH10 could possibly play a role in the progression of p53 signatures to STICs, while its role may be less significant in the STIC to HGSOC progression step. It is perhaps more likely that UbcH10 expression levels might mirror the increased proliferative indices from p53 signatures to STICs to HGSOC.

6.5 The heterogeneous relationship between UbcH10 and p53 in HGSOC precursor lesions

6.5.1 Overview

We have previously determined a heterogeneous relationship between p53 and UbcH10 protein levels in HGSOC in the Birmingham cohort. In this section we extend these studies to explore the relationship between p53 and UbcH10 in p53 signatures, and STICs to determine if these proteins show any correlative expression in the early stages of HGSOC pathogenesis. Multiplex immunohistochemical staining was done with both anti-p53 and anti-UbcH10 antibodies. Scoring of UbcH10 protein expression was done on dual staining and compared to single stained slides.

6.5.2 UbcH10 and p53 protein expression in p53 signatures and their corresponding STICs and HGSOCs

6.5.2.1 P53 expression in the p53 signature-STIC-HGSOC sequence

In our cohort, we had only 9 cases for which we had samples for all stages of HGSOC carcinogenesis: namely p53 signatures, STICs and invasive high-grade serous carcinomas. Whilst we previously demonstrated that the p53 IHC staining pattern was identical in STICs and their corresponding tumours (Figure 6.3), this was not the case for p53 signatures. Of the 9 cases, concordant p53 overexpression was observed in p53 signatures and their corresponding intra-epithelial and invasive carcinomas in only 6 cases (66.7%, Figure 6.17). Two cases (22.2%) had discordant p53 overexpression in the p53 signature in an otherwise p53 null tumour (Figure 6.18), whilst one case (11.1%) demonstrated a previously unreported cytoplasmic staining pattern in the p53 signature and corresponding tumour (Figure 6.19).

6.5.2.2 UbcH10 expression in the p53 signature-STIC-HGSOC sequence

To determine the relationship between UbcH10 and p53 in these 9 patients, dual staining for both proteins was performed. It was noticeable on multiplex staining that UbcH10 expression levels were low in p53 signatures (Median IRS 4, Median H-score 12) and increased significantly in STICs (Median IRS 7, Median H-score 106) as well as HGSOC (Median IRS 7, Median H-score 109). This increase in UbcH10 expression was noted irrespective of the p53 expression pattern as shown in Figures 6.18 to 6.20. From a statistical point of view, this rise from p53 signatures to STIC and HGSOC was statistically significant [for IRS H=15.1, p=<0.001, for H-score H=17.7, p=<0.001]. Taken together, these data further corroborate a heterogeneous relationship between UbcH10 and p53 in HGSOC and their precursor lesions.

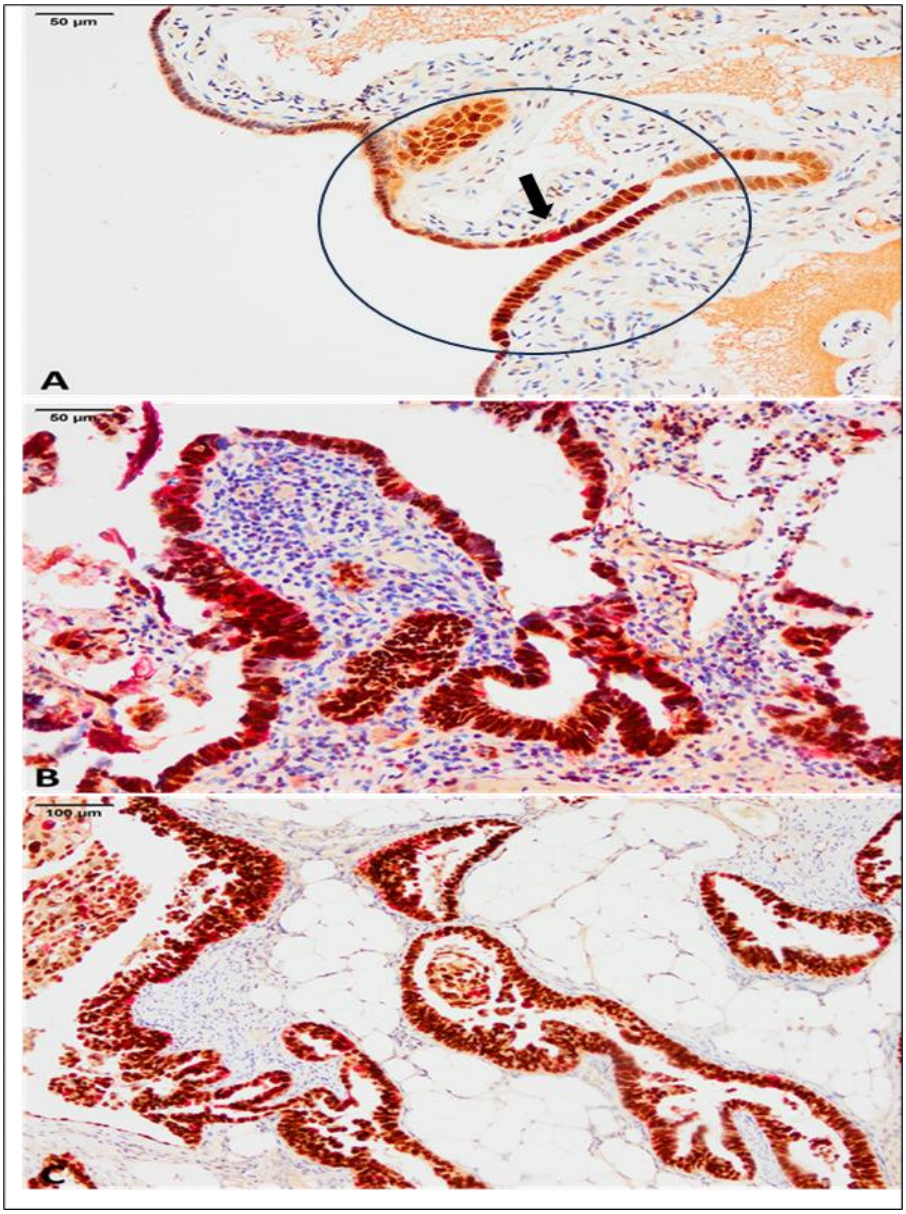

Figure 6. 17: UbcH10 and p53 dual expression throughout the spectrum of precursor lesions in HGSOC with concordant p53 overexpression in all lesions. A) A focus of p53 signature (circle) demonstrating p53 overexpression (brown) and very focal UbcH10 expression (red, arrow) (anti-p53, anti-UbcH10, x20 magnification). B) A focus of STIC from the same patient showing p53 overexpression (brown) and high UbcH10 expression (red, IRS 8, H-score 115) (anti-p53, anti-UbcH10, x20 magnification). C) Invasive HGSOC in the omental fat of the same patient showing p53 overexpression (brown) and comparable UbcH10 expression to the STIC (red, IRS 8, H-score 147.4) (anti-p53, anti-UbcH10, x10 magnification).

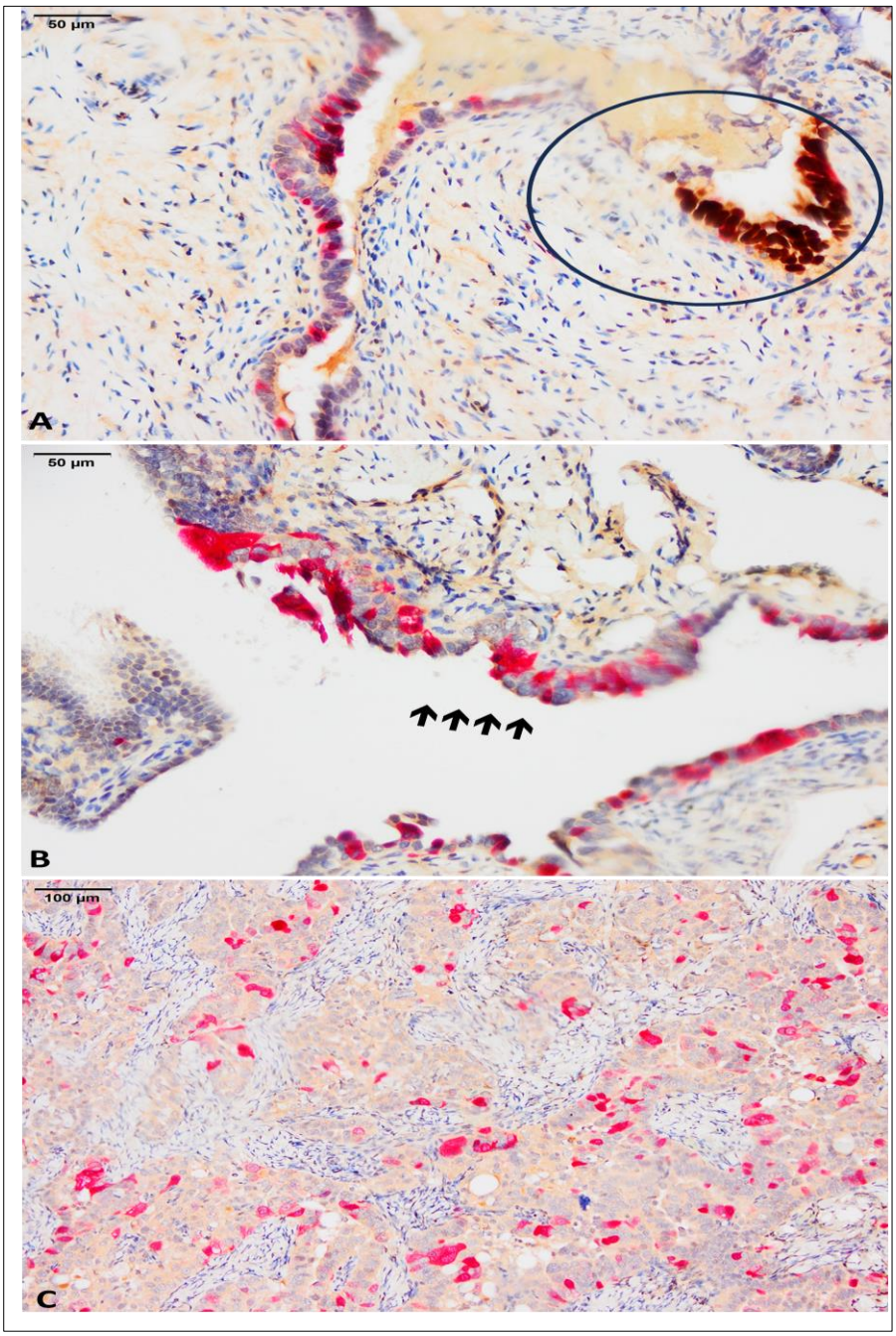

Figure 6. 18: UbcH10 and p53 dual expression in a HGSOC patient with discordant p53 overexpression signature in a p53 null tumour. A) A focus of p53 signature (circle) showing p53 overexpression (brown) and focal UbcH10 expression (red, IRS 3, H-score 9). Note the remaining normal tubal epithelium to the left showing focal UbcH10 expression as well. (anti-p53, anti-UbcH10, x20 magnification). B) A focus of STIC from the same patient (arrows) with p53 null pattern (no brown stain) and higher UbcH10 expression (red, IRS 6, H-score 90) (anti-p53, anti-UbcH10, x20 magnification). C) Invasive HGSOC in the same patient with completely absent p53 expression (no brown stain) and comparable UbcH10 expression to the intra-epithelial carcinoma (red, IRS 6, H-score 106) (anti-p53, anti-UbcH10, x10 magnification).

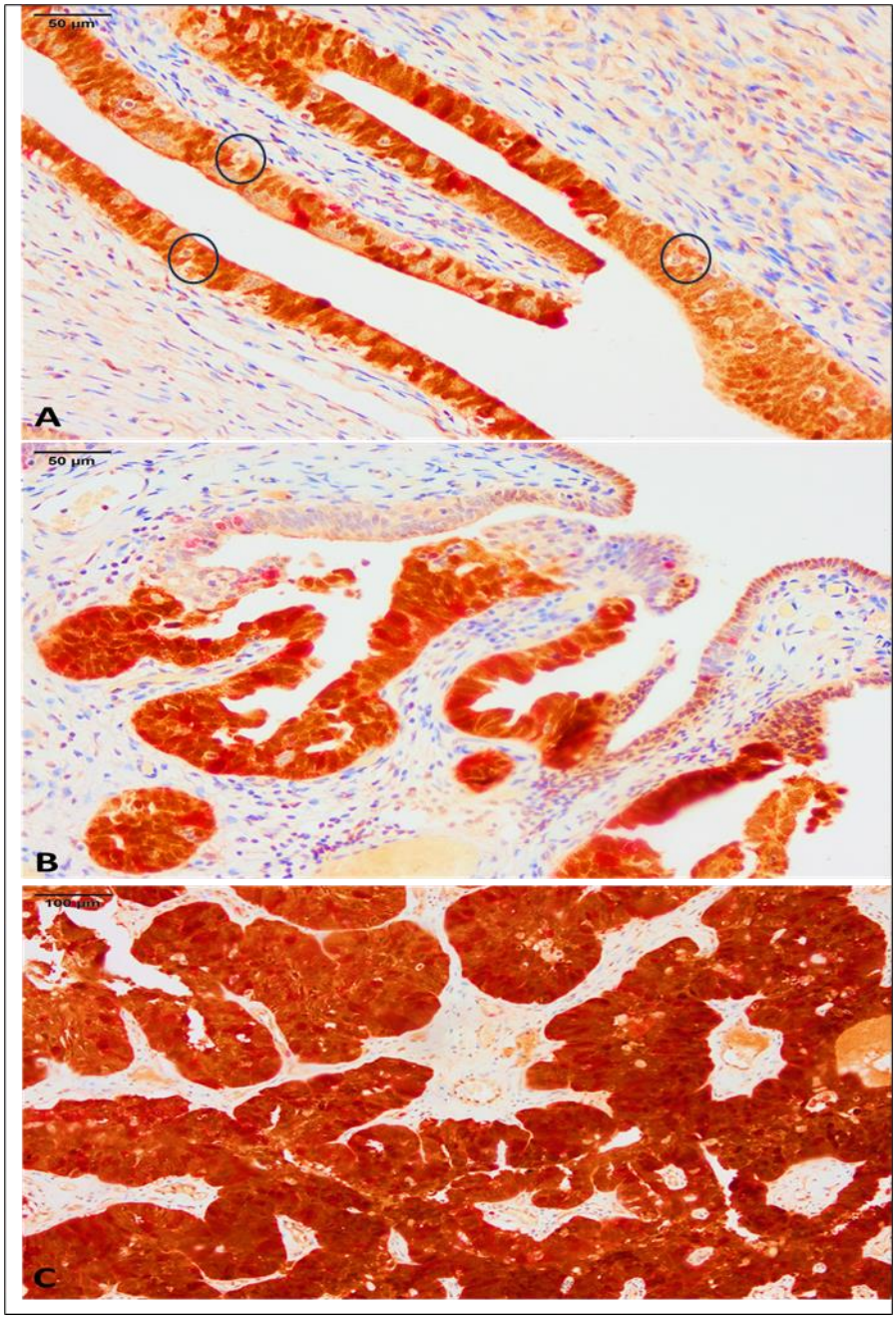

Figure 6. 19: UbcH10 and p53 dual expression throughout the spectrum of precursor lesions in a HGSOC case with cytoplasmic p53 expression. A) A p53 signature stretch of tubal epithelium with prominent secretory cells (circles) and ciliated cells characteristic of normal tubal epithelium showing cytoplasmic p53 expression (brown) and focal UbcH10 expression (red, IRS 5, H-score 38) (anti-p53, anti-UbcH10, x20 magnification). B) A STIC in the same patient with cytoplasmic p53 expression (brown) and higher UbcH10 expression (red, IRS 6, H-score 92) (anti-p53, anti-UbcH20, x20 magnification). C) Invasive carcinoma showing cytoplasmic p53 expression (brown) and high UbcH10 expression (red, IRS 11, H-score 175) (anti-p53, anti-UbcH10, x10 magnification).

6.5.3 Heterogeneous relationship between UbcH10 and p53 in serous tubal intra-epithelial carcinomas

To look more closely at the relationship between UbcH10 and p53, we performed dual staining for both proteins in the 24 cases of serous tubal intra-epithelial carcinomas in this cohort. We then put the STICs with p53 overexpression (19 cases, 79.2%) in one group and grouped the STICs with null (2 cases), cytoplasmic (1 case), and wild type-like (2 cases) p53 into a second group (5 cases, 20.8%). We also divided the cohort into high and low UbcH10 expression categories based on the previously defined cut-offs of 7 and 120 for IRS and H-scores, respectively. Fisher's exact test was then used to see if any significant association was found between the UbcH10 and p53 expression groups.

6.5.3.1 p53 and UbcH10 protein levels in STIC using IRS

The STIC samples which over-expressed UbcH10 protein (>7) represented a minority (9 cases, 37.5%) of the whole cohort, whilst 15 cases (62.5%) had low UbcH10 protein levels (≤7). When considering the expression levels of both UbcH10 and p53, only 9 (37.5%) STIC samples showed p53 overexpression and high UbcH10 expression. The remaining 10 cases (41.7%) with p53 overexpression polarized to the low UbcH10 expression group. All the STIC samples with null, cytoplasmic, and wild type-like p53 staining (20.8%) showed low or absent UbcH10 levels (≤7). The association between both proteins in STICs was found to be statistically not significant (Fisher's exact 2-sided significance=0.118).

6.5.3.2 p53 and UbcH10 protein levels in STIC using H-score

When considering UbcH10 expression by H-score, 10 STIC samples (41.7%) overexpressed UbcH10 (>120) whilst 14 (58.3%) had low UbcH10 expression. Similar to IRS, only 9 STIC samples (37.5%) showed both p53 and UbcH10 overexpression, and the majority of cases with p53 overexpression (10 cases, 41.7%) polarized to the low UbcH10 expression category, and the p53 null and cytoplasmic cases polarized to the low UbcH10 expression group. One wild type-like p53 STIC samples had low UbcH10 expression, whilst the other had high UbcH10 expression. The association between p53 and UbcH10 proteins in STICs was found to be statistically not significant (Fisher's exact 2-sided significance=0.358).

Figure 6.20 shows an example of STIC and corresponding HGSOC with both p53 and UbcH10 overexpression. Figures 6.21 and 6.22 show examples of STICs with null p53 and low UbcH10 expression.

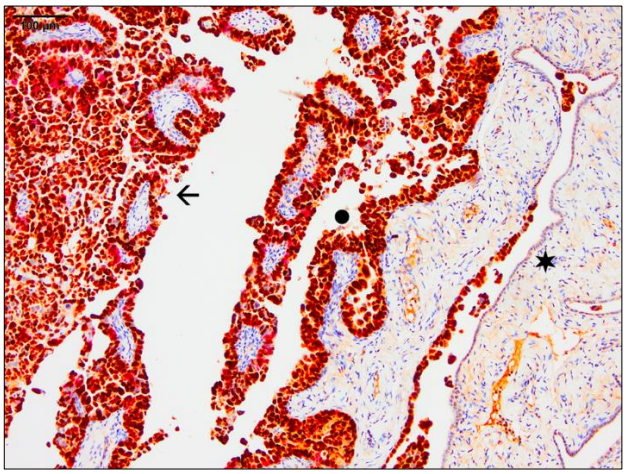

Figure 6. 20: The relationship between UbcH10 and p53 expression in STIC and HGSOC from a patient with p53 overexpression. A stretch of normal tubal epithelium with virtually no p53 or UbcH10 expression is appreciated (star). In the center of the field, a focus of STIC (dot) with p53 overexpression (brown) and high UbcH10 expression (red, IRS 8, H-score 138.8) is seen. Invasive HGSOC (arrow) with both p53 (brown) and UbcH10 overexpression (red, IRS 11, H-score 190) (anti-p53, anti-UbcH10, x10 magnification). This is the same sample shown in Figure 6.11.

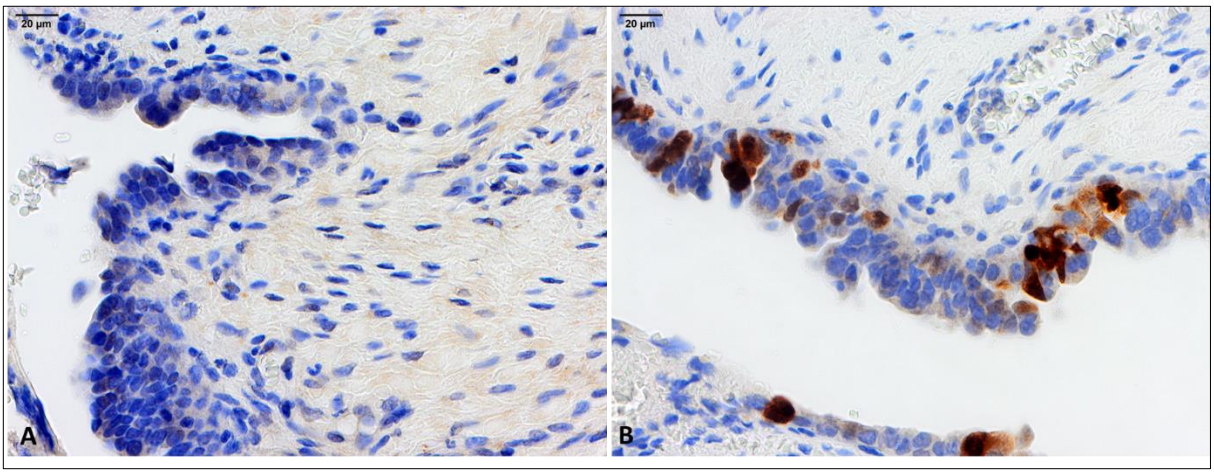

Figure 6. 21: The relationship between UbcH10 and p53 in serous tubal intra-epithelial carcinoma with null p53 pattern. A) Serous tubal intra-epithelial carcinoma demonstrating nuclear stratification, enlargement, and atypia with completely absent p53 expression (anti-p53, x40 magnification). B) Low UbcH10 expression in the STIC focus with an IRS of 6 and H-score of 90 (anti-UbcH10, x40 magnification).

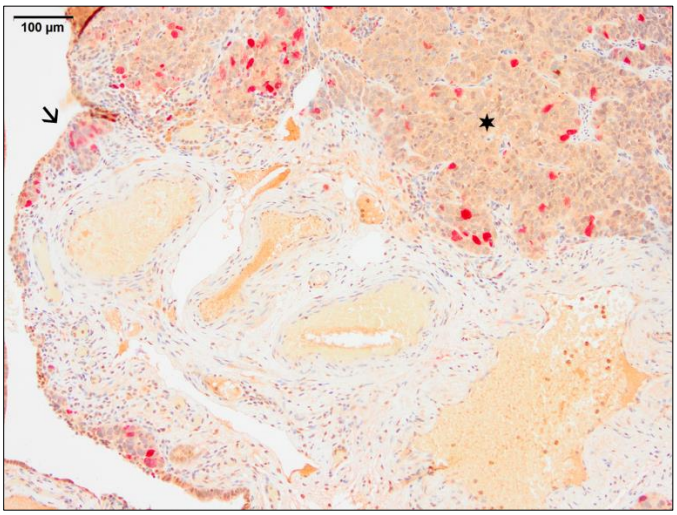

Figure 6. 22: The relationship between UbcH10 and p53 expression in STIC and HGSOC from a patient with p53 null pattern. An intra-epithelial carcinoma (arrow) with null p53 pattern (no brown staining) and low UbcH10 expression (red, IRS 7, H-score 109). The invasive tumour (star) shows the same staining pattern for both markers as well (anti-p53, anti-UbcH10, x10 magnification).

Taken together, the above data indicate that both UbcH10 and p53 are expressed early in the precursor lesions of HGSOC. In addition, our results exclude any positive correlation between the two proteins.

6.6 UbcH10 protein levels correlate positively with the proliferative state of the cell

6.6.1 Overview

As discussed in chapters 3 and 5, UbcH10 has the characteristics of a proliferative marker in HGSOC. Moreover, UbcH10 levels are low in p53 signatures which, by definition, have a low proliferative index. Furthermore, its expression levels are high in both STICs and HGSOC, both of which are characterized by high proliferation rates. To explore the possibility further that UbcH10 is a proliferative marker here we explore the relationship between UbcH10 and the well-known proliferative marker Ki-67 in our cohort of STICs and HGSOC. One case out of the 24 patients was omitted from analysis because its FFPE tissue block was exhausted, leaving 23 patients in this cohort for analysis. Normal fallopian tube and tonsillar tissue sections were used as controls for both proteins.

In this section we used a stepwise approach from single to multiplex staining to assess multiple parameters for Ki-67 and UbcH10 as previously described in Materials and Methods section 2.2.1.3). These parameters were measured for both STICs and HGSOCs separately. We then used the Mann-Whitney test to detect if these parameters (as continuous variables) differed significantly between STICs and their corresponding HGSOC samples. Spearman's correlation coefficient was then applied

to look for a significant correlation between Ki-67 and UbcH10 protein expression in both STICs and HGSOCs.

6.6.2 UbcH10 and Ki-67 protein levels in normal tissue

In normal fallopian tubes both the Ki-67 index and UbcH10 TPS was low. The Ki-67 index in normal tubal epithelium ranged from 0 to 4% whilst the UbcH10 TPS ranged from 0 to 10.2%. In tonsillar tissue both UbcH10 and Ki-67 polarized to the proliferating centroblasts located in the dark zone of the germinal centre with near total co-localisation between the two proteins. Less intense staining for both proteins was noted in the centrocytes, representing post-mitotic memory cells, located in the light zone of the germinal centre. Figure 6.23 illustrates Ki-67 and UbcH10 co-expression patterns in normal tubal and tonsillar tissue.

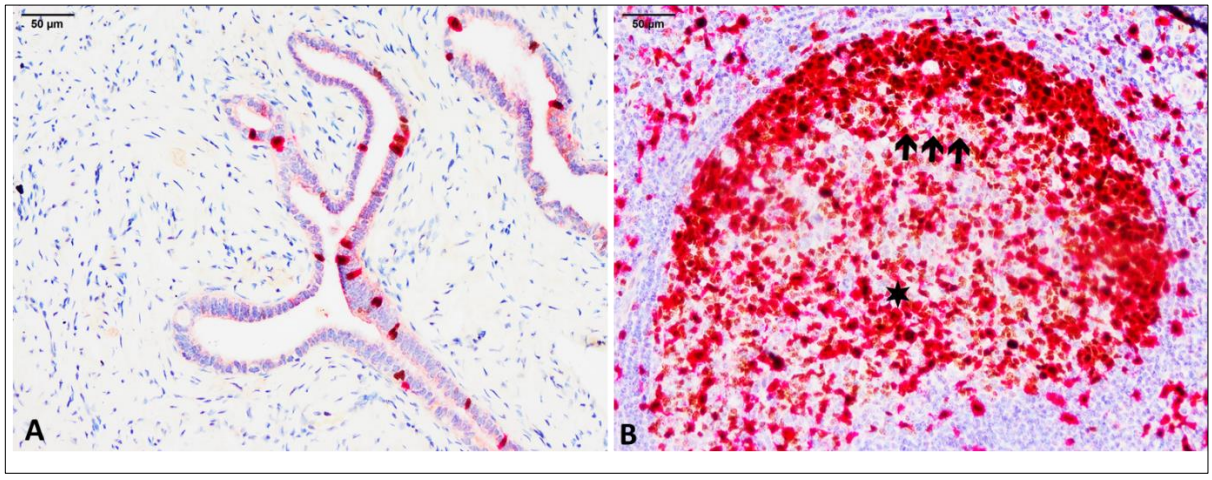

Figure 6. 23: Multiplex staining for Ki-67 (brown) and UbcH10 (red) in normal fallopian tube and tonsillar tissue. A) Normal tubal epithelium showing focal Ki-67 expression (brown nuclear) and low UbcH10 expression (red cytoplasmic and nuclear) [anti-Ki67 (MM-1), anti-UbcH10, x20 magnification]. B) A tonsillar germinal centre showing strong diffuse brown nuclear staining for Ki-67 and red cytoplasmic staining for UbcH10 in the proliferating centroblasts (dark zone, arrows). Near total co-localisation between both proteins is noted. In the post-mitotic centrocytes located in the light zone of the germinal centre (star), staining for both proteins is less intense [anti-Ki67 (MM-1), anti-UbcH10, x20 magnification].

6.6.3 UbcH10 and Ki-67 protein expression in STIC

The Ki-67 index ranged from 10 to 60% (*Mdn*=40) in the 23 serous tubal intra-epithelial carcinoma samples, whilst the UbcH10 TPS ranged from 20 to 83% (*Mdn*=35). The total TPS in dual-stained STICs ranged from 25 to 90% (*Mdn*=60), whilst the percentage of tumour cells that co-expressed both Ki-67 and UbcH10 in relation to the whole tumour ranged from 10 to 50% (*Mdn*=27). Furthermore, the percentage of tumour cells that co-expressed Ki-67 and UbcH10 as a percentage of the TPS ranged from 16.7 to 84.8% (*Mdn*=50). Figure 6.24 shows two examples of STIC with Ki-67 and UbcH10 co-expression.

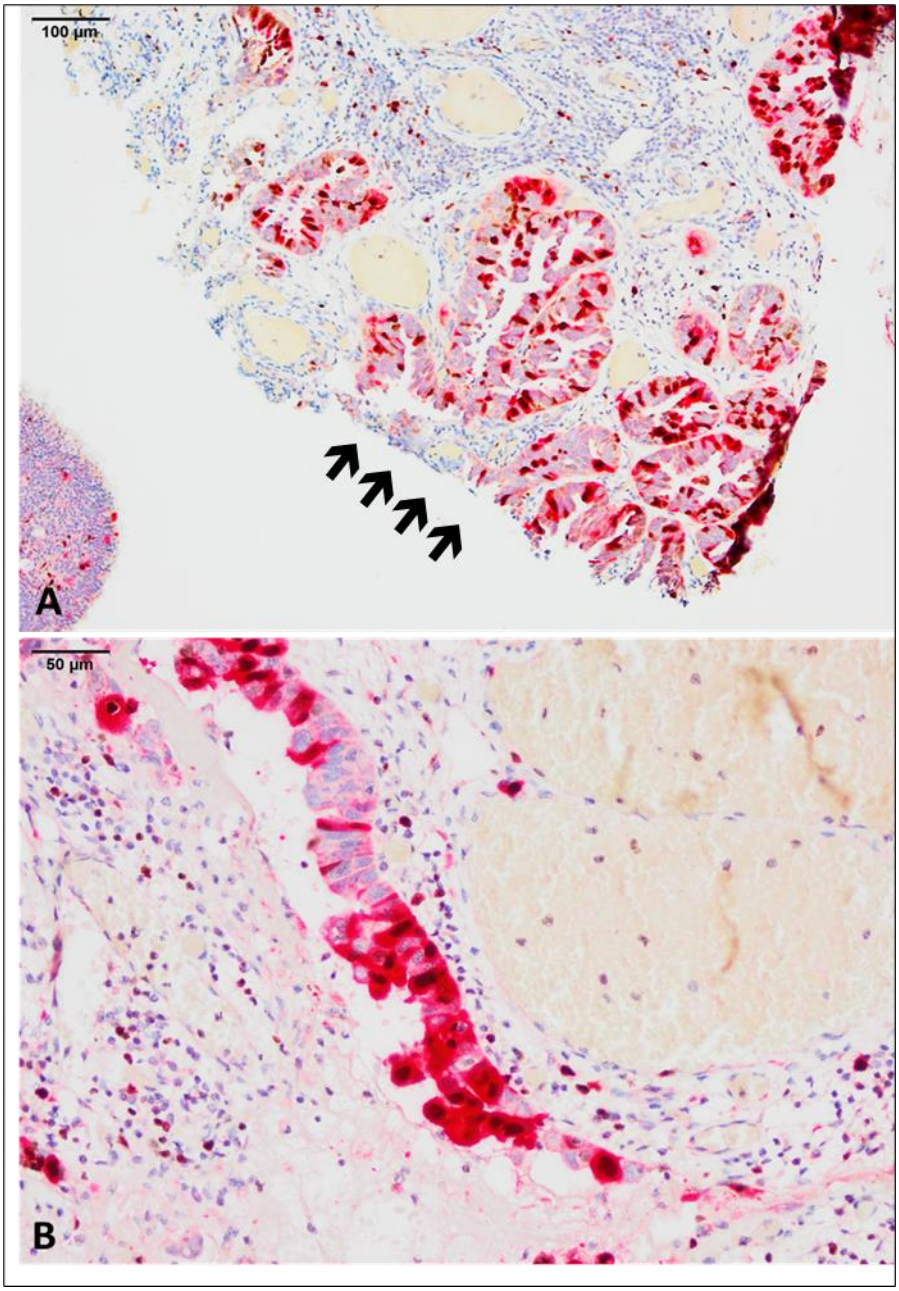

Figure 6. 24: Multiplex staining for Ki-67 (brown) and UbcH10 (red) in two different cases of STICs with significant colocalization of both proteins. A) A serous tubal intra-epithelial carcinoma with a Ki-67 index (brown nuclear) and UbcH10 tumour proportion score (red cytoplasmic and nuclear) of 50%. The total tumour proportion score for both Ki-67 and UbcH10 in this case was 60%. Around 44% of tumour cells showed co-expression of both proteins in relation to the whole intra-epithelial carcinoma, while 73.3% of tumour cells showed co-expression of both proteins in relation to the total tumour proportion score [anti-Ki-67 (MM-1), anti-UbcH10, x10 magnification]. B) Another intra-epithelial carcinoma showing a Ki-67 index and UbcH10 total proportion score of 50% with near total colocalization between both proteins [anti-Ki67 (MM-1), anti-UbcH10, x20 magnification].

6.6.4 UbcH10 and Ki-67 protein levels in HGSOC

We next considered the invasive carcinomas corresponding to the intra-epithelial carcinomas in the 23 patients. The Ki-67 index ranged from 11 to 90% (*Mdn*=50), whilst the UbcH10 TPS ranged from 20.2 to 84% (*Mdn*=50).

Dual staining indicated that the total TPS in HGSOC ranged from 35 to 95% (*Mdn*=68) and that the percentage of tumour cells that co-expressed both Ki-67 and UbcH10 in relation to the whole tumour ranged from 14 to 69% (*Mdn*=35). Additionally, the percentage of tumour cells that co-expressed Ki-67 and UbcH10 as a percentage of the TPS ranged from 20 to 76.7% (*Mdn*=55.5). Figure 6.25 shows two examples of HGSOCs with Ki-67 and UbcH10 co-expression.

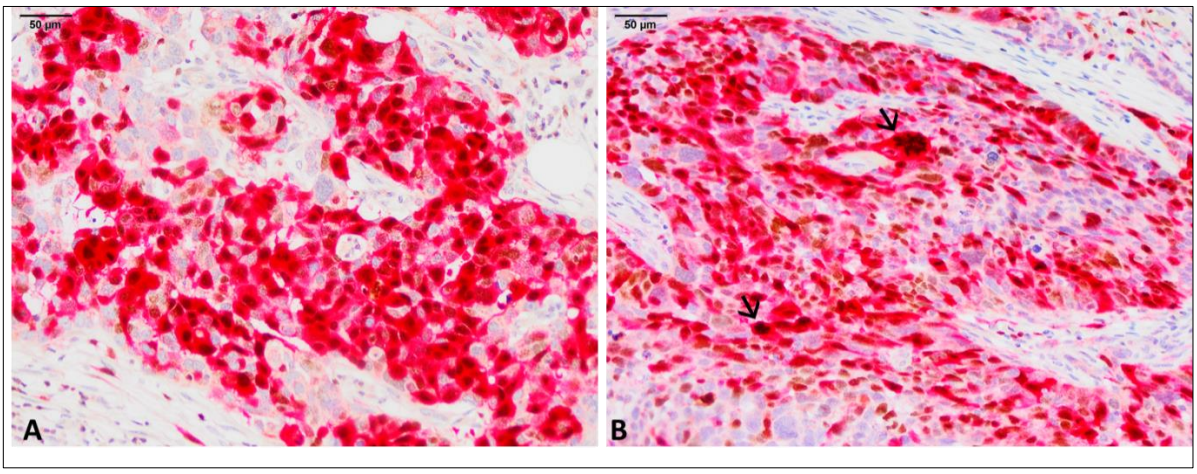

Figure 6. 25: Multiplex staining for Ki-67 (brown) and UbcH10 (red) in two different cases of HGSOC with significant colocalization of both proteins. A) A HGSOC showing diffuse strong expression for both Ki-67 (brown nuclear) and UbcH10 (red cytoplasmic). This case was assigned a Ki-67 index of 75% and a UbcH10 tumour proportion score of 84%. The total tumour proportion score for both Ki-67 and UbcH10 was 90%. Around 69% of tumour cells showed co-expression of both proteins in relation to the whole tumour, while 76.6% of tumour cells showed co-expression of both proteins in relation to the total tumour proportion score [anti-Ki-67 (MM-1), anti-UbcH10, x20 magnification]. B) Another HGSOC with a Ki-67 index of 47% and a UbcH10 tumour proportion score of 60%. Note the mitotically active cells (arrows) expressing both markers [anti-Ki-67 (MM-1), anti-UbcH10, x20 magnification].

6.6.5 Ki-67 and UbcH10 protein levels in STIC compared to HGSOC

After exploring the dual expression of Ki-67 and UbcH10 proteins in STICs and HGSOC we compared their expression levels between intra-epithelial and invasive carcinomas using the Mann-Whitney test. The Ki-67 index was significantly higher in HGSOC compared to their matched STICs (U=170.5, p=0.038; Figure 6.26). However, the UbcH10 total tumour proportion score, although higher in the HGSOC, was not significantly different between the invasive and intra-epithelial carcinomas (U=177, p=0.054).

Concerning both Ki-67 and UbcH10, the total TPS was higher in HGSOC compared to STIC, but the difference was not statistically significant (U=195, p=0.124).

Dual staining, co-localisation studies indicated that the percentage of tumour cells that co-expressed both proteins in relation to the whole tumour was significantly higher in HGSOC compared to their STICs (U=170, p=0.037; Figure 6.27). However, the percentage of tumour cells that co-expressed both proteins in relation to the TPS was not significantly higher in HGSOC compared to their matched STICs (U=212.5, p=0.253). These data are summarized in Table 6.3.

Overall, this data reflects the higher proliferative nature of HGSOC compared to STICs and point to the significant co-expression of both UbcH10 and Ki-67 in STICs and HGSOC.

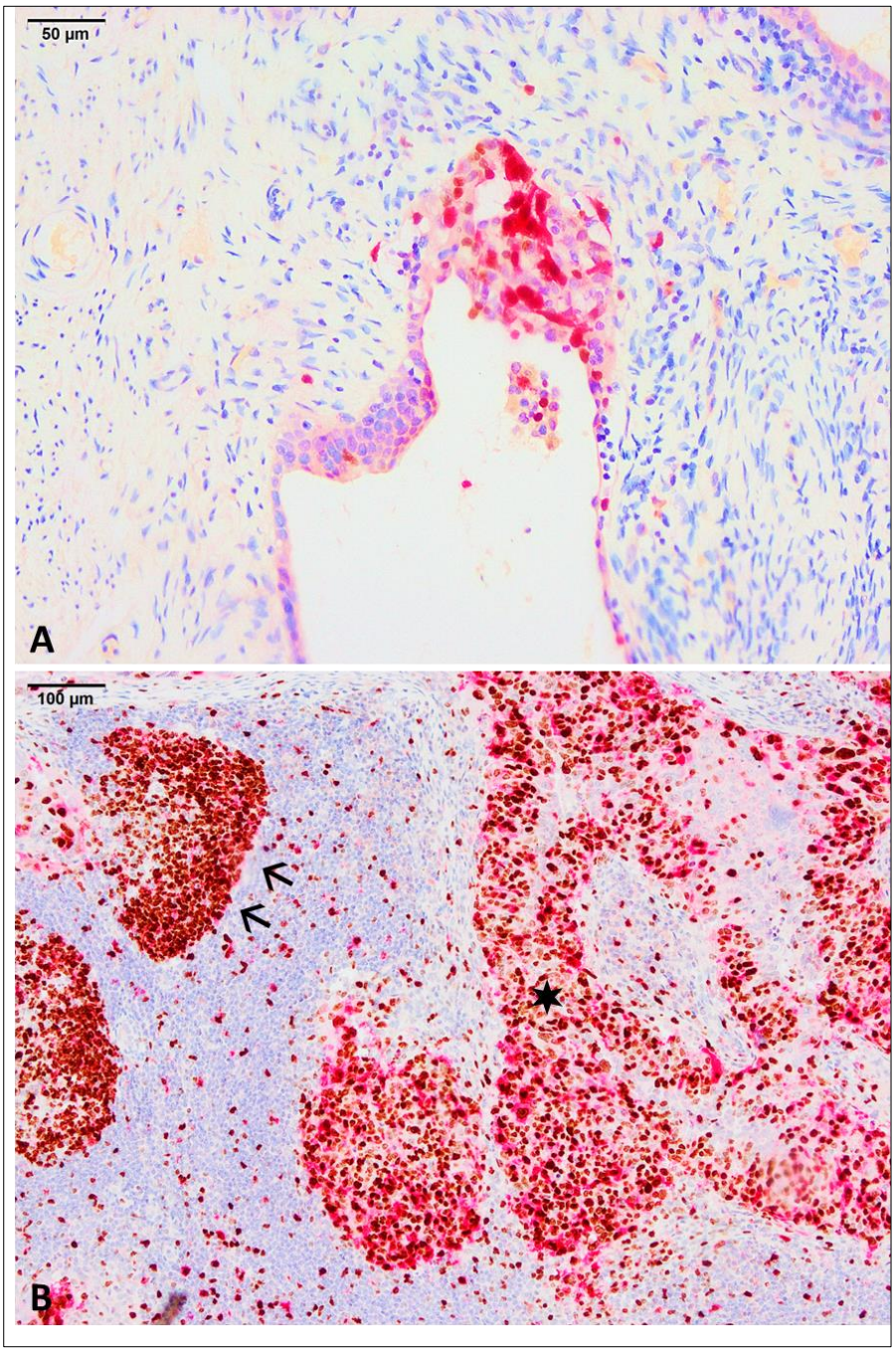

Figure 6. 26: Comparative Ki-67 (brown) and UbcH10 (red) expression between a STIC and HGSOC from the same patient. A) Serous tuba intra-epithelial carcinoma with a Ki-67 index (brown nuclear) of 45% and a UbcH10 tumour proportion score (red cytoplasmic) of 33% [anti-Ki-67 (MM-1), anti-UbcH10, x20 magnification). B) Invasive high-grade serous carcinoma (star) in a lymph node (arrows) from the same patient. The Ki-67 index in this case was significantly higher (90%) than the intra-epithelial carcinoma. The UbcH10 tumour proportion score in this case was also higher than STIC at 65%. Note the polarization of both Ki-67 and UbcH10 in the germinal centre (arrows) of the native nodal tissue to the left of the invasive tumour [anti-Ki67 (MM-1), anti-UbcH10, x10 magnification).

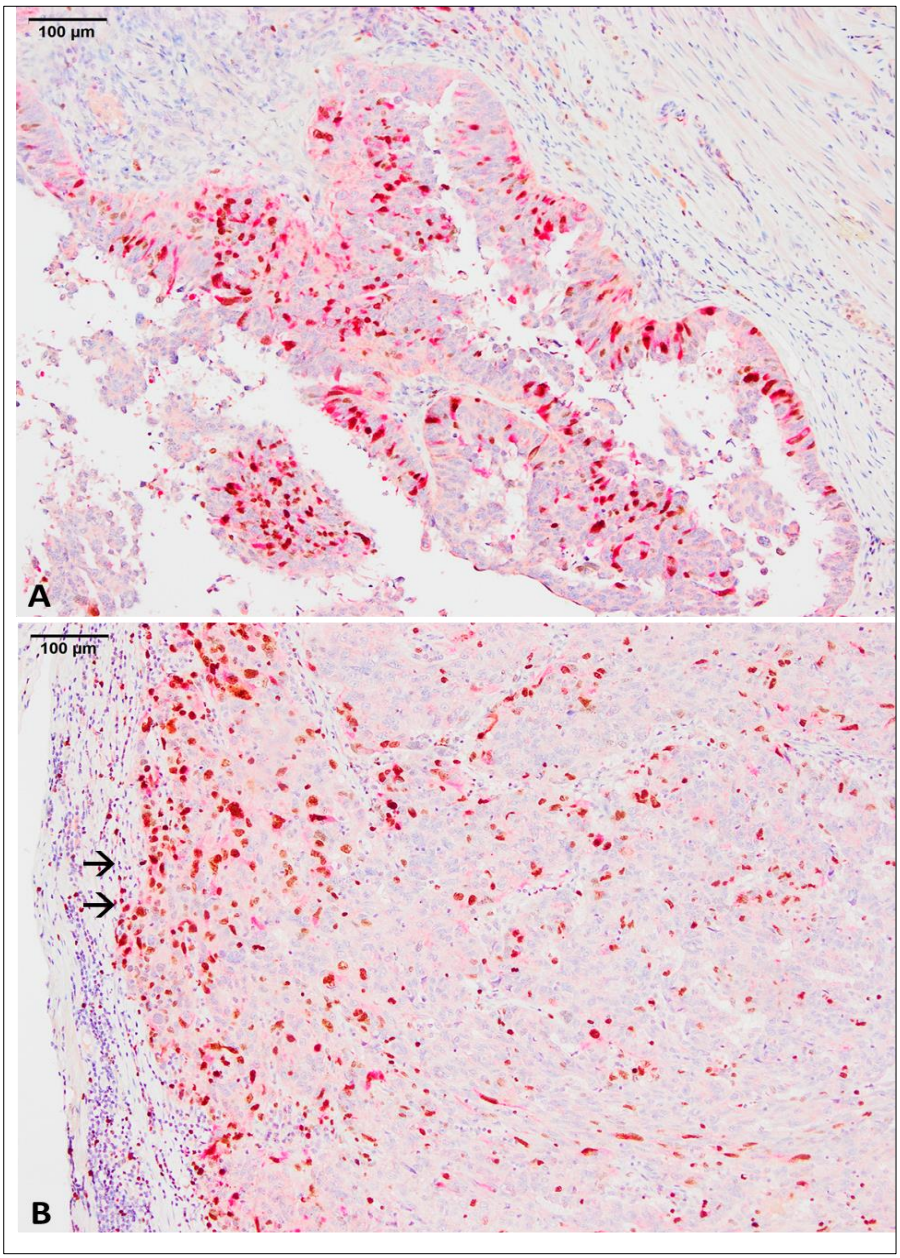

Figure 6. 27: Comparative Ki-67 (brown) and UbcH10 (red) expression between a STIC and HGSOC from the same patient with significant higher co-localisation in the invasive component. A) Serous tubal intra-epithelial carcinoma with a Ki-67 index (brown nuclear) of 22% and a UbcH10 tumour proportion score of 40%. The co-localisation of both proteins was estimated at 15% in relation to the whole intra-epithelial carcinoma [anti-Ki-67 (MM-1), anti-UbcH10, x10 magnification]. B) Invasive carcinoma from the same patient with a higher Ki-67 index at 35% and a similar UbcH10 tumour proportion score of 40% compared to the intra-epithelial carcinoma. The co-localisation of both proteins here was significantly higher at 35% particularly noticeable at the invasive front of the tumour (arrows) [anti-Ki-67 (MM-1), anti-UbcH10, x10 magnification].

Table 6. 3: The relationship between UbcH10 and Ki-67 protein expression in matched STICs and HGSOCs matched from 23 patients.

Type of sample	Number of samples	Ki-67 index *Mdn* *(Min, Max)*	Mann-Whitney *(U)*
STIC	23	40 (10, 60)	**170.5** **(*p*=0.038)***
HGSOC	23	50 (11, 90)	
		UbcH10 TPS *Mdn* *(Min, Max)*	**177** **(*p*=0.054)**
STIC	23	35 (20, 83)	
HGSOC	23	50 (20.2, 84)	
		Total TPS (Ki-67+UbcH10) *Mdn* *(Min, Max)*	**195** **(*p*=0.124)**
STIC	23	60 (25, 90)	
HGSOC	23	68 (35, 95)	
		Colocalization of UbcH10 & Ki-67 (% of whole tumour) *Mdn* *(Min, Max)*	**170** **(*p*=0.037)***
STIC	23	27 (10, 50)	
HGSOC	23	35 (14, 69)	
		Colocalization of UbcH10 & Ki-67 (% of TPS) *Mdn* *(Min, Max)*	**212.5** **(*p*=0.253)**
STIC	23	50 (16.7, 84.8)	
HGSOC	23	55.5 (20, 76.7)	

Mdn: Median, **Min**: minimum, **Max**: maximum, **TPS**: tumour proportion score

6.6.6 Ki-67 and UbcH10 are positively co-expressed in HGSOC and their precursor lesions

Given the similarities in Ki-67 and UbcH10 staining patterns we next applied statistical correlations to define the relationship between Ki-67 and UbcH10 in STICs and their corresponding invasive tumours. We used Spearman's correlation coefficient as the most appropriate test to correlate Ki-67 and UbcH10 protein expression. Spearman's correlation coefficient was first applied to STICs and matched invasive carcinomas separately. The STICs and HGSOCs were then divided into high and low UbcH10 expression groups based on the previously identified cut-offs for UbcH10 expression by IRS (7) and H-score (120). The difference in Ki-67 proliferative index between the two groups was then explored in STICs and HGSOCs using the Mann-Whitney test.

6.6.6.1 Ki-67 and UbcH10 are weakly correlated in STICs

In the 23 STIC samples, the UbcH10 TPS weakly and positively correlated with the Ki-67 index but the relationship was not statistically significant (ρ=0.172, p=0.434; Figure 6.28). When the STIC samples were divided into low and high UbcH10 expression groups, the Ki-67 index was higher in the high UbcH10 group (IRS>7, H-score >120) compared to the low UbcH10 group (IRS≤7, H-score≤120) but the difference was not statistically significant. Data are shown in Table 6.4.

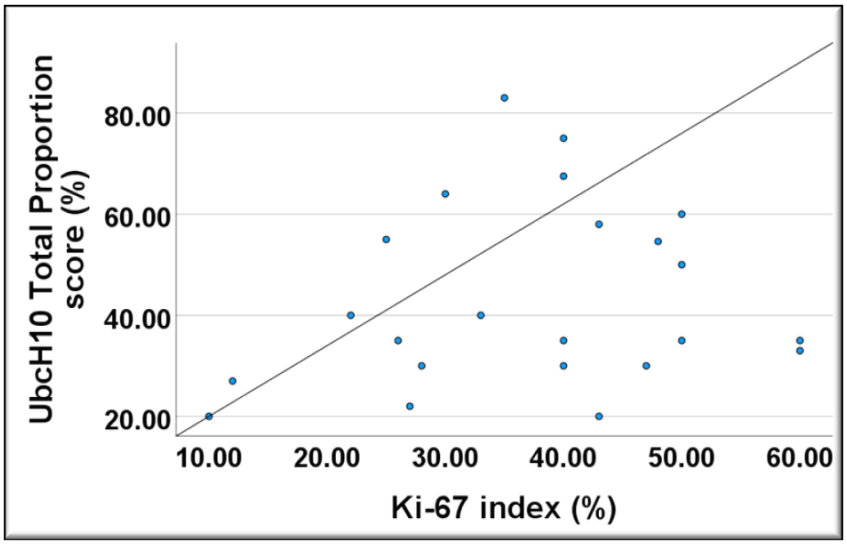

Figure 6. 28: The correlation between the Ki-67 index and UbcH10 tumour proportion score in 23 STIC samples. A weak positive correlation exists between the two proteins, but the association was not statistically significant (Spearman's ρ=0.172, p=0.434).

Table 6. 4: The relationship between Ki-67 index and UbcH10 protein expression categories by IRS and H-scores in 23 STIC samples. The Ki-67 index was higher in the high UbcH10 expression group whether by IRS or H-score, but the difference was not statistically significant.

UbcH10 protein expression	**Number of STIC samples**	**Ki-67 index** ***Mdn*** ***(Min, Max)***	**Mann-Whitney** ***(U)***
IRS category			**50.5 (*p*=0.429)**
Low (≤7)	14	36.5 (10, 60)	
High (>7)	9	40 (25 ,50)	
Total	23	40 (10, 60)	
H-score category			**49.5 (*p*=0.334)**
Low (≤120)	13	33 (10, 60)	
High (>120)	10	40 (25, 60)	
Total	23	40 (10, 60)	

Mdn: Median, **Min**: minimum, **Max**: maximum

Together, these data indicate a weak positive correlation between Ki-67 and UbcH10 protein expression in STIC samples.

6.6.6.2 Ki-67 and UbcH10 are significantly correlated in HGSOC

In the 23 invasive high-grade serous carcinomas, the UbcH10 TPS was moderately and positively correlated with the Ki-67 index and the relationship was statistically significant (ρ=0.478, p=0.021; Figure 6.29). When the HGSOC samples were divided into low and high UbcH10 expression groups, the Ki-67 index was significantly higher in the high UbcH10 group (IRS>7, H-score >120) compared to the low UbcH10 group (IRS≤7, H-score≤120). Data are shown in Table 6.5.

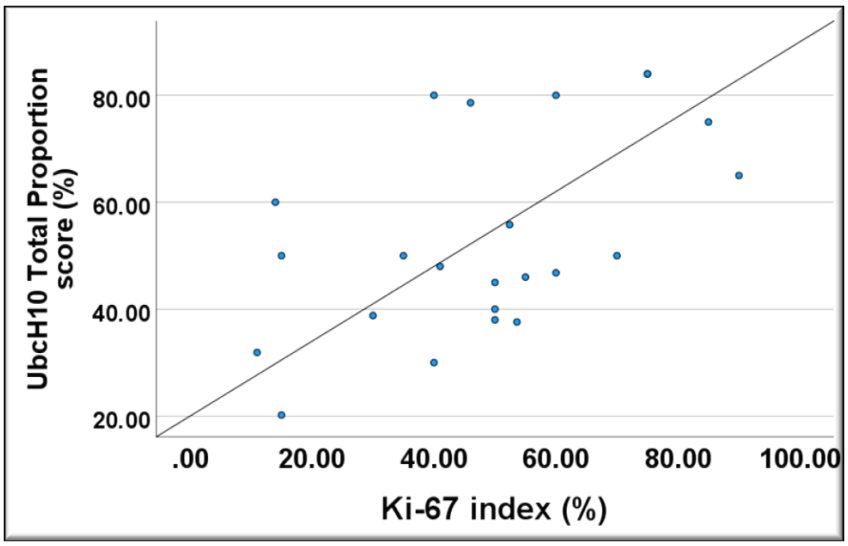

Figure 6. 29: The correlation between Ki-67 index and UbcH10 tumour proportion score in 23 HGSOC specimens. A significant moderate positive correlation is demonstrated between the two proteins (Spearman's ρ=0.478, p=0.021).

Table 6. 5: The relationship between Ki-67 index and UbcH10 protein expression categories by IRS and H-scores in 23 HGSOC samples. The Ki-67 index was significantly higher in the high UbcH10 expression group whether by IRS or H-score as indicated by the *p*-value of the Mann-Whitney test.

UbcH10 protein expression	**Number of HGSOC samples**	**Ki-67 index** ***Mdn*** ***(Min, Max)***	**Mann-Whitney** ***(U)***
IRS category			**23.5 (*p*=0.01)**
Low (≤7)	10	32.5 (11, 60)	
High (>7)	13	52.4 (40, 90)	
Total	23	50 (11, 90)	
H-score category			**23.5 (*p*=0.01)**
Low (≤120)	10	33 (10, 60)	
High (>120)	13	52.4 (40, 90)	
Total	23	50 (11, 90)	

Mdn: Median, **Min**: minimum, **Max**: maximum

We can infer from the above data the significant positive co-expression of Ki-67 and UbcH10 in high grade serous carcinomas.

6.7 The correlation of UbcH10 and Ki-67 protein expression with clinico-pathological/treatment variables in the STIC-HGSOC cohort

6.7.1 Overview

We next correlated UbcH10 protein expression and Ki-67 index with the various clinico-pathological and treatment variables in the 23 patients with matched STICs and HGSOC samples. Both UbcH10 and Ki-67 protein expression were measured as continuous variables without cut-off values. The UbcH10 TPS and the Ki-67 index in the invasive samples were considered for the statistical correlations and expression in the STICs was overlooked since the invasive tumour supersedes the intra-epithelial carcinoma.

6.7.2 UbcH10 and Ki-67 protein levels do not correlate with older patient age

When the UbcH10 TPS was correlated with the age of patients at diagnosis, a weak negative correlation was detected that was statistically not significant (ρ=-0.077, p=0.72). Similarly, a weak and non-significant but positive correlation existed between the Ki-67 index and age of the female patients at diagnosis (Figure 6.30). We conclude therefore that neither UbcH10 nor Ki-67 protein expression levels correlate with age at diagnosis in this cohort.

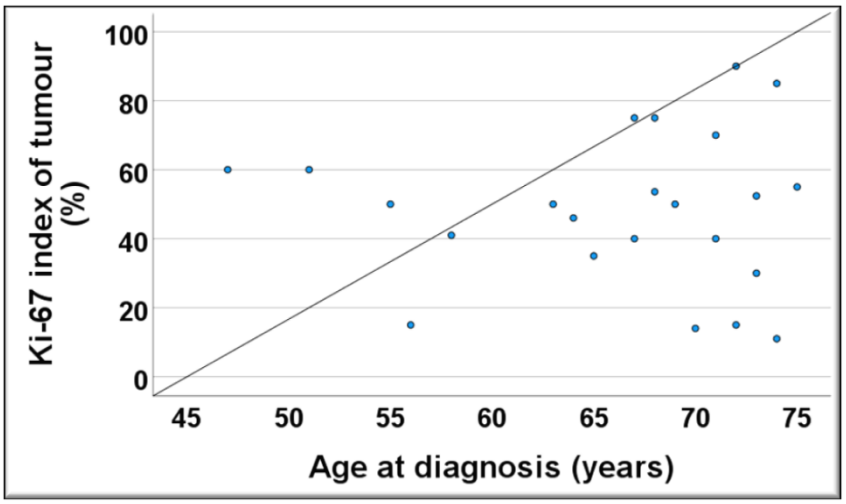

Figure 6. 30: The correlation between the Ki-67 index and age at diagnosis in 23 HGSOC females. A weak positive correlation was found between the two parameters that was statistically not significant (ρ=0.003, 0.99).

6.7.3 UbcH10 and Ki-67 protein levels do not correlate with FIGO stage

The UbcH10 TPS was higher in early FIGO stage patients (*n*=5, *Mdn*=50) compared to late FIGO stage patients *(n*=19, *Mdn*=49). The difference however was statistically not significant (*U*=39.5, *p*=0.681). Similarly, the median Ki-67 index was higher in early FIGO stage patients compared to late FIGO stage patients, but again the difference was not statistically significant (*U*=32.5, *p*=0.351). These data show that neither UbcH10 nor Ki-67 protein expression levels correlate with FIGO stage in these 23 HGSOC patients.

6.7.4 UbcH10 and Ki-67 protein levels do not correlate with Lymph node metastasis

The median UbcH10 TPS was higher in N0 and Nx patients (n=18, *Mdn*=50) compared to those with nodal metastasis (N1, n=5, *Mdn*=46). The difference was not, however,

statistically significant (*U*=34.5, *p*=0.433). Similarly, the Ki-67 index was higher in patients with N0 or Nx disease (*Mdn*=50) compared to those with N1 disease (*Mdn*=40), and again the difference was not statistically significant (*U*=42.5, *p*=0.852). Thus, neither UbcH10 nor Ki-67 protein levels correlate with nodal metastasis.

6.7.5 UbcH10 and Ki-67 protein levels are affected by pre-operative chemotherapy

To examine the effect of chemotherapy on UbcH10 and Ki-67 from this cohort we compared expression levels in patients who underwent PDS (n=11) and those who underwent DDS after NACT (n=12). The median UbcH10 TPS was higher in patients who underwent PDS (*Mdn*=65) compared to those who underwent DDS (*Mdn*=47), though the difference was not statistically significant (*U*=38, *p*=0.084).

Likewise, the median Ki-67 index in patients who underwent PDS, was higher than patients who underwent DDS. This difference was statistically significant (*U*=24.5, *p*=0.01; Figure 6.31).

These data indicate that both UbcH10 and Ki-67 protein levels are reduced by pre-operative chemotherapy administration.

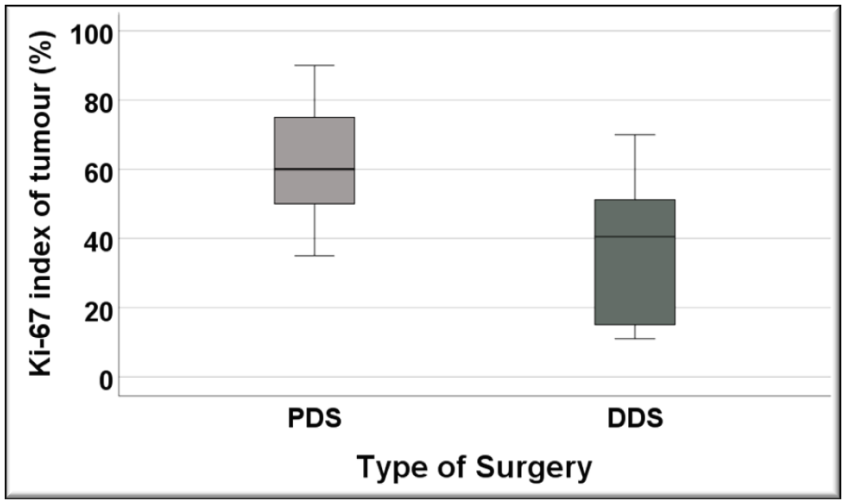

Figure 6. 31: A box plot diagram demonstrating the difference in Ki-67 proliferative index between patients who underwent primary debulking surgery and those who underwent delayed debulking surgery after neoadjuvant chemotherapy treatment. The median Ki-67 index was higher in patients who underwent PDS (n=11, *Mdn*=60) compared to those who underwent DDS after pre-operative chemotherapy (n=12, *Mdn*=40.5). This difference was statistically significant (*U*=24.5, *p*=0.01).

6.7.6 UbcH10 and Ki-67 protein levels do not correlate with volume of residual disease after surgery

The median UbcH10 TPS was lowest in R0 patients (n=13, *Mdn*=46.8), followed by R2 patients (n=3, *Mdn*=50) and highest in R1 patients (n=7, *Mdn*=60). The difference was not statistically significant (*H*=2.96, *p*=0.227).

The median Ki-67 index was lowest in R0 patients (*Mdn*=41), followed by R1 patients (*Mdn*=52.4) and highest in R1 patients (*Mdn*=70). The difference was also statistically not significant (*H*=3.28, *p*=0.193). These data indicate no correlation between UbcH10 and Ki-67 protein expression and the level of cytoreduction following surgery.

6.7.7 UbcH10 and Ki-67 protein levels are not predictive of chemotherapy response

To correlate UbcH10 and Ki-67 protein expression levels with measures of treatment response, we analysed their expression levels with CRS in the 12 patients who had received NACT and underwent DDS. Patients with a minimal CRS had a higher median UbcH10 TPS (n=4, *Mdn*=51.9) compared to those with partial and complete response (n=8, *Mdn*=45.5). The difference was not statistically significant (*U*=12, *p*=0.496).

Similarly, the median Ki-67 index was higher in patients with minimal CRS (*Mdn*=43.5) compared to patients with partial and complete CRS (*Mdn*=35). The difference was again not statistically significant (*U*=13.5, *p*=0.671). We can infer that neither UbcH10 nor Ki-67 protein expression levels are predictive of chemotherapy response in this cohort.

6.7.8 UbcH10 and Ki-67 protein levels do not differ significantly between p53 IHC staining patterns

To explore the relationship between total UbcH10 and Ki-67 protein expression and p53 mutational status, we compared their expression levels between patients with p53 overexpression by IHC (n=18) and those with p53 null, cytoplasmic, and wild type-like staining (n=5). The median UbcH10 TPS was slightly higher in patients with p53 overexpression (*Mdn*=50) compared to those with p53 null, cytoplasmic, and wild type-like (*Mdn*=46), however, the difference was not statistically significant (*U*=40.5, *p*=0.737). In contrast, the median Ki-67 index was higher in patients with p53 null, cytoplasmic, and wild type-like IHC staining (*Mdn*=55) compared to those with p53

overexpression (*Mdn*=43.5), though again the difference was statistically not significant (*U*=22.5, *p*=0.093).

These data do not corroborate a significant association between p53 protein expression and UbcH10 and Ki-67 protein levels.

6.8 Discussion

Serous tubal intra-epithelial carcinoma (STIC) is the earliest morphologically identifiable step in the carcinogenic sequence that leads to the development of invasive tubo-ovarian high grade serous malignancy (47). These lesions are characterized by early *TP53* mutations and a high Ki-67 proliferative index. A postulated earlier step known as 'p53 signature' is recognized by p53 protein overexpression and a low Ki-67 index (47). Therefore, the current model of HGSOC carcinogenesis includes p53 signatures, STICs and invasive high grade serous carcinomas. In the previous chapters we hypothesized that UbcH10 behaved more like a proliferative marker in HGSOC rather than an oncogene product that promotes tumourigenesis. Therefore, in this chapter we studied the relationship between UbcH10 and Ki-67 in a cohort of STICs and their corresponding invasive tumours. We also looked at UbcH10 and p53 protein expression in these precursor lesions to support our earlier conclusions of a lack of a directly proportional relationship between the two proteins.

Our findings confirm that UbcH10 is a feature of malignant tissue with very low to nil expression in normal ovarian and tubal tissue as well as benign and borderline serous tumours (Figure 6.3). These finding are consistent with our findings from chapter 3 (Figure 3.2) as well as both Berlingieri *et al (86)* and Gong *et al* (116) who also detected low UbcH10 protein expression in normal ovarian tissue as well as benign ovarian

tumours. Furthermore, because p53 signatures are morphologically normal tubal epithelium, UbcH10 expression levels in these structures were comparable to the normal tubal control tissue (Figures 6.4 and 6.5). UbcH10 expression levels then significantly increased in STICs and their corresponding HGSOC (Figures 6.9 and 6.10). This differential pattern of UbcH10 expression in the above sequence means that it is expressed early in the model of HGSOC carcinogenesis similar to *TP53* mutations. This could be one of the reasons UbcH10 does not correlate with any prognostic or predictive parameters in HGSOC because it is a ubiquitous finding in all these tumours like p53. However, another plausible explanation is that the different UbcH10 expression levels in p53 signatures versus STICs and invasive carcinomas reflects the difference in the proliferative nature of these lesions.

To our knowledge the present study is the first to examine UbcH10 expression in the p53 signature-STIC-HGSOC sequence. However, studies have reported that p53 signatures have a low Ki-67 index comparable to background tubal epithelium with a mean Ki-67 index of 3% (47, 165). STICs and HGSOC on the other hand are proliferative lesions by definition (8). Indeed, we determined a Ki-67 index ranging from 10 to 60% with a median of 40% in our STIC samples (Table 6.3) and ranging from 11 to 90% with a median of 50% in our HGSOC samples. These Ki-67 expression levels are comparable to one previous study by Kuhn *et al* (166) who reported a Ki-67 index in STICs ranging from 12-71% with a mean index of 36%. Another study by Jarboe *et al* (165) reported a higher mean Ki-67 proliferative index at 72% with a range from 40 to 95% in their STIC samples. Chen *et al* (167) reported a Ki-67 index ranging from 3 to 95% with a median of 40% in their HGSOC samples which are more comparable to our samples. While there are no reports on UbcH10 expression in p53 signatures and

STICs, studies mainly investigated the expression of γ-H2AX as a marker of DNA damage and telomere shortening in p53 signatures (168). Even the presence of *TP53* mutations in p53 signatures is a source of debate in the literature and from a clinical perspective most of these lesions do not progress and are clinically harmless (59, 169). STICs on the other hand are more genetically complex with *TP53* mutations, chromosomal abnormalities, and *CCNE1/cyclin E* amplifications (59, 170). Accordingly, UbcH10 may be expressed as early as the p53 signature step of the model due to the low proliferative nature of these lesions and not because it is necessarily amplified or mutated in those lesions. UbcH10 subsequently becomes overexpressed in STICs and invasive carcinomas probably due to the high proliferative nature of these lesions.

Our hypothesis that UbcH10 behaves like a proliferative marker is supported by the significant co-expression we detected between Ki-67 and UbcH10 in STICs (Figure 6.24) and HGSOC (Figure 6.25). Furthermore, Ki-67 and UbcH10 protein levels were positively correlated in STICs (Figure 6.28) and significantly correlated in their corresponding invasive carcinomas (Figure 6.29). Although the association between UbcH10 and Ki-67 was not statistically significant in STICs, it still reflects the significant association between UbcH10 and the proliferative state of the cell. These findings are corroborated by Fujita *et al* (101) who demonstrated that UbcH10 overexpression promoted an accelerated rate of cellular proliferation in colon cancer cell lines. Similarly, Kariri *et al* (159) demonstrated a strong association between UbcH10 protein expression and cell-cycle proliferative markers like *CDKN2A*, *CCNB1* and *CCNE1* in TCGA cohort of breast carcinomas.

Additionally, from a clinical perspective, both UbcH10 and Ki-67 total protein expression levels did not correlate with any prognostic or predictive parameters in our small cohort of 23 STIC/HGSOC patients. This is in line with our analysis on UbcH10 as a prognostic and predictive marker in the HGSOC females from the Birmingham and Barts cohorts in chapter 3. However, in the present small cohort we used the UbcH10 TPS for analysis as opposed to the IRS and H-scores we used in chapter 3. These different analyses indicate that whichever way UbcH10 protein levels are quantified in HGSOC specimens, it is a weak prognostic biomarker. Moreover, both UbcH10 and Ki-67 protein levels were reduced by chemotherapy administration (Figure 6.31). Although the reduction in UbcH10 levels were not significant as opposed to the Ki-67 index, this is likely due to the small number of patients in this cohort. This is because in both our training and validation cohorts from chapter 3 with 100 and 81 HGSOC females respectively, the reduction in UbcH10 levels after NACT administration was significant (Table 3.5). Similar to our own analysis, several studies reported the significant reduction in Ki-67 expression levels after NACT administration in breast cancer (125-127). However, the prognostic and predictive role of Ki-67 in the literature on ovarian cancer is controversial. One study associated high Ki-67 expression with worse PFS and prognosis in EOCs (171). However, this study included various subtypes of EOCs of both low- and high-grade morphology and hence different outcomes by default. Other studies found that high Ki-67 expression (>50%) was associated with prolonged PFS in HGSOC patients, but this effect was not independent on multivariate analysis but rather due to enhanced platinum sensitivity in tumours with high Ki-67 expression (172). Similarly, one study of 318 HGSOC patients showed a significant association between low Ki-67 (≤40%) expression and platinum resistance

(167). Another study also demonstrated that Ki-67 index at 50% was predictive of worse OS in HGSOC patients with minimal and partial response to chemotherapy (173). While platinum resistance and survival data were not available in the present small cohort of STIC/HGSOC, it is most likely that any prognostic role for Ki-67 in HGSOC is directly related to its effect on chemotherapy response. We consider further the prognostic effect of Ki-67 on patient survival in comparison with UbcH10 in chapter 7.

In relation to other malignancies, a study of 280 females with the aggressive triple negative breast cancer, high Ki-67 expression before chemotherapy was significantly associated with better pathological response to chemotherapy (125). While we did not demonstrate any significant association between Ki-67 expression and the CRS in the present cohort, the Ki-67 index was lower in patients with a pathological complete response. This was also true for the UbcH10 TPS (section 6.7.7). Therefore, studying both Ki-67 and UbcH10 in a larger cohort of matched chemo-naïve and chemo-responsive tubo-ovarian high grade serous carcinomas might prove useful in establishing UbcH10 and Ki-67 as predictive markers in HGSOC.

As a counterargument, it was notable that the Ki-67 index was significantly higher in HGSOC compared to their matched STICs, while the UbcH10 TPS was comparable in the matched lesions (Table 6.3). So, while Ki-67 showed a graded manner of expression (Figure 6.26), UbcH10 was maintained at high levels in STICs and their invasive tumours (Figure 6.27). Therefore, one cannot totally exclude the possibility of an oncogenic role of UbcH10 through early amplification in STICs and subsequently their invasive HGSOC. This is especially true since STICs are genetically complex and are thought to even have a low metastatic potential on their own without developing

into invasive HGSOC (37). Moreover, they demonstrate early *CCNE1* copy number gains as well as laminin overexpression. That said, we had previously demonstrated a moderate significant positive correlation between *Ube2C* and *CCNE1* expression in TCGA cohort of HGSOC patients in chapter 5 (Table 5.1). *CCNE1* amplifications are also particularly associated with aggressive behaviour in HGSOC as shown in TCGA data analysed in the HPA as well as other studies (50, 174). Therefore, the possibility that UbcH10 amplifications contribute to aggressive behaviour in STIC, and HGSOC is worth studying through molecular analysis of STIC samples. To this end, whilst we have demonstrated the strong proliferative properties of UbcH10 in HGSOC and their precursor lesions at the protein level, this can only be confirmed by looking at the molecular profile of HGSOC patients and correlating that with *Ube2C* gene expression levels. We address this in more detail in chapter 7.

With respect to the relationship between UbcH10 and p53 in HGSOC precursor lesions, our results confirm a heterogeneous relationship between the two proteins (Figures 6.20 to 6.22). Furthermore, in the p53 signature-STIC-HGSOC sequence there was a significant rise in UbcH10 expression from p53 signatures to STICs and HGSOC irrespective of the p53 staining pattern (Figures 6.17 to 6.19). These results exclude a directly proportional relationship between the two proteins and confirm our speculations from the previous chapters that UbcH10 akin to p53 is expressed early in the HGSOC model. Findings from this cohort are consistent with our results from chapter 4 (Figures 4.6 to 4.8) which similarly failed to find a directly proportional relationship between UbcH10 and p53 protein expression in HGSOC patients in the Birmingham cohort. In addition, we could not find a relationship between *Ube2C* gene expression levels and *TP53* mutations from TCGA cohort of HGSOC patients (Figures

5.14 to 5.16). Therefore, to reiterate, if UbcH10 is expressed in the early steps of HGSOC carcinogenesis, its use in the prognostication of these tumours becomes diluted like p53. Following the same line of reasoning, UbcH10 might play an oncogenic role in the early progression and contribute to the aggressive behaviour of HGSOC like *TP53* mutations, but it is not a robust marker for the prediction of patient outcomes.

To discuss the relatively ambiguous p53 signature as precursors of STICs, there has been a debate in the literature with regards to linking p53 signatures to STICs and HGSOC. Authors proposing p53 signatures as the earliest step in the model of HGSOC carcinogenesis argue that p53 signatures are more common and multifocal in fallopian tube with STICs and are also located in the fimbrial end of the fallopian tubes (164). In addition, like STICs, p53 signatures show p53 protein overexpression, DNA damage, and some can show *TP53* mutations as well (165). Moreover, both p53 signature and STIC arise from the secretory cells in the fallopian tube epithelium. Secretory cells have been shown to evolve into carcinomas in mouse models (175). The 9 p53 signatures from the present cohort were all in the fimbrial end of the fallopian tube and mostly in close proximity to STIC consistent with these reports (Figure 6.1).

However, the clonal relationship between p53 signatures and STIC/HGSOC is controversial. While there are reports of *TP53* missense mutations in p53 signatures, this is not consistent in the literature. One study demonstrated *TP53* mutations in 8 out of 14 p53 signatures in their samples (169), while another demonstrated *TP53* mutations in 100% of their p53 signatures (59). In that same study, Wu *et al (59)* had 4 cases with concomitant STIC and HGSOC, one of which also had a p53 signature. They detected a clonal relationship between STIC and HGSOC in 3 out of 4 patients due to the presence of identical *TP53* mutations and sub-chromosomal loss of

heterozygosity (LOH) in both lesions. In one patient, the p53 signature did not share a similar *TP53* mutation or sub-chromosomal LOH with the corresponding ovarian carcinoma and hence were not clonally related. On the other hand, Lee *et al* (169) demonstrated identical *TP53* mutations in one patient with p53 signature that was in direct continuity with a STIC. Similarly, Carlson *et al (176)* reported identical *TP53* mutations in a p53 signature and peritoneal serous carcinomas in one patient. These studies suggest that while p53 signatures can show *TP53* missense mutations, a very small proportion of those develop the second hit in the form of chromosome 17 loss/sub-chromosomal loss to develop into STIC and eventually into full blown malignancies.

To compare these studies to our own, it is true we did not perform any sequencing on our samples, but we did find identical p53 IHC staining in STICs and their corresponding HGSOC suggesting a shared clonal origin (Figure 6.2). In p53 signatures on the other hand, only 6 cases demonstrated concordant p53 overexpression with the corresponding STIC and HGSOC samples (Figure 6.17). Two cases had p53 signatures with discordant p53 overexpression in an otherwise p53 null STIC and HGSOC (Figure 6.18). Finally, one case had a cytoplasmic p53 signature identical to cytoplasmic staining in its corresponding STIC and HGSOC (Figure 6.19). The latter three cases probably add to the ambiguity of the clonal origin of some p53 signatures. This is because while the cytoplasmic p53 signature suggests a clonal relationship with its corresponding STIC/HGSOC, the discordant p53 signature in a p53 null tumour suggests otherwise. However, similar to our two cases, Hatano *et al (177)* reported discordant p53 signature in a p53 null tumour. Although they did not sequence that p53 signature, they demonstrated nuclear overexpression of γ-H2AX in

that p53 signature as well as in the adjacent benign tubal epithelium without p53 overexpression. Accordingly, they proposed these γ-H2AX expressing foci of normal tubal epithelium without p53 overexpression as precursors of *TP53* null mutations in HGSOC. We argue their conclusions are largely speculative, especially since γ-H2AX overexpression without p53 overexpression has been reported in normal fallopian tube epithelium without from *BRCA*1/2 mutation carriers undergoing risk-reducing salpingo-oophorectomy (178). However, it is possible that p53 overexpression signatures serve as precursors of p53 overexpression STIC/HGSOC. On the other hand, given that p53 overexpression signatures are mostly discovered fortuitously, it is also possible that p53 signatures with null p53 are simply overlooked. This is because they are morphologically normal and the lack of p53 expression by IHC would not necessarily indicate an aberrant null pattern since normal tubal epithelium shows very low p53 immunohistochemical expression by default. To elaborate further, the discordant p53 signature in our cases most likely represents a DNA damage response that led to p53 protein accumulation, and there is probably another p53 null signature which developed into a p53 null STIC/HGSOC that we are missing. To follow the same line of reasoning, our case with cytoplasmic p53 throughout the p53 signature-STIC-HGSOC spectrum is an unprecedented finding. Again, we argue that cytoplasmic p53 signatures are probably misinterpreted as p53 overexpression signatures given the rarity of these lesions. It would therefore be interesting to sequence those p53 signatures and their corresponding STICs and HGSOC samples to identify a relevant relationship. Taken together, our findings provide new insights into the clonal evolution of HGSOC from p53 signatures and suggest that not all p53 signatures are created equal.

6.9 Conclusion

UbcH10 is expressed as early as the ‘p53 signature’ stage of the HGSOC carcinogenesis model but with levels comparable to the normal fallopian tube. UbcH10 overexpression begins at the STIC stage of the model with levels comparable to their corresponding invasive high-grade serous carcinomas. UbcH10 behaves like a proliferative marker with a significant association with the Ki-67 proliferative index in HGSOC and their precursor lesions. No significant association was found between UbcH10 and p53 protein expression in serous tubal intra-epithelial carcinomas. P53, UbcH10 and Ki-67 protein expression levels seem to play a weak role in the prognostication of HGSOC patient. Finally, we report two relatively new patterns of p53 signatures (discordant and cytoplasmic) that might provide useful insights into the pathogenesis of HGSOC.

Chapter 7. TCGA molecular subtypes of HGSOC and its relationship to *Ube2C* gene expression in TCGA cohort and UbcH10 protein expression in the Birmingham cohort

7.1 Introduction

In 2011, investigators form The Cancer Genome Atlas (TCGA) identified four molecular subtypes of HGSOC based on mRNA, miRNA, DNA methylation analysis and exonic sequencing of more than 18,500 genes (50). The four subtypes were termed *Immunoreactive*, *Proliferative, Mesenchymal and Differentiated.* The *Immunoreactive* subtype is characterized by T-cell chemokine ligands *CXCL10* and *CXCL11* expression, whilst the *Proliferative* subtype is characterized by high expression of proliferation markers such as *MCM2*, *PCNA.* The *Differentiated* subtype shows a more mature stage of development with the expression of *SLPI*, a marker of secretory fallopian tube epithelium, and the *Mesenchymal* subtype is characterized by overexpression of genes associated with increased stromal myofibroblasts and perivascular pericytes. Investigators from TCGA however, did not identify any survival differences between the 4 molecular subtypes (50). Further gene expression characterization from Verhaak and colleagues, however, identified an increased number of tumour infiltrating T-lymphocytes in the Immunoreactive group with overall and recurrence-free survival benefits (60). They also determined that the Mesenchymal subtype demonstrated worse overall and recurrence-free survival (60). Further validation studies by Konecny *et al* also demonstrated poor survival for the

both the Mesenchymal and Proliferative subtypes and good survival advantage for the Immunoreactive subtype (61).

More recently, Murakami and colleagues used unsupervised hierarchical clustering to correlate gene expression with transcriptomic data in two different datasets of HGSOC (114). Their study identified four histopathological subtypes of HGSOC that overlap with TCGA characterized molecular groups. They also identified an algorithm based on a combination of morphology and immunohistochemistry to identify these subtypes.

In the previous chapter, we demonstrated the strong proliferative properties of UbcH10 and its significant association with the proliferative marker Ki-67 in HGSOC and their precursor lesions. In this chapter, we expand on these findings further by correlating *Ube2C* gene expression with the molecular subtypes in TCGA cohort of HGSOC patients previously discussed in chapter 5. We also attempt to classify our previously characterized Birmingham cohort into the 4 molecular subtypes based on the study by Murakami *et al* (114) using a combination of morphology and IHC. The aim of these analyses is to identify if UbcH10 correlates significantly with any of the molecular subtypes either at the gene level in TCGA cohort or at the protein level in the Birmingham cohort.

7.2 *Ube2C* gene expression and the molecular subtypes in TCGA cohort of HGSOC patients

7.2.1 Characterization of molecular subtypes in TCGA cohort

The MetaGxData package compendium is the largest source of curated transcriptomic, pathological, and clinical metadata for breast, ovarian and pancreatic cancer (179). We used the MetaGx ovarian dataset as the source of TCGA ovarian serous carcinoma patient identifiers. The dataset was then filtered using the best probe set from across 12823 genes which identified 1000 intrinsically variable genes that were used for consensus clustering. The Verhaak/TCGA subtypes (60) were applied using the Bioconductor package (180) to assign molecular subtype to a total of 536 ovarian serous carcinoma patients from TCGA. We then narrowed our cohort to 163 HGSOC patients with both *TP53* mutations and *Ube2C* gene expression data.

Out of 163 HGSOC patients from TCGA, 52 (31.9%) were of the Immunoreactive (IMR) subtype, 33 (20.2%) were of the Proliferative (PRO), 30 (18.4%) were of the Mesenchymal (MES) subtype and 48 (29.5%) were of the Differentiated (DIF) subtype.

The clinico-pathological profile of these 163 HGSOC females from TCGA was previously characterized in Table 5.3.

7.2.2 *Ube2C* gene expression levels are significantly higher in the Proliferative subtype of HGSOC

After identifying the number of HGSOC patients belonging to each molecular subtype from TCGA cohort, we next proceeded to compare *Ube2C* gene expression levels in each of 4 subtypes. The log normalized *Ube2C* mRNA expression levels ranged from

8.27 to 13.28 (*Mdn*=10.63) in the 163 patients collectively. When we analysed *Ube2C* mRNA levels as a continuous variable, we found that *Ube2C* gene expression levels were significantly higher in the Proliferative subtype of HGSOC (*H*=28.152, *p*=<0.001; Figure 7.1 and Table 7.1).

We then applied the previously generated *X*-tile generated cut-off of 11.236 to divide TCGA cohort into high (>11.236) and low (≤11.236) *Ube2C* gene expression groups. and used Pearson's Chi-square test to identify any significant association between the *Ube2C* expression groups and the molecular subtypes of HGSOC. Analysis indicated that both the Proliferative and Immunoreactive subtypes were significantly associated with the high *Ube2C* gene expression group, while the Mesenchymal and Differentiated subtypes were significantly associated with the low *Ube2C* gene expression group (Pearson's X^2=22.965, *p*=<0.001). Data are shown in Table 7.2.

These data confirm the strong proliferative properties of UbcH10 at the molecular level in HGSOC patients from TCGA.

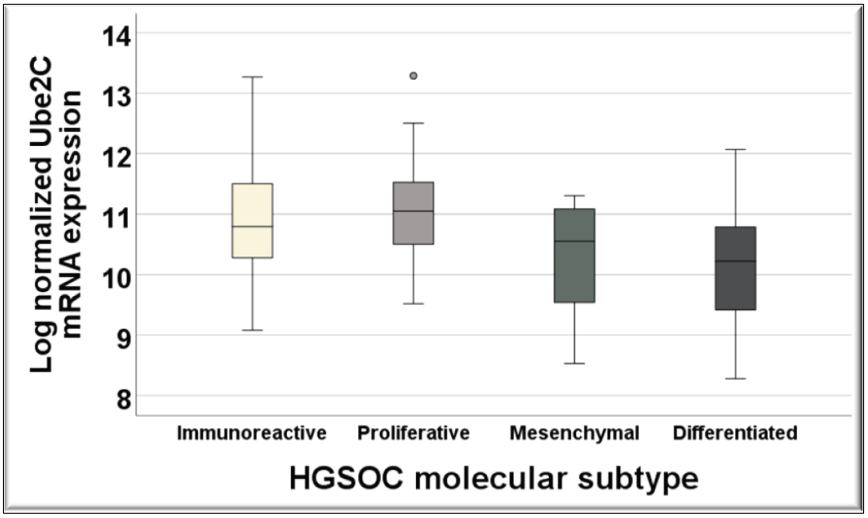

Figure 7. 1: A box plot diagram demonstrating the difference in *Ube2C* mRNA expression levels between the different TCGA defined molecular subtypes in TCGA cohort of HGSOC patients. The median $\log_2$ normalized *Ube2C* gene expression levels were significantly higher in the Proliferative subtype (n=33, *Mdn*=11.04), followed by the Immunoreactive subtype (n=52, *Mdn*=10.8), and the Mesenchymal subtype (n=30, *Mdn*=10.6). The lowest gene expression levels were in the Differentiated subtype (n=48, *Mdn*=10.2). This difference was strongly statistically significant as indicated by the *p*-value of the Kruskal-Wallis test (*H*=28.15, *p*=<0.001).

Table 7. 1: The relationship between *Ube2C* mRNA expression levels and the molecular subtypes of HGSOC females from TCGA. *Ube2C* gene expression levels were significantly higher in the Proliferative subtype compared to the three other subtypes as indicated by the strong *p*-value of the Kruskal-Wallis test.

Molecular subtype of HGSOC	**Number of patients**	***Ube2C* mRNA expression[a] *Mdn* *(Min, Max)***	**Kruskal-Wallis *(H)* test (*p*-value)**
Immunoreactive	52	10.8 (9.1, 13.3)	**28.152 (*p*=<0.001)***
Proliferative	33	11.04 (9.5, 13.3)	
Mesenchymal	30	10.6 (8.5, 11.3)	
Differentiated	48	10.2 (8.3,12.1)	
Total	**163**	**10.63 (8.27, 13.28)**	

Mdn: median, **Min:** minimum**, Max:** maximum

a: normalized mRNA expression data were calculated as $\log_2$ value using the formula: $X=\log_2(X+1)$

Table 7. 2: The relationship between the *Ube2C* gene expression groups and the molecular subtypes of HGSOC patients from TCGA. Patients in the Proliferative and Immunoreactive subtypes were significantly associated with the high *Ube2C* mRNA expression group. On the other hand, patients with the Mesenchymal and Differentiated subtypes were significantly associated with the low expression group. This association is strongly significant as indicated by the *p*-value of the Chi-square test.

***Ube2C* gene expression group[a]**	**Molecular subtype of HGSOC**				**Total**	**Chi-square test (X^2)**
	IMR	PRO	MES	DIF		
Low (≤11.236)	31	20	28	44	**123**	**22.965 (*p*=<0.001)***
High (>11.236)	21	13	2	4	**40**	
Total	**52**	**33**	**30**	**48**	**163**	

IMR: immunoreactive**, PRO:** proliferative, **MES:** mesenchymal**, DIF:** Differentiated

a: normalized mRNA expression data were calculated as $\log_2$ value using the formula: $X=\log_2(X+1)$

7.2.3 TCGA defined molecular subtypes do not correlate significantly with clinical parameters from TCGA cohort of HGSOC patients

7.2.3.1 Overview

As previously shown in Table 5.3, the 163 HGSOC females from TCGA were aged between 34 and 87 years (*Mdn*=58). All those patients underwent debulking surgery in the primary setting without NACT administration. They were staged according to the AJCC staging system into stage II (10 patients), stage III (130 patients) and stage IV (23 patients) disease.

In this section we tried to correlate the molecular subtypes with age and AJCC stage as the two clinical parameters available to us from this cohort. The main aim was to try and identify any significant association these molecular subtypes might have with prognostic parameters in HGSOC patients. We used the Kruskal-Wallis and Fisher's exact tests for this analysis.

7.2.3.2 TCGA defined molecular subtypes do not correlate significantly with age at diagnosis in HGSOC patients from TCGA

The patients with the Mesenchymal subtype had the highest median age at diagnosis (*Mdn*=62). All patients with the Immunoreactive, Proliferative and Differentiated subtypes had a median age at diagnosis of 57 years. The difference was therefore not statistically significant (H=0.883, p=0.83). Data are shown in Figure 7.2.

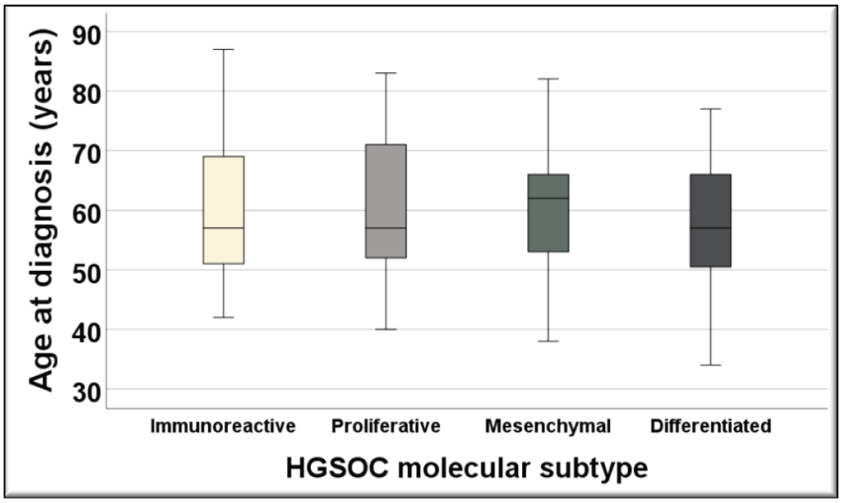

Figure 7. 2: A box plot diagram showing the relationship between the different TCGA defined molecular subtypes and the age of patients at diagnosis in HGSOC from TCGA cohort. Patients with the Mesenchymal subtype had the highest median age at diagnosis (n=30, *Mdn*=62). Patients with the Immunoreactive (n=52), Proliferative (n=33) and Differentiated subtypes (n=48) all had a median age at diagnosis of 57 years. The difference was statistically not significant (*H*=0.883, *p*=0.83).

7.2.3.3 TCGA defined molecular subtypes do not correlate significantly with AJCC stage in HGSOC patients from TCGA

We next correlated TCGA defined molecular subtypes of HGSOC to the AJCC stage of the patients. Because early-stage patients were very low in number (n=10) compared to late-stage patients (n=153) we did the statistical analysis differently to avoid losing statistical power. We compared each molecular group with the other 3 groups as dichotomous variables instead of 4 groups. For example, we compared patients with Mesenchymal HGSOC (n=30) as one group to Immunoreactive, Proliferative and Differentiated subtypes as another group (n=133) and checked the distribution of AJCC stage patients among the two groups using the Fisher's exact test. Analysis for the other three subtypes was done similarly. We could not find any

significant association between any of the molecular subtypes and AJCC stage in HGSOC patients from TCGA (Table 7.3).

Table 7. 3: The relationship between the Molecular subtype of HGSOC and the AJCC stage in TCGA cohort.

Clinical Characteristic	**Molecular subtype of HGSOC**				**Total (%)**
	IMR	PRO	MES	DIF	
Number of patients (%)	52 (31.9)	33 (20.2)	30 (18.4)	48 (29.5)	**163 (100)**
AJCC stage					
Early (II)	4	1	1	4	**10 (6.1)**
Late (III & IV)	48	32	29	44	**153 (93.9)**
Fisher's exact 2-sided significance[a]	**0.73**	**0.69**	**0.69**	**0.48**	

IMR: Immunoreactive**, PRO:** Proliferative**, MES:** Mesenchymal**, DIF:** Differentiated

AJCC: American Joint Committee on Cancer Staging

a: Statistics were computed by comparing each subtype with the other three subtypes as 2 groups. No significant association was found between the two parameters as indicated by the p-values of the Fisher's exact test.

Taken together, the above data indicate no significant difference in age at diagnosis or AJCC stage between the 4 molecular subtypes of HGSOC patients from TCGA.

7.2.4 The prognostic impact of TCGA defined molecular subtypes on HGSOC patient outcomes from TCGA cohort

7.2.4.1 Overview

After exploring the relationship between molecular subtypes of HGSOC and prognostic parameters in TCGA cohort, we proceeded to explore their impact on the overall and

progression-free survival of those patients to confirm previous reports form TCGA investigators (50).

As previously discussed in section 5.3.3, OS data was available for a total of 162 patients from this cohort with a median OS of 44.05 months. Progression-free survival data on the other hand was available for 130 patients with a median PFS of 17.3 months.

7.2.4.2 TCGA defined molecular subtypes do not impact HGSOC mortality from TCGA cohort

Concerning the 162 patients with OS data, patients with the Mesenchymal subtype had the shortest median OS whilst patients with the Immunoreactive subtype showed the longest median OS. These differences however were not significant as indicated in Figure 7.3.

HGSOC patients of the Differentiated subtype exhibited the highest death rate, while patients of the Immunoreactive subtype exhibited the lowest death rate. The difference was again statistically not significant as shown in Table 7.4. Taken together, these data confirm that the molecular subtypes of HGSOC do not impact the mortality of those patients from TCGA cohort.

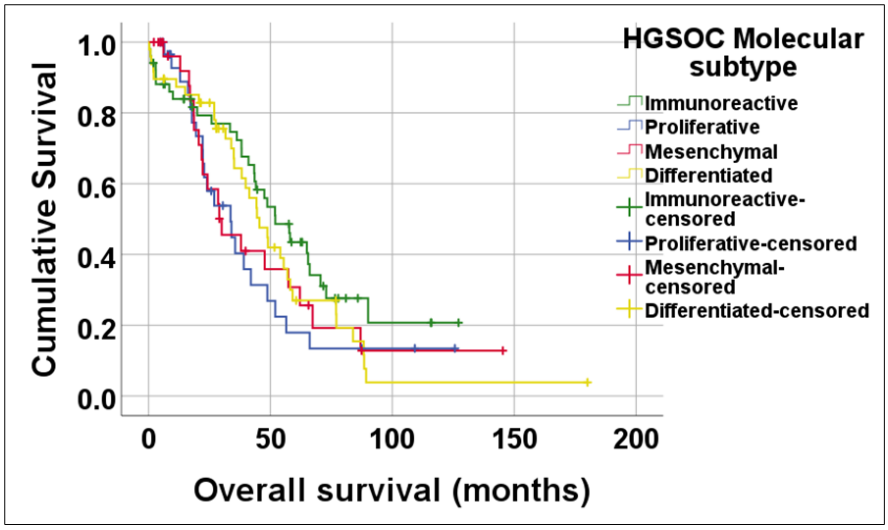

Figure 7. 3: A Kaplan-Meier curve demonstrating the difference in overall survival between the 4 molecular subtypes of HGSOC females from TCGA cohort. HGSOC patients of the Mesenchymal subtype had the shortest median OS (n=30, *Mdn* OS=30.03 months), followed by patients with the Proliferative subtype (n=33, *Mdn* OS=33.64 months). HGSOC patients of the Differentiated subtype (n=48) showed a median OS of 45.47 months. Lastly, patients with the Immunoreactive subtype (n=51) exhibited the longest median OS (*Mdn* OS=52 months). The difference was not statistically significant (Log rank X^2=3.93, p=0.268).

Table 7. 4: The effect of molecular subtype on the overall survival of HGSOC patients from TCGA cohort. Patients with the Mesenchymal subtype exhibited the shortest median OS and a death rate of 63.3%. Patients with the Proliferative subtype exhibited the second shortest median OS and a death rate of 63.6%. Patients with the Differentiated subtype exhibited the highest death rate (70.8%) but an intermediate median OS. Patients with the Immunoreactive subtype exhibited the longest median OS and the lowest death rate (60.8%). These differences were however statistically not significant (Log rank X^2=3.93, p=0.268).

Molecular subtype of HGSOC	Number of patients	Number of events	Median OS (95% CI)
Immunoreactive	51	31	52.00 (39.35,64.64)
Proliferative	33	21	33.64 (18.72,48.55)
Mesenchymal	30	19	30.03 (14.23,45.82)
Differentiated	48	34	45.47 (34.97,55.96)
Total	**162**	**105**	**44.05 (36.40, 51.70)**

OS: overall survival, **95% C.I**: 95% confidence interval

7.2.4.3 TCGA defined molecular subtypes do not impact HGSOC progression from TCGA cohort

Concerning the 130 patients with PFS data, the median PFS followed the same trend as the overall survival. Patients with the Mesenchymal subtype had the shortest median PFS whilst patients with the Immunoreactive subtype showed the longest median PFS. These differences however were not statistically significant as indicated in Figure 7.4.

HGSOC patients of the Immunoreactive subtype exhibited the highest progression rate, while patients of the Mesenchymal subtype exhibited the lowest progression rate. The difference was again statistically not significant as shown in Table 7.5. Taken together, these data indicate that the molecular subtypes of HGSOC do not impact the progression rates of those patients from TCGA cohort.

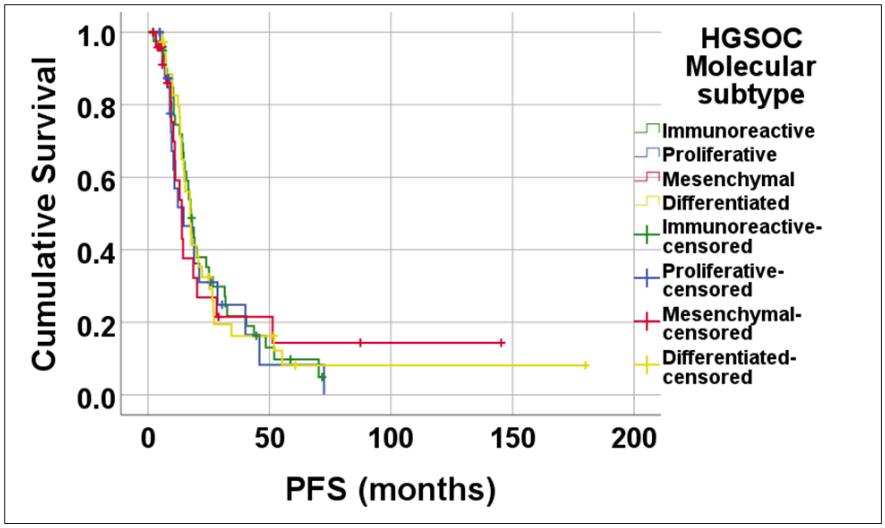

Figure 7. 4: A Kaplan-Meier curve demonstrating the difference in progression-free survival between the 4 molecular subtypes of HGSOC females from TCGA cohort. HGSOC patients of the Mesenchymal subtype had the shortest median PFS (n=25, *Mdn* PFS=13.93 months), followed by patients with the Proliferative subtype (n=27, *Mdn* PFS=14.68 months). HGSOC patients of the Differentiated subtype (n=37) showed a median PFS of 17.51 months. Lastly, patients with the Immunoreactive subtype (n=41) exhibited the longest median PFS (*Mdn* OS=17.71 months). The difference was not statistically significant (Log rank X^2=0.423, p=0.935).

Table 7. 5: The effect of molecular subtype on the progression-free survival of HGSOC patients from TCGA cohort. Patients with the Immunoreactive subtype exhibited the longest median PFS but the highest progression/recurrence rate (85.4%). Patients with the Differentiated subtype exhibited the 2nd highest progression/recurrence rate (81.1%) and 2nd longest median PFS. Patients with the Proliferative subtype exhibited a progression/recurrence rate of 66.7%, while those with the Mesenchymal subtype exhibited the shortest median PFS and the lowest progression/recurrence rate (64%). These differences were not statistically significant (Log rank X^2=0.423, p=0.935).

Molecular subtype of HGSOC	Number of patients	Number of events	Median PFS (95% CI)
Immunoreactive	41	35	17.71 (14.96, 20.46)
Proliferative	27	18	14.68 (4.71, 24.64)
Mesenchymal	25	16	13.93 (10.09,17.76)
Differentiated	37	30	17.51 (14.15, 20.86)
Total	**130**	**99**	**17.30 (14.60, 19.90)**

PFS: Progression-free survival, **95% C.I**: 95% confidence interval

7.3 UbcH10 protein expression and the molecular subtypes of HGSOC in the Birmingham cohort

7.3.1 Characterization of the Molecular subtypes in the Birmingham cohort

7.3.1.1 Tissues, samples, and criteria for selection

After analysis of the molecular subtypes in TCGA cohort in relation to the *Ube2C* gene expression levels, we wanted to apply the same principles to the Birmingham cohort. Due to the poor quality of nucleic acids extracted from FFPE tissue blocks, we could sequence our samples, so we followed recommendations from Murakami and colleagues (114). All 32 chemo-naïve patients who underwent PDS were included in the analysis. Two relatively new HGSOC cases who had also undergone PDS were included bringing the total of chemo-naïve cases in this cohort to 34 patients. With respect to the 68 patients who received pre-operative chemotherapy, a total of 12 patients were excluded due to extensive chemotherapy associated changes that hindered proper tumour classification. In the remaining 56 post-chemotherapy cases, we managed to obtain diagnostic pre-chemotherapy samples for 10 patients, leaving 46 cases where we did the classification on the post-chemotherapy samples. This brought the total number of cases in this cohort to 90 HGSOC patients. In 61 (67.8%) patients, subtyping was performed on ovarian and tubal sections and in 11 (12.2%) patients subtyping was performed on omental tumours. There were 10 patients (11.1%) where subtyping was performed on pre-operative diagnostic laparoscopy biopsies. In the remaining 8 (8.9%) patients, subtyping was done on other metastatic sites (groin lymph nodes, serosal large bowel deposits and pelvic side wall peritoneal deposits).

7.3.1.2 Molecular subtype diagnostic algorithm

According to the study by Murakami *et al (114),* identification of the molecular subtypes started with looking at an average of 2 to 3 H&E-stained sections to look for the characteristic morphological features of the Mesenchymal subtype. These included the presence of either isolated and spindled single cells with destructive stromal invasion (mesenchymal transition pattern; Figure 7.5) or broadly compressed papillae (labyrinthine pattern; Figure 7.6) along with a desmoplastic stromal response that occupied more than 10% of the tumour area. If either of these features were present, then the Mesenchymal subtype was assigned Figure 7.7 shows a HGSOC with both patterns of Mesenchymal subtype.

After exclusion of Mesenchymal features, counting of CD8 positive tumour infiltrating lymphocytes (TILs) was performed according to previous recommendations (Materials and Methods section 2.2.1.3) (113). A tumour which had a smooth invasive border and high CD8+ TILs (stromal >100/HPF and intraepithelial >50/HPF) was diagnosed as the Immunoreactive subtype. Figure 7.8 is representative of the Immunoreactive subtype of HGSOC from the Birmingham cohort.

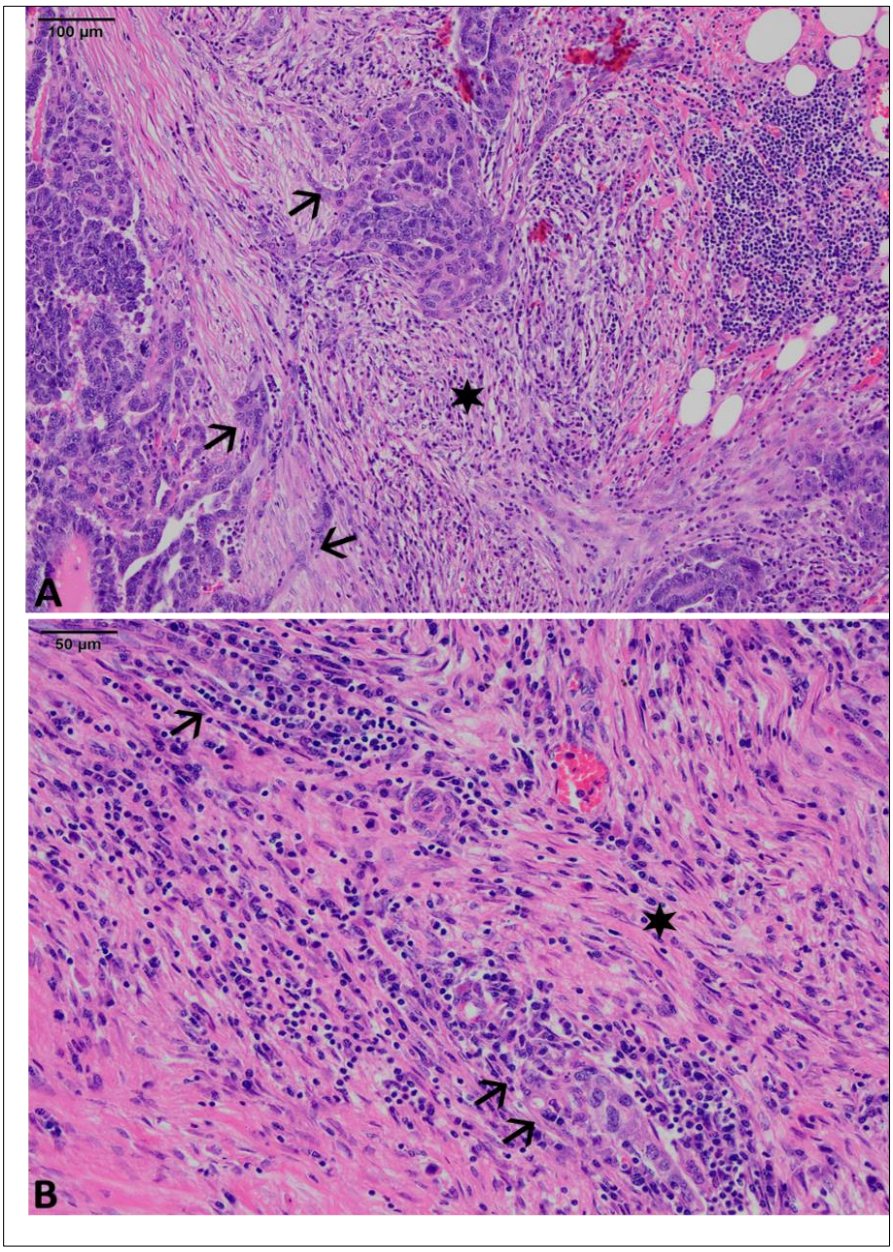

Figure 7. 5: A patient from the Birmingham cohort with the mesenchymal transition pattern characteristic of the Mesenchymal subtype of HGSOC. A) Invasive tumour islands infiltrating omental fat and surrounded by intense inflammation and desmoplasia (star). The mesenchymal transition pattern is apparent here with spindled cells emanating from the main tumour and infiltrating as single cells (arrows, H&E, x10 magnification). B) Higher power view showing the spindled malignant cells (arrows) blending with the stroma and infiltrating in a single cell pattern. This tumour has an intense desmoplastic stromal response >10% of tumour area (star) characteristic of this molecular subtype (H&E, x20 magnification).

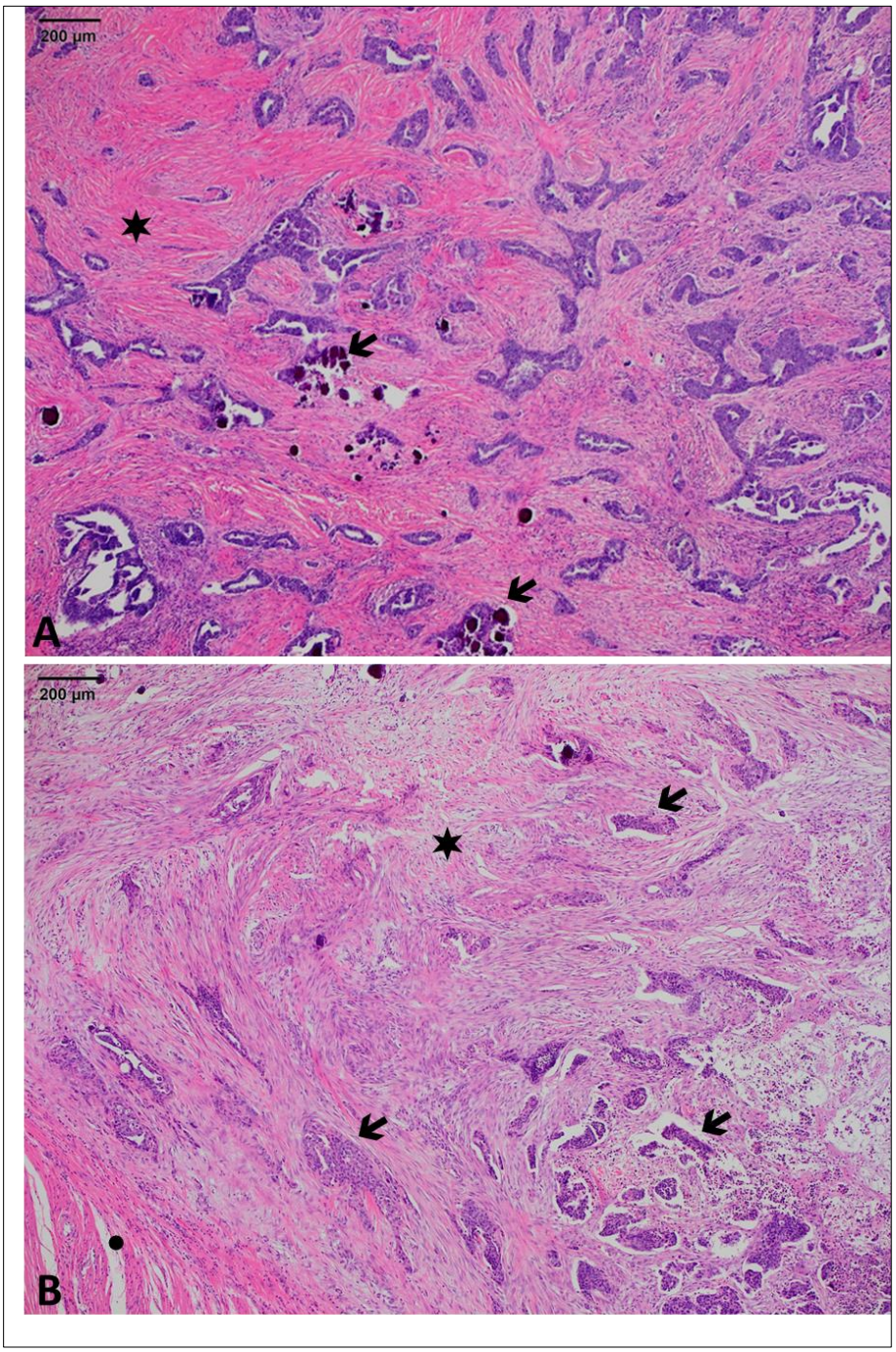

Figure 7. 6: Two different patients from the Birmingham cohort with the labyrinthine pattern characteristic of the Mesenchymal subtype of HGSOC. A) Invasive ovarian tumour nests arranged in the form of broad compressed papillae with some showing psammomatous calcifications (arrows) surrounded by a dense desmoplastic stroma (star) which constitutes more than 10% of the tumour (H&E, x4 magnification). B) Another HGSOC patients demonstrating the broad compressed papillary structures (arrows) and intense desmoplasia (star) characteristic of the Mesenchymal subtype. This tumour is infiltrating into outer muscular coat of the sigmoid colon shown in the lower left corner of the field (dot, H&E, x4 magnification).

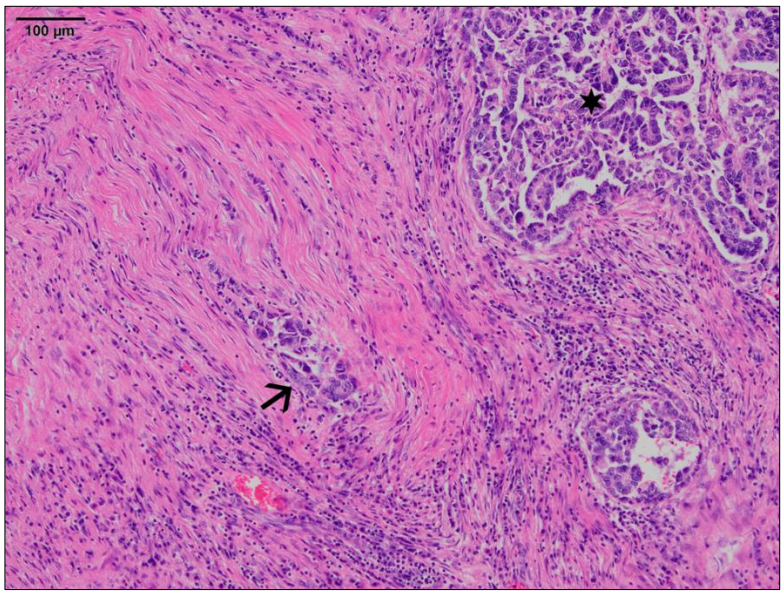

Figure 7. 7: A HGSOC patient from the Birmingham cohort demonstrating both the mesenchymal transition and labyrinthine patterns characteristic of the Mesenchymal subtype. In the upper right corner of the photomicrograph the tumour infiltrates as broadly compressed papillae (star, labyrinthine pattern). The arrow marks tumour cells that infiltrate singly into an intense desmoplastic stroma (mesenchymal transition pattern, H&E, x10 magnification).

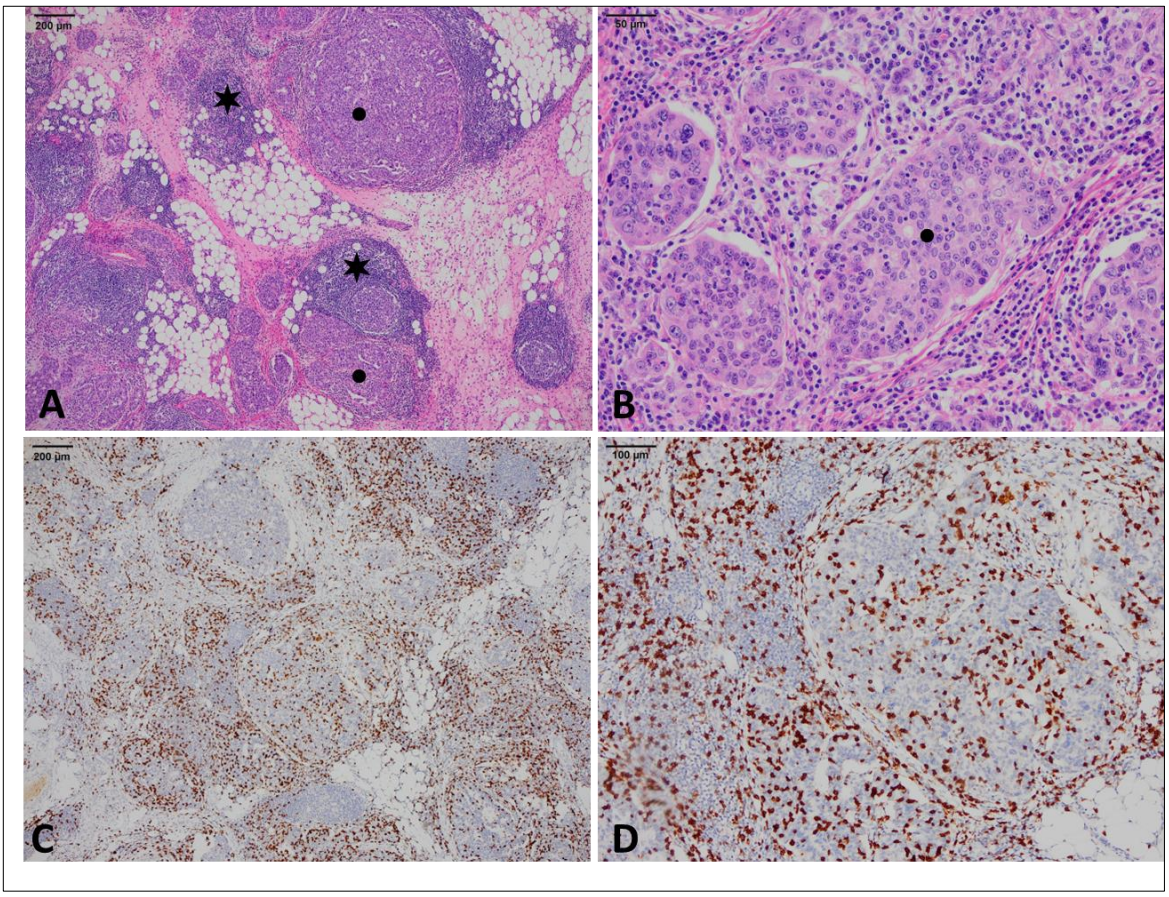

Figure 7. 8: The Immunoreactive subtype of HGSOC from one patient in the Birmingham cohort. A) Omental tumour showing rounded nests of malignant cells with a smooth and pushing border (dots) and lots of tumour infiltrating lymphocytes in the stroma around the tumour (stars, H&E, x4 magnification). B) Higher power view of the tumour nests (dot) in panel A with intraepithelial lymphocytic infiltration (H&E, x20 magnification) .C) Immunostaining highlighting the membranous staining pattern of tumour infiltrating CD8+ lymphocytes around the tumour (215/HPF) (anti-CD8, x4 magnification). D) Higher power view of panel C showing intraepithelial CD8+ cells (134/HPF) (anti-CD8, x10 magnification).

After exclusion of Mesenchymal and Immunoreactive features, scoring for a Ki-67 index was performed as previously discussed in Materials and Methods section 2.2.1.3. Tumours with a pure solid growth pattern and a Ki-67 proliferative index of >40% were categorized as the Solid Proliferative subtype. The 40% cut-off was determined

according to recommendations from Chen and colleagues (167). Figure 7.9 is representative of the Solid Proliferative subtype of HGSOC in our cohort.

Finally, if a tumour lacks any features suggestive of the above 3 subtypes and has a well-differentiated papillary and glandular growth pattern with no overt desmoplasia, it was assigned to the Differentiated/Papillary glandular subtype (Figures 7.10).

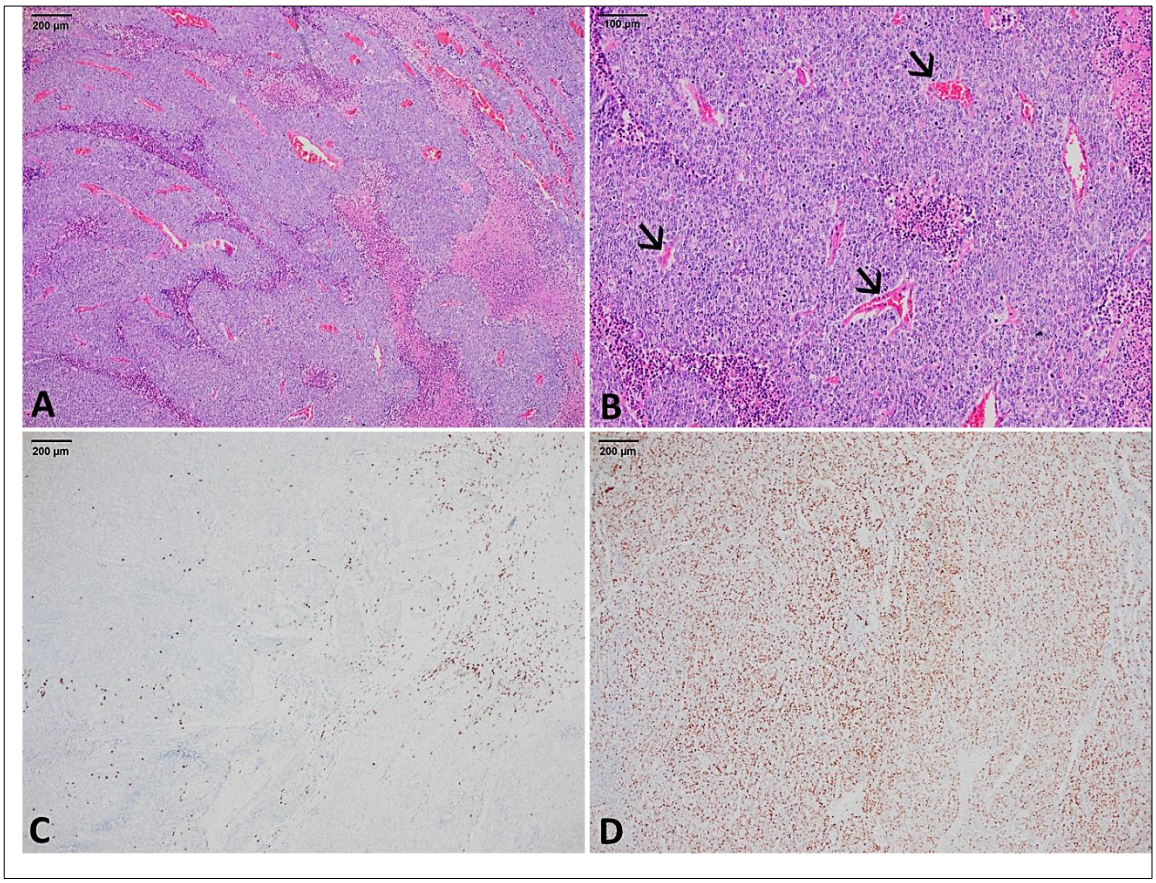

Figure 7. 9: A HGSOC patient of the Solid Proliferative subtype from the Birmingham cohort. A) Rounded solid nests of high-grade serous carcinoma with smooth invasive front from the ovary of one patient (H&E, x4 magnification). B) A higher power view of the tumour in panel A showing the solid nests composed of very closely packed papillae with fibrovascular cores (arrows) imparting a solid growth pattern (H&E, x10 magnification). C) Immunostaining for CD8 showing some tumour infiltrating lymphocytes but not reaching the threshold for the Immunoreactive subtype (stromal 65/HPF, Intraepithelial 35/HPF) (anti-CD8, x4 magnification). D) Ki-67 immunostaining showing strong diffuse nuclear staining in 67% of the tumour cells [anti-Ki67 (MM-1), x4 magnification].

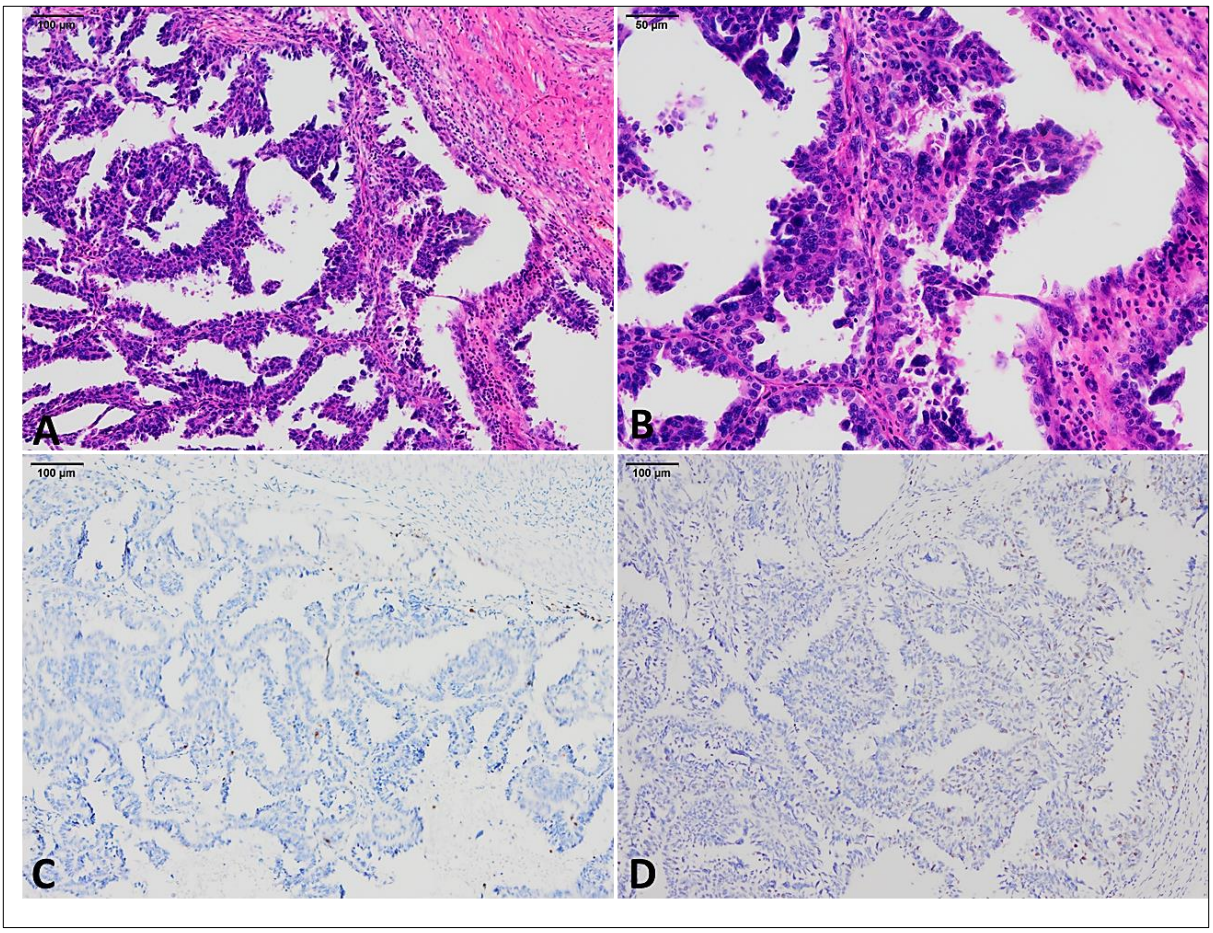

Figure 7. 10: The differentiated (papillary glandular) subtype of HGSOC from one patient in the Birmingham cohort. A) A tumour with a papillary architecture reminiscent of borderline serous tumours with no solid areas or mesenchymal transition pattern (H&E, x10 magnification) B) Higher power view of the tumour in panel A showing the high grade wildly pleomorphic nuclei characteristic of HGSOC (H&E, x20 magnification). C) CD8 immunostaining in the tumour showing very focal and scattered tumour infiltrating CD8+ cells indicating the absence of immunoreactive features (anti-CD8, x10). D) Ki-67 staining showing low levels of expression (23%). Together with the absence of a solid growth pattern, this excludes the Solid Proliferative subtype [anti-Ki67 (MM-1), x10 x10 magnification).

When applying the above algorithm to our 90 patients from the Birmingham cohort, the majority of patients 43 (47.8%) fell into the Mesenchymal category, followed by 25 patients (27.8%) who had the Differentiated phenotype (Papillary glandular) as the second most frequent subtype. A total of 12 patients (13.3%) displayed the Solid

Proliferative phenotype, whilst only 10 patients (11.1%) displayed the Immunoreactive phenotype.

7.3.1.3 Extensive tumour infiltrating lymphocytes and high proliferative activity were associated significantly with the Immunoreactive and Solid Proliferative subtypes of HGSOC, respectively

To confirm the robustness of our diagnostic parameters, we first compared the density of stromal and intraepithelial CD8+ T-lymphocytes between the 4 molecular subgroups in the Birmingham cohort using the Kruskal-Wallis test. The median stromal CD8+ TILs per HPF was significantly higher in the Immunoreactive subtype compared to the other three subtypes (H=24.25, p=<0.001; Figure 7.11). Similarly, the median intraepithelial CD8+ TILs per HPF was significantly higher in the Immunoreactive subtype compared to the other 3 subtypes (H=21.64, p=<0.001; Figure 7.12). These data indicate that the different molecular subtypes of HGSOC can show immunoreactive features but with significant higher levels in the Immunoreactive subtype.

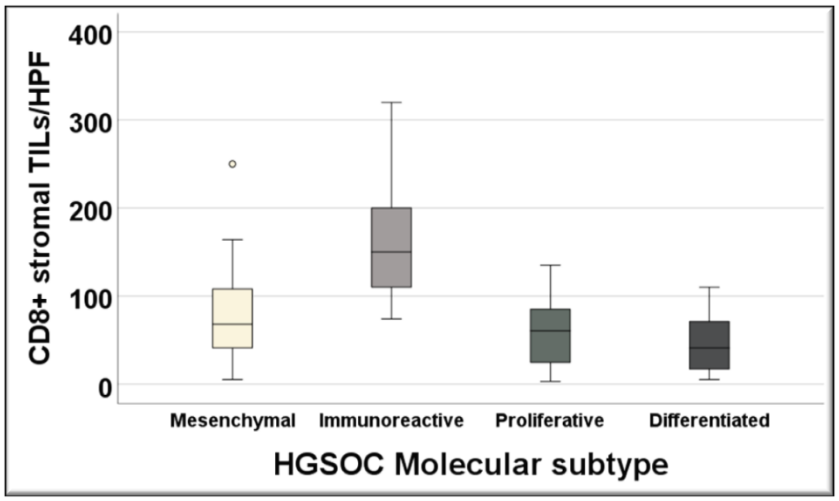

Figure 7. 11: A box plot diagram demonstrating the difference in the density of peri-tumoral/stromal tumour infiltrating CD8+ lymphocytes amongst the 4 molecular subtypes of HGSOC in the Birmingham cohort. The median stromal CD8 count per high power field was highest in the Immunoreactive subtype (n=10, *Mdn*=150/HPF), followed by the Mesenchymal subtype (n=43, *Mdn*=68). The Solid Proliferative subtype (n=12) had a median stromal CD8 count of 60.5/HPF. The lowest median stromal CD8 count was in the Differentiated/Papillary glandular subtype (n=25, *Mdn*=41). These differences were statistically significant (*H*=24.25, .001).

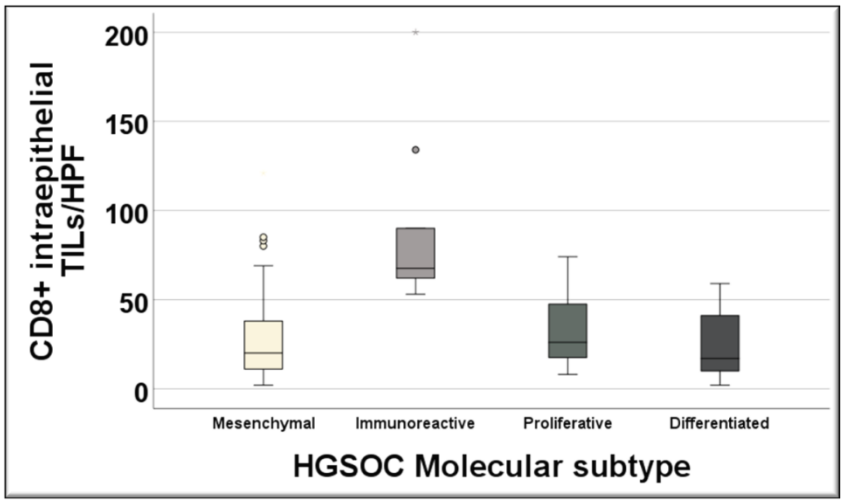

Figure 7. 12: A box plot diagram demonstrating the difference in the density of intraepithelial tumour infiltrating CD8+ lymphocytes amongst the 4 molecular subtypes of HGSOC in the Birmingham cohort. The median intraepithelial CD8 count per high power field was highest in the Immunoreactive subtype (n=10, *Mdn*=67.5/HPF), followed by the Proliferative subtype (n=12, *Mdn*=26). The Mesenchymal subtype (n=43) had a median intraepithelial CD8 count of 20/HPF. The lowest median intraepithelial CD8 count was in the Differentiated/Papillary glandular subtype (n=25, *Mdn*=17). These differences were statistically significant (*H*=21.64, *p*=<0.001).

The next step was to determine the Ki-67 index in the 4 molecular subgroups of HGSOC to study the difference in the proliferative nature of these tumours. The median Ki-67 index was highest in the Solid Proliferative subtype and lowest in the Immunoreactive subtype. This difference was statistically significant when applying the Kruskal-Wallis test (Figure 7.13).

A formal mitotic index was then calculated by counting the number of mitoses in 10 HPFs equivalent to $2mm^2$ in total and then compared amongst the 4 molecular subgroups. Similar to the Ki-67 index, the median mitotic index was highest in the Solid Proliferative subtype and lowest in the Immunoreactive subtype. This difference was also statistically significant (Table 7.6).

To confirm the concordance between the mitotic and Ki-67 indices we found a strong significant positive correlation between the 2 variables using Spearman's correlation coefficient (ρ=0.75, p=<0.001). To test the sensitivity of the 40% cut-off we applied for the Ki-67 index, we compared the mitotic index in the low (≤40%) versus high (>40%) Ki-67 expression group. The mitotic index/10HPFs was significantly higher in the high Ki-67 expression group (U=253.5, p=<0.001). Taken together, these data indicate that the Ki-67 and mitotic indices are significantly higher in the Solid Proliferative subtype of HGSOC from the Birmingham cohort consistent with their underlying biology.

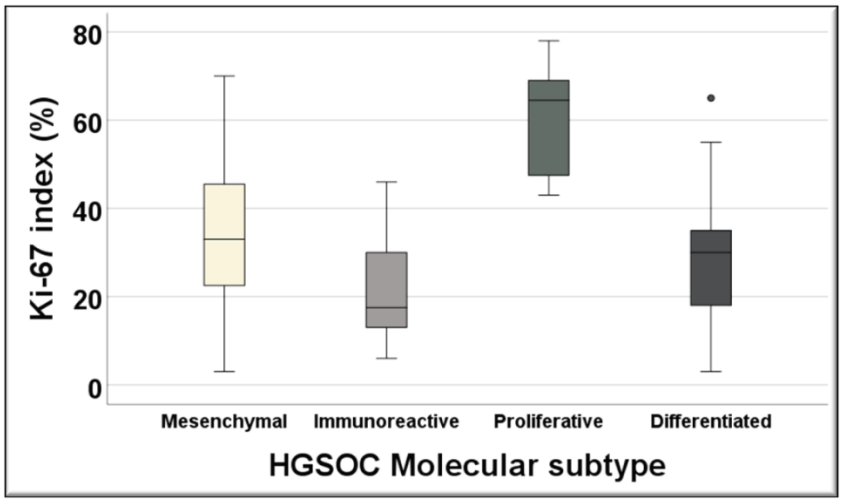

Figure 7. 13: A box plot diagram demonstrating the difference in the Ki-67 proliferative index between the molecular subgroups of HGSOC from the Birmingham cohort. The median Ki-67 index was highest in the Solid Proliferative subtype (n=12, *Mdn*=64.5%), followed by the Mesenchymal subtype (n=43, *Mdn*=33%), and the Differentiated subtype (n=25, Mdn=30%). The Immunoreactive subgroup (n=10) had the lowest median Ki-67 index at 17.5%. The difference was statistically significant using the Kruskal-Wallis test (*H*=26.194, *p*=<0.001).

Table 7. 6: The difference in the mitotic index between the 4 molecular subgroups of HGSOC from the Birmingham cohort. The Solid Proliferative subtype had a significantly higher median mitotic count per 10 high power fields compared to the other 3 subtypes.

Molecular Subtype of HGSOC	**Number of patients**	**Mitotic index[a]** ***Mdn*** ***(Min, Max)***	**Kruskal Wallis test *(H)*** ***(p-value)***
Mesenchymal	43	26 (3, 60)	**10.74** ***(p=0.013)****
Immunoreactive	10	18 (4, 46)	
Solid Proliferative	12	43 (10, 70)	
Differentiated	25	20 (5, 58)	
Total	**90**	**25 (3, 70)**	

Mdn: median**, Min:** minimum**, Max:** maximum

a: Mitotic index was calculated in 10 high power fields=2mm^2

7.3.2 Overlapping morphology between the Molecular subtypes and morphological features associated with *BRCA* mutations

Although the patients in this cohort were categorised into one molecular subtype following the above algorithm, we have evidence to show the morphological/molecular heterogeneity of HGSOC. To this end, we noticed a percentage of the patients who had overlapping morphological features between two subtypes. In addition, we noticed some unique morphological features associated with *BRCA* mutant HGSOC patients.

To elaborate, there were 6 patients with the Mesenchymal subtype who also showed immunoreactive features (Figure 7.14). One of these 6 patients was a *BRCA*-1 mutation carrier, and another patient was *BRCA* wild type. In addition, there were 16 patients with the Mesenchymal subtype who also showed proliferative features (Figure 7.15). One of these patients had a *BRCA*-2 frameshift mutation in exon 13 and two other patients were *BRCA* wild type. Two patients with the Immunoreactive subtype also showed proliferative features one of which showed a *BRCA-2* frameshift mutation (Figure 7.16). A total of 5 patients with the Differentiated/Papillary Glandular subtype also showed focal areas with a solid proliferative pattern. In the latter subtype, two patients were *BRCA* mutant (one with *BRCA-1* deletion and the other with *BRCA-2* mutation) and one patient was *BRCA* wild type.

Although numbers were small for statistical correlations, we noted that the combination of Papillary Glandular and Solid Proliferative patterns is particularly observed in *BRCA* mutant patients which is referred to in the literature as the SET pattern. Figure 7.17 demonstrates a *BRCA*-1 mutant patient from our cohort with this SET pattern that was classified as Differentiated/Papillary glandular with proliferative

features due to the dominance of the former pattern. Taken together, these data indicate the morphological and molecular heterogeneity of HGSOC tumours which in some cases may indicate the presence of *BRCA* mutations.

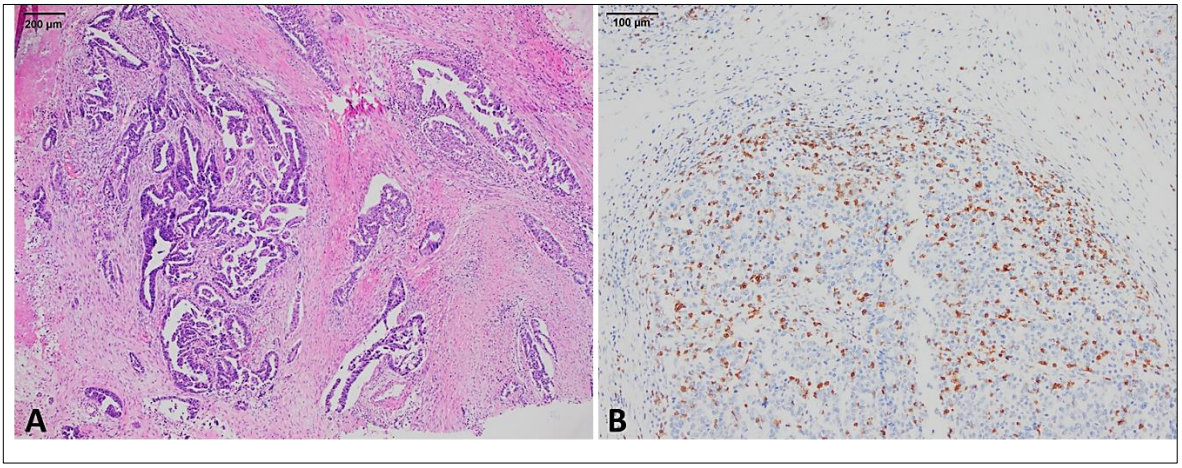

Figure 7. 14: The Mesenchymal subtype of HGSOC with immunoreactive features in one patient from the Birmingham cohort. A) The classic mesenchymal labyrinthine pattern with extensive desmoplasia is apparent in this tumour (H&E, x4 magnification). B) CD8 immunostaining in a different part of the same tumour showing extensive tumour infiltrating lymphocytes (stromal 132/HPF, intraepithelial 85/HPF) (anti-CD8, x10 magnification). This demonstrates the morphological and molecular heterogeneity of these neoplasms.

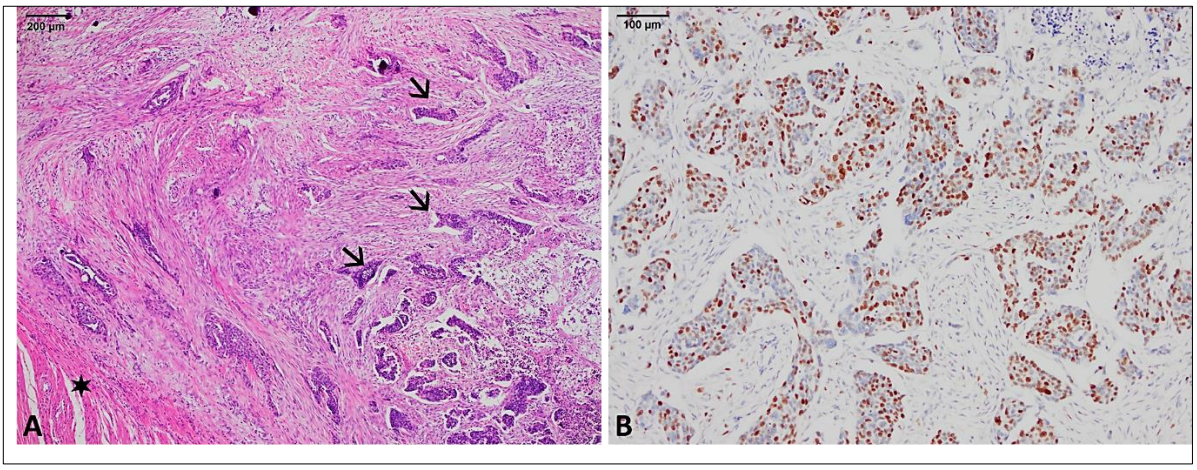

Figure 7. 15: A HGSOC patient of the Mesenchymal subtype which showed proliferative features in the Birmingham cohort. A) Invasive papillae (arrows) with a labyrinthine pattern invading the serosal and muscular coat (star) of the colonic wall and eliciting an extensive desmoplastic response characteristic of the Mesenchymal subtype of HGSOC (H&E, x4 magnification). B) The Ki-67 index in the invasive nests was 50% indicating a high proliferative activity [anti-Ki67 (MM-1), x10 magnification].

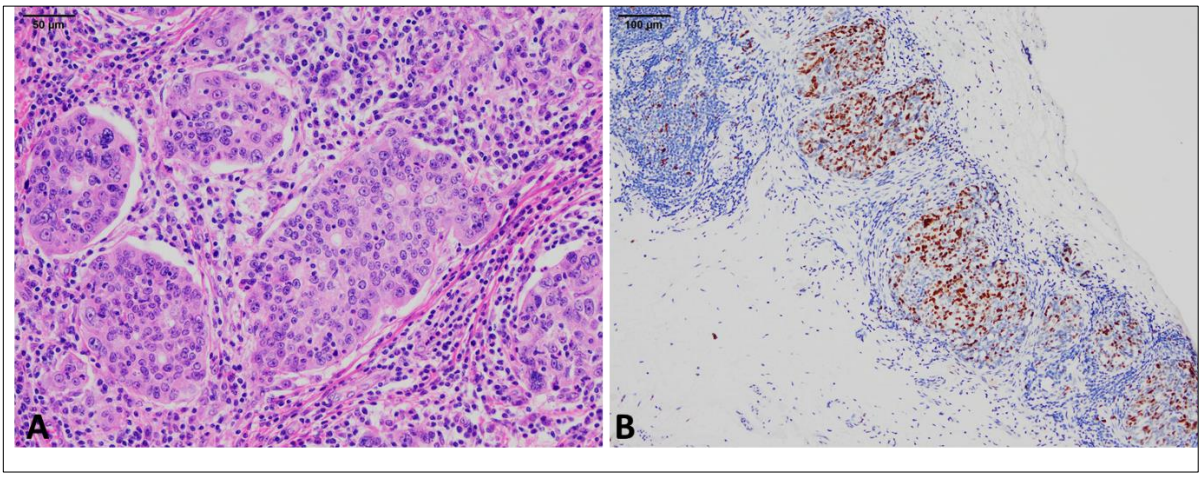

Figure 7. 16: A *BRCA-2* mutant HGSOC patient from the Birmingham cohort with the Immunoreactive subtype of HGSOC that also showed proliferative features. A) The smooth and well-defined invasive nests characteristic of the Immunoreactive subtype of HGSOC are apparent in this case (H&E, x20 magnification). B) The Ki-67 index was 46% in these tumour nests indicating proliferative features [anti-Ki67 (MM-1), x10 magnification].

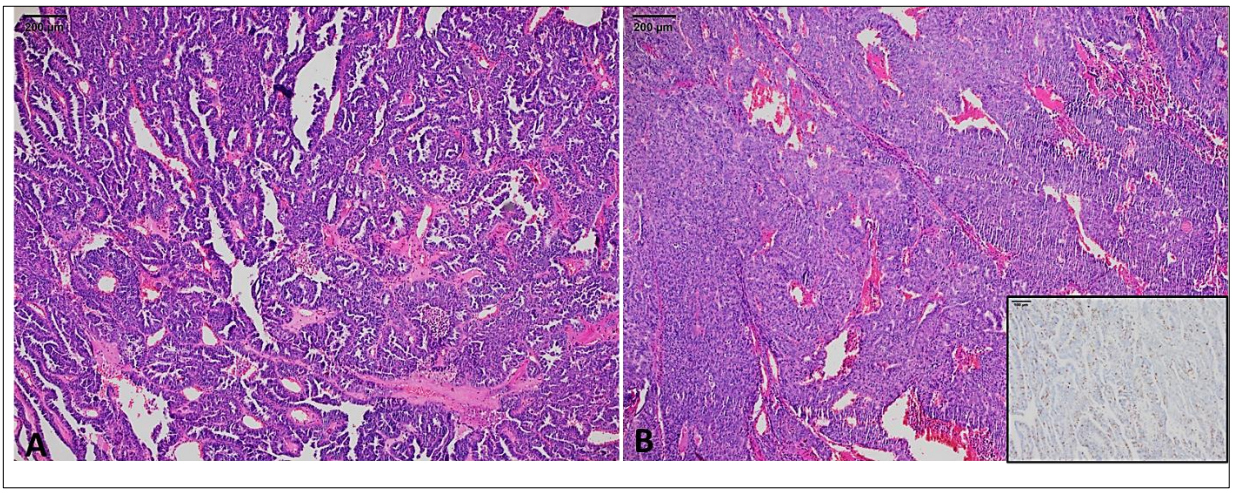

Figure 7. 17: A *BRCA*-1 mutant patient with the Differentiated/Papillary Glandular subtype of HGSOC that showed solid proliferative areas as well. A) The classic papillary glandular subtype is noted in one part of the tumour, and this was the dominant pattern (H&E, x4 magnification). B) Another focus in the same tumour showing a solid, pseudo-glandular and transitional-like pattern (SET pattern) with a Ki-67 index of 41% (inset) indicating proliferative features (H&E, x4 magnification). These features are characteristic of *BRCA* mutant HGSOC patients.

In addition to the SET pattern, another morphological feature that we noted in *BRCA* mutant patients was the presence of invasive micropapillary structures without fibrovascular cores that were surrounded by a clear space. Figure 7.18 demonstrates a *BRCA-2* mutant patient that showed heterogeneous morphology with a predominant Papillary Glandular architecture with proliferative features as well as invasive micropapillary architecture in some areas. It is interesting to note that this is the same patient from Figures 4.11 and 4.12 in chapter 4 that showed mosaic p53 expression and differential UbcH10 and Ki-67 expression in different parts of the same tumour. Collectively, these data indicate that different biological mechanisms and molecular abnormalities might underpin the morphological heterogeneity of *BRCA* mutant HGSOC patients.

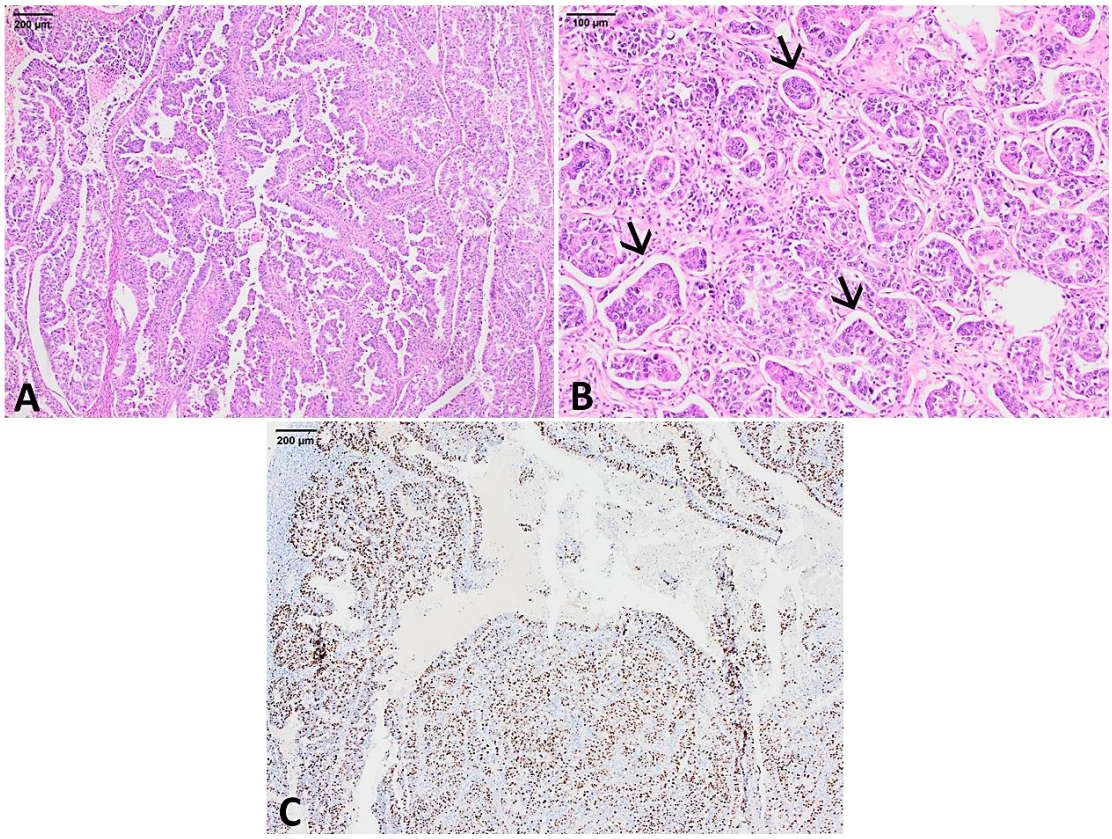

Figure 7. 18: A *BRCA-2* mutant patient with the Differentiated/Papillary Glandular subtype of HGSOC that showed proliferative features and micropapillary architecture. A) Invasive high-grade serous carcinoma with a papillary glandular architecture (H&E, x4 magnification). B) Another focus in the same tumour showing invasive micropapillae surrounded by a stromal retraction artefact (arrows, H&E, x10 magnification). C) This tumour was very proliferative particularly in the papillary areas with a Ki-67 index of 53% [anti-Ki67 (MM-1), x4 magnification). Of note, this is one of the cases with mosaic p53 expression seen in Figures 4.11 and 4.12 in chapter 4.

7.3.3 The Immunoreactive subtype of HGSOC is significantly associated with *BRCA* mutations and new morphological features identified in the Mesenchymal subtype

To investigate further the morphological features in *BRCA* mutant HGSOC patients, we next investigated whether there was any significant association between the molecular subtypes and *BRCA* mutations. In addition, we also investigated whether

the aforementioned invasive micropapillary architecture was pathognomonic to *BRCA* mutant HGSOC.

7.3.3.1 The Immunoreactive subtype of HGSOC is significantly associated with BRCA-1 mutations

Of the 28 patients that were tested for *BRCA* mutations in this cohort, 16 (57.1%) of which were *BRCA* mutant and 12 (42.9%) were *BRCA* wild type. Out of 16 BRCA mutant patients, 9 where *BRCA-1* and 7 were *BRCA-2* mutants. We then compared the distribution of *BRCA* mutant and *BRCA* wild type patients among the 4 molecular subgroups using Pearson's Chi-square test. Due to the small number of patients in each of the 4 molecular subgroups, statistics were done by comparing each molecular subgroup to the other 3 subgroups combined. We found a significant association between the Immunoreactive subtype and *BRCA* mutations in HGSOC from this cohort (Table 7.7).

Table 7. 7: The relationship between the molecular subtype of HGSOC and *BRCA* mutation status in the 28 patients that were tested for *BRCA* mutations from the Birmingham cohort. The *p*-value of the Chi-square test indicates a significant association between the Immunoreactive subtype and *BRCA* mutations in this cohort.

***BRCA* mutation status**	**Molecular subtype of HGSOC**				**Total**
	MES (n=9)	IMR (n=5)	PRO (n=5)	DIF (n=9)	28
Wild type	4	0	4	4	12
Mutant	5	5	1	5	16
Pearson's Chi-square test (*p*-value)[a]	**0.014 (1)**	**4.6 (0.04)***	**3.43 (0.13)**	**0.014 (1)**	

MES: Mesenchymal**, IMR:** Immunoreactive**, PRO:** Solid Proliferative**, DIF:** Differentiated/Papillary Glandular.

a: Statistics were computed by comparing each subtype with the other three subtypes as 2 groups.

We next considered the type of *BRCA* mutations in each molecular subtype in more detail. Out of 5 HGSOC patients with the *Immunoreactive* subtype who were tested for *BRCA*, 4 patients had *BRCA-1* mutations (Two were frameshift mutations and two were unspecified) and one had a *BRCA-2* frameshift mutation. The *BRCA-2* mutant patient was the same patient shown in Figure 7.16 who also had proliferative features. Figure 7.19 demonstrates a *BRCA-1* mutant HGSOC patients from our cohort with the Immunoreactive subtype which also showed an invasive micropapillary architecture. These data indicate the higher frequency of *BRCA-1* mutations in the Immunoreactive subtype of HGSOC.

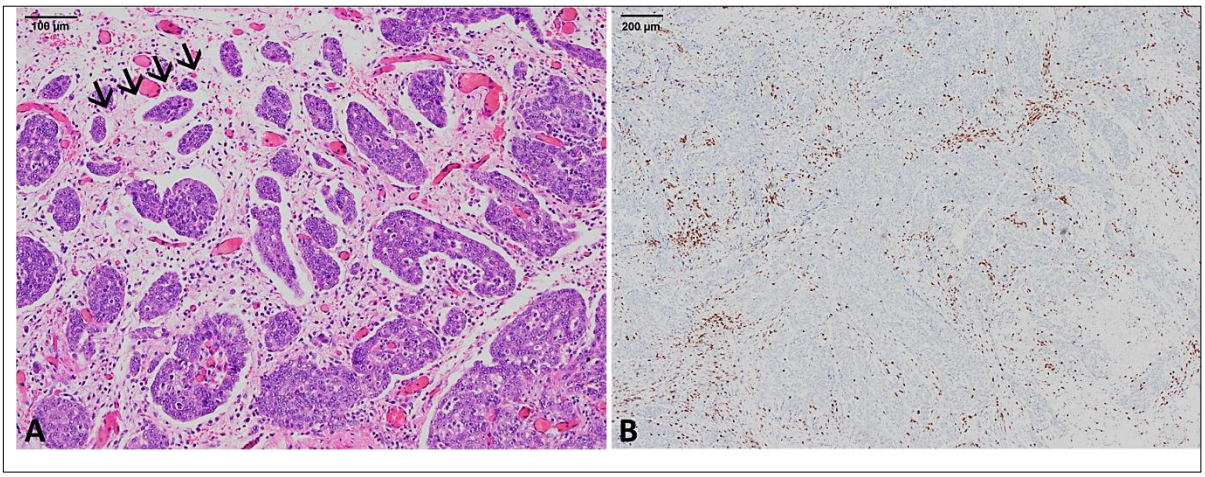

Figure 7. 19: A *BRCA-1* mutant patient with Immunoreactive HGSOC from the Birmingham cohort. A) Smooth nests with pushing border characteristic of this subtype are present as well as invasive micropapillae (arrows) surrounded by a stromal retraction artefact (H&E, x10 magnification). B) CD8 immunostaining highlighting extensive tumour infiltrating lymphocytes (stromal 110/HPF, intraepithelial 84/HPF) (anti-CD8, x4 magnification).

Concerning the 5 patients with the *Solid Proliferative* subtype that were tested for *BRCA* mutations, the one patient that was *BRCA* mutant had a *BRCA-1* deletion, and that particular patient showed a focal papillary glandular architecture in one part of the tumour (Figure 7.20). This again highlights the higher frequency of a combined Papillary Glandular and Solid Proliferative or SET pattern in *BRCA* mutant patients.

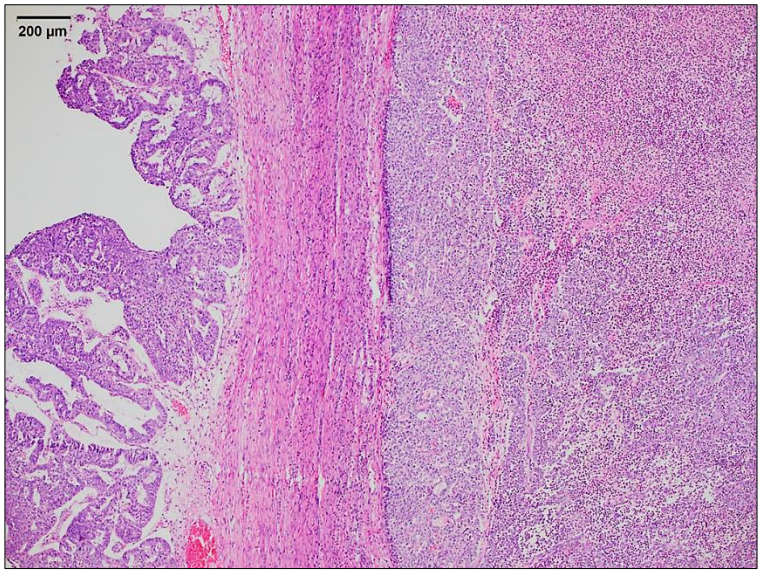

Figure 7. 20: A *BRCA-1* mutant patient from the Birmingham cohort with a predominantly Solid Proliferative subtype of HGSOC (right-hand side) and a focal papillary glandular architecture (left-hand side). This is another example of the SET (solid, pseudo-endometrioid and transitional-like) pattern seen in *BRCA* mutant HGSOC patients (H&E, x4 magnification).

With respect to the 9 *BRCA*-tested patients with the *Differentiated/Papillary Glandular* subtype, 5 were *BRCA* mutant. Two patients were mutant for *BRCA-1* and three were mutant for *BRCA-2.* One of three *BRCA-2* mutant patients showed proliferative features. Figures 7.17 and 7.18 display examples of patients with the Differentiated subtype who had *BRCA-1* and *BRCA-2* mutations, respectively. This indicates the

higher frequency of *BRCA-2* mutations in the Differentiated/Papillary Glandular subtype of HGSOC.

Finally, to consider the 9 *BRCA* tested HGSOC patients with the *Mesenchymal* subtype, 5 were *BRCA* mutant. Two patients were *BRCA-1* mutant, one of which had immunoreactive features, whilst three patients were *BRCA-2* mutant, one of which showed proliferative features. This indicates the higher frequency of *BRCA-2* mutations in the Mesenchymal subtype.

From a statistical perspective, the numbers are too low to do any further associations, but the above data collectively indicate that *BRCA-1* mutations confer more immunoreactive properties to the tumours, whilst *BRCA-2* mutations confer more proliferative features.

To test the association between the invasive micropapillary architecture and *BRCA* mutations statistically in our cohort, we used Fisher's exact test to compare the presence of an invasive micropapillary architecture between *BRCA* mutant patients (n=16) and *BRCA* wild type patients (n=12). The association was found to be statistically not significant (Fisher's exact 2-sided significance=1) indicating equal distribution of an invasive micropapillary architecture between *BRCA* mutant and *BRCA* wild type patients.

7.3.3.2 New morphological features significantly associated with Mesenchymal HGSOC

After finding no significant association between the micropapillary architecture and *BRCA* mutations *per se*, we next investigated the frequency and distribution of this architecture amongst the 4 molecular subgroups in our cohort using the Chi-square

test. We found that the invasive micropapillary architecture was significantly associated with the Mesenchymal subtype of HGSOC (X^2=22.4, p=<0.001). This pattern was noted in 22 out of 43 patients with the Mesenchymal subtype, 6 of which were chemonaïve and 16 had received pre-operative chemotherapy. It was completely absent in the Solid Proliferative pattern by definition. However, once the Mesenchymal subtype was excluded, the presence of a micropapillary architecture in the Immunoreactive or Differentiated subtypes was highly suggestive of the presence of *BRCA* mutations as previously shown in Figures 7.18 and 7.19.

In addition, we identified two previously unreported histopathological features that were exclusive to the Mesenchymal subtype; a sarcomatoid/syncytial pattern and paradoxical differentiation. The sarcomatoid/syncytial pattern is where the tumour grows as a cell continuum with wildly pleomorphic sarcomatous looking nuclei. The paradoxical differentiation phenomenon is where invasive small nests derived from the main tumour acquire a densely eosinophilic cytoplasm with low nuclear to cytoplasmic (N/C) ratio that contrasts with the intense hyperchromasia and high N/C ratio of the cells in the main tumour mass. These two morphological features were noted in 10 out of 43 patients with the Mesenchymal subtype of HGSOC, 5 of which were chemo-naïve and 5 had received pre-operative chemotherapy. Figure 7.21 is representative of a chemonaïve Mesenchymal HGSOC with both a micropapillary architecture and a syncytial pattern. Figure 7.22 is representative of another chemonaïve Mesenchymal HGSOC with both the sarcomatoid/syncytial pattern and paradoxical differentiation phenomenon. Data on the association between micropapillary, sarcomatoid/syncytial pattern and paradoxical differentiation with the 4 molecular subtypes of HGSOC in this cohort are summarized in Table 7.8.

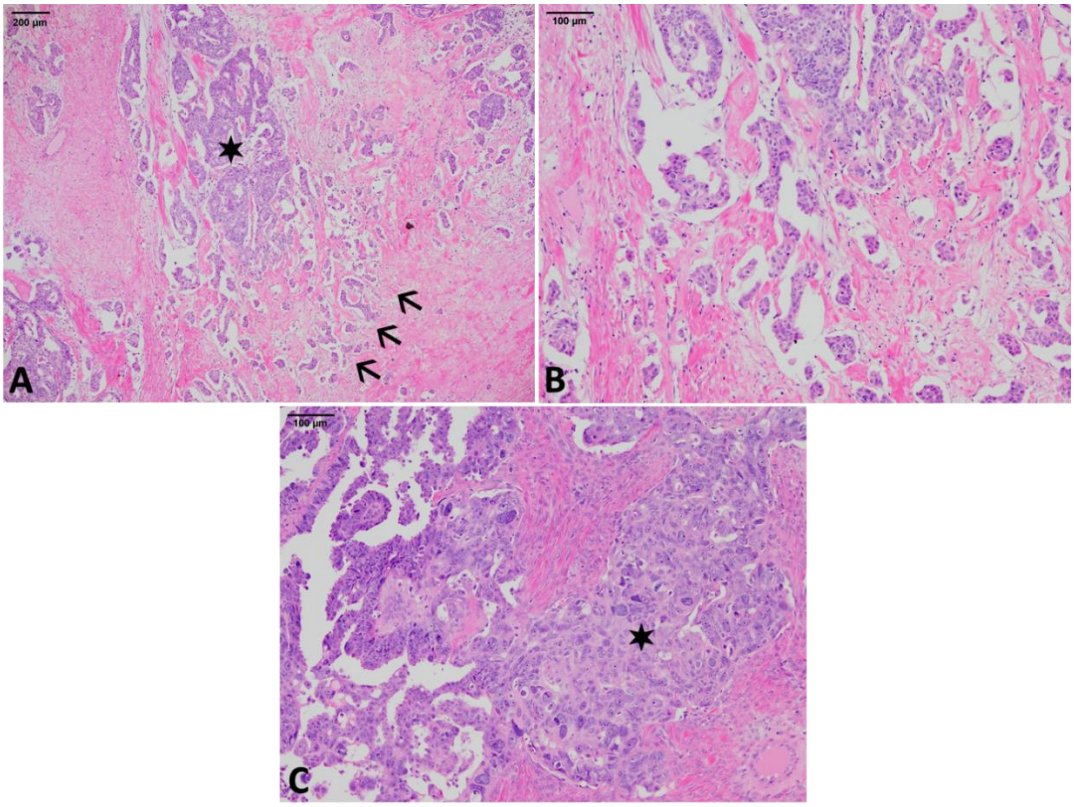

Figure 7. 21: Invasive micropapillary architecture and sarcomatoid/syncytial pattern observed predominantly in the Mesenchymal subtype of HGSOC from the Birmingham cohort. A) The classic labyrinthine pattern (star) seen in a chemonaïve Mesenchymal tumour surrounded by invasive micropapillae emanating from the main tumour (arrows, H&E, x4 magnification). B) Higher power view of the tumour in panel A demonstrating the micropapillae arising from the main tumour and surrounded by a clear space (H&E, x10 magnification).C) Another focus in the same tumour showing cells growing in a syncytial sheet like pattern (star) with very ugly looking large nuclei reminiscent of an undifferentiated carcinoma or sarcoma (H&E, x10 magnification).

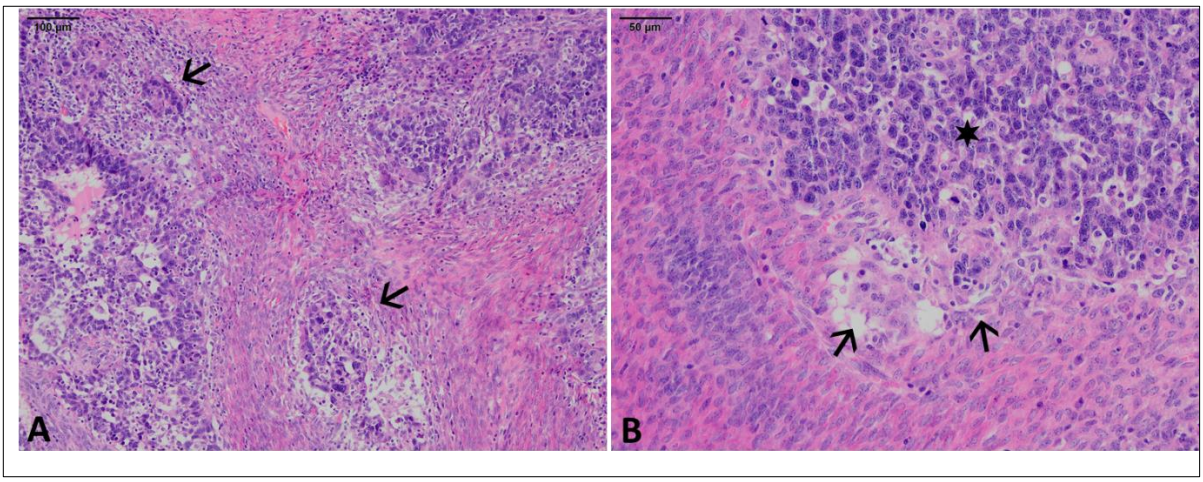

Figure 7. 22: Sarcomatoid/syncytial pattern and paradoxical differentiation observed exclusively in the Mesenchymal subtype of HGSOC from the Birmingham cohort. A) Chemonaïve Invasive nests that are loosely cohesive (arrows) and blend into a desmoplastic stroma characteristic of the Mesenchymal pattern. The tumour cells have ugly looking pleomorphic nuclei reminiscent of a sarcoma or undifferentiated carcinoma (H&E, x10 magnification). B) Another area in the same tumour where the main tumour mass is composed of cells with hyperchromatic nuclei (star) that grow as a syncytium. Two small nests acquiring ample eosinophilic cytoplasm emanating from the main tumour with low N/C ratio (arrows; paradoxical differentiation phenomenon) (H&E, x20 magnification).

Table 7. 8: The distribution of the invasive micropapillary architecture, sarcomatoid/syncytial pattern, and paradoxical differentiation phenomenon amongst the molecular subtypes of HGSOC in the Birmingham cohort. The *p*-values of the Fisher's exact and Chi-square tests indicate that invasive micropapillae, sarcomatoid/syncytial pattern and paradoxical differentiation were significantly associated with Mesenchymal subtype of HGSOC. The Solid Proliferative subtype showed complete absence of both micropapillary architecture and sarcomatoid/syncytial pattern by definition. The Differentiated subtype showed significantly less invasive micropapillary architecture and the two patients that had micropapillae were *BRCA*-mutant patients.

Morphological parameter	**Molecular subtype of HGSOC**				**Total**
	MES (n=43)	**IMR (n=10)**	**PRO (n=12)**	**DIF (n=25)**	**90**
Sarcomatoid/ syncytial pattern and paradoxical differentiation					
Present	10	0	0	0	**10**
Absent	33	10	12	25	**80**
Fisher's exact test (*p*-value)[a]	**(<0.001)***	**(0.6)**	**(0.35)**	**(0.056)**	
Invasive Micropapillary architecture					
Present	22	1[b]	0	2[b]	**25**
Absent	21	9	12	23	**65**
Chi-square test (*p*-value)[a]	**22.4 (<0.001)***	**1.7 (0.27)**	**5.3 (0.032)***	**6.7 (0.009)***	

MES: Mesenchymal**, IMR:** Immunoreactive**, PRO:** Solid Proliferative**, DIF:** Differentiated/Papillary Glandular.

a: Statistics were computed by comparing each subtype with the other three subtypes as 2 groups.

b: The three patients (2 Differentiated and 1 Immunoreactive) that showed micropapillae were *BRCA*-mutant.

We can conclude from the above data that the Immunoreactive subtype of HGSOC is significantly correlated with *BRCA* mutations particularly *BRCA-1*. The invasive micropapillary architecture and the newly identified sarcomatoid/syncytial pattern and paradoxical differentiation phenomenon are morphological features significantly associated with the Mesenchymal subtype of HGSOC. In the absence of features of Mesenchymal differentiation, invasive micropapillary architecture is highly suggestive of *BRCA* mutations.

7.3.4 UbcH10 protein expression levels are significantly higher in the Solid Proliferative subtype of HGSOC

In order to recapitulate results with *Ube2C* gene expression and its association with the Proliferative subtype of HGSOC from TCGA cohort, we next examined the association between UbcH10 protein expression and the molecular subtypes in the Birmingham cohort.

In the first instance, we looked at UbcH10 protein expression by IRS and H-scores in the 90 HGSOC patients from this cohort. In those 90 patients, UbcH10 protein expression by IRS ranged from 0 to 12 (*Mdn*=7), and by H-score it ranged from 0 to 229 (*Mdn*=106.7). The total UbcH10 protein expression ranged from 0 to 89.6% (*Mdn*=47.8).

When comparing UbcH10 protein expression by IRS in the 4 molecular subgroups as a continuous variable, the median UbcH10 expression was highest in the Solid Proliferative subgroup (*Mdn*=8), followed by the Immunoreactive and Mesenchymal subtypes (*Mdn*=7). The lowest median UbcH10 expression by IRS was in the

Differentiated/Papillary glandular subgroup (*Mdn*=6). The difference was not statistically significant (*H*=5.031, *p*=0.17).

The median UbcH10 expression by H-score was again highest in the Solid Proliferative subtype (*Mdn*=125.9), followed by the Immunoreactive (*Mdn*=111.6) and Mesenchymal subtypes (*Mdn*=106.6). The lowest median UbcH10 expression by H-score was in the Differentiated subtype *(Mdn*=102.8). The difference was again not statistically significant (*H*=2.79, *p*=0.425).

The median UbcH10 TPS was also highest in the Solid Proliferative subtype (Mdn=61.7%), followed by the Immunoreactive subtype (Mdn=60.7%) and the Mesenchymal subtype (46%). The lowest median UbcH10 TPS was in the Differentiated subtype (Mdn=43.6%). The difference was also statistically not significant (*H*=6.519, *p*=0.089).

To try and gain statistical significance, we combined the Mesenchymal, Immunoreactive and Differentiated subtypes into one group and we termed it the 'Non-Solid Proliferative' group. We then compared UbcH10 protein expression levels between the Solid Proliferative (n=12) and the Non-Solid Proliferative (n=78) as two groups. The median UbcH10 expression by IRS was significantly higher in the Solid Proliferative subtype (Figure 7.23). However, when comparing the median UbcH10 expression by H-score between the two groups, although it was higher in the Solid Proliferative subtype (*Mdn*=125.9) compared to the Non-Solid Proliferative subtype (*Mdn*=104.5), the difference was not statistically significant (*U*=334, *p*=0.112). When considering the median UbcH10 total tumour proportion score, it was again higher in the Solid Proliferative subgroup (Mdn=61.7%) compared to the Non-Solid Proliferative

group (Mdn=47.3%) but the difference was also statistically not significant (*U*=309, *p*=0.059). These results although borderline, indicate that UbcH10 protein expression is significantly higher in the Solid Proliferative subtype of HGSOC.

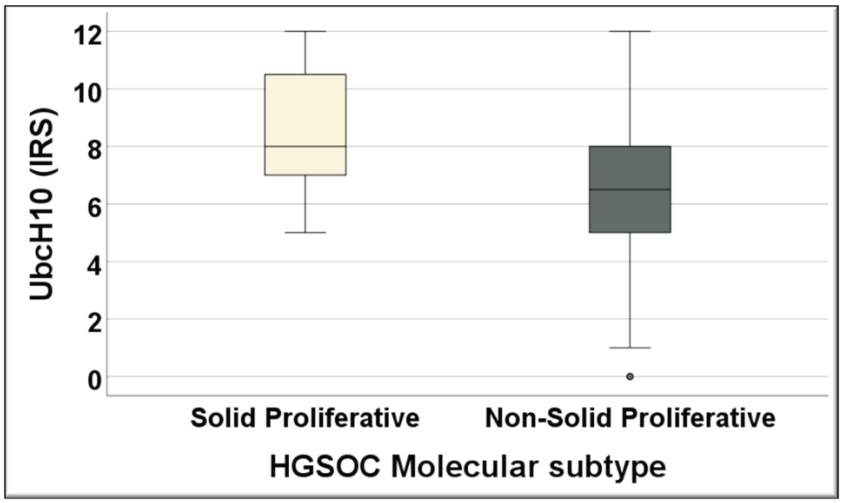

Figure 7. 23: The association between UbcH10 protein levels by IRS and the Solid Proliferative subtype of HGSOC from the Birmingham cohort. Patients with the Solid Proliferative subtype (n=12) had a higher median UbcH10 expression by IRS (*Mdn*=8) compared to the three other molecular subtypes (Immunoreactive, Mesenchymal and Differentiated) combined as one group (Non-Solid Proliferative, n=78, *Mdn*=6.5). The difference was statistically significant when applying the Mann-Whitney test (*U*=288.5, *p*=0.031).

7.3.5 UbcH10 protein levels correlate positively and significantly with the Ki-67 and mitotic indices in HGSOC

To expand more on the proliferative properties of UbcH10, we wanted to look at its correlation with both the Ki-67 and mitotic indices in the 90 HGSOC patients from this cohort to prove its significant association with the proliferative state of the cell.

For this analysis we used both the UbcH10 TPS and the H-score but not the IRS because both the UbcH10 TPS and H-score unlike the IRS are continuous and can be applied in bivariate analysis using Spearman's correlation coefficient.

We found a significant strong positive correlation between UbcH10 expression by H-score and the Ki-67 index (Figure 7.24), and a significant moderate positive correlation between the UbcH10 TPS and the Ki-67 index (ρ=0.498, p=<0.001).

Additionally, we found a significant strong positive correlation between UbcH10 expression by H-score and the mitotic index (ρ=0.667, p=<0.001). Similarly, we found a significant strong positive correlation between the UbcH10 TPS and the mitotic index (Figure 7.25). Figure 7.26 is representative of a HGSOC case from our cohort of the Solid Proliferative subtype with high Ki-67 and mitotic indices and high UbcH10 protein expression. Taken together, these data confirm the strong proliferative properties of UbcH10 and its significant association with the more proliferative subtypes of HGSOC in the Birmingham cohort.

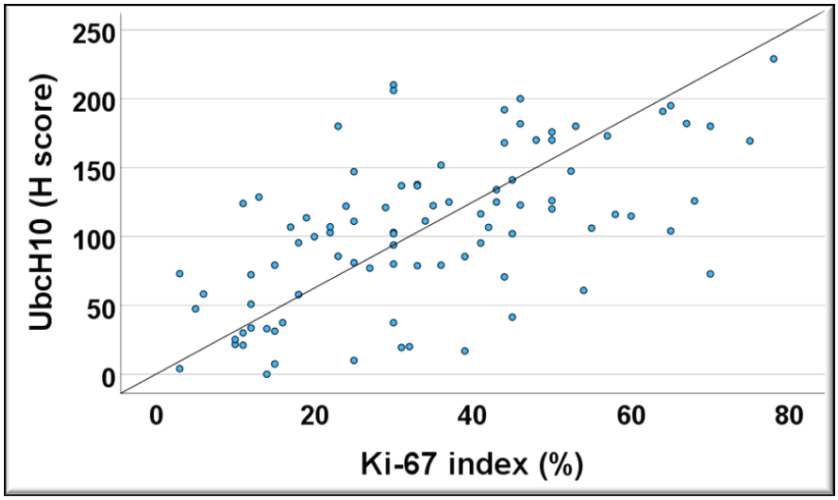

Figure 7. 24: A scatter plot demonstrating the strong correlation between UbcH10 protein expression by H-score and the Ki-67 index in HGSOC patients from the Birmingham cohort. A statistically significant strong positive correlation exists between the two variables (ρ=0.592, p=<0.001).

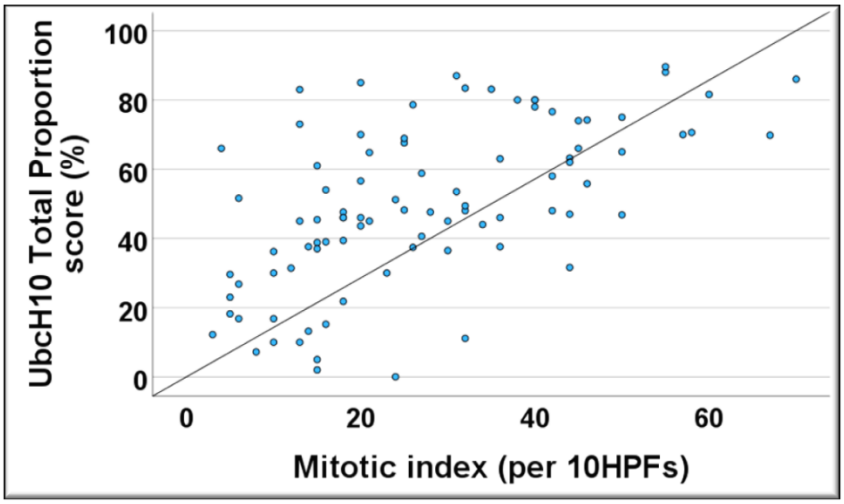

Figure 7. 25: A scatter plot demonstrating the strong correlation between the UbcH10 total tumour proportion score and the mitotic index per 10 high power fields in HGSOC patients from the Birmingham cohort. A statistically significant strong positive correlation exists between the two variables (ρ=0.614, p=<0.001).

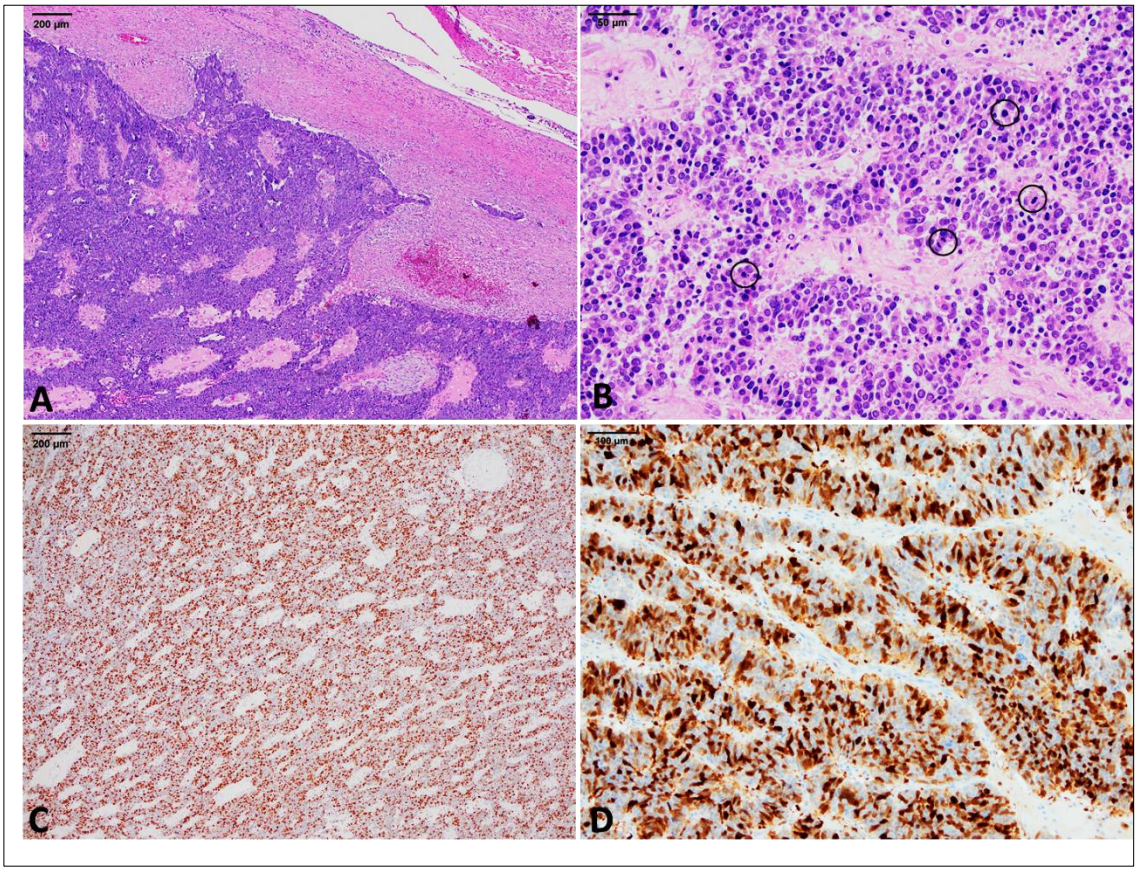

Figure 7. 26: High UbcH10 expression in the Solid Proliferative subtype of HGSOC from the Birmingham cohort and its strong association with the Ki-67 and mitotic indices in this tumour. A) Scanning power view of a high-grade serous carcinoma with solid growth and a pushing pattern of invasion without overt desmoplasia characteristic of the Solid Proliferative subtype of HGSOC (H&E, x4 magnification). B) Higher power view of the tumour in panel A showing brisk mitotic activity (circles) with 45 mitoses per 10HPFs (H&E, x20 magnification). C) Immunostaining of the tumour for Ki-67 showing strong diffuse nuclear staining in 80% of tumour cell nuclei [anti-Ki67 (MM-1), x4 magnification). D) High UbcH10 expression in the same tumour (IRS 12, H-score 229) (anti-UbcH10, x10 magnification).

7.3.6 Pre-operative chemotherapy significantly reduces UbcH10 and Ki-67 protein levels but does not impact tumour infiltrating lymphocytes

Because we had a significant number of patients who had received pre-operative chemotherapy, we wanted to study the effect of chemotherapy on UbcH10 protein levels and the two diagnostic parameters in our cohort: Ki-67 and CD8+ TILs. To this end, we had 10 patients with matched pre- and post-chemotherapy biopsies where we compared UbcH10 and Ki-67 protein expression levels as well as CD8+ stromal and intraepithelial TILs. The Wilcoxon signed ranks test was used for this type of analysis.

The median UbcH10 protein levels by both IRS and H-scores were significantly reduced by pre-operative chemotherapy administration. In addition, the UbcH10 TPS was significantly reduced in post-chemotherapy specimens.

The median Ki-67 index was also significantly reduced in post-chemotherapy specimens.

With respect to the CD8+ TILs, both stromal and intraepithelial tumour infiltrating lymphocyte density were slightly increased in post-chemotherapy specimens, but the increase was not statistically significant. Data are summarized in Table 7.9.

Collectively, these data indicate that UbcH10 akin to Ki-67 behaves like a proliferative marker with significant reductions in their protein levels by chemotherapy administration. This might indicate an underrepresentation of the Solid Proliferative subtype in our cohort because of the effect of chemotherapy. On the other hand, chemotherapy increases the density of TILs but not to a level that would alter the classification of the molecular subtypes in our cohort.

Table 7. 9: The effect of Chemotherapy on UbcH10 and Ki-67 protein expression levels as well as the density of CD8+ tumour infiltrating lymphocytes in 10 HGSOC patients with matched pre-and post-operative chemotherapy biopsies in the Birmingham cohort. The p-values of the Wilcoxon singed ranks test indicates that both UbcH10 and Ki-67 protein expression levels are significantly reduced by pre-operative chemotherapy administration. On the other hand, chemotherapy increases the density of stromal and intraepithelial CD8+ TILs but not significantly.

Diagnostic parameter	**Pre-chemotherapy value** ***Mdn (Min, Max)***	**Post-Chemotherapy value** ***Mdn (Min, Max)***	**Wilcoxon signed ranks test (*p-value*)**
Stromal CD8+ TILs	62 (3, 150)	65 (10, 150)	0.678
Intraepithelial CD8+ TILs	9.5 (2, 41)	20.5 (3, 110)	0.285
Ki-67 index	40 (15, 70)	21 (1, 50)	0.008*
UbcH10 (IRS)	8 (5, 10)	5 (1, 8)	0.018*
UbcH10 (H-score)	125 (80, 195)	51 (2, 120)	0.008*
UbcH10 tumour proportion score	46 (30, 80)	23.6 (2, 47)	0.008*

Mdn: median**, Min:** minimum**, Max:** maximum, **TILs:** Tumour infiltrating lymphocytes.

7.3.7 The correlation between the molecular subtypes of HGSOC and the clinicopathological parameters in the Birmingham cohort

7.3.7.1 Overview

Similar to analysis done on TCGA cohort, in this section we correlate the molecular subtypes with the prognostic and predictive parameters of HGSOC patients from the Birmingham cohort to identify any significant associations. Due to the small number of patients in the subgroups, statistics were done by comparing one subtype to the other three subtypes combined as two groups. Continuous quantitative variables such as the age at diagnosis were analysed using the Mann-Whitney test. Otherwise, qualitative variables were compared between the molecular groups using the Chi-square test.

7.3.7.2 The molecular subtypes of HGSOC do not correlate with any prognostic parameters in the Birmingham cohort

To establish a prognostic role for the 4 molecular subgroups in this cohort, we correlated these groups with the various prognostic indicators available to us from this cohort. Firstly, we considered the age of patients at diagnosis. The median age at diagnosis was highest in the Mesenchymal subgroup at 65 years followed by the Differentiated subtype at 64 years and the Immunoreactive at 63 years. The lowest median age at diagnosis was in the Solid Proliferative subtype at 55 years. These differences were not statistically significant.

Concerning FIGO stage, Lymph node metastasis, type of surgery performed and the volume of residual disease after surgery, the number of patients were proportionately distributed between the molecular subtypes indicating no statistically significant association. The statistical correlations performed are detailed in Table 7.10. These data indicate that the molecular subtypes of HGSOC do not correlate significantly with any of the prognostic parameters of HGSOC in the Birmingham cohort.

7.3.7.3 The Mesenchymal subtype of HGSOC is significantly associated with minimal chemotherapy response and platinum resistance

To consider the predictive role of the molecular subgroups of HGSOC in this cohort, we next correlated the 4 subgroups with the predictive parameters: namely the CRS and platinum resistance. The Mesenchymal subtype was significantly associated with a minimal response to chemotherapy and platinum resistance, whilst, in contrast, the Differentiated/Papillary glandular subtype was significantly associated with a complete or partial response to chemotherapy and platinum sensitivity. The statistical correlations performed are detailed in Table 7.11. These data indicate that the

Mesenchymal subtype of HGSOC portends a poor response to chemotherapy whilst the Differentiated subtype portends a better response to chemotherapy in this cohort.

Table 7. 10: The relationship between the molecular subtypes of HGSOC and the prognostic parameters in the Birmingham cohort. The *p*-values of the Mann-Whitney and the Chi-square tests indicate the absence of a significant association between the molecular subtypes and the prognostic parameters from this cohort.

Prognostic parameter	**Molecular subtype of HGSOC**				**Total (%)**
	MES	**IMR**	**PRO**	**DIF**	
No. of patients (%)	**43 (47.8)**	**10 (11.1)**	**12 (13.3)**	**25 (27.8)**	**90 (100)**
Age, year					
Mdn	65	63	55	64	**90 (100)**
(Min,Max)	(40, 81)	(40, 84)	(63, 81)	(40, 78)	
Mann-Whitney (p-value)[a]	**861.5 (0.228)**	**359.5 (0.603)**	**317 (0.073)**	**770 (0.702)**	
FIGO stage, *n*					
Early (I &II)	3	1	1	4	**9 (10)**
Late (III & IV)	40	9	11	21	**81 (90)**
Chi-square (p-value)[a]	**0.84 (0.49)**	**0.0 (1)**	**0.043 (1)**	**1.4 (0.26)**	
LN status, *n*					
Nx & N0	26	7	8	19	**60 (66.7)**
N1	17	3	4	6	**30 (33.3)**
Chi-square (p-value)[a]	**1.43 (0.23)**	**0.056 (1)**	**0.0 (1)**	**1.4 (0.24)**	
Type of surgery, *n*					
PDS	16	4	6	8	**34 (37.8)**
DDS[b]	27	6	6	17	**56 (62.2)**
Chi-square (p-value)[a]	**0.011 (0.92)**	**0.024 (0.878)**	**0.0 (1)**	**1.35 (0.321)**	
Cytoreduction, *n*					
R0 &R1	36	10	9	21	**76 (84.4)**
R2	7	0	3	4	**14 (15.6)**
Chi-square (p-value)[a]	**0.033 (0.856)**	**2.07 (0.351)**	**0.94 (0.39)**	**0.005 (1)**	

MES: Mesenchymal**, IMR:** Immunoreactive**, PRO:** Solid Proliferative**, DIF:** Differentiated/Papillary Glandular, **Mdn**: median, **Min**: minimum, **Max**: maximum, **LN:** Lymph node, **PDS**: Primary debulking surgery, **DDS**: Delayed debulking surgery, **R0** (complete):no gross residual disease, **R1** (optimal): gross residual disease between 0.1 to 1 cm, **R2** (sub-optimal): gross residual disease >1cm.

a: Statistics were computed by comparing each subtype with the other three subtypes as 2 groups.
b: Preoperative biopsy was retrieved in 10 out of 56 patients who underwent DDS (8 Mesenchymal, 1 Solid Proliferative, 1 Differentiated).

Table 7. 11: The relationship between the molecular subtypes of HGSOC and the predictive parameters in the Birmingham cohort. The Mesenchymal subtype and is significantly associated with minimal chemotherapy response and platinum resistance. The Differentiated subtype on the other hand is associated with partial or complete response to treatment and platinum sensitivity.

Predictive parameter	**Molecular subtype of HGSOC**				**Total (%)**
	MES	**IMR**	**PRO**	**DIF**	
CRS, *n*[a]					
Minimal	18	3	2	4	**27 (49.2)**
Partial & Complete	10	3	4	12	**29 (51.8)**
***Chi-square test (p-value)*[c]**	**5.24 (0.022)***	**0.02 (1)**	**0.525 (0.672)**	**4.5 (0.034)***	
Platinum resistance, *n*[b]					
Yes	14	2	3	2	**21 (30.8)**
No	19	6	7	15	**47 (69.2)**
***Chi-square test (p-value)*[c]**	**4 (0.045)***	**0.15 (1)**	**0.004 (1)**	**3.881 (0.049)***	

MES: Mesenchymal**, IMR:** Immunoreactive**, PRO:** Solid Proliferative**, DIF:** Differentiated/Papillary Glandular, **CRS**: Chemotherapy response score.

a: Analysis done on the 56 patients who underwent delayed debulking surgery.

b: Analysis done on 68 patients with available platinum resistance data.

c: Statistics were computed by comparing each subtype with the other three subtypes as 2 groups.

7.3.7.4 The Molecular subtypes of HGSOC do not correlate significantly with p53 protein expression patterns in the Birmingham cohort

We next investigated the correlation between the molecular subtypes and the p53 IHC staining pattern in the Birmingham cohort. The aim was to identify if any specific IHC staining pattern/mutation for p53 was associated with a particular molecular subtype. Similar to previous analysis, we used the Chi-square test to compare the distribution of patients with p53 overexpression (including mosaic) as well as null and cytoplasmic patterns amongst the 4 molecular subgroups. We found no significant association

between the p53 IHC staining patterns and the molecular subgroups in this cohort. Statistical correlations are detailed in Table 7.12.

Table 7. 12: The relationship between the molecular subtypes of HGSOC and the p53 immunohistochemical staining pattern in the Birmingham cohort. No significant association was found between the molecular subgroups and the various p53 IHC staining patterns.

	Molecular subtype of HGSOC				**Total (%)**
	MES	**IMR**	**PRO**	**DIF**	
No. of patients (%)	**43 (47.8)**	**10 (11.1)**	**12 (13.3)**	**25 (27.8)**	**90 (100)**
P53 IHC staining pattern, *n*					
Overexpression & Mosaic	33	8	10	15	**66 (73.3)**
Null & cytoplasmic	10	2	2	10	**24 (26.7)**
Chi-square test (p-value)	0.49 (0.48)	0.26 (1)	0.71 (0.5)	3.14 (0.076)	

MES: Mesenchymal**, IMR:** Immunoreactive**, PRO:** Solid Proliferative**, DIF:** Differentiated/Papillary Glandular**, IHC**: immunohistochemistry

a: Statistics were computed by comparing each subtype with the other three subtypes as 2 groups.

7.3.8 The prognostic impact of the molecular subtypes on patient outcomes in the Birmingham cohort

7.3.8.1 Overview

After exploring the relationship between molecular subtypes of HGSOC and prognostic parameters in the Birmingham cohort, we proceeded to explore their impact on the overall and progression-free survival of those 90 patients to see if results mirrored our previous analyses in TCGA cohort (Figures 7.3 and 7.4).

Overall and progression-free survival were available for 88 out of 90 patients from this cohort. Overall survival ranged from 1.9 to 126.1 months [Median OS=49.77*, 95% C.I* (38.72, 60.82)]. Progression-free survival ranged from 1.5 to 126.1 months [Median PFS=15.81, 95% C.I (13.51, 18.11)].

7.3.8.2 The molecular subgroups significantly impact HGSOC mortality in the Birmingham cohort

Concerning OS, patients with the Mesenchymal subtype exhibited the worst median OS, whilst patients with the Immunoreactive subtype had the longest median OS. In addition, the Solid Proliferative and Differentiated subtypes had intermediate OS rates. These differences were statistically significant as indicated in Figure 7.27 and Table 7.13. These data indicate that the Immunoreactive subtype of HGSOC confers a better OS whilst the Mesenchymal subtype confers a worse OS.

On univariate Cox regression analysis, only the Mesenchymal subtype was found to be a strong significant positive predictor of mortality and conferred an increased risk of death compared to patients with non-Mesenchymal (reference category) subtypes [HR=2.48, 95% C.I (1.42, 4.31), p=0.001]. On the other hand, the Differentiated/Papillary Glandular subtype of HGSOC decreased the risk of death compared to the non-Differentiated (reference category) subtypes. However, this was only borderline significant as indicated by the p-value and confidence interval [HR=0.54, 95% C.I (0.30, 0.99), p=0.045]. Although the Immunoreactive subtype decreased the risk of death compared to non-Immunoreactive (reference category) subtypes, it did not achieve statistical significance in this cohort [HR=0.67, 95% C.I (0.28, 1.56), p=0.352]. This indicates that the Immunoreactive subtype although

experiencing better OS, was not a significant negative predictor of mortality in this cohort.

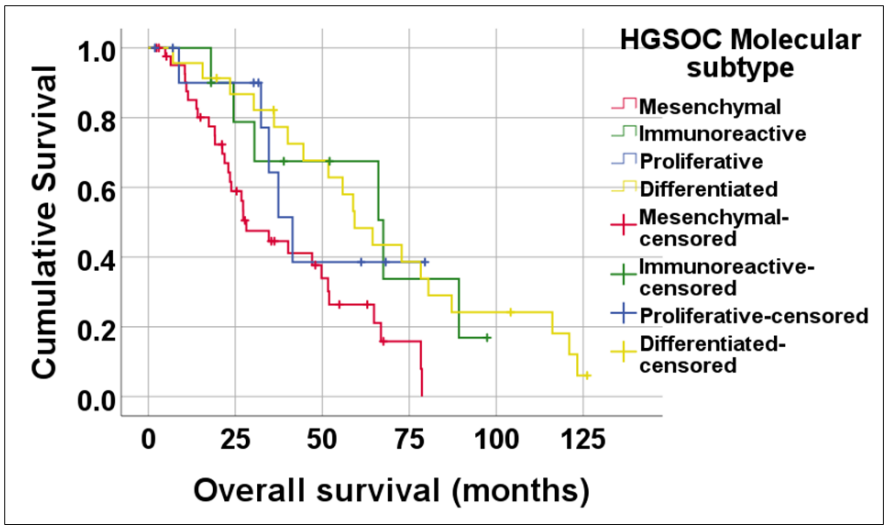

Figure 7. 27: A Kaplan-Meier curve demonstrating the difference in overall survival between the 4 molecular subgroups of HGSOC from the Birmingham cohort. HGSOC patients of the Mesenchymal subtype had the shortest median OS (n=43, *Mdn* OS=28.17 months), followed by patients with the Solid Proliferative subtype (n=12, *Mdn* OS=41.45 months). HGSOC patients of the Differentiated/Papillary Glandular subtype (n=23) showed a median OS of 59.27 months. Lastly, patients with the Immunoreactive subtype (n=10) exhibited the longest median OS (*Mdn* OS=67.52 months). These differences were statistically significant (Log rank X^2=11.157, p=0.011).

Table 7. 13: The effect of molecular subtype on the overall survival of HGSOC patients from the Birmingham cohort. Patients with the Mesenchymal subtype exhibited the worst median OS and a death rate of 69.8%. Patients with the Solid Proliferative subtype exhibited the second shortest median OS and the lowest death rate at 41.6%. Patients with the Differentiated subtype exhibited the highest death rate (82.6%) but an intermediate median OS. Patients with the Immunoreactive subtype exhibited the best median OS and a death rate of 60%. These differences were statistically significant (Log rank X^2=11.157, p=0.011).

Molecular subtype of HGSOC	Number of patients	Number of events	Median OS (95% CI)
Mesenchymal	43	30	28.17 (17.21, 39.14)
Immunoreactive	10	6	67.52 (27.60, 107.45)
Solid Proliferative	12	5	41.45 (32.47, 50.44)
Differentiated	23	19	59.27 (46.58, 71.97)
Total	**88**	**60**	**49.77 (38.72, 60.82)**

OS: overall survival, **95% C.I**: 95% confidence interval

7.3.8.3 The molecular subgroups do not impact HGSOC progression in the Birmingham cohort

Concerning the PFS, patients with the Mesenchymal subtype had the shortest median PFS whilst patients with the Differentiated/Papillary Glandular subtype showed the longest median PFS. These differences however were not statistically significant as indicated in Figure 7.28.

HGSOC patients of the Solid Proliferative subtype exhibited the highest progression rate, while patients of the Mesenchymal subtype exhibited the lowest progression rate. The difference was statistically not significant as shown in Table 7.14. Taken together, these data indicate that the molecular subtypes of HGSOC do not impact the progression rates in the Birmingham cohort.

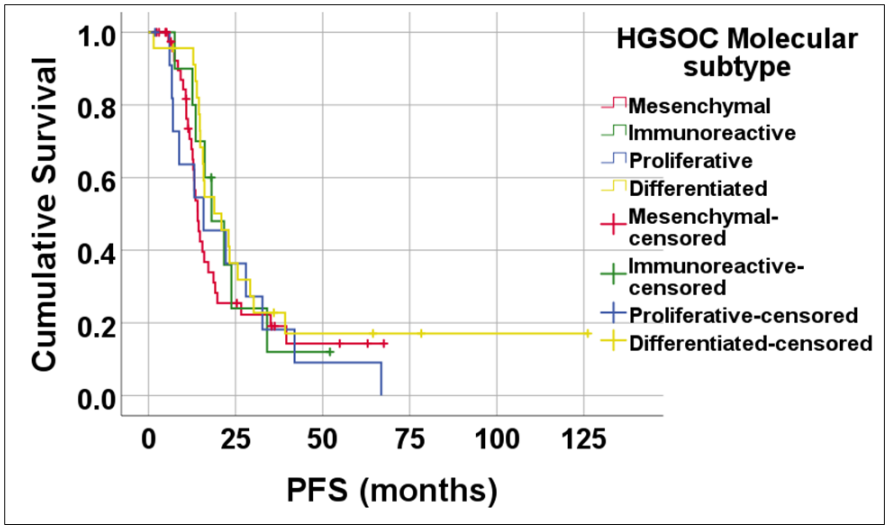

Figure 7. 28: A Kaplan-Meier curve demonstrating the difference in progression-free survival between the 4 molecular subgroups of HGSOC from the Birmingham cohort. HGSOC patients of the Mesenchymal subtype had the shortest median PFS (n=43, *Mdn* PFS=14.13 months), followed by patients with the Solid Proliferative subtype (n=12, *Mdn* PFS=15.81 months). HGSOC patients of the Immunoreactive subtype (n=10) showed a median PFS of 18.11 months. Lastly, patients with the Differentiated/Papillary Glandular subtype (n=23) exhibited the longest median OS (*Mdn* PFS=20.94 months). These differences were statistically not significant (Log rank X^2=1.99, p=0.574).

Table 7. 14: The effect of molecular subtype on the progression-free survival of HGSOC patients from the Birmingham cohort. Patients with the Mesenchymal subtype exhibited the worst median PFS and the lowest progression/recurrence rate at 69.8%. Patients with the Solid Proliferative subtype exhibited the second shortest median PFS and the highest progression/recurrence rate at 91.6%. Patients with the Immunoreactive subtype exhibited an intermediate median PFS and a progression/recurrence rate of 80%. Patients with the Differentiated subtype exhibited the longest median PFS and a progression/recurrence rate of 78.3%. These differences were however not statistically significant (Log rank X^2=1.99, p=0.574).

Molecular subtype of HGSOC	Number of patients	Number of events	Median PFS (95% CI)
Mesenchymal	43	30	14.13 (12.27, 15.99)
Immunoreactive	10	8	18.11 (10.67, 25.55)
Solid Proliferative	12	11	15.81 (1.37, 30.25)
Differentiated	23	18	20.94 (12.71, 29.16)
Total	**88**	**67**	**15.81 (13.51, 18.11)**

PFS: progression-free survival, **95% C.I**: 95% confidence interval

7.3.9 The prognostic impact of Ki-67 protein levels on HGSOC patient outcomes in the Birmingham cohort

7.3.9.1 Overview

In the final section of this chapter, we discuss the prognostic role that Ki-67 plays in HGSOC patients from the Birmingham cohort. We aimed to identify if Ki-67 affects the mortality or progression rates of HGSOC to compare with the borderline poor prognostic role UbcH10 played in the same cohort in chapter 3. We applied the 40% cut-off to divide patients into low (≤40%) and high (>40%) Ki-67 expression groups and used the Kaplan-Meier curves and the Log rank X^2 test to compare survival functions between the two groups.

7.3.9.2 Ki-67 protein expression does not impact HGSOC mortality in the Birmingham cohort

When looking at the OS of the 88 patients from this cohort, the high Ki-67 expression group experienced a shorter median OS compared to the low Ki-67 expression group. This difference however was not statistically significant as shown in Figure 7.29. This indicates that Ki-67 protein expression does not impact the OS of HGSOC females from this cohort.

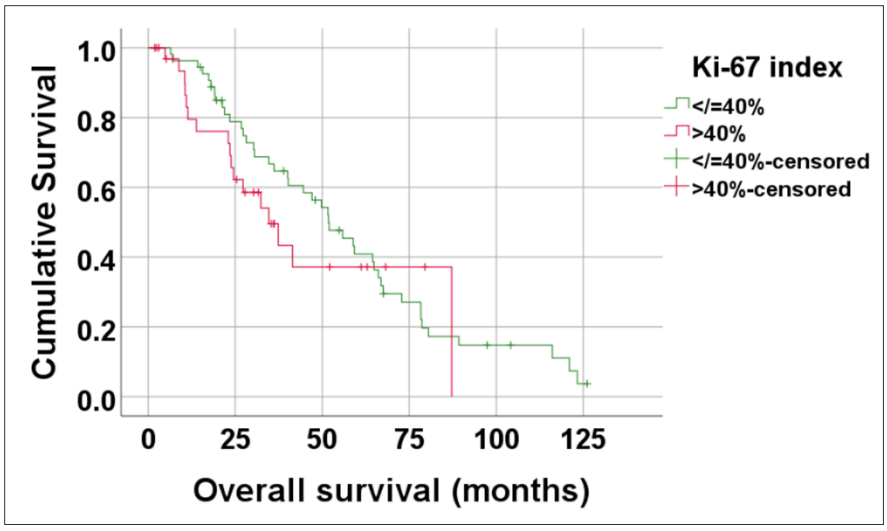

Figure 7. 29: A Kaplan-Meier curve demonstrating the effect of Ki-67 protein expression on the overall survival of HGSOC females in the Birmingham cohort. HGSOC patients with high Ki-67 protein expression (n=34, red line) experienced a worse median OS (*Mdn*=34.65 months) compared to the low Ki-67 protein expression (n=54, green line, *Mdn* OS=51.78 months). This difference was not statistically significant (Log rank X^2=0.721, p=0.396).

7.3.9.3 Ki-67 protein expression does not impact HGSOC progression in the Birmingham cohort

When considering the PFS in the 88 patients from this cohort, patients with high Ki-67 expression experienced a slightly worse median PFS compared to patients with low Ki-67 expression. The difference was again not statistically significant as indicated in Figure 7.30. This indicates that Ki-67 protein expression does not impact HGSOC progression in the Birmingham cohort.

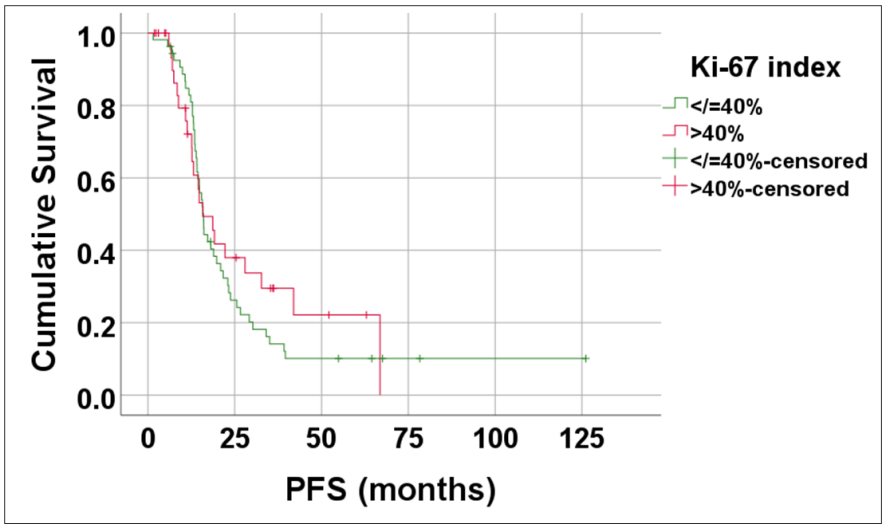

Figure 7. 30: A Kaplan-Meier curve demonstrating the effect of Ki-67 protein expression on the progression of HGSOC females from the Birmingham cohort. HGSOC patients with high Ki-67 protein expression (n=34, red line) experienced a slightly worse median PFS (*Mdn*=15.81 months) compared to the low Ki-67 protein expression (n=54, green line, *Mdn* PFS=16.01 months). This difference was not statistically significant (Log rank X^2=0.466, p=0.495).

7.4 Discussion

The Cancer Genome Atlas benchmark study in 2011 identified four transcriptomic subgroups of HGSOC; *Mesenchymal*, *Immunoreactive*, *Proliferative* and *Differentiated* (50). The literature has been conflicting on the prognostic role and survival risk of these four molecular subtypes (50, 60, 61). In the previous chapters we found strong evidence of the proliferative properties of UbcH10. Therefore, in this chapter we aimed to correlate *Ube2C* gene expression with the molecular subtypes of HGSOC in TCGA cohort. In addition, we attempted to apply the molecular classification on the HGSOC specimens from the Birmingham cohort based on previous studies (114, 181) and correlate the subgroups with UbcH10 protein expression. Moreover, we aimed to study the prognostic and predictive role of these molecular subgroups in these two cohorts to expand on the aforementioned studies.

7.4.1 UbcH10 is strongly associated with the Proliferative subtype of HGSOC and the proliferative state of the cell

In TCGA HGSOC cohort we found a strong significant association between *Ube2C* gene expression and the Proliferative subtype of HGSOC (Figure 7.1 and Table 7.1). In addition, in the Birmingham cohort we found a significant association between UbcH10 protein expression and the Solid Proliferative subtype of HGSOC (Figure 7.23). Moreover, we found a strong and significant positive correlation between UbcH10 protein expression (both by H-score and total proportion score) and the Ki-67 and mitotic indices in HGSOC patients in the Birmingham cohort (Figures 7.24, 7.25 and 7.26). Findings from these two cohorts validate our findings from chapter 6 where we also found a significant positive correlation between the UbcH10 total proportion

score, and the Ki-67 index in HGSOC with corresponding STIC samples (Figure 6.29). Additionally, we found that UbcH10 and Ki-67 were significantly co-expressed in HGSOC and their matched STICs (Figures 6.24 and 6.25). Taken together, these data confirm that UbcH10 behaves like a proliferative marker in HGSOC and is significantly upregulated in the more proliferative subtypes of these tumours.

To our knowledge, the present study is the first to correlate UbcH10 with the Proliferative subtype of HGSOC both at the gene and protein expression levels. Murakami and colleagues identified several gene expression signatures enriched in the Proliferative subtype of HGSOC in their cohorts which overlapped with TCGA defined signatures (50, 114). Commonly enriched gene sets in the Proliferative subtype of HGSOC included BENPORATH_PROLIFERATION and REACTOME_G2_M_CHECKPOINTS (114). Whilst both proliferation-related gene sets do not include *Ube2C*/UbcH10, they do include some of the *Ube2C* strongly and significantly co-expressed genes we identified in TCGA cohort in chapter 5 (Table 5.1 and Figure 5.1). Examples of genes included in the two aforementioned gene sets were *CENP-A, MYBL2, AURKB, AURKA, PLK1, CCNB2, CDC25C, CCNB1, UBE2T, TOP2A and RAD51.* Similarly*, Konecny et al (61)* also detected the differential expression of certain marker genes in the Proliferative subtype of HGSOC in their analysis. Gene sets involved in ubiquitin-mediated proteolysis were particularly upregulated in the Proliferative subtype in their study. These genes include those that encode components of the Anaphase Promoting Complex: *ANAPC1, ANAPC5, ANAPC7 and ANAPC13* as well as other genes: *BTRC, UBE2G1, SKP2, HERC4, UBE2NL, CDC26, UBE2N, UBE2E3, UBA2, UBE2CBP and MDM2*. All these genes

share similar molecular and biological functions with UbcH10 and are involved in cell-cycle regulation.

More recently, Hollis and colleagues (182) performed correlative genomic and transcriptomic characterization of 362 chemonaïve HGSOC samples. They demonstrated a significantly higher frequency of *CCNE1* amplifications in the Proliferative subtype of HGSOC in their cohort. Similar to the above-mentioned genes, *CCNE1* is significantly correlated with *Ube2C* gene expression in HGSOC patients from TCGA (Table 5.1). Moreover, and similar to UbcH10 we could not demonstrate a prognostic role for the proliferative maker Ki-67 on the mortality (Figure 7.29) and progression (Figure 7.30) of HGSOC patients in the Birmingham cohort. Collectively, these findings corroborated by previously discussed studies (101, 159) prove the strong proliferative properties of UbcH10 in malignancies in general and in HGSOC in particular.

7.4.2 The molecular classification of HGSOC and overlapping morphology between the molecular subgroups

In the Birmingham cohort we used morphological features as well as CD8 and Ki-67 immunohistochemistry to classify our cohort into the 4 molecular subgroups. The Mesenchymal subgroup represented the majority of our samples (47.8%) followed by the Differentiated/Papillary glandular subgroup (27.8%). Both the Solid Proliferative and Immunoreactive subgroups represented a minority in our cohort at 13.3% and 11.1%, respectively. When looking at the study by Murakami *et al* (114) who applied the same classification algorithm in a cohort of 132 chemo-naïve HGSOC samples, the Mesenchymal subgroup also represented the majority of their cohort at 36%.

However, both the Immunoreactive and Solid Proliferative subtypes constituted a larger proportion of their cohort at 26% and 24% respectively. We suggest that the inclusion of a significant number of post-chemotherapy samples in our cohort (51.1%) is the source of this discrepancy. This is especially true since both UbcH10 and Ki-67 protein levels were found to significantly reduced by pre-operative chemotherapy administration (Table 7.9). In addition, both taxanes and platinum-based therapy are known to induce desmoplasia which is an important diagnostic criterion for the Mesenchymal subtype of HGSOC (183, 184). This may account for the underrepresentation of the Solid Proliferative subtype and the overrepresentation of the Mesenchymal subtype of HGSOC in our cohort. To consider other studies, Khashaba *et al* (181) also used a diagnostic algorithm closely similar to ours on a cohort of 85 HGSOC patients. In their cohort, they also included a significant number (49.5%) of post-chemotherapy samples. Concordant with our results, they also had a higher number of Mesenchymal tumours and a minority of the Immunoreactive and Proliferative subtypes.

Another possible explanation for the low number of Solid Proliferative HGSOC in our cohort is the 40% cut-off for the Ki-67 index we applied to classify these tumours. Combined with the pure solid growth pattern these represented strict criteria for the diagnosis of the Proliferative subtype in our cohort as opposed to Murakami *et al* (114) who used only the solid growth pattern as the basis for their diagnosis. We contend that the application of the 40% Ki-67 cut-off improved the reproducibility of diagnosing the Solid Proliferative subtype by immunohistochemistry. This is because we demonstrated a significantly higher mitotic count and Ki-67 index in the Solid Proliferative subtype of HGSOC (Table 7.6 and Figure 7.13) as well as a strong

concordance between Ki-67 IHC and mitotic indices. On the other hand, Murakami *et al* did not demonstrate a difference in the mitotic indices between the 4 molecular subgroups of HGSOC in their cohort (114). Our results are concordant with Khashaba and colleagues who also found a significant association between a high Ki-67 index (>40%) and the Proliferative subtype of HGSOC in their cohort (181). However, while we have refined the diagnostic algorithm used by Murakami *et al* for the molecular classification of HGSOC, our classification is not without its limitations (114). We acknowledge that the robustness of our classification is limited by the lack of correlation between the protein and gene expression profiles as opposed to Murakami and colleagues (114), and a prospect for future research on the molecular classification of HGSOC in the Birmingham cohort.

To consider the Immunoreactive cases in our cohort, we demonstrated a significantly higher number of infiltrating CD8 positive lymphocytes in these tumours with low levels detected in the Solid Proliferative and Differentiated subtypes (Figures 7.11 and 7.12) This is consistent with reports from both Murakami *et al* and Khashaba *et al* albeit with different cut-off points (114, 181). Whilst Murakami *et al* applied our own cut-off for stromal (>100/HPF) and intraepithelial (>50/HPF) TILs in their study (114), Khashaba *et al* applied a cut-off of >20 intraepithelial TILs/HPF and ignored stromal TILs (181). However, while we used full-faced tumour sections like Murakami *et al (114)*, Khashaba *et al* used TMA cores, and therefore, their smaller cut-off can be justified (181). Hollis *et al* on the other hand quantified tumour infiltrating lymphocytes in their study as a percentage of intra-epithelial CD8+ cells in relation to the tumour islet infiltrated (182). They also showed a significant increase in immune cell infiltration (both CD3+ and CD8+ T-lymphocytes) in the Immunoreactive subtype of HGSOC in their study with

consistent low levels in the Proliferative subtype. However, unlike Murakami *et al* and Hollis *et al* (114, 182), we included post-chemotherapy samples in our cohort, and since both platinum and taxanes increase T-cell activation (185), it was important to consider the effect of chemotherapy on tumour infiltrating lymphocytes in our study. We found that chemotherapy did not significantly impact the number of TILs in matched pre- and post-chemotherapy samples from the same patients (Table 7.9). This means that while chemotherapy might have impacted the classification of the Mesenchymal and Solid Proliferative subtypes in our cohort it did not affect the classification of the Immunoreactive subtype. Similarly, the Differentiated/Papillary Glandular subtype does not have a specific immunohistochemical profile or morphological feature that would have been impacted by chemotherapy.

Concordant with previous studies we attempted to classify our HGSOC patients into one molecular subgroup. However, our samples demonstrated considerable morphological heterogeneity and morphological overlap between two subtypes. Particularly noted was the overlap between the Mesenchymal and Immunoreactive features (Figure 7.14) as well as the Solid Proliferative and Differentiated subtypes (Figure 7.17). The morphological heterogeneity of HGSOC was acknowledged in the study by Murakami and colleagues where they demonstrated a considerable overlap between the Mesenchymal and Immunoreactive subtypes of HGSOC (114).

Our results are also corroborated by results from Konecney *et al* who studied gene expression signatures in a cohort of 174 HGSOC patients and externally validated their results in a cohort of 185 HGSOC patients (61). They detected a considerable overlap in the expression matrix between the Mesenchymal and Immunoreactive subtypes as well as the Differentiated and Proliferative subtypes. These findings at the molecular

level explain the overlap that we detected at the morphological level in a proportion of our samples. Similarly, Verhaak and colleagues who studied prognostic gene signatures in 489 HGSOC samples from TCGA demonstrated that genes related to immune cells are upregulated in both the Mesenchymal and Immunoreactive gene expression subtypes (60). In fact, they found that 82% of their samples were assigned to at least 2 gene expression subtypes and every possible combination between the 4 molecular subgroups was observed in at least one of their samples. However, molecular subtype was assigned based on the dominant signature. Moreover, they detected a negative correlation between the Proliferative and Immunoreactive gene expression signatures as well as between the Differentiated and Mesenchymal signatures. Konecny and colleagues also detected a distinct downregulation of immune response genes in the Proliferative subtype of HGSOC in their cohort (61). These findings presumably explain why we did not detect any morphological overlap between the Differentiated and Mesenchymal HGSOC in our cohort and why the Immunoreactive HGSOC with proliferative features were among the least common subtypes in our cohort (Figure 7.16). In addition, this might also explain why CD8 immune cell infiltration was low in the Solid Proliferative subtype in our cohort (Figures 7.11 and 7.12). Taken together, our findings corroborated by the above studies indicate that HGSOC does not harbour mutually exclusive gene expression signatures but rather multiple gene signatures with differential activation levels. This might mean that the application of double classifiers e.g., Differentiated/Proliferative, Mesenchymal/Immunoreactive might be more informative in HGSOC given the genetic complexity of these tumours.

7.4.3 *BRCA* mutations and the molecular subtypes of HGSOC

We demonstrated a wide range of morphological features in *BRCA* mutant patients in our cohort. Firstly, we noticed the combination of the Differentiated and Solid Proliferative subtypes (Figures 7.17 and 7.20). We inferred that this was the "SET" pattern that is well described in the literature in association with *BRCA* mutant HGSOC patients (62). This notion has providence since the SET pattern described by Soslow *et al* demonstrated a significant association with a high mitotic index *(62)*.

In addition, we also demonstrated the association between the micropapillary architecture and *BRCA* mutations in HGSOC (Figure 7.18). However, statistically speaking the micropapillary architecture was equally distributed between *BRCA* mutant and *BRCA* wild type patients in our cohort. This means that on its own, the micropapillary architecture is not pathognomonic for *BRCA* mutant HGSOC. This is also consistent with findings by Soslow *et al* who described the micropapillary architecture in *BRCA1/2* mutant HGSOC patients, but their finding did not achieve statistical significance (62). However, similar to the case illustrated in Figure 7.18, they did describe a wide range of morphological patterns in *BRCA1/2* mutant patients. In addition, *BRCA1/2* mutant HGSOC have been shown to harbour a high tumour mutational burden which makes them more likely to express tumour specific neoantigens (186). Combined with the fact that we detected previously unreported differential patterns of Ki-67, UbcH10 and p53 expression in these tumours (Figure 4.11 and 4.12), this might reflect that molecular heterogeneity and different subcellular pathways might underpin the morphologic heterogeneity of *BRCA* mutant HGSOC. Therefore, studying the association between *BRCA* mutations and p53 mosaicism at

the molecular level represents a promising outlook for a better understanding of these tumours.

Furthermore, we demonstrated a significant association between the Immunoreactive subtype of HGSOC and *BRCA*-1 mutations in HGSOC in the Birmingham cohort (Table 7.7). High numbers of TILs are a well described feature in *BRCA-1* mutant triple negative breast cancer. They have also been described in several studies in association with *BRCA-1* mutant HGSOC, however, this was not previously interpreted in the context of the molecular subgroup in HGSOC (62, 187). Only very recently, and similar to our results, the study by Hollis *et al* demonstrated a higher rate of *BRCA1/2* mutations in the Immunoreactive subtype of HGSOC (182). In addition, they demonstrated improved survival benefit for *BRCA1/2* mutant HGSOC across all molecular subtypes of HGSOC. This is contrary to our results where the improved survival of *BRCA* mutant compared to *BRCA* wild type patients did not achieve statistical significance in the Birmingham cohort previously discussed in chapter 3 (Table 3.8 and 3.9). It is likely, however, that the limited availability of *BRCA* mutational data (only 33 patients) from this cohort impacted our statistical analysis. This is especially true since large studies have demonstrated the survival advantage of *BRCA1/2* mutant HGSOC (50, 188). As a counterargument, some studies suggested that the survival benefit of *BRCA* mutations in HGSOC seems to attenuate with long follow-up periods exceeding 10 years. This was the case in the Birmingham cohort where the follow-up period of *BRCA* mutant patients exceeded 10 years (189). This might be one of the reasons we did not detect survival differences between *BRCA*-mutant and non *BRCA*-mutant HGSOC. Nonetheless, our findings have significant implications, since the Immunoreactive subtype can be easily identified on routine H&E

and immunohistochemical staining and would therefore portend a better response to PARP inhibitors without the need for *BRCA1/2* mutational testing.

We also noticed the higher prevalence of proliferative features in *BRCA-2* mutant HGSOC samples in the Birmingham cohort (Figure 7.18). Because of the relatively small numbers of *BRCA-2* mutant patients (only 7 out of 16 *BRCA* mutant patients) we could not test this association statistically. This association thus merits further investigation. However, the Solid Proliferative subtype of HGSOC was not significantly associated with *BRCA* mutations. In fact, it was the least common subtype to show *BRCA* mutations (Table 7.7). Since UbcH10 is significantly associated with the Solid Proliferative subtype of HGSOC, this corroborates our findings from chapter 3 where we could not demonstrate a significant association between UbcH10 and *BRCA* mutations (Figure 3. 11 and Table 3.7). When looking at other studies, Verhaak *et al* reported that the Proliferative subtype of HGSOC was less likely to show *BRCA1/2* germline mutations *(60)*. Similarly, Hollis *et al* demonstrated a lower frequency of *BRCA1/2* mutations in the Proliferative subtype of HGSOC (182). However, interestingly, both Verhaak *et al* and Konecny *et al* reported the significant upregulation of gene sets involved in chromatin remodelling and DNA double strand break repairs in the Proliferative subtype of HGSOC (60, 61). These gene sets include genes such as *MMS22L, OBFC2B, RAD51AP1, RAD51D, PARP1 and PARP2* indicating that the Proliferative subtype undergoes high levels of homologous recombination. Combined with the low levels of immune cell infiltration we detected in Solid Proliferative HGSOC, this means that UbcH10 is particularly upregulated in a subset of HGSOC that are inherently aggressive and less likely to respond to PARP inhibition and immune-checkpoint inhibition currently under research. In fact, a recent study suggested that

the Proliferative subtype of HGSOC might benefit more from anti-angiogenic agents such as bevacizumab (190). Accordingly, we propose that the upregulation of UbcH10 might be used as a marker to tailor therapy for HGSOC patients. So, whilst UbcH10 is only a borderline prognostic marker in HGSOC, it is more beneficial as a predictor of treatment response when interpreted in the context of the molecular subgroup of HGSOC.

To expand more on the invasive micropapillary architecture in our cohort, we found it to be significantly associated with the Mesenchymal subtype of HGSOC (Figure 7.21 and Table 7.8). This is a previously unreported morphological feature in this subtype as neither Murakami *et al n*or Khashaba *et al* reported this finding (114, 181). However, other than the Mesenchymal subtype, micropapillary architecture was detected in the Immunoreactive (Figure 7.19) and Differentiated subtypes (Figure 7.18) of HGSOC and those were all *BRCA* mutant patients. Combined with the lack of statistically significant association between the micropapillary architecture and *BRCA* mutations this means that on its own, the micropapillary architecture is not indicative of the presence of an underlying *BRCA* mutation unless interpreted in the context of the molecular subtype it is associated with. We therefore propose the exclusion of the Mesenchymal subtype of HGSOC in the first instance and using the micropapillary architecture in the context of Immunoreactive and Differentiated subtypes as a more specific feature for *BRCA* mutant HGSOC.

7.4.4 New morphological criteria identified in Mesenchymal HGSOC

In addition to the invasive micropapillary architecture, we found two new morphological features to be indicative of the Mesenchymal subtype of HGSOC: sarcomatoid/syncytial pattern and paradoxical differentiation (Figure 7.22). Murakami

and colleagues described the mesenchymal transition pattern as spindled dyscohesive tumour cells associated with destructive stromal invasion (114). Similarly, Verhaak and colleagues described infiltrating single cells as a diagnostic clue to the Mesenchymal subtype of HGSOC (60). We propose the sarcomatoid/syncytial pattern as part of the spectrum of epithelial to mesenchymal transition that is well known to contribute to aggressive behaviour in these tumours (191).

We also detected the paradoxical differentiation phenomenon which is well described in cervical squamous cell carcinoma (SCC) and urothelial carcinoma but not in high-grade serous ovarian cancer (192, 193). Similar to the sarcomatoid/syncytial pattern, the paradoxical differentiation phenomenon was found exclusively in the Mesenchymal subtype of HGSOC in our cohort (Table 7.8). In cervical SCC, paradoxical differentiation is associated with early invasion (192). Ultra-structurally, these invasive nests have been associated with the accumulation of smooth muscle actin filaments that contribute to cytoplasmic eosinophilia. In addition, they have been shown to harbour cytoplasmic vesicles that open directly onto the extracellular matrix and contribute to basement membrane destruction, cellular dyscohesion and migration (194). Therefore, the paradoxical differentiation phenomenon might be part of the spectrum of EMT seen in the Mesenchymal subtype of HGSOC and is worthy of further ultrastructural investigation.

7.4.5 The Prognostic/Predictive role of the molecular subtypes of HGSOC

In TCGA cohort of HGSOC, we found no difference in overall or progression-free survival between the 4 molecular subgroups (Figures 7.3 and 7.4). In addition, the

molecular subgroups did not correlate significantly with age at diagnosis (Figure 7.2) or AJCC stage (Table 7.3). Since we applied the TCGA subtype classifier, these findings are consistent with the original study by TCGA investigators who similarly did not demonstrate any survival differences between the 4 Molecular subgroups in 489 HGSOC samples (50). However, later the TCGA research network along with Verhaak and colleagues identified a significant OS benefit for the Immunoreactive subtype and worse survival for the mesenchymal subtype in an independent validation dataset of 879 HGSOC specimens (60). This can be explained because the TCGA research network modified the original molecular classification by combining the original TCGA gene signatures with prognostic expression signatures and termed it Classification of Ovarian Cancer (CLOVAR) which allowed for a more robust survival classification.

In the Birmingham cohort, we demonstrated better OS for the Immunoreactive and Differentiated subtypes and worse survival for the Solid Proliferative and Mesenchymal subtypes (Figure 7.27). The trend was maintained in PFS between the molecular groups but did not achieve statistical significance (Figure 7.28). Our findings are consistent with findings from Verhaak and colleagues as detailed above (60). However, contrary to our results, the study by Verhaak demonstrated a recurrence-free survival benefit for the Immunoreactive subtype as well as worsened recurrence-free survival for the Mesenchymal subgroup. Similarly, Konecny and colleagues (61) who applied a *de novo* clustering method also demonstrated better OS for the Immunoreactive and Differentiated subtypes and worse survival for the Proliferative and Mesenchymal subtypes. They did not however report on the PFS differences between the molecular groups (61).

When looking at studies at the protein level, Murakami *et al* used two independent datasets to compare survival between the 4 molecular subgroups which included 132 and 89 HGSOC samples respectively (114). They showed significantly better OS and PFS for the Immunoreactive subgroup and worse OS and PFS for the Mesenchymal subgroups in both datasets. We contend that our small sample size (n=88) was a huge hindrance in achieving statistical significance with respect to the PFS compared to the above studies.

The better survival for the Immunoreactive subtype can be explained by the upregulation of KEGG gene sets involved in immune engagement as well as B and T cell activation. Additionally, high expression of MHC class I and II genes in this subtype facilitate antigen presentation and cell-mediated cytotoxicity (61, 114). These factors, in addition to the significant association with *BRCA1/2* mutations which confer a better survival and enhanced platinum sensitivity, likely underpin the better outcome of the Immunoreactive subtype (180). Conversely, the worse outcome observed in the Solid Proliferative subtype is likely explained by the low levels of immune cell infiltration indicating poor activation of the immune system against the tumour (182). In addition, these tumours show lower rates of *BRCA1/2* mutations but higher frequencies of *CCNE1* amplification which have been traditionally associated with poorer survival in HGSOC (50, 174, 182).

When we applied univariate Cox regression analysis in the Birmingham cohort, only the Mesenchymal subtype was associated with a significant increased risk of mortality, whilst the Differentiated subtype was only borderline significant as a negative predictor of mortality. In addition, we demonstrate a significant association between the Mesenchymal subtype and minimal chemotherapy response as well as platinum

resistance. The Differentiated subtype on the contrary was associated with partial/complete chemotherapy response and platinum sensitivity (Table 7.11). These findings partially explain the poorer outcome associated with the Mesenchymal subtype and the better outcome associated with Differentiated subtype.

Our study is the first to correlate the molecular subgroups classified at the protein level with response to chemotherapy. This was one of the advantages of including post-chemotherapy samples as opposed to Murakami and colleagues who only used chemonaïve HGSOC specimens for immunohistochemical analysis in their cohort (114). However, Murakami *et al* investigated an independent gene expression microarray dataset (GSE15622) that included ovarian cancer specimens treated with carboplatin single therapy (114). They found that the CLOVAR Mesenchymal gene expression signature was particularly low in carboplatin responders. Congruous with these results, Verhaak *et al* also demonstrated a higher frequency of platinum resistance in the Mesenchymal subtype of HGSOC (60).

At the gene expression level, the Mesenchymal subtype of HGSOC shows upregulation of genes related to: extracellular matrix remodelling, such as TGFBI; proteolysis such as Matrix metalloproteinases (MMPs); angiogenesis, such as VEGFB; activation of transcription factors that regulate EMT (61). Collectively, these factors contribute to invasion, metastasis, and aggressive behaviour in these tumours (191, 195). In addition, studies have reported the significant association between EMT and resistance to platinum therapy in ovarian cancer (196). The Differentiated subtype on the other hand shows an increased expression of genes involved in ovarian folliculo-genesis and secretory fallopian tube markers indicating more terminal differentiation (60, 61). Interestingly, *LAD1* a gene that regulates the anchoring of the epithelium to

the underlying mesenchyme was found to be significantly upregulated in the Differentiated subtype. These findings explain the better outcome associated with these tumours (60).

7.5 Conclusions

Here, we have validated the strong proliferative properties of UbcH10 both at the gene level in TCGA cohort and the protein level in the Birmingham cohort. UbcH10 is significantly and strongly associated with the Proliferative subtype of HGSOC which is an aggressive subtype explained by its molecular properties. UbcH10 overexpression, although weak in the prognostication of HGSOC *per se*, can be used as a marker to tailor therapy for HGSOC when interpreted in the context of the molecular subgroup of these tumours.

We refined the diagnostic algorithm developed in previous studies for the molecular classification of HGSOC using a combination of morphology and immunohistochemistry for Ki-67 and CD8 in the Birmingham cohort. We also identified new morphological features to aid in the molecular subtyping of HGSOC. These include the sarcomatoid/syncytial pattern and paradoxical differentiation phenomenon both exclusive to the Mesenchymal subtype. Furthermore, we identified the invasive micropapillary to be significantly associated with the Mesenchymal subtype. However, after exclusion of the Mesenchymal subtype, if observed in the Differentiated or Immunoreactive subgroups it suggests the potential for underlying *BRCA* mutations.

We also detected a significant and relatively new association between the Immunoreactive subtype of HGSOC and *BRCA* mutations. Concerning treatment response, the Mesenchymal subtype was significantly associated with minimal

response to chemotherapy and platinum resistance, whilst the Differentiated subtype was significantly associated with partial or complete response to chemotherapy and no platinum resistance.

We also clarified the conflicting literature on the survival differences between the 4 molecular subgroups. To this end, we confirm the significant difference in overall survival between the 4 molecular subgroups in the Birmingham cohort. Consistent with previous reports we demonstrated the survival benefit of the Immunoreactive and Differentiated subtypes and the worse survival of the Mesenchymal and Proliferative subtypes.

Our findings from the Birmingham cohort are, however, limited by the small sample size and the lack of correlation between protein expression and gene expression data which represent a prospect for future research.

Chapter 8. Ovarian cancer organoids are 3D-models that recapitulate the tumour from which they are derived

8.1 Introduction

As discussed in previous chapters, it is clear that HGSOC, as a subset of epithelial ovarian cancers, is a molecularly heterogeneous disease (61, 84). Some of the major hurdles that face researchers studying HGSOC is a lack of understanding of the molecular mechanisms that drive disease development and progression. Additionally, the current models used to study the disease have many drawbacks (197). As such, the most common models used to study ovarian cancer include 2D tumour cell lines and patient-derived tumour xenografts (198-201). Establishing a two-dimensional tumour cell line is a time-consuming task involving multiple passages that inevitably results in genetic drift with loss of tumour molecular characteristics and intratumoural heterogeneity (202). Xenografts, on the other hand, reliably recapitulate the characteristics of the tumour microenvironment but this comes at a significant cost in time and resources for their maintenance (46). Moreover, they undergo rapid evolution specific to the host in which they are transplanted (203). Therefore, there is a need to develop novel platforms to study ovarian cancer and allow for a more personalized approach to cancer treatment (204).

Organoids are three-dimensional, *in vitro,* models that faithfully recapitulate the tumour from which they are derived (205). First described for colorectal cancer, organoid culture has become an important technique for cancer research due to its ability to

allow the cells to differentiate and form multicellular units, more closely resembling tumour heterogeneity *in vivo* (206-208). In addition, organoids allow for rapid phenotype-genotype correlations. Therefore, they represent an attractive tool for drug sensitivity and resistance testing since they recapitulate patient response (208, 209). Studies with patient-derived organoids will ultimately improve our understanding of the tumour microenvironment and allow for a more tailored therapeutic approach as well as development of therapeutic drug strategies for each patient.

Organoid technology is based on using a three-dimensional matrix to support the cells that mimics the basement membrane. This is then supplemented with a cocktail of growth factors and small molecules to recreate the ecosystem of the tumour microenvironment enabling the cells to cluster into aggregates resembling organisation within an organ (210). Patient-derived organoids have been generated from breast, lung, prostate, bladder, liver, and stomach tumours (211). Recently, some studies investigated drug responses in short-term 3D models derived from HGSOC patients (212). However, only a few studies have described culture conditions suitable for long term expansion of ovarian cancer organoids (213-215).

Studies on ovarian cancer-derived organoids report successful organoid derivation from borderline tumours as well as a variety of epithelial ovarian cancers. These include low and high-grade serous, endometroid, mucinous and clear cell carcinomas. In addition, studies demonstrate that ovarian cancer-derived organoids capture the genomic and molecular landscape of the primary tumour. They also identify these models as a suitable platform for personalised drug testing (213, 214). However, some of these studies report slow growth of some of their organoid models suggesting suboptimal conditions (213).

As a starting point for ovarian cancer organoid derivation, studies used a culture medium originally used for organoid derivation from healthy fallopian tube epithelium termed “Fallopian tube organoid medium”. This culture medium consisted of a base culture medium supplemented with a cocktail of niche factors that modulate Wnt/β-catenin, fibroblast growth factor-10 (FGF-10), epidermal growth factor (EGF), transforming growth factor-β (TGF-β), bone morphogenetic protein (BMP) and ROCK signalling pathways (216).

In this chapter we optimise the culture conditions required to derive, develop, and sustain organoid models from HGSOC patients as well as other epithelial ovarian neoplasms. As such, we also demonstrate how these models accurately recapitulate patients’ cancers and reflect their histological complexity and genetic heterogeneity.

8.2 Development of patient-derived organoid growth conditions

8.2.1 Sample collection and tissue processing

The collection of fresh ovarian cancer tissues was performed intraoperatively at City hospital NHS Trust. Patients signed informed consent forms before the operation and appropriate ethical approval for all tissue collected was obtained from the relevant Ethics Committee Committee (Health Resource Authority reference 18/NE/0011). Samples were collected from a total of 19 patients between 2020 and 2022.

During surgery and immediately after extraction of the primary tumour, samples were dissected freshly inside the operating theatre and were then transported to the laboratory in 40ml of sample storage solution at 4 °C in a polystyrene ice box. The

sample storage solution consisted of Advanced DMEM/F12 (Thermo Fisher Scientific) supplemented with 10% (v/v) foetal-bovine serum (FBS; Sigma-Aldrich) and 1% (v/v) penicillin/streptomycin (Thermo Fisher Scientific). The sample delivery time was 90-120 min.

Upon arrival in the laboratory, the tissue samples were put on a sterile 10 cm tissue culture dish (Falcon) in a biological safety cabinet. They were then washed twice with ice-cold D-PBS (Gibco) and diced into approximately 2mm pieces. Any necrotic and fatty tissue was removed, and the greyish white tumorous tissue was retained for organoid generation. A few pieces were put in a cryovial and stored at -80 °C for biobanking. The remaining pieces were then incubated in 4ml of tissue digestion medium (Table 8.1) for 60 min on a shaking platform inside a humidified incubator at 37°C until the medium became cloudy to the naked eye.

Table 8. 1: Fresh tissue digestion medium.

Reagent	Supplier (catalogue number)	Stock concentration	Final concentration	Amount	Storage
Advanced DMEM/F12	Thermo Fisher Scientific (12634010)	x1	x1	3.96 ml	4°C
Collagenase type II	Thermo Fisher Scientific (17101015)	250 mg/ml[a]	2.5 mg/ml	40 µl	-20°C
ROCK inhibitor (Y-27632)*	APExBIO (B1293)	10 mM[b]	10 µM	4 µl	-20°C
Total	**-**	**-**	**-**	**4 ml**	**-**

a: collagenase type II stock was reconstituted as 1 g powder dissolved in 4ml of advanced DMEM/F12 and filtered with a 0.22 µm filter.

b: ROCK inhibitor stock was reconstituted as 10 mg powder in 4.043 ml of DMSO (Sigma).

*ROCK inhibitor was used to inhibit dissociation-induced apoptosis and improve cellular viability of digested tumour cells.

The resulting tissue/digestion medium mixture was then diluted 1:1 with Advanced DMEM/F12 at room temperature to deactivate the collagenase. The mixture was then filtered through a 70µM filter (Falcon, Catalogue number 352350) into a 50ml Falcon tube. Any remaining tissue pieces inside the filter were then ground using the rubber guard of a syringe plunge and homogenised to increase the cellular yield in the filtered cellular suspension. The filtered cell suspension was then centrifuged at 1000 rpm for 5 min to form a cell pellet and the supernatant was discarded. If the cell pellet contained a considerable number of erythrocytes, it was washed with 2ml of red blood cell lysis buffer (Merck, Catalogue number 11814389001) up to 3 times, 5-10 min incubation per time, until the red pellet turned grey/white to the naked eye. The cells were then

washed twice in 2ml of Advanced DMEM/F12 at room temperature to deactivate the lysis buffer. The cell suspension was then re- centrifuged at 1000 rpm for 5 min and the supernatant discarded. The resulting cell pellet was then resuspended in 1ml of Advanced DMEM/F12 at room temperature. The cell suspension was then pipetted up and down a few times using P1000 tips pre-wetted with D-PBS to break any cell clumps into a single cell suspension. The dispersion status of the cells was then checked under a light microscope by applying a 4μl drop of the cell suspension onto a glass slide. A single cell suspension was determined if more than 90% of the cells were dispersed as single cells without clumps. The cells were then counted and checked for viability using Trypan blue, as described below.

8.2.2 Cell counting and viability assessment

To determine the number and viability of cells in the prepared suspension, a haemocytometer/Neubauer chamber was used. The haemocytometer was first washed with 70% (v/v) ethanol and allowed to dry. A coverslip was then placed over the haemocytometer counting chambers. Subsequently, 30μl of the cellular suspension containing the tumour cells was mixed with an equal volume of 0.4% trypan blue stain (Gibco) in a microcentrifuge tube and left to stand for 5 min at room temperature. About 15μl of the cell/trypan blue mixture was then applied to the haemocytometer chamber between the coverslip and the V-shaped groove in the chamber. The haemocytometer was then placed on the stage of a binocular light microscope. The outer four corner quadrants of the haemocytometer were used for counting, each of which has a volume of $0.1mm^3$ or $1x10^{-4}$ ml. The number of viable (unstained) and non-viable cells (stained) in each of the 4 corner chambers was counted manually under the 10x objective using a hand tally counter. The average of

the 4 readings was then taken and multiplied by 10^4 to get the total number of cells (viable and non-viable) per ml of the sample applied to the haemocytometer. The resulting number was then multiplied by 2 to consider the 1:1 dilution of the sample in trypan blue. This determines the number of cells per ml of the original cell suspension. Cellular viability was then determined as the percentage of viable (unstained) cells to the total number of cells (stained and unstained).

8.2.3 Organoid culture

8.2.3.1 Preparation of reagents and solutions

Before starting, sufficient aliquots of the growth factor reduced basement membrane matrix (Matrigel; Corning, catalogue number 356231) were thawed on ice overnight at 4°C in a refrigerator. Additionally, P200 tips were pre-cooled in a refrigerator at 4°C to avoid clotting of the Matrigel whilst pipetting. Finally, a 24 well plate (Corning Costar) labelled with patient study number and date was placed in a humidified incubator at 37°C for at least 2 hours. The fallopian tube organoid medium previously described was used as our starting point for ovarian cancer medium optimization (216). The fallopian tube medium was then supplemented with factors used to support the growth of ovarian cancer and other tumour type organoids (205, 208, 213, 215). We experimented with various combinations of niche factors including growing organoids with and without ROCK inhibitor, with and without human Gastrin and with and without Wnt-3A conditioned medium before settling on the optimal conditions described below. As such, final organoid base and complete culture medium were prepared at room temperature according to Tables 8.2 and 8.3.

Table 8. 2: Organoid base medium.

Reagent	Supplier (catalogue number)	Stock concentration	Final concentration	Amount	Long term storage
Advanced DMEM/F12	Thermo Fisher Scientific (12634010)	x1	x1	48.4 ml	4 °C
HEPES	Thermo Fisher Scientific (15630080)	1 M	10 mM	500 µl	4 °C
GlutaMAX	Thermo Fisher Scientific (35050-061)	x100	x1	500 µl	4 °C
N-2MAX	R&D (AR009)	x100	x1	500 µl	-20 °C
Primocin	InvivoGen (ant-pm-1)	50 mg/ml	100 µg/ml	100 µl	-20 °C
Total	**-**	**-**	**-**	**50 ml**	**-**

Table 8. 3: Organoid complete growth medium.

Reagent	Supplier (catalogue number)	Stock concentration*	Final concentration	Amount
Organoid base medium	Refer to Table 8.3	-	35.75% (v/v)	7.15 ml
R-spondin 1 conditioned medium	Prepared in house from HA-R-Spondin1-Fc 293T Cells (Cultrex)	-	10% (v/v)	2 ml
Wnt-3A conditioned medium	Prepared in house using L Wnt-3A cell line from ATCC (CRL-2647)	-	50% (v/v)	10 ml
Human Noggin	PeproTech (120-10C-20μg)	20 μg/ml[a]	100 ng/ml	100 μl
B27-supplement	Gibco (17504-044)	X50	1x	400 μl
N-Acetyl-L-Cysteine	Sigma (A9165-5g)	625mM[b]	1.25 mM	40 μl
Nicotinamide	Sigma (N0636-100g)	1M[c]	10 mM	200 μl
A83-01	Sigma (SML0788-5mg)	10 mM[d]	500 nM	1 μl
Recombinant human FGF-10	PeproTech (100-26-25μg)	25 μg/ml[e]	100 ng/ml	80 μl
Recombinant human EGF	PeproTech (AF-100-15-100μg)	50 μg/ml[f]	50 ng/ml	20 μl
Total	-	-	-	**20 ml**

FGF-10: Fibroblast growth factor-10, **EGF**: Epidermal growth factor. *Aliquots of reconstituted stocks of reagents were kept at -20°C for long term storage.

a: Human Noggin stock was reconstituted as 20 μg powder in 200 μl of water to yield a 0.1 mg/ml solution. This was then diluted with 800 μl of 0.1% (w/v) Bovine serum albumin (BSA; Sigma) in Phosphate buffered saline (PBS; Gibco).

b: N-Acetyl-L-Cysteine stock was reconstituted as 1g powder in 10 ml of ultra-pure water.

c: Nicotinamide stock was reconstituted as 1.2 g powder in 10 ml of PBS (Gibco).

d: A83-01 stock was reconstituted as 5 mg powder in 1.18 ml of DMSO (Sigma).

e: FGF-10 stock was reconstituted as 25 μg powder in 250 μl of 5mM Sodium Phosphate pH 7.4 to yield a 0.1 mg/ml solution. This was then diluted with 750 μl of 0.1% (w/v) BSA in PBS.

f: EGF stock was reconstituted as 100 μg powder in 100 μl of water to yield a 1mg/ml solution. This was then diluted with 1900μl of 0.1% (w/v) BSA in PBS

8.2.3.2 R-spondin-1 conditioned medium

To prepare R-spondin-1 conditioned medium, HA-R-Spondin1-Fc 293T Cells from Cultrex (Catalogue number 3710-001-01) were used. The basal growth medium for this cell line is Dulbecco's Modified Eagle Medium (DMEM; Sigma-Aldrich). The base medium was supplemented with 10% (v/v) foetal-bovine serum (FBS; Sigma-Aldrich), 1% (v/v) penicillin/streptomycin (Thermo Fisher Scientific) and 1% GlutaMax (Thermo Fisher Scientific). The cells were seeded in a T25 tissue culture flask and grown in a humidified incubator at 37 ºC with 5% (v/v) CO2. The following day the cells were supplemented with fresh selection growth medium in a T75 flask. The selection growth medium consisted of basal growth medium supplemented with 100mg/ml Zeocin (Thermo Fisher Scientific) at a final concentration of 300 μg/ml. The selection growth medium was changed every 2 to 3 days and the cells were passaged when 80-90% confluent at a density of 1:4 to 1:6 for one week. For passaging, the culture medium was aspirated, and the cells washed in D-PBS (Gibco) twice. To facilitate detachment, cells were then incubated in Trypsin (TrypLE express, Gibco) for 5 minutes at 37 ºC. To inactivate the trypsin, the detached cells were resuspended in basal growth medium and then centrifuged at 1000 rpm for 3 minutes. The cells were then resuspended in selection growth medium and plated out at the appropriate passage density.

On the second week and after the cells were passaged 1:4 from a culture flask, they were grown in basal growth medium without Zeocin for 7-10 days without passaging. After this time medium would have turned yellow, and the cells detached from the culture flask and grown in suspension indicating production of R-spondin. The medium was then collected and centrifuged at 2000 rpm for 15 min at 4°C. The supernatant was then filtered through a 0.22 μm filter at 4 °C to remove cells and debris. R-spondin-

1 presence in the medium was verified by Western blot analysis with a validated antibody (R&D, Catalogue number MAB4658) that recognise the protein at 70-75 kDa. Aliquots of R-spondin-1 conditioned medium were stored at -20°C.

8.2.3.3 Wnt-3A conditioned medium

To prepare Wnt-3A conditioned medium, L Wnt-3A cell line from ATCC (CRL-2647) was used. The base medium for this cell line is ATCC Dulbecco's Modified Eagle Medium (DMEM; Sigma-Aldrich). The base medium was supplemented with 10% (v/v) foetal-bovine serum (FBS; Sigma-Aldrich), 1% (v/v) penicillin/streptomycin (Thermo Fisher Scientific) and G-418 (Thermo Fisher Scientific, Catalogue number 10131035) at a final concentration of 0.4 mg/ml. The cells were grown in a 75 cm^2 flask (Falcon) in a humidified incubator at 37 ºC with 5% (v/v) CO2. At 80-90% confluence the cells were passaged twice a week at a 1:8-1:10 ratio for two weeks. For passaging, the culture medium was aspirated, and the cells washed in D-PBS (Gibco) twice. To facilitate detachment, cells were then incubated in Trypsin (TrypLE express, Gibco) for 5 minutes at 37 ºC. To inactivate the trypsin, the detached cells were resuspended in complete growth medium and then centrifuged at 1600 rpm for 3 minutes. The cells were then resuspended in complete growth medium and plated out at the appropriate passage density.

On the third week and after splitting the cells 1:10 from a confluent flask, 18 ml of complete medium was added (without G-418) to the cells in a 75 cm^2 flask and the cells were grown for 4 days. The medium was then collected and centrifuged at 2000 rpm for 3 minutes to remove the cellular debris. The medium was then filtered with a 0.22μm filter to yield the first batch of medium. Another 18 ml of fresh culture medium (without G-418) was then added to the cells and grown for another 3 days. The medium

was then aspirated, spun, and filtered to yield the second batch of medium. The overgrown cells were discarded, and the two batches of media were mixed 1:1 to yield Wnt-3A conditioned medium. Aliquots of Wnt-3A conditioned medium were stored at -20°C.

8.2.3.4 Organoid growth

Organoids were normalised to 25,000 cells/50 μl droplet of Matrigel. Two organoids were grown from each patient i.e. 50,000 cells were required from the prepared cellular suspension. The following method was used to normalise and culture the organoids.

Using the method described in section 8.2.2, the number of tumour cells per 1ml of the previously prepared cellular suspension was determined (y). The volume (x in μl) of the cellular suspension required to collect 50,000 cells was then worked out using the following formula: X=50,000x1000/y. The 50,000 cells were collected and centrifuged at 1000 rpm for 5 min in a 1.5 ml microcentrifuge tube at 4°C and the supernatant was discarded. The cell pellet was then resuspended in 30μl of cold advanced DMEM/F12 to counteract the viscosity of the Matrigel. Using the pre-cooled and pre-wetted P200 tips, 100 μl of Matrigel was then added to the cell suspension. The cell suspension was then mixed gently and slowly with the Matrigel on ice and care was taken not to introduce air bubbles. Subsequently, the Matrigel/tumour cell suspension was dispensed as two 50 μl droplets inside two separate wells in the pre-warmed 24 well plate and left in a humidified incubator at 37°C for 30 min to allow Matrigel polymerisation. After solidification of the Matrigel, 500μl of complete organoid medium (Table 8.3) at room temperature was added gently on the side of each well to cover the organoid droplet totally. The surrounding empty wells were filled with D-PBS to ensure

organoid humidification. The lid was then placed on the culture plate and organoids were incubated at 37°C and 5% (v/v) CO2. The organoid medium was supplemented with 10 μM ROCK inhibitor (1μl of ROCK inhibitor for 1 ml of media) in the first 3 days to prevent dissociation-induced apoptosis. The culture medium was changed three times per week and the organoids were passaged at the appropriate density at 1:2 - 1:4 every 2-5 weeks. Phase contrast microscope images were taken every 3 days to monitor organoid growth and development. Organoid base and complete media were stored at 4°C and ideally, used-up within a month.

8.2.4 Organoid passaging

When organoids reached an appropriate size, density, and confluence, they were passaged. Before passaging, D-PBS was kept on ice, sufficient aliquots of Matrigel were thawed on ice and a 24 well plate was kept overnight in an incubator at 37 °C. In addition, organoid complete medium was left to warm at room temperature (15-25°C) and ROCK inhibitor was thawed from -20°C to room temperature.

The culture medium was aspirated from the organoid wells and 500 μl of ice-cold D-PBS was added to each well to liquify the Matrigel. Using a plastic pipette (Sigma Aldrich) the organoids along with the Matrigel and D-PBS were collected and transferred to a 15 ml tube (Falcon). The plastic pipette was then used to vigorously pipette the organoid/Matrigel mixture up and down several times to break down the Matrigel. The 15 ml tube with the organoids was then centrifuged at 1600 rpm for 4 min at 4°C and the supernatant was discarded. The cell pellet was then resuspended in 1 ml of Trypsin (TrypLE express, Gibco) to digest the Matrigel and was supplemented with 1 μl of ROCK inhibitor at a final concentration of 10 μM to prevent

dissociation-induced apoptosis. A P1000 pipette-tip was then used to pipette the organoids up and down 10 times to dissociate them into single cells. The 15 ml tube with the cell suspension was then incubated at 37°C in a water bath for between 5 and 30 minutes. Every 5-8 minutes, a 4μl drop of the cellular suspension was checked under the microscope until 90% of the cells were seen dispersed singly with no clumps. To inactivate the Trypsin, the cells were resuspended in 9 ml of ice-cold D-PBS for every 1 ml of Trypsin and centrifuged at 1600 rpm for 4 min at 4°C. The supernatant was discarded, and the cell pellet was resuspended in 1 ml of ice-cold D-PBS and a cell count was performed according to section 8.2.2. The cell suspension was centrifuged again at 1600 rpm for 4 min at 4°C and the supernatant was discarded. The organoids were passaged at 1:2 -1:4 according to the cell count. Using pre-cooled and pre-wetted tips, the cell pellet was resuspended gently and slowly in the appropriate amount of Matrigel. Subsequently, the Matrigel/tumour cell suspension was dispensed as 50 μl droplets inside separate wells in the pre-warmed 24 well plate and left in a humidified incubator at 37°C for 30 min to allow Matrigel polymerisation. After solidification of the Matrigel, 500μl of complete organoid medium (Table 8.3) at room temperature was added gently on the side of each well to cover the organoid droplets. The lid was then placed on the culture plate and organoids were incubated at 37°C and 5% (v/v) CO2. The organoid medium was supplemented with 10 μM ROCK inhibitor (1μl of ROCK inhibitor for 1 ml of media) in the first 3 days to prevent dissociation-induced apoptosis. Organoid growth was monitored as previously discussed in section 8.2.3.3.

8.2.5 Organoid cryopreservation

To freeze down organoids for long term storage, the media was aspirated from the wells and 500 μl of ice-cold D-PBS was added to each well containing a growing organoid. The Matrigel droplet containing the organoid along with the D-PBS was then collected with a plastic pipette and transferred to a 15 ml Falcon tube. The tube was then centrifuged at 1600 rpm for 4 min at 4 °C after which the supernatant was discarded. The organoid was then added to a labelled cryovial containing 2 ml of Recovery cell culture freezing medium (Gibco, Catalogue number 12648010) using a P1000 pipette-tip. The cryovial was placed inside a Freezing container (Nalgene, Mr Frosty) in a -80 °C freezer before they were transferred to liquid nitrogen after 24 hours.

8.2.6 Organoid retrieval from liquid nitrogen

To thaw organoids from frozen, 10 ml of advanced DMEM/F12 medium was pre-warmed to 37°C for each organoid model. A cryovial containing the selected organoid model was taken out of the liquid nitrogen tank and transferred to a polystyrene box with dry ice. The cryovial was then thawed in a water bath at 37 °C until only small flecks of frozen material remained. The cryovial was then removed from the water bath and wiped down with 70% (v/v) ethanol and transferred to a biosafety cabinet. Using a plastic Pasteur pipette, 500 μl of warm advanced DMEM/F12 was added dropwise to the vial before transferring the contents of the vial dropwise to the 15 ml Falcon tube containing 10 ml of warm media. The organoid/medium suspension was then centrifuged at 1600 rpm for 4 min at room temperature. The supernatant was discarded, and the organoid pellet was resuspended in the appropriate amount of Matrigel (50μl per well for a 24 well plate). Using a P200 pipette tip, the

organoid/Matrigel suspension was dispensed into a labelled 24 well plate as 50μl droplets. The plate containing the organoids was then placed in an incubator for 30 min at 37°C to allow Matrigel polymerisation. After Matrigel polymerisation, 500 μl of complete organoid media (Table 8.3) was added to each well and the organoids were transferred back to the incubator. The organoid medium was supplemented with ROCK inhibitor at a final concentration of 10 μM for the first 10 days to aid organoid growth.

8.2.7 Organoid fixation

When organoids reached maximum size, density, and confluence, they were fixed to facilitate subsequent staining.

To prepare organoids for fixation, the medium was aspirated from the wells containing the organoid droplets and then they were washed with 500 μl of ice-cold D-PBS for 1 min before discarding the D-PBS. Subsequently, 500 μl of organoid recovery solution (Corning, catalogue number 354253) was added. The organoid containing Matrigel droplet was then gently collected using a P1000 pipette tip and transferred to a sterile 15 ml Falcon tube. The tube containing the organoid was then placed on ice in a polystyrene box that was put on a shaker for 30-40 min to dissociate the Matrigel. Subsequently, 5 ml of cold advanced DMEM/F12 was added to the organoids and centrifuged at 1000 rpm for 5 min at 4 °C. The supernatant was discarded and then the organoids were resuspended gently in 1 ml of 10% (v/v) neutral-buffered Formalin solution for 30 min at room temperature. Care was taken with pipetting to avoid breaking down of the organoids. Around 10 ml of D-PBS was then added to the organoids and the tube was centrifuged at 1000 rpm for 5 min at 4 °C. The supernatant was discarded and only 50 μl of D-PBS was left to counteract the viscosity of the

subsequently added agar. Then, 1ml of 3% (w/v) agar solution was added dropwise to the fixed organoid pellet at 37 ºC and left to set at 4 ºC for 30 min. The agar solution was used to prevent the fragmentation of the fixed organoid pellet during subsequent processing. The agar-embedded organoid pellet was then placed in tissue cassettes and processed for paraffin embedding using the automated tissue processor at the Birmingham Women's hospital (Thermo Scientific Shandon Pathcentre). The FFPE tissue blocks containing the organoid pellet were then sectioned into 3µm sections using a microtome onto coated slides (Colorfrost plus, Thermo Scientific).

8.2.8 Organoid H&E and immunohistochemical staining

To visualize organoids under Bright field microscopy (Leica Bright field microscope Dm500) using standard H&E staining, organoid sections were deparaffinised, rehydrated, followed by Haematoxylin and Eosin staining, dehydration and finally clearing. These steps were performed inside a Leica ST5010 Auto stainer at the Birmingham Women's hospital.

All organoids generated during this study were stained for both UbcH10 and p53 to compare with the parent tumour. Immunohistochemical staining for organoids followed the automated protocol previously outlined in section 2.2.1.2 but with some modifications to suit the delicate nature of the organoids. The BOND Polymer Refine detection kit was used. UbcH10 was diluted to 1:300 instead of 1:200 and HIER was performed at pH 6.0 for 10 min instead of the 20 min used on tissue sections. Similarly, p53 was diluted to 1:5 instead of 1:2.5 and HIER was performed at pH 6.0 for 10 min instead of 30 min.

8.3 Results

8.3.1 Establishment of primary ovarian cancer organoids and Patient Characteristics

Using the methodology described, we successfully established a protocol to derive organoids from primary ovarian tumours. In the first instance, we established a protocol to extract single tumour cells from fresh ovarian tumours of various histological subtypes, stages, and chemotherapy status (Table 8.4). We then used a combination of basement membrane material (Matrigel) and a cocktail of niche factors to derive the organoid models within 2-4 weeks. Experimentation with various cellular concentrations and volumes of Matrigel were performed before settling on the optimal conditions used (25,000 cells/50 μl of Matrigel). Guidance was taken from work done by previous colleagues who had grown spheroids from MG75, A2780 and SKOV-3 ovarian cancer cell lines (Danielle O'Neille and Jason Yap unpublished observation). We monitored the growth of the organoids for 2 to 3 passages using different combinations of niche factor cocktails (with and without human Gastrin, with and without ROCK inhibitor, with and without Wnt-3A conditioned medium). The growth factors shown in Table 8.3 were decided to be the ones most optimal for long term maintenance and expansion of ovarian cancer organoid models. Finally, various fixation protocols were experimented with to establish optimal conditions for organoid visualisation and staining. These included various fixation times, temperatures and with and without Triton X-100 (Sigma-Aldrich) as a permeabilization buffer.

Out of 19 patients recruited, successful organoid models were established from 8 patients with an overall success rate of 42%. All 8 successfully established organoid

models were cryopreserved for stocking and successfully retrieved from liquid Nitrogen. The clinicopathological characteristics of the 8 patients are shown in Table 8.4.

Table 8. 4: The clinicopathological features of the 8 ovarian cancer patients with successfully generated organoid models.

Patient Study number	Histopathological diagnosis	Sample for organoid	Age at diagnosis	Type of surgery	FIGO stage
SWBH250	Serous borderline tumour	Left ovarian tumour	54	Staging laparotomy	IC2
SWBH270	Low-grade serous carcinoma	Right ovarian tumour	68	Staging laparotomy	IIA
SWBH271	HGSOC	Right groin lymph node	72	PDS	IVB
SWBH286	Endometrioid carcinoma	Right ovarian tumour	65	PDS	IC2
SWBH290	HGSOC	Left ovarian tumour	74	DDS after NACT	IIIC
SWBH291	HGSOC	Omental tumour	64	DDS after NACT	IIIC
SWBH297	HGSOC	Omental tumour	61	DDS after NACT	IIIC
SWBH298	HGSOC	Omental tumour	68	DDS after NACT	IVB

HGSOC: High-grade serous ovarian cancer, **PDS**: Primary debulking surgery, **DDS**: Delayed debulking surgery, **NACT**: Neo-adjuvant chemotherapy.

For the remaining 11 patients, organoid culture failed to show proper vitality and confluence. The clinicopathological features of the 11 failed organoid models are shown in Table 8.5.

It is our experience that two important factors impacted organoid growth: cell viability and cellular concentration. To this end, cellular viability by Trypan blue assay after tissue processing from patients SWBH266, SWBH284, SWBH285 and SWBH296 was below 50%. Tumour cells from all 4 patients failed to grow into organoid models after 4 weeks of culture. Hence, it was determined that a cellular viability of >50% was an important factor in establishing successful organoid models. In patients SWBH282 and SWBH294 although cellular viability was more than 50% after tissue processing, tumour cells failed to form organoid models and the cells disintegrated in the first two weeks after culture because ROCK inhibitor was not used in these models.

Additionally, cellular concentrations of less than 5000 cells/50 μl droplet of Matrigel either died in the early days after culture or remained as a singe cell suspension. This was particularly evident in patient SWBH272 with benign serous cystadenoma and patients SWBH280 and SWBH287 with borderline tumours. This was also apparent with patient SWBH277 with clear cell carcinoma where the cellular yield was also very low. Similarly, cellular concentrations of more than 40,000 cells/50μl droplet of Matrigel (patient SWBH268) did not have enough room to grow in the basement membrane matrix and the cells mostly remained as a single cell suspension.

Table 8. 5: The clinicopathological features of the patients with failed organoid models.

Patient Study number	Histopathological diagnosis	Sample for organoid	Age at diagnosis	Type of surgery	FIGO stage
SWBH266	HGSOC	Omentum tumour	65	DDS after NACT	IIIC
SWBH268	HGSOC	Rt ovarian tumour	82	PDS	IIIC
SWBH272	Serous cystadenoma	Lt ovarian tumour	67	Staging laparotomy	-
SWBH277	CCC	Lt ovarian tumour	63	Staging laparotomy	IC2
SWBH280	Serous borderline tumour	Rt ovarian tumour	66	Staging laparotomy	IC2
SWBH282	HGSOC	Lt ovarian tumour	64	PDS	IIIC
SWBH284	HGSOC	Omental tumour	63	DDS after NACT	IVB
SWBH285	HGSOC	Omental tumour	66	DDS after NACT	IIIC
SWBH287	Mucinous borderline tumour	Rt ovarian tumour	73	Staging laparotomy	IA
SWBH294	LGSOC	Rt ovarian tumour	48	Staging laparotomy	IIIB
SWBH296	HGSOC	Lt ovarian tumour	66	DDS after NACT	IIIB

HGSOC: High-grade serous ovarian cancer, **PDS**: Primary debulking surgery, **DDS**: Delayed debulking surgery, **NACT**: Neo-adjuvant chemotherapy, **CCC:** Clear cell carcinoma, **LGSOC**: low-grade serous ovarian cancer.

8.3.2 Organoid growth varies between different ovarian tumours

The rate of organoid growth showed significant variability between different patients. Tumour cells would usually aggregate into small multicellular unit clusters by days 3-7. The clusters then became larger and more multicellular by days 10-13. Organoid rings usually started to form after 2-3 weeks, and the organoid rings reached maximum size, density, and confluence at 4-5 weeks. Figure 8.1 demonstrates the stages of growth of organoids derived from a patient with HGSOC and is representative of most of the HGSOC derived organoid models. The serous borderline tumour showed the slowest growth rate with organoid rings forming after 3 weeks, whilst HGSOC showed the fastest growth rate with organoid rings forming after 2 weeks. In patients SWBH271 and SWBH286 where organoids were derived from chemonaïve cells, it was noted that ring formation was achieved as early as Day 10 compared to organoids from chemotherapy treated patients. Passaging intervals ranged from 2-5 weeks and the split ratios ranged from 1:2 to 1:4. Figure 8.2 demonstrates organoids ready for passaging.

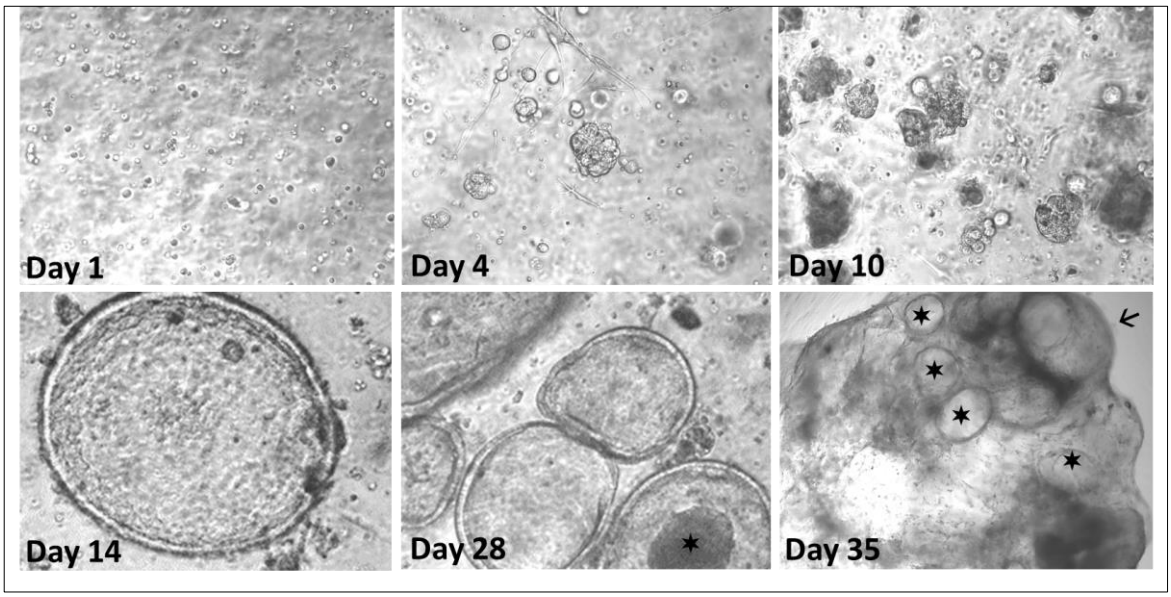

Figure 8. 1: Phase contrast imaging demonstrating the growth of organoids derived from a HGSOC patient (SWBH290). Tumour cells started from a single cell solution on Day 1, subsequently, they formed small cellular aggregates and clusters on Day 4. Cell aggregates started to become larger and more complex and cellular by Day 10. Rings form at the edge of the cellular clusters by Day 14 which highlights organoid formation. By Day 28, organoids become larger, more confluent and cells become denser at their centre (star). By Day 35, organoids become very confluent (stars) that they fill up and outgrow the edge of the supporting basement membrane matrix (arrow) and become darker. This signals that the organoids are ready for either passaging or fixation. All images taken at x20 magnification except for images at Day14 and Day 28 taken at x40 magnification.

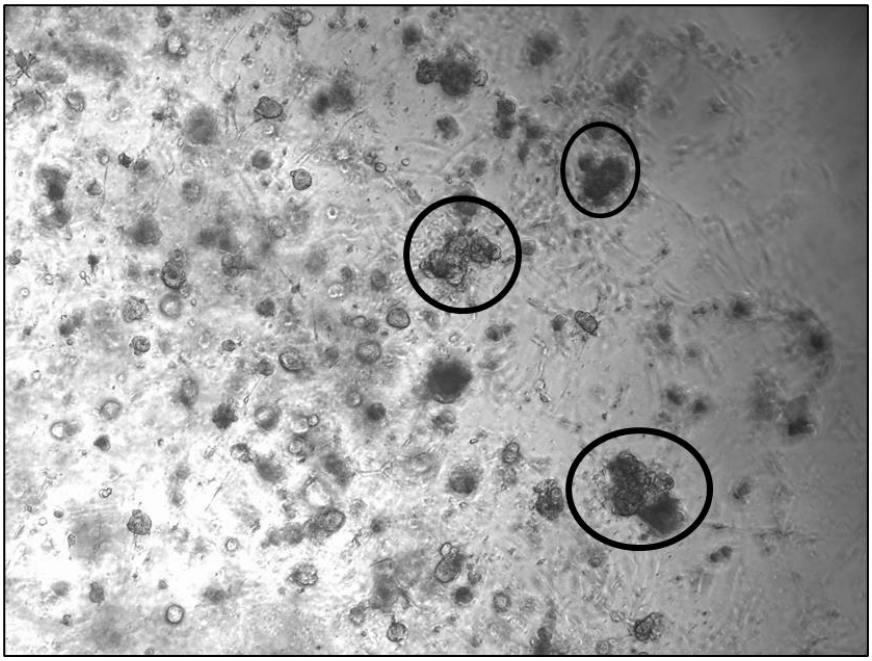

Figure 8. 2: Phase contrast image of organoids derived from a HGSOC patient (SWBH298) ready for passaging on Day 32. Multiple organoids/spheroids are dispersed in basement membrane matrix. Some organoids have become very large, confluent, and cellularly dense (circles) resembling morules or grape-like clusters indicating a need for passaging (x4 magnification).

8.3.3 Organoids faithfully recapitulate their parent tumours both morphologically and immunohistochemically

8.3.3.1 Morphological characterization of ovarian cancer organoids

After establishing protocols for fixation and staining, organoids were visualized under Bright field microscopy. Organoids were compared to their parent tumours where they consistently recapitulated both at the cellular and architectural levels. Mostly, organoids consisted of the transformed epithelial component of the parent tumour. However, in some instances a fibroblastic stroma was noted supporting the epithelial component similar to the parent tumour (Figure 8.3). Organoids derived from serous borderline tumour displayed a cystic morphology with simple non atypical epithelial lining (Figure 8.4). On the contrary, organoids derived from low and high-grade serous

carcinoma as well as endometrioid carcinoma showed more complexity at the architectural level and more atypia at the cellular level. Figure 8.5 demonstrates comparative histological features of two different organoid models derived from HGSOC and LGSOC patients.

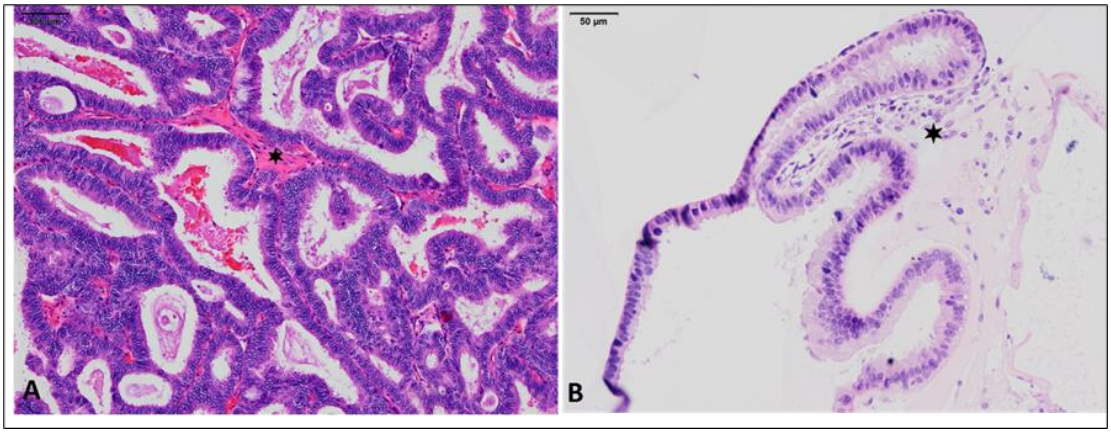

Figure 8. 3: Organoid model derived from a patient with endometrioid carcinoma (SWBH286). A) An endometrioid carcinoma with a complex and confluent glandular architecture lined by atypical endometrioid type epithelial lining with a wisp of supporting fibroblastic stroma in between (star; H&E, x10 magnification). B) The organoid model derived from the tumour consists of epithelial lining that assumes a similar glandular architecture with some stratification and atypia. The epithelium in this case is supported by a fibroblastic stroma (star; H&E, x20 magnification).

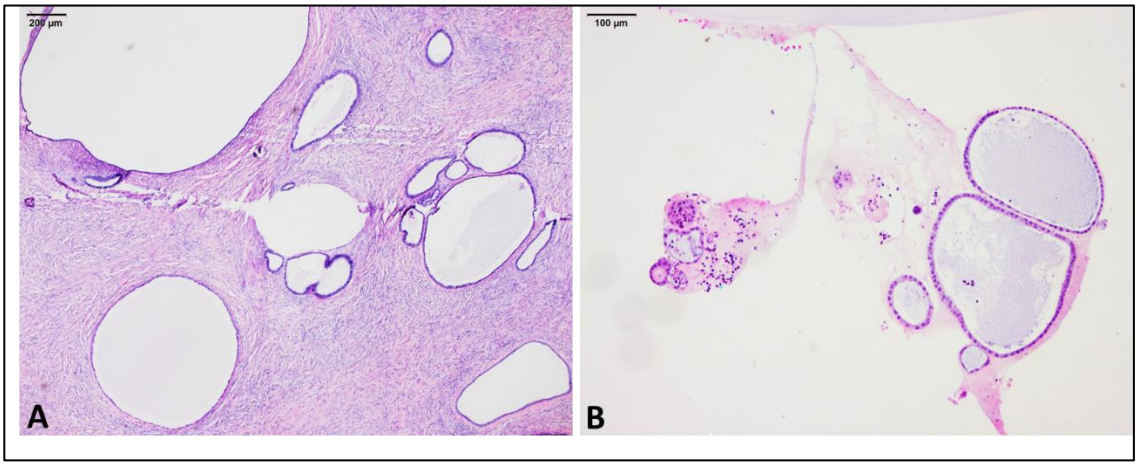

Figure 8. 4: Organoid model developed from a patient with serous borderline tumour (SWBH250). A) Ovarian tumour showing cystic spaces lined by benign serous type epithelium. (H&E, x4 magnification). B) An organoid model derived from the tumour showing similar growth pattern and benign simple non-atypical serous type epithelial lining. (H&E, x10 magnification).

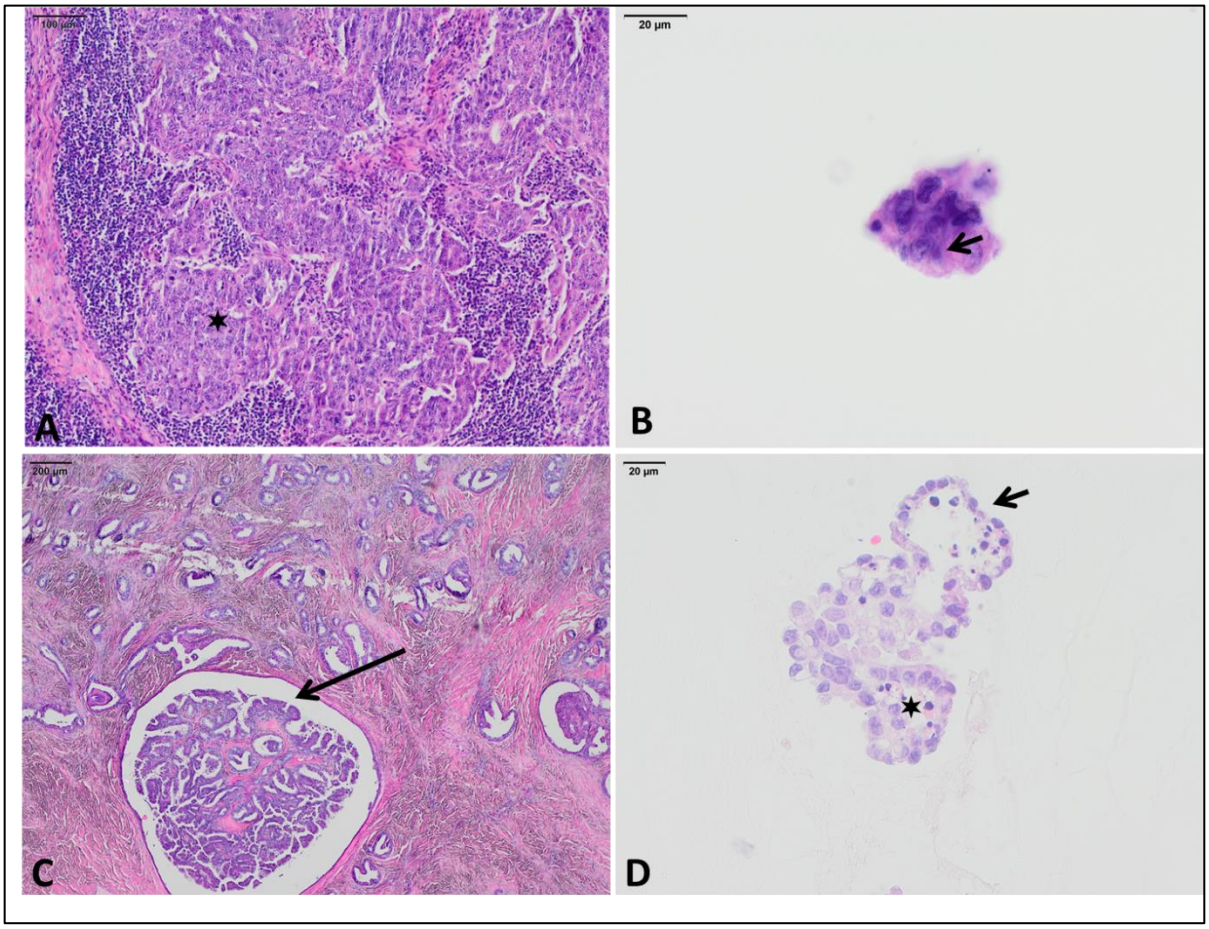

Figure 8. 5: Organoid models morphologically recapitulate the tumours from which they are derived. A) Infiltrative nests of HGSOC (star) in a lymph node from patient SWBH271 (H&E, x10 magnification). B) An organoid model derived from the HGSOC tumour in Figure A showing high-grade nuclear atypia and prominent nucleoli (arrow; H&E, x40 magnification). C) Ovarian stroma infiltrated by glandular structures and macro-papillae surrounded by a cleft like space (arrow) with low-grade nuclear atypia characteristic of low-grade serous carcinoma from patient SWBH270 (H&E, x4 magnification). D) An organoid model derived from the LGSOC in Figure C showing a similar glandular (star) and papillary (arrow) architectural growth pattern and low-grade nuclear atypia (H&E, x40 magnification).

8.3.3.2 Immunohistochemical characterization of ovarian cancer organoids

After confirming morphological similarity between the organoids and their parent tumours we wanted to establish whether these similarities were also evident at the molecular level. Accordingly, we investigated the expression of UbcH10 and p53 by IHC in both the organoids and their parent tumours.

Organoids showed comparable protein expression levels for both UbcH10 and p53 relative to their parent tumours. Serous borderline tumour and its corresponding organoid model displayed low UbcH10 expression levels (IRS 2, H-score 6) and wild-type p53 staining. Similarly, the Low-grade serous carcinoma and its derived organoid model showed low levels of UbcH10 expression and wild-type p53 staining (Figure 8.6). The endometroid carcinoma and its organoid displayed moderate levels of UbcH10 expression (IRS 6, H-score 102) and wild-type p53 expression. Two of the HGSOC cases displayed null p53 expression and moderate UbcH10 expression (Figure 8.7), whilst the three remaining cases displayed p53 overexpression and high UbcH10 expression (Figure 8.8).

With respect to subcellular localization, UbcH10 was mostly cytoplasmic in the organoid models as opposed to both nuclear and cytoplasmic in the parent tumours (Figure 8.7). In 5 out of the 8 organoid models, nuclear staining was also noted albeit with a more focal distribution (Figure 8.8). P53 on the other hand was nuclear in both the organoids and the tumours (Figure 8.8).

We can therefore conclude that organoids capture the molecular characteristics of the tumours from which they are derived.

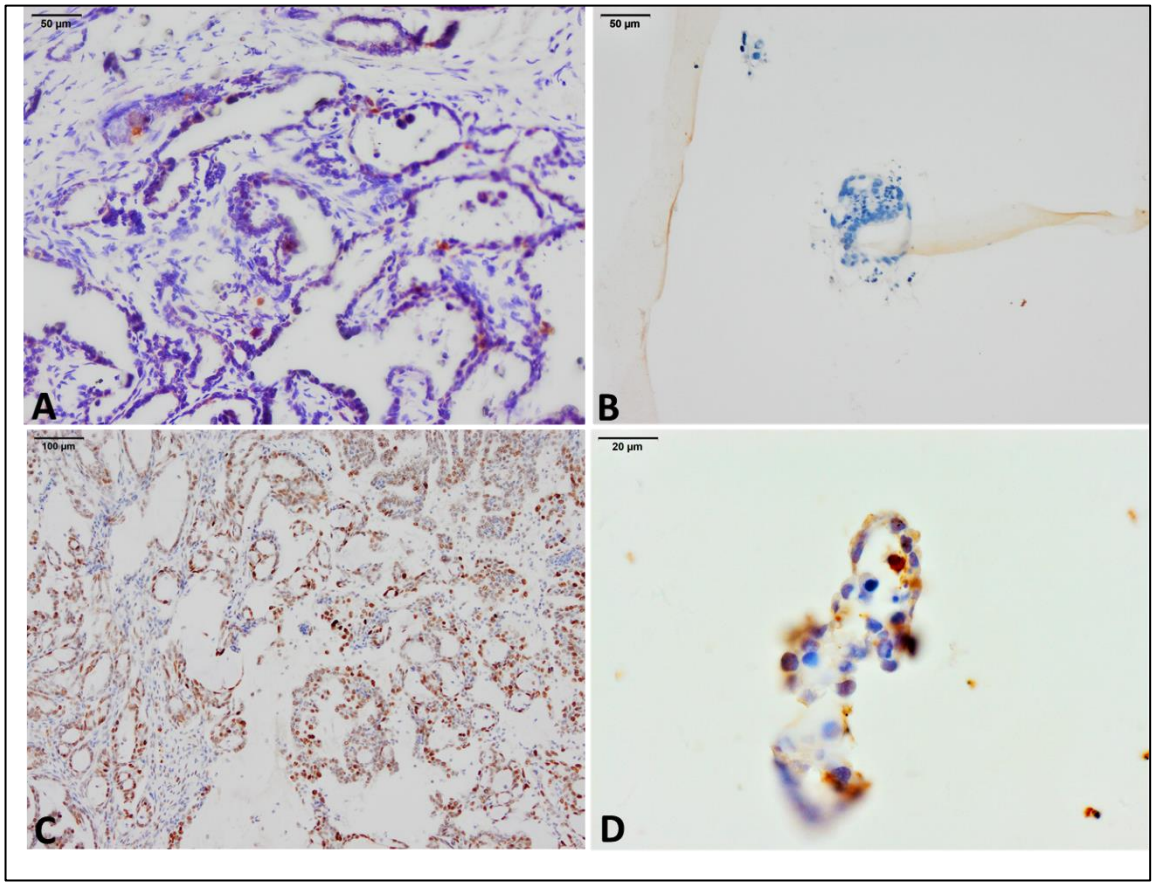

Figure 8. 6: An organoid model that recapitulates the parent tumour immunohistochemically in a case of low-grade serous carcinoma (SWBH270). A) Low grade serous carcinoma showing focal weak staining for UbcH10 (IRS 1, H-score 2) (anti-UbcH10, x20 magnification). B) A small organoid derived from the tumour in A showing no staining for UbcH10 (anti-UbcH10, x20 magnification). C) Wild type p53 expression in the low-grade serous carcinoma (same tumour in panel A) with nuclei showing variably intense nuclear staining for p53 (anti-p53, x10 magnification). D) The organoid derived from the same tumour with similar p53 wild type staining (anti-p53, x40 magnification).

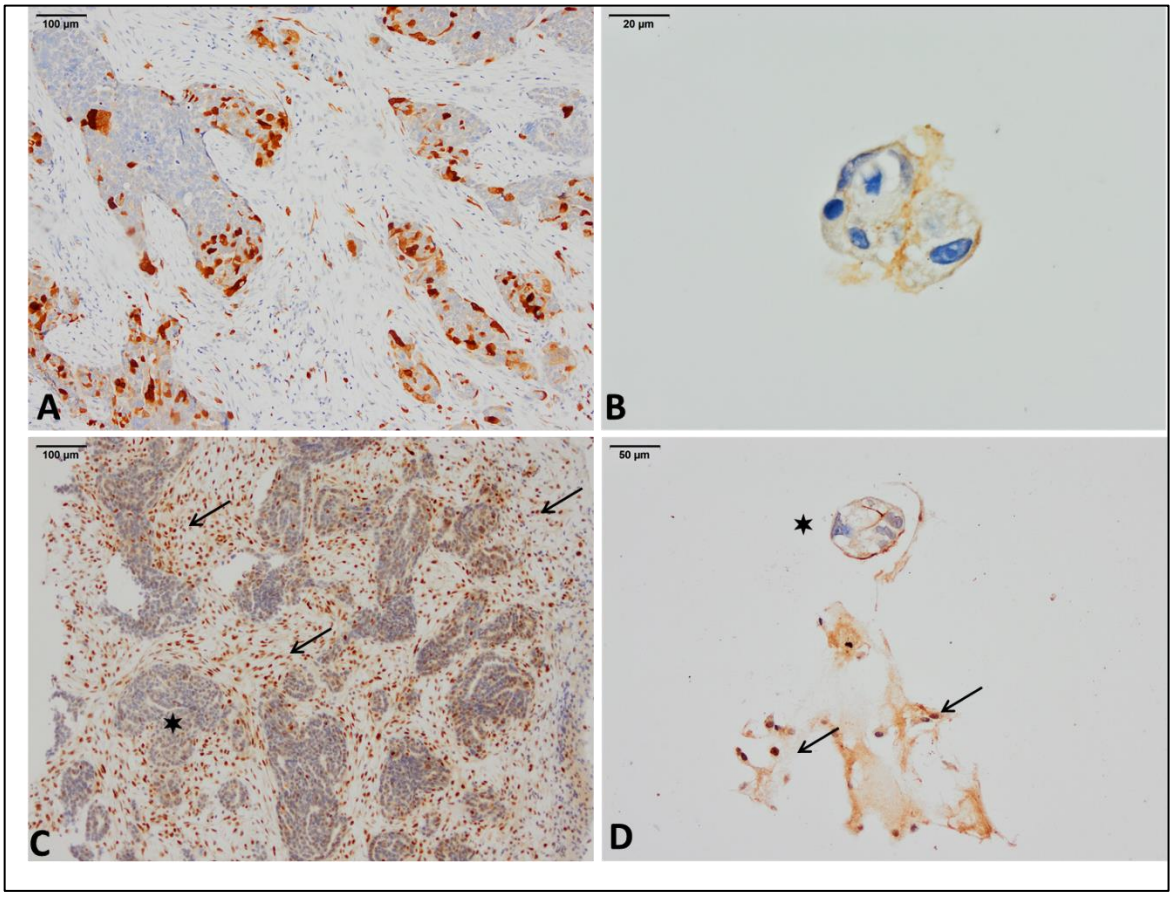

Figure 8. 7: An organoid model that recapitulates the parent tumour immunohistochemically in a case of high-grade serous carcinoma (SWBH298) with moderate UbcH10 expression and p53 null phenotype. A) High grade serous carcinoma showing moderately intense cytoplasmic and nuclear staining for UbcH10 (IRS 7, H-score 119) (anti-UbcH10, x10 magnification). B) An organoid/spheroid derived from the tumour in A showing similar intensity cytoplasmic staining for UbcH10 (anti-UbcH10, x40 magnification). C) P53 null pattern in the tumour shown in panel A (star) as opposed to wild type staining in the background stroma (arrows; anti-p53, x10 magnification). D) The derived organoid with null p53 expression (star) and wild staining in the supportive stroma (arrows; anti-p53, x20 magnification).

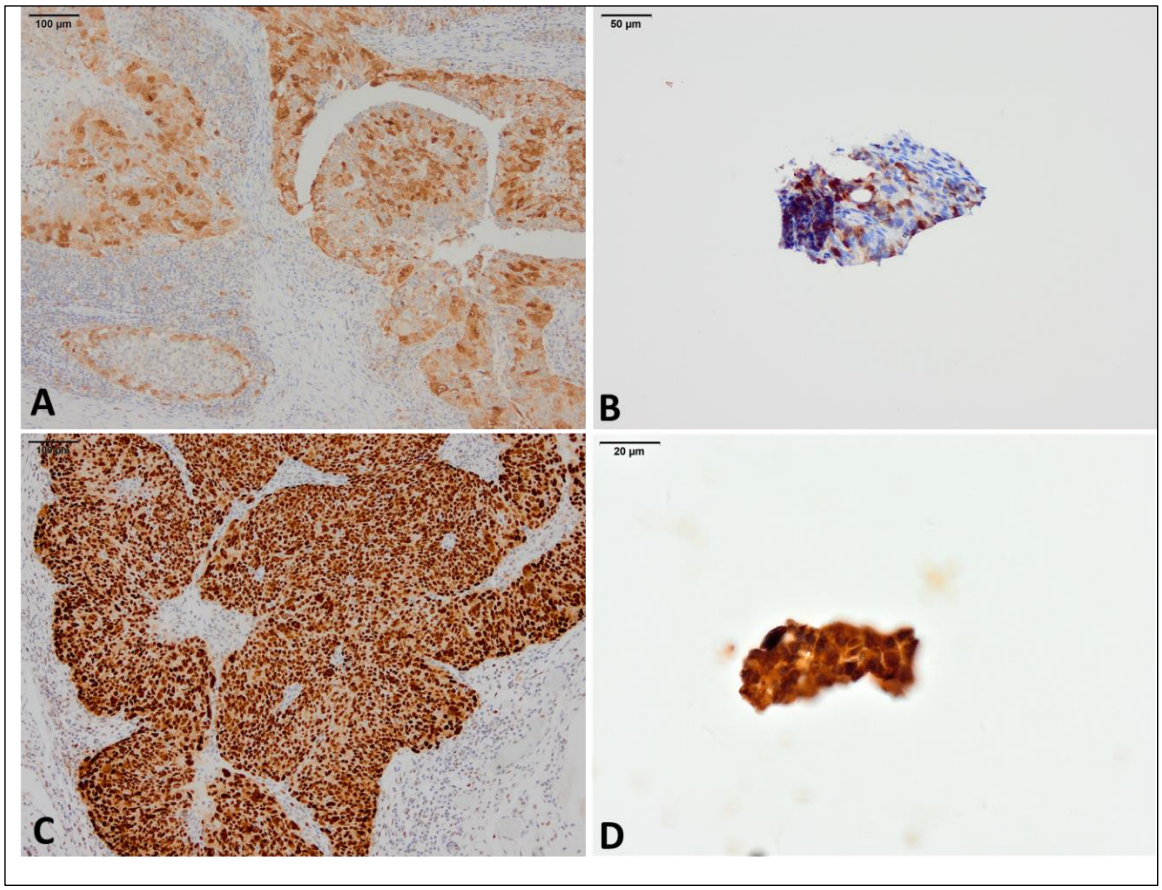

Figure 8. 8: An organoid model that recapitulates the parent tumour immunohistochemically in a case of high-grade serous carcinoma (SWBH271) with high UbcH10 expression and p53 overexpression. A) High grade serous carcinoma showing strong diffuse cytoplasmic and nuclear staining for UbcH10 (IRS 11, H-score 165) (anti-UbcH10, x10 magnification). B) An organoid derived from the tumour in A showing similar intensity cytoplasmic and focal nuclear staining for UbcH10 (anti-UbcH10, x20 magnification). C) Diffuse nuclear p53 overexpression in the high-grade serous carcinoma cells (anti-p53, x10 magnification). D) Nuclear P53 overexpression seen in the derived organoid (anti-p53, x40 magnification).

8.4 Discussion

Ovarian cancer is a complex heterogeneous disease that needs reliable experimental models to address its clinical changes such as acquired chemoresistance and disease recurrence. In addition, new tumour models are required to allow for drug testing and the development of novel therapeutics. To this end, we successfully developed *in vitro* patient-derived ovarian cancer organoid models that capture the *in vivo* characteristics of the parent tumours. In accordance with various studies carried out on various tumours, our ovarian cancer organoid models retained both the histological (Figures 8.3 to 8.5) and immunohistochemical features (Figures 8.6 to 8.8) of the parent tumour (205-208, 213). In addition, we developed culture conditions that allows long-term expansion of organoid models of various epithelial ovarian tumour subtypes (Tables 8.2 and 8.3).

Our success rate in establishing organoid cell lines was 8/19 (42%). This rate was lower than success rates from other studies that derived ovarian cancer organoids (213, 215). Nanki *et al* (215) who used culture conditions similar to ours as well as similar cellular concentrations reported an 80% success rate (28/35). We hypothesize that this is the result of the difference in cellular viability of the tumours used in both studies. Nanki *et al* (215) used mostly chemonaïve cases whilst most of our patients had received pre-operative chemotherapy, which might have lowered cellular viability in our tumours resulting in a lower success rate. Additionally, success rates were lower in some of our patients due to experimentation with culture conditions that directly impacted cellular viability. This included the use of ROCK inhibitor which improved organoid derivation in the early phases of culture due to enhanced cellular viability as opposed to culture conditions without this factor. Kopper *et al* (213) also reported a

success rate of 65% for ovarian cancer derived organoids. In contrast to Nanki et al and similar to our patients, Kopper *et al* (213) derived organoid models from both pre- and post-chemotherapy samples. However, they found that the addition of hydrocortisone, oestradiol, forskolin and heregulinβ-1 improved organoid derivation from ovarian cancer specimens which could account for their higher success rates. On the other hand, Hoffmann *et al* (214) reported success rates as low as 33% for HGSOC-derived organoids. In contrast to the various epithelial ovarian tumours used in our study, Hoffmann *et al* (214) derived organoids only from HGSOC patients. As opposed to our cases, they used only chemonaïve samples, however, similar to our study design, they experimented with various combinations of organoid growth factors which might account for their low success rate.

For successful organoid derivation, we used a basic culture medium that consisted of advanced DMEM/F12 supplemented with the nutrient GlutaMAX, the buffer HEPES and the broad-spectrum antibiotic, Primocin (Table 8.2). The serum-free supplement which contains human transferrin “N2-MAX” was added to aid the appropriate differentiation of pluripotent stem cells (217). Essential for the derivation of ovarian cancer organoids, several factors were added to promote cellular growth. These included a B27 supplement which improves the survival and growth of cancer stem cells without differentiation and nicotinamide which acts as a coenzyme precursor and promotor of cellular survival (218). Wnt-3A conditioned medium was used to activate the Wnt/β-catenin signalling pathway. R-spondin-1 conditioned medium synergistically activates the Wnt/β-catenin pathway resulting in increased activation levels compared to Wnt-3A alone. Finally, FGF-10 and EGF were used as activators of their respective signalling pathways (214, 218).

In addition, the inhibition of detrimental signalling pathways was found as important as promotors of cellular growth. For this, we used A83-01 as an inhibitor of the TGF-β signalling pathway known to be detrimental for organoid growth by inhibition of cellular proliferation and promotion of cellular differentiation (219). Noggin was also used as an antagonist of BMP that acts as a ligand for the TGF-β family. A ROCK inhibitor was found essential to prevent dissociation-induced cellular apoptosis both in the digestion and culture media (218).

Our culture conditions were similar to conditions described in colorectal, pancreatic and lung organoids (208, 220). However, we found human Gastrin mostly used in colorectal and intestinal-derived organoids was not required for ovarian cancer organoid derivation. Additionally, ovarian cancer organoids did not benefit from a MAP kinase inhibitor like lung and colorectal organoids. Importantly, we found R-spondin and Wnt-3A conditioned media essential for the growth of all our ovarian cancer organoid lines. Wnt-3A conditioned medium use particularly improved the viability of the organoid models and lowered apoptosis and necrosis upon fixation. This is based on previous reports which described Wnt signalling to be essential for the regulation of stemness both in the ovary and fallopian tube epithelium (216, 221). Similarly, Nanki and colleagues (215) used R-spondin and Wnt-3A conditioned media with a success rate of 80% for ovarian cancer organoid derivation and expansion. On the other hand, Kopper and colleagues (213) found Wnt-3A conditioned medium to be detrimental for the growth of some of their organoid cell lines. They resorted this to the presence of serum in the conditioned medium and not Wnt-3A. However, Hoffmann *et al* (214) also found Wnt-3A conditioned medium to be detrimental for the maintenance of all their HGSOC-derived organoid models. They showed evidence that Wnt activation while

important for the derivation of healthy organoid models from the fallopian tube, intestine, and liver, it was less important for HGSOC organoids. To explain this difference in methodology, we contend that while Hoffmann *et al* (214) monitored the growth of their organoid models for more than a year, we only monitored organoid growth for 3 months maximum. Therefore, while Wnt-3A might be important for the initial derivation of organoid models, it may not benefit on their long-term growth. This would represent a prospect for future research that would be interesting to explore.

We found that organoids faithfully recapitulate the tumours from which they are derived both morphologically and immunohistochemically. Morphologically, we found that organoids derived from serous borderline tumour (Figure 8.4) were cystic with no nuclear atypia while those derived from LGSOC (Figure 8.5 C and D) are glandular with papillary-like formations and low-grade nuclear atypia. HGSOC-derived organoids were more complex architecturally with high-grade nuclear atypia (Figure 8.5 A and B). These results are in line with Kopper *et al* (213) who also found similar morphology for the organoid models derived from borderline, low-grade and high-grade serous carcinomas. Similarly, Nanki *et al* (215) found similar results for their HGSOC-derived organoids. At the immunohistochemical level we also found comparable UbcH10 and p53 staining between the organoids and their parent tumours (Figures 8.6 and 8.7). Similarly, both Kopper *et al* (213) and Nanki *et al* (215) showed similar p53 immunohistochemical expression in their organoid models and the tumours from which they were derived. Although there are no reports of UbcH10 expression in ovarian cancer models, Kopper *et al* (213) did demonstrate comparable expression of the proliferative marker Ki-67 in the HGSOC cases and their derived organoids. This is consistent with the proliferative property of UbcH10 described in Chapters 6 and 7.

Additionally, both Kopper *et al* (213) and Nanki *et al* (215) validated their results at the genetic level, where they identified in the HGSOC organoid lines identical *TP53* mutations to the parent tumour. Due to the COVID-19 pandemic and the need for mitigation, we could not perform any sequencing or drug testing on the organoid models. However, this would represent an attractive platform for future endeavours.

8.5 Conclusions

We have successfully established protocols for the derivation and maintenance of organoids from various epithelial ovarian tumours. We have also demonstrated that these organoid models recapitulate their parent tumours both morphologically and immunohistochemically. We believe these organoid models hold great potential for personalised future drug sensitivity and resistance testing as well as studying the biological mechanisms that underpin the development and progression of ovarian cancer.

Chapter 9. General discussion and future work

9.1 UbcH10 as a prognostic and predictive marker in HGSOC

Previous studies on ovarian and non-ovarian malignancies identified UbcH10 as a proto-oncogene which promotes aggressive tumour behaviour (96-101), however, its role solely in HGSOC has not been investigated before. Given these earlier findings, UbcH10 represented an attractive cancer biomarker of potential use in the prognostication of HGSOC. In Chapter 3, we set out to study the prognostic and predictive role that UbcH10 plays in HGSOC. We used two well characterized retrospective cohorts of HGSOC patients as training (n=100, full-faced sections) and validation (n=81, tissue microarrays) sets. Patients were mostly advanced FIGO stage and more than 60% had received preoperative chemotherapy (Table 3.1 and 3.12). We used immunohistochemistry as the primary method of investigation and implemented two widely recognised scoring systems for UbcH10 quantification (IRS and H-score). We then used the robust bioinformatics tool *X-tile* to generate biologically significant cut-off points for UbcH10 expression. This allowed us to divide each cohort into high and low expression groups to compare overall survival, progression-free survival and correlate UbcH10 expression in these groups with the well-established prognostic and predictive indicators in ovarian cancer.

In the training set, UbcH10 only correlated weakly with advanced age at diagnosis (Figure 3.6). Otherwise, it did not correlate significantly with any of the other prognostic parameters studied; FIGO stage, lymph node metastasis, volume of residual disease after surgery and *BRCA* mutation status (Tables 3.3 and 3.4, Figures 3.8 and 3.11). Additionally, UbcH10 expression did not correlate significantly with the predictive

parameters including chemotherapy response score and platinum resistance (Figures 3.9 and 3.10). High UbcH10 expression did not significantly influence overall survival in that cohort (Figure 3.19). Finally, although univariate analysis seemed to suggest a *favourable* effect of high Ubch10 expression (Table 3.10), multivariate analysis against FIGO stage and level of cytoreduction failed to confirm UbcH10 as an *independent* risk factor for HGSOC progression in the training set (Table 3.11).

In the validation cohort, UbcH10 did not correlate significantly with FIGO stage as the only prognostic parameter available to us in this cohort (Table 3.14). This was concordant with results from the training set. However, contradictory to the training set, high UbcH10 expression negatively impacted on overall-survival (Figure 3.26 and Table 3.16) and multivariate analysis against FIGO stage confirmed UbcH10 as an independent, but weak, risk factor for HGSOC mortality in the validation cohort (Table 3.17).

The fact that UbcH10 did not correlate significantly with any of the strong and well-established prognostic or predictive parameters in both the training and validation sets suggests that UbcH10 is not a strong parameter that can be used in the prognostication of HGSOC. Moreover, UbcH10 exerted only a weak negative effect on OS in the validation set but not the training set. This was very clear from the HR of increased UbcH10 expression in the validation set (1.006 to 1.11 for overall survival). This means that high UbcH10 expression increased the risk of mortality in HGSOC in the validation cohort by only 0.6 to 11%. Failure to recapitulate results in two independent datasets with respect to patient survival drove the general conclusion that UbcH10 is only a marker of *weak/borderline* prognostic effect in HGSOC patients. The significant independent negative effect of UbcH10 on OS in the validation dataset coupled with

the weak association with advanced age at diagnosis in the training set tipped the scale in favour of a *poor* yet weak prognostic effect. This argues against the use of UbcH10 as a *standalone* marker to predict patient outcome in HGSOC patients, contradictory to what the literature seemed to suggest for EOCs as well as other malignancies (see section 3.5.2). While the present study design is one of the main strengths of this thesis, the two experimental cohorts, however, were not without their limitations. The sample size was relatively small and the missing clinical data (age, level of cytoreduction, *BRCA* mutation) from the validation set hindered further analysis. Furthermore, UbcH10 protein expression levels were found to be significantly reduced by pre-operative chemotherapy (Table 3.5 and Figure 3.23). Therefore, we further explored the above conclusions at the molecular level in TCGA cohort in Chapter 5.

In TCGA cohort of ovarian serous carcinomas (*n*=585), we chose 163 patients who were *TP53* mutant to ensure they were High-grade serous carcinomas. The clinicopathological profile of the cohort (Table 5.3) was mostly similar to our two experimental cohorts utilised in chapter 3 except that none of the patients had received pre-operative chemotherapy. Furthermore, we used *Ube2C* mRNA expression levels to validate protein expression data from our two experimental cohorts. The *X*-tile was again applied to generate biologically significant cut-off values for *Ube2C* mRNA expression. *Ube2C* gene expression levels did not correlate significantly with age or stage of disease (Figures 5.4 and 5.5). Additionally, it did not impact HGSOC mortality (Figure 5.6) or progression rates (Figure 5.7). These results are mostly concordant with results from the two experimental cohorts. The only exception is the weak association with advanced age at diagnosis in the training set which we contend is the result of chemotherapy effect on UbcH10 protein expression levels (see section 5.4.2). Results

from TCGA cohort presented a robust refinement of our study design by offering a larger sample size and eliminating pre-analytical confounding factors such as pre-operative chemotherapy. Furthermore, they validated protein expression data at the molecular level. Accordingly, these results further confirm our conclusions from the experimental cohorts and argue against the use of UbcH10 as an independent prognostic marker in HGSOC. Accordingly, studies that previously advocated UbcH10 as a prognostic parameter in ovarian cancer (86, 116) probably overstated its significance as it was probably contingent on other well established prognostic parameters in ovarian cancer like stage, grade, and histological subtype. To clarify, these studies mostly compared UbcH10 expression in different histological subtypes of epithelial ovarian cancers which inherently have different prognosis, stage, and outcome. This highlights the importance of looking at epithelial ovarian cancers (EOCs) as distinct groups of diseases with discrete molecular profiles rather than just one disease. Future work should therefore avoid studying cancer biomarkers in EOCs as a whole, but rather as genetically distinct diseases similar to our study design where we focused on HGSOC.

With respect to UbcH10 as a predictive marker, although we could not find a significant association with measures of treatment response in the training set, one cannot not totally exclude the possibility due to the lack of treatment response data (platinum resistance and CRS) in the validation dataset. We also acknowledge the heterogeneity of the sample biopsy site and the number of cycles of NACT administered in the training set. To study the relationship between UbcH10 levels and treatment parameters adequately, it is therefore important to standardize these parameters in future studies. In addition, matched pre-and post-operative samples should ideally be

used to further clarify the role of UbcH10 in chemotherapy resistance/sensitivity in HGSOC.

9.2 UbcH10 as a proliferative marker in HGSOC

In both the training and validation sets in Chapter 3, we observed that UbcH10 protein expression levels were reduced significantly in patients who underwent DDS after neoadjuvant chemotherapy compared to patients who underwent PDS without pre-operative chemotherapy (Table 3.5 and Figure 3.23). This indicated that UbcH10 expression levels were affected by chemotherapy administration in a manner akin to well-known proliferative markers such as Ki-67 (125-127). Moreover, UbcH10 expression polarized to the proliferative cells in the germinal centres of tonsillar tissue similar to Ki-67 (Figure 2.1). Therefore, we sought to explore this relationship further in Chapter 6 in an independent experimental cohort of 24 HGSOC patients. We also aimed to study the role of UbcH10 expression in the progression of HGSOC by studying their expression in the putative precursors of HGSOC namely STICs and p53 signatures.

In the STIC/HGSOC cohort, we found that UbcH10 was expressed at a level comparable to normal tubal epithelium in p53 signatures with a significant rise in its expression in STICs and their corresponding invasive malignancies (Table 6.2 and Figure 6.9). This meant that UbcH10 was overexpressed as *early* as the STIC stage of the HGSOC carcinogenesis model which could explain why it did not correlate significantly with any prognostic parameters in these patients. Moreover, when applying multiplex IHC, UbcH10 expression closely mirrored Ki-67 expression in normal tubal epithelia, intraepithelial and invasive high-grade serous malignancy with

significant colocalization of both proteins (Figures 6.23 to 6.25). A significant moderate positive correlation was particularly found between Ki-67 index and UbcH10 total tumour proportion score in HGSOC in that cohort (Figure 6.29). These data indicate that UbcH10 protein levels correlate positively with the proliferative state of the cell. This is why its expression levels were low in p53 signatures which by definition have low Ki-67 indices and were high in STICs and HGSOC which are highly proliferative by nature. Neither UbcH10 nor Ki-67 correlated significantly with any clinicopathological parameters in that cohort (Figures 6.30 and 6.31). This again indicates that UbcH10 behaves more like a proliferative marker rather than a proto-oncogene product in HGSOC.

To confirm our conclusion at the molecular level, we looked at TCGA cohort of ovarian serous carcinoma (*n*=585). Firstly, we found that *Ube2C* was significantly and positively co-expressed with genes involved in mitosis and cell-cycle regulation (Table 5.1 and Figure 5.1). Secondly, when using the Bioconductor package(180) to assign Verhaak/TCGA molecular (60) subtypes to TCGA cohort of HGSOC (*n*=163), we found that *Ube2C* gene expression levels were significantly higher in the Proliferative and clinically aggressive subtype of HGSOC (Table 7.1 and Figure 7.1). Lastly, we attempted a molecular characterization of the Birmingham cohort (training set) at the protein level using Ki-67 and CD8 expression by immunohistochemistry following recommendations from Murakami and colleagues (114). Our findings were concordant with TCGA cohort and STIC/HGSOC cohort. We found that UbcH10 protein expression levels were significantly higher in the Solid Proliferative subtype of HGSOC (Figure 7.23). Additionally, UbcH10 protein expression levels correlated positively with Ki-67 and mitotic indices in the Birmingham cohort (Figures 7.24 to 7.26). When we used

matched pre-and post-chemotherapy samples from the same patients to compare Ki-67 and UbcH10 protein expression levels, a significant reduction was noted in the level of both proteins (Table 7.9). Moreover, and similar to UbcH10 we could not demonstrate a prognostic role for the proliferative maker Ki-67 on the mortality (Figure 7.29) and progression (Figure 7.30) of HGSOC patients in the Birmingham cohort. It is therefore clear from three different cohorts that UbcH10/*Ube2C* has strong proliferative properties and a limited role in the prognostication of these tumours. However, if used to identify the aggressive Proliferative subgroup of HGSOC, UbcH10 might prove of more clinical significance. Future studies should therefore not focus on a single marker like UbcH10 to prognosticate a genetically complex disease like HGSOC. Instead, the focus should be on biological markers in the context of a molecular subtype to yield more meaningful and clinically translatable results. This was one of the main reasons we investigated and established a molecular classification of HGSOC by use of immunohistochemistry in Chapter 7.

9.3 Insights into the molecular classification of HGSOC

One of the main objectives of the present study was to identify a clinically significant molecular classification for HGSOC by use of immunohistochemistry. We achieved this objective successfully in Chapter 7. Investigators from TCGA followed by several studies had previously identified four molecular subtypes for HGSOC based on transcriptomic and DNA methylation data (50, 60, 61). Their clinical significance however was doubtful and conflicting in the literature. Initially, we set out to look at the clinical significance of the molecular subtypes in TCGA cohort of HGSOC. We found no significant correlation between the molecular subtypes and the clinical parameters available in that cohort; age and AJCC stage (Figure 7.2 and Table 7.3). Additionally,

we found no significant impact of the molecular subtypes on the mortality or progression of HGSOC patients in TCGA cohort (Figure 7.3 and 7.4). More recently, Murakami and colleagues used unsupervised hierarchical clustering to correlate gene expression with transcriptomic data in two different datasets of HGSOC (114). Their study identified four histopathological subtypes of HGSOC that overlap with TCGA characterized molecular groups. They also identified an algorithm based on a combination of morphology and immunohistochemistry to identify these subtypes. Using that study as a guide, we applied the same principles at the protein level with further refinement by incorporating Ki-67 in the algorithm to identify the Solid Proliferative subtype of HGSOC. Additionally, we described new morphological features to help identify the Mesenchymal subtype including: the sarcomatoid/syncytial pattern and paradoxical differentiation phenomenon (Figure 7.21 and 7.22). We propose these new features as part of the spectrum of epithelial to mesenchymal transition (EMT) that is well known to contribute to metastasis and invasion in these tumours (191) and worthy of future investigations.

Our diagnostic algorithm proved clinically significant in several ways. Firstly, we identified a relatively new association between the Immunoreactive subgroup of HGSOC and *BRCA* mutations (Table 7.7). Although premature, this might prove promising in easily identifying *BRCA*-mutant HGSOC as early candidates for PARP inhibition (55). Moreover, we identified the invasive micropapillary architecture when interpreted in the context of the Immunoreactive or Differentiated subtypes of HGSOC to be highly suggestive of *BRCA* mutations (Figure 7.18 and 7.19). Additionally, we found the combination of Differentiated and Solid Proliferative subtypes to be particularly common in *BRCA*-mutant HGSOC patients (Figure 7.17 and 7.20). These

represent new and cost-effective methods ways of morphologically identifying *BRCA*-mutant HGSOC which are well-known to have a more favourable outcome (50, 188). Future work should focus on confirming these criteria at the molecular level through RNA sequencing and hierarchical clustering. A deeper investigation into the specific types of *BRCA*-mutations might also prove useful since most of the Immunoreactive subgroup had *BRCA-1* mutations. Statistical testing to prove this association was not possible in our cases due to the small number of the Immunoreactive cases (n=10).

Secondly, we found significant differences in outcome and treatment response among the 4 molecular subgroups. The Mesenchymal subgroup exhibited the worst overall-survival (Figure 7.27) and were more resistant to chemotherapy (Table 7.11) whilst the Immunoreactive subgroup exhibited the best OS. The Differentiated subgroup showed intermediate OS and were more treatment responsive. These results advocate a prognostic and predictive role for the molecular subgroups similar to previous studies (61, 114). We could not however find a significant difference in progression rates between the 4 molecular subgroups (Figure 7.28).

Whilst these results are promising, we contend that our small sample size might have hindered drawing stronger conclusions. In addition, the pre-operative chemotherapy administered in a proportion of our samples would have altered the morphology and affected the proliferation indices (Table 7.9). Although including such samples allowed us to correlate molecular subgroups to treatment response measures, nonetheless, it might account for the overrepresentation of the Mesenchymal subtype in our cohort and the underrepresentation of the Solid Proliferative subgroup. We therefore suggest standardising future cohorts when applying the diagnostic algorithm by using only chemo-naïve samples. Furthermore, our results need validation at the molecular level

RNA sequencing and hierarchical clustering. Future work should therefore focus on correlating protein expression with gene expression data when applying the molecular classification for HGSOC.

9.4 The role of p53 in HGSOC, its relationship to UbcH10 and prospects for the future

In Chapter 4 we mainly aimed to address the prognostic and predictive role of the different *TP53* mutations through their IHC expression patterns in the Birmingham cohort. A review of the literature revealed conflicting results concerning the prognostic role that p53 played in HGSOC patients (82, 83). Additionally, because studies suggested that p53 GOF mutants promoted the transcriptional upregulation of UbcH10, we thought to tackle this relationship with therapeutic and prognostic goals in mind (104).

In the Birmingham cohort we failed to identify a significant impact of the various p53 IHC expression patterns on HGSOC mortality (Figure 4.9) and progression (Figure 4.10). In addition, we found that aberrant p53 expression patterns were not predictive of chemotherapy resistance in the Birmingham cohort (Table 4.5). Although we failed to recapitulate these results in the Barts cohort due to the missing data, we did confirm these results at the molecular level in TCGA cohort in Chapter 5.

In TCGA cohort of HGSOC, we divided *TP53* mutations into 5 major subtypes (missense, nonsense, frameshift, in-frame, and splice site). We also divided the mutations based on their functional impact on the p53 protein (absent vs overexpressed protein). Moreover, we grouped *TP53* missense mutations based on their location within the DBD tertiary structure (Table 5.4), and whether they conferred

GOF activity (Table 5.5). Irrespective of how we partitioned the *TP53* mutations in the TCGA cohort, we did not determine a significant impact on overall or progression-free survival (Figures 5.8 to 5.15).This corroborates our results from the Birmingham cohort and is supported by conclusive new evidence from the literature with large multicentre cohorts (81, 138, 160). Nonetheless, it was interesting to note that Tuna *et al (161)* identified certain hotspot missense mutations (G266, Y163, R282) to be associated with worse OS in HGSOC females. While the number of such mutations in our cohort of HGSOC females from TCGA are too low to achieve any robust conclusions, this might point that individual mutation analysis might be more clinically relevant than categorising mutations based on their functional impact on the p53 protein. In the era of personalised medicine, these might even represent attractive targets for therapy. Taken together the above studies support the notion that functional and structural groups of *TP53* mutations do not impact survival in HGSOC, while individual mutation analysis might be a more promising prospect for future investigation.

Consistent with the notion that p53 mutational status should be explored for individual patients to help determine personal outcomes, we discovered a mosaic pattern for p53 expression that is rarely reported in HGSOC. These included 9% of our cases with a combination of overexpression and wild-like or cytoplasmic staining (Figures 4.4 and 4.5). We could not find a significant survival difference for the mosaic cases (Figures 4.9 and 4.10) nor a significant correlation with any clinicopathological parameters (Table 4.6). Nonetheless, we argue that because patient numbers were too low, we could not achieve statistical significance. We also contend that these cases are overlooked in routine practice because of the rarity of cytoplasmic and wild-like p53 staining in HGSOC and hence unfamiliarity with these patterns. We acknowledge that

pre-analytical factors (pre-operative chemotherapy and poor fixation) could have affected p53 staining by IHC. Therefore, investigation is currently underway to harvest more p53 mosaic HGSOC cases to study their molecular basis and effect on patient outcome. We believe these cases hold great promise for future studies on HGSOC especially since we noted differential morphology, UbcH10 and Ki-67 expression in some of these cases which were particularly *BRCA*-mutant (Figures 4.11, 4.12 and 7.18). Collectively, these data indicate that different biological mechanisms and molecular abnormalities might underpin the morphological heterogeneity of *BRCA* mutant HGSOC patients. It would, therefore, be interesting to interpret the mosaic cases in the context of the molecular subtype of HGSOC and type of *BRCA* mutation.

As a final point, when we addressed the relationship between p53 and UbcH10 at the protein level in the Birmingham cohort, we found it rather heterogeneous with no evidence to support a directly proportional relationship between the two proteins (Table 4.1 and Figure 4.6). This is contrary to what the literature seemed to suggest (104). We confirmed this at the molecular level in TCGA cohort in Chapter 5 when we again failed to identify a significant relationship between *Ube2C* mRNA expression and *TP53* mutations grouped both structurally and functionally (Table 5.15 and Figures 5.16 to 5.18). When we looked at this proposed relationship between the two proteins in the precursors of HGSOC, we again found the relationship to be heterogeneous (Figures 6.20 to 6.22). These results exclude any positive correlation between the two proteins and confirm our speculations that UbcH10 akin to p53 is expressed early in the HGSOC carcinogenesis model and hence has a limited role in the prognostication of these tumours.

9.5 Concluding remarks

The study detailed herein used 3 different experimental cohorts of HGSOC as well as the publicly available TCGA cohort. Such study design provided a platform to draw solid conclusions from our results. We achieved most of the objectives we set out to identify, including identifying the role UbcH10 played in the prognosis of HGSOC and the prediction of treatment response. We also identified the prognostic and predictive role that p53 played in HGSOC and its relationship to UbcH10. Moreover, we unprecedently studied UbcH10 in the HGSOC carcinogenesis model and correlated it to the proliferative state of the cell. We were successful in establishing a molecular classification for HGSOC at by the simple use of immunohistochemistry with clinically significant results. A great amount of work is however still required to validate our results at the molecular level and to incorporate our results into routine clinical practice.

10. Appendices

10.1 Appendix: Western blot analysis for UbcH10 and p53 in the Pilot cohort

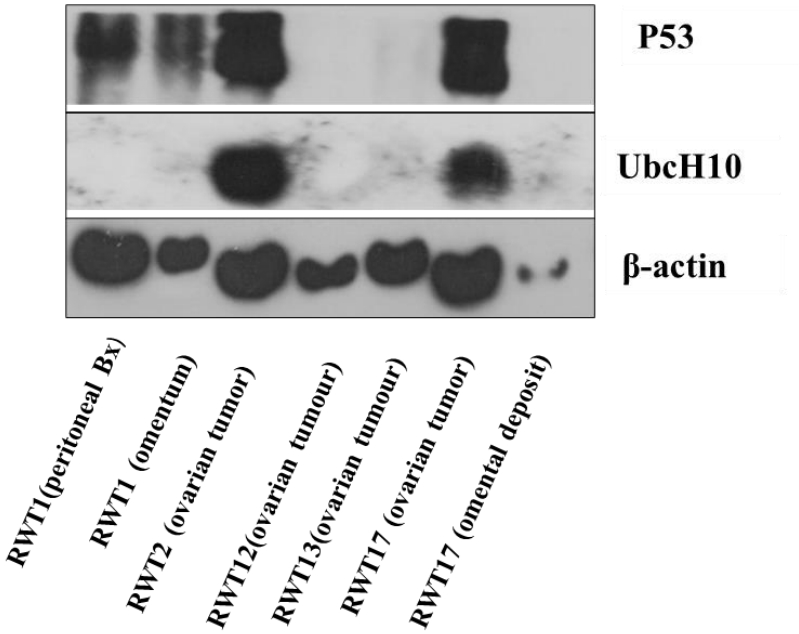

Appendix 10. 1: Expression levels of UbcH10 and p53 by Western blot analysis in 7 samples belonging to 5 HGSOC patients from the Pilot cohort. Biopsies were disrupted in UTB buffer solution, sonicated and centrifuged; the protein lysate was run on SDS-PAGE and subject to Western blot analysis. The ovarian tumour in cases RWT2 and RWT17 overexpressed both UbcH10 and p53 whilst the two RWT1 samples overexpressed p53 but not UbcH10. Note that in patient RWT17 the omental sample does not show detectable UbcH10 or p53 protein expression contradictory to the ovarian tumour.

10.2 Appendix: Discrepant results between Western blot analysis and immunohistochemistry in the Pilot cohort.

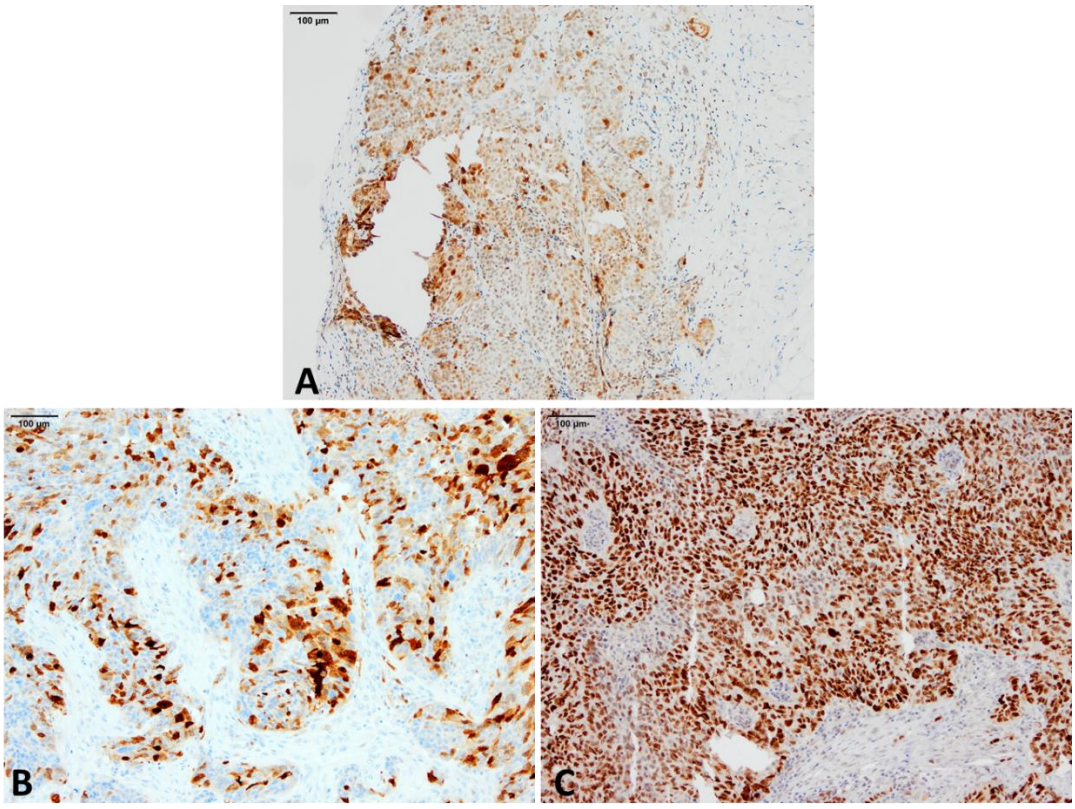

Appendix 10. 2: Two HGSOC patients with discrepant UbcH10 and p53 expression on immunohistochemistry compared to Western blot analysis. A) Patient RWT1 showing HGSOC in a peritoneal biopsy with low but detectable UbcH10 expression (IRS 5, H-score 41). This case showed no detectable UbcH10 expression on Western blot analysis (see Appendix 10.1) (anit-UbcH10, x10 magnification). B) Patient RWT13 showing HGSOC in an ovarian section with moderate UbcH10 expression (IRS 7, H-score 114). This case showed no detectable UbcH10 expression on Western blot analysis (see Appendix 10.1) (anti-UbcH10, x10 magnification). C) Patient RWT13 showing p53 overexpression despite a negative p53 band on Western blot analysis (Appendix 10.1) (anti-p53, x10 magnification)

10.3 Appendix: List of presentations, prizes, and published work from the present study

10.3.1 Presentations from the present study

- Oral presentation titled “Investigating the role of the UbcH10 proto-oncogene product in High-grade serous ovarian cancer” in the post graduate research festival at the Institute of Cancer and Genomic Sciences, University of Birmingham in March 2020, and May 2022.
- Poster presentation titled “UbcH10 is a proto-oncogene and cell-cycle proliferative marker of borderline prognostic significance in tubo-ovarian high grade serous cancer” at the joint meeting of the British division of the international academy of pathology (BDIAP) and Pathological Society of Great Britain and Ireland in Liverpool in June 2023.
- Poster presentation titled “Mosaic P53 expression in tubo-ovarian high grade serous cancer: a report of 9 cases” at the at the joint meeting of the British division of the international academy of pathology (BDIAP) and Pathological Society of Great Britain and Ireland in Liverpool in June 2023.

10.3.2 Published work from the present study

- Accepted two abstracts for poster presentation at the USCAP annual meeting in New Orleans, LA on the 11-16th of March 2023. The abstracts were later published (no. 890 and 891) in the USCAP’s 112th annual meeting abstract book, volume 103, issue 3 of Laboratory investigations: **https://doi.org/10.1016/j.labinv.2023.100091.**
- Two manuscripts in preparation for submission to “Histopathology” journal.

10.3.3 Prizes received for this study

- Commendation for best presentation at the postgraduate research festival, Institute of Cancer and Genomic Sciences, University of Birmingham, 16th March, 2020.
- Young member investigator award for the year 2021 from the International Society of Gynaecological Pathologists for my project titled “Investigating the role of the UbcH10 proto-oncogene product in High grade serous ovarian cancer”.
- BDIAP 1st poster prize Winner at the 14th Joint meeting of the British division of the International Academy of Pathology and the Pathological Society of Great Britain and Ireland for the poster titled “UbcH10 is a Proto-oncogene and Cell-cycle proliferative marker of borderline prognostic significance in tubo-ovarian high grade serous ovarian cancer”. The poster was judged by Professor Simon Herrington and Professor Nafisa Wilkinson.

REFERENCES

1. Wild CP, Stewart BW, Wild C. World cancer report 2014: World Health Organization Geneva, Switzerland; 2014.

2. Sung H, Ferlay J, Siegel RL, Laversanne M, Soerjomataram I, Jemal A, et al. Global Cancer Statistics 2020: GLOBOCAN Estimates of Incidence and Mortality Worldwide for 36 Cancers in 185 Countries. CA Cancer J Clin. 2021;71(3):209-49.

3. Siegel RL, Miller KD, Jemal A. Cancer Statistics, 2017. CA Cancer J Clin. 2017;67(1):7-30.

4. Delon C, Brown KF, Payne NWS, Kotrotsios Y, Vernon S, Shelton J. Differences in cancer incidence by broad ethnic group in England, 2013–2017. British Journal of Cancer. 2022;126(12):1765-73.

5. Yoneda A, Lendorf ME, Couchman JR, Multhaupt HA. Breast and ovarian cancers: a survey and possible roles for the cell surface heparan sulfate proteoglycans. The journal of histochemistry and cytochemistry : official journal of the Histochemistry Society. 2012;60(1):9-21.

6. Malvezzi M, Carioli G, Rodriguez T, Negri E, La Vecchia C. Global trends and predictions in ovarian cancer mortality. Annals of oncology : official journal of the European Society for Medical Oncology. 2016;27(11):2017-25.

7. Cooke A, Butt A, Nasir R, Windsor-Shellard B. Mortality from leading causes of death by ethnic group, England and Wales: 2012 to 2019. Experimental analysis of ethnic differences in mortality and cause-specific mortality in England and Wales based on 2011 Census and death registrations: Office for National Statistics; 2021.

8. Cheung AN, Ellenson LH, Gilks GB, Kim K-R, Kong CS, Lax SF, et al. WHO Classification of Tumours, Female Genital Tumours. IARC WHO Classification of Tumours, Fifth Edition Lyon: IARC. 2020.

9. Kumar V, Abbas AK, Aster JC, Cotran RS, Robbins SL. Robbins & Cotran pathologic basis of disease. Philadelphia, Pa.: Elsevier Philadelphia, Pa.; 2021.

10. Seidman JD, Ronnett BM, Shih I-M, Cho KR, Kurman RJ. Epithelial Tumors of the Ovary. In: Kurman RJ, Hedrick Ellenson L, Ronnett BM, editors. Blaustein's Pathology of the Female Genital Tract. Cham: Springer International Publishing; 2019. p. 841-966.

11. Cabasag CJ, Arnold M, Butler J, Inoue M, Trabert B, Webb PM, et al. The influence of birth cohort and calendar period on global trends in ovarian cancer incidence. Int J Cancer. 2020;146(3):749-58.

12. Gong TT, Wu QJ, Vogtmann E, Lin B, Wang YL. Age at menarche and risk of ovarian cancer: a meta-analysis of epidemiological studies. Int J Cancer. 2013;132(12):2894-900.

13. Wentzensen N, Poole EM, Trabert B, White E, Arslan AA, Patel AV, et al. Ovarian Cancer Risk Factors by Histologic Subtype: An Analysis From the Ovarian Cancer Cohort Consortium. Journal of clinical oncology : official journal of the American Society of Clinical Oncology. 2016;34(24):2888-98.

14. Bahar-Shany K, Brand H, Sapoznik S, Jacob-Hirsch J, Yung Y, Korach J, et al. Exposure of fallopian tube epithelium to follicular fluid mimics carcinogenic changes in precursor lesions of serous papillary carcinoma. Gynecol Oncol. 2014;132(2):322-7.

15. Rasmussen CB, Kjaer SK, Albieri V, Bandera EV, Doherty JA, Høgdall E, et al. Pelvic Inflammatory Disease and the Risk of Ovarian Cancer and Borderline Ovarian

Tumors: A Pooled Analysis of 13 Case-Control Studies. American journal of epidemiology. 2017;185(1):8-20.

16. Yang HP, Murphy KR, Pfeiffer RM, George N, Garcia-Closas M, Lissowska J, et al. Lifetime Number of Ovulatory Cycles and Risks of Ovarian and Endometrial Cancer Among Postmenopausal Women. American journal of epidemiology. 2016;183(9):800-14.

17. Brown KF, Rumgay H, Dunlop C, Ryan M, Quartly F, Cox A, et al. The fraction of cancer attributable to modifiable risk factors in England, Wales, Scotland, Northern Ireland, and the United Kingdom in 2015. Br J Cancer. 2018;118(8):1130-41.

18. Kyrgiou M, Kalliala I, Markozannes G, Gunter MJ, Paraskevaidis E, Gabra H, et al. Adiposity and cancer at major anatomical sites: umbrella review of the literature. BMJ (Clinical research ed). 2017;356:j477.

19. Dixon SC, Nagle CM, Thrift AP, Pharoah PD, Pearce CL, Zheng W, et al. Adult body mass index and risk of ovarian cancer by subtype: a Mendelian randomization study. International journal of epidemiology. 2016;45(3):884-95.

20. Kuchenbaecker KB, Hopper JL, Barnes DR, Phillips KA, Mooij TM, Roos-Blom MJ, et al. Risks of Breast, Ovarian, and Contralateral Breast Cancer for BRCA1 and BRCA2 Mutation Carriers. Jama. 2017;317(23):2402-16.

21. Vierkoetter KR, Ayabe AR, VanDrunen M, Ahn HJ, Shimizu DM, Terada KY. Lynch Syndrome in patients with clear cell and endometrioid cancers of the ovary. Gynecol Oncol. 2014;135(1):81-4.

22. Tavassoli FA, Devilee P. Tumours of the ovary and peritoneum. In: Tavassoli FA, Devilee P. WHO classification of tumours, Pathology and genetics of tumours of the breast and female genital organs. Lyon; IARC Press; 2003. p.114-202.

23. Kurman RJ, Shih Ie M. The origin and pathogenesis of epithelial ovarian cancer: a proposed unifying theory. Am J Surg Pathol. 2010;34(3):433-43.

24. Kurman RJ, Shih Ie M. Molecular pathogenesis and extraovarian origin of epithelial ovarian cancer--shifting the paradigm. Hum Pathol. 2011;42(7):918-31.

25. Organization WH, Kurman RJ. WHO classification of tumours of female reproductive organs: Internat. Agency for Research on Cancer; 2014.

26. McCluggage WG. Overview of Epithelial Ovarian Carcinoma (EOC): Pathogenesis and General Considerations. In: Wilkinson N (ed). Pathology of the Ovary, Fallopian Tube and Peritoneum, Essentials of Diagnostic Gynecological Pathology. London: Springer; 2014. p. 177-95.

27. Shih I, Kurman RJ. Ovarian tumorigenesis: a proposed model based on morphological and molecular genetic analysis. Am J Pathol 2004;164(5):1511-8.

28. Kurman RJ, Shih Ie M. The Dualistic Model of Ovarian Carcinogenesis: Revisited, Revised, and Expanded. Am J Pathol. 2016;186(4):733-47.

29. Kurman RJ, Shih I. The Origin and pathogenesis of epithelial ovarian cancer-a proposed unifying theory. The American journal of surgical pathology. 2010;34(3):433.

30. Boyd C, McCluggage WG. Low-grade ovarian serous neoplasms (low-grade serous carcinoma and serous borderline tumor) associated with high-grade serous carcinoma or undifferentiated carcinoma: report of a series of cases of an unusual phenomenon. The American journal of surgical pathology. 2012;36(3):368-75.

31. Garg K, Park KJ, Soslow RA. Low grade serous neoplasms of the ovary with transformation to high grade carcinomas: Report of 3 cases. International journal of gynecological pathology: official journal of the International Society of Gynecological Pathologists. 2012;31(5):423.

32. Böhm S, Faruqi A, Said I, Lockley M, Brockbank E, Jeyarajah A, et al. Chemotherapy response score: Development and validation of a system to quantify histopathologic response to neoadjuvant chemotherapy in tubo-ovarian high-grade serous carcinoma. Journal of Clinical Oncology. 2015;33(22):2457-63.

33. van Zyl B, Tang D, Bowden NA. Biomarkers of platinum resistance in ovarian cancer: what can we use to improve treatment. Endocr Relat Cancer. 2018;25(5):R303-r18.

34. Coghlan E, Meniawy TM, Munro A, Bulsara M, Stewart CJ, Tan A, et al. Prognostic Role of Histological Tumor Regression in Patients Receiving Neoadjuvant Chemotherapy for High-Grade Serous Tubo-ovarian Carcinoma. International journal of gynecological cancer : official journal of the International Gynecological Cancer Society. 2017;27(4):708-13.

35. Prat J. FIGO's staging classification for cancer of the ovary, fallopian tube, and peritoneum: abridged republication. J Gynecol Oncol. 2015;26(2):87-9.

36. Labidi-Galy SI, Papp E, Hallberg D, Niknafs N, Adleff V, Noe M, et al. High grade serous ovarian carcinomas originate in the fallopian tube. Nature communications. 2017;8(1):1093.

37. Schneider S, Heikaus S, Harter P, Heitz F, Grimm C, Ataseven B, et al. Serous Tubal Intraepithelial Carcinoma Associated With Extraovarian Metastases. International journal of gynecological cancer : official journal of the International Gynecological Cancer Society. 2017;27(3):444-51.

38. Pölcher M, Zivanovic O, Chi DS. Cytoreductive surgery for advanced ovarian cancer. Women’s Health. 2014;10(2):179-90.

39. Wimberger P, Lehmann N, Kimmig R, Burges A, Meier W, Hoppenau B, et al. Impact of age on outcome in patients with advanced ovarian cancer treated within a prospectively randomized phase III study of the Arbeitsgemeinschaft Gynaekologische Onkologie Ovarian Cancer Study Group (AGO-OVAR). Gynecol Oncol. 2006;100(2):300-7.

40. Tetsche MS, Dethlefsen C, Pedersen L, Sorensen HT, Norgaard M. The impact of comorbidity and stage on ovarian cancer mortality: a nationwide Danish cohort study. BMC Cancer. 2008;8:31.

41. Lisio MA, Fu L, Goyeneche A, Gao ZH, Telleria C. High-Grade Serous Ovarian Cancer: Basic Sciences, Clinical and Therapeutic Standpoints. International journal of molecular sciences. 2019;20(4).

42. Garg R, Zahurak ML, Trimble EL, Armstrong DK, Bristow RE. Abdominal carcinomatosis in women with a history of breast cancer. Gynecol Oncol. 2005;99(1):65-70.

43. Fotopoulou C, Hall M, Cruickshank D, Gabra H, Ganesan R, Hughes C, et al. British Gynaecological Cancer Society (BGCS) epithelial ovarian/fallopian tube/primary peritoneal cancer guidelines: recommendations for practice. European journal of obstetrics, gynecology, and reproductive biology. 2017;213:123-39.

44. Piek JM, van Diest PJ, Zweemer RP, Jansen JW, Poort-Keesom RJ, Menko FH, et al. Dysplastic changes in prophylactically removed Fallopian tubes of women predisposed to developing ovarian cancer. J Pathol. 2001;195(4):451-6.

45. Gilks CB, Irving J, Köbel M, Lee C, Singh N, Wilkinson N, et al. Incidental nonuterine high-grade serous carcinomas arise in the fallopian tube in most cases:

further evidence for the tubal origin of high-grade serous carcinomas. Am J Surg Pathol. 2015;39(3):357-64.

46. Jones PM, Drapkin R. Modeling High-Grade Serous Carcinoma: How Converging Insights into Pathogenesis and Genetics are Driving Better Experimental Platforms. Frontiers in oncology. 2013;3:217.

47. Vang R, Shih IM. Serous tubal intra-epithelial carcinoma: what do we really know at this point? Histopathology. 2022;81(5):542-55.

48. Singh N, Gilks CB, Hirshowitz L, Wilkinson N, McCluggage WG. Adopting a Uniform Approach to Site Assignment in Tubo-Ovarian High-Grade Serous Carcinoma: The Time has Come. International journal of gynecological pathology : official journal of the International Society of Gynecological Pathologists. 2016;35(3):230-7.

49. Cole AJ, Dwight T, Gill AJ, Dickson KA, Zhu Y, Clarkson A, et al. Assessing mutant p53 in primary high-grade serous ovarian cancer using immunohistochemistry and massively parallel sequencing. Sci Rep. 2016;6:26191.

50. Bell D, Berchuck A, Birrer M, Chien J, Cramer DW, Dao F, et al. Integrated genomic analyses of ovarian carcinoma. Nature. 2011;474(7353):609-15.

51. Vang R, Levine DA, Soslow RA, Zaloudek C, Shih Ie M, Kurman RJ. Molecular Alterations of TP53 are a Defining Feature of Ovarian High-Grade Serous Carcinoma: A Rereview of Cases Lacking TP53 Mutations in The Cancer Genome Atlas Ovarian Study. International journal of gynecological pathology : official journal of the International Society of Gynecological Pathologists. 2016;35(1):48-55.

52. Alsop K, Fereday S, Meldrum C, deFazio A, Emmanuel C, George J, et al. BRCA mutation frequency and patterns of treatment response in BRCA mutation-positive women with ovarian cancer: a report from the Australian Ovarian Cancer Study

Group. Journal of clinical oncology : official journal of the American Society of Clinical Oncology. 2012;30(21):2654-63.

53. Rebbeck TR, Mitra N, Wan F, Sinilnikova OM, Healey S, McGuffog L, et al. Association of type and location of BRCA1 and BRCA2 mutations with risk of breast and ovarian cancer. Jama. 2015;313(13):1347-61.

54. Baldwin RL, Nemeth E, Tran H, Shvartsman H, Cass I, Narod S, et al. BRCA1 promoter region hypermethylation in ovarian carcinoma: a population-based study. Cancer Res. 2000;60(19):5329-33.

55. Konstantinopoulos PA, Ceccaldi R, Shapiro GI, D'Andrea AD. Homologous Recombination Deficiency: Exploiting the Fundamental Vulnerability of Ovarian Cancer. Cancer discovery. 2015;5(11):1137-54.

56. Pennington KP, Walsh T, Harrell MI, Lee MK, Pennil CC, Rendi MH, et al. Germline and somatic mutations in homologous recombination genes predict platinum response and survival in ovarian, fallopian tube, and peritoneal carcinomas. Clinical cancer research : an official journal of the American Association for Cancer Research. 2014;20(3):764-75.

57. Rudaitis V, Zvirblis T, Kanopiene D, Janulynaite D, Griskevicius L, Janavicius R. BRCA1/2 mutation status is an independent factor of improved survival for advanced (stage III-IV) ovarian cancer. International journal of gynecological cancer : official journal of the International Gynecological Cancer Society. 2014;24(8):1395-400.

58. Kroeger PT, Jr., Drapkin R. Pathogenesis and heterogeneity of ovarian cancer. Current opinion in obstetrics & gynecology. 2017;29(1):26-34.

59. Wu RC, Wang P, Lin SF, Zhang M, Song Q, Chu T, et al. Genomic landscape and evolutionary trajectories of ovarian cancer precursor lesions. J Pathol. 2019;248(1):41-50.

60. Verhaak RG, Tamayo P, Yang JY, Hubbard D, Zhang H, Creighton CJ, et al. Prognostically relevant gene signatures of high-grade serous ovarian carcinoma. The Journal of clinical investigation. 2013;123(1):517-25.

61. Konecny GE, Wang C, Hamidi H, Winterhoff B, Kalli KR, Dering J, et al. Prognostic and therapeutic relevance of molecular subtypes in high-grade serous ovarian cancer. Journal of the National Cancer Institute. 2014;106(10).

62. Soslow RA, Han G, Park KJ, Garg K, Olvera N, Spriggs DR, et al. Morphologic patterns associated with BRCA1 and BRCA2 genotype in ovarian carcinoma. Modern pathology : an official journal of the United States and Canadian Academy of Pathology, Inc. 2012;25(4):625-36.

63. Howitt BE, Hanamornroongruang S, Lin DI, Conner JE, Schulte S, Horowitz N, et al. Evidence for a dualistic model of high-grade serous carcinoma: BRCA mutation status, histology, and tubal intraepithelial carcinoma. Am J Surg Pathol. 2015;39(3):287-93.

64. Tan PH, Ellis I, Allison K, Brogi E, Fox SB, Lakhani S, et al. The 2019 World Health Organization classification of tumours of the breast. Histopathology. 2020;77(2):181-5.

65. Reyes MC, Arnold AG, Kauff ND, Levine DA, Soslow RA. Invasion patterns of metastatic high-grade serous carcinoma of ovary or fallopian tube associated with BRCA deficiency. Modern pathology : an official journal of the United States and Canadian Academy of Pathology, Inc. 2014;27(10):1405-11.

66. Kastenhuber ER, Lowe SW. Putting p53 in Context. Cell. 2017;170(6):1062-78.

67. Cho Y, Gorina S, Jeffrey PD, Pavletich NP. Crystal structure of a p53 tumor suppressor-DNA complex: understanding tumorigenic mutations. Science. 1994;265(5170):346-55.

68. Wanka C, Steinbach JP, Rieger J. Tp53-induced glycolysis and apoptosis regulator (TIGAR) protects glioma cells from starvation-induced cell death by up-regulating respiration and improving cellular redox homeostasis. The Journal of biological chemistry. 2012;287(40):33436-46.

69. Hainaut P, Pfeifer GP. Somatic TP53 Mutations in the Era of Genome Sequencing. Cold Spring Harbor perspectives in medicine. 2016;6(11).

70. Vousden KH, Lu X. Live or let die: the cell's response to p53. Nat Rev Cancer. 2002;2(8):594-604.

71. Seagle BL, Eng KH, Dandapani M, Yeh JY, Odunsi K, Shahabi S. Survival of patients with structurally-grouped TP53 mutations in ovarian and breast cancers. Oncotarget. 2015;6(21):18641-52.

72. Rivlin N, Brosh R, Oren M, Rotter V. Mutations in the p53 Tumor Suppressor Gene: Important Milestones at the Various Steps of Tumorigenesis. Genes & cancer. 2011;2(4):466-74.

73. Boettcher S, Miller PG, Sharma R, McConkey M, Leventhal M, Krivtsov AV, et al. A dominant-negative effect drives selection of TP53 missense mutations in myeloid malignancies. Science. 2019;365(6453):599-604.

74. Alexandrova EM, Mirza SA, Xu S, Schulz-Heddergott R, Marchenko ND, Moll UM. p53 loss-of-heterozygosity is a necessary prerequisite for mutant p53 stabilization and gain-of-function in vivo. Cell Death Dis. 2017;8(3):e2661.

75. Shirole NH, Pal D, Kastenhuber ER, Senturk S, Boroda J, Pisterzi P, et al. TP53 exon-6 truncating mutations produce separation of function isoforms with pro-tumorigenic functions. eLife. 2016;5.

76. Köbel M, Ronnett BM, Singh N, Soslow RA, Gilks CB, McCluggage WG. Interpretation of P53 Immunohistochemistry in Endometrial Carcinomas: Toward Increased Reproducibility. International journal of gynecological pathology : official journal of the International Society of Gynecological Pathologists. 2019;38 Suppl 1(Iss 1 Suppl 1):S123-s31.

77. Köbel M, Piskorz AM, Lee S, Lui S, LePage C, Marass F, et al. Optimized p53 immunohistochemistry is an accurate predictor of TP53 mutation in ovarian carcinoma. The journal of pathology Clinical research. 2016;2(4):247-58.

78. Yemelyanova A, Vang R, Kshirsagar M, Lu D, Marks MA, Shih Ie M, et al. Immunohistochemical staining patterns of p53 can serve as a surrogate marker for TP53 mutations in ovarian carcinoma: an immunohistochemical and nucleotide sequencing analysis. Modern pathology : an official journal of the United States and Canadian Academy of Pathology, Inc. 2011;24(9):1248-53.

79. Reles A, Wen WH, Schmider A, Gee C, Runnebaum IB, Kilian U, et al. Correlation of p53 mutations with resistance to platinum-based chemotherapy and shortened survival in ovarian cancer. Clinical cancer research : an official journal of the American Association for Cancer Research. 2001;7(10):2984-97.

80. He C, Li L, Guan X, Xiong L, Miao X. Mutant p53 Gain of Function and Chemoresistance: The Role of Mutant p53 in Response to Clinical Chemotherapy. Chemotherapy. 2017;62(1):43-53.

81. Kang HJ, Chun SM, Kim KR, Sohn I, Sung CO. Clinical relevance of gain-of-function mutations of p53 in high-grade serous ovarian carcinoma. PLoS One. 2013;8(8):e72609.

82. Laframboise S, Chapman W, McLaughlin J, Andrulis IL. p53 mutations in epithelial ovarian cancers: possible role in predicting chemoresistance. Cancer journal (Sudbury, Mass). 2000;6(5):302-8.

83. Xu J, Reumers J, Couceiro JR, De Smet F, Gallardo R, Rudyak S, et al. Gain of function of mutant p53 by coaggregation with multiple tumor suppressors. Nature chemical biology. 2011;7(5):285-95.

84. Wang C, Armasu SM, Kalli KR, Maurer MJ, Heinzen EP, Keeney GL, et al. Pooled Clustering of High-Grade Serous Ovarian Cancer Gene Expression Leads to Novel Consensus Subtypes Associated with Survival and Surgical Outcomes. Clinical cancer research : an official journal of the American Association for Cancer Research. 2017;23(15):4077-85.

85. Presta I, Novellino F, Donato A, La Torre D, Palleria C, Russo E, et al. UbcH10 a Major Actor in Cancerogenesis and a Potential Tool for Diagnosis and Therapy. International journal of molecular sciences. 2020;21(6).

86. Berlingieri M, Pallante P, Guida M, Nappi C, Masciullo V, Scambia G, et al. UbcH10 expression may be a useful tool in the prognosis of ovarian carcinomas. 2007;26(14):2136-40.

87. Sivakumar S, Gorbsky GJ. Spatiotemporal regulation of the anaphase-promoting complex in mitosis. Nature reviews Molecular cell biology. 2015;16(2):82-94.

88. Swatek KN, Komander D. Ubiquitin modifications. Cell research. 2016;26(4):399-422.

89. Barford D. Structure, function and mechanism of the anaphase promoting complex (APC/C). Quarterly reviews of biophysics. 2011;44(2):153-90.

90. Berndsen CE, Wolberger C. New insights into ubiquitin E3 ligase mechanism. Nature structural & molecular biology. 2014;21(4):301-7.

91. Hyer ML, Milhollen MA, Ciavarri J, Fleming P, Traore T, Sappal D, et al. A small-molecule inhibitor of the ubiquitin activating enzyme for cancer treatment. Nature medicine. 2018;24(2):186-93.

92. Musacchio A, Salmon ED. The spindle-assembly checkpoint in space and time. Nature reviews Molecular cell biology. 2007;8(5):379-93.

93. van Ree JH, Jeganathan KB, Malureanu L, van Deursen JM. Overexpression of the E2 ubiquitin-conjugating enzyme UbcH10 causes chromosome missegregation and tumor formation. The Journal of cell biology. 2010;188(1):83-100.

94. Weaver BA. How Taxol/paclitaxel kills cancer cells. Molecular biology of the cell. 2014;25(18):2677-81.

95. Walker A, Acquaviva C, Matsusaka T, Koop L, Pines J. UbcH10 has a rate-limiting role in G1 phase but might not act in the spindle checkpoint or as part of an autonomous oscillator. Journal of cell science. 2008;121(Pt 14):2319-26.

96. Okamoto Y, Ozaki T, Miyazaki K, Aoyama M, Miyazaki M, Nakagawara A. UbcH10 is the cancer-related E2 ubiquitin-conjugating enzyme. Cancer Res. 2003;63(14):4167-73.

97. Wagner KW, Sapinoso LM, El-Rifai W, Frierson HF, Butz N, Mestan J, et al. Overexpression, genomic amplification and therapeutic potential of inhibiting the

UbcH10 ubiquitin conjugase in human carcinomas of diverse anatomic origin. Oncogene. 2004;23(39):6621-9.

98. Pallante P, Berlingieri MT, Troncone G, Kruhoffer M, Orntoft TF, Viglietto G, et al. UbcH10 overexpression may represent a marker of anaplastic thyroid carcinomas. Br J Cancer. 2005;93(4):464-71.

99. Yang M, Qu Y, Shi R, Wu X, Su C, Hu Z, et al. Ubiquitin-conjugating enzyme UbcH10 promotes gastric cancer growth and is a potential biomarker for gastric cancer. Oncology reports. 2016;36(2):779-86.

100. Perrotta I, Bruno L, Maltese L, Russo E, Donato A, Donato G. Immunohistochemical analysis of the ubiquitin-conjugating enzyme UbcH10 in lung cancer: a useful tool for diagnosis and therapy. The journal of histochemistry and cytochemistry : official journal of the Histochemistry Society. 2012;60(5):359-65.

101. Fujita T, Ikeda H, Taira N, Hatoh S, Naito M, Doihara H. Overexpression of UbcH10 alternates the cell cycle profile and accelerate the tumor proliferation in colon cancer. BMC Cancer. 2009;9:87.

102. Rape M, Reddy SK, Kirschner MW. The processivity of multiubiquitination by the APC determines the order of substrate degradation. Cell. 2006;124(1):89-103.

103. Wang C, Pan YH, Shan M, Xu M, Bao JL, Zhao LM. Knockdown of UbcH10 enhances the chemosensitivity of dual drug resistant breast cancer cells to epirubicin and docetaxel. International journal of molecular sciences. 2015;16(3):4698-712.

104. Bajaj S, Alam SK, Roy KS, Datta A, Nath S, Roychoudhury S. E2 Ubiquitin-conjugating Enzyme, UBE2C Gene, Is Reciprocally Regulated by Wild-type and Gain-of-Function Mutant p53. The Journal of biological chemistry. 2016;291(27):14231-47.

105. Gao J, Aksoy BA, Dogrusoz U, Dresdner G, Gross B, Sumer SO, et al. Integrative analysis of complex cancer genomics and clinical profiles using the cBioPortal. Science signaling. 2013;6(269):pl1.

106. Zeppernick F, Meinhold-Heerlein I. The new FIGO staging system for ovarian, fallopian tube, and primary peritoneal cancer. Archives of gynecology and obstetrics. 2014;290(5):839-42.

107. McCluggage WG, Judge MJ, Clarke BA, Davidson B, Gilks CB, Hollema H, et al. Data set for reporting of ovary, fallopian tube and primary peritoneal carcinoma: recommendations from the International Collaboration on Cancer Reporting (ICCR). Modern pathology : an official journal of the United States and Canadian Academy of Pathology, Inc. 2015;28(8):1101-22.

108. Camp RL, Dolled-Filhart M, Rimm DL. X-tile: a new bio-informatics tool for biomarker assessment and outcome-based cut-point optimization. Clinical cancer research : an official journal of the American Association for Cancer Research. 2004;10(21):7252-9.

109. Howat WJ, Lewis A, Jones P, Kampf C, Pontén F, van der Loos CM, et al. Antibody validation of immunohistochemistry for biomarker discovery: recommendations of a consortium of academic and pharmaceutical based histopathology researchers. Methods (San Diego, Calif). 2014;70(1):34-8.

110. Fedchenko N, Reifenrath J. Different approaches for interpretation and reporting of immunohistochemistry analysis results in the bone tissue – a review. Diagnostic pathology. 2014;9(1):221.

111. Dabbs DJ. Diagnostic Immunohistochemistry: Diagnostic Immunohistochemistry E-Book: Elsevier Health Sciences; 2021.

112. Nagtegaal ID, Odze RD, Klimstra D, Paradis V, Rugge M, Schirmacher P, et al. The 2019 WHO classification of tumours of the digestive system. Histopathology. 2020;76(2):182-8.

113. Hamanishi J, Mandai M, Iwasaki M, Okazaki T, Tanaka Y, Yamaguchi K, et al. Programmed cell death 1 ligand 1 and tumor-infiltrating CD8+ T lymphocytes are prognostic factors of human ovarian cancer. Proc Natl Acad Sci U S A. 2007;104(9):3360-5.

114. Murakami R, Matsumura N, Mandai M, Yoshihara K, Tanabe H, Nakai H, et al. Establishment of a Novel Histopathological Classification of High-Grade Serous Ovarian Carcinoma Correlated with Prognostically Distinct Gene Expression Subtypes. Am J Pathol. 2016;186(5):1103-13.

115. Coan M, Rampioni Vinciguerra GL, Cesaratto L, Gardenal E, Bianchet R, Dassi E, et al. Exploring the Role of Fallopian Ciliated Cells in the Pathogenesis of High-Grade Serous Ovarian Cancer. International journal of molecular sciences. 2018;19(9).

116. Gong Y, Wang D, Lin L, Dai J, Yu L. The expression of ubiquitin-conjugating enzyme E2C and KAI1 in ovarian carcinoma and their clinical significance. Medicine. 2019;98(46):e17896.

117. Kefeli M, Yildiz L, Celik H, Tosun M, Karagoz F. UbcH10 expression in benign, hyperplastic, and malignant endometrial curetted materials: a tissue microarray study. International journal of surgical pathology. 2012;20(4):360-6.

118. Wang R, Song Y, Liu X, Wang Q, Wang Y, Li L, et al. UBE2C induces EMT through Wnt/β-catenin and PI3K/Akt signaling pathways by regulating phosphorylation levels of Aurora-A. International journal of oncology. 2017;50(4):1116-26.

119. Jia B, Lynn HS. A sample size planning approach that considers both statistical significance and clinical significance. Trials. 2015;16:213.

120. Singh R, Som AJb. Identification of potential biomarkers in subtypes of epithelial ovarian cancer. 2020:2020.02. 24.962472.

121. Fedchenko N, Reifenrath J. Different approaches for interpretation and reporting of immunohistochemistry analysis results in the bone tissue - a review. Diagnostic pathology. 2014;9:221.

122. Dabbs DJ. Diagnostic Immunohistochemistry E-Book: Theranostic and Genomic Applications: Elsevier Health Sciences; 2017.

123. Altman DG, Lausen B, Sauerbrei W, Schumacher MJJJotNCI. Dangers of using “optimal” cutpoints in the evaluation of prognostic factors. 1994;86(11):829-35.

124. Mo CH, Gao L, Zhu XF, Wei KL, Zeng JJ, Chen G, et al. The clinicopathological significance of UBE2C in breast cancer: a study based on immunohistochemistry, microarray and RNA-sequencing data. Cancer cell international. 2017;17:83.

125. Wang R-X, Chen S, Jin X, Shao Z-M. Value of Ki-67 expression in triple-negative breast cancer before and after neoadjuvant chemotherapy with weekly paclitaxel plus carboplatin. Scientific Reports. 2016;6(1):30091.

126. Lee J, Im YH, Lee SH, Cho EY, Choi YL, Ko YH, et al. Evaluation of ER and Ki-67 proliferation index as prognostic factors for survival following neoadjuvant chemotherapy with doxorubicin/docetaxel for locally advanced breast cancer. Cancer chemotherapy and pharmacology. 2008;61(4):569-77.

127. Mukai H, Yamaguchi T, Takahashi M, Hozumi Y, Fujisawa T, Ohsumi S, et al. Ki-67 response-guided preoperative chemotherapy for HER2-positive breast cancer: results of a randomised Phase 2 study. Br J Cancer. 2020;122(12):1747-53.

128. Mitchison TJ. The proliferation rate paradox in antimitotic chemotherapy. Molecular biology of the cell. 2012;23(1):1-6.

129. Chen X, He C, Han D, Zhou M, Wang Q, Tian J, et al. The predictive value of Ki-67 before neoadjuvant chemotherapy for breast cancer: a systematic review and meta-analysis. Future oncology (London, England). 2017;13(9):843-57.

130. Santoro A, Angelico G, Piermattei A, Inzani F, Valente M, Arciuolo D, et al. Pathological Chemotherapy Response Score in Patients Affected by High Grade Serous Ovarian Carcinoma: The Prognostic Role of Omental and Ovarian Residual Disease. Frontiers in oncology. 2019;9:778.

131. Cohen PA, Powell A, Böhm S, Gilks CB, Stewart CJR, Meniawy TM, et al. Pathological chemotherapy response score is prognostic in tubo-ovarian high-grade serous carcinoma: A systematic review and meta-analysis of individual patient data. Gynecol Oncol. 2019;154(2):441-8.

132. Ahmed AA, Etemadmoghadam D, Temple J, Lynch AG, Riad M, Sharma R, et al. Driver mutations in TP53 are ubiquitous in high grade serous carcinoma of the ovary. J Pathol. 2010;221(1):49-56.

133. Testa U, Petrucci E, Pasquini L, Castelli G, Pelosi E. Ovarian Cancers: Genetic Abnormalities, Tumor Heterogeneity and Progression, Clonal Evolution and Cancer Stem Cells. Medicines (Basel, Switzerland). 2018;5(1).

134. Olivier M, Hollstein M, Hainaut P. TP53 mutations in human cancers: origins, consequences, and clinical use. Cold Spring Harbor perspectives in biology. 2010;2(1):a001008.

135. Köbel M, Reuss A, du Bois A, Kommoss S, Kommoss F, Gao D, et al. The biological and clinical value of p53 expression in pelvic high-grade serous carcinomas. J Pathol. 2010;222(2):191-8.

136. Sazonova EV, Kopeina GS, Imyanitov EN, Zhivotovsky B. Platinum drugs and taxanes: can we overcome resistance? Cell Death Discovery. 2021;7(1):155.

137. Psyrri A, Kountourakis P, Yu Z, Papadimitriou C, Markakis S, Camp RL, et al. Analysis of p53 protein expression levels on ovarian cancer tissue microarray using automated quantitative analysis elucidates prognostic patient subsets. Annals of Oncology. 2007;18(4):709-15.

138. Köbel M, Kang EY, Weir A, Rambau PF, Lee CH, Nelson GS, et al. p53 and ovarian carcinoma survival: an Ovarian Tumor Tissue Analysis consortium study. The journal of pathology Clinical research. 2023;9(3):208-22.

139. Rabban JT, Garg K, Ladwig NR, Zaloudek CJ, Devine WP. Cytoplasmic Pattern p53 Immunoexpression in Pelvic and Endometrial Carcinomas With TP53 Mutation Involving Nuclear Localization Domains: An Uncommon But Potential Diagnostic Pitfall With Clinical Implications. Am J Surg Pathol. 2021;45(11):1441-51.

140. Vermij L, Léon-Castillo A, Singh N, Powell ME, Edmondson RJ, Genestie C, et al. p53 immunohistochemistry in endometrial cancer: clinical and molecular correlates in the PORTEC-3 trial. Modern Pathology. 2022;35(10):1475-83.

141. Yen TT, Wang TL, Fader AN, Shih IM, Gaillard S. Molecular Classification and Emerging Targeted Therapy in Endometrial Cancer. International journal of gynecological pathology : official journal of the International Society of Gynecological Pathologists. 2020;39(1):26-35.

142. Wu Q, Zhang N, Xie X. The clinicopathological characteristics of POLE-mutated/ultramutated endometrial carcinoma and prognostic value of POLE status: a meta-analysis based on 49 articles incorporating 12,120 patients. BMC Cancer. 2022;22(1):1157.

143. Anczuków O, Ware MD, Buisson M, Zetoune AB, Stoppa-Lyonnet D, Sinilnikova OM, et al. Does the nonsense-mediated mRNA decay mechanism prevent the synthesis of truncated BRCA1, CHK2, and p53 proteins? Human mutation. 2008;29(1):65-73.

144. Sabapathy K, Lane DP. Understanding p53 functions through p53 antibodies. Journal of molecular cell biology. 2019;11(4):317-29.

145. Yang B, Ma C, Chen Z, Yi W, McNutt MA, Wang Y, et al. Correlation of immunoglobulin G expression and histological subtype and stage in breast cancer. PLoS One. 2013;8(3):e58706.

146. Elliott K, McQuaid S, Salto-Tellez M, Maxwell P. Immunohistochemistry should undergo robust validation equivalent to that of molecular diagnostics. J Clin Pathol. 2015;68(10):766-70.

147. Park E, Han H, Choi SE, Park H, Woo HY, Jang M, et al. p53 Immunohistochemistry and Mutation Types Mismatching in High-Grade Serous Ovarian Cancer. Diagnostics (Basel, Switzerland). 2022;12(3).

148. Casey L, Köbel M, Ganesan R, Tam S, Prasad R, Böhm S, et al. A comparison of p53 and WT1 immunohistochemical expression patterns in tubo-ovarian high-grade serous carcinoma before and after neoadjuvant chemotherapy. Histopathology. 2017;71(5):736-42.

149. Pallante P, Malapelle U, Berlingieri MT, Bellevicine C, Sepe R, Federico A, et al. UbcH10 overexpression in human lung carcinomas and its correlation with EGFR and p53 mutational status. European journal of cancer (Oxford, England : 1990). 2013;49(5):1117-26.

150. Huang DW, Sherman BT, Tan Q, Collins JR, Alvord WG, Roayaei J, et al. The DAVID Gene Functional Classification Tool: a novel biological module-centric algorithm to functionally analyze large gene lists. Genome Biology. 2007;8(9):R183.

151. Roulland Y, Ouararhni K, Naidenov M, Ramos L, Shuaib M, Syed SH, et al. The Flexible Ends of CENP-A Nucleosome Are Required for Mitotic Fidelity. Mol Cell. 2016;63(4):674-85.

152. AJCC Staging System. National Cancer Institute. Available at https://www.cancer.gov/publications/dictionaries/cancer-terms/def/ajcc-staging-system Accessed 2/3/2021.

153. Ioannidis NM, Rothstein JH, Pejaver V, Middha S, McDonnell SK, Baheti S, et al. REVEL: An Ensemble Method for Predicting the Pathogenicity of Rare Missense Variants. American journal of human genetics. 2016;99(4):877-85.

154. Musa J, Aynaud M-M, Mirabeau O, Delattre O, Grünewald TGP. MYBL2 (B-Myb): a central regulator of cell proliferation, cell survival and differentiation involved in tumorigenesis. Cell Death & Disease. 2017;8(6):e2895-e.

155. Carvalhal S, Ribeiro SA, Arocena M, Kasciukovic T, Temme A, Koehler K, et al. The nucleoporin ALADIN regulates Aurora A localization to ensure robust mitotic spindle formation. Molecular biology of the cell. 2015;26(19):3424-38.

156. Wheatley SP, Henzing AJ, Dodson H, Khaled W, Earnshaw WC. Aurora-B phosphorylation in vitro identifies a residue of survivin that is essential for its

localization and binding to inner centromere protein (INCENP) in vivo. The Journal of biological chemistry. 2004;279(7):5655-60.

157. Han J, Xie R, Yang Y, Chen D, Liu L, Wu J, et al. CENPA is one of the potential key genes associated with the proliferation and prognosis of ovarian cancer based on integrated bioinformatics analysis and regulated by MYBL2. Translational cancer research. 2021;10(9):4076-86.

158. Liu Q, Liu H, Huang X, Fan X, Xiao Z, Yan R, et al. A targetable MYBL2-ATAD2 axis governs cell proliferation in ovarian cancer. Cancer gene therapy. 2023;30(1):192-208.

159. Kariri Y, Toss MS, Alsaleem M, Elsharawy KA, Joseph C, Mongan NP, et al. Ubiquitin-conjugating enzyme 2C (UBE2C) is a poor prognostic biomarker in invasive breast cancer. Breast Cancer Research and Treatment. 2022;192(3):529-39.

160. Mandilaras V, Garg S, Cabanero M, Tan Q, Pastrello C, Burnier J, et al. TP53 mutations in high grade serous ovarian cancer and impact on clinical outcomes: a comparison of next generation sequencing and bioinformatics analyses. International journal of gynecological cancer : official journal of the International Gynecological Cancer Society. 2019;29(2):346-52.

161. Tuna M, Ju Z, Yoshihara K, Amos CI, Tanyi JL, Mills GB. Clinical relevance of TP53 hotspot mutations in high-grade serous ovarian cancers. Br J Cancer. 2020;122(3):405-12.

162. Serrano M, Lin AW, McCurrach ME, Beach D, Lowe SW. Oncogenic ras provokes premature cell senescence associated with accumulation of p53 and p16INK4a. Cell. 1997;88(5):593-602.

163. Li J, Yang L, Gaur S, Zhang K, Wu X, Yuan YC, et al. Mutants TP53 p.R273H and p.R273C but not p.R273G enhance cancer cell malignancy. Human mutation. 2014;35(5):575-84.

164. Meserve EEK, Brouwer J, Crum CP. Serous tubal intraepithelial neoplasia: the concept and its application. Modern pathology : an official journal of the United States and Canadian Academy of Pathology, Inc. 2017;30(5):710-21.

165. Jarboe E, Folkins A, Nucci MR, Kindelberger D, Drapkin R, Miron A, et al. Serous carcinogenesis in the fallopian tube: a descriptive classification. International journal of gynecological pathology : official journal of the International Society of Gynecological Pathologists. 2008;27(1):1-9.

166. Kuhn E, Kurman RJ, Sehdev AS, Shih Ie M. Ki-67 labeling index as an adjunct in the diagnosis of serous tubal intraepithelial carcinoma. International journal of gynecological pathology : official journal of the International Society of Gynecological Pathologists. 2012;31(5):416-22.

167. Chen M, Yao S, Cao Q, Xia M, Liu J, He M. The prognostic value of Ki67 in ovarian high-grade serous carcinoma: an 11-year cohort study of Chinese patients. Oncotarget. 2017;8(64):107877-85.

168. Asaka S, Davis C, Lin SF, Wang TL, Heaphy CM, Shih IM. Analysis of Telomere Lengths in p53 Signatures and Incidental Serous Tubal Intraepithelial Carcinomas Without Concurrent Ovarian Cancer. Am J Surg Pathol. 2019;43(8):1083-91.

169. Lee Y, Miron A, Drapkin R, Nucci MR, Medeiros F, Saleemuddin A, et al. A candidate precursor to serous carcinoma that originates in the distal fallopian tube. J Pathol. 2007;211(1):26-35.

170. Shih IM, Wang Y, Wang TL. The Origin of Ovarian Cancer Species and Precancerous Landscape. Am J Pathol. 2021;191(1):26-39.

171. Liu P, Sun YL, Du J, Hou XS, Meng H. CD105/Ki67 coexpression correlates with tumor progression and poor prognosis in epithelial ovarian cancer. International journal of gynecological cancer : official journal of the International Gynecological Cancer Society. 2012;22(4):586-92.

172. Feng Z, Wen H, Bi R, Ju X, Chen X, Yang W, et al. A clinically applicable molecular classification for high-grade serous ovarian cancer based on hormone receptor expression. Scientific Reports. 2016;6(1):25408.

173. Heayn M, Skvarca LB, Zhu L, Edwards RP, Olawaiye AB, Modugno F, et al. Impact of Ki-67 Labeling Index on Prognostic Significance of the Chemotherapy Response Score in Women With Tubo-ovarian Cancer Treated With Neoadjuvant Chemotherapy. 2021;40(3):278-85.

174. Petersen S, Wilson AJ, Hirst J, Roby KF, Fadare O, Crispens MA, et al. CCNE1 and BRD4 co-amplification in high-grade serous ovarian cancer is associated with poor clinical outcomes. Gynecol Oncol. 2020;157(2):405-10.

175. Perets R, Wyant GA, Muto KW, Bijron JG, Poole BB, Chin KT, et al. Transformation of the fallopian tube secretory epithelium leads to high-grade serous ovarian cancer in Brca;Tp53;Pten models. Cancer cell. 2013;24(6):751-65.

176. Carlson JW, Miron A, Jarboe EA, Parast MM, Hirsch MS, Lee Y, et al. Serous tubal intraepithelial carcinoma: its potential role in primary peritoneal serous carcinoma and serous cancer prevention. Journal of clinical oncology : official journal of the American Society of Clinical Oncology. 2008;26(25):4160-5.

177. Hatano Y, Fukuda S, Makino H, Tomita H, Morishige KI, Hara A. High-grade serous carcinoma with discordant p53 signature: report of a case with new insight regarding high-grade serous carcinogenesis. Diagnostic pathology. 2018;13(1):24.

178. Staff S, Tolonen T, Laasanen SL, Mecklin JP, Isola J, Mäenpää J. Quantitative analysis of γ-H2AX and p53 nuclear expression levels in ovarian and fallopian tube epithelium from risk-reducing salpingo-oophorectomies in BRCA1 and BRCA2 mutation carriers. International journal of gynecological pathology : official journal of the International Society of Gynecological Pathologists. 2014;33(3):309-16.

179. Gendoo DMA, Zon M, Sandhu V, Manem VSK, Ratanasirigulchai N, Chen GM, et al. MetaGxData: Clinically Annotated Breast, Ovarian and Pancreatic Cancer Datasets and their Use in Generating a Multi-Cancer Gene Signature. Sci Rep. 2019;9(1):8770.

180. Chen GM, Kannan L, Geistlinger L, Kofia V, Safikhani Z, Gendoo DMA, et al. Consensus on Molecular Subtypes of High-Grade Serous Ovarian Carcinoma. Clinical cancer research : an official journal of the American Association for Cancer Research. 2018;24(20):5037-47.

181. Khashaba M, Fawzy M, Abdel-Aziz A, Eladawei G, Nagib R. Subtyping of high grade serous ovarian carcinoma: histopathological and immunohistochemical approach. Journal of the Egyptian National Cancer Institute. 2022;34(1):6.

182. Hollis RL, Meynert AM, Michie CO, Rye T, Churchman M, Hallas-Potts A, et al. Multiomic Characterization of High-Grade Serous Ovarian Carcinoma Enables High-Resolution Patient Stratification. Clinical cancer research : an official journal of the American Association for Cancer Research. 2022;28(16):3546-56.

183. Matsuda Y, Inoue Y, Hiratsuka M, Kawakatsu S, Arai T, Matsueda K, et al. Encapsulating fibrosis following neoadjuvant chemotherapy is correlated with outcomes in patients with pancreatic cancer. PLOS ONE. 2019;14(9):e0222155.

184. Anscher MS, Peters WP, Reisenbichler H, Petros WP, Jirtle RL. Transforming growth factor beta as a predictor of liver and lung fibrosis after autologous bone marrow transplantation for advanced breast cancer. The New England journal of medicine. 1993;328(22):1592-8.

185. Zhu L, Chen L. Progress in research on paclitaxel and tumor immunotherapy. Cellular & Molecular Biology Letters. 2019;24(1):40.

186. Birkbak NJ, Kochupurakkal B, Izarzugaza JM, Eklund AC, Li Y, Liu J, et al. Tumor mutation burden forecasts outcome in ovarian cancer with BRCA1 or BRCA2 mutations. PLoS One. 2013;8(11):e80023.

187. Strickland KC, Howitt BE, Shukla SA, Rodig S, Ritterhouse LL, Liu JF, et al. Association and prognostic significance of BRCA1/2-mutation status with neoantigen load, number of tumor-infiltrating lymphocytes and expression of PD-1/PD-L1 in high grade serous ovarian cancer. 2016;7(12).

188. Bolton KL, Chenevix-Trench G, Goh C, Sadetzki S, Ramus SJ, Karlan BY, et al. Association between BRCA1 and BRCA2 mutations and survival in women with invasive epithelial ovarian cancer. Jama. 2012;307(4):382-90.

189. Kotsopoulos J, Rosen B, Fan I, Moody J, McLaughlin JR, Risch H, et al. Ten-year survival after epithelial ovarian cancer is not associated with BRCA mutation status. Gynecol Oncol. 2016;140(1):42-7.

190. Kommoss S, Winterhoff B, Oberg AL, Konecny GE, Wang C, Riska SM, et al. Bevacizumab May Differentially Improve Ovarian Cancer Outcome in Patients with

Proliferative and Mesenchymal Molecular Subtypes. Clinical cancer research : an official journal of the American Association for Cancer Research. 2017;23(14):3794-801.

191. Yang D, Sun Y, Hu L, Zheng H, Ji P, Pecot Chad V, et al. Integrated Analyses Identify a Master MicroRNA Regulatory Network for the Mesenchymal Subtype in Serous Ovarian Cancer. Cancer cell. 2013;23(2):186-99.

192. Kalof AN, Cooper K. Our approach to squamous intraepithelial lesions of the uterine cervix. J Clin Pathol. 2007;60(5):449-55.

193. Cheng L, Montironi R, Davidson DD, Lopez-Beltran A. Staging and reporting of urothelial carcinoma of the urinary bladder. Modern Pathology. 2009;22(2):S70-S95.

194. Kudo R, Sato T, Mizuuchi H. Ultrastructural and immunohistochemical study of infiltration in microinvasive carcinoma of the uterine cervix. Gynecol Oncol. 1990;36(1):23-9.

195. Cheon DJ, Tong Y, Sim MS, Dering J, Berel D, Cui X, et al. A collagen-remodeling gene signature regulated by TGF-β signaling is associated with metastasis and poor survival in serous ovarian cancer. Clinical cancer research : an official journal of the American Association for Cancer Research. 2014;20(3):711-23.

196. Marchini S, Fruscio R, Clivio L, Beltrame L, Porcu L, Nerini IF, et al. Resistance to platinum-based chemotherapy is associated with epithelial to mesenchymal transition in epithelial ovarian cancer. European Journal of Cancer. 2013;49(2):520-30.

197. Sachs N, Clevers H. Organoid cultures for the analysis of cancer phenotypes. Current opinion in genetics & development. 2014;24:68-73.

198. Thu KL, Papari-Zareei M, Stastny V, Song K, Peyton M, Martinez VD, et al. A comprehensively characterized cell line panel highly representative of clinical ovarian high-grade serous carcinomas. Oncotarget. 2017;8(31):50489-99.

199. Kreuzinger C, Gamperl M, Wolf A, Heinze G, Geroldinger A, Lambrechts D, et al. Molecular characterization of 7 new established cell lines from high grade serous ovarian cancer. Cancer letters. 2015;362(2):218-28.

200. Ince TA, Sousa AD, Jones MA, Harrell JC, Agoston ES, Krohn M, et al. Characterization of twenty-five ovarian tumour cell lines that phenocopy primary tumours. Nature communications. 2015;6:7419.

201. Fleury H, Communal L, Carmona E, Portelance L, Arcand SL, Rahimi K, et al. Novel high-grade serous epithelial ovarian cancer cell lines that reflect the molecular diversity of both the sporadic and hereditary disease. Genes & cancer. 2015;6(9-10):378-98.

202. Domcke S, Sinha R, Levine DA, Sander C, Schultz N. Evaluating cell lines as tumour models by comparison of genomic profiles. Nature communications. 2013;4:2126.

203. Ben-David U, Ha G, Tseng YY, Greenwald NF, Oh C, Shih J, et al. Patient-derived xenografts undergo mouse-specific tumor evolution. Nature genetics. 2017;49(11):1567-75.

204. Vaughan S, Coward JI, Bast RC, Jr., Berchuck A, Berek JS, Brenton JD, et al. Rethinking ovarian cancer: recommendations for improving outcomes. Nat Rev Cancer. 2011;11(10):719-25.

205. Sachs N, de Ligt J, Kopper O, Gogola E, Bounova G, Weeber F, et al. A Living Biobank of Breast Cancer Organoids Captures Disease Heterogeneity. Cell. 2018;172(1-2):373-86.e10.

206. Sato T, Stange DE, Ferrante M, Vries RG, Van Es JH, Van den Brink S, et al. Long-term expansion of epithelial organoids from human colon, adenoma, adenocarcinoma, and Barrett's epithelium. Gastroenterology. 2011;141(5):1762-72.

207. Fujii M, Shimokawa M, Date S, Takano A, Matano M, Nanki K, et al. A Colorectal Tumor Organoid Library Demonstrates Progressive Loss of Niche Factor Requirements during Tumorigenesis. Cell stem cell. 2016;18(6):827-38.

208. van de Wetering M, Francies HE, Francis JM, Bounova G, Iorio F, Pronk A, et al. Prospective derivation of a living organoid biobank of colorectal cancer patients. Cell. 2015;161(4):933-45.

209. Vlachogiannis G, Hedayat S, Vatsiou A, Jamin Y, Fernández-Mateos J, Khan K, et al. Patient-derived organoids model treatment response of metastatic gastrointestinal cancers. Science. 2018;359(6378):920-6.

210. Roerink SF, Sasaki N, Lee-Six H, Young MD, Alexandrov LB, Behjati S, et al. Intra-tumour diversification in colorectal cancer at the single-cell level. Nature. 2018;556(7702):457-62.

211. Bleijs M, van de Wetering M, Clevers H, Drost J. Xenograft and organoid model systems in cancer research. The EMBO journal. 2019;38(15):e101654.

212. Hill SJ, Decker B, Roberts EA, Horowitz NS, Muto MG, Worley MJ, Jr., et al. Prediction of DNA Repair Inhibitor Response in Short-Term Patient-Derived Ovarian Cancer Organoids. Cancer discovery. 2018;8(11):1404-21.

213. Kopper O, de Witte CJ, Lõhmussaar K, Valle-Inclan JE, Hami N, Kester L, et al. An organoid platform for ovarian cancer captures intra- and interpatient heterogeneity. Nature medicine. 2019;25(5):838-49.

214. Hoffmann K, Berger H, Kulbe H, Thillainadarasan S, Mollenkopf HJ, Zemojtel T, et al. Stable expansion of high-grade serous ovarian cancer organoids requires a low-Wnt environment. The EMBO journal. 2020;39(6):e104013.

215. Nanki Y, Chiyoda T, Hirasawa A, Ookubo A, Itoh M, Ueno M, et al. Patient-derived ovarian cancer organoids capture the genomic profiles of primary tumours applicable for drug sensitivity and resistance testing. Sci Rep. 2020;10(1):12581.

216. Kessler M, Hoffmann K, Brinkmann V, Thieck O, Jackisch S, Toelle B, et al. The Notch and Wnt pathways regulate stemness and differentiation in human fallopian tube organoids. Nature communications. 2015;6:8989.

217. Surina, Tanggis, Suzuki T, Hisata S, Fujita K, Fujiwara S, et al. Patient-derived spheroids and patient-derived organoids simulate evolutions of lung cancer. Heliyon. 2023;9(3):e13829.

218. Yip HYK, Tan CW, Hirokawa Y, Burgess AW. Colon organoid formation and cryptogenesis are stimulated by growth factors secreted from myofibroblasts. PLoS One. 2018;13(6):e0199412.

219. Ng-Blichfeldt J-P, Guryev V, Hiemstra P, Jong TD, Kortekaas R, Stolk J, et al. Late Breaking Abstract - TGF-ß impairs fibroblast ability to support lung organoid formation: pharmacological restoration by GSK-3 inhibition and secreted niche factor supplementation. 2018;52(suppl 62):OA520.

220. Li Z, Yu L, Chen D, Meng Z, Chen W, Huang W. Protocol for generation of lung adenocarcinoma organoids from clinical samples. STAR protocols. 2021;2(1):100239.

221. Ng A, Tan S, Singh G, Rizk P, Swathi Y, Tan TZ, et al. Lgr5 marks stem/progenitor cells in ovary and tubal epithelia. Nature cell biology. 2014;16(8):745-57.